2.8 Special Form

This section is not applicable to the NAC-LWT cask because the fuel to be transported in the cask fails to satisfy the definition for special form radioactive material in 10 CFR 71.4

2.9 Spent Fuel Contents

2.9.1 PWR and BWR Fuel Rods

Regulatory Guide 7.9 requires that analysis or test data be provided showing that the fuel rod cladding has structural integrity, justifying the amount of integrity claimed. This section is not applicable to the NAC-LWT cask, since no fuel rod structural integrity is claimed. However, it is noted that according to "Dynamic Impact Effects on Spent Fuel Assemblies" (Chun), damage is not likely to occur to the Westinghouse 17 × 17 fuel assembly for a 63 g side drop or an 82 g end drop load. (Of the fuel assemblies examined, the Westinghouse 17 × 17 had the "weakest" structural parameters.) Fuel rod resistance to impact load is dependent on clad temperature and cool time. The NAC-LWT cask impact limiter analyses (Section 2.6.7.4) demonstrate that the maximum design side drop and end drop are 49.7 g and 60 g, respectively. Since the cask g loads are less than the g loads reported in the reference noted above, damage to the fuel rods in the NAC-LWT cask is not likely to occur.

2.9.2 TRIGA Fuel Elements

This section shows that the TRIGA fuel cladding remains intact when hypothetical accident deceleration loads (end and side drops) are applied to the NAC-LWT cask. Hand calculations are used to analyze the TRIGA fuel cladding. All analyses are performed using temperature dependent material properties and a bounding temperature value of 600°F. The following table summarizes the properties used to evaluate the aluminum cladding (1100-0 alloy) and stainless steel cladding (Type 304).

	Aluminum	Steel
Ultimate tensile strength, S_u	2,900 psi	63,500 psi
Tensile yield strength, S_y	2,000 psi	18,200 psi
Modulus of Elasticity, E	7.0×10^6 psi	25.3×10^6 psi 28.3×10^6 psi @70°F (conservative value for bearing)
Poisson's ratio, ν	0.3	0.275
Density, ρ	0.1	0.288 lb/in^3

ASME Code Section III, Subsection NG stress allowables are used for this evaluation. As stated in the previous section, design g values are 60.0 g and 49.7 g for the end and side drops, respectively.

The weight of the standard stainless steel fuel element is 4 kg (8.82 lbs) and the weight of the fuel follower control elements is 6 kg (13.2 lbs). There are a maximum of four (4) elements in any fuel can resulting in a maximum weight of 53 lbs. The aluminum (0.03-inches thick) and stainless steel (0.02-inches thick) cladding are described in TRIGA fuel characterization reports (Tomsio). The bounding weight of the cladding is:

$$W_{cladding} = \frac{\pi}{4}(D_o^2 - D_i^2) \times L \times \rho = 2 \text{ lbs}$$

where:

Do = 1.47 inches, outside diameter of cladding
Di = 1.41 inches, inside diameter of cladding
L = 45 inches, length of cladding (fuel follower rod)
ρ = 0.288 lb/in^3, density of steel

2.9.2.1 End Drop

The end drop evaluation determines if the cladding is structurally stable under its own weight with dynamic load factors to account for cask drop deceleration. Because it is longer and heavier, the fuel follower control element is investigated for buckling. For conservatism, the thinnest cladding is used in conjunction with stainless steel density and aluminum properties. The fuel is taken as self supporting. The buckling load is the weight of the cladding times the end drop design g value of 60g.

$$P_c = 60 \times 2 = 120 \text{ lbs}$$

The critical buckling load is:

$$P_{cr} = \frac{\pi^2 EI}{(2L)^2} = 205 \text{ lbs}$$

where:

I = 0.0491 × (1.47^4-1.43^4) = 0.024 in^4
E = 7.0 × 10^6 psi
L = 45 inches, length of the fuel follower control element

The effective length factor is taken as 2.

The margin of safety is:

$$MS = \frac{P_{cr}}{P_c} - 1 = +0.71$$

Therefore, the cladding will not buckle under its own weight due to the cask end drop.

2.9.2.2 Side Drop

In the side drop, two fuel elements can bear on each other and two elements (one on top of the other) can bear on the flat surface of the module cell wall.

Because of aluminum's lower strength, the bearing stress in the aluminum clad fuel element is the governing case.

For the aluminum clad fuel elements, the bearing stresses will cause local cladding deformation in the radial direction along the line of contact. The deformation will be limited to the distance producing an area, A, sufficient to limit bearing stress to the yield stress of the aluminum cladding.

$$A = \frac{p}{S_y} = \frac{0.51(49.7)}{2{,}000} = 0.0127 \text{in}^2$$

where:

$$p = \frac{W}{L} = \frac{15.2 \text{ lb}}{30} = 0.51 \text{ lb / in.}$$

W = ss clad fuel element, 8.8 lbs (4 kg) + aluminum clad fuel element, 6.4 lbs (2.9 kg) = 15.2 lbs. (Tomsio)

L= fuel element length = 30 inches (Tomsio)

Acceleration from side drop = 49.7 g

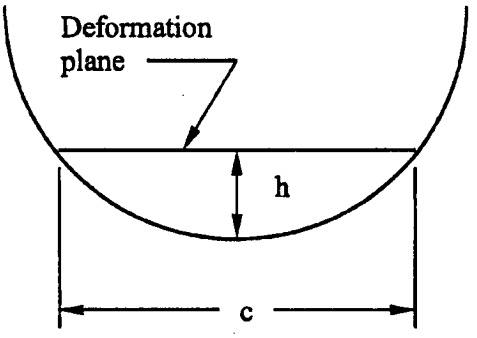

The area, A, of the deformation plane is:

$A = c \times \text{unit length} = 0.0127 \text{ in}^2$, therefore,

$c = 0.0127$ inches

The deformation depth, h, is then:

$$h = r - \frac{1}{2}\sqrt{4r^2 - c^2} = 0.735 - \frac{1}{2}\sqrt{4(0.735)^2 - 0.0127^2} = 2.7 \times 10^{-5} \text{ inches}$$

This deformation is insignificant when compared to the 0.030-inch wall thickness of the aluminum cladding.

The slight local deformation (0.000027 in) along the line of contact between fuel elements reduces the bearing stress in the aluminum cladding at this point to the yield strength of the cladding. The small linear deformation of the cladding has no adverse effect on its ability to contain the fuel and does not impede its insertion into or removal from the fuel basket cell.

Therefore, the integrity and function of the fuel element cladding is not impaired.

2.9.3 PULSTAR Intact Fuel Elements

There are two configurations for the PULSTAR intact fuel elements:

1. Intact PULSTAR fuel assemblies that are comprised of a 5 × 5 array of fuel elements. Elements in the assembly are spaced by a tie plate at each end and by periodic spacer tabs on each fuel element (see Figure 1.2-13).
2. Intact PULSTAR fuel elements that are loaded into the TRIGA fuel rod insert (Drawing 315-40-096).

In the item a) configuration, the PULSTAR fuel assembly is inserted in a cell of a MTR basket module that provides full-length support of the fuel assembly. The tabs connecting the individual fuel elements are separated by 6.37 inches and each fuel element has a 0.47-inch outer diameter. The span between PULSTAR fuel element supports is bounded by a standard PWR fuel assembly, while the outer diameter of 0.47 inch bounds a standard PWR rod diameter of 0.37 inch. As the PULSTAR fuel assembly is fully supported, similar to a PWR assembly in the LWT basket, it is concluded that the PULSTAR fuel assembly will remain intact during normal and accident conditions, as is presented for a PWR assembly in the LWT SAR.

In the item b) configuration, the individual elements are supported for the full length of the fuel element. The stresses being developed in the fuel element for the normal and accident conditions for either the end drop or the side drop are considered to be minimal since the fuel element is supported for the full length of the element. The tube has been evaluated in Section 2.6.12.7.9 for the normal transport condition 1-foot drops and in Section 2.7.7.9.8 for the hypothetical accident condition 30-foot drops. The evaluations concluded that in either of the configurations described, the fuel assembly, or the individual fuel elements, will remain intact for the normal transport and hypothetical accident conditions.

2.9.4 ANSTO Fuels

The structural integrity of the MARK III spiral fuel assemblies and the MOATA plate bundles is evaluated in this section for normal and accident conditions of transport.

2.9.4.1 MARK III Spiral Fuel Assemblies

The Mark III spiral fuel assembly is comprised of a center tube, an outer tube and 10 fuel plates that are 25 inches long (see Figure 1.2.3-14). The fuel plates are curved and are positioned between the center tube and the outer tube in a spiral configuration, as opposed to forming a radial type "spoke" between the center and the outer tubes. Evaluations are performed for the center tube and the outer tube since they are the components that must transfer the weight of the plates during normal and accident conditions. Aluminum 1100 properties, which are considered to provide minimal values for the stress allowables, are used in the plates and tubes.

Center Tube

A structural evaluation of the center tube of the MARK III spiral fuel is performed. Two loads are considered: the tube self-weight and 50% of the weight of the fuel plates. Five out of 10 of the fuel plates can transfer their weight to the inner tube; therefore, 50% of the weight of the fuel plates is considered. The weight of the center tube is increased to account for 50% of the fuel plate weight. The formula for the circular rings from Case 15 (ring supported at the base at a single point and loaded by their own weight per unit length of circumference w) of Table 17 in Roark is used for this evaluation. It is conservatively assumed that the tube weight and 50% of the fuel plate weight are supported at a single point.

There are 10 fuel plates in a fuel assembly. A fuel plate of MARK III spiral fuel weighs 0.4431 lb (201 g). The weight of the five fuel plates (2.22 lbs) contributes to the load and pushes the tube down during the basket side drop. The weight of the five plates, converted to its own weight per unit length of circumference, w_p, is (before considering the g load factor):

$$w_p = \frac{m_p}{L \times 2\pi R} = 0.0121 \text{ lb/in}$$

where:

m_p = 2.22 lbs, the weight of five plates

L = 25 inches, the length of the plate

R = 1.1678, median radius of the fuel inner tube

The tube weight per unit length of circumference, w_t, is (before considering the g load factor):

$$w_t = \frac{m_t}{2\pi R} = 0.0058 \text{ lb/in.}$$

where:

m_t = 1.0582/25 = 0.0423 lb, the weight of tube (480 g) per inch

R = 1.1678, median radius of the fuel inner tube

Normal Condition

The maximum bending moment at the support point for the normal condition is:

$$M_c = \frac{3}{2} \times f_{GN} \times (w_p + w_t) \times R^2 = 0.9154 \text{ lb-in}$$

where:

f_{GN} = 25, the side drop g load for the normal condition

The circumferential bending stress in the tube for the normal condition is:

$$\sigma_c = \frac{6M_c}{bt^2} = \frac{6 \times 0.9154}{1 \times 0.0443^2} = 2{,}799 \text{ psi}$$

where:

t = 0.0443 inch, tube thickness

b = 1 inch, unit length of tube

The margin of safety corresponding to the allowable for the normal condition is:

$$MS = \frac{1.5S_m}{\sigma_c} - 1 = +0.58$$

where:

Sm = 2.95 ksi, Design Stress Intensity, Aluminum 1100, 250°F (Table 2.2, "Aluminum Standards and Data," The Aluminum Association)
(S_m is the lesser of $S_u/3$ and $2S_y/3$)

Accident Condition

The maximum bending moment at the support point for the accident condition is:

$$M_c = \frac{3}{2} \times f_{GA} \times (w_p + w_t) \times R^2 = 2.197 \text{ lb-in}$$

where:

f_{GA} = 60, the side drop g load for the accident condition

The circumferential bending stress in the fuel tube for the accident condition is:

$$\sigma_c = \frac{6M_c}{bt^2} = \frac{6 \times 2.197}{1 \times 0.0443^2} = 6{,}717 \text{ psi}$$

The margin of safety corresponding to the allowable for the accident condition is:

$$MS = \frac{S_u}{\sigma_c} - 1 = +0.36$$

where:

Su = 9.14 ksi, ultimate stress of Aluminum 1100 at 250°F (Table 2.2, "Aluminum Standards and Data," The Aluminum Association)

Outer Tube

A structural evaluation of the outer tube of the MARK III spiral fuel is performed. Three loads are considered: the tube self-weight, the weight of the fuel plates, and the weight of the inner tube. The weight of the outer tube is increased to account for the fuel plate weight and the weight of the inner tube. The formula for a curved beam (pinned arch under uniform load) from Blake is used for this evaluation. Since the diametrical gap between the MARK III spiral fuel and the basket tube inner surface is 0.125 inch, the use of the pin-pin configuration is adequate.

There are 10 fuel plates in a fuel assembly. A fuel plate of MARK III spiral fuel weighs 0.4431 pound (201 g). The weight of the inner tube (1.0582 lbs) and the 10 fuel plates (4.431 lbs) contributes to the load and pulls the tube down during the basket side drop. The weight of the inner tube and the fuel plates, converted to its own weight per unit length of circumference, q_c, is (before considering the g load factor):

$$q_c \approx \frac{m_p + m_i}{Lp \times 2\pi R} = 0.0177 \text{ lb/in}$$

where:

m_p = 4.431 lbs, the weight of 10 plates

m_i = 1.0582 lbs, the weight of inner tube (480 g)

Lp = 25 inches, the length of the plate

R = 1.9695, median radius of the fuel outer tube

The outer tube weight per unit length of circumference, q_t, is (before considering the g load factor):

$$q_t = \frac{m_t}{2\pi R} = 0.0078 \text{ lb/in.}$$

where:

m_t = 2.4251/25 = 0.0970 lb, the weight of outer tube (1,100 g) per inch

R = 1.9695, median radius of the fuel outer tube

The combined load factor, q_{total}, is 1.53 lb/in [$60\times(q_c+q_t)$, 60 is the side drop g load factor] for the accident condition of the side drop case.

The maximum moment (Equation 27.63, Blake) for the accident conditions is:

$$M = q_{total} \times R^2 \times B = 0.5460 \text{ lb}-\text{in} \quad \text{for accident condition}$$

where:

R = 1.9695, median radius of the fuel outer tube

B = 0.092, the maximum absolute value of the bending moment factor
(B is from Figure 27.17 in Blake)

Based on Equation 28.1 from Blake, the stress due to this bending is:

$$S = \frac{M}{A\times R}\left[1+\frac{c}{\lambda(R+c)}\right] = 879 \text{ psi} \quad \text{for accident condition}$$

where:

A = 0.061 in^2, the cross-section area (thickness of the outer tube is 0.061 in)

R = 1.9695, median radius of the fuel outer tube

c = 0.03 in, half of the thickness of the outer tube

λ = 7.8×10^{-5}, the Winkler's factor for rectangular cross-section, as calculated:
(Table 28.1, Blake)

$$\lambda = \frac{1}{3}\left(\frac{c}{R}\right)^2+\frac{1}{5}\left(\frac{c}{R}\right)^4+\frac{1}{7}\left(\frac{c}{R}\right)^6+\cdots = 7.8\times10^{-5}$$

Conservatively, the allowable for the normal condition is used for calculating the margin of safety in the accident condition. The margin of safety corresponding to the allowable for the normal condition is:

$$MS = \frac{1.5S_m}{S}-1 = +4.0$$

where:

S_m = 2.95 ksi, Design Stress Intensity, Aluminum 1100, 250°F

Therefore, the Mark III spiral fuel remains intact for the normal and accident conditions of transport.

2.9.4.2 MOATA Plate Bundles

Two 6.35-mm aluminum plates are required to carry the weight of the MOATA plate bundle during transport. The aluminum plates sandwich the 14 or the 9 aluminum fuel plates (see the following illustration). At each end of the plate bundle is an end fitting that permits handling. Each end fitting also contains a bolt assembly that threads into the walls of the end fitting. The outer diameter of the end fitting is 3.449 inches. The diametrical gap between the end fitting and the inner diameter of the basket tube is 4.125 – 3.449 or 0.68 inch. During transport, it is not possible for the bolt to become disengaged from the end fitting due to the 0.68-inch gap. Therefore, the configuration of the fuel plates and the aluminum plates will not be altered during transport. The bolt assembly is considered to experience negligible loading stress due to its own weight. Likewise, the stresses occurring in the end fittings are expected to be minimal and are bounded by stresses occurring in the aluminum plates.

For the stress evaluation of the aluminum plates, the bounding condition is the side drop. To compute the minimum margin for both the normal condition and the accident condition, the stress is computed using the accident loading case, but the margin of safety is computed using the stress allowable for the normal condition.

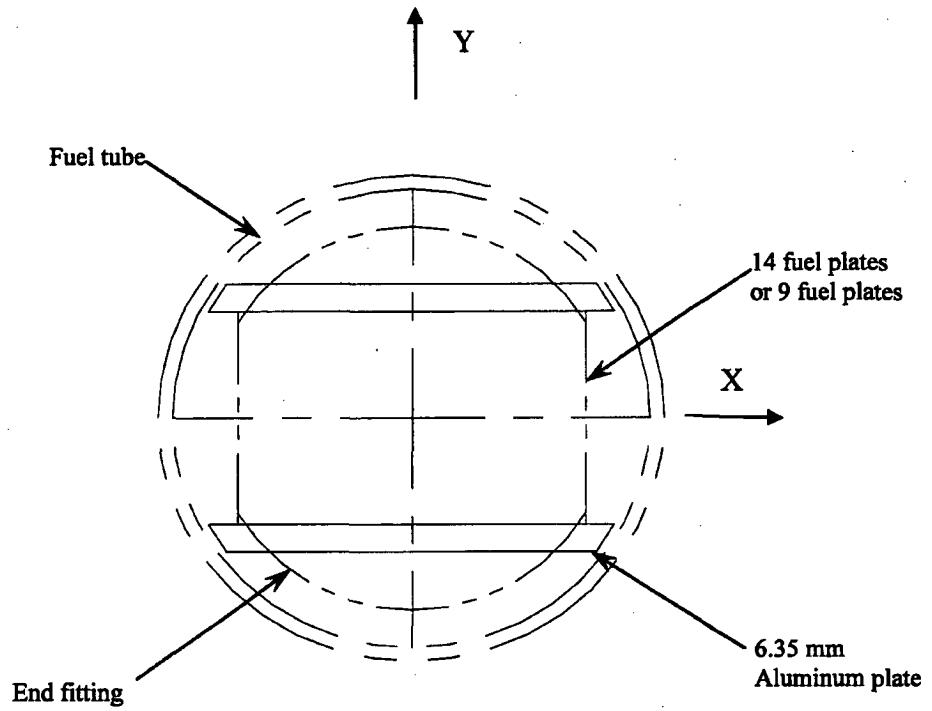

For a 30-foot side drop in the direction aligned with the Y axis, the maximum stress in the aluminum plate is calculated by representing the plate as a uniformly loaded, simply supported beam. Since the plate is supported at the edges along the 26-inch length of the plate, the length of the beam in this calculation is its width, or 3.7 inches. The bending moment on the center of the plate is:

$$M = \frac{Pw^2}{8} = \frac{36.5 \times 3.7^2}{8} = 62.5 \text{ in-lb}$$

where:

$$P = \frac{Wg}{L} = \frac{15.8 \times 60}{26} = 36.5 \text{ lb/in}$$

W =18-2.2 = 15.8 lbs, since the top aluminum plate is significantly stiffer than the fuel elements below the top aluminum plate and does not load the bottom plate

w = 3.7 inches (94 mm), maximum plate width

L = 26 inches, length of the aluminum plate

The bending stress in the plate (0.25-in thick) is:

$$\sigma = \frac{6M}{bt^2} = \frac{6 \times 62.5}{1 \times 0.25^2} = 6.0 \text{ ksi}$$

Conservatively using the membrane plus bending allowable for normal conditions, the margin of safety is:

$$MS = \frac{1.5S_m}{\sigma} - 1 = +1.9$$

where:

S_u = 34.6, ultimate strength, 6061-T6, 250°F

(design stress intensity, S_m, is the lesser of $S_u/3$ and $2 \times S_y/3$)

For a 30-foot side drop of the fuel aligned with the X axis, the fuel plates are not supported by the 6.35-mm aluminum plates. The maximum stress in the fuel plate (Aluminum 1100) is calculated by representing the plate (26 inches long) as a uniformly loaded, simply supported beam. The bending moment on the center of the plate is:

$$M = \frac{PL^2}{8} = \frac{1.53 \times 26^2}{8} = 129.3 \text{ in-lb}$$

where:

$$P = \frac{Wg}{L} = \frac{0.66 \times 60}{26} = 1.53 \text{ lb/in}$$

W = 0.66 lb (300 g);

L = 26 inches, length of the fuel plate

The bending stress in the plate (0.08-in thick) is:

$$\sigma = \frac{6M}{bt^2} = \frac{6 \times 129.3}{0.08 \times 3^2} = 1.1 \text{ ksi}$$

Conservatively using the allowable for normal conditions, the margin of safety is:

$$MS = \frac{1.5S_m}{\sigma} - 1 = +3.0$$

where:

S_m = 2.95 ksi, Design Stress Intensity, Aluminum 1100, 250°F

(design stress intensity, S_m, is the lesser of $S_u/3$ and $2 \times S_y/3$)

During an end drop, a compressive load is developed in the aluminum plates and in the fuel elements. Due to the proximity of the end of the fuel elements to the lifting bracket or to the bottom of the basket, the axial load of the fuel elements will be transmitted directly into the lifting bracket or the bottom of the basket. The compressive load on the aluminum plates is the weight of the end fittings and the self-weight of the aluminum plates. However, the inertial load in the end drop of the aluminum plates is not uniform, but rather is at a maximum at the bottom of the plate nearest the plane of impact. The maximum compressive stress is the product of the 26-inch length, the density of 0.098 lb/in^3, and the acceleration of 60g's or 153 psi. This compressive stress is considered to be minimal and only occurs at the base. The load that is considered to be uniform over the length of the aluminum plate is the weight of the end fitting, or 4.34 lbs. Since there are two plates of equal stiffness, the load is considered to be distributed equally to the two plates.

For a 60g end drop, the load on one plate is:

$$P = W_a g = \left(\frac{4.34}{2}\right) \times 60 = 130.2 \text{ lbs}$$

The stress in the aluminum plate is:

$$\sigma = \frac{P}{bt} = \frac{130.2}{3.38 \times 0.25} = 154 \text{ psi}$$

Using the Euler buckling methodology from the "Manual of Steel Construction," the critical buckling stress, for $KL/r > C_c$ is:

$$F_a = \frac{12\pi^2 E}{23(KL/r)^2} = 371 \text{ psi}$$

where:

b = 3.38 inches, plate width

t = 0.25 in (6.35 mm), plate thickness

L = 26.0 inches, plate length between bolt supports

K = 1.0, buckling end fixity constant – simply supported at each end due to the retaining pin

E = 9.1×10^6 psi, modulus of elasticity, 6061-T6, 250°F

F_y = 29.8 ksi, yield strength, 6061-T6, 250°F

$$r = \sqrt{\frac{I}{A}} = 0.072$$

$$I = \frac{bt^3}{12} = 0.0044 \text{ in}^4$$

$A = bt = 0.84 \text{ in}^2$

KL/r = 361

$$C_c = \sqrt{\frac{2\pi^2 E}{F_y}} = 79$$

The safety factor against the plate buckling is calculated to be larger than unity, as shown in the following equation. Therefore, aluminum plates will not buckle.

$$FS = \frac{F_a}{\sigma} = \frac{371}{154} = 2.4$$

Since the aluminum plates do not buckle, the fuel elements will only be loaded by their own self-weight. The compressive loading on the fuel elements also varies uniformly from zero at the top of the fuel element to the base. This stress is the ratio of the total compressive load (0.66 lb × 60g's) to the cross-sectional area (7.6 cm × 0.203 cm or 0.24 in^2), or 166 psi. This is considered to be a minimal compressive stress that would not result in damage to the fuel element. Since the aluminum plates do not buckle and are further restrained by the fuel basket tubes, the buckling of the fuel elements cannot occur during the end drop. Therefore, the fuel is not damaged.

2.10 Appendices

2.10.1 Computer Program Descriptions

Structural evaluation of the NAC-LWT cask body is accomplished by two computer codes, ANSYS and RBCUBED. Each program is described in the following sections.

2.10.1.1 ANSYS

The structural analysis of the main body of the NAC-LWT cask is performed using a finite element model and the ANSYS structural analysis computer program ('ANSYS' Computer Code for Large-Scale General Purpose Engineering Analysis). The ANSYS computer program is a large-scale, general purpose computer program for the solution of several classes of engineering analyses, including: static and dynamic; elastic, plastic, creep and swelling; buckling; and small and large deflections. The matrix displacement method of analysis based on finite element idealization is employed throughout the program. The large variety of element types available gives ANSYS the capability of analyzing 2- and 3-dimensional frame structures, piping systems, 2-dimensional plane and axisymmetric solids, 3-dimensional solids, flat plates, axisymmetric and 3-dimensional shells, and nonlinear problems, including gap element interfaces. The use of the axisymmetric elements permits accurate modeling of the cask body with a half-section model. The interface gap elements provide the capability of realistic modeling and evaluation of the interactions between the lead and the stainless steel shells and between the upper ring, closure lid and bolts.

Typically, the ANSYS program is run by sequential implementation of three options: pre-processing (or model building); analysis (calculation of stiffness matrix, displacements and reaction forces solution, element stresses); and post-processing (selection of analysis results). Each option may be run in the interactive or batch mode computer environment.

The ANSYS pre-processor (PREP7) is used to construct the finite element mesh, describe each cask component material (temperature-dependent) property, assign unique identifiers for cask components, model displacement boundary conditions and prescribe temperature, point loads, or surface tractions of appropriate element faces or nodes. The PREP7 graphics option is a valuable tool that permits the user to check the model for completeness. The ANSYS analysis option uses the PREP7 file to generate a solution file and to provide a user-oriented printout of the solution phase. In general, each solution provides: a complete echo of the model data, model displacement solution, element stresses, nodal forces, reaction forces, and any warnings or errors related to the analysis.

A variety of ANSYS post-processors (e.g., Postl and Post29) utilize the solution file to sort, print, or plot selected results from the ANSYS analysis. The post-processors can provide many useful features including a maximum set of variables (such as stress components or displacements) or section stresses along a designated path. Additionally, the structural behavior can be viewed by model displacement and stress contour plots.

2.10.1.2 RBCUBED - A Program to Calculate Impact Limiter Dynamics

This section presents a general description of the RBCUBED program. The methods described in this section are used by the RBCUBED program in the NAC-LWT cask impact limiter analyses.

RBCUBED, an impact limiter analysis computer program, utilizes quasistatic methodology; that is, each iteration freezes an instant in time during which all calculations are performed, and then, proceeds to the next time increment. The methodology employed in the program sizes the impact limiter and calculates the deceleration forces used to calculate the stresses imposed on the cask structure, but does not implement any load factor. There are several assumptions that are attendant to this methodology:

- Gravity is the only force that acts on the cask during free fall. While falling, the cask is translating vertically and continues to do so until the initial (first) impacting end has been brought to rest. In oblique and side drop cases after the first end has been stopped, the cask rotates until the second limiter strikes the unyielding surface and absorbs the remaining kinetic energy.
- There is no sliding or lateral motion of the cask at any time during the impact(s).
- The cask weight includes the impact limiters, but the length of the cask does not.
- The deceleration force generated during crushing of the isotropic absorption material acts at the area centroid of the area engaged in crushing for that increment in time.
- Crushing of the absorption material occurs from the outside toward the cask body.
- The component of the cask weight acting downward and the crush force acting upward are assumed to act colinearly. The magnitude of the weight component is very small compared to the crush force.
- The impact limiter material that is not between the cask and the unyielding surface does not absorb any kinetic energy. The extraneous limiter material is ineffective for the purposes of this impact limiter analysis.

RBCUBED is capable of analyzing any cask impact orientation from vertical (0°) to horizontal (90°).

The input data for RBCUBED includes the following: (1) height of drop; (2) weight of cask system; (3) cask length; (4) impact orientation angle; (5) deflection increment; (6) material crush properties (stress-strain curve or force deflection curve); and (7) impact limiter geometry.

Geometric modeling of the impact limiter is performed using combinatorial geometry based on the MORSE-CG computer program.

The output data from RBCUBED includes the following: (1) a verbatim input return; (2) a processed input of general problem parameters and material properties; (3) the results of the RBCUBED execution - deflection; (4) resultant force; (5) remaining kinetic energy; (6) velocity; (7) elapsed time since the beginning of impact; (8) area currently involved in crushing; and (9) a series of crush "footprints" at crush intervals of one inch.

The computer program, RBCUBED--A Program to Calculate Impact Limiter Dynamics, was benchmarked for validity by comparison of analysis results to manual calculations using crush areas determined by drafting methods.

2.10.2 Finite Element Model Description

The finite element analysis technique is well suited for the evaluation of the axisymmetric cask body structure, especially with respect to the following: (1) the interaction between the lead cylinder and the stainless steel shells and end plates; (2) the discontinuity effects at the shell and bottom forging intersections; and (3) the interaction of the top ring forging, closure lid and bolts in the vicinity of the bolted region. Furthermore, finite element analysis must consider (1) the stresses in the inner and outer shell induced by the lateral pressure from the lead during 30-foot drop conditions; (2) the differential thermal expansion of the lead and stainless steel shells under both hot and cold temperature conditions; and (3) the fact that no physical bonding exists between the lead and the surrounding stainless steel.

The finite element model of the NAC-LWT cask body is generated utilizing the ANSYS PREP7 routine. The cask body is modeled as an assembly of axisymmetric elements about its longitudinal centerline (Figure 2.10.2-1). The aspect ratio of finite elements and the density of geometric mesh are carefully arranged, especially at the locations of geometric discontinuity and force boundary. This minimizes the numerical instability situation incurred by the finite element method.

The cask components considered in the finite element model include the cask closure lid, top ring, closure lid bolts, inner and outer shells, lead middle shell, bottom, bottom cover plate, and lead bottom plate. All of the cask components, except the closure lid bolts, are modeled with isoparametric quadrilateral axisymmetric elements.

The closure lid bolt is modeled as a beam element connected just below the countersink in the lid to the cask body at the bolt circle centerline. The cross-sectional properties of the bolt are input on a "per radian" basis. The bolt preload is applied to the finite element model as an initial strain on the beam element.

A significant number of gap elements are used to model (1) the interfaces between the lead shell and the inner and outer stainless steel shells, and (2) the interface between the lead bottom plate and the bottom. The "gap" element represents two surfaces, which may maintain or break physical contact and may slide relative to each other. Note that the gap element is only capable of supporting compression in the direction normal to the surfaces and friction in the tangential direction. Gap elements completely surround the lead shell in the cask wall. According to whether or not there is contact between the lead and stainless steel surfaces, the gap elements transmit compressive load, but permit no tensile load between the lead and stainless steel. This means that the gap element allows the lead to move freely inside the space surrounded by the stainless steel. When an acceleration is imposed on the entire mass of the cask model, which includes the lead shell, to account for the inertial effect of a drop impact condition, the

acceleration applied to the lead shell causes the lead to slump and, consequently, creates lateral pressures on the inner and outer shells, wherever the lead contacts them.

Similarly, when the lead shell has a higher thermal expansion coefficient than the stainless steel, the lead has a larger thermal growth or contraction and is restrained by the surrounding stainless steel. The gap element again allows the lead to move freely inside the space surrounded by the stainless steel. Pressures resulting from the thermal expansion restraints develop wherever the lead contacts the surrounding stainless steel.

Thus, accurate modeling is achieved for the lead slump during an impact load condition and for differential thermal expansion and contraction during temperature excursions.

A large stiffness of 10^9 is specified to maintain the boundary between the lead/steel surfaces. Similarly, gap elements are used to model the interface between the closure lid and the top ring. A stiffness of 10^9 is specified to maintain the boundary between these surfaces.

It should be noted that there are tapered transitions at each end of the outer shell. The results of parametric studies combined with previous cask analyses have shown that a tapered transition region will not significantly affect the stress concentration on the junctions of the outer shell and the end forgings. The finite element model of the NAC-LWT cask, therefore, conservatively gives no consideration to tapered transitions at each end of the outer shell.

License drawings in Section 1.4 are used to define the cask dimensions for the model. The material properties used in the ANSYS analyses are tabulated in Section 2.3.

Figure 2.10.2-1 presents an entire cask view of the finite element model identifying view regions. There are a total of 2,013 nodes and 1,890 elements. Figure 2.10.2-2 through Figure 2.10.2-8 are detailed views of each region showing the nodal point numbers on the edge nodes. The broken lines represent the gap between the lead and the steel.

For identification and ease of evaluation of component critical section stresses, the finite element cask components are uniquely designated as shown in Figure 2.10.2-9.

A list of nodal coordinates is reported in Table 2.10.2-1. This helps to identify the actual locations of component critical sections, which are widely used in the expression of finite element stress results.

2.10.2.1 Boundary and Loading Conditions Used in the 30-Foot Drop Finite Element Analysis

The constrained nodes and the loading conditions for each 30-foot drop finite element analysis are summarized below for illustration purposes. The 1-foot drop conditions are identical to those of the 30-foot drops, except that the g-load factors are different.

2.10.2.1.1 Displacement Boundary Conditions

Case 1	Top end drop,	$\phi = 0°$
	Boundary constraint	UX: all the nodes located on the cask vertical centerline; for example, 1, 26, 51, 76, etc. UY: node 25
Case 2	Side drop,	$\phi = 90°$
	Boundary constraint	UX: node 1, 2561 UY: node 1 UZ: node 1, 2561
Case 3	Bottom end drop,	$\phi = 180°$
	Boundary constraint	UX: all the nodes located on the cask vertical centerline; for example, 1, 26, 51, 76, etc. UY: node 2176
Case 4	Top oblique drop,	$\phi = 15.74°, 30°, 45°, 60°$
	Boundary constraint	UX: node 1, 25, 2561 UY: node 1 UZ: node 1, 25, 2561
Case 5	Bottom oblique drop,	$\phi = 120°, 135°, 150°, 164.26°$
	Boundary constraint	UX: node 1, 2176, 2561 UY: node 2561 UZ: node 1, 2176, 2561

where:

ϕ = drop orientation or, in other words, the angle between the impact direction and the cask centerline. When ϕ equals 120°, 135°, 150° or 164.26°, it represents the bottom oblique drops at 60°, 45°, 30° and 15.74°.

UX = translational displacement restraints along the cask radial direction.

UY = translational displacement restraints along the longitudinal (vertical) direction.

UZ = translational displacement restraints along the circumferential direction.

2.10.2.1.2 Loading Conditions

For each of the side or oblique drop orientations, the impact loads are applied as a cosine-shaped distribution over the impact region (See Figure 2.7.1-6 and Figure 2.7.1-9). This cosine-shaped pressure distribution is represented in terms of a Fourier series of harmonic functions, as discussed in Section 2.7.1.2.2, equations 1 through 4, for the side drop condition and Table 2.7.1-22 for the oblique drop condition. The applied impact pressure loadings for each of the 30-foot hypothetical accident conditions are tabulated in Table 2.10.2-2. In addition, the inertial load is applied on the mass of the cask model for each drop. Table 2.6.7-34 provides the cask drop g load factors. The impact pressures for each of the 1-foot drop conditions are calculated by multiplying the 31-foot impact pressure by the ratio of the 1-foot g load to the 31-foot g load.

Figure 2.10.2-1 ANSYS Finite Element Model – NAC-LWT Cask

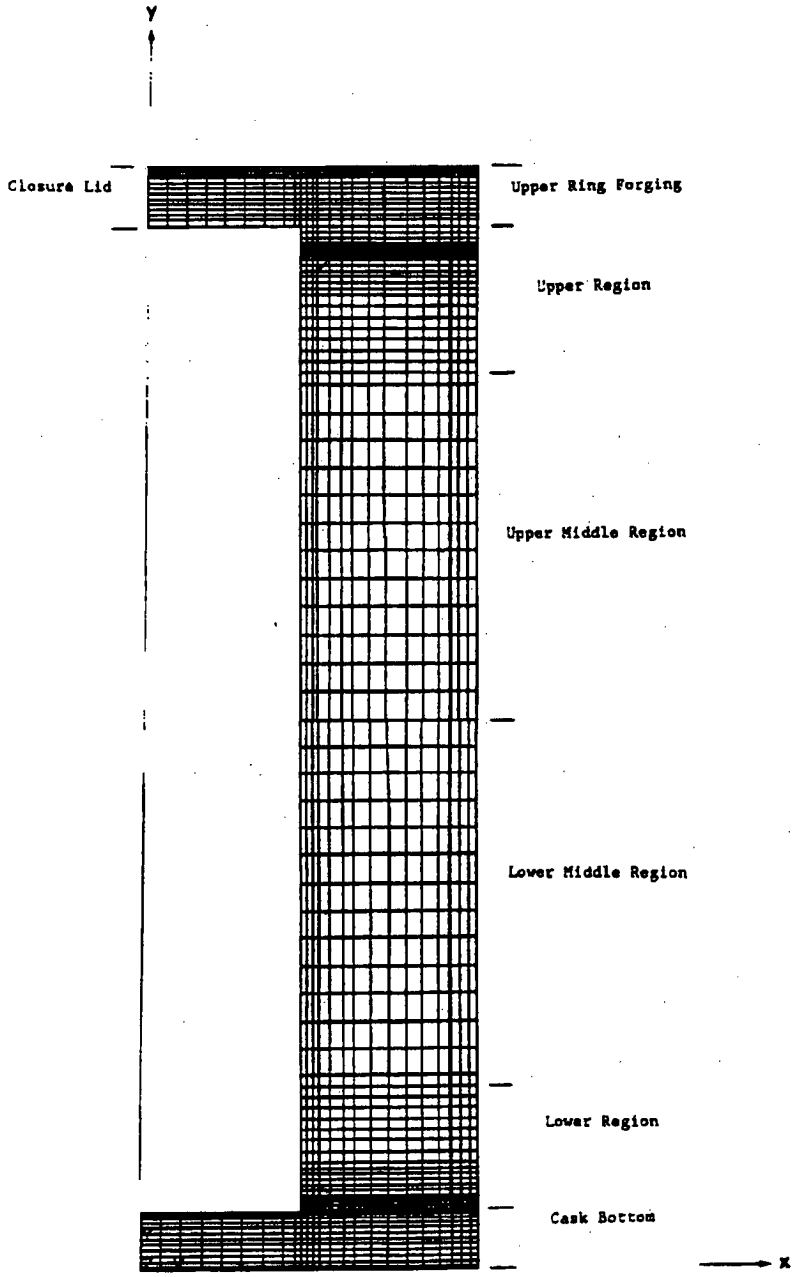

Figure 2.10.2-2 Cask Bottom of Model

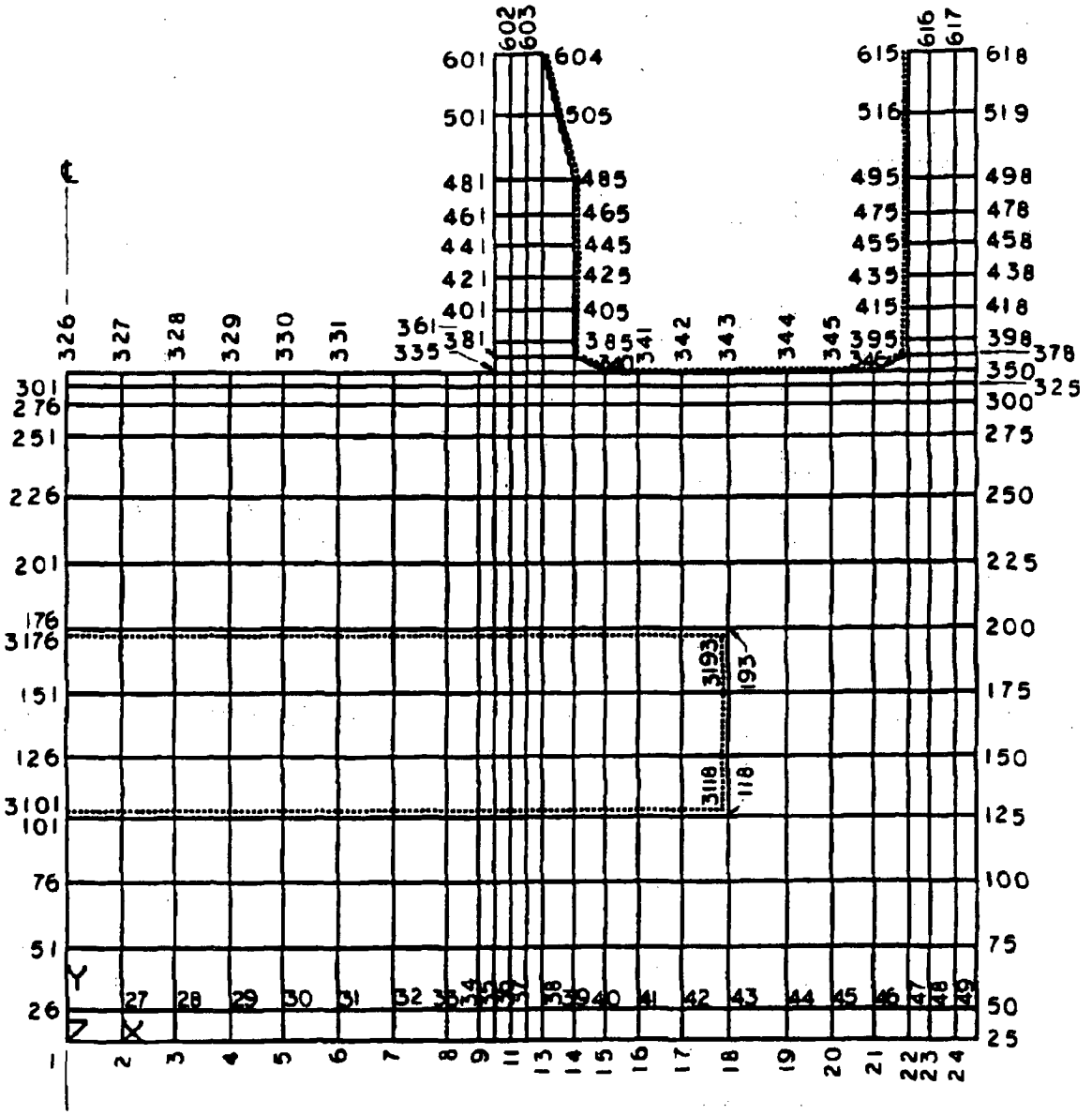

Broken lines indicate where the ANSYS gap element was used to represent no physical bonding.

Figure 2.10.2-3 Inner, Lead and Outer Shells – Lower Region of Model

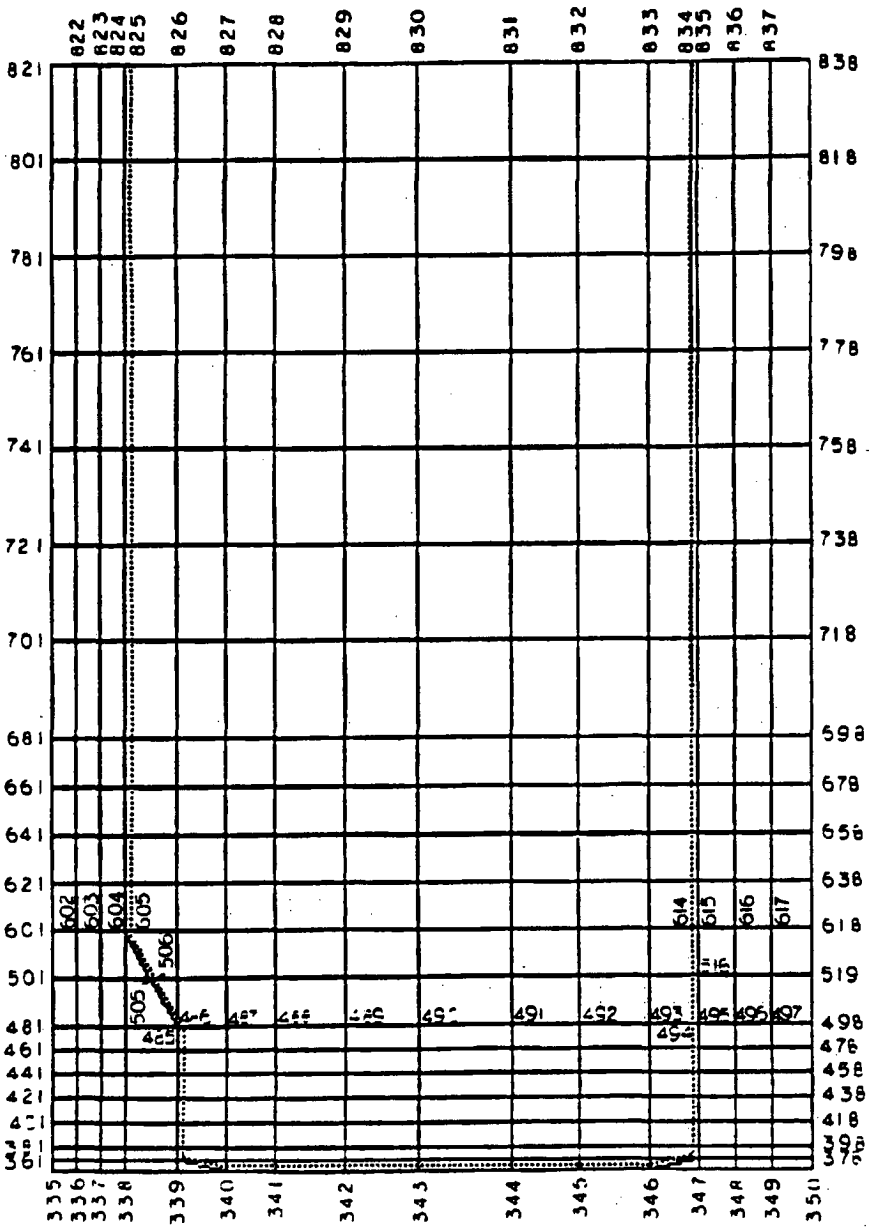

Broken lines indicate where the ANSYS gap element was used to represent no physical bonding.

Figure 2.10.2-4 Inner, Lead and Outer Shells – Lower Middle Region of Model

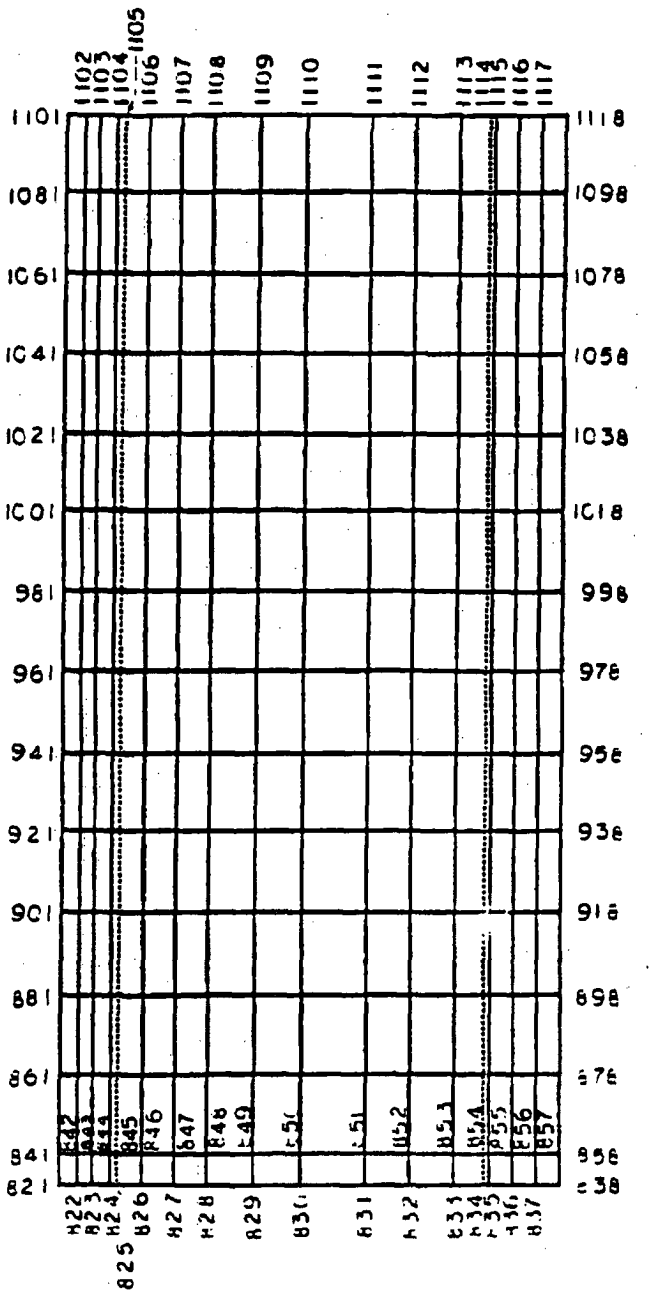

Broken lines indicate where the ANSYS gap element was used to represent no physical bonding.

Figure 2.10.2-5 Inner, Lead and Outer Shells – Upper Middle Region of Model

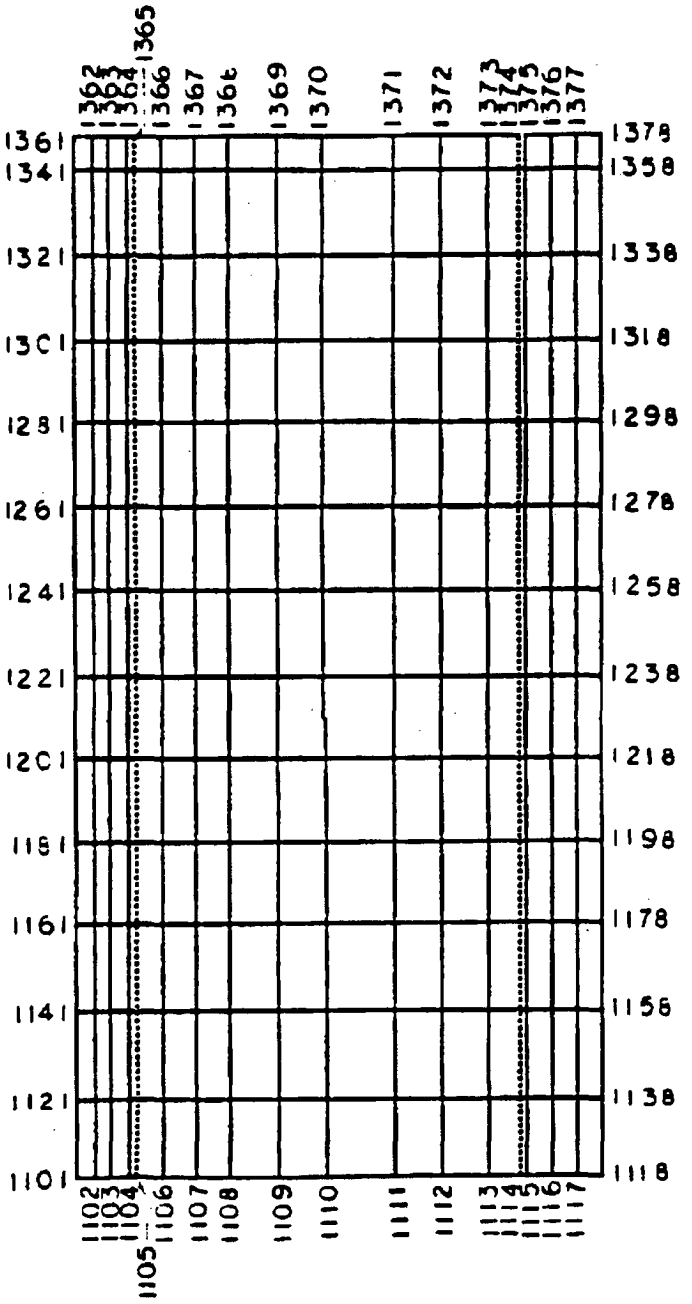

Broken lines indicate where the ANSYS gap element was used to represent no physical bonding.

Figure 2.10.2-6 Inner, Lead and Outer Shells – Upper Region of Model

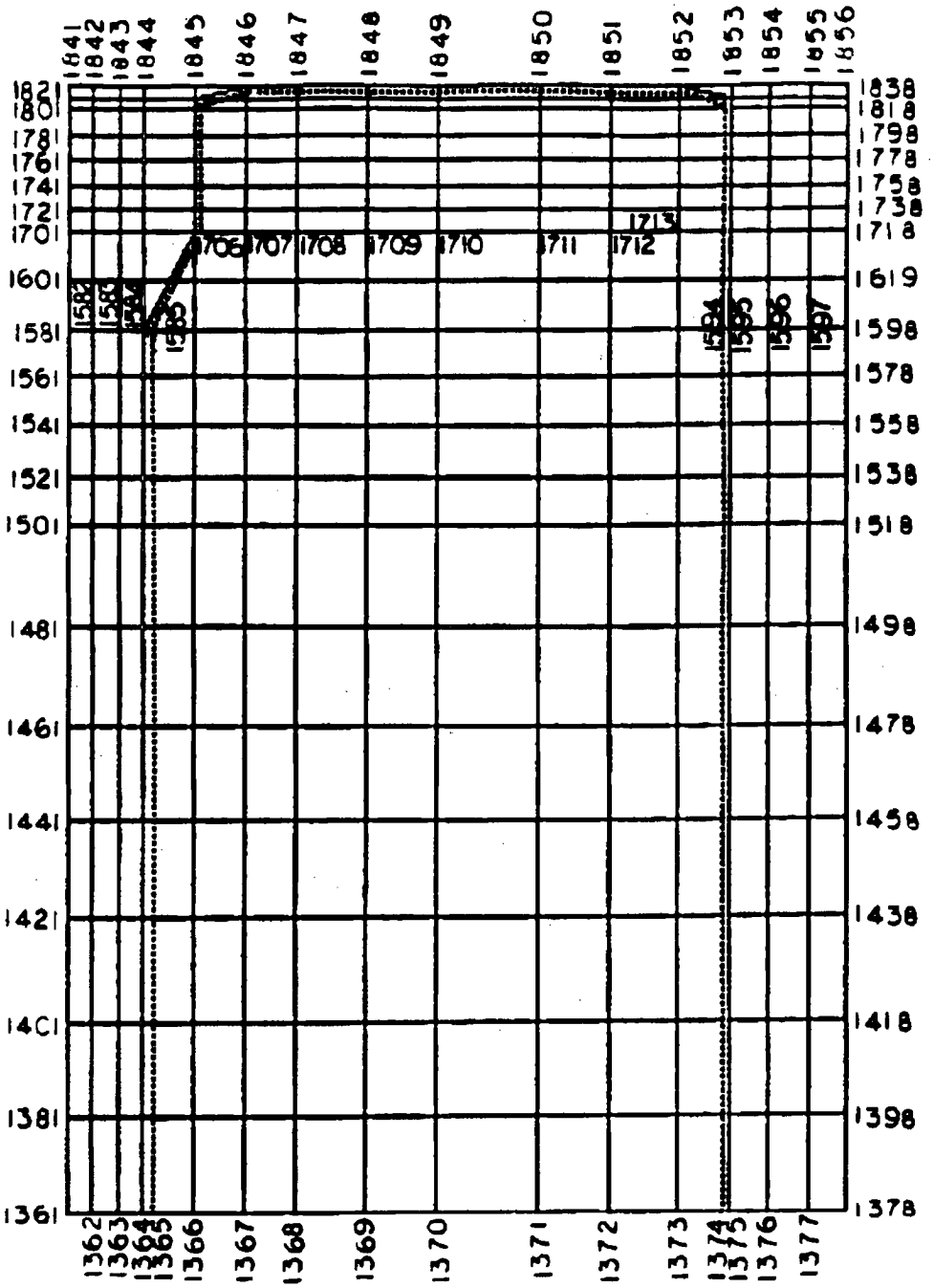

Broken lines indicate where the ANSYS gap element was used to represent no physical bonding.

Figure 2.10.2-7 Upper Ring Forging on Model

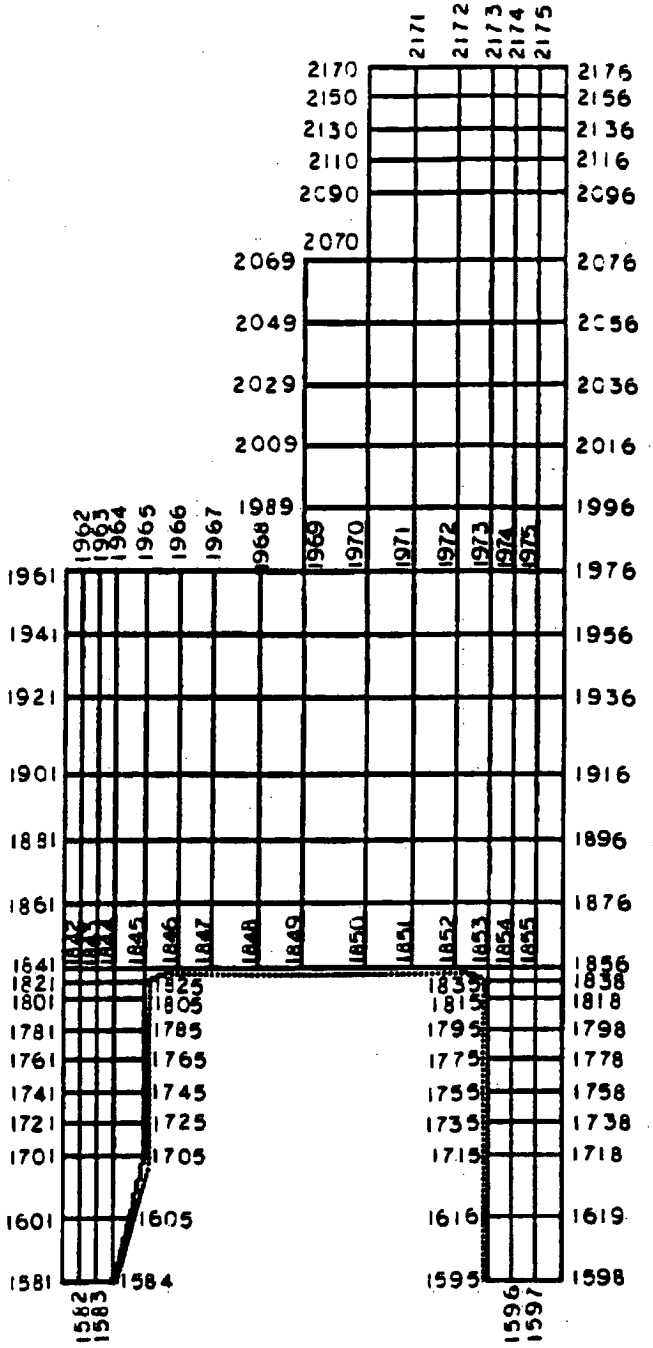

Broken lines indicate where the ANSYS gap element was used to represent no physical bonding.

Figure 2.10.2-8 Closure Lid on Model

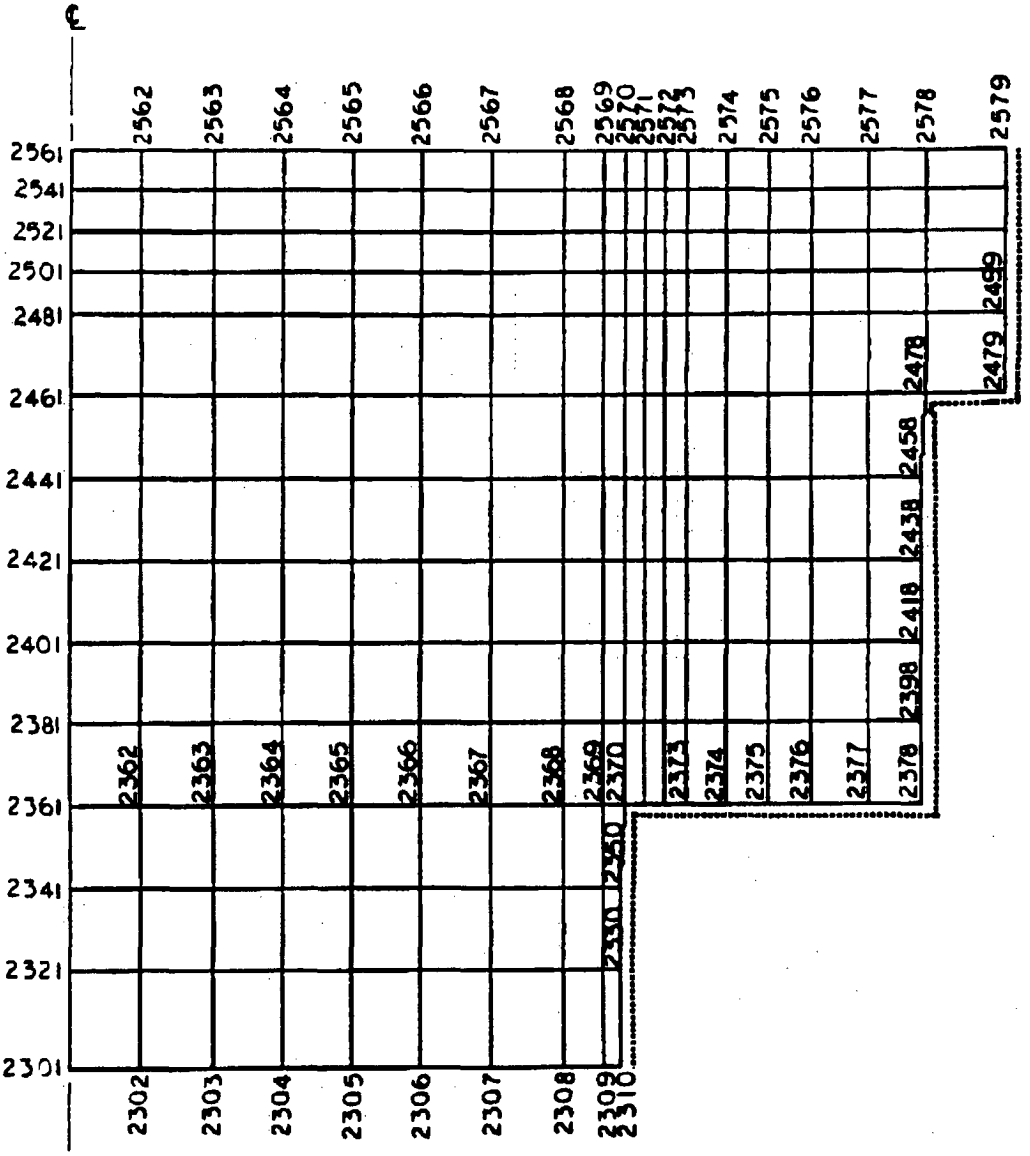

Broken lines indicate where the ANSYS gap element was used to represent no physical bonding.

Figure 2.10.2-9 ANSYS Finite Element Model – Component Identification

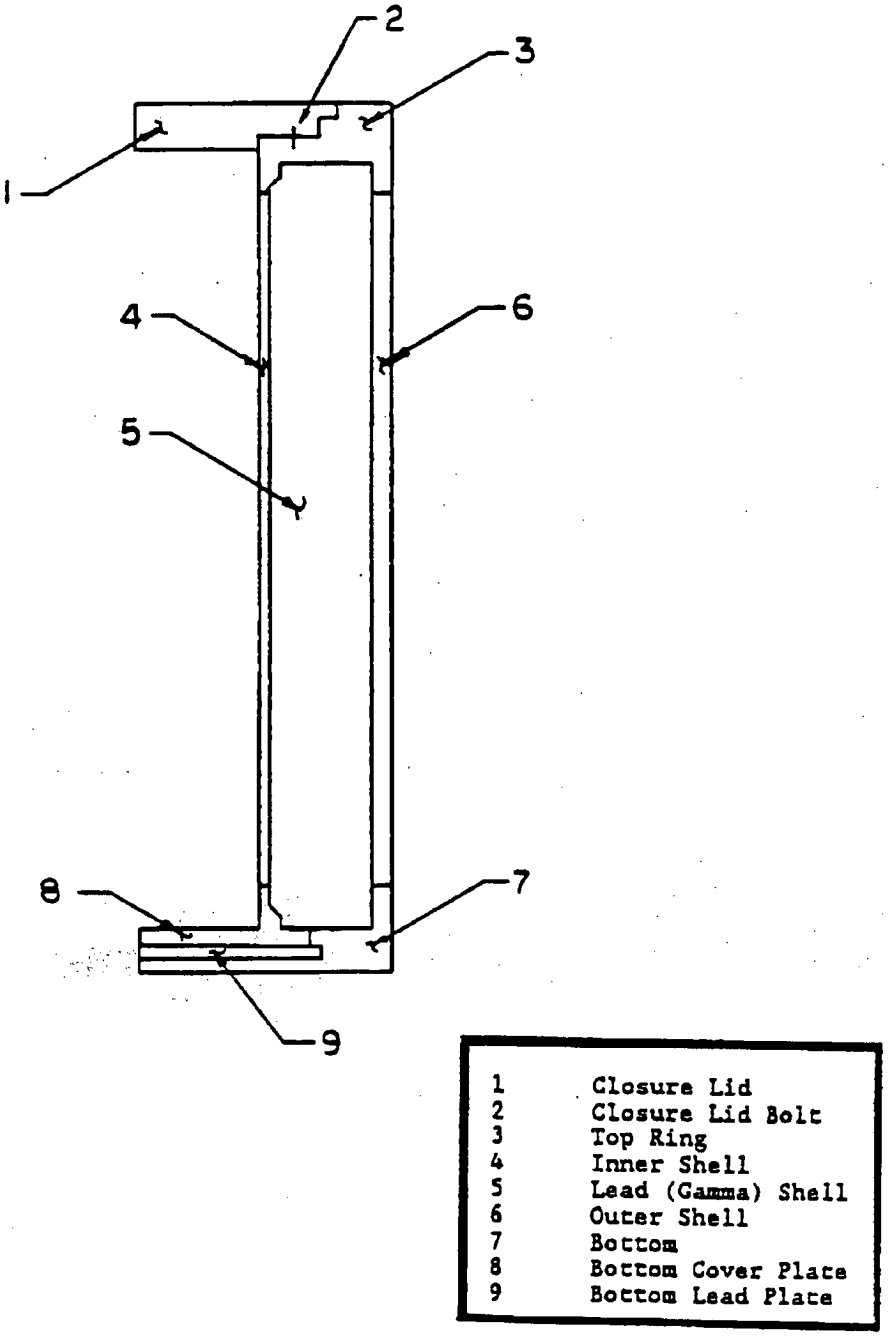

Table 2.10.2-1 Node Definitions

NODE	X (inch)	Y (inch)
1	.00000	.00000
2	.85000	.00000
3	1.7000	.00000
4	2.5500	.00000
5	3.4000	.00000
6	4.2500	.00000
7	5.1000	.00000
8	5.9500	.00000
9	6.4375	.00000
10	6.6875	.00000
11	6.9375	.00000
12	7.1875	.00000
13	7.4375	.00000
14	7.9375	.00000
15	8.4375	.00000
16	8.9375	.00000
17	9.6375	.00000
18	10.375	.00000
19	11.315	.00000
20	12.001	.00000
21	12.688	.00000
22	13.188	.00000
23	13.561	.00000
24	13.934	.00000
25	14.301	.00000
26	.00000	.50000
27	.85000	.50000
28	1.7000	.50000
29	2.5500	.50000
30	3.4000	.50000
31	4.2500	.50000
32	5.1000	.50000
33	5.9500	.50000
34	6.4375	.50000
35	6.6875	.50000
36	6.9375	.50000
37	7.1875	.50000
38	7.4375	.50000
39	7.9375	.50000
40	8.4375	.50000
41	8.9375	.50000
42	9.6375	.50000
43	10.375	.50000
44	11.315	.50000
45	12.001	.50000
46	12.688	.50000
47	13.188	.50000
48	13.561	.50000
49	13.934	.50000
50	14.307	.50000
51	.00000	1.5000
52	.85000	1.5000
53	1.7000	1.5000
54	2.5500	1.5000

Table 2.10.2-1 Node Definitions (continued)

NODE	X (inch)	Y (inch)
55	3.4000	1.5000
56	4.2500	1.5000
57	5.1000	1.5000
58	5.9500	1.5000
59	6.4375	1.5000
60	6.6875	1.5000
61	6.9375	1.5000
62	7.1875	1.5000
63	7.4375	1.5000
64	7.9375	1.5000
65	8.4375	1.5000
66	8.9375	1.5000
67	9.6375	1.5000
68	10.375	1.5000
69	11.315	1.5000
70	12.001	1.5000
71	12.688	1.5000
72	13.188	1.5000
73	13.561	1.5000
74	13.934	1.5000
75	14.307	1.5000
76	.00000	2.5000
77	.85000	2.5000
78	1.7000	2.5000
79	2.5500	2.5000
80	3.4000	2.5000
81	4.2500	2.5000
82	5.1000	2.5000
83	5.9500	2.5000
84	6.4375	2.5000
85	6.6875	2.5000
86	6.9375	2.5000
87	7.1875	2.5000
88	7.4375	2.5000
89	7.9375	2.5000
90	8.4375	2.5000
91	8.9375	2.5000
92	9.6375	2.5000
93	10.375	2.5000
94	11.315	2.5000
95	12.001	2.5000
96	12.688	2.5000
97	13.188	2.5000
98	13.561	2.5000
99	13.964	2.5000
100	14.307	2.5000
101	.00000	3.5000
102	.85000	3.5000
103	1.7000	3.5000
104	2.5500	3.5000
105	3.4000	3.5000
106	4.2500	3.5000
107	5.1000	3.5000
108	5.9500	3.5000
109	6.4375	3.5000
110	6.6875	3.5000
111	6.9375	3.5000
112	7.1875	3.5000
113	7.4375	3.5000
114	7.9375	3.5000

Table 2.10.2-1 Node Definitions (continued)

NODE	X (inch)	Y (inch)
115	8.4375	3.5000
116	8.9375	3.5000
117	9.6375	3.5000
118	10.375	3.5000
119	11.315	3.5000
120	12.001	3.5000
121	12.688	3.5000
122	13.188	3.5000
123	13.561	3.5000
124	13.934	3.5000
125	14.307	3.5000
126	.00000	4.5000
127	.85000	4.5000
128	1.7000	4.5000
129	2.5500	4.5000
130	3.4000	4.5000
131	4.2500	4.5000
132	5.1000	4.5000
133	5.9500	4.5000
134	6.4375	4.5000
135	6.6875	4.5000
136	6.9375	4.5000
137	7.1875	4.5000
138	7.4375	4.5000
139	7.9375	4.5000
140	8.4375	4.5000
141	8.9375	4.5000
142	9.6375	4.5000
143	10.375	4.5000
144	11.315	4.5000
145	12.001	4.5000
146	12.683	4.5000
147	13.188	4.5000
148	13.561	4.5000
149	13.934	4.5000
150	14.307	4.5000
151	.00000	5.5000
152	.85000	5.5000
153	1.7000	5.5000
154	2.5500	5.5000
155	3.4000	5.5000
156	4.2500	5.5000
157	5.1000	5.5000
158	5.9500	5.5000
159	6.4375	5.5000
160	6.6875	5.5000
161	6.9375	5.5000
162	7.1875	5.5000
163	7.4375	5.5000
164	7.9375	5.5000
165	8.4375	5.5000
166	8.9375	5.5000
167	9.6375	5.5000
168	10.375	5.5000
169	11.315	5.5000
170	12.001	5.5000
171	12.688	5.5000
172	13.188	5.5000
173	13.561	5.5000
174	13.934	5.5000

Table 2.10.2-1 Node Definitions (continued)

NODE	X (inch)	Y (inch)
175	14.307	5.5000
176	.00000	6.5000
177	.85000	6.5000
178	1.7000	6.5000
179	2.5500	6.5000
180	3.4000	6.5000
181	4.2500	6.5000
182	5.1000	6.5000
183	5.9500	6.5000
184	6.4375	6.5000
185	6.6875	6.5000
186	6.9378	6.5000
187	7.1875	6.5000
188	7.4375	6.5000
189	7.9375	6.5000
190	8.4375	6.5000
191	8.9375	6.5000
192	9.6375	6.5000
193	10.375	6.5000
194	11.315	6.5000
195	12.001	6.5000
196	12.688	6.5000
197	13.188	6.5000
198	13.561	6.5000
199	13.934	6.5000
200	14.307	6.5000
201	.00000	7.5000
202	.85000	7.5000
203	1.7000	7.5000
204	2.5500	7.5000
205	3.4000	7.5000
206	4.2500	7.5000
207	5.1000	7.5000
208	5.9500	7.5000
209	6.4375	7.5000
210	6.6875	7.5000
211	6.9375	7.5000
212	7.1875	7.5000
213	7.4375	7.5000
214	7.9375	7.5000
215	8.4375	7.5000
216	8.9375	7.5000
217	9.6375	7.5000
218	10.375	7.5000
219	11.315	7.5000
220	12.001	7.5000
221	12.688	7.5000
222	13.188	7.5000
223	13.561	7.5000
224	13.934	7.5000
225	14.307	7.5000
226	.00000	8.5000
227	.85000	8.5000
228	1.7000	8.5000
229	2.5500	8.5000
230	3.4000	8.5000
231	4.2500	8.5000
232	5.1000	8.5000
233	5.9500	8.5000
234	6.4375	8.5000

Table 2.10.2-1 Node Definitions (continued)

NODE	X (inch)	Y (inch)
235	6.6875	8.5000
236	6.9375	8.5000
237	7.1875	8.5000
238	7.4375	8.5000
239	7.9375	8.5000
240	8.4375	8.5000
241	8.9375	8.5000
242	9.6375	8.5000
243	10.375	8.5000
244	11.315	8.5000
245	12.001	8.5000
246	12.688	8.5000
247	13.188	8.5000
248	13.561	8.5000
249	13.934	8.5000
250	14.307	8.5000
251	.00000	9.5000
252	.85000	9.5000
253	1.7000	9.5000
254	2.5500	9.5000
255	3.4000	9.5000
256	4.2500	9.5000
257	5.1000	9.5000
258	5.9500	9.5000
259	6.4375	9.5000
260	6.6875	9.5000
261	6.9375	9.5000
262	7.1875	9.5000
263	7.4375	9.5000
264	7.9375	9.5000
265	8.4375	9.5000
266	8.9375	9.5000
267	9.6375	9.5000
268	10.375	9.5000
269	11.315	9.5000
270	12.001	9.5000
271	12.688	9.5000
272	13.188	9.5000
273	13.561	9.5000
274	13.934	9.5000
275	14.307	9.5000
276	.00000	10.000
277	.85000	10.000
278	1.7000	10.000
279	2.5500	10.000
280	3.4000	10.000
281	4.2500	10.000
282	5.1000	10.000
283	5.9500	10.000
284	643.75	10.000
285	6.6875	10.000
286	6.9375	10.000
287	7.1875	10.000
288	7.4375	10.000
289	7.9375	10.000
290	8.4375	10.000
291	8.9375	10.000
292	9.6375	10.000
293	10.375	10.000
294	11.315	10.000

Table 2.10.2-1 Node Definitions (continued)

NODE	X (inch)	Y (inch)
295	12.001	10.000
296	12.688	10.000
297	13.188	10.000
298	13.561	10.000
299	13.934	10.000
300	14.307	10.000
301	.00000	10.250
302	.85000	10.250
303	1.7000	10.250
304	2.5500	10.250
305	3.4000	10.250
306	4.2500	10.250
307	5.1000	10.250
308	5.9500	10.250
309	6.4375	10.250
310	6.6875	10.250
311	6.9375	10.250
312	7.1875	10.250
313	7.4375	10.250
314	7.9375	10.250
315	8.4375	10.250
316	8.9375	10.250
317	9.6375	10.250
318	10.375	10.250
319	11.315	10.250
320	12.001	10.250
321	12.688	10.250
322	13.188	10.250
323	13.561	10.250
324	13.934	10.250
325	14.307	10.250
326	.00000	10.500
327	.85000	10.500
328	1.7000	10.500
329	2.5500	10.500
330	3.4000	10.500
331	4.2500	10.500
332	5.1000	10.500
333	5.9500	10.500
334	6.4375	10.500
335	6.6875	10.500
336	6.9375	10.500
337	7.1875	10.500
338	7.4375	10.500
339	7.9375	10.500
340	8.4375	10.500
341	8.9375	10.500
342	9.6375	10.500
343	10.375	10.500
344	11.315	10.500
345	12.001	10.500
346	12.688	10.500
347	13.188	10.500
348	13.561	10.500
349	13.934	10.500
350	14.307	10.500
361	6.6875	10.750
362	6.9375	10.750
363	7.1875	10.750
364	7.4375	10.750

Table 2.10.2-1 Node Definitions (continued)

NODE	X (inch)	Y (inch)
365	7.9375	10.750
366	7.9375	10.750
367	8.4375	10.750
368	8.9375	10.750
369	9.6375	10.750
370	10.375	10.750
371	11.315	10.750
372	12.001	10.750
373	12.688	10.750
374	13.133	10.750
375	13.188	10.750
376	13.561	10.750
377	13.934	10.750
378	14.307	10.750
381	6.6875	11.000
382	6.9375	11.000
383	7.1875	11.000
384	7.4375	11.000
385	7.9375	11.000
386	7.9375	11.000
387	8.4375	11.000
388	8.9375	11.000
389	9.6375	11.000
390	10.375	11.000
391	11.315	11.000
392	12.001	11.000
393	12.688	11.000
394	13.133	11.000
395	13.188	11.000
396	13.561	11.000
397	13.934	11.000
398	14.307	11.000
401	6.6875	11.500
402	6.9375	11.500
403	7.1875	11.500
404	7.4375	11.500
405	7.9375	11.500
406	7.9375	11.500
407	8.4375	11.500
408	8.9375	11.500
409	9.6375	11.500
410	10.375	11.500
411	11.315	11.500
412	12.001	11.500
413	12.688	11.500
414	13.133	11.500
415	13.188	11.500
416	13.561	11.500
417	13.934	11.500
418	14.307	11.500
421	6.6875	12.000
422	6.9375	12.000
423	7.1875	12.000
424	7.4375	12.000
425	7.9375	12.000
426	7.9375	12.000
427	8.4375	12.000
428	8.9375	12.000
429	9.6375	12.000
430	10.375	12.000

Table 2.10.2-1 Node Definitions (continued)

NODE	X (inch)	Y (inch)
431	11.315	12.000
432	12.001	12.000
433	12.688	12.000
434	13.133	12.000
435	13.188	12.000
436	13.561	12.000
437	13.934	12.000
438	14.307	12.000
441	6.6875	12.500
442	6.9375	12.500
443	7.1875	12.500
444	7.4375	12.500
445	7.9375	12.500
446	7.9375	12.500
447	8.4375	12.500
448	8.9375	12.500
449	9.6375	12.500
450	10.375	12.500
451	11.315	12.500
452	12.001	12.500
453	12.688	12.500
454	13.133	12.500
455	13.188	12.500
456	13.561	12.500
457	13.934	12.500
458	14.307	12.500
461	6.6875	13.000
462	6.9375	13.000
463	7.1875	13.000
464	7.4375	13.000
465	7.9375	13.000
466	7.9375	13.000
467	8.4375	13.000
468	8.9375	13.000
469	9.6375	13.000
470	10.375	13.000
471	11.315	13.000
472	12.001	13.000
473	12.688	13.000
474	13.133	13.000
475	13.188	13.000
476	13.561	13.000
477	13.934	13.000
478	14.307	13.000
481	6.6875	13.500
482	6.9375	13.500
483	7.1875	13.500
484	7.4375	13.500
485	7.9375	13.500
486	7.9375	13.500
487	8.4375	13.500
488	8.9375	13.500
489	9.6375	13.500
490	10.375	13.500
491	11.315	13.500
492	12.001	13.500
493	12.688	13.500
494	13.133	13.500
495	13.188	13.500
496	13.561	13.500

Table 2.10.2-1 Node Definitions (continued)

NODE	X (inch)	Y (inch)
497	13.934	13.500
498	14.307	13.500
501	6.6875	14.500
502	6.9375	14.500
503	7.1875	14.500
504	7.4375	14.500
505	7.6875	14.500
506	7.6875	14.500
507	7.9375	14.500
508	8.4375	14.500
509	8.9375	14.500
510	9.6375	14.500
511	10.375	14.500
512	11.315	14.500
513	12.001	14.500
514	12.688	14.500
515	13.133	14.500
516	13.188	14.500
517	13.561	14.500
518	13.934	14.500
519	14.307	14.500
601	6.6875	15.500
602	6.9375	15.500
603	7.1875	15.500
604	7.4375	15.500
605	7.4375	15.500
606	7.9375	15.500
607	8.4375	15.500
608	8.9375	15.500
609	9.6375	15.500
610	10.375	15.500
611	11.315	15.500
612	12.001	15.500
613	12.688	15.500
614	13.133	15.500
615	13.188	15.500
616	13.561	15.500
617	13.934	15.500
618	14.307	15.500
621	6.6875	16.500
622	6.9375	16.500
623	7.1875	16.500
624	7.4375	16.500
625	7.4375	16.500
626	7.9375	16.500
627	8.4375	16.500
628	8.9375	16.500
629	9.6375	16.500
630	10.375	16.500
631	11.315	16.500
632	12.001	16.500
633	12.688	16.500
634	13.133	16.500
635	13.188	16.500
636	13.561	16.500
637	13.934	16.500
638	14.307	16.500
641	6.6875	17.500
642	6.9375	17.500
643	7.1875	17.500

Table 2.10.2-1 Node Definitions (continued)

NODE	X (inch)	Y (inch)
644	7.4375	17.500
645	7.4375	17.500
646	7.9375	17.500
647	8.4375	17.500
648	8.9375	17.500
649	9.6375	17.500
650	10.375	17.500
651	11.315	17.500
652	12.001	17.500
653	12.688	17.500
654	13.133	17.500
655	13.188	17.500
656	13.561	17.500
657	13.934	17.500
658	14.307	17.500
661	6.6875	18.500
662	6.9375	18.500
663	7.1875	18.500
664	7.4375	18.500
665	7.4375	18.500
666	7.9375	18.500
667	8.4378	18.500
668	8.9375	18.500
669	9.6375	18.500
670	10.375	18.500
671	11.315	18.500
672	12.001	18.500
673	12.688	18.500
674	13.133	18.500
675	13.188	18.500
676	13.561	18.500
677	13.934	18.500
678	14.307	18.500
681	6.6875	19.500
682	6.9375	19.500
683	7.1875	19.500
684	7.4375	19.500
685	7.4375	19.500
686	7.9375	19.500
687	8.4375	19.500
688	8.9375	19.500
689	9.6375	19.500
690	10.375	19.500
691	11.315	19.500
692	12.001	19.500
693	12.688	19.500
694	13.133	19.500
695	13.188	19.500
696	13.561	19.500
697	13.934	19.500
698	14.307	19.500
701	6.6875	21.500
702	6.9375	21.500
703	7.1875	21.500
704	7.4375	21.500
705	7.4375	21.500
706	7.9375	21.500
707	8.4375	21.500
708	8.9375	21.500
709	9.6375	21.500

Table 2.10.2-1 Node Definitions (continued)

NODE	X (inch)	Y (inch)
710	10.375	21.500
711	11.315	21.500
712	12.001	21.500
713	12.688	21.500
714	13.133	21.500
715	13.188	21.500
716	13.561	21.500
717	13.934	21.500
718	14.307	21.500
721	6.6875	23.500
722	6.9375	23.500
723	7.1875	23.500
724	7.4375	23.500
725	7.4375	23.500
726	7.9375	23.500
727	8.4375	23.500
728	8.9375	23.500
729	9.6375	23.500
730	10.375	23.500
731	11.315	23.500
732	12.001	23.500
733	12.688	23.500
734	13.133	23.500
735	13.188	23.500
736	13.561	23.500
737	13.934	23.500
738	14.307	23.500
741	6.6875	25.500
742	6.9375	25.500
743	7.1875	25.500
744	7.4375	25.500
745	7.4375	25.500
746	7.9375	25.500
747	8.4375	25.500
748	8.9375	25.500
749	9.6375	25.500
750	10.375	25.500
751	11.315	25.500
752	12.001	25.500
753	12.688	25.500
754	13.133	25.500
755	13.188	25.500
756	13.561	25.500
757	13.934	25.500
758	14.307	25.500
761	6.6875	27.500
762	6.9375	27.500
763	7.1875	27.500
764	7.4375	27.500
765	7.4375	27.500
766	7.9375	27.500
767	8.4375	27.500
768	8.9375	27.500
769	9.6375	27.500
770	10.375	27.500
771	11.315	27.500
772	12.001	27.500
773	12.688	27.500
774	13.133	27.500
775	13.188	27.500

Table 2.10.2-1 Node Definitions (continued)

NODE	X (inch)	Y (inch)
776	13.561	27.500
777	16.934	27.500
778	14.307	27.500
781	6.6875	29.500
782	6.9375	29.500
783	7.1875	29.500
784	7.4375	29.500
785	7.4375	29.500
786	7.9375	29.500
787	8.4375	29.500
788	8.9375	29.500
789	9.6375	29.500
790	10.375	29.500
791	11.315	29.500
792	12.001	29.500
793	12.688	29.500
794	13.133	29.500
795	13.188	29.500
796	13.561	29.500
797	13.934	29.500
798	14.307	29.500
801	6.6875	31.500
802	6.9375	31.500
803	7.1875	31.500
804	7.4375	31.500
805	7.4375	31.500
806	7.9375	31.500
807	8.4375	31.500
808	8.9375	31.500
809	9.6375	31.500
810	10.375	31.500
811	11.315	31.500
812	12.001	31.500
813	12.688	31.500
814	13.133	31.500
815	13.183	31.500
816	13.561	31.500
817	13.934	31.500
818	14.307	31.500
821	6.6875	33.500
822	6.9375	33.500
823	7.1875	33.500
824	7.4375	33.500
825	7.4375	33.500
826	7.9375	33.500
827	8.4375	33.500
828	8.9375	33.500
829	9.6375	33.500
830	10.375	33.500
831	11.315	33.500
832	12.001	33.500
833	12.688	33.500
834	13.133	33.500
835	13.188	33.500
836	13.561	33.500
837	13.934	33.500
838	14.307	33.500
841	6.6875	35.500
842	6.9375	35.500
843	7.1875	35.500

Table 2.10.2-1 Node Definitions (continued)

NODE	X (inch)	Y (inch)
844	7.4375	35.500
845	7.4375	35.500
846	7.9375	35.500
847	8.4375	35.500
848	8.9375	35.500
849	9.6375	35.500
850	10.375	35.500
851	11.315	35.500
852	12.001	35.500
853	12.688	35.500
854	13.133	35.500
855	13.188	35.500
856	13.561	35.500
857	13.934	35.500
858	14.307	35.500
861	6.6875	40.500
862	6.9375	40.500
863	7.1875	40.500
834	7.4375	40.500
835	7.4375	40.500
866	7.9375	40.500
867	8.4375	40.500
868	8.9375	40.500
869	9.6375	40.500
870	10.373	40.500
871	11.315	40.500
872	12.001	40.500
873	12.688	40.500
874	13.133	40.500
875	13.188	40.500
876	13.561	40.500
877	13.934	40.500
878	14.307	40.500
881	6.6875	45.500
882	6.9375	45.500
883	7.1875	45.500
884	7.4375	45.500
885	7.4375	45.500
886	7.9375	45.500
887	8.4375	45.500
888	8.9375	45.500
889	9.6375	45.500
890	10.370	45.500
891	11.315	45.500
892	12.001	45.500
893	12.688	45.500
894	13.133	45.500
895	13.188	45.500
896	13.561	45.500
897	13.934	45.500
898	14.307	45.500
901	6.6875	50.500
902	6.9375	50.500
903	7.1875	50.500
904	7.4375	50.500
905	7.4375	50.500
906	7.9375	50.500
907	8.4375	50.500
908	8.9375	50.500
909	9.6375	50.500

Table 2.10.2-1 Node Definitions (continued)

NODE	X (inch)	Y (inch)
910	10.368	50.500
911	11.315	50.500
912	12.001	50.500
913	12.688	50.500
914	13.133	50.500
915	13.188	50.500
916	13.561	50.500
917	13.934	50.500
918	14.307	50.500
921	6.6875	55.500
922	6.9375	55.500
923	7.1875	55.500
924	7.4375	55.500
925	7.4375	55.500
926	7.9375	55.500
927	8.4375	55.500
928	8.9375	55.500
929	9.6375	55.500
930	10.365	55.500
931	11.315	55.500
932	12.001	55.500
933	12.688	55.500
934	13.133	55.500
935	13.188	55.500
936	13.561	55.500
937	13.934	55.500
938	14.307	55.500
941	6.6875	60.500
942	6.9375	60.500
943	7.1875	60.500
944	7.4375	60.500
945	7.4375	60.500
946	7.9375	60.500
947	8.4375	60.500
948	8.9375	60.500
949	9.6375	60.500
950	10.363	60.500
951	11.315	60.500
952	12.001	60.500
953	12.688	60.500
954	13.133	60.500
955	13.188	60.500
956	13.561	60.500
957	13.934	60.500
958	14.307	60.500
961	6.6875	65.500
962	6.9375	65.500
963	7.1875	65.500
964	7.4375	65.500
965	7.4375	65.500
966	7.9375	65.500
967	8.4375	65.500
968	8.9375	65.500
969	9.6375	65.500
970	10.361	65.500
971	11.315	65.500
972	12.001	65.500
973	12.688	65.500
974	13.133	65.500
975	13.188	65.500

Table 2.10.2-1 Node Definitions (continued)

NODE	X (inch)	Y (inch)
976	13.561	65.500
977	13.934	65.500
978	14.307	65.500
981	6.6875	70.500
982	6.9375	70.500
983	7.1875	70.500
984	7.4375	70.500
985	7.4375	70.500
986	7.9375	70.500
987	8.4375	70.500
988	8.9375	70.500
989	9.6375	70.500
990	10.358	70.500
991	11.315	70.500
992	12.001	70.500
993	12.688	70.500
994	13.133	70.500
995	13.188	70.500
996	13.561	70.500
997	13.934	70.500
998	14.307	70.500
1001	6.6875	75.500
1002	6.9375	75.500
1003	7.1875	75.500
1004	7.4375	75.500
1005	7.4375	75.500
1006	7.9375	75.500
1007	8.4375	75.500
1008	8.9375	75.500
1009	9.6375	75.500
1010	10.356	75.500
1011	11.315	75.500
1012	12.001	75.500
1013	12.688	75.500
1014	13.133	75.500
1015	13.188	75.500
1016	13.561	75.500
1017	13.934	75.500
1018	14.307	75.500
1021	6.6875	80.500
1022	6.9375	80.500
1023	7.1875	80.500
1024	7.4375	80.500
1025	7.4375	80.500
1026	7.9375	80.500
1027	8.4375	80.500
1028	8.9375	80.500
1029	9.6375	80.500
1030	10.353	80.500
1031	11.315	80.500
1032	12.001	80.500
1033	12.688	80.500
1034	13.133	80.500
1035	13.188	80.500
1036	13.561	80.500
1037	13.934	80.500
1038	14.307	80.500
1041	6.6875	85.500
1042	6.9375	85.500
1043	7.1875	85.500

Table 2.10.2-1 Node Definitions (continued)

NODE	X (inch)	Y (inch)
1044	7.4375	85.500
1045	7.4375	85.500
1046	7.9375	85.500
1047	8.4375	85.500
1048	8.9375	85.500
1049	9.6375	85.500
1050	10.351	85.500
1051	11.315	85.500
1052	12.001	85.500
1053	12.688	85.500
1054	13.133	85.500
1055	13.188	85.500
1056	13.561	85.500
1057	13.934	85.500
1058	14.307	85.500
1061	6.6875	90.500
1062	6.9375	90.500
1063	7.1875	90.500
1064	7.4375	90.500
1065	7.4375	90.500
1066	7.9375	90.500
1067	8.4375	90.500
1068	8.9375	90.500
1069	9.6375	90.500
1070	10.349	90.500
1071	11.315	90.500
1072	12.001	90.500
1073	12.688	90.500
1074	13.133	90.500
1075	13.188	90.500
1076	13.561	90.500
1077	13.934	90.500
1078	14.307	90.500
1081	6.6875	95.500
1082	6.9375	95.500
1083	7.1875	95.500
1084	7.4375	95.500
1085	7.4375	95.500
1086	7.9375	95.500
1087	8.4375	95.500
1088	8.9375	95.500
1089	9.6375	95.500
1090	10.346	95.500
1091	11.315	95.500
1092	12.001	95.500
1093	12.688	95.500
1094	13.133	95.500
1095	13.188	95.500
1096	13.561	95.500
1097	13.934	95.500
1098	14.307	95.500
1101	6.6875	100.50
1102	6.9375	100.50
1103	7.1875	100.50
1104	7.4375	100.50
1105	7.4375	100.50
1106	7.9375	100.50
1107	8.4375	100.50
1108	8.9375	100.50
1109	9.6375	100.50

Table 2.10.2-1 Node Definitions (continued)

NODE	X (inch)	Y (inch)
1110	10.344	100.50
1111	11.315	100.50
1112	12.001	100.50
1113	12.688	100.50
1114	13.133	100.50
1115	13.188	100.50
1116	13.561	100.50
1117	13.934	100.50
1118	14.307	100.50
1121	6.6875	105.50
1122	6.9375	105.50
1123	7.1875	105.50
1124	7.4375	105.50
1125	7.4375	105.50
1126	7.9375	105.50
1127	8.4375	105.50
1128	8.9375	105.50
1129	9.6375	105.50
1130	10.341	105.50
1131	11.315	105.50
1132	12.001	105.50
1133	12.688	105.50
1134	13.133	105.50
1135	13.188	105.50
1136	13.561	105.50
1137	13.934	105.50
1138	14.307	105.50
1141	6.6875	110.50
1142	6.9375	110.50
1143	7.1875	110.50
1144	7.4375	110.50
1145	7.4375	110.50
1146	7.9375	110.50
1147	8.4375	110.50
1148	8.9375	110.50
1149	9.6375	110.50
1150	10.339	110.50
1151	11.315	110.50
1152	12.001	110.50
1153	12.688	110.50
1154	13.133	110.50
1155	13.188	110.50
1156	13.561	110.50
1157	13.934	110.50
1158	14.307	110.50
1161	6.6875	115.50
1162	6.9375	115.50
1163	7.1875	115.50
1164	7.4375	115.50
1165	7.4375	115.50
1166	7.9375	115.50
1167	8.4375	115.50
1168	8.9375	115.50
1169	9.6375	115.50
1170	10.337	115.50
1171	11.315	115.50
1172	12.001	115.50
1173	12.688	115.50
1174	13.133	115.50
1175	13.188	115.50

Table 2.10.2-1 Node Definitions (continued)

NODE	X (inch)	Y (inch)
1176	13.561	115.50
1177	13.934	115.50
1178	14.307	115.50
1181	6.6875	120.50
1182	6.9375	120.50
1183	7.1875	120.50
1184	7.4375	120.50
1185	7.4375	120.50
1186	7.9375	120.50
1187	8.4375	120.50
1188	8.9375	120.50
1189	9.6375	120.50
1190	10.334	120.50
1191	11.315	120.50
1192	12.001	120.50
1193	12.688	120.50
1194	13.133	120.50
1195	13.188	120.50
1196	13.561	120.50
1197	13.934	120.50
1198	14.307	120.50
1201	6.6875	125.50
1202	6.9375	125.50
1203	7.1875	125.50
1204	7.4375	125.50
1205	7.4375	125.50
1206	7.9375	125.50
1207	8.4375	125.50
1208	8.9375	125.50
1209	9.6375	125.50
1210	10.332	125.50
1211	11.315	125.50
1212	12.001	125.50
1213	12.688	125.50
1214	13.133	125.50
1215	13.188	125.50
1216	13.561	125.50
1217	13.934	125.50
1218	14.307	125.50
1221	6.6875	130.50
1222	6.9375	130.50
1223	7.1875	130.50
1224	7.4375	130.50
1225	7.4375	130.50
1226	7.9375	130.50
1227	8.4375	130.50
1228	8.9375	130.50
1229	9.6375	130.50
1230	10.339	130.50
1231	11.315	130.50
1232	12.001	130.50
1233	12.688	130.50
1234	13.133	130.50
1235	13.188	130.50
1236	13.561	130.50
1237	13.934	130.50
1238	14.307	130.50
1241	6.6875	135.50
1242	6.9375	135.50
1243	7.1875	135.50

Table 2.10.2-1 Node Definitions (continued)

NODE	X (inch)	Y (inch)
1244	7.4375	135.50
1245	7.4375	135.50
1246	7.9375	135.50
1247	8.4375	135.50
1248	8.9375	135.50
1249	9.6375	135.50
1250	10.327	135.50
1251	11.315	135.50
1252	12.001	135.50
1253	12.688	135.50
1254	13.133	135.50
1255	13.188	135.50
1256	13.561	135.50
1257	13.934	135.50
1258	14.307	135.50
1261	6.6875	140.50
1262	6.9375	140.50
1263	7.1875	140.50
1264	7.4375	140.50
1265	7.4375	140.50
1266	7.9375	140.50
1267	8.4375	140.50
1268	8.9375	140.50
1269	9.6375	140.50
1270	10.325	140.50
1271	11.315	140.50
1272	12.001	140.50
1273	12.688	140.50
1274	13.133	140.50
1275	13.188	140.50
1276	13.561	140.50
1277	13.934	140.50
1278	14.307	140.50
1281	6.6875	145.50
1282	6.9375	145.50
1283	7.1875	145.50
1284	7.4375	145.50
1285	7.4375	145.50
1286	7.9375	145.50
1287	8.4375	145.50
1288	8.9375	145.50
1289	9.6375	145.50
1290	10.322	145.50
1291	11.315	145.50
1292	12.001	145.50
1293	12.688	145.50
1294	13.133	145.50
1295	13.188	145.50
1296	13.561	145.50
1297	13.934	145.50
1298	14.307	145.50
1301	6.6875	150.50
1302	6.9375	150.50
1303	7.1875	150.50
1304	7.4375	150.50
1305	7.4375	150.50
1306	7.9375	150.50
1307	8.4375	150.50
1308	8.9375	150.50
1309	9.6375	150.50

Table 2.10.2-1 Node Definitions (continued)

NODE	X (inch)	Y (inch)
1310	10.320	150.50
1311	11.315	150.50
1312	12.001	150.50
1313	12.688	150.50
1314	13.133	150.50
1315	13.188	150.50
1316	13.561	150.50
1317	13.934	150.50
1318	14.307	150.50
1321	6.6875	155.50
1322	6.9375	155.50
1323	7.1875	155.50
1324	7.4375	155.50
1325	7.4375	155.50
1326	7.9375	155.50
1327	8.4375	155.50
1328	8.9375	155.50
1329	9.6375	155.50
1330	10.317	155.50
1331	11.315	155.50
1332	12.001	155.50
1333	12.688	155.50
1334	13.133	155.50
1335	13.188	155.50
1336	13.561	155.50
1337	13.934	155.50
1338	14.307	155.50
1341	6.6875	160.50
1342	6.9375	160.50
1343	7.1875	160.50
1344	7.4375	160.50
1345	7.4375	160.50
1346	7.9375	160.50
1347	8.4375	160.50
1348	8.9375	160.50
1349	9.6375	160.50
1350	10.315	160.50
1351	11.315	160.50
1352	12.001	160.50
1353	12.688	160.50
1354	13.133	160.50
1355	13.188	160.50
1356	13.561	160.50
1357	13.934	160.50
1358	14.307	160.50
1361	6.6875	162.50
1362	6.9375	162.50
1363	7.1875	162.50
1364	7.4375	162.50
1365	7.4375	162.50
1366	7.9375	162.50
1367	8.4375	162.50
1368	8.9375	162.50
1369	9.6375	162.50
1370	10.315	162.50
1371	11.315	162.50
1372	12.001	162.50
1373	12.688	162.50
1374	13.133	162.50
1375	13.188	162.50

Table 2.10.2-1 Node Definitions (continued)

NODE	X (inch)	Y (inch)
1376	13.561	162.50
1377	13.934	162.50
1378	14.307	162.50
1381	6.6875	164.50
1382	6.9375	164.50
1383	7.1875	164.50
1384	7.4375	164.50
1385	7.4375	164.50
1386	7.9375	164.50
1387	8.4375	164.50
1388	8.9375	164.50
1389	9.6375	164.50
1390	10.315	164.50
1391	11.315	164.50
1392	12.001	164.50
1393	12.688	164.50
1394	13.133	164.50
1395	13.188	164.50
1396	13.561	164.50
1397	13.934	164.50
1398	14.307	164.50
1401	6.6875	166.50
1402	6.9375	166.50
1403	7.1875	166.50
1404	7.4375	166.50
1405	7.4375	166.50
1406	7.9375	166.50
1407	8.4375	166.50
1408	8.9375	166.50
1409	9.6375	166.50
1410	10.315	166.50
1411	11.315	166.50
1412	12.001	166.50
1413	12.688	166.50
1414	13.133	166.50
1415	13.188	166.50
1416	13.561	166.50
1417	13.934	166.50
1418	14.307	166.50
1421	6.6875	168.50
1422	6.9375	168.50
1423	7.1875	168.50
1424	7.4375	168.50
1425	7.4375	168.50
1426	7.9375	168.50
1427	8.4375	168.50
1428	8.9375	168.50
1429	9.6375	168.50
1430	10.315	168.50
1431	11.315	168.50
1432	12.001	168.50
1433	12.688	168.50
1434	13.133	168.50
1435	13.188	168.50
1436	13.561	168.50
1437	13.934	168.50
1438	14.307	168.50
1441	6.6875	170.50
1442	6.9375	170.50
1443	7.1875	170.50

Table 2.10.2-1 Node Definitions (continued)

NODE	X (inch)	Y (inch)
1444	7.4375	170.50
1445	7.4375	170.50
1446	7.9375	170.50
1447	8.4375	170.50
1448	8.9375	170.50
1449	9.6375	170.50
1450	10.315	170.50
1451	11.315	170.50
1452	12.001	170.50
1453	12.688	170.50
1454	13.133	170.50
1455	13.188	170.50
1456	13.561	170.50
1457	13.934	170.50
1458	14.307	170.50
1461	6.6875	172.50
1462	6.9375	172.50
1463	7.1875	172.50
1464	7.4375	172.50
1465	7.4375	172.50
1466	7.9375	172.50
1467	8.4375	172.50
1468	8.9375	172.50
1469	9.6375	172.50
1470	10.315	172.50
1471	11.315	172.50
1472	12.001	172.50
1473	12.688	172.50
1474	13.133	172.50
1475	13.188	172.50
1476	13.561	172.50
1477	13.934	172.50
1478	14.307	172.50
1481	6.6875	174.50
1482	6.9375	174.50
1483	7.1875	174.50
1484	7.4375	174.50
1485	7.4375	174.50
1486	7.9375	174.50
1487	8.4375	174.50
1488	8.9375	174.50
1489	9.6375	174.50
1490	10.315	174.50
1491	11.315	174.50
1492	12.001	174.50
1493	12.688	174.50
1494	13.133	174.50
1495	13.188	174.50
1496	13.561	174.50
1497	13.934	174.50
1498	14.307	174.50
1501	6.6875	176.50
1502	6.9375	176.50
1503	7.1875	176.50
1504	7.4375	176.50
1505	7.4375	176.50
1506	7.9375	176.50
1507	8.4375	176.50
1508	8.9375	176.50
1509	9.6375	176.50

Table 2.10.2-1 Node Definitions (continued)

NODE	X (inch)	Y (inch)
1510	10.315	176.50
1511	11.315	176.50
1512	12.001	176.50
1513	12.688	176.50
1514	13.133	176.50
1515	13.188	176.50
1516	13.561	176.50
1517	13.934	176.50
1518	14.307	176.50
1521	6.6875	177.50
1522	6.9375	177.50
1523	7.1875	177.50
1524	7.4375	177.50
1525	7.4375	177.50
1526	7.9375	177.50
1527	8.4375	177.50
1528	8.9375	177.50
1529	9.6375	177.50
1530	10.315	177.50
1531	11.315	177.50
1532	12.001	177.50
1533	12.688	177.50
1534	13.133	177.50
1535	13.188	177.50
1536	13.561	177.50
1537	13.934	177.50
1538	14.307	177.50
1541	6.6875	178.50
1542	6.9375	178.50
1543	7.1875	178.50
1544	7.4375	178.50
1545	7.4375	178.50
1546	7.9375	178.50
1547	8.4375	178.50
1548	8.9375	178.50
1549	9.6375	178.50
1550	10.315	178.50
1551	11.315	178.50
1552	12.001	178.50
1553	12.688	178.50
1554	13.133	178.50
1555	13.188	178.50
1556	13.561	178.50
1557	13.934	178.50
1558	14.307	178.50
1561	6.6875	179.50
1562	6.9375	179.50
1563	7.1875	179.50
1564	7.4375	179.50
1565	7.4375	179.50
1566	7.9375	179.50
1567	8.4375	179.50
1568	8.9375	179.50
1569	9.6375	179.50
1570	10.315	179.50
1571	11.315	179.50
1572	12.001	179.50
1573	12.688	179.50
1574	13.133	179.50
1575	13.188	179.50

Table 2.10.2-1 Node Definitions (continued)

NODE	X (inch)	Y (inch)
1576	13.561	179.50
1577	13.934	179.50
1578	14.307	179.50
1581	6.6875	180.50
1582	6.9375	180.50
1583	7.1875	180.50
1584	7.4375	180.50
1585	7.4375	180.50
1586	7.9375	180.50
1587	8.4375	180.50
1588	8.9375	180.50
1589	9.6375	180.50
1590	10.315	180.50
1591	11.315	180.50
1592	12.001	180.50
1593	12.688	180.50
1594	13.133	180.50
1595	13.188	180.50
1596	13.561	180.50
1597	13.934	180.50
1598	14.307	180.50
1601	6.6875	181.50
1602	6.9375	181.50
1603	7.1875	181.50
1604	7.4375	181.50
1605	7.6875	181.50
1606	7.6880	181.50
1607	7.9375	181.50
1608	8.4375	181.50
1609	8.9375	181.50
1610	9.6375	181.50
1611	10.315	181.50
1612	11.315	181.50
1613	12.001	181.50
1614	12.688	181.50
1615	13.133	181.50
1616	13.188	181.50
1617	13.561	181.50
1618	13.934	181.50
1619	14.307	181.50
1701	6.6875	182.50
1702	6.9375	182.50
1703	7.1875	182.50
1704	7.4375	182.50
1705	7.9375	182.50
1706	7.9385	182.50
1707	8.4375	182.50
1708	8.9375	182.50
1709	9.6375	182.50
1710	10.315	182.50
1711	11.315	182.50
1712	12.001	182.50
1713	12.688	182.50
1714	13.133	182.50
1715	13.188	182.50
1716	13.561	182.50
1717	13.934	182.50
1718	14.307	182.50
1721	6.6875	183.00
1722	6.9375	183.00

Table 2.10.2-1 Node Definitions (continued)

NODE	X (inch)	Y (inch)
1723	7.1875	183.00
1724	7.4375	183.00
1725	7.9375	183.00
1726	7.9385	183.00
1727	8.4375	183.00
1728	8.9375	183.00
1729	9.6375	183.00
1730	10.315	183.00
1731	11.315	183.00
1732	12.001	183.00
1733	12.688	183.00
1734	13.133	183.00
1735	13.188	183.00
1736	13.561	183.00
1737	13.934	183.00
1738	14.307	183.00
1741	6.6875	183.50
1742	6.9375	183.50
1743	7.1875	183.50
1744	7.4375	183.50
1745	7.9375	183.50
1746	7.9385	183.50
1747	8.4375	183.50
1748	8.9375	183.50
1749	9.6375	183.50
1750	10.315	183.50
1751	11.315	183.50
1752	12.001	183.50
1753	12.688	183.50
1754	13.133	183.50
1755	13.188	183.50
1756	13.561	183.50
1757	13.934	183.50
1758	14.307	183.50
1761	6.6875	184.00
1762	6.9375	184.00
1763	7.1875	184.00
1764	7.4375	184.00
1765	7.9375	184.00
1766	7.9385	184.00
1767	8.4375	184.00
1768	8.9375	184.00
1769	9.6375	184.00
1770	10.315	184.00
1771	11.315	184.00
1772	12.001	184.00
1773	12.688	184.00
1774	13.133	184.00
1775	13.188	184.00
1776	13.561	184.00
1777	13.934	184.00
1778	14.307	184.00
1781	6.6875	184.50
1782	6.9375	184.50
1783	7.1875	184.50
1784	7.4375	184.50
1785	7.9375	184.50
1786	7.9385	184.50
1787	8.4375	184.50
1788	8.9375	184.50

Table 2.10.2-1 Node Definitions (continued)

NODE	X (inch)	Y (inch)
1789	9.6375	184.50
1790	10.315	184.50
1791	11.315	184.50
1792	12.001	184.50
1793	12.688	184.50
1794	13.133	184.50
1795	13.188	184.50
1796	13.561	184.50
1797	13.934	184.50
1798	14.307	184.50
1801	6.6875	185.00
1802	6.9375	185.00
1803	7.1875	185.00
1804	7.4375	185.00
1805	7.9375	185.00
1806	7.9385	185.00
1807	8.4375	185.00
1808	8.9375	185.00
1809	9.6375	185.00
1810	10.315	185.00
1811	11.315	185.00
1812	12.001	185.00
1813	12.688	185.00
1814	13.133	185.00
1815	13.188	185.00
1816	13.561	185.00
1817	13.934	185.00
1818	14.307	185.00
1821	6.6875	185.25
1822	6.9375	185.25
1823	7.1875	185.25
1824	7.4375	185.25
1825	7.9375	185.25
1826	7.9385	185.25
1827	8.4375	185.25
1828	8.9375	185.25
1829	9.6375	185.25
1830	10.315	185.25
1831	11.315	185.25
1832	12.001	185.25
1833	12.688	185.25
1834	13.133	185.25
1835	13.188	185.25
1836	13.561	185.25
1837	13.934	185.25
1838	14.307	185.25
1841	6.6875	185.50
1842	6.9375	185.50
1843	7.1875	185.50
1844	7.4375	185.50
1845	7.9375	185.50
1846	8.4375	185.50
1847	8.9375	185.50
1848	9.6375	185.50
1849	10.315	185.50
1850	11.315	185.50
1851	12.001	185.50
1852	12.688	185.50
1853	13.188	185.50
1854	13.561	185.50

Table 2.10.2-1 Node Definitions (continued)

NODE	X (inch)	Y (inch)
1855	13.934	185.50
1856	14.307	185.50
1861	6.6875	186.50
1862	6.9375	186.50
1863	7.1875	186.50
1864	7.4375	186.50
1865	7.9375	186.50
1866	8.4375	186.50
1867	8.9375	186.50
1868	9.6375	186.50
1869	10.315	186.50
1870	11.315	186.50
1871	12.001	186.50
1872	12.688	186.50
1873	13.188	186.50
1874	13.561	186.50
1875	13.934	186.50
1876	14.307	186.50
1881	6.6875	187.50
1882	6.9375	187.50
1883	7.1875	187.50
1884	7.4375	187.50
1885	7.9375	187.50
1886	8.4375	187.50
1887	8.9375	187.50
1888	9.6375	187.50
1889	10.315	187.50
1890	11.315	187.50
1891	12.001	187.50
1892	12.688	187.50
1893	13.188	187.50
1894	13.561	187.50
1895	13.934	187.50
1896	14.307	187.50
1901	6.6875	188.50
1902	6.9375	188.50
1903	7.1875	188.50
1904	7.4375	188.50
1905	7.9375	188.50
1906	8.4375	188.50
1907	8.9375	188.50
1908	9.6375	188.50
1909	10.315	188.50
1910	11.315	188.50
1911	12.001	188.50
1912	12.688	188.50
1913	13.188	188.50
1914	13.561	188.50
1915	13.934	188.50
1916	14.307	188.50
1921	6.6875	189.75
1922	6.9375	189.75
1923	7.1875	189.75
1924	7.4375	189.75
1925	7.9375	189.75
1926	8.4375	189.75
1927	8.9375	189.75
1928	9.6375	189.75
1929	10.315	189.75
1930	11.315	189.75

Table 2.10.2-1 Node Definitions (continued)

NODE	X (inch)	Y (inch)
1931	12.001	189.75
1932	12.688	189.75
1933	13.188	189.75
1934	13.561	189.75
1935	13.934	189.75
1936	14.307	189.75
1941	6.6875	190.75
1942	6.9375	190.75
1943	7.1875	190.75
1944	7.4375	190.75
1945	7.9375	190.75
1946	8.4375	190.75
1947	8.9375	190.75
1948	9.6375	190.75
1949	10.315	190.75
1950	11.315	190.75
1951	12.001	190.75
1952	12.688	190.75
1953	13.188	190.75
1954	13.561	190.75
1955	13.934	190.75
1956	14.307	190.75
1961	6.6875	191.75
1962	6.9375	191.75
1963	7.1875	191.75
1964	7.4375	191.75
1965	7.9375	191.75
1966	8.4375	191.75
1967	8.9375	191.75
1968	9.6375	191.75
1969	10.315	191.75
1970	11.315	191.75
1971	12.001	191.75
1972	12.688	191.75
1973	13.188	191.75
1974	13.561	191.75
1975	13.934	191.75
1976	14.307	191.75
1989	10.315	192.75
1990	11.315	192.75
1991	12.001	192.75
1992	12.688	192.75
1993	13.188	192.75
1994	13.561	192.75
1995	13.934	192.75
1996	14.307	192.75
2009	10.315	193.75
2010	11.315	193.75
2011	12.001	193.75
2012	12.688	193.75
2013	13.188	193.75
2014	13.561	193.75
2015	13.934	193.75
2016	14.307	193.75
2029	10.315	194.75
2030	11.315	194.75
2031	12.001	194.75
2032	12.688	194.75
2033	13.188	194.75
2034	13.561	194.75

Table 2.10.2-1 Node Definitions (continued)

NODE	X (inch)	Y (inch)
2035	13.934	194.75
2036	14.307	194.75
2049	10.315	195.75
2050	11.315	195.75
2051	12.001	195.75
2052	12.688	195.75
2053	13.188	195.75
2054	13.561	195.75
2055	13.934	195.75
2056	14.307	195.75
2069	10.315	196.69
2070	11.315	196.69
2071	12.001	196.69
2072	12.688	196.69
2073	13.188	196.69
2074	13.561	196.69
2075	13.934	196.69
2076	14.307	196.69
2090	11.315	197.75
2091	12.001	197.75
2092	12.688	197.75
2093	13.188	197.75
2094	13.561	197.75
2095	13.934	197.75
2096	14.307	197.75
2110	11.315	198.25
2111	12.001	198.25
2112	12.688	198.25
2113	13.188	198.25
2114	13.561	198.25
2115	13.934	198.25
2116	14.307	198.25
2130	11.315	198.25
2131	12.001	198.25
2132	12.688	198.25
2133	13.188	198.25
2134	13.561	198.25
2135	13.934	198.25
2136	14.307	198.25
2150	11.315	199.25
2151	12.001	199.25
2152	12.688	199.25
2153	13.188	199.25
2154	13.561	199.25
2155	13.934	199.25
2156	14.307	199.25
2170	11.315	199.25
2171	12.001	199.25
2172	12.688	199.25
2173	13.188	199.25
2174	13.561	199.25
2175	13.934	199.25
2176	14.307	199.25
2301	.00000	188.50
2302	.85000	188.50
2303	1.7000	188.50
2304	2.5500	188.50
2305	3.4000	188.50
2306	4.2500	188.50
2307	5.1000	188.50

Table 2.10.2-1 Node Definitions (continued)

NODE	X (inch)	Y (inch)
2308	5.9500	188.50
2309	6.4375	188.50
2310	6.6250	188.50
2321	.00000	189.75
2322	.85000	189.75
2323	1.7000	189.75
2324	2.5500	189.75
2325	3.4000	189.75
2326	4.2500	189.75
2327	5.1000	189.75
2328	5.9500	189.75
2329	6.4375	189.75
2330	6.6250	189.75
2341	.00000	190.75
2342	.85000	190.75
2343	1.7000	190.75
2344	2.5500	190.75
2345	3.4000	190.75
2346	4.2500	190.75
2347	5.1000	190.75
2348	5.9500	190.75
2349	6.4375	190.75
2350	6.6250	190.75
2361	.00000	191.75
2362	.85000	191.75
2363	1.7000	191.75
2364	2.5500	191.75
2365	3.4000	191.75
2366	4.2500	191.75
2367	5.1000	191.75
2368	5.9500	191.75
2369	6.4375	191.75
2370	6.6875	191.75
2371	6.9375	191.75
2372	7.1875	191.75
2373	7.4375	191.75
2374	7.9375	191.75
2375	8.4375	191.75
2376	8.9375	191.75
2377	9.6375	191.75
2378	10.250	191.75
2381	.00000	192.75
2382	.85000	192.75
2383	1.7000	192.75
2384	2.5500	192.75
2385	3.4000	192.75
2386	4.2500	192.75
2387	5.1000	192.75
2388	5.9500	192.75
2389	6.4375	192.75
2390	6.6875	192.75
2391	6.9375	192.75
2392	7.1875	192.75
2393	7.4375	192.75
2394	7.9375	192.75
2395	8.4375	192.75
2396	8.9375	192.75
2397	9.6375	192.75
2398	10.250	192.75
2401	.00000	193.75

Table 2.10.2-1 Node Definitions (continued)

NODE	X (inch)	Y (inch)
2402	.85000	193.75
2403	1.7000	193.75
2404	2.5500	193.75
2405	3.4000	193.75
2406	4.2500	193.75
2407	5.1000	193.75
2408	5.9500	193.75
2409	6.4375	193.75
2410	6.6875	193.75
2411	6.9375	193.75
2412	7.1875	193.75
2413	7.4375	193.75
2414	7.9375	193.75
2415	8.4375	193.75
2416	8.9375	193.75
2417	9.6375	193.75
2418	10.250	193.75
2421	.00000	194.75
2422	.85000	194.75
2423	1.7000	194.75
2424	2.5500	194.75
2425	3.4000	194.75
2426	4.2500	194.75
2427	5.1000	194.75
2428	5.9500	194.75
2429	6.4375	194.75
2430	6.6875	194.75
2431	6.9375	194.75
2432	7.1875	194.75
2433	7.4375	194.75
2434	7.9375	194.75
2435	8.4375	194.75
2436	8.9375	194.75
2437	9.6375	194.75
2438	10.250	194.75
2441	.00000	195.75
2442	.85000	195.75
2443	1.7000	195.75
2444	2.5500	195.75
2445	3.4000	195.75
2446	4.2500	195.75
2447	5.1000	195.75
2448	5.9500	195.75
2449	6.4375	195.75
2450	6.6875	195.75
2451	6.9375	195.75
2452	7.1875	195.75
2453	7.4375	195.75
2454	7.9375	195.75
2455	8.4375	195.75
2456	8.9375	195.75
2457	9.6375	195.75
2458	10.250	195.75
2461	.00000	196.75
2462	.85000	196.75
2463	1.7000	196.75
2464	2.5500	196.75
2465	3.4000	196.75
2466	4.2500	196.75
2467	5.1000	196.75

Table 2.10.2-1 Node Definitions (continued)

NODE	X (inch)	Y (inch)
2468	5.9500	196.75
2469	6.4375	196.75
2470	6.6875	196.75
2471	6.9375	196.75
2472	7.1875	196.75
2473	7.4375	196.75
2474	7.9375	196.75
2475	8.4375	196.75
2476	8.9375	196.75
2477	9.6375	196.75
2478	10.315	196.75
2479	11.250	196.75
2481	.00000	197.75
2482	.85000	197.75
2483	1.7000	197.75
2484	2.5500	197.75
2485	3.4000	197.75
2486	4.2500	197.75
2487	5.1000	197.75
2488	5.9500	197.75
2489	6.4375	197.75
2490	6.6875	197.75
2491	6.9375	197.75
2492	7.1875	197.75
2493	7.4375	197.75
2494	7.9375	197.75
2495	8.4375	197.75
2496	8.9375	197.75
2497	9.6375	197.75
2498	10.315	197.75
2499	11.250	197.75
2501	.00000	198.25
2502	.85000	198.25
2503	1.7000	198.25
2504	2.5500	198.25
2505	3.4000	198.25
2506	4.2500	198.25
2507	5.1000	198.25
2508	5.9500	198.25
2509	6.4375	198.25
2510	6.6875	198.25
2511	6.9375	198.25
2512	7.1875	198.25
2513	7.4375	198.25
2514	7.9375	198.25
2515	8.4375	198.25
2516	8.9375	198.25
2517	9.6375	198.25
2518	10.315	198.25
2519	11.250	198.25
2521	.00000	198.75
2522	.85000	198.75
2523	1.7000	198.75
2524	2.5500	198.75
2525	3.4000	198.75
2526	4.2500	198.75
2527	5.1000	198.75
2528	5.9500	198.75
2529	6.4375	198.75
2530	6.6875	198.75

Table 2.10.2-1 Node Definitions (continued)

NODE	X (inch)	Y (inch)
2531	6.9375	198.75
2532	7.1875	198.75
2533	7.4375	198.75
2534	7.9375	198.75
2535	8.4375	198.75
2536	8.9375	198.75
2537	9.6375	198.75
2538	10.315	198.75
2539	11.250	198.75
2541	.00000	199.25
2542	.85000	199.25
2543	1.7000	199.25
2544	2.5500	199.25
2545	3.4000	199.25
2546	4.2500	199.25
2547	5.1000	199.25
2548	5.9500	199.25
2549	6.4375	199.25
2550	6.6875	199.25
2551	6.9375	199.25
2552	7.1875	199.25
2553	7.4375	199.25
2554	7.9375	199.25
2555	8.4375	199.25
2556	8.9375	199.25
2557	9.6375	199.25
2558	10.315	199.25
2559	11.250	199.25
2561	.00000	199.25
2562	.85000	199.25
2563	1.7000	199.25
2564	2.5500	199.25
2565	3.4000	199.25
2566	4.2500	199.25
2567	5.1000	199.25
2568	5.9500	199.25
2569	6.4375	199.25
2570	6.6875	199.25
2571	6.9375	199.25
2572	7.1875	199.25
2573	7.4375	199.25
2574	7.9375	199.25
2575	8.4375	199.25
2576	8.9375	199.25
2577	9.6375	199.25
2578	10.315	199.25
2579	11.250	199.25
3101	.00000	3.5010
3102	.85000	3.5010
3103	1.7000	3.5010
3104	2.5500	3.5010
3105	3.4000	3.5010
3106	4.2500	3.5010
3107	5.1000	3.5010
3108	5.9500	3.5010
3109	6.4375	3.5010
3110	6.6875	3.5010
3111	6.9375	3.5010
3112	7.1875	3.5010
3113	7.4375	3.5010

Table 2.10.2-1 Node Definitions (continued)

NODE	X (inch)	Y (inch)
3114	7.9375	3.5010
3115	8.4375	3.5010
3116	8.9375	3.5010
3117	9.6375	3.5010
3118	10.375	3.5010
3143	10.374	4.5000
3168	10.374	5.5000
3176	.00000	6.4990
3177	.85000	6.4990
3178	1.7000	6.4990
3179	2.5500	6.4990
3180	3.4000	6.4990
3181	4.2500	6.4990
3182	5.1000	6.4990
3183	5.9500	6.4990
3184	6.4375	6.4990
3185	6.6875	6.4990
3186	6.9375	6.4990
3187	7.1875	6.4990
3188	7.4375	6.4990
3189	7.9375	6.4990
3190	8.4375	6.4990
3191	8.9375	6.4990
3192	9.6375	6.4990
3193	10.375	6.4990
3340	8.4375	10.501
3341	8.9375	10.501
3342	9.6375	10.501
3343	10.375	10.501
3344	11.315	10.501
3345	12.001	10.501
3346	12.688	10.501
3846	8.4375	185.50
3847	8.9375	185.50
3848	9.6375	185.50
3849	10.315	185.50
3850	11.315	185.50
3851	12.001	185.50
3852	12.688	185.50

Table 2.10.2-2 Applied Impact Pressure Loadings – 30-Foot Hypothetical Accident Conditions

Impact Case	ϕ[1] (degree)	θ[2] (degree)	Node to Node		Impact Pressure[3] (psi)	Impact Type
1	0	360	1	25	4852	Bottom End
			326	335	1708	Content End
2	90	45	25	418	8495	Bottom Side
			1916	2176	8693	Top Side
			335	1901	177.1	Content Side
3	180	360	2176	2561	4852	Top End
			2301	2310	1740	Content End
4	15.74	60.4	2176	2561	14768	Top End
			1916	2176	3370	Top Side
			2301	2310	5299	Content End
			335	1901	35	Content Side
4	30	54.4	2176	2561	12925	Top End
			1916	2176	5831	Top Side
			2301	2310	4638	Content End
			335	1901	61	Content Side
4	45	43.8	2176	2561	10840	Top End
			1916	2176	7812	Top Side
			2301	2310	3889	Content End
			335	1901	81	Content Side
4	60	44.4	2176	2561	9599	Top End
			1916	2176	11470	Top Side
			2301	2310	3444	Content End
			335	1901	119	Content Side

Table 2.10.2-2 Applied Impact Pressure Loadings – 30-Foot Hypothetical Accident Conditions (continued)

Impact Case	ϕ[1] (degree)	θ[2] (degree)	Node to Node		Impact Pressure[3] (psi)	Impact Type
5	120	44.4	1	25	9191	Bottom End
			25	418	10820	Bottom Side
			326	335	3236	Content End
			335	1901	115	Content Side
5	135	43.8	1	25	10359	Bottom End
			25	418	7389	Bottom Side
			326	335	3647	Content End
			335	1901	78	Content Side
5	150	54.4	1	25	12294	Bottom End
			25	418	5549	Bottom Side
			326	335	4329	Content End
			335	1901	59	Content Side
5	164.26	60.4	1	25	14768	Bottom End
			25	418	3292	Bottom Side
			326	335	5200	Content End
			335	1901	35	Content Side

1 ϕ = drop orientation

2 The angle θ determines the pressure distribution arc in the circumferential direction. (See Figure 2.7.1-6 and Figure 2.7.1-9.) The same arc is applied for both the impact pressure and the content pressure.

3 See Section 2.7.1 for the methodology used to calculate the impact pressures for the 30-foot end drop, the 30-foot side drop and the 30-foot oblique drops, respectively.

2.10.3 Finite Element Evaluations

This section presents (1) the temperature information required for the finite element stress analysis of the NAC-LWT cask, and (2) the NAC procedures to determine the maximum stress intensities for each cask component (designated in Section 2.10.2).

2.10.3.1 Isothermal Plot - Hot Case

This section presents the temperature distribution in the body of the NAC-LWT cask for the hot case (130°F ambient temperature with maximum insolation and decay heat load). The cask temperatures are obtained from the results of the heat transfer analysis for the hot environment (Section 3.4.2). The plot is shown in Figure 2.10.3-1.

2.10.3.2 Isothermal Plot - Cold Case

This section presents the results obtained from the heat transfer analysis performed in Section 3.4.3 for the cold case. The cask temperatures are determined for the cold environment (-40°F ambient temperature with maximum decay heat load and no insolation). The plot is shown in Figure 2.10.3-2.

2.10.3.3 Determination of Component Critical Stresses

This section presents the procedure that is used to determine the maximum stress intensities for each cask component for the analyses performed by the ANSYS finite element program. As required by Regulatory Guide 7.6, the calculated stresses are categorized into the P_m stress intensity, the $P_m + P_b$ stress intensity, the S_n stress intensity, and the total stress intensity categories. These stress intensities must be less than the allowable stress intensities defined by Regulatory Guide 7.6. The procedure is explained in the following steps:

1. Apply the ANSYS plotting option to produce a stress intensity contour plot for each cask component.
2. Review the plot and identify the component cross sections where significant P_m, $P_m + P_b$, and S_n stresses occur (close contour spacing).
3. Run the ANSYS post-processing program to determine the P_m, $P_m + P_b$, and S_n stress intensities for each cross section identified.
4. Sort through all of the P_m, $P_m + P_b$, and S_n stresses to obtain the maximum value for each stress category.
5. Tabulate the critical cross section, the stress intensity, and the resulting margin of safety for each component of the cask.

A FORTRAN program is set up to execute the evaluation of the stress data generated in step 3. The program then applies an algorithm to search for the maximum stress intensity for each cask

component. In addition, the program prints out the cask component, the critical cross section, the stress intensity, etc. Because steps 3 and 4 are performed by computer, many cross sections can be identified and evaluated.

An example is provided to illustrate the aforementioned procedures. Figure 2.10.2-3 is the stress contour plot of cask component 3 (upper ring), resulting from the normal operations heat condition with 130°F ambient temperature; see Section 2.6.1 for a detailed description of this load case.

In reviewing the plot, it is expected that the maximum stress intensity will occur at section (1) or (2). However, P_m and $P_m + P_b$ stresses are calculated for 44 sections at different locations of the upper ring to assure that the maximum stress locations are identified. These stress data are listed in Table 2.10.3-1 and Table 2.10.3-2, and the sections with maximum P_m or $P_m + P_b$ stresses are identified by the algorithm mentioned in step 4.

Figure 2.10.3-1 NAC-LWT Cask Isotherms (Hot Case)

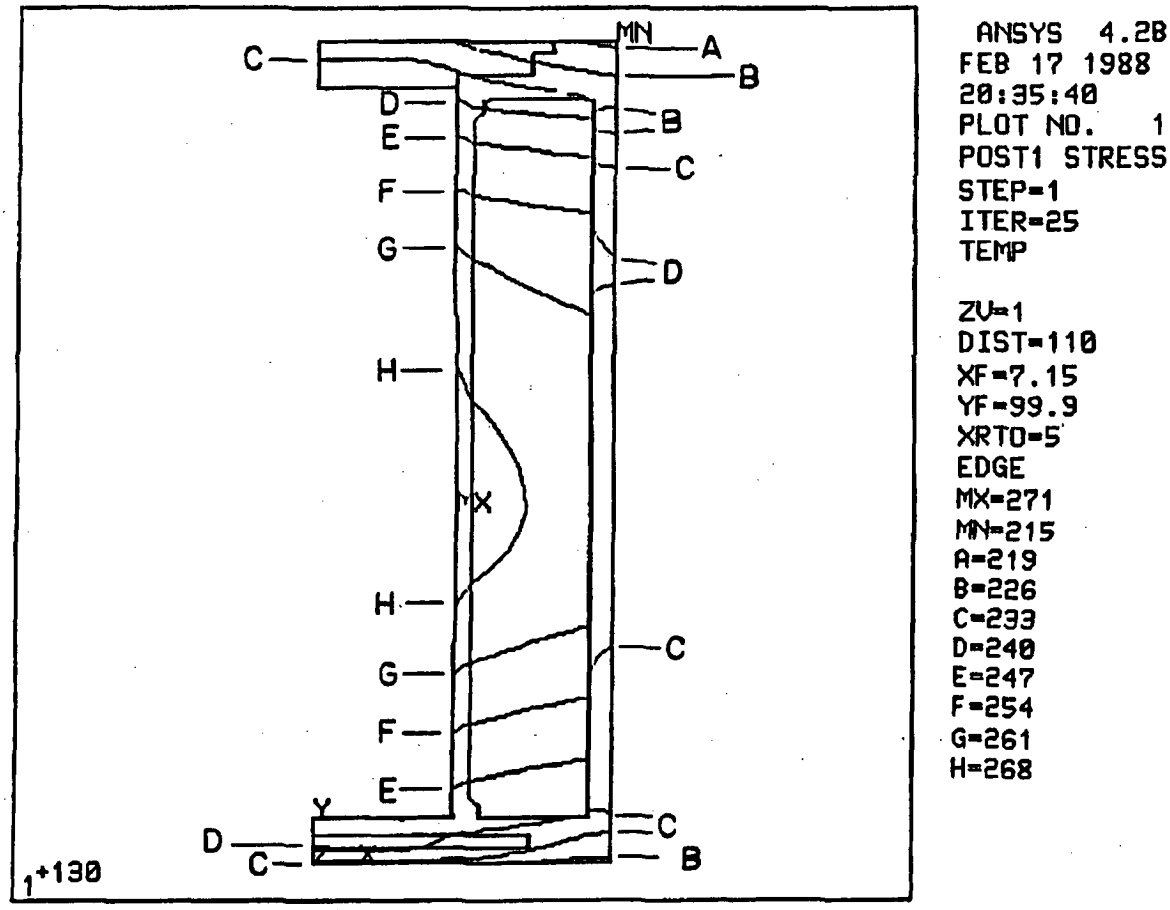

Figure 2.10.3-2 NAC-LWT Cask Isotherms (Cold Case)

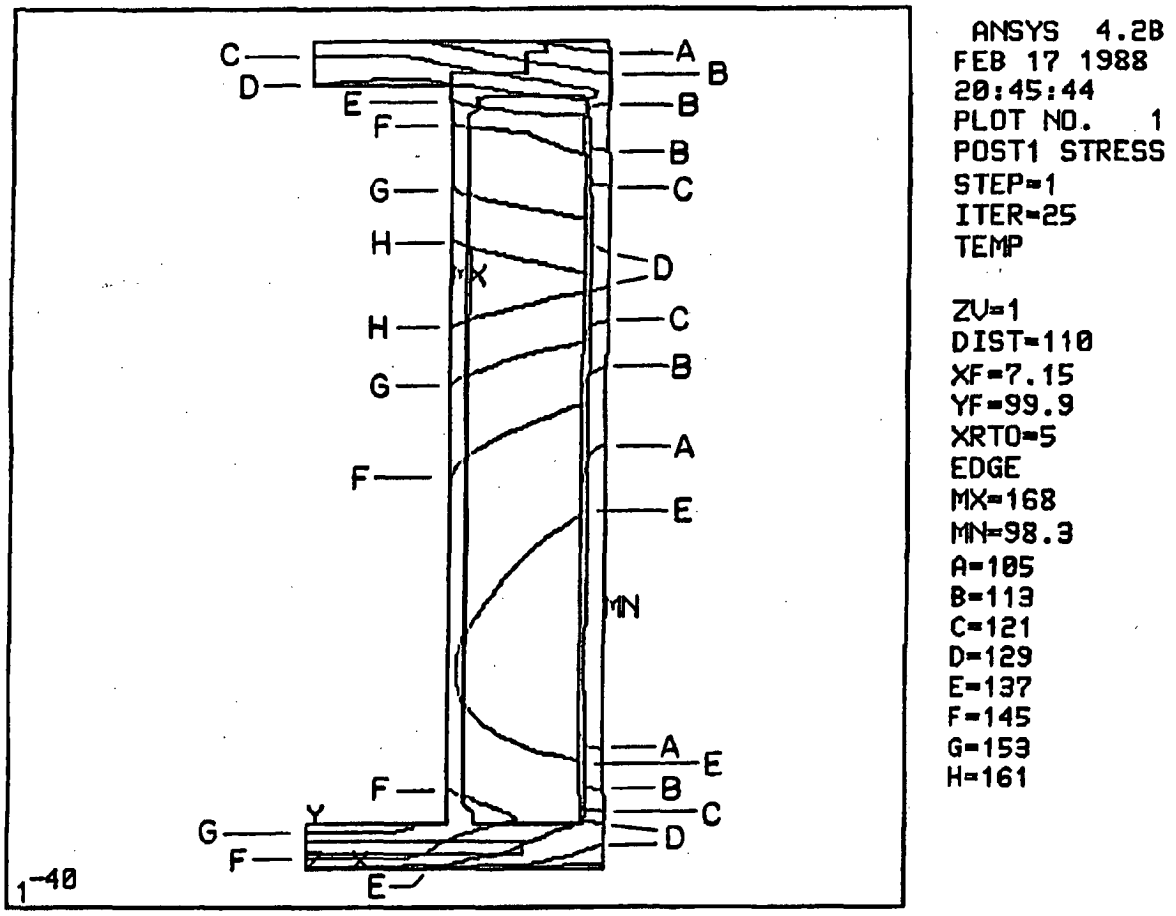

Figure 2.10.3-3 Stress Contour Plot – Hot Case

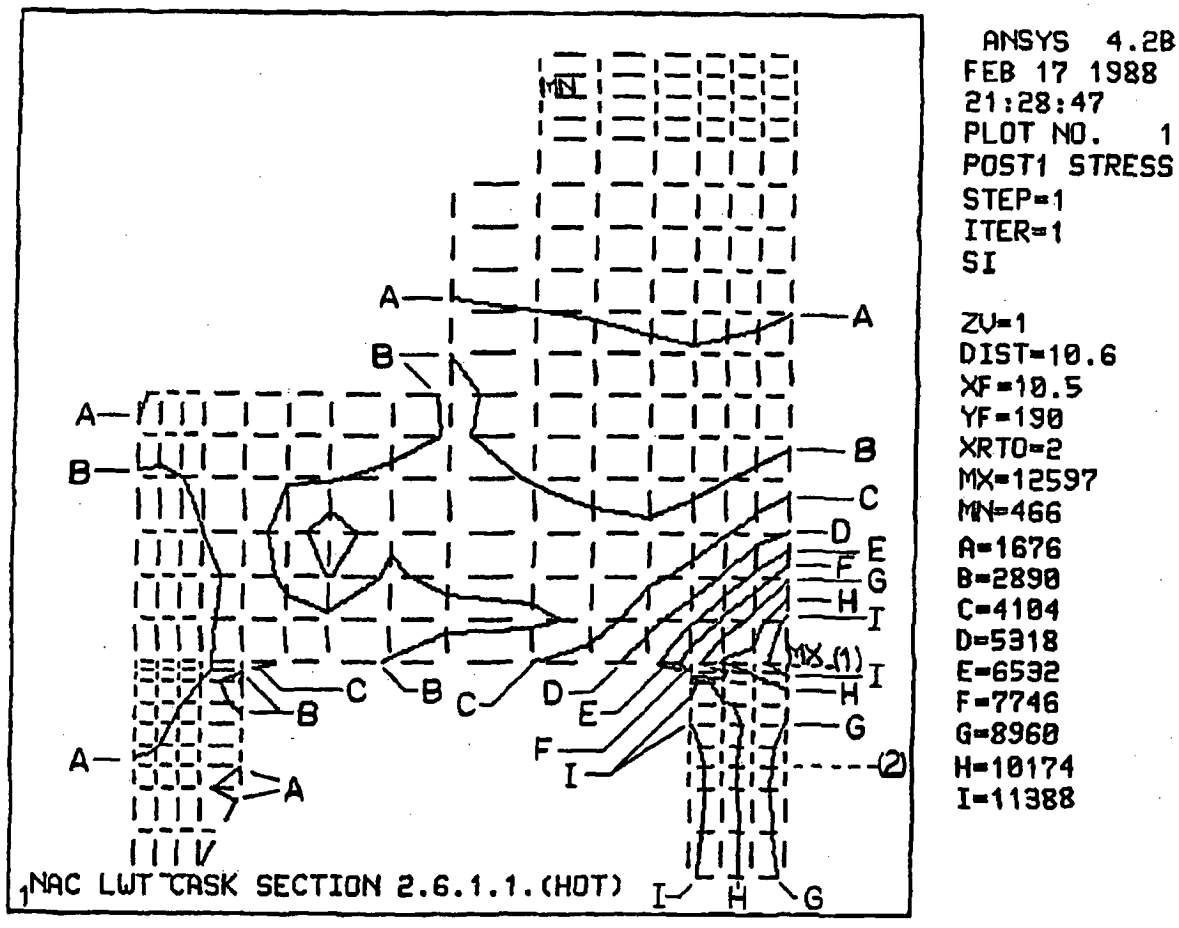

Table 2.10.3-1 P_m Stress Summary – Upper Ring Critical Section

LOADING CONDITION: SEC261(HEAT)
COMPONENT TYPE: TYPE3.

THE MAXIMUM PM STRESS OCCURS AT SECTION

FROM NODE 1595 TO NODE 1598

SX =	3.
SY =	10200.
SZ =	269.
SXY =	-63.
SYZ =	0.
SXZ =	0.
SIG1=	10200.
SIG2=	269.
SIG3=	2.
SI =	10200.
SIGE=	10070.

INSIDE NODE = 1581 OUTSIDE NODE = 1584

** MEMBRANE **

SX	SY	SZ	SXY	SYZ	SXZ
10.84	2754.	924.2	125.9	.0000	.0000
SIG1	SIG2	SIG3	SI	SIGE	
2760.	924.2	5.073	2754.	2429.	

INSIDE NODE = 1601 OUTSIDE NODE = 1605

** MEMBRANE **

SX	SY	SZ	SXY	SYZ	SXZ
22.03	2407.	749.2	196.2	.0000	.0000
SIG1	SIG2	SIG3	SI	SIGE	
2423.	749.2	5.992	2417.	2144.	

INSIDE NODE = 1701 OUTSIDE NODE = 1705

** MEMBRANE **

SX	SY	SZ	SXY	SYZ	SXZ
-28.80	1743.	515.3	177.2	.0000	.0000
SIG1	SIG2	SIG3	SI	SIGE	
1760.	515.3	-46.35	1807.	1601.	

INSIDE NODE = 1721 OUTSIDE NODE = 1725

** MEMBRANE **

SX	SY	SZ	SXY	SYZ	SXZ
-39.65	1750.	526.7	186.0	.0000	.0000
SIG1	SIG2	SIG3	SI	SIGE	
1769.	526.7	-58.78	1828.	1616.	

Table 2.10.3-1 P_m Stress Summary – Upper Ring Critical Section (continued)

INSIDE NODE =	1741	OUTSIDE NODE =	1745		
** MEMBRANE **					
SX	SY	SZ	SXY	SYZ	SXZ
-32.68	1746.	550.0	205.8	.0000	.0000
SIG1	SIG2	SIG3	SI	SIGE	
1770.	550.0	-56.19	1826.	1611.	
INSIDE NODE =	1761	OUTSIDE NODE =	1765		
** MEMBRANE **					
SX	SY	SZ	SXY	SYZ	SXZ
-38.52	1743.	557.1	226.2	.0000	.0000
SIG1	SIG2	SIG3	SI	SIGE	
1771.	557.1	-66.79	1838.	1619.	
INSIDE NODE =	1781	OUTSIDE NODE =	1785		
** MEMBRANE **					
SX	SY	SZ	SXY	SYZ	SXZ
-2.336	1741.	531.6	242.9	.0000	.0000
SIG1	SIG2	SIG3	SI	SIGE	
1774.	531.6	-35.55	1810.	1604.	
INSIDE NODE =	1801	OUTSIDE NODE =	1805		
** MEMBRANE **					
SX	SY	SZ	SXY	SYZ	SXZ
166.1	1734.	465.4	238.8	.0000	.0000
SIG1	SIG2	SIG3	SI	SIGE	
1769.	465.4	130.6	1639.	1499.	
INSIDE NODE =	1821	OUTSIDE NODE =	1825		
** MEMBRANE **					
SX	SY	SZ	SXY	SYZ	SXZ
372.6	1401.	340.4	157.0	.0000	.0000
SIG1	SIG2	SIG3	SI	SIGE	
1424.	349.1	340.4	1084.	1079.	
INSIDE NODE =	1841	OUTSIDE NODE =	1846		
** MEMBRANE **					
SX	SY	SZ	SXY	SYZ	SXZ
67.89	1119.	112.2	283.9	.0000	.0000
SIG1	SIG2	SIG3	SI	SIGE	
1191.	112.2	-3.883	1195.	1141.	
INSIDE NODE =	1595	OUTSIDE NODE =	1598		
** MEMBRANE **					
SX	SY	SZ	SXY	SYZ	SXZ
2.844	.1020+005	269.4	-62.79	.0000	.0000
SIG1	SIG2	SIG3	SI	SIGE	
.1020+005	269.4	2.458	.1020+005	.1007+005	
INSIDE NODE =	1616	OUTSIDE NODE =	1619		
** MEMBRANE **					
SX	SY	SZ	SXY	SYZ	SXZ
3.317	.1018+005	547.6	-41.72	.0000	.0000
SIG1	SIG2	SIG3	SI	SIGE	
.1018+005	547.6	3.146	.1017+005	9912.	
INSIDE NODE =	1715	OUTSIDE NODE =	1718		
** MEMBRANE **					
SX	SY	SZ	SXY	SYZ	SXZ
1.050	.1015+005	968.7	3.222	.0000	.0000
SIG1	SIG2	SIG3	SI	SIGE	
.1015+005	968.7	1.049	.1015+005	9702.	
INSIDE NODE =	1735	OUTSIDE NODE =	1738		
** MEMBRANE **					
SX	SY	SZ	SXY	SYZ	SXZ
-6.316	.1014+005	1224.	33.66	.0000	.0000
SIG1	SIG2	SIG3	SI	SIGE	
.1014+005	1224.	-6.428	.1014+005	9588.	

Table 2.10.3-1 P_m Stress Summary – Upper Ring Critical Section (continued)

INSIDE NODE =	1755	OUTSIDE NODE =	1758		
** MEMBRANE **					
SX	SY	SZ	SXY	SYZ	SXZ
-11.67	.1012+005	1512.	71.43	.0000	.0000
SIG1	SIG2	SIG3	SI	SIGE	
.1013+005	1512.	-12.17	.1014+005	9468.	
INSIDE NODE =	1775	OUTSIDE NODE =	1778		
** MEMBRANE **					
SX	SY	SZ	SXY	SYZ	SXZ
-36.04	.1011+005	1812.	116.7	.0000	.0000
SIG1	SIG2	SIG3	SI	SIGE	
.1011+005	1812.	-37.38	.1015+005	9364.	
INSIDE NODE =	1795	OUTSIDE NODE =	1798		
** MEMBRANE **					
SX	SY	SZ	SXY	SYZ	SXZ
68.56	.1010+005	2155.	170.4	.0000	.0000
SIG1	SIG2	SIG3	SI	SIGE	
.1010+005	2155.	65.66	.1004+005	9173.	
INSIDE NODE =	1795	OUTSIDE NODE =	1818		
** MEMBRANE **					
SX	SY	SZ	SXY	SYZ	SXZ
2019.	8317.	2367.	3901.	.0000	.0000
SIG1	SIG2	SIG3	SI	SIGE	
.1018+005	2367.	155.2	.1003+005	9123.	
INSIDE NODE =	1795	OUTSIDE NODE =	1838		
** MEMBRANE **					
SX	SY	SZ	SXY	SYZ	SXZ
3571.	6865.	2479.	4792.	.0000	.0000
SIG1	SIG2	SIG3	SI	SIGE	
.1029+005	2479.	151.0	.1013+005	9194.	
INSIDE NODE =	1815	OUTSIDE NODE =	1818		
** MEMBRANE **					
SX	SY	SZ	SXY	SYZ	SXZ
264.1	.1009+005	2521.	238.5	.0000	.0000
SIG1	SIG2	SIG3	SI	SIGE	
.1009+005	2521.	258.3	9836.	8922.	
INSIDE NODE =	1815	OUTSIDE NODE =	1838		
** MEMBRANE **					
SX	SY	SZ	SXY	SYZ	SXZ
770.4	9536.	2591.	2400.	.0000	.0000
SIG1	SIG2	SIG3	SI	SIGE	
.1015+005	2591.	156.5	9993.	9026.	
INSIDE NODE =	1815	OUTSIDE NODE =	1856		
** MEMBRANE **					
SX	SY	SZ	SXY	SYZ	SXZ
1872.	8251.	2622.	3914.	.0000	.0000
SIG1	SIG2	SIG3	SI	SIGE	
.1011+005	2622.	13.23	.1010+005	9078.	
INSIDE NODE =	1835	OUTSIDE NODE =	1838		
** MEMBRANE **					
SX	SY	SZ	SXY	SYZ	SXZ
149.0	9430.	2449.	349.3	.0000	.0000
SIG1	SIG2	SIG3	SI	SIGE	
9443.	2449.	135.9	9307.	8393.	
INSIDE NODE =	1835	OUTSIDE NODE =	1856		
** MEMBRANE **					
SX	SY	SZ	SXY	SYZ	SXZ
154.4	8850.	2375.	2151.	.0000	.0000
SIG1	SIG2	SIG3	SI	SIGE	
9353.	2375.	-348.5	9701.	8667.	

Table 2.10.3-1 P_m Stress Summary – Upper Ring Critical Section (continued)

INSIDE NODE = 1852			OUTSIDE NODE = 1856		
** MEMBRANE **					
SX	SY	SZ	SXY	SYZ	SXZ
-2286.	6576.	1023.	-558.9	.0000	.0000
SIG1	SIG2	SIG3	SI	SIGE	
6611.	1023.	-2321.	8932.	7816.	
INSIDE NODE = 1861			OUTSIDE NODE = 1876		
** MEMBRANE **					
SX	SY	SZ	SXY	SYZ	SXZ
-1032.	128.8	-294.6	-502.6	.0000	.0000
SIG1	SIG2	SIG3	SI	SIGE	
316.2	-294.6	-1219.	1536.	1339.	
INSIDE NODE = 1901			OUTSIDE NODE = 1916		
** MEMBRANE **					
SX	SY	SZ	SXY	SYZ	SXZ
301.2	-444.4	222.5	-488.2	.0000	.0000
SIG1	SIG2	SIG3	SI	SIGE	
542.7	222.5	-685.8	1229.	1104.	
INSIDE NODE = 1941			OUTSIDE NODE = 1956		
** MEMBRANE **					
SX	SY	SZ	SXY	SYZ	SXZ
179.9	-451.5	554.6	-404.6	.0000	.0000
SIG1	SIG2	SIG3	SI	SIGE	
554.6	377.4	-649.0	1204.	1125.	
INSIDE NODE = 1969			OUTSIDE NODE = 1976		
** MEMBRANE **					
SX	SY	SZ	SXY	SYZ	SXZ
-143.6	141.0	1091.	-485.3	.0000	.0000
SIG1	SIG2	SIG3	SI	SIGE	
1091.	504.4	-507.0	1598.	1400.	
INSIDE NODE = 1969			OUTSIDE NODE = 1996		
** MEMBRANE **					
SX	SY	SZ	SXY	SYZ	SXZ
-378.2	233.0	1038.	-363.6	.0000	.0000
SIG1	SIG2	SIG3	SI	SIGE	
1038.	402.3	-547.6	1585.	1382.	
INSIDE NODE = 1969			OUTSIDE NODE = 2016		
** MEMBRANE **					
SX	SY	SZ	SXY	SYZ	SXZ
-528.5	258.3	982.6	-231.4	.0000	.0000
SIG1	SIG2	SIG3	SI	SIGE	
982.6	321.3	-591.5	1574.	1369.	
INSIDE NODE = 1969			OUTSIDE NODE = 2036		
** MEMBRANE **					
SX	SY	SZ	SXY	SYZ	SXZ
-599.5	240.7	927.8	-133.4	.0000	.0000
SIG1	SIG2	SIG3	SI	SIGE	
927.8	261.4	-620.2	1548.	1345.	
INSIDE NODE = 1989			OUTSIDE NODE = 1996		
** MEMBRANE **					
SX	SY	SZ	SXY	SYZ	SXZ
-151.2	-4.381	1006.	-409.8	.0000	.0000
SIG1	SIG2	SIG3	SI	SIGE	
1006.	338.5	-494.1	1500.	1302.	
INSIDE NODE = 2009			OUTSIDE NODE = 2016		
** MEMBRANE **					
SX	SY	SZ	SXY	SYZ	SXZ
-71.20	-3.681	948.3	-331.7	.0000	.0000
SIG1	SIG2	SIG3	SI	SIGE	
948.3	296.0	-370.9	1319.	1143.	

Table 2.10.3-1 P_m Stress Summary – Upper Ring Critical Section (continued)

INSIDE NODE = 2029			OUTSIDE NODE = 2036		
** MEMBRANE **					
SX	SY	SZ	SXY	SYZ	SXZ
-21.69	-2.435	867.2	-256.9	.0000	.0000
SIG1	SIG2	SIG3	SI	SIGE	
867.2	245.0	-269.2	1136.	985.6	
INSIDE NODE = 2049			OUTSIDE NODE = 2056		
** MEMBRANE **					
SX	SY	SZ	SXY	SYZ	SXZ
-2.420	-1.452	779.8	-189.0	.0000	.0000
SIG1	SIG2	SIG3	SI	SIGE	
779.8	187.1	-191.0	970.7	847.5	
INSIDE NODE = 2070			OUTSIDE NODE = 2076		
** MEMBRANE **					
SX	SY	SZ	SXY	SYZ	SXZ
-104.0	33.41	765.9	-146.4	.0000	.0000
SIG1	SIG2	SIG3	SI	SIGE	
765.9	126.4	-197.0	962.9	848.8	
INSIDE NODE = 2070			OUTSIDE NODE = 2096		
** MEMBRANE **					
SX	SY	SZ	SXY	SYZ	SXZ
-161.8	66.08	720.3	-77.73	.0000	.0000
SIG1	SIG2	SIG3	SI	SIGE	
720.3	90.06	-185.8	906.1	804.5	
INSIDE NODE = 2070			OUTSIDE NODE = 2116		
** MEMBRANE **					
SX	SY	SZ	SXY	SYZ	SXZ
-172.8	63.77	699.7	-52.64	.0000	.0000
SIG1	SIG2	SIG3	SI	SIGE	
699.7	74.95	-184.0	883.7	786.9	
INSIDE NODE = 2070			OUTSIDE NODE = 2136		
** MEMBRANE **					
SX	SY	SZ	SXY	SYZ	SXZ
-180.7	56.78	679.9	-35.13	.0000	.0000
SIG1	SIG2	SIG3	SI	SIGE	
679.9	61.87	-185.8	865.7	772.3	
INSIDE NODE = 2090			OUTSIDE NODE = 2096		
** MEMBRANE **					
SX	SY	SZ	SXY	SYZ	SXZ
-23.81	-.4666	694.1	-109.8	.0000	.0000
SIG1	SIG2	SIG3	SI	SIGE	
694.1	98.32	-122.6	816.7	731.7	
INSIDE NODE = 2110			OUTSIDE NODE = 2116		
** MEMBRANE **					
SX	SY	SZ	SXY	SYZ	SXZ
-19.01	-.4233	665.4	-83.96	.0000	.0000
SIG1	SIG2	SIG3	SI	SIGE	
665.4	74.76	-94.19	759.6	690.8	
INSIDE NODE = 2130			OUTSIDE NODE = 2136		
** MEMBRANE **					
SX	SY	SZ	SXY	SYZ	SXZ
-43.37	-.2781	632.9	-59.62	.0000	.0000
SIG1	SIG2	SIG3	SI	SIGE	
632.9	41.57	-85.23	718.1	663.9	
INSIDE NODE = 2150			OUTSIDE NODE = 2156		
** MEMBRANE **					
SX	SY	SZ	SXY	SYZ	SXZ
-149.4	-.1861	590.7	-37.46	.0000	.0000
SIG1	SIG2	SIG3	SI	SIGE	
590.7	8.687	-158.3	749.0	681.1	

Table 2.10.3-2 $P_m + P_b$ Stress Summary – Upper Ring Critical Section

LOADING CONDITION: SEC261(HEAT)
COMPONENT TYPE: TYPE3.

THE MAXIMUM PM + PB STRESS OCCURS AT SECTION

FROM NODE 1852 TO NODE 1856

SX =	-297.
SY =	13090.
SZ =	3904.
SXY =	-559.
SYZ =	0.
SXZ =	0.
SIG1=	13110.
SIG2=	3904.
SIG3=	-321.
SI =	13430.
SIGE=	11900.

INSIDE NODE = 1581 OUTSIDE NODE = 1584
** MEMBRANE PLUS BENDING ** I=INSIDE C=CENTER O=OUTSIDE

	SX	SY	SZ	SXY	SYZ	SXZ
I	-23.79	2331.	781.4	125.9	.0000	.0000
C	-13.15	2746.	924.2	125.9	.0000	.0000
O	-2.511	3162.	1067.	125.9	.0000	.0000
	SIG1	SIG2	SIG3	SI	SIGE	
I	2337.	781.4	-30.51	2368.	2084.	
C	2752.	924.2	-18.89	2771.	2440.	
O	3167.	1067.	-7.515	3175.	2797.	

INSIDE NODE = 1601 OUTSIDE NODE = 1605
** MEMBRANE PLUS BENDING ** I=INSIDE C=CENTER O=OUTSIDE

	SX	SY	SZ	SXY	SYZ	SXZ
I	-66.43	2278.	636.4	196.2	.0000	.0000
C	62.08	2404.	749.2	196.2	.0000	.0000
O	190.6	2530.	862.0	196.2	.0000	.0000
	SIG1	SIG2	SIG3	SI	SIGE	
I	2294.	636.4	-82.74	2377.	2111.	
C	2420.	749.2	45.76	2374.	2112.	
O	2546.	862.0	174.3	2372.	2114.	

Table 2.10.3-2 $P_m + P_b$ Stress Summary – Upper Ring Critical Section (continued)

INSIDE NODE = 1701 OUTSIDE NODE = 1705
** MEMBRANE PLUS BENDING ** I=INSIDE C=CENTER O=OUTSIDE

	SX	SY	SZ	SXY	SYZ	SXZ
I	-76.27	2299.	585.7	177.2	.0000	.0000
C	-12.63	1758.	515.3	177.2	.0000	.0000
O	51.01	1218.	445.0	177.2	.0000	.0000

	SIG1	SIG2	SIG3	SI	SIGE
I	2312.	585.7	-89.42	2401.	2145.
C	1776.	515.3	-30.18	1806.	1604.
O	1244.	445.0	24.70	1219.	1073.

INSIDE NODE = 1721 OUTSIDE NODE = 1725
** MEMBRANE PLUS BENDING ** I=INSIDE C=CENTER O=OUTSIDE

	SX	SY	SZ	SXY	SYZ	SXZ
I	-52.67	1829.	477.1	186.0	.0000	.0000
C	-34.90	1752.	526.7	186.0	.0000	.0000
O	-17.13	1675.	576.4	186.0	.0000	.0000

	SIG1	SIG2	SIG3	SI	SIGE
I	1848.	477.1	-70.88	1918.	1712.
C	1771.	526.7	-54.06	1825.	1615.
O	1695.	576.4	-37.34	1732.	1521.

INSIDE NODE = 1741 OUTSIDE NODE = 1745
** MEMBRANE PLUS BENDING ** I=INSIDE C=CENTER O=OUTSIDE

	SX	SY	SZ	SXY	SYZ	SXZ
I	-64.41	1351.	365.5	205.8	.0000	.0000
C	-27.54	1735.	550.0	205.8	.0000	.0000
O	9.334	2119.	734.5	205.8	.0000	.0000

	SIG1	SIG2	SIG3	SI	SIGE
I	1381.	365.5	-93.73	1474.	1307.
C	1759.	550.0	-51.25	1810.	1597.
O	2139.	734.5	-10.56	2150.	1891.

INSIDE NODE = 1761 OUTSIDE NODE = 1765
** MEMBRANE PLUS BENDING ** I=INSIDE C=CENTER O=OUTSIDE

	SX	SY	SZ	SXY	SYZ	SXZ
I	-53.49	828.0	231.6	226.2	.0000	.0000
C	-27.07	1717.	557.1	226.2	.0000	.0000
O	-.6480	2607.	882.6	226.2	.0000	.0000

	SIG1	SIG2	SIG3	SI	SIGE
I	882.7	231.6	-108.1	990.8	872.1
C	1746.	557.1	-55.92	1802.	1587.
O	2626.	882.6	-20.13	2647.	2330.

INSIDE NODE = 1781 OUTSIDE NODE = 1785
** MEMBRANE PLUS BENDING ** I=INSIDE C=CENTER O=OUTSIDE

	SX	SY	SZ	SXY	SYZ	SXZ
I	-27.39	257.3	35.40	242.9	.0000	.0000
C	11.46	1700.	531.6	242.9	.0000	.0000
O	50.32	3143.	1028.	242.9	.0000	.0000

	SIG1	SIG2	SIG3	SI	SIGE
I	396.5	35.40	-166.6	563.1	494.1
C	1734.	531.6	-22.79	1757.	1556.
O	3162.	1028.	31.35	3131.	2770.

INSIDE NODE = 1801 OUTSIDE NODE = 1805
** MEMBRANE PLUS BENDING ** I=INSIDE C=CENTER O=OUTSIDE

	SX	SY	SZ	SXY	SYZ	SXZ
I	2.605	-264.9	-222.6	238.8	.0000	.0000
C	50.43	1678.	465.4	238.8	.0000	.0000
O	98.25	3621.	1153.	238.8	.0000	.0000

	SIG1	SIG2	SIG3	SI	SIGE
I	142.6	-222.6	-404.9	547.4	482.8
C	1712.	465.4	16.12	1696.	1522.
O	3637.	1153.	82.13	3555.	3159.

Table 2.10.3-2 $P_m + P_b$ Stress Summary – Upper Ring Critical Section (continued)

INSIDE NODE = 1821 OUTSIDE NODE = 1825
** MEMBRANE PLUS BENDING ** I=INSIDE C=CENTER O=OUTSIDE

	SX	SY	SZ	SXY	SYZ	SXZ
I	9.905	3.544	-373.6	157.0	.0000	.0000
C	440.8	1362.	340.4	157.0	.0000	.0000
O	871.7	2720.	1054.	157.0	.0000	.0000
	SIG1	SIG2	SIG3	SI	SIGE	
I	163.7	-150.3	-373.6	537.4	467.6	
C	1388.	414.8	340.4	1048.	1012.	
O	2734.	1054.	858.5	1875.	1785.	

INSIDE NODE = 1841 OUTSIDE NODE = 1846
** MEMBRANE PLUS BENDING ** I=INSIDE C=CENTER O=OUTSIDE

	SX	SY	SZ	SXY	SYZ	SXZ
I	-78.52	883.3	-232.8	283.9	.0000	.0000
C	109.6	1110.	112.2	283.9	.0000	.0000
O	297.6	1338.	457.2	283.9	.0000	.0000
	SIG1	SIG2	SIG3	SI	SIGE	
I	960.8	-156.1	-232.8	1194.	1157.	
C	1185.	112.2	34.63	1151.	1114.	
O	1410.	457.2	225.2	1185.	1088.	

INSIDE NODE = 1595 OUTSIDE NODE = 1598
** MEMBRANE PLUS BENDING ** I=INSIDE C=CENTER O=OUTSIDE

	SX	SY	SZ	SXY	SYZ	SXZ
I	-8.812	.1159+005	482.7	-62.79	.0000	.0000
C	.1007	.1022+005	269.4	-62.79	.0000	.0000
O	9.014	8843.	56.14	-62.79	.0000	.0000
	SIG1	SIG2	SIG3	SI	SIGE	
I	.1159+005	482.7	-9.152	.1160+005	.1137+005	
C	.1022+005	269.4	-.2852	.1022+005	.1009+005	
O	8843.	56.14	8.567	8835.	8811.	

INSIDE NODE = 1616 OUTSIDE NODE = 1619
** MEMBRANE PLUS BENDING ** I=INSIDE C=CENTER O=OUTSIDE

	SX	SY	SZ	SXY	SYZ	SXZ
I	-17.39	.1183+005	852.5	-41.72	.0000	.0000
C	-.7916	.1020+005	547.6	-41.72	.0000	.0000
O	15.81	8565.	242.8	-41.72	.0000	.0000
	SIG1	SIG2	SIG3	SI	SIGE	
I	.1183+005	852.5	-17.54	.1185+005	.1144+005	
C	.1020+005	547.6	-.9623	.1020+005	9937.	
O	8565.	242.8	15.61	8549.	8438.	

INSIDE NODE = 1715 OUTSIDE NODE = 1718
** MEMBRANE PLUS BENDING ** I=INSIDE C=CENTER O=OUTSIDE

	SX	SY	SZ	SXY	SYZ	SXZ
I	-26.58	.1191+005	1331.	3.222	.0000	.0000
C	-4.097	.1017+005	968.7	3.222	.0000	.0000
O	18.38	8437.	606.8	3.222	.0000	.0000
	SIG1	SIG2	SIG3	SI	SIGE	
I	.1191+005	1331.	-26.58	.1194+005	.1132+005	
C	.1017+005	968.7	-4.098	.1018+005	9728.	
O	8437.	606.8	18.38	8419.	8141.	

INSIDE NODE = 1735 OUTSIDE NODE = 1738
** MEMBRANE PLUS BENDING ** I=INSIDE C=CENTER O=OUTSIDE

	SX	SY	SZ	SXY	SYZ	SXZ
I	-38.11	.1185+005	1594.	33.66	.0000	.0000
C	-11.76	.1016+005	1224.	33.66	.0000	.0000
O	14.58	8467.	854.4	33.66	.0000	.0000
	SIG1	SIG2	SIG3	SI	SIGE	
I	.1185+005	1594.	-38.21	.1189+005	.1116+005	
C	.1016+005	1224.	-11.88	.1017+005	9614.	
O	8467.	854.4	14.45	8453.	8065.	

Table 2.10.3-2 $P_m + P_b$ Stress Summary – Upper Ring Critical Section (continued)

INSIDE NODE = 1755 OUTSIDE NODE = 1758
** MEMBRANE PLUS BENDING ** I=INSIDE C=CENTER O=OUTSIDE

	SX	SY	SZ	SXY	SYZ	SXZ
I	-46.78	.1169+005	1861.	71.43	.0000	.0000
C	-15.64	.1015+005	1512.	71.43	.0000	.0000
O	15.49	8600.	1162.	71.43	.0000	.0000
	SIG1	SIG2	SIG3	SI	SIGE	
I	.1169+005	1861.	-47.21	.1174+005	.1091+005	
C	.1015+005	1512.	-16.15	.1016+005	9491.	
O	8601.	1162.	14.89	8586.	8073.	

INSIDE NODE = 1775 OUTSIDE NODE = 1778
** MEMBRANE PLUS BENDING ** I=INSIDE C=CENTER O=OUTSIDE

	SX	SY	SZ	SXY	SYZ	SXZ
I	-83.33	.1142+005	2107.	116.7	.0000	.0000
C	-39.87	.1013+005	1812.	116.7	.0000	.0000
O	3.589	8844.	1517.	116.7	.0000	.0000
	SIG1	SIG2	SIG3	SI	SIGE	
I	.1142+005	2107.	-84.52	.1150+005	.1058+005	
C	.1013+005	1812.	-41.21	.1017+005	9384.	
O	8845.	1517.	2.049	8843.	8191.	

INSIDE NODE = 1795 OUTSIDE NODE = 1798
** MEMBRANE PLUS BENDING ** I=INSIDE C=CENTER O=OUTSIDE

	SX	SY	SZ	SXY	SYZ	SXZ
I	47.28	.1101+005	2344.	170.4	.0000	.0000
C	82.92	.1011+005	2155.	170.4	.0000	.0000
O	118.6	9219.	1965.	170.4	.0000	.0000
	SIG1	SIG2	SIG3	SI	SIGE	
I	.1101+005	2344.	44.63	.1096+005	.1001+005	
C	.1012+005	2155.	80.03	.1004+005	9176.	
O	9222.	1965.	115.4	9106.	8337.	

INSIDE NODE = 1795 OUTSIDE NODE = 1818
** MEMBRANE PLUS BENDING ** I=INSIDE C=CENTER O=OUTSIDE

	SX	SY	SZ	SXY	SYZ	SXZ
I	1928.	8893.	2245.	3901.	.0000	.0000
C	2031.	8325.	2367.	3901.	.0000	.0000
O	2134.	7756.	2489.	3901.	.0000	.0000
	SIG1	SIG2	SIG3	SI	SIGE	
I	.1064+005	2245.	181.5	.1046+005	9594.	
C	.1019+005	2367.	166.1	.1002+005	9124.	
O	9753.	2489.	137.0	9616.	8682.	

INSIDE NODE = 1795 OUTSIDE NODE = 1838
** MEMBRANE PLUS BENDING ** I=INSIDE C=CENTER O=OUTSIDE

	SX	SY	SZ	SXY	SYZ	SXZ
I	3532.	7244.	2184.	4792.	.0000	.0000
C	3747.	6870.	2479.	4792.	.0000	.0000
O	3962.	6496.	2773.	4792.	.0000	.0000
	SIG1	SIG2	SIG3	SI	SIGE	
I	.1053+005	2184.	249.2	.1028+005	9460.	
C	.1035+005	2479.	268.7	.1008+005	9177.	
O	.1019+005	2773.	272.7	9913.	8930.	

INSIDE NODE = 1815 OUTSIDE NODE = 1818
** MEMBRANE PLUS BENDING ** I=INSIDE C=CENTER O=OUTSIDE

	SX	SY	SZ	SXY	SYZ	SXZ
I	98.74	.1051+005	2531.	238.5	.0000	.0000
C	116.5	.1009+005	2521.	238.5	.0000	.0000
O	134.3	9683.	2510.	238.5	.0000	.0000
	SIG1	SIG2	SIG3	SI	SIGE	
I	.1051+005	2531.	93.28	.1042+005	9437.	
C	.1010+005	2521.	110.8	9989.	9028.	
O	9689.	2510.	128.4	9560.	8620.	

T

Table 2.10.3-2 $P_m + P_b$ Stress Summary – Upper Ring Critical Section (continued)

INSIDE NODE = 1815 OUTSIDE NODE = 1838
** MEMBRANE PLUS BENDING ** I=INSIDE C=CENTER O=OUTSIDE

	SX	SY	SZ	SXY	SYZ	SXZ
I	511.0	9585.	2393.	2400.	.0000	.0000
C	627.9	9537.	2591.	2400.	.0000	.0000
O	744.9	9488.	2789.	2400.	.0000	.0000
	SIG1	SIG2	SIG3	SI	SIGE	
I	.1018+005	2393.	-84.49	.1027+005	9278.	
C	.1014+005	2591.	22.74	.1012+005	9111.	
O	.1010+005	2789.	129.7	9974.	8946.	

INSIDE NODE = 1815 OUTSIDE NODE = 1856
** MEMBRANE PLUS BENDING ** I=INSIDE C=CENTER O=OUTSIDE

	SX	SY	SZ	SXY	SYZ	SXZ
I	1806.	8043.	2289.	3914.	.0000	.0000
C	1847.	8248.	2622.	3914.	.0000	.0000
O	1888.	8454.	2955.	3914.	.0000	.0000
	SIG1	SIG2	SIG3	SI	SIGE	
I	9929.	2289.	-79.45	.1001+005	9059.	
C	.1010+005	2622.	-8.103	.1011+005	9086.	
O	.1028+005	2955.	62.44	.1022+005	9121.	

INSIDE NODE = 1835 OUTSIDE NODE = 1838
** MEMBRANE PLUS BENDING ** I=INSIDE C=CENTER O=OUTSIDE

	SX	SY	SZ	SXY	SYZ	SXZ
I	-2.180	7501.	1824.	349.3	.0000	.0000
C	-3.885	9404.	2449.	349.3	.0000	.0000
O	-5.590	.1131+005	3074.	349.3	.0000	.0000
	SIG1	SIG2	SIG3	SI	SIGE	
I	7517.	1824.	-18.40	7536.	6804.	
C	9417.	2449.	-16.84	9434.	8474.	
O	.1132+005	3074.	-16.37	.1133+005	.1015+005	

INSIDE NODE = 1835 OUTSIDE NODE = 1856
** MEMBRANE PLUS BENDING ** I=INSIDE C=CENTER O=OUTSIDE

	SX	SY	SZ	SXY	SYZ	SXZ
I	120.5	6844.	1564.	2151.	.0000	.0000
C	242.9	8823.	2375.	2151.	.0000	.0000
O	365.3	.1080+005	3186.	2151.	.0000	.0000
	SIG1	SIG2	SIG3	SI	SIGE	
I	7473.	1564.	-508.7	7982.	7174.	
C	9332.	2375.	-266.1	9598.	8588.	
O	.1123+005	3186.	-60.60	.1129+005	.1007+005	

INSIDE NODE = 1852 OUTSIDE NODE = 1856
** MEMBRANE PLUS BENDING ** I=INSIDE C=CENTER O=OUTSIDE

	SX	SY	SZ	SXY	SYZ	SXZ
I	-5378.	-203.5	-1857.	-558.9	.0000	.0000
C	-2838.	6443.	1023.	-558.9	.0000	.0000
O	-297.2	.1309+005	3904.	-558.9	.0000	.0000
	SIG1	SIG2	SIG3	SI	SIGE	
I	-143.8	-1857.	-5438.	5294.	4679.	
C	6477.	1023.	-2871.	9348.	8133.	
O	.1311+005	3904.	-320.5	.1343+005	.1190+005	

INSIDE NODE = 1861 OUTSIDE NODE = 1876
** MEMBRANE PLUS BENDING ** I=INSIDE C=CENTER O=OUTSIDE

	SX	SY	SZ	SXY	SYZ	SXZ
I	-87.62	-3319.	-1662.	-502.6	.0000	.0000
C	-182.7	-243.3	-294.6	-502.6	.0000	.0000
O	-277.9	2833.	1073.	-502.6	.0000	.0000
	SIG1	SIG2	SIG3	SI	SIGE	
I	-11.26	-1662.	-3396.	3384.	2931.	
C	290.5	-294.6	-716.5	1007.	875.9	
O	2912.	1073.	-357.1	3269.	2838.	

Table 2.10.3-2 $P_m + P_b$ Stress Summary – Upper Ring Critical Section (continued)

INSIDE NODE = 1901 OUTSIDE NODE = 1916
** MEMBRANE PLUS BENDING ** I=INSIDE C=CENTER O=OUTSIDE

	SX	SY	SZ	SXY	SYZ	SXZ
I	7.805	-3976.	-1710.	-488.2	.0000	.0000
C	72.37	-825.5	222.5	-488.2	.0000	.0000
O	136.9	2325.	2155.	-488.2	.0000	.0000
	SIG1	SIG2	SIG3	SI	SIGE	
I	66.76	-1710.	-4035.	4102.	3563.	
C	286.7	222.5	-1040.	1327.	1296.	
O	2429.	2155.	32.94	2396.	2272.	

INSIDE NODE = 1941 OUTSIDE NODE = 1956
** MEMBRANE PLUS BENDING ** I=INSIDE C=CENTER O=OUTSIDE

	SX	SY	SZ	SXY	SYZ	SXZ
I	141.5	-3071.	-841.4	-404.6	.0000	.0000
C	87.81	-734.2	554.6	-404.6	.0000	.0000
O	34.09	1603.	1951.	-404.6	.0000	.0000
	SIG1	SIG2	SIG3	SI	SIGE	
I	191.7	-841.4	-3122.	3313.	2936.	
C	554.6	253.5	-900.0	1455.	1330.	
O	1951.	1701.	-64.12	2015.	1902.	

INSIDE NODE = 1969 OUTSIDE NODE = 1976
** MEMBRANE PLUS BENDING ** I=INSIDE C=CENTER O=OUTSIDE

	SX	SY	SZ	SXY	SYZ	SXZ
I	-239.2	-2119.	248.0	-485.3	.0000	.0000
C	-115.5	25.14	1091.	-485.3	.0000	.0000
O	8.328	2170.	1935.	-485.3	.0000	.0000
	SIG1	SIG2	SIG3	SI	SIGE	
I	248.0	-121.4	-2237.	2485.	2323.	
C	1091.	445.2	-535.5	1627.	1419.	
O	2273.	1935.	-95.64	2369.	2219.	

INSIDE NODE = 1969 OUTSIDE NODE = 1996
** MEMBRANE PLUS BENDING ** I=INSIDE C=CENTER O=OUTSIDE

	SX	SY	SZ	SXY	SYZ	SXZ
I	-739.1	-1522.	273.5	-363.6	.0000	.0000
C	-338.2	143.0	1038.	-363.6	.0000	.0000
O	62.72	1808.	1802.	-363.6	.0000	.0000
	SIG1	SIG2	SIG3	SI	SIGE	
I	273.5	-596.3	-1665.	1938.	1682.	
C	1038.	338.4	-533.6	1571.	1363.	
O	1881.	1802.	-9.987	1891.	1852.	

INSIDE NODE = 1969 OUTSIDE NODE = 2016
** MEMBRANE PLUS BENDING ** I=INSIDE C=CENTER O=OUTSIDE

	SX	SY	SZ	SXY	SYZ	SXZ
I	-1312.	-948.8	300.9	-231.4	.0000	.0000
C	-557.9	196.4	982.6	-231.4	.0000	.0000
O	196.1	1342.	1664.	-231.4	.0000	.0000
	SIG1	SIG2	SIG3	SI	SIGE	
I	300.9	-836.3	-1424.	1725.	1519.	
C	982.6	261.7	-623.2	1606.	1393.	
O	1664.	1387.	151.1	1513.	1395.	

INSIDE NODE = 1969 OUTSIDE NODE = 2036
** MEMBRANE PLUS BENDING ** I=INSIDE C=CENTER O=OUTSIDE

	SX	SY	SZ	SXY	SYZ	SXZ
I	-1794.	-522.4	330.4	-133.4	.0000	.0000
C	-760.9	201.6	927.8	-133.4	.0000	.0000
O	272.0	925.6	1525.	-133.4	.0000	.0000
	SIG1	SIG2	SIG3	SI	SIGE	
I	330.4	-508.6	-1808.	2138.	1866.	
C	927.8	219.7	-779.0	1707.	1485.	
O	1525.	951.7	245.8	1279.	1110.	

Table 2.10.3-2 $P_m + P_b$ Stress Summary – Upper Ring Critical Section (continued)

INSIDE NODE = 1989 OUTSIDE NODE = 1996
** MEMBRANE PLUS BENDING ** I=INSIDE C=CENTER O=OUTSIDE

	SX	SY	SZ	SXY	SYZ	SXZ
I	-117.5	-2025.	230.3	-409.8	.0000	.0000
C	-58.36	-108.0	1006.	-409.8	.0000	.0000
O	.8085	1809.	1782.	-409.8	.0000	.0000
	SIG1	SIG2	SIG3	SI	SIGE	
I	230.3	-33.20	-2109.	2339.	2219.	
C	1006.	327.4	-493.7	1500.	1301.	
O	1897.	1782.	-87.74	1985.	1930.	

INSIDE NODE = 2009 OUTSIDE NODE = 2016
** MEMBRANE PLUS BENDING ** I=INSIDE C=CENTER O=OUTSIDE

	SX	SY	SZ	SXY	SYZ	SXZ
I	-71.13	-1430.	315.8	-331.7	.0000	.0000
C	-33.63	-76.82	948.3	-331.7	.0000	.0000
O	3.869	1276.	1581.	-331.7	.0000	.0000
	SIG1	SIG2	SIG3	SI	SIGE	
I	315.8	5.536	-1507.	1822.	1689.	
C	948.3	277.2	-387.7	1336.	1157.	
O	1581.	1358.	-77.43	1658.	1559.	

INSIDE NODE = 2029 OUTSIDE NODE = 2036
** MEMBRANE PLUS BENDING ** I=INSIDE C=CENTER O=OUTSIDE

	SX	SY	SZ	SXY	SYZ	SXZ
I	-26.70	-955.9	338.9	-256.9	.0000	.0000
C	-9.613	-51.33	867.2	-256.9	.0000	.0000
O	7.470	853.2	1395.	-256.9	.0000	.0000
	SIG1	SIG2	SIG3	SI	SIGE	
I	338.9	39.61	-1022.	1361.	1239.	
C	867.2	227.3	-288.2	1155.	1003.	
O	1395.	925.2	-64.46	1460.	1291.	

INSIDE NODE = 2049 OUTSIDE NODE = 2056
** MEMBRANE PLUS BENDING ** I=INSIDE C=CENTER O=OUTSIDE

	SX	SY	SZ	SXY	SYZ	SXZ
I	42.19	-599.4	337.9	-189.0	.0000	.0000
C	24.09	-32.11	779.8	-189.0	.0000	.0000
O	5.988	535.2	1222.	-189.0	.0000	.0000
	SIG1	SIG2	SIG3	SI	SIGE	
I	337.9	93.75	-650.9	988.9	892.2	
C	779.8	187.1	-195.1	974.9	850.8	
O	1222.	595.7	-54.60	1276.	1105.	

INSIDE NODE = 2070 OUTSIDE NODE = 2076
** MEMBRANE PLUS BENDING ** I=INSIDE C=CENTER O=OUTSIDE

	SX	SY	SZ	SXY	SYZ	SXZ
I	-237.7	-408.0	397.1	-146.4	.0000	.0000
C	-116.1	16.87	765.9	-146.4	.0000	.0000
O	5.387	441.7	1135.	-146.4	.0000	.0000
	SIG1	SIG2	SIG3	SI	SIGE	
I	397.1	-153.5	-492.2	889.3	777.4	
C	765.9	111.2	-210.4	976.3	861.8	
O	1135.	486.3	-39.17	1174.	1018.	

INSIDE NODE = 2070 OUTSIDE NODE = 2096
** MEMBRANE PLUS BENDING ** I=INSIDE C=CENTER O=OUTSIDE

	SX	SY	SZ	SXY	SYZ	SXZ
I	-379.8	-204.8	411.0	-77.73	.0000	.0000
C	-175.0	55.93	720.3	-77.73	.0000	.0000
O	29.87	316.7	1030.	-77.73	.0000	.0000
	SIG1	SIG2	SIG3	SI	SIGE	
I	411.0	-175.3	-409.3	820.4	732.0	
C	720.3	79.66	-198.7	919.0	816.2	
O	1030.	336.4	10.16	1019.	901.7	

Table 2.10.3-2 $P_m + P_b$ Stress Summary – Upper Ring Critical Section (continued)

INSIDE NODE = 2070 OUTSIDE NODE = 2116
** MEMBRANE PLUS BENDING ** I=INSIDE C=CENTER O=OUTSIDE

	SX	SY	SZ	SXY	SYZ	SXZ
I	-439.7	-128.0	416.1	-52.64	.0000	.0000
C	-196.4	56.58	699.7	-52.64	.0000	.0000
O	47.04	241.1	983.4	-52.64	.0000	.0000
	SIG1	SIG2	SIG3	SI	SIGE	
I	416.1	-119.3	-448.4	864.5	755.7	
C	699.7	67.10	-206.9	906.6	805.4	
O	983.4	254.5	33.68	949.7	860.8	

INSIDE NODE = 2070 OUTSIDE NODE = 2136
** MEMBRANE PLUS BENDING ** I=INSIDE C=CENTER O=OUTSIDE

	SX	SY	SZ	SXY	SYZ	SXZ
I	-487.3	-72.28	420.3	-35.13	.0000	.0000
C	-209.7	51.94	679.9	-35.13	.0000	.0000
O	67.85	176.2	939.5	-35.13	.0000	.0000
	SIG1	SIG2	SIG3	SI	SIGE	
I	420.3	-69.33	-490.2	910.5	789.3	
C	679.9	56.58	-214.3	894.3	794.3	
O	939.5	186.6	57.45	882.1	825.1	

INSIDE NODE = 2090 OUTSIDE NODE = 2096
** MEMBRANE PLUS BENDING ** I=INSIDE C=CENTER O=OUTSIDE

	SX	SY	SZ	SXY	SYZ	SXZ
I	15.34	-296.5	383.3	-109.8	.0000	.0000
C	10.44	-11.56	694.1	-109.8	.0000	.0000
O	5.536	273.4	1005.	-109.8	.0000	.0000
	SIG1	SIG2	SIG3	SI	SIGE	
I	383.3	50.14	-331.3	714.7	619.4	
C	694.1	109.8	-110.9	805.0	720.5	
O	1005.	312.7	-33.74	1039.	915.9	

INSIDE NODE = 2110 OUTSIDE NODE = 2116
** MEMBRANE PLUS BENDING ** I=INSIDE C=CENTER O=OUTSIDE

	SX	SY	SZ	SXY	SYZ	SXZ
I	-22.61	-153.0	385.8	-83.96	.0000	.0000
C	-8.556	-6.142	665.4	-83.96	.0000	.0000
O	5.495	140.8	945.0	-83.96	.0000	.0000
	SIG1	SIG2	SIG3	SI	SIGE	
I	385.8	18.49	-194.1	579.9	508.1	
C	665.4	76.62	-91.32	756.7	688.3	
O	945.0	180.9	-34.68	979.7	891.7	

INSIDE NODE = 2130 OUTSIDE NODE = 2136
** MEMBRANE PLUS BENDING ** I=INSIDE C=CENTER O=OUTSIDE

	SX	SY	SZ	SXY	SYZ	SXZ
I	-20.71	-76.97	374.5	-59.62	.0000	.0000
C	-7.937	-3.152	632.9	-59.62	.0000	.0000
O	4.831	70.66	891.2	-59.62	.0000	.0000
	SIG1	SIG2	SIG3	SI	SIGE	
I	374.5	17.09	-114.8	489.3	438.5	
C	632.9	54.13	-65.22	698.1	646.7	
O	891.2	105.9	-30.36	921.6	861.6	

INSIDE NODE = 2150 OUTSIDE NODE = 2156
** MEMBRANE PLUS BENDING ** I=INSIDE C=CENTER O=OUTSIDE

	SX	SY	SZ	SXY	SYZ	SXZ
I	-109.4	-26.89	355.8	-37.46	.0000	.0000
C	-77.32	-1.187	590.7	-37.46	.0000	.0000
O	-45.28	24.52	825.6	-37.46	.0000	.0000
	SIG1	SIG2	SIG3	SI	SIGE	
I	355.8	-12.42	-123.8	479.6	434.7	
C	590.7	14.15	-92.66	683.4	636.7	
O	825.6	40.81	-61.58	887.2	840.7	

2.10.4 Oblique Drop Slapdown

The NAC-LWT cask is analyzed and a scale model was tested for the secondary impact resulting from a 30-foot oblique drop (hypothetical accident condition) onto a flat, unyielding, horizontal surface.

2.10.4.1 Discussion

The NAC-LWT cask geometry is presented in the license drawings of Section 1.4 and in Figure 2.10.4-1. Section 2.6.7.4 has outlined an analysis of the NAC-LWT cask impact forces developed during the 30-foot hypothetical accident free drop. This analysis assumes that the impact limiter is crushed by a 1-foot fall before the 30-foot accident begins, for a total of 31 feet. The analysis of Section 2.6.7.4 addresses the maximum force imparted to one limiter resulting from the initial impact with the unyielding surface for various cask orientation angles. This section addresses the primary impact loads on the cask structure and the adequacy of the impact limiter to absorb the remaining energy during the secondary impact on the unyielding surface for an oblique cask orientation based on test results.

2.10.4.2 Analysis

In Section 2.10.12, the total amount of energy (ET) to be dissipated after the cask has fallen is calculated as:

$$ET = EI + ER + EP + ES$$

where:

EI = energy absorbed during the first impact

ER = remaining energy after the first impact

EP = rotational potential energy

ES = elastically stored energy

The sum of the last three terms equals the energy absorbed by the second impact limiter (secondary impact). Terms EI, ER and EP can be calculated; however, testing of the aluminum honeycomb in an impact limiter configuration was necessary to determine ES.

A quarter-scale model of the NAC-LWT cask has been tested and the secondary impact phenomenon has been reviewed. It has been concluded that the rebound energy (5 to 10 percent of the primary impact energy) may be restored to the cask in such a manner as to cause the first impacted end of the cask to lift from the ground several inches during the secondary impact (slapdown). Thus, the stored rebound energy must be dissipated by the second impact limiter.

Table 2.10.4-1 shows that at a drop angle of 75 degrees, the energy dissipated in the secondary impact (E2) is greater than energy dissipated in a secondary side impact, so that the cask "slaps down." This is because the residual drop energy not absorbed in the first impact (energy transformed to rotational energy), impact limiter rebound energy (elastic rebound), and potential energy converted to kinetic energy as the cask rotates to the second impact, all combine to exceed the energy absorbed by one limiter in a pure side drop orientation. Results of the scale impact limiter tests show that the impact limiters do have sufficient energy dissipation margin to absorb the 75-degree oblique secondary impact energy.

The calculation of El in RBCUBED is done by solving the equations of motion for the cask. These equations are based on the force developed by the impact limiter as it crushes. The limiter force is equal to the crush strength of the aluminum honeycomb multiplied by the backed-up crush area. The RBCUBED program calculates this area as a function of impact angle and crush depth using a system of solid geometry subroutines developed by Oak Ridge National Laboratories as part of the MORSE shielding code. These crush area calculations have been verified by manual calculation of crush area using graphical drafting techniques for several impact angles and crush depths. The accuracy of the area calculation may be shown by inspection of the scale limiter results presented in Figure 2.10.4-2 through Figure 2.10.4-4, which show that the RBCUBED force (the crush area times the crush strength) accurately tracks the measured force.

The impact limiter force is normal to the unyielding surface and is applied to the cask body, as shown in Figure 2.10.4-5. The weight of the cask continues to accelerate the cask downward as the impact limiter decelerates, producing a crush force (FD), decelerating the cask. During the initial contact of an impact limiter with the unyielding surface, the cask weight may cause the net force to accelerate the cask downward until the crush area (footprint) becomes large enough to overcome the cask weight and produce a net deceleration.

The net force applied to the cask produces a force and deceleration parallel to the cask long axis and a force and angular acceleration perpendicular to the cask axis, as shown in Figure 2.10.4-5 The parallel force component acts on the cask center of mass to slow the cask down, but the perpendicular component transforms translational kinetic energy from the drop into rotational energy that must be absorbed in the secondary impact.

The calculations to determine the energy to be dissipated for each drop angle shown in Figure 2.10.4-1 include the potential energy resulting from the cask tipping over (for $0° \leq \theta \leq 15°$) and elastically stored rebound energy from the first impact.

2.10.4.3 Energy Calculation

The cask and impact limiters are considered to be a mass (m). When the mass is released from rest a distance (H), it is accelerated uniformly by gravity (g). Because the mass is not acted upon by any off-center forces while free falling, it will remain in the same attitude that it had when it was released. The change in potential energy equals the change in kinetic energy. The vertical velocity of the mass at the time of contact with the unyielding surface is calculated as:

where:

V_i = initial vertical velocity of cask at time of impact (t = 0 sec)

g = the gravitational constant (ft/sec^2)

H = the drop height (ft)

The cask may impact at any angle (0° to 90°). In the case of impact angles from 0 degrees (end drop) through 15 degrees (corner drop), the cask could be expected to remain upright after the total energy of the first impact is absorbed; as a result, the center of gravity does not have a moment arm, which would provide a rotational moment about the cask base, causing the cask to tip over. However, the calculated energies shown in Table 2.10.4-1 do include the energy of the tip-over for conservatism. Ignoring elastically stored energy, which is absorbed by one impact limiter, the total kinetic energy is:

$$ET = mgH,\ 0° \leq 0 \leq 15°$$

where:

E_T = total energy to be absorbed (in-lbf)

m = mass of the cask and limiters (lbm)

g = acceleration due to gravity (ft/sec^2)

H = height of drop (ft)

For oblique drops within the angular range from corner drop to side drop, the total energy absorbed is greater than that for the 0-degree to 15-degree range, if one ignores cask tip-over and elastically stored energy. Cask impact angles greater than 75 degrees are considered to be side drops because the first impact limiter stops the cask as the second begins to absorb energy.

Oblique drops ($15° \leq \theta \leq 75°$) have four constituent energy dissipation components, which account for all the potential energy given to a cask prior to being dropped. Oblique drops are two-step phenomena. First, the cask vertically translates toward the unyielding surface and the lower impact limiter decelerates the lower end of the cask. The amount of energy dissipated while stopping the vertical translation of the lower end of the cask is El (inch-pounds). Second, the cask pivots on the crushed impact limiter until the cask is near horizontal and the second impact limiter begins to crush. The remaining three constituent energy components (remaining energy from the free drop, ER, which is transformed to rotational energy; potential energy from

pivoting to the horizontal, EP; and elastically stored energy, ES) are all absorbed in the second limiter in the side drop orientation (A more detailed discussion of potential to kinetic energy conversion, cask motion and energy dissipation is found in Appendix 2.10.12).

Thus, in oblique drops, the center of gravity will fall a distance greater than the drop height, H. The additional distance the center of gravity must fall is L/2 (cosθ) (Figure 2.10.4-2), where L is the length of the cask body. Therefore, the total kinetic energy that must be absorbed to bring the cask to rest for angles greater than 15 degrees is:

$$E_T = mg\,(H + \frac{L}{2}\cos\theta),\ 15° \le \theta \le 90°$$

The total energy to be absorbed is greatest for the 0-degree cask impact angle because the first impact limiter stops the cask and the second impact limiter absorbs the other energy components (ER + EP + ES). The total energy absorption is determined by summing El and E2 for each drop angle.

2.10.4.4 Rotational Velocity Change

For cask angles greater than 15 degrees, the center of gravity of the cask is unsupported. The net crush force is applied at one end of the cask, resulting in a torque (T), possibly causing rotation of the cask about its center of gravity. As the cask is translating vertically while decelerating, it is also rotating around the end that is crushing. The cask is also attempting to rotate around the center of gravity due to the torque applied to the decelerating end of the cask by the perpendicular component ($F_{d\perp}$) of the crush force. The applied torque is:

$$T = F_{d\perp}\frac{L}{2}$$

$$= Fd \sin\theta\frac{L}{2}$$

where:

T = torque (in-lb)

L = cask length (in)

F_d = deceleration force (lb)

The impulse equation for an applied torque is:

$$T\Delta t = I\Delta\omega$$

where:

Δt = increment of time (sec)

I = moment of inertia of a cylinder (cask) about its center of gravity

$$= \frac{mL^2}{12}$$

$\Delta\omega =$ change in angular velocity (rad/sec)

The angular velocity is equal to the rotational velocity change (ΔVt) divided by the radius:

$$\Delta\omega = \frac{\Delta V_t}{L/2}$$

Substituting for $\Delta\omega$ in the impulse equation:

$$T\Delta t = I\frac{\Delta V_t}{L/2}$$

Substituting and solving for ΔV_t:

$$\Delta V_t = \frac{F_d \sin\theta\ \Delta t\ L^2}{4I}$$

Substituting the formula for I_{cofm} for a cylinder yields:

$$\Delta V_t = \frac{F_d \sin\theta\ \Delta t\ 3g}{W_T}$$

Note that the same result for ΔV_t is obtained by regarding the cask as rotating about one end.

This change in transverse velocity is subtracted from the transverse component of the initial velocity to determine the transverse velocity of the cask at the beginning of the next deformation step (δ'). When the sum of the transverse velocity changes equals the initial velocity, the impacting end of the cask has been stopped along an axis normal to the longitudinal axis of the cask.

Figure 2.10.4-1 Cask Slapdown Geometry

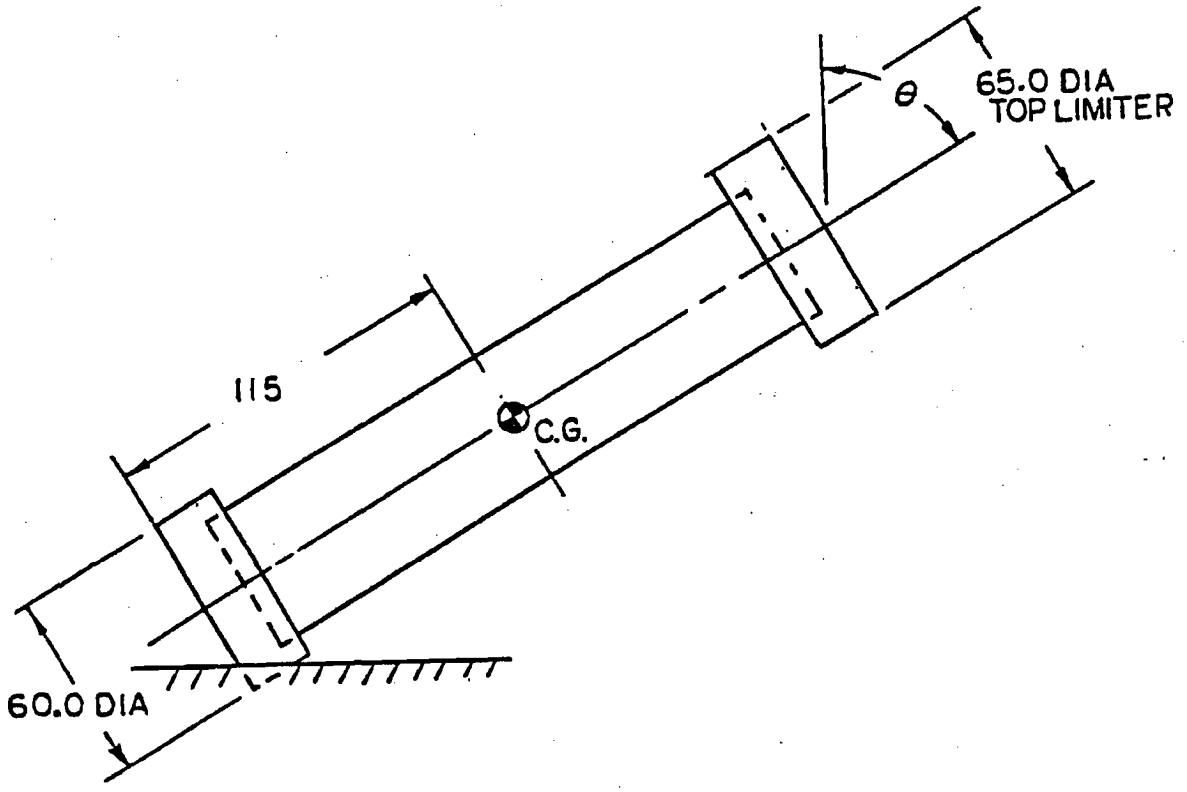

Figure 2.10.4-2 Force Deflection Curve of Drop Tested Limiter – 0-Degree Impact

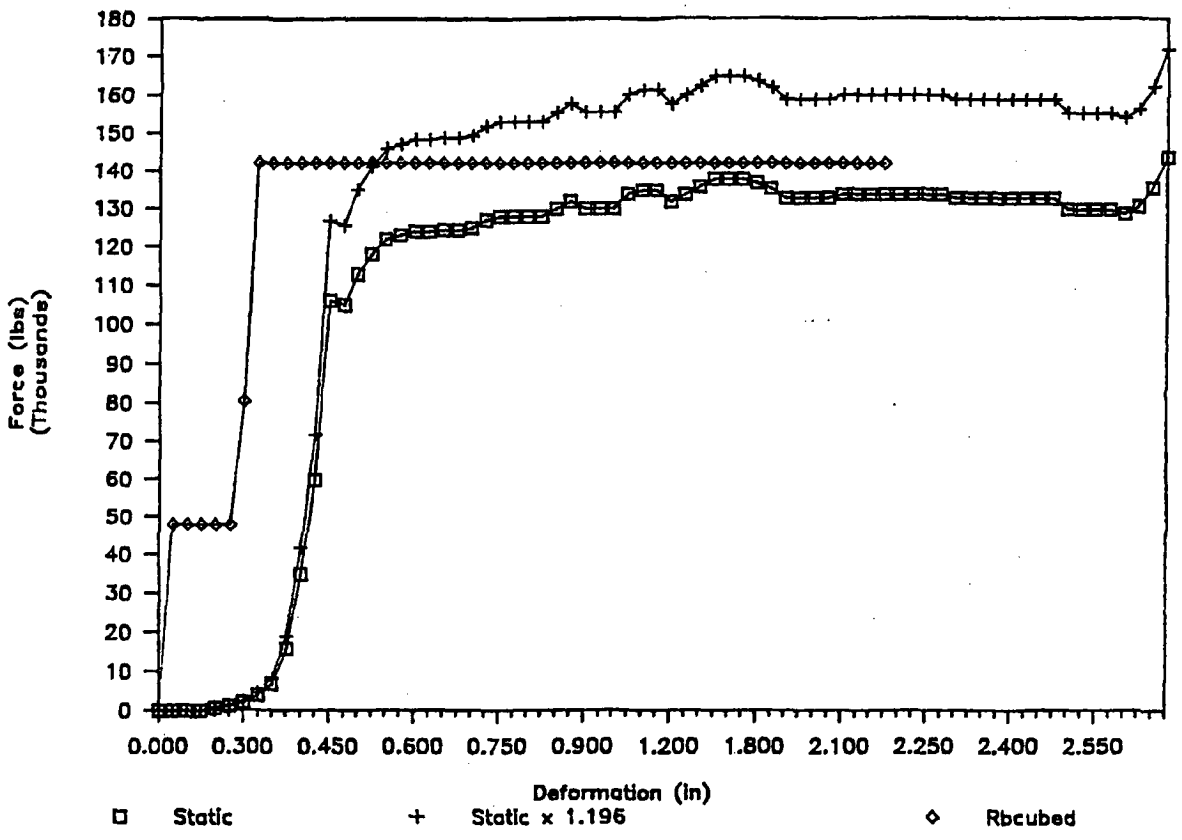

Figure 2.10.4-3 Force Deflection Curve of Drop Tested Limiter – 14-Degree Impact

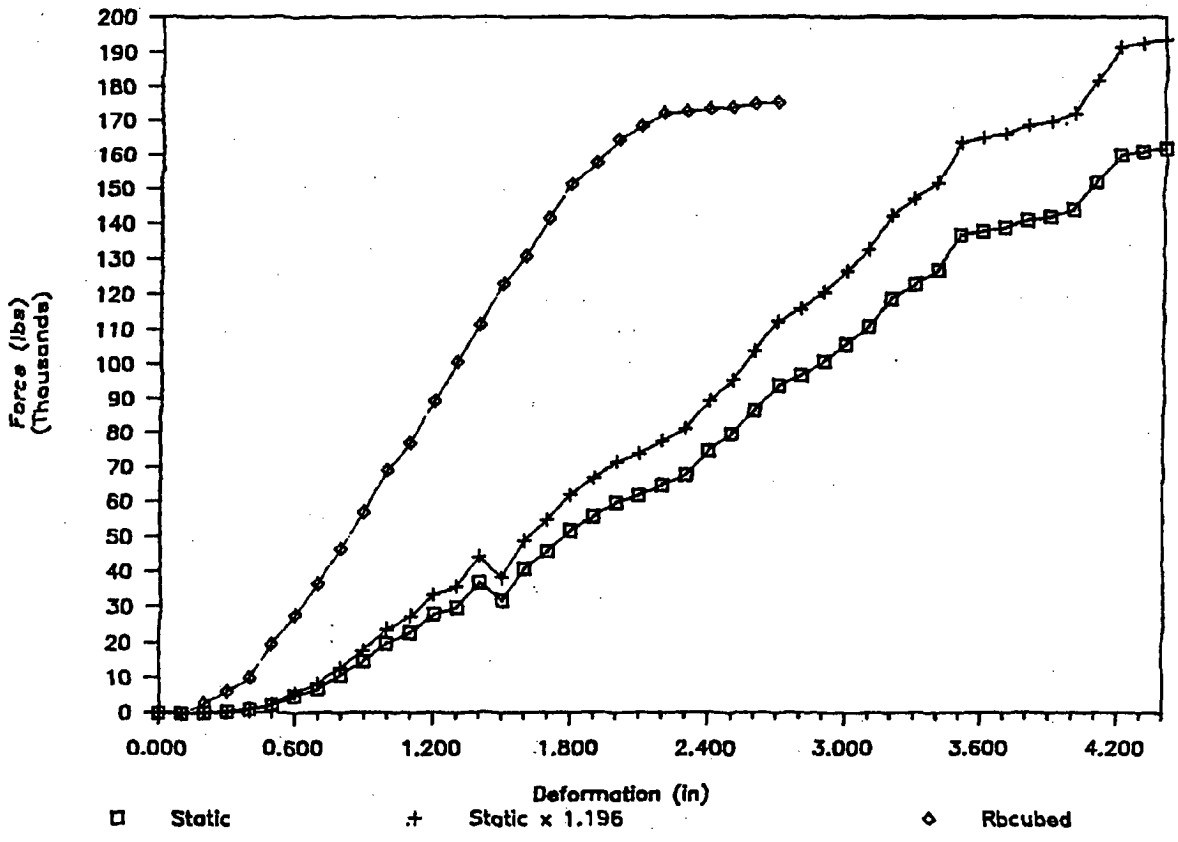

Figure 2.10.4-4 Force Deflection Curve of Drop Tested Limiter – 90-Degree Impact

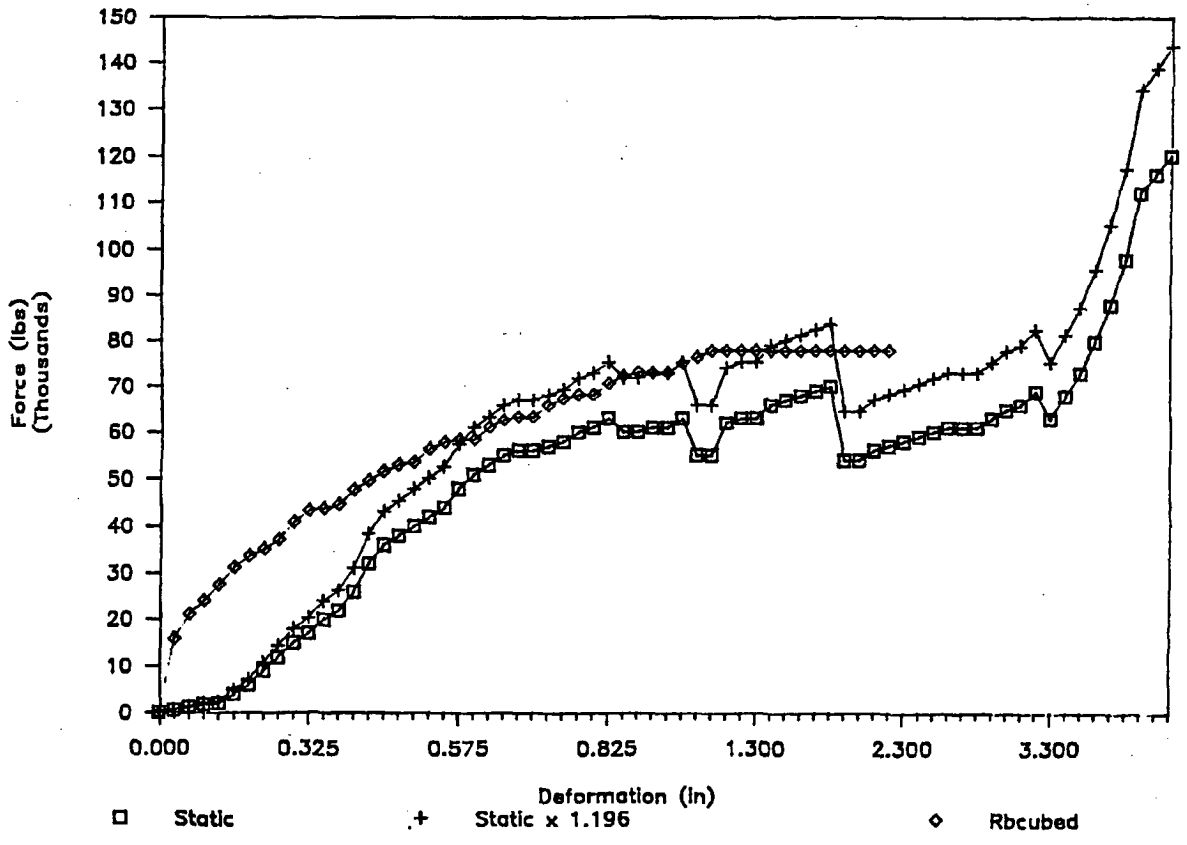

Figure 2.10.4-5 Oblique Drop

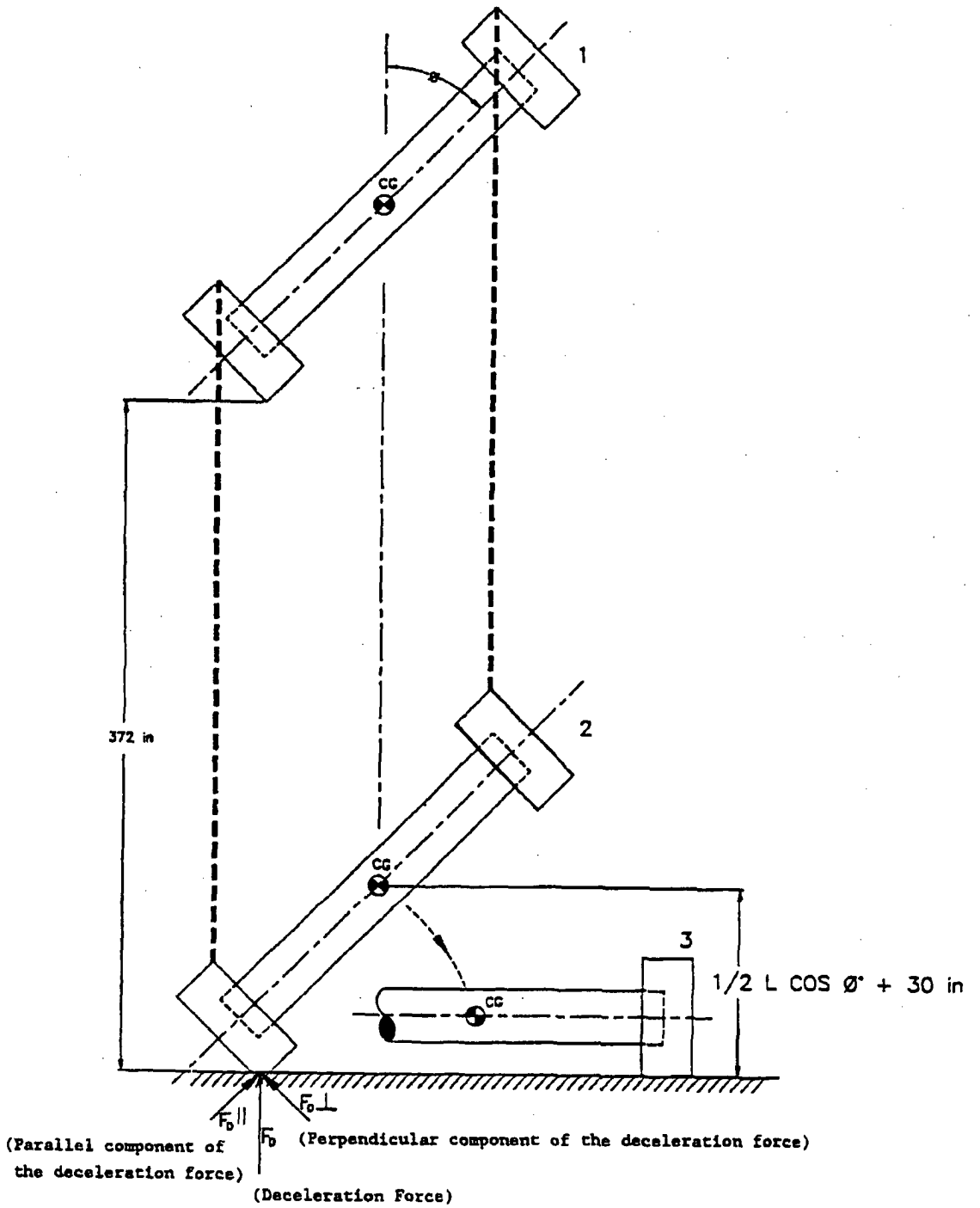

Table 2.10.4-1 Determination of Maximum Energy for Secondary Impact – Full-Scale Impact Limiter

Drop Angle (degrees)	0	15	30	45	60	75	90
EI Energy absorbed by first limiter (in-lb).	1.93×10^7	1.88×10^7	1.74×10^7	1.52×10^7	1.23×10^7	1.03×10^7	9.67×10^6
ER Energy remaining after first impact (in-lb).	0.00	5.40×10^5	1.94×10^6	4.14×10^6	7.04×10^6	9.02×10^6	9.67×10^6
EP Potential energy of cask after first impact (in-lb).	$6.04 \times 10^{6*}$	4.97×10^6	4.40×10^6	3.45×10^6	2.21×10^6	7.68×10^5	0.00
ES Energy stored in first limiter; absorbed in second limiter in side drop orientation (in-lb).	1.87×10^6 (9.7%)	1.24×10^6 (6.6%)	1.04×10^6 (6.0%)**	8.66×10^5 (5.7%)**	6.77×10^5 (5.5%)**	5.56×10^5 (5.4%)**	5.13×10^5 (5.3%)
E2 Secondary impact total of ER + EP + ES (in-lb).	7.91×10^6	6.75×10^6	7.38×10^6	8.46×10^6	9.93×10^6	1.03×10^7	1.02×10^7
E_{max}-Side Drop Maximum energy absorption capability of impact limiter in side drop orientation (in-lb).	1.49×10^7	1.49×10^7	1.49×10^7	1.49×10^7	1.49×10^7	1.49×10^7	1.49×10^7
Energy Absorption Margin	88.32%	120.71%	101.79%	76.20%	50.10%	44.04%	46.33%

* Assumes tip-over of cask onto the second impact limiter.
** Interpolated values.

2.10.5 Lead Slump - End Drop

The magnitude of lead slump that occurs during the end drop accident is assessed from the results of the finite element analyses as previously addressed in Section 2.7.1.1. Since ANSYS gap elements are used to model the interfaces between the lead shell and the stainless steel shells, the finite element model of the cask is adequate to represent the lead slump effect during an end drop condition. The maximum axial gap that occurs between the lead and the steel due to the 30-foot end drop is summarized as follows:

Condition*	Gap (inch)
(1)	0.0**
(2)	0.0658***
(3)	0.3216
(4)	0.0**
(5)	0.0693***

* (1) Bottom end drop with 130°F ambient temperature and maximum decay heat load.

(2) Bottom end drop with -40°F ambient temperature and maximum decay heat load.

(3) Bottom end drop with -40°F ambient temperature and no decay heat load.

(4) Top end drop with 130°F ambient temperature and maximum decay heat load.

(5) Top end drop with -40°F ambient temperature and maximum decay heat load.

** The lead slump effect has been offset by the thermal expansion effect, which is equal to:

$$175\ (16.9 \times 10^{-6})(250 - 70) = 0.532 \text{ in}$$

*** The lead slump effect has been offset by the thermal expansion of the lead, which is evaluated as:

$$175\ (16.5 \times 10^{-6})(160 - 70) = 0.260 \text{ in}$$

This slump assessment includes the initial gaps, developed at the top and bottom ends of the lead shell, induced by the fabrication process. The maximum lead slump, based on the finite element analysis, due to the end drop, is 0.33 inch.

2.10.6 Inner Shell Buckling Design Criteria and Evaluation

Code Case N-284 (Metal Containment Shell Buckling Design Methods) of the "ASME Boiler and Pressure Vessel Code," is used to analyze the NAC-LWT cask inner shell for structural stability. Structural stability assures that the inner shell does not buckle during cask fabrication, normal operations, or hypothetical accident conditions. The buckling evaluation requirements of Regulatory Guide 7.6, Paragraph C.5, are shown to be satisfied by the results of the interaction equation calculations of Code Case N-284.

2.10.6.1 Code Case N-284

The "ASME Boiler and Pressure Vessel Code," sets forth service limits that are analogous to load conditions found in 10 CFR 71. As stated in Regulatory Guide 7.6, the normal transport conditions correspond to Level A Service Limits and the hypothetical accident conditions correspond to Level D Service Limits. Service condition A and D allowable stresses are used in performing the buckling assessment of the inner shell. Level A (normal transport) conditions use a buckling factor of safety of 2.0 and Level D (accident) conditions use a buckling factor of safety of 1.34. Code Case N-284 addresses both elastic and inelastic buckling. Interaction equations are used to combine hoop compressive, axial compressive, and in-plane shear loadings. Also, Appendix F of the "ASME Boiler and Pressure Vessel Code," (for Level D Service Loadings) specifically identifies use of "a code case for metal containment shell buckling" as an acceptable means of addressing buckling issues (paragraph F-1331.5(c)).

Buckling of the inner shell, which is the primary component of containment, is evaluated in the following manner:

1. Determine the theoretical elastic buckling stresses using classical theory.
2. Apply the appropriate factors of safety and interaction equations to elastic and inelastic buckling cases and establish the worst case compressive and in-plane shear stresses.
3. Calculate and apply capacity reduction factors, which account for differences between classical theory and predicted instability stress for fabricated shells.
4. Calculate plasticity reduction factors and apply them in cases where elastically determined buckling stresses are above the proportional limit.

2.10.6.2 Theoretical Elastic Buckling Stresses

Inner shell geometric parameters and material properties necessary for the elastic buckling evaluation are presented in Table 2.10.6-1 and Table 2.10.6-2. The theoretical elastic buckling stresses for the inner shell are calculated using the equations of Code Case N-284 and the data presented in Table 2.10.6-1 and Table 2.10.6-2. The values of the theoretical elastic buckling stresses for the inner shell are presented in Table 2.10.6-3 and Table 2.10.6-4.

The equations from Code Case N-284 are:

$$S_{\phi cL} = C_{\phi} \frac{Et}{R}$$

$$S_{\theta cL} = S_{rcL} = C_{\theta r} \frac{Et}{R}$$

$$S_{hcL} = C_{\theta h} \frac{Et}{R}$$

$$S_{\phi\theta cL} = C_{\phi\theta} \frac{Et}{R}$$

These elastic buckling stress formulas are for cylindrical shells that are unstiffened. The values tabulated in Table 2.10.6-3 are resultant numerical values, excluding the modulus of elasticity (E). The modulus of elasticity is excluded because of its temperature dependent nature.

Table 2.10.6-4 is generated by substituting the value of E, corresponding to the temperature of interest, into the formulas in Table 2.10.6-3.

2.10.6.3 Capacity Reduction Factors

Capacity reduction factors, as stated earlier, compensate for differences between classically determined and predicted instability stresses for fabricated shells. The capacity reduction factors were determined using methods described in Section-1500 of Code Case N-284. For the NAC-LWT cask inner shell geometry, the factors are determined by the following expression:

1. Axial Compression

   $\alpha_{\phi L} = \left[1.0 \times 10^{-5} \ (S_y)\right] - 0.033$

2. Hoop Compression

   $\alpha_{\theta L} = 0.8$

3. Shear

   $\alpha_{\phi\theta L} = 0.8$

Table 2.10.6-5 summarizes the capacity reduction factors for the NAC-LWT cask inner shell (Type XM-19 stainless steel) based on the material yield strengths tabulated in Table 2.10.6-2.

In order to directly use the capacity reduction factors from Table 2.10.6-5, the tolerance requirements of NE-4220 of the "ASME Boiler and Pressure Vessel Code," Subsection NE, must be satisfied. NE-4221.1 and NE-4221.2 set forth the "maximum difference in cross-sectional diameters" and "maximum deviation from true theoretical form for external pressure." Table 2.10.6-6 shows that the requirements of NE-4221.1 and NE-4221.2 are satisfied, if the maximum tolerances and configuration constraints are met during manufacturing.

2.10.6.4 Plasticity Reduction Factors

Plasticity reduction factors account for nonlinear material behavior, occurring when buckling stresses exceed the proportional limit of the material. Reduction factors chosen are dependent on the magnitude of the applied compressive or in-plane shear stress, S_i. Because values for S_i are not directly calculated, the equations used to determine the reduction factors (Section-1600 of Code Case N-284) are presented.

1. Axial Compression

   $\eta_\phi = 1.0$; if $[(S_\phi)(FS)/S_y] < 0.55$

   $\eta_\phi = 0.18/(1 - [0.45S_y/(S_\phi)(FS)])$;

   if $0.55 < [(S_\phi)(FS)/S_y] \leq 0.738$

   $\eta_\phi = 1.31 - [1.15(S_\phi)(FS)/S_y]$; if $0.738 < [(S_\phi)(FS)/S_y] < 1.0$

2. Hoop Compression

   $\eta_\theta = 1.0$; if $[(S_\theta)(FS)/S_y] < 0.67$

   $\eta_\theta = 2.53 - 2.29[(S_\theta)(FS)/S_y]$; if $0.67 < [(S_\theta)(FS)/S_y] < 1.0$

3. Shear

   $\eta_{\phi\theta} = 1.0$; if $[(S_{\phi\theta})(FS)/S_y] \leq 0.48$

   $\eta_{\phi\theta} = 0.1/1 - [0.43S_y/(S_{\phi\theta})(FS)]$;

   if $0.48 < [(S_{\phi\theta})(FS)/S_y] \leq 0.6$

2.10.6.5 Upper Bound Magnitudes for Compressive Stresses and In-Plane Shear Stresses

From Section-1600 of Code Case N-284, as an upper limit, the compressive stresses, S_i ($i = \phi$ or θ) must be less than the yield strength, S_y, divided by the appropriate factor of safety ($S_i < S_y/FS$). Similarly, for shear, $S_{\phi\theta}$ must be less than, or equal to, 0.6 S_y divided by the appropriate factor of safety ($S_{\phi\theta} < 0.6\ S_y/FS$). As stated in Section 2.10.6, there is a factor of safety of 2.0 for normal transport and a factor of safety of 1.34 for hypothetical accident conditions. Table 2.10.6-7 presents the elastic upper bound compressive and shear stresses, evaluated using normal and accident condition factors of safety. Under no circumstances can the elastic values presented in the table be exceeded. However, satisfying these limits alone is not sufficient to demonstrate that buckling will not occur. As stated in Section 2.10.6, the interaction equations must also be satisfied.

2.10.6.6 Interaction Equations

Elastic and inelastic interaction equations must be satisfied for all states of compressive and in-plane shear stress. The interaction equations for cylindrical shells are directly available from paragraph-1713.1.1 and paragraph-1713.2.1 of Code Case N-284. Once a stress state is established for a specific shell, plasticity reduction factors can be determined and all appropriate interaction equations checked. Elastic interaction equations must be satisfied, and if any of the uniaxial critical stress values exceed the proportional limit of the fabricated material, the inelastic interaction equations must also be satisfied.

2.10.6.7 Detailed Buckling Evaluation - Sample Calculation

The maximum P_m stress in the NAC-LWT cask inner shell for each load condition is identified and tabulated in Table 2.10.6-8. Stresses shown for the normal operations conditions 1-foot bottom and top end drops are obtained by ratioing from the corresponding accident condition 30-foot bottom or top end drop stress; the ratio (15.8/60.0 - 0.263) represents the 1-foot drop condition g factor divided by the actual 30-foot drop condition g factor used in the ANSYS finite element analysis (Section 2.6.1.1). The stresses shown for the 30-foot side drop accident condition are obtained from Table 2.7.1-17 for component No. 4. All other stresses tabulated in Table 2.10.6-8 are obtained directly from the ANSYS analysis results (Sections 2.6 and 2.7). Load condition "r" is used to demonstrate the step-by-step analysis procedure, which reflects the procedure diagrammed in paragraph-1800 of Code Case N-284.

Step 1

Stresses for each specified loading are found in Table 2.10.6-8. Load condition "r", accident condition, 130°F, maximum decay heat load (inner shell maximum temperature = 280°F), is examined below.

Step 2

For load condition "r" (Table 2.10.6-9), the maximum compressive stresses are:

S_ϕ = 23,247 psi

S_0 = 360 psi

$S_{\phi 0}$ = 0 psi

Step 3

For accident conditions, the factor of safety (FS) is 1.34. Multiplying the stress components by this factor of safety yields:

FS (S_ϕ) = 31,151 psi

FS (S_θ) = 482 psi

FS ($S_{\phi\theta}$) = 0 psi

Step 4

Capacity reduction factors are available from Section 2.10.6.3 and are as follows for the load condition "r" inner shell temperature of 280°F:

$\alpha_{\phi L} = 0.408$

$\alpha_{\theta L} = 0.8$

$\alpha_{\phi\theta L} = 0.8$

Step 5

Plasticity reduction factors are determined using the equations presented in Section 2.10.6.4 as follows (S_y available from Table 2.10.6-2):

1. Axial Compression

   $S_\phi (FS)/S_y = 31{,}151/44{,}120 = 0.7060$

   $\eta_\phi = 0.18/[1 - (0.45)(1/0.7060)] = 0.496$

2. Hoop Compression

   $S_\theta (FS)/S_y = 482/44{,}120 = 0.0109$

   $\eta_\theta = 1.0$

3. Shear

   $S_{\phi\theta} (FS)/S_y = 0/44{,}120 = 0.00$

   $\eta_{\phi\theta} = 1.0$

Step 6

Compute elastic stress components per the following equation:

$S_{is} = S_i (FS)/\alpha_{iL}$

$S_{\phi s} = S_\phi (FS)/\alpha_{\phi L} = 31{,}151/0.408 = 76{,}349$ psi

$S_{\theta s} = S_\theta (FS)/\alpha_{\theta L} = 482/0.8 = 603$ psi

$S_{\phi\theta s} = S_{\phi\theta} (FS)/\alpha_{\phi\theta L} = 0/0.8 = 0$ psi

Step 7

Compute inelastic stress components per the following equation:

$S_{ip} = S_{is}/\eta_i$

$S_{\phi p} = S_{\phi s} / \eta_{\phi} = 76,349 / 0.496 = 153,820$ psi

$S_{\theta p} = S_{\theta s} / \eta_{\theta} = 603 / 1.0 = 603$ psi

$S_{\phi\theta p} = S_{\phi\theta s} / \eta_{\phi\theta} = 0 / 1.0 = 0$ psi

Step 8

For the NAC-LWT cask, the buckling evaluation approach, consistent with the vessel design and method of analysis, is that of paragraph-1710 of Code Case N-284 (By Formulae).

Step 9

Theoretical uniaxial buckling values are available from Section 2.10.6.2. For the outer cask inner shell at 280°F, these theoretical values are as follows:

$S_{\phi eL} = 1,742,406$

$S_{\theta eL} = S_{reL} = 84,262$

$S_{heL} = 84,262$

$S_{\phi\theta eL} = 246,385$

Applicable elastic and inelastic interaction equations in paragraph-1713.1.1 and paragraph-1713.2.1 of Code Case N-284 are checked as follows:

1. Elastic Buckling (paragraph-1713.1.1)
   a. Axial Compression Plus Hoop Compression

   $(S_{\phi s} < 0.5\ S_{\theta s})$

   $76,349 > (0.5)(603)$; therefore, not applicable.

   b. Axial Compression Plus Hoop Compression

   $(S_{\phi s} < 0.5\ S_{\theta s})$

   $[(S_{\phi s} - 0.5\ S_{heL}) / (S_{\phi eL} - 0.5\ S_{heL})] + (S_{\phi s} / S_{heL})^2 \leq 1.0$

   $[76,349 - (0.5)(84,262)] / [1,742,406 - (0.5)(84,262) +$

   $(76,349/84,262)^2 = 0.8411 \leq 1.0$

   c. Axial Compression Plus Shear

   $(S_{\phi s} / S_{\phi eL}) + (S_{\phi\theta s} / S_{\phi\theta eL})^2 \leq 1.0$

   $(76,349/1,742,406) + (0/246,385)^2 = 0.0438 < 1.0$

   d. Hoop Compression Plus Shear

   $(S_{\theta s} / S_{reL}) + (S_{\phi\theta s} / S_{\phi\theta eL})^2 \leq 1.0$

   $(603/84,262) + (0/246,385)^2 = 0.0072 < 1.0$

   e. Axial Compression Plus Hoop Compression Plus Shear

$K = 1 - (S_{\phi\theta s} / S_{\phi\theta eL})^2 = 1 - (0/246{,}385)^2 = 1.00$

and equations a and b above remain unchanged.

2. Inelastic Buckling (paragraph-1713.2.1)
   a. Axial Compression Plus Shear

   (153,820/1,742,406)2 + (0/246,385)2 = 0.0078 < 1.0

   b. Hoop Compression Plus Shear

   $(S_{\theta p} / S_{reL})^2 + (S_{\phi\theta p} / S_{\phi\theta eL})^2 \leq 1.0$

   $(603/84{,}262)^2 + (0/246{,}385)^2 = 0.0001 < 1.0$

Since all interaction equations are satisfied, and there are no concentrated loads on the shell which, lead to localized buckling, it is concluded that buckling of the NAC-LWT cask inner shell will not occur.

The remainder of this section presents tabulations (Table 2.10.6-10) of the results from the interaction equations for the maximum P_m load cases identified in Table 2.10.6-8. As shown, all interaction equations yield values less than 1.0; thus, it is concluded that buckling of the NAC-LWT cask inner shell will not occur.

2.10.6.8 Conclusion

The buckling interaction equations yield values less than 1.0 for all of the NAC-LWT cask load conditions. Therefore, it is concluded that the cask inner shell will not buckle.

Table 2.10.6-1 Inner Shell Geometry Parameters

Parameter	Inner Shell
R = Radius (in) [to centerline of shell]	7.0625
t = thickness (in)	0.75
$(Rt)^{0.5}$	2.3015
L_ϕ = length (in)	175.00
$L_\theta = 2\pi R$ = circumference (in)	44.375
$M_\phi = L_\phi/(Rt)^{0.5}$	76.0374
$M_\theta = L_\theta/(Rt)^{0.5}$	19.2809
M = lesser of M_ϕ or M_θ	19.2809
ν = Poisson's Ratio	0.275

Table 2.10.6-2 Material Properties of Type XM-19 Stainless Steel for Buckling Analysis Input (ASME, Section III, Appendix I)

Parameter/Temperature (°F)	-40	170	280
E (psi)	28.82×10^6	27.76×10^6	27.12×10^6
S_y (psi)	66.2×10^3	49.4×10^3	44.1×10^3

Table 2.10.6-3 Theoretical Elastic Buckling Stress Values (Temperature Independent Form)

Elastic Buckling Stress	Inner Shell	Load Description
$S_{\phi eL}$	0.064248E	axial
$S_{\theta eL} = S_{reL}$	0.003107E	hoop, without end pressure
S_{heL}	0.003107E	hoop, with end pressure
$S_{\phi\theta eL}$	0.009085E	shear

Table 2.10.6-4 Theoretical Elastic Buckling Stresses for Selected Temperatures

Parameter	Location	Theoretical Elastic Buckling Stress (psi)		
Modulus of Elasticity		T = -40°F E = 28.82 × 10^6	T= 170°F E = 27.76 × 10^6	T = 280°F E = 27.12 × 10^6
$S_{\phi eL}$	Inner Shell	1,851,627	1,784,167	1,742,406
$S_{\theta eL} = S_{reL}$	Inner Shell	89,544	86,281	84,262
S_{heL}	Inner Shell	89,544	86,281	84,262
$S_{\phi\theta eL}$	Inner Shell	261,830	254,290	246,385

Table 2.10.6-5 Capacity Reduction Factors for the Type XM-19 Stainless Steel Inner Shell

Capacity Reduction Factor	Temperature (°F)		
	-40	170	280
$\alpha_{\phi L}$ (axial)	0.629	0.461	0.408
$\alpha_{\theta L}$ (hoop)	0.8	0.8	0.8
$\alpha_{\phi\theta L}$ (shear)	0.8	0.8	0.8

Table 2.10.6-6 Fabrication Tolerances for the NAC-LWT Cask Inner Shell

Requirement	Parameter	Inner Shell Data (in)
NE-4221.1	Maximum Inside Diameter (I.D.) Minimum I.D. Nominal I.D.	13.390 13.360 13.375
	a) (Max I.D. – Min I.D.) b) (0.01) × (Nominal I.D.)	0.030 0.134
	Tolerance Check (a < b)	Yes (0.030 in < 0.134 in)
NE-4221.2	Nominal Shell Thickness Minimum Shell Thickness Shell Length Nominal Shell Outside Diameter (O.D.) Minimum Shell O.D.	0.7575 0.745 181.25 14.890 14.880
	c) Permissible Deviation, e (Figure –4221.2-1) d) Actual Deviation*	0.225 0.005
	Tolerance Check (d < c)	Yes (0.005 in < 0.225 in)

* (Nominal O.D. – Minimum O.D.)/2 = (14.890 – 14.880)/2 = 0.005

Table 2.10.6-7 Upper Bound Buckling Stresses

	Load Condition	-40°F	170°F	280°F
Elastic, Upper Bound Compressive Stress S_ϕ or S_θ (psi)	Normal	33,100	24,700	22,060
	Accident	49,403	36,866	32,925
Elastic, Upper Bound In-Plane Shear Stress $S_{\phi\theta}$ (psi)	Normal	19,860	14,820	13,236
	Accident	29,642	22,120	19,755

Table 2.10.6-8 Calculated Maximum Compressive Stresses in the Inner Shell

Load Case	Load Condition (Peak Shell Temperature Shown)	Primary Membrane		
		S-Axial	S-Hoop	S-Shear
	Fabrication (l)			
a	at 170°F	9515	4136	0
b	Heat	3380	450	0
c	Cold	2590	130	10
	Normal – 1-Foot Top End Drop			
d	at 170°F – Max. Decay Heat	11770	240	40
e	at 280°F – Max. Decay Heat	8190	520	20
	Normal – 1-Foot Bottom End Drop			
f	at -40°F – No Decay Heat	7760	1050	240
g	at 170°F – Max. Decay Heat	12080	200	30
h	at 280°F – Max. Decay Heat	8440	510	20
	Normal – 1-Foot Side Drop			
i	at 250°F – Max. Decay Heat	15430	250	0
	Normal – 1-Foot Corner Drop Top End			
j	at -40°F – No Decay Heat	2720	330	110
k	at 280°F – Max. Decay Heat	3110	360	10
	Normal – 1-Foot Corner Drop Bottom End			
l	at 280°F – Max. Decay Heat	2980	280	20

Table 2.10.6-8 Calculated Maximum Compressive Stresses in the Inner Shell (continued)

Load Case	Load Condition (Peak Shell Temperature Shown)	Primary Membrane		
		S-Axial	S-Hoop	S-Shear
	Accident – 30-Foot Top End Drop			
m	at 170°F – Max. Decay Heat	11170	240	40
n	at 280°F – Max. Decay Heat	8190	520	20
	Accident – 30-Foot Bottom End Drop			
o	at -40°F – No Decay Heat	7760	1050	240
p	at 170°F – Max. Decay Heat	12080	200	30
q	at 280°F – Max. Decay Heat	8440	510	20
	Accident – 30-Foot Side Drop			
r	at 280°F – Max. Decay Heat	31550	520	0
	Accident – 30-Foot Oblique Top End Drop			
s	at -40°F – No Decay Heat – 15.74° D.O.	13570	2030	540
t	at -40°F – No Decay Heat – 30° D.O.	11940	150	0
u	at -40°F – No Decay Heat – 45° D.O.	14900	160	0
v	at -40°F – No Decay Heat – 60° D.O.	19850	180	0
w	at 280°F – Max. Decay Heat – 15.74° D.O.	17160	2010	630
x	at 280°F – Max. Decay Heat – 30° D.O.	14410	820	0
y	at 280°F – Max. Decay Heat – 45° D.O.	17880	840	10
z	at 280°F – Max. Decay Heat – 60° D.O.	23480	650	30
	Accident – 30-Foot Oblique Bottom End Drop			
A	at 280°F – Max. Decay Heat – 15.74° D.O.	16150	1450	480
B	at 280°F – Max. Decay Heat – 30° D.O.	16360	810	0
C	at 280°F – Max. Decay Heat – 45° D.O.	19420	870	0
D	at 280°F – Max. Decay Heat – 60° D.O.	24940	910	20

Table 2.10.6-9 Calculated Stresses with ASME Factors of Safety

Load Case	Normal or Accident	Inner Shell Temp. (°F)	Meridonal Stress (psi)	Circ. Stress (psi)	Inplane Shear Stress (psi)	Factor of Safety	Meridonal Stress (psi)	Circ. Stress (psi)	Inplane Shear Stress (psi)
a	Normal	170	9515	4136	0	2.00	19030	8272	0
b	Normal	280	3380	450	0	2.00	6760	900	0
c	Normal	-40	2590	130	10	2.00	5180	260	20
d	Normal	170	11770	240	40	2.00	23540	480	80
e	Normal	280	8190	520	20	2.00	16380	1040	40
f	Normal	-40	7760	1050	240	2.00	15520	2100	480
g	Normal	170	12080	200	30	2.00	24160	400	60
h	Normal	280	8440	510	20	2.00	16880	1020	40
i	Normal	250	15430	250	0	2.00	30860	500	0
j	Normal	-40	2720	330	110	2.00	5440	660	220
k	Normal	280	3110	360	10	2.00	6220	720	20
l	Normal	280	2980	280	20	2.00	5960	560	40
m	Accident	170	11170	240	40	1.34	14968	322	54
n	Accident	280	8190	520	20	1.34	10975	697	27
o	Accident	-40	7760	1050	240	1.34	10398	1407	322
p	Accident	170	12080	200	30	1.34	16187	268	40
q	Accident	280	8440	510	20	1.34	11310	683	27
r	Accident	250	31550	520	0	1.34	42277	697	0
s	Accident	-40	13570	2030	540	1.34	18184	2720	724
t	Accident	-40	11940	150	0	1.34	16000	201	0
u	Accident	-40	14900	160	0	1.34	19966	214	0
v	Accident	-40	19850	180	0	1.34	26599	241	0
w	Accident	280	17160	2010	630	1.34	22994	2693	844
x	Accident	280	14410	820	0	1.34	19309	1099	0
y	Accident	280	17880	840	10	1.34	23959	1126	13
z	Accident	280	23480	650	30	1.34	31463	871	40
A	Accident	280	16150	1450	480	1.34	21641	1943	643
B	Accident	280	16360	810	0	1.34	21922	1085	0
C	Accident	280	19420	870	0	1.34	26023	1166	0
D	Accident	280	24940	910	20	1.34	33420	1219	27

Table 2.10.6-10 Results – Interaction Equations

Load Case	Elastic Interaction*					Inelastic Interaction*	
	(1)	(2)	(3)	(4)	(5)	(6)	(7)
a	N/A	N/A	0.0231	0.1199	N/A	0.0005	0.0144
b	N/A	N/A	0.0093	0.0133	N/A	0.0001	0.0002
c	N/A	N/A	0.0044	0.0036	N/A	0.0000	0.0000
d	N/A	0.0046	0.0286	0.0070	0.0046	0.0008	0.0000
e	N/A	N/A	0.0224	0.0153	N/A	0.0005	0.0002
f	N/A	N/A	0.0132	0.0293	N/A	0.0002	0.0009
g	N/A	0.0054	0.0294	0.0058	0.0054	0.0009	0.0000
h	N/A	N/A	0.0231	0.0151	N/A	0.0005	0.0002
i	N/A	0.0185	0.0422	0.0074	0.0185	0.0065	0.0001
j	N/A	N/A	0.0047	0.0092	N/A	0.0000	0.0001
k	N/A	N/A	0.0085	0.0106	N/A	0.0001	0.0001
l	N/A	N/A	0.0082	0.0083	N/A	0.0001	0.0001
m	N/A	N/A	0.0182	0.0047	N/A	0.0003	0.0000
n	N/A	N/A	0.0150	0.0103	N/A	0.0002	0.0001
o	N/A	N/A	0.0088	0.0196	N/A	0.0001	0.0004
p	N/A	N/A	0.0197	0.0039	N/A	0.0004	0.0000
q	N/A	N/A	0.0155	0.0101	N/A	0.0002	0.0001
r	N/A	0.0346	0.0578	0.0103	0.0346	0.0632	0.0001

Table 2.10.6-10 Results – Interaction Equations (continued)

Load Case	Elastic Interaction*					Inelastic Interaction*	
	(1)	(2)	(3)	(4)	(5)	(6)	(7)
s	N/A	N/A	0.0156	0.0380	N/A	0.0003	0.0015
t	N/A	N/A	0.0137	0.0028	N/A	0.0002	0.0000
u	N/A	N/A	0.0171	0.0030	N/A	0.0003	0.0000
v	N/A	N/A	0.0228	0.0034	N/A	0.0005	0.0000
w	N/A	0.0091	0.0315	0.0398	0.0091	0.0010	0.0016
x	N/A	0.0026	0.0264	0.0162	0.0026	0.0007	0.0003
y	N/A	0.0091	0.0328	0.0166	0.0091	0.0011	0.0003
z	N/A	0.0195	0.0431	0.0129	0.0195	0.0073	0.0002
A	N/A	0.0064	0.0296	0.0287	0.0064	0.0009	0.0008
B	N/A	0.0062	0.0300	0.0160	0.0062	0.0009	0.0003
C	N/A	0.0120	0.0356	0.0172	0.0120	0.0019	0.0003
D	N/A	0.0224	0.0457	0.0180	0.0224	0.0100	0.0003

All values are less than or equal to 1.0; therefore, buckling of the inner shell will not occur.

*1 – Axial compression plus hoop compression (< 0.5).
2 – Axial compression plus hoop compression (> 0.5).
3 – Axial compression plus shear.
4 – Hoop compression plus shear.
5 – Axial compression plus hoop compression plus shear.
6 – Axial compression plus shear.
7 – Hoop compression plus shear.

2.10.7 Detailed Finite Element Stress Summary

This section presents the finite element stresses at representative sections throughout the cask components resulting from the different loading cases for normal operations conditions and hypothetical accident conditions. The representative sections are plotted in Figure 2.10.7-1 and their locations are tabulated in Table 2.10.7-1.

2.10.7.1 Finite Element Stress Tables - Normal Operation Hot Condition

This section presents the detailed stress Table 2.10.7-2 and Table 2.10.7-3 to document the critical stresses reported in Section 2.6.1.

2.10.7.2 Finite Element Stress Tables - Normal Operation Cold Condition

This section presents the detailed stress Table 2.10.7-4 and Table 2.10.7-5 to document the critical stresses reported in Section 2.6.2.

2.10.7.3 Finite Element Stress Tables - 1-Foot End Drop

This section presents the detailed stress Table 2.10.7-6 through Table 2.10.7-15 to document the critical stresses reported in Section 2.6.7.1.

2.10.7.4 Finite Element Stress Tables - 1-Foot Side Drop

This section presents the detailed stress Table 2.10.7-16 through Table 2.10.7-18 to document the critical stresses reported in Section 2.6.7.2.

2.10.7.5 Finite Element Stress Tables - 1-Foot Corner Drop

This section presents the detailed stress Table 2.10.7-19 through Table 2.10.7-27 to document the critical stresses reported in Section 2.6.7.3.

2.10.7.6 Finite Element Stress Tables - 30-Foot End Drop

This section presents the detailed stress Table 2.10.7-28 through Table 2.10.7-37 to document the critical stresses reported in Section 2.7.1.1.

2.10.7.7 Finite Element Stress Tables - 30-Foot Side Drop

This section presents the detailed stress Table 2.10.7-38 and Table 2.10.7-39 to document the critical stresses reported in Section 2.7.1.2.

2.10.7.8 Finite Element Stress Tables - 30-Foot Oblique Drop

This section presents the detailed stress Table 2.10.7-40 through Table 2.10.7-63 to document the critical stresses reported in Section 2.7.1.3.

Figure 2.10.7-1 Representative Section Cut Diagram

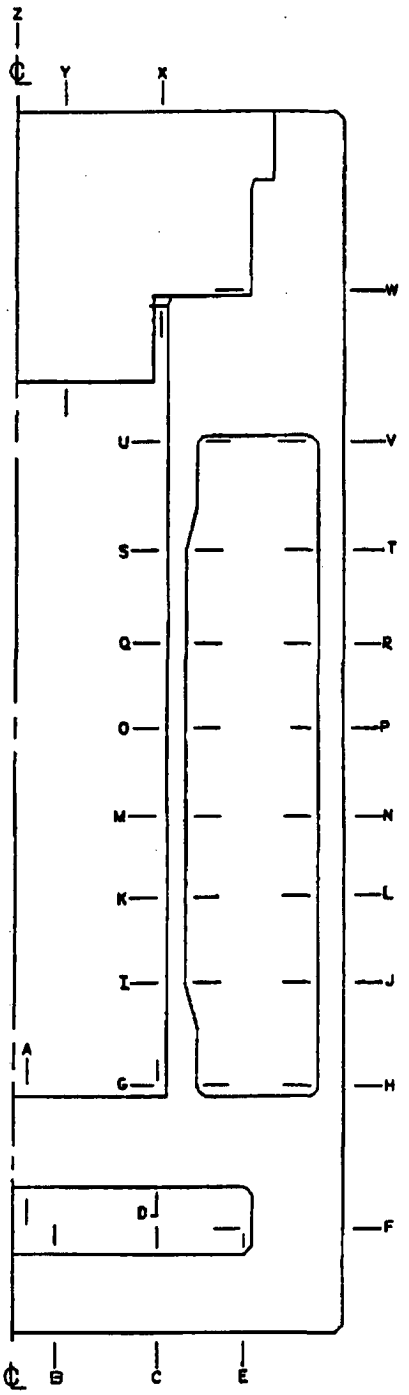

Table 2.10.7-1 Section Cut Identification

Section[1]	Node to Node	Location[2] (in)
A	177 - 327	0.85
B	4 - 104	2.55
C	10 – 110	6.6875
D	185 – 335	6.6875
E	18 – 118	10.375
F	143 – 150	4.50
G	335 – 340	10.50
H	346 – 350	10.50
I	621 – 624	16.50
J	635 – 638	16.50
K	841 – 844	35.50
L	855 – 858	35.50
M	941 – 944	60.50
N	955 – 958	60.50
O	1101 – 1104	100.50
P	1115 – 1118	100.50
Q	1261 – 1264	140.50
R	1275 – 1278	140.50
S	1561 – 1564	179.50
T	1575 – 1578	179.50
U	1841 – 1846	185.50
V	1852 – 1856	185.50
W	1969 – 1976	191.75
X	2370 – 2570	6.6875
Y	2305 – 2565	3.40
Z	2301 - 2561	0.0

[1] Refer to Figure 2.10.7-1 for section cut diagram.
[2] Location of section is measured either from the cask centerline or from the cask bottom surface.

Table 2.10.7-2 P_m Stress Summary (Hot Case)

Section	Node to Node	S_X	S_Y	S_Z	S_{XY}	SI
A	177 - 327	-0.11	-1.62	-1.54	0.03	1.51
B	4 - 104	0.11	2.77	1.79	-0.31	2.73
C	10 – 110	-0.41	2.34	2.29	-0.25	2.80
D	185 – 335	-2.24	-1.22	-1.54	0.30	1.18
E	18 – 118	-0.10	1.51	2.77	-1.43	3.71
F	143 – 150	-4.52	1.94	1.23	1.25	6.93
G	335 – 340	3.78	1.47	5.30	-1.32	4.44
H	346 – 350	-3.33	6.67	1.98	0.01	10.00
I	621 – 624	-0.02	2.94	0.79	0.01	2.96
J	635 – 638	0.00	10.13	0.17	0.06	10.13
K	841 – 844	-0.03	3.11	0.44	0.02	3.14
L	855 – 858	0.00	10.55	0.04	0.00	10.55
M	941 – 944	-0.03	3.27	0.44	0.00	3.30
N	955 – 958	-0.01	10.94	0.05	0.00	10.94
O	1101 – 1104	-0.03	3.38	0.45	0.00	3.41
P	1115 – 1118	-0.01	11.18	0.05	0.00	11.19
Q	1261 – 1264	-0.03	3.30	0.47	0.00	3.33
R	1275 – 1278	-0.01	10.91	-0.05	0.00	10.97
S	1561 – 1564	-0.04	3.06	0.92	0.07	3.10
T	1575 – 1578	0.00	10.22	0.09	-0.07	10.22
U	1841 – 1846	0.07	1.12	0.11	0.28	1.19
V	1852 – 1856	-2.29	6.58	1.02	-0.56	8.93
W	1969 – 1976	-0.14	0.14	1.09	-0.48	1.60
X	2370 – 2570	-0.20	-0.27	0.09	0.16	0.48
Y	2305 – 2565	-0.09	-0.19	-0.47	0.13	0.47
Z	2301 - 2561	0.04	0.00	-0.35	0.00	0.39

Table 2.10.7-3 $P_m + P_b$ Stress Summary (Hot Case)

Section	Node to Node	S_X	S_Y	S_Z	S_{XY}	SI
A	177 - 327	0.02	-1.62	-1.54	0.03	1.64
B	4 - 104	0.00	2.77	1.79	-0.31	2.85
C	10 – 110	-0.80	2.34	2.29	-0.25	3.18
D	185 – 335	-7.81	-1.22	-1.54	0.30	6.61
E	18 – 118	-2.94	1.51	2.77	-1.43	6.13
F	143 – 150	-10.01	0.44	-0.32	1.25	10.75
G	335 – 340	0.51	-4.89	2.41	-1.32	7.61
H	346 – 350	-0.22	15.10	5.80	0.01	15.32
I	621 – 624	-0.05	3.40	0.88	0.01	3.45
J	635 – 638	-0.01	11.23	0.36	0.06	11.24
K	841 – 844	0.00	3.34	0.62	0.02	3.34
L	855 – 858	0.00	10.82	0.29	0.00	10.82
M	941 – 944	0.00	3.56	0.68	0.00	3.56
N	955 – 958	0.00	11.31	0.36	0.00	11.31
O	1101 – 1104	0.00	3.68	0.68	0.00	3.68
P	1115 – 1118	0.00	11.58	0.38	0.00	11.58
Q	1261 – 1264	0.00	3.54	0.65	0.00	3.54
R	1275 – 1278	-0.01	11.30	0.20	0.00	11.32
S	1561 – 1564	-0.04	3.57	1.08	0.07	3.62
T	1575 – 1578	0.00	11.27	0.20	-0.07	11.28
U	1841 – 1846	-0.08	0.88	-0.23	0.28	1.19
V	1852 – 1856	-0.30	13.09	3.90	-0.56	13.43
W	1969 – 1976	-0.24	-2.12	0.25	-0.48	2.48
X	2370 – 2570	-0.40	-0.27	0.09	0.16	0.59
Y	2305 – 2565	0.00	-0.19	-0.47	0.13	0.54
Z	2301 - 2561	0.01	0.00	-0.35	0.00	0.36

Table 2.10.7-4 P_m Stress Summary (Cold Case)

Section	Node to Node	S_X	S_Y	S_Z	S_{XY}	SI
A	177 - 327	-0.15	-2.55	-2.48	0.03	2.40
B	4 - 104	0.07	0.81	-0.16	-0.30	1.08
C	10 – 110	-0.20	0.43	0.93	-0.37	1.30
D	185 – 335	-1.38	-2.01	-1.58	0.22	0.77
E	18 – 118	-0.40	0.51	2.05	-0.66	2.80
F	143 – 150	-2.06	0.82	1.64	0.90	3.97
G	335 – 340	-1.22	-1.08	0.32	-0.26	1.74
H	346 – 350	-2.74	4.43	2.04	-0.29	7.19
I	621 – 624	0.00	-2.64	-0.13	0.06	2.64
J	635 – 638	0.00	6.79	0.36	0.06	6.78
K	841 – 844	-0.01	-2.47	0.11	0.01	2.58
L	855 – 858	0.00	7.19	0.05	0.00	7.20
M	941 – 944	-0.01	-2.31	0.11	0.00	2.42
N	955 – 958	-0.01	7.58	0.05	0.00	7.59
O	1101 – 1104	-0.01	-2.20	0.11	0.00	2.31
P	1115 – 1118	-0.01	7.82	0.06	0.00	7.83
Q	1261 – 1264	-0.01	-2.27	-0.10	0.00	2.27
R	1275 – 1278	-0.02	7.55	-0.16	0.00	7.70
S	1561 – 1564	-0.01	-2.52	-0.02	-0.02	2.51
T	1575 – 1578	0.00	6.88	0.31	-0.05	6.88
U	1841 – 1846	-0.96	-1.14	-2.43	-0.25	1.64
V	1852 – 1856	-1.96	4.45	0.93	-0.19	6.42
W	1969 – 1976	-0.46	0.17	1.13	-0.50	1.87
X	2370 – 2570	-0.29	-0.39	0.05	0.15	0.55
Y	2305 – 2565	-0.06	-0.29	-0.59	0.13	0.58
Z	2301 - 2561	0.11	0.00	-0.44	0.00	0.55

Table 2.10.7-5 $P_m + P_b$ Stress Summary (Cold Case)

Section	Node to Node	S_X	S_Y	S_Z	S_{XY}	SI
A	177 - 327	-0.02	-2.55	-2.48	0.03	2.53
B	4 - 104	0.03	0.81	-0.16	-0.30	1.08
C	10 – 110	-0.40	0.43	0.93	-0.37	1.47
D	185 – 335	-5.15	-2.01	-1.58	0.22	3.58
E	18 – 118	-2.34	0.51	2.05	-0.66	4.55
F	143 – 150	-4.52	-1.72	-0.03	0.90	4.76
G	335 – 340	-3.04	-3.44	-0.90	-0.26	2.66
H	346 – 350	-0.23	11.86	5.77	-0.29	12.10
I	621 – 624	0.04	-2.84	0.02	0.06	2.89
J	635 – 638	-0.01	8.06	0.50	0.06	8.07
K	841 – 844	-0.01	-2.71	-0.11	0.01	2.70
L	855 – 858	0.00	7.57	0.42	0.00	7.56
M	941 – 944	-0.01	-2.62	-0.16	0.00	2.61
N	955 – 958	0.00	8.03	0.46	0.00	8.03
O	1101 – 1104	-0.01	-2.52	-0.16	0.00	2.51
P	1115 – 1118	0.00	8.30	0.48	0.00	8.30
Q	1261 – 1264	0.00	-2.66	-0.38	0.00	2.66
R	1275 – 1278	-0.03	8.26	0.31	0.00	8.29
S	1561 – 1564	-0.02	-2.85	-0.28	-0.02	2.83
T	1575 – 1578	-0.01	8.01	0.33	-0.05	8.02
U	1841 – 1846	-0.08	-0.57	-2.64	-0.25	2.66
V	1852 – 1856	-0.26	10.30	3.87	-0.19	10.57
W	1969 – 1976	0.00	2.48	2.30	-0.50	2.68
X	2370 – 2570	-0.47	-0.39	0.05	0.15	0.64
Y	2305 – 2565	0.00	-0.29	-0.59	0.13	0.64
Z	2301 - 2561	0.01	0.00	-0.44	0.00	0.45

Table 2.10.7-6 P_m Stress Summary (1-Foot Bottom End Drop) – Loading Condition 1

LOADING CONDITION 1: 130°F Ambient Temperature and Maximum Decay Heat Load

Section	Node to Node	S_X	S_Y	S_Z	S_{XY}	SI
A	177 - 327	-2.81	0.86	0.86	0.25	3.70
B	4 - 104	-4.47	1.22	1.22	0.20	5.70
C	10 – 110	-5.23	1.26	1.61	-0.09	6.84
D	185 – 335	-5.81	0.88	0.56	2.15	7.96
E	18 – 118	-3.44	1.18	2.81	-1.27	6.58
F	143 – 150	-3.86	-3.70	1.95	0.98	6.71
G	335 – 340	-0.98	-4.20	3.28	-1.13	7.84
H	346 – 350	-1.69	-2.09	1.96	-0.23	4.15
I	621 – 624	0.03	-8.53	-0.81	0.28	8.58
J	635 – 638	0.00	-1.55	0.20	0.04	1.75
K	841 – 844	-0.03	-8.11	0.44	0.02	8.55
L	855 – 858	0.00	-1.12	0.00	0.00	1.12
M	941 – 944	-0.03	-7.57	0.44	0.00	8.01
N	955 – 958	0.00	-0.58	0.00	0.00	0.58
O	1101 – 1104	-0.03	-6.69	0.44	0.00	7.13
P	1115 – 1118	0.00	0.30	0.00	0.00	0.31
Q	1261 – 1264	-0.03	-5.80	0.47	0.00	6.27
R	1275 – 1278	-0.01	1.18	-0.10	0.00	1.28
S	1561 – 1564	-0.01	-4.94	-0.08	-0.08	4.93
T	1575 – 1578	0.00	2.05	0.26	-0.03	2.05
U	1841 – 1846	-1.11	-2.08	-2.04	-0.27	1.10
V	1852 – 1856	-0.96	1.43	0.61	0.07	2.39
W	1969 – 1976	-0.31	-0.07	0.68	-0.29	1.19
X	2370 – 2570	-0.30	-0.37	0.12	-0.03	0.50
Y	2305 – 2565	-0.18	-0.35	-0.40	-0.03	0.23
Z	2301 - 2561	0.03	0.00	-0.33	0.00	0.35

Table 2.10.7-7 $P_m + P_b$ Stress Summary (1-Foot Bottom End Drop) – Loading Condition 1

LOADING CONDITION 1: 130°F Ambient Temperature and Maximum Decay Heat Load

Section	Node to Node	S_X	S_Y	S_Z	S_{XY}	SI
A	177 - 327	-3.80	0.86	0.86	0.25	4.69
B	4 - 104	-4.84	1.22	1.22	0.20	6.07
C	10 – 110	-5.54	1.26	1.61	-0.09	7.15
D	185 – 335	-13.08	0.88	0.56	2.15	14.61
E	18 – 118	-4.79	1.18	2.81	-1.27	7.87
F	143 – 150	-9.99	-5.56	0.41	0.98	10.60
G	335 – 340	-3.75	-8.88	1.98	-1.13	11.11
H	346 – 350	-4.78	-5.93	-0.12	-0.23	5.86
I	621 – 624	0.15	-10.37	-1.16	0.28	10.54
J	635 – 638	0.01	-2.43	0.07	0.04	2.50
K	841 – 844	-0.05	-8.31	0.27	0.02	8.58
L	855 – 858	0.00	-1.36	-0.24	0.00	1.35
M	941 – 944	-0.05	-7.84	0.21	0.00	8.05
N	955 – 958	0.00	-0.90	-0.31	0.00	0.90
O	1101 – 1104	-0.05	-6.96	0.21	0.00	7.17
P	1115 – 1118	0.00	0.63	0.32	0.00	0.63
Q	1261 – 1264	-0.05	-6.01	0.30	0.00	6.31
R	1275 – 1278	-0.01	1.52	0.15	0.00	1.53
S	1561 – 1564	0.06	-5.15	-0.04	-0.08	5.21
T	1575 – 1578	-0.01	2.92	0.32	-0.03	2.92
U	1841 – 1846	-0.11	-1.72	-2.00	-0.27	1.93
V	1852 – 1856	-0.13	4.34	2.22	0.07	4.47
W	1969 – 1976	-0.75	-1.72	-0.15	-0.29	1.66
X	2370 – 2570	-1.36	-0.37	0.12	-0.03	1.49
Y	2305 – 2565	0.00	-0.35	-0.40	-0.03	0.40
Z	2301 - 2561	0.01	0.00	-0.33	0.00	0.34

Table 2.10.7-8 P_m Stress Summary (1-Foot Bottom End Drop) – Loading Condition 2

LOADING CONDITION 2: -40°F Ambient Temperature and Maximum Decay Heat Load

Section	Node to Node	S_X	S_Y	S_Z	S_{XY}	SI
A	177 - 327	-2.90	-0.61	-0.61	0.27	2.36
B	4 - 104	-4.58	-0.59	-0.57	0.15	4.02
C	10 – 110	-4.67	-0.41	0.50	0.20	5.18
D	185 – 335	-5.31	-0.38	-0.11	1.93	6.26
E	18 – 118	-5.85	0.23	1.56	0.09	7.41
F	143 – 150	-2.63	-5.32	2.26	0.39	7.64
G	335 – 340	-3.57	-5.67	0.67	-0.42	6.41
H	346 – 350	-1.82	-3.00	2.18	-0.45	5.33
I	621 – 624	0.05	-12.18	-1.52	0.32	12.24
J	635 – 638	0.00	-2.83	0.37	0.04	3.19
K	841 – 844	-0.01	-11.75	0.11	0.01	11.86
L	855 – 858	0.00	-2.39	0.01	0.00	2.40
M	941 – 944	-0.01	-11.21	0.10	0.00	11.32
N	955 – 958	-0.01	-1.86	0.00	0.00	1.86
O	1101 – 1104	-0.01	-10.33	0.11	0.00	10.44
P	1115 – 1118	0.00	-0.97	0.00	0.00	0.98
Q	1261 – 1264	-0.01	-9.44	-0.10	0.00	9.44
R	1275 – 1278	-0.02	-0.10	-0.20	0.00	0.18
S	1561 – 1564	0.01	-8.58	-0.82	-0.16	8.60
T	1575 – 1578	0.00	0.77	0.44	-0.02	0.77
U	1841 – 1846	-1.37	-3.46	-3.17	-0.61	2.43
V	1852 – 1856	-1.26	0.57	0.90	0.27	2.20
W	1969 – 1976	-0.42	-0.06	0.76	-0.31	1.36
X	2370 – 2570	-0.29	-0.44	0.14	-0.04	0.60
Y	2305 – 2565	-0.16	-0.40	-0.47	-0.04	0.31
Z	2301 - 2561	0.07	0.00	-0.37	0.00	0.45

Table 2.10.7-9 $P_m + P_b$ Stress Summary (1-Foot Bottom End Drop) – Loading Condition 2

LOADING CONDITION 2: -40°F Ambient Temperature and Maximum Decay Heat Load

Section	Node to Node	S_X	S_Y	S_Z	S_{XY}	SI
A	177 - 327	-4.00	-0.61	-0.61	0.27	3.44
B	4 - 104	-4.81	-0.59	-0.57	0.15	4.24
C	10 – 110	-4.83	-0.41	0.50	0.20	5.34
D	185 – 335	-12.66	-0.38	-0.11	1.93	12.87
E	18 – 118	-8.64	0.23	1.56	0.09	10.20
F	143 – 150	-5.57	-11.51	-0.28	0.39	11.25
G	335 – 340	-6.48	-8.95	-0.32	-0.42	8.70
H	346 – 350	-4.85	-7.40	-0.46	-0.45	7.02
I	621 – 624	0.18	-13.91	-1.67	0.32	14.10
J	635 – 638	0.01	-4.00	0.25	0.04	4.26
K	841 – 844	-0.01	-11.96	-0.11	0.01	11.95
L	855 – 858	0.00	-2.73	-0.36	0.00	2.73
M	941 – 944	-0.01	-11.49	-0.16	0.00	11.48
N	955 – 958	0.00	-2.26	-0.41	0.00	2.26
O	1101 – 1104	-0.01	-10.61	-0.16	0.00	10.59
P	1115 – 1118	0.00	-1.39	-0.42	0.00	1.39
Q	1261 – 1264	0.00	-9.79	-0.39	0.00	9.79
R	1275 – 1278	0.00	-0.77	-0.67	0.00	0.77
S	1561 – 1564	0.10	-8.94	-0.67	-0.16	9.04
T	1575 – 1578	-0.01	1.90	0.46	-0.02	1.91
U	1841 – 1846	-0.09	-3.21	-3.39	-0.61	3.42
V	1852 – 1856	-0.16	4.29	3.11	0.27	4.48
W	1969 – 1976	-0.01	1.50	1.80	-0.31	1.87
X	2370 – 2570	-1.48	-0.44	0.14	-0.04	1.62
Y	2305 – 2565	0.00	-0.40	-0.47	-0.04	0.47
Z	2301 - 2561	0.01	0.00	-0.37	0.00	0.39

Table 2.10.7-10 P_m Stress Summary (1-Foot Bottom End Drop) – Loading Condition 3

LOADING CONDITION 3: -40°F Ambient Temperature and No Decay Heat Load

Section	Node to Node	S_X	S_Y	S_Z	S_{XY}	SI
A	177 - 327	-1.79	1.47	1.47	0.41	3.37
B	4 - 104	-4.27	-1.47	-1.45	0.40	2.91
C	10 – 110	-3.52	-1.43	-1.29	1.50	3.66
D	185 – 335	-2.89	1.55	1.16	2.22	6.28
E	18 – 118	-10.02	-0.60	-2.85	2.62	10.78
F	143 – 150	-1.23	-8.11	0.50	-1.39	8.88
G	335 – 340	-3.07	-3.85	0.69	-0.47	4.76
H	346 – 350	0.68	-5.74	-0.06	0.10	6.43
I	621 – 624	0.04	-7.76	-1.05	0.24	7.81
J	635 – 638	0.00	-6.83	-0.06	-0.01	6.83
K	841 – 844	-0.05	-7.34	-0.82	-0.04	7.28
L	855 – 858	0.00	-6.39	0.00	0.00	6.40
M	941 – 944	-0.11	-6.80	-1.78	0.00	6.69
N	955 – 958	0.00	-5.86	0.00	0.00	5.86
O	1101 – 1104	-0.19	-5.91	-3.29	0.00	5.73
P	1115 – 1118	0.00	-4.97	0.00	0.00	4.97
Q	1261 – 1264	-0.27	-5.03	-4.81	0.00	4.76
R	1275 – 1278	0.00	-4.09	0.00	0.00	4.09
S	1561 – 1564	-0.28	-4.17	-5.87	-0.07	5.59
T	1575 – 1578	0.00	-3.23	0.06	0.01	3.29
U	1841 – 1846	0.70	-1.62	-0.89	0.36	2.43
V	1852 – 1856	0.44	-2.22	-0.21	0.13	2.67
W	1969 – 1976	-0.06	-0.96	-0.19	-0.12	0.93
X	2370 – 2570	-0.16	0.02	-0.03	-0.08	0.23
Y	2305 – 2565	-0.02	0.02	0.01	-0.04	0.08
Z	2301 - 2561	-0.01	0.00	0.02	0.00	0.02

Table 2.10.7-11 $P_m + P_b$ Stress Summary (1-Foot Bottom End Drop) – Loading Condition 3

LOADING CONDITION 3: -40°F Ambient Temperature and No Decay Heat Load

Section	Node to Node	S_X	S_Y	S_Z	S_{XY}	SI
A	177 - 327	-3.42	1.47	1.47	0.41	4.96
B	4 - 104	-4.73	-1.47	-1.45	0.40	3.35
C	10 – 110	-4.75	-1.43	-1.29	1.50	4.48
D	185 – 335	-8.83	1.55	1.16	2.22	11.29
E	18 – 118	-20.14	-0.60	-2.85	2.62	20.23
F	143 – 150	0.08	-19.42	-2.13	-1.39	19.70
G	335 – 340	-5.11	-5.41	0.81	-0.47	6.56
H	346 – 350	0.08	-8.13	-0.82	0.10	8.21
I	621 – 624	0.12	-8.99	-1.30	0.24	9.13
J	635 – 638	0.00	-7.03	-0.12	-0.01	7.03
K	841 – 844	-0.01	-7.36	-0.87	-0.04	7.34
L	855 – 858	0.00	-6.39	0.00	0.00	6.40
M	941 – 944	-0.01	-6.80	-1.87	0.00	6.78
N	955 – 958	0.00	-5.86	0.00	0.00	5.86
O	1101 – 1104	-0.01	-5.91	-3.46	0.00	5.90
P	1115 – 1118	0.00	-4.97	0.00	0.00	4.97
Q	1261 – 1264	-0.01	-5.03	-5.05	0.00	5.03
R	1275 – 1278	0.00	-4.09	0.00	0.00	4.09
S	1561 – 1564	0.01	-3.85	-6.08	-0.07	6.10
T	1575 – 1578	0.00	-3.34	0.03	0.01	3.37
U	1841 – 1846	0.06	-4.16	-2.04	0.36	4.29
V	1852 – 1856	0.07	-3.50	-0.65	0.13	3.58
W	1969 – 1976	-0.01	-1.47	-0.29	-0.12	1.48
X	2370 – 2570	-0.59	0.02	-0.03	-0.08	0.63
Y	2305 – 2565	-0.01	0.02	0.01	-0.04	0.08
Z	2301 - 2561	-0.01	0.00	0.02	0.00	0.02

Table 2.10.7-12 P_m Stress Summary (1-Foot Top End Drop) – Loading Condition 1

LOADING CONDITION 1: 130°F Ambient Temperature and Maximum Decay Heat Load

Section	Node to Node	S_X	S_Y	S_Z	S_{XY}	SI
A	177 - 327	-0.06	-0.20	-0.20	0.02	0.14
B	4 - 104	-0.05	1.35	1.34	-0.04	1.41
C	10 – 110	-0.96	1.39	1.70	-0.81	2.91
D	185 – 335	-2.42	-0.20	-0.32	0.76	2.69
E	18 – 118	3.42	1.02	3.52	-2.23	5.06
F	143 – 150	-2.34	2.43	1.38	1.32	5.46
G	335 – 340	-0.11	-1.73	1.65	-0.40	3.47
H	346 – 350	-1.87	1.69	1.73	-0.33	3.64
I	621 – 624	0.00	-4.69	-0.19	0.14	4.70
J	635 – 638	0.00	2.47	0.27	0.03	2.46
K	841 – 844	-0.02	-5.13	0.44	0.02	5.57
L	855 – 858	0.00	2.03	0.00	0.00	2.03
M	941 – 944	-0.03	-5.67	0.44	0.00	6.11
N	955 – 958	0.00	1.49	0.00	0.00	1.50
O	1101 – 1104	-0.03	-6.55	0.44	0.00	7.00
P	1115 – 1118	0.00	0.61	0.00	0.00	0.61
Q	1261 – 1264	-0.03	-7.43	0.47	0.00	7.91
R	1275 – 1278	-0.01	-0.28	-0.10	0.00	0.27
S	1561 – 1564	0.02	-8.29	-0.70	-0.22	8.32
T	1575 – 1578	0.00	-1.13	0.35	-0.04	1.48
U	1841 – 1846	-0.23	-4.69	0.73	0.55	5.48
V	1852 – 1856	-1.43	-1.80	1.55	0.03	3.35
W	1969 – 1976	0.37	-3.95	0.29	-0.20	4.34
X	2370 – 2570	-4.28	-0.22	0.01	-1.02	4.54
Y	2305 – 2565	-3.45	-0.16	-0.21	-0.43	3.40
Z	2301 - 2561	-3.26	0.00	-0.14	0.00	3.26

Table 2.10.7-13 $P_m + P_b$ Stress Summary (1-Foot Top End Drop) – Loading Condition 1

LOADING CONDITION 1: 130°F Ambient Temperature and Maximum Decay Heat Load

Section	Node to Node	S_X	S_Y	S_Z	S_{XY}	SI
A	177 - 327	-0.01	-0.20	-0.20	0.02	0.20
B	4 - 104	-0.21	1.35	1.34	-0.04	1.56
C	10 – 110	-1.71	1.39	1.70	-0.81	3.61
D	185 – 335	-6.70	-0.20	-0.32	0.76	6.67
E	18 – 118	9.55	1.02	3.52	-2.23	9.62
F	143 – 150	-7.67	6.60	1.37	1.32	14.52
G	335 – 340	-1.76	-5.05	0.40	-0.40	5.50
H	346 – 350	-0.18	6.27	4.03	-0.33	6.49
I	621 – 624	0.08	-5.54	-0.31	0.14	5.62
J	635 – 638	0.00	3.41	0.42	0.03	3.42
K	841 – 844	-0.05	-5.34	0.27	0.02	5.60
L	855 – 858	0.00	2.26	0.24	0.00	2.26
M	941 – 944	-0.05	-5.94	0.21	0.00	6.14
N	955 – 958	0.00	1.80	0.30	0.00	1.80
O	1101 – 1104	-0.05	-6.82	0.21	0.00	7.03
P	1115 – 1118	0.00	0.94	0.32	0.00	0.94
Q	1261 – 1264	-0.05	-7.64	0.30	0.00	7.94
R	1275 – 1278	0.00	-0.63	-0.35	0.00	0.63
S	1561 – 1564	0.12	-9.50	-0.89	-0.22	9.64
T	1575 – 1578	0.01	-2.28	0.20	-0.04	2.48
U	1841 – 1846	-0.11	-6.10	0.36	0.55	6.51
V	1852 – 1856	-3.44	-5.74	-0.38	0.03	5.36
W	1969 – 1976	0.02	-4.40	0.51	-0.20	4.92
X	2370 – 2570	-4.84	-0.22	0.01	-1.02	5.07
Y	2305 – 2565	-4.82	-0.16	-0.21	-0.43	4.74
Z	2301 - 2561	-4.79	0.00	-0.14	0.00	4.79

Table 2.10.7-14 P_m Stress Summary (1-Foot Top End Drop) – Loading Condition 2

LOADING CONDITION 2: -40°F Ambient Temperature and Maximum Decay Heat Load

Section	Node to Node	S_X	S_Y	S_Z	S_{XY}	SI
A	177 - 327	-0.15	-1.64	-1.64	0.04	1.50
B	4 - 104	-0.16	-0.49	-0.49	-0.09	0.38
C	10 – 110	-0.36	-0.32	0.56	-0.48	1.38
D	185 – 335	-1.87	-1.43	-0.96	0.51	1.25
E	18 – 118	0.91	0.06	2.21	-0.82	2.66
F	143 – 150	-1.12	0.77	1.69	0.70	3.04
G	335 – 340	-2.64	-3.14	-0.92	0.33	2.38
H	346 – 350	-2.05	0.79	1.95	-0.54	4.10
I	621 – 624	0.02	-8.27	-0.89	0.18	8.30
J	635 – 638	0.00	1.25	0.43	0.04	1.25
K	841 – 844	-0.01	-8.71	0.10	0.01	8.81
L	855 – 858	0.00	0.81	0.00	0.00	0.81
M	941 – 944	-0.01	-9.25	0.10	0.00	9.35
N	955 – 958	-0.01	0.28	0.00	0.00	0.28
O	1101 – 1104	-0.01	-10.13	0.11	0.00	10.24
P	1115 – 1118	0.00	-0.61	0.00	0.00	0.61
Q	1261 – 1264	-0.01	-11.02	-0.10	0.00	11.01
R	1275 – 1278	-0.02	-1.51	-0.20	0.00	1.48
S	1561 – 1564	0.04	-11.87	-1.44	-0.30	11.93
T	1575 – 1578	0.00	-2.35	0.53	-0.03	2.88
U	1841 – 1846	-0.48	-6.05	-0.39	0.20	5.67
V	1852 – 1856	-1.74	-2.62	1.84	0.23	4.52
W	1969 – 1976	0.27	-3.94	0.38	-0.21	4.32
X	2370 – 2570	-4.27	-0.30	0.03	-1.03	4.55
Y	2305 – 2565	-3.43	-0.21	-0.28	-0.44	3.34
Z	2301 - 2561	-3.21	0.00	-0.18	0.00	3.21

Table 2.10.7-15 $P_m + P_b$ Stress Summary (1-Foot Top End Drop) – Loading Condition 2

LOADING CONDITION 2: -40°F Ambient Temperature and Maximum Decay Heat Load

Section	Node to Node	S_X	S_Y	S_Z	S_{XY}	SI
A	177 - 327	-0.02	-1.64	-1.64	0.04	1.62
B	4 - 104	-0.02	-0.49	-0.49	-0.09	0.51
C	10 – 110	-0.67	-0.32	0.56	-0.48	1.56
D	185 – 335	-6.21	-1.43	-0.96	0.51	5.31
E	18 – 118	0.04	0.06	2.21	-0.82	2.99
F	143 – 150	-3.24	0.51	0.66	0.70	4.02
G	335 – 340	-4.44	-5.12	-1.91	0.33	3.35
H	346 – 350	-0.23	6.01	4.87	-0.54	6.34
I	621 – 624	0.11	-9.00	-0.82	0.18	9.12
J	635 – 638	-0.01	2.50	0.56	0.04	2.51
K	841 – 844	-0.01	-8.93	-0.11	0.01	8.92
L	855 – 858	0.00	1.14	0.37	0.00	1.14
M	941 – 944	-0.01	-9.52	-0.16	0.00	9.51
N	955 – 958	0.00	0.67	0.41	0.00	0.67
O	1101 – 1104	-0.01	-10.41	-0.16	0.00	10.40
P	1115 – 1118	0.00	-1.03	-0.42	0.00	1.03
Q	1261 – 1264	0.00	-11.37	-0.39	0.00	11.37
R	1275 – 1278	0.00	-2.17	-0.67	0.00	2.17
S	1561 – 1564	0.17	-13.22	-1.52	-0.30	13.40
T	1575 – 1578	0.02	-3.75	0.43	-0.03	4.18
U	1841 – 1846	-0.08	-7.57	-1.01	0.20	7.50
V	1852 – 1856	-4.13	-7.44	-0.71	0.23	6.74
W	1969 – 1976	0.01	-4.33	0.80	-0.21	5.14
X	2370 – 2570	-4.84	-0.30	0.03	-1.03	5.10
Y	2305 – 2565	-4.82	-0.21	-0.28	-0.44	4.69
Z	2301 - 2561	-4.79	0.00	-0.18	0.00	4.79

Table 2.10.7-16 P_m Stress Summary (1-Foot Side Drop) – Loading Condition 1

LOADING CONDITION 1: 100°F Ambient Temperature and Maximum Decay Heat Load

Section	Node to Node	S_X	S_Y	S_Z	S_{XY}	SI
A	177 - 327	-3.76	-0.84	0.93	-0.22	4.71
B	4 - 104	-3.19	-0.78	0.05	-0.44	3.32
C	10 – 110	-3.91	-0.21	-1.00	0.22	3.72
D	185 – 335	-4.37	-0.09	-1.47	-0.18	4.29
E	18 – 118	-4.44	0.61	-2.66	-0.03	5.05
F	143 – 150	-2.31	0.18	-4.82	-0.39	5.06
G	335 – 340	-2.47	-0.66	-1.12	0.42	2.00
H	346 – 350	-3.13	3.07	-5.60	-0.24	8.68
I	621 – 624	-0.08	2.48	1.09	-0.03	2.56
J	635 – 638	-0.07	7.31	1.23	-0.06	7.37
K	841 – 844	-0.08	8.97	0.56	0.01	9.05
L	855 – 858	-0.02	17.11	0.95	-0.01	17.13
M	941 – 944	-0.09	13.34	0.44	0.01	13.44
N	955 – 958	-0.03	26.18	1.12	0.01	26.21
O	1101 – 1104	-0.10	15.36	0.27	0.00	15.46
P	1115 – 1118	-0.05	31.36	1.31	0.00	31.40
Q	1261 – 1264	-0.08	14.15	0.55	-0.01	14.24
R	1275 – 1278	-0.04	25.93	1.00	0.00	25.98
S	1561 – 1564	-0.08	4.01	1.20	0.06	4.10
T	1575 – 1578	-0.07	11.86	1.38	0.03	11.93
U	1841 – 1846	0.25	0.24	1.04	-0.09	0.88
V	1852 – 1856	2.33	6.99	-0.91	-1.26	8.22
W	1969 – 1976	10.14	1.89	-4.53	-1.65	12.47
X	2370 – 2570	-1.94	-0.89	0.09	0.52	2.24
Y	2305 – 2565	-1.50	-0.03	0.56	0.26	2.10
Z	2301 - 2561	-1.10	0.08	0.66	1.09	2.47

Table 2.10.7-17 $P_m + P_b$ Stress Summary (1-Foot Side Drop) – Loading Condition 1

LOADING CONDITION 1: 100°F Ambient Temperature and Maximum Decay Heat Load

Section	Node to Node	S_X	S_Y	S_Z	S_{XY}	SI
A	177 - 327	-8.25	-1.80	0.27	-1.47	8.85
B	4 - 104	-4.89	-1.65	-1.52	-0.64	3.49
C	10 – 110	-5.50	-0.44	-2.48	0.01	5.07
D	185 – 335	-6.75	-0.75	-2.88	-0.01	5.99
E	18 – 118	-4.23	1.45	-2.97	-0.41	5.74
F	143 – 150	-0.95	3.51	-1.76	-0.39	5.30
G	335 – 340	-4.63	-2.10	-2.43	0.42	2.66
H	346 – 350	-2.52	8.15	-2.54	-0.24	10.69
I	621 – 624	-0.05	3.05	1.14	-0.03	3.10
J	635 – 638	-0.01	9.61	1.08	-0.06	9.63
K	841 – 844	-0.03	9.69	1.13	0.01	9.72
L	855 – 858	0.02	17.90	0.66	-0.01	17.88
M	941 – 944	-0.05	14.24	1.05	0.02	14.29
N	955 – 958	0.01	27.38	1.03	0.01	27.37
O	1101 – 1104	-0.07	16.34	0.88	0.00	16.41
P	1115 – 1118	0.01	33.37	1.50	0.00	33.36
Q	1261 – 1264	-0.04	15.10	1.16	-0.01	15.14
R	1275 – 1278	0.02	27.35	1.67	0.00	27.34
S	1561 – 1564	-0.07	4.88	1.57	0.06	4.95
T	1575 – 1578	0.01	13.85	2.29	0.03	13.84
U	1841 – 1846	-0.07	0.04	1.42	-0.09	1.54
V	1852 – 1856	4.97	9.12	0.92	-1.26	8.56
W	1969 – 1976	-21.00	-6.92	-5.29	-1.65	15.91
X	2370 – 2570	-5.54	-1.99	-0.67	0.84	5.06
Y	2305 – 2565	-1.21	-0.19	0.78	0.76	2.40
Z	2301 - 2561	-0.78	0.06	0.82	3.96	7.96

Table 2.10.7-18 S_n Stress Summary (1-Foot Side Drop) – Loading Condition 1

LOADING CONDITION 1: 100°F Ambient Temperature and Maximum Decay Heat Load

Section	Node to Node	S_X	S_Y	S_Z	S_{XY}	SI
A	177 - 327	-16.56	-1.93	-8.01	-1.48	14.92
B	4 - 104	2.59	0.13	5.70	-0.30	5.60
C	10 – 110	1.72	0.02	5.07	0.50	5.18
D	185 – 335	-12.37	-1.73	-9.50	0.51	10.69
E	18 – 118	-2.16	0.74	-0.97	2.43	5.67
F	143 – 150	-10.70	3.74	-1.87	0.84	14.53
G	335 – 340	-1.23	-4.19	2.34	-0.84	6.76
H	346 – 350	-11.73	6.02	-4.40	-0.30	17.76
I	621 – 624	-0.14	4.66	1.54	0.00	4.80
J	635 – 638	-0.01	17.65	1.00	0.01	17.66
K	841 – 844	-0.04	12.03	1.49	0.02	12.07
L	855 – 858	0.02	27.31	0.90	-0.01	27.29
M	941 – 944	-0.06	16.64	1.47	0.01	16.70
N	955 – 958	0.01	36.87	1.33	0.00	36.86
O	1101 – 1104	-0.08	18.74	1.30	0.00	18.81
P	1115 – 1118	0.01	42.87	1.82	0.00	42.86
Q	1261 – 1264	-0.05	17.43	1.55	-0.01	17.48
R	1275 – 1278	0.00	36.86	1.82	0.00	36.86
S	1561 – 1564	-0.11	7.38	2.24	0.11	7.49
T	1575 – 1578	0.01	21.87	2.22	-0.04	21.86
U	1841 – 1846	-0.09	0.59	1.04	0.12	1.14
V	1852 – 1856	0.05	17.35	1.18	-1.71	17.63
W	1969 – 1976	-21.77	-8.80	-5.04	-2.15	17.08
X	2370 – 2570	-6.17	-3.00	-1.15	1.18	5.42
Y	2305 – 2565	-1.62	-0.34	0.33	0.70	2.26
Z	2301 - 2561	-1.17	0.13	0.43	3.97	8.06

Table 2.10.7-19 P_m Stress Summary (1-Foot Top Corner Drop) – Loading Condition 1 – Drop Orientation = 15.74 Degrees

LOADING CONDITION 1: 130°F Ambient Temperature and Maximum Decay Heat Load

Section	Node to Node	S_X	S_Y	S_Z	S_{XY}	SI
A	177 - 327	-1.30	-0.47	0.11	-0.05	1.42
B	4 - 104	-1.10	1.05	1.32	-0.18	2.43
C	10 – 110	-2.22	1.28	1.32	-0.71	3.78
D	185 – 335	-3.79	-0.22	-0.80	0.68	3.81
E	18 – 118	1.85	1.19	2.54	-2.17	4.40
F	143 – 150	-3.03	2.42	-0.25	1.15	5.92
G	335 – 340	-0.92	-1.90	1.23	-0.25	3.19
H	346 – 350	-2.85	2.65	-0.17	-0.40	5.56
I	621 – 624	-0.03	-3.73	0.18	0.13	3.91
J	635 – 638	-0.02	4.81	0.67	0.01	4.83
K	841 – 844	-0.03	1.44	0.40	0.02	1.47
L	855 – 858	0.00	2.53	0.13	0.00	2.53
M	941 – 944	-0.03	1.49	0.40	0.00	1.52
N	955 – 958	0.00	2.93	0.16	0.00	2.93
O	1101 – 1104	-0.04	0.72	0.35	0.00	0.75
P	1115 – 1118	-0.01	2.31	0.20	0.00	2.32
Q	1261 – 1264	-0.03	-0.56	0.40	0.00	0.96
R	1275 – 1278	0.00	-0.03	0.16	0.00	0.19
S	1561 – 1564	0.00	-3.39	-0.14	-0.13	3.40
T	1575 – 1578	-0.01	-3.82	0.45	0.01	4.26
U	1841 – 1846	0.66	-1.96	2.32	0.23	4.30
V	1852 – 1856	0.60	-3.51	0.76	0.07	4.27
W	1969 – 1976	-1.80	-2.28	-0.95	0.05	1.33
X	2370 – 2570	-2.86	-0.60	-0.40	-0.59	2.60
Y	2305 – 2565	-1.90	-0.69	-0.10	-0.30	1.87
Z	2301 - 2561	-0.63	0.00	0.07	0.00	0.69

Table 2.10.7-20 $P_m + P_b$ Stress Summary (1-Foot Top Corner Drop) – Loading Condition 1 – Drop Orientation = 15.74 Degrees

LOADING CONDITION 1: 130°F Ambient Temperature and Maximum Decay Heat Load

Section	Node to Node	S_X	S_Y	S_Z	S_{XY}	SI
A	177 - 327	-2.73	-0.79	-0.10	-0.47	2.73
B	4 - 104	-1.82	0.77	0.80	-0.25	2.64
C	10 – 110	-3.47	1.20	0.83	-0.78	4.93
D	185 – 335	-8.73	-0.44	-1.26	0.73	8.41
E	18 – 118	7.87	1.47	2.43	-2.30	7.88
F	143 – 150	-7.75	7.56	0.75	1.15	15.49
G	335 – 340	-3.24	-5.59	-0.41	-0.25	5.20
H	346 – 350	-1.01	8.77	3.07	-0.40	9.81
I	621 – 624	0.06	-4.37	0.08	0.13	4.45
J	635 – 638	-0.00	6.48	0.76	0.01	6.48
K	841 – 844	-0.01	1.52	0.41	0.02	1.53
L	855 – 858	0.00	2.62	0.14	0.00	2.62
M	941 – 944	-0.01	1.57	0.41	0.00	1.59
N	955 – 958	0.00	3.04	0.16	0.00	3.04
O	1101 – 1104	-0.02	0.77	0.36	0.00	0.78
P	1115 – 1118	0.00	2.41	0.17	0.00	2.41
Q	1261 – 1264	-0.06	-0.56	0.41	0.00	0.96
R	1275 – 1278	-0.01	-0. 01	0.27	0.00	0.28
S	1561 – 1564	0.06	-4.51	-0.67	-0.13	4.58
T	1575 – 1578	0.00	-4.01	0.34	0.01	4.35
U	1841 – 1846	0.00	-3.90	1.88	0.23	5.79
V	1852 – 1856	0.12	-5.06	0.00	0.07	5.19
W	1969 – 1976	-4.00	-2.57	-1.31	0.05	2.70
X	2370 – 2570	-2.97	-0.60	-0.40	-0.59	2.71
Y	2305 – 2565	-2.96	-0.69	-0.10	-0.30	2.90
Z	2301 - 2561	-1.28	0.00	0.07	0.00	1.34

Table 2.10.7-21 S_n Stress Summary (1-Foot Top Corner Drop) – Loading Condition 1 – Drop Orientation = 15.74 Degrees

LOADING CONDITION 1: 130°F Ambient Temperature and Maximum Decay Heat Load

Section	Node to Node	S_X	S_Y	S_Z	S_{XY}	SI
A	177 - 327	-5.52	-0.83	-2.84	-0.47	4.78
B	4 - 104	0.81	1.35	3.18	-0.14	2.41
C	10 – 110	-0.36	1.35	3.32	-0.62	3.89
D	185 – 335	-6.43	-0.76	-3.45	0.91	5.95
E	18 – 118	2.60	1.23	3.09	-1.36	3.05
F	143 – 150	-5.80	3.59	0.72	1.56	9.90
G	335 – 340	-0.51	-3.06	2.37	-0.36	5.60
H	346 – 350	-5.68	3.63	0.23	-0.42	9.35
I	621 – 624	-0.05	-3.01	0.32	0.14	3.34
J	635 – 638	-0.00	8.22	0.59	0.03	8.22
K	841 – 844	0.00	4.24	0.70	0.02	4.24
L	855 – 858	0.01	12.46	0.38	0.00	12.45
M	941 – 944	0.00	4.36	0.76	0.00	4.36
N	955 – 958	0.00	12.96	0.47	0.00	12.96
O	1101 – 1104	-0.01	3.55	0.71	0.00	3.55
P	1115 – 1118	0.00	12.34	0.50	0.00	12.34
Q	1261 – 1264	0.00	2.16	0.72	-0.01	2.16
R	1275 – 1278	-0.01	9.88	0.20	0.00	9.89
S	1561 – 1564	0.04	-1.61	-0.01	-0.07	1.65
T	1575 – 1578	-0.03	7.13	0.72	-0.06	7.16
U	1841 – 1846	0.02	-3.14	1.53	0.43	4.73
V	1852 – 1856	-0.19	7.89	4.10	-0.42	8.12
W	1969 – 1976	-4.79	-4.26	-1.11	-0.42	3.92
X	2370 – 2570	-6.19	-0.98	-0.29	-0.51	5.95
Y	2305 – 2565	-2.96	-1.07	-0.53	-0.31	2.47
Z	2301 - 2561	-1.26	0.00	-0.29	0.00	1.26

Table 2.10.7-22 P_m Stress Summary (1-Foot Bottom Corner Drop) – Loading Condition 1 – Drop Orientation = 15.74 Degrees

LOADING CONDITION 1: 130°F Ambient Temperature and Maximum Decay Heat Load

Section	Node to Node	S_X	S_Y	S_Z	S_{XY}	SI
A	177 - 327	-1.05	-1.53	-0.54	0.19	1.06
B	4 - 104	-2.40	-2.97	-0.90	0.14	2.10
C	10 – 110	-2.22	-1.94	-1.62	0.53	1.11
D	185 – 335	-1.77	-1.33	-0.84	0.25	1.05
E	18 – 118	-4.30	-1.41	-2.63	1.27	3.84
F	143 – 150	-0.64	-4.15	-1.80	-1.19	4.25
G	335 – 340	-1.05	-1.97	0.05	0.05	2.03
H	346 – 350	-0.13	-4.31	-0.68	-0.16	4.19
I	621 – 624	-0.01	-3.18	-0.02	0.09	3.17
J	635 – 638	-0.01	-4.79	0.33	-0.03	5.13
K	841 – 844	-0.03	-1.49	0.42	0.02	1.90
L	855 – 858	0.00	-2.51	0.15	0.00	2.66
M	941 – 944	-0.03	-0.14	0.40	0.00	0.54
N	955 – 958	0.00	-0.12	0.17	0.00	0.29
O	1101 – 1104	-0.04	1.05	0.36	0.00	1.08
P	1115 – 1118	-0.01	2.23	0.20	0.00	2.24
Q	1261 – 1264	-0.03	1.89	0.40	0.00	1.92
R	1275 – 1278	0.00	2.78	0.15	0.00	2.78
S	1561 – 1564	-0.04	-3.47	0.32	-0.06	3.79
T	1575 – 1578	-0.02	5.90	0.71	-0.02	5.93
U	1841 – 1846	-0.99	-1.94	-1.64	-0.29	1.11
V	1852 – 1856	-0.16	3.69	0.29	-0.35	3.92
W	1969 – 1976	3.05	0.56	-0.84	-0.83	4.13
X	2370 – 2570	-0.93	-0.65	0.15	0.14	1.14
Y	2305 – 2565	-0.67	-0.35	-0.20	0.06	0.48
Z	2301 - 2561	-0.33	0.03	-0.10	0.36	0.80

Table 2.10.7-23 $P_m + P_b$ Stress Summary (1-Foot Bottom Corner Drop) – Loading Condition 1 – Drop Orientation = 15.74 Degrees

LOADING CONDITION 1: 130°F Ambient Temperature and Maximum Decay Heat Load

Section	Node to Node	S_X	S_Y	S_Z	S_{XY}	SI
A	177 - 327	-1.14	-1.53	-0.54	0.19	1.07
B	4 - 104	-3.16	-2.97	-0.90	0.14	2.33
C	10 – 110	-2.94	-1.94	-1.62	0.53	1.55
D	185 – 335	-3.44	-1.33	-0.84	0.25	2.63
E	18 – 118	-7.08	-1.41	-2.63	1.27	6.21
F	143 – 150	-1.59	-4.78	-2.29	-1.19	3.98
G	335 – 340	-1.79	-2.62	-0.09	0.05	2.53
H	346 – 350	-0.63	-6.85	-1.64	-0.16	6.23
I	621 – 624	0.04	-4.09	-0.52	0.09	4.14
J	635 – 638	-0.02	-4.90	0.42	-0.03	5.32
K	841 – 844	-0.05	-1.39	0.57	0.02	1.97
L	855 – 858	0.00	-2.31	0.49	0.00	2.80
M	941 – 944	-0.06	-0.14	0.41	0.00	0.55
N	955 – 958	-0.01	-0.07	0.41	0.00	0.48
O	1101 – 1104	-0.02	1.10	0.36	0.00	1.12
P	1115 – 1118	0.00	2.32	0.15	0.00	2.32
Q	1261 – 1264	-0.01	1.98	0.41	0.00	1.99
R	1275 – 1278	0.00	2.89	0.16	0.00	2.89
S	1561 – 1564	0.04	-3.39	0.48	-0.06	3.87
T	1575 – 1578	-0.01	7.40	1.07	-0.02	7.41
U	1841 – 1846	-0.13	-1.66	-1.47	-0.29	1.63
V	1852 – 1856	1.51	7.22	2.46	-0.35	5.75
W	1969 – 1976	-7.66	-3.95	-1.89	-0.83	5.94
X	2370 – 2570	-3.15	-1.02	-0.10	0.25	3.07
Y	2305 – 2565	-0.40	-0.40	-0.13	0.22	0.49
Z	2301 - 2561	-0.25	0.02	-0.05	1.31	2.63

Table 2.10.7-24 S_n Stress Summary (1-Foot Bottom Corner Drop) – Loading Condition 1 – Drop Orientation = 15.74 Degrees

LOADING CONDITION 1: 130°F Ambient Temperature and Maximum Decay Heat Load

Section	Node to Node	S_X	S_Y	S_Z	S_{XY}	SI
A	177 - 327	-1.07	-3.11	-2.11	0.20	2.08
B	4 - 104	-3.18	-0.96	1.11	0.11	4.29
C	10 – 110	-2.96	0.13	0.81	0.36	3.82
D	185 – 335	-11.74	-2.52	-2.35	0.61	9.43
E	18 – 118	-10.29	-0.03	0.29	-0.13	10.58
F	143 – 150	-11.56	-4.53	-2.48	0.01	9.08
G	335 – 340	-1.71	-7.85	2.18	-1.29	10.29
H	346 – 350	-0.86	8.07	4.25	-0.20	8.94
I	621 – 624	0.06	-2.14	-0.21	0.11	2.21
J	635 – 638	-0.02	5.88	0.71	0.03	5.90
K	841 – 844	0.00	1.15	0.55	0.02	1.15
L	855 – 858	0.00	7.14	0.07	0.00	7.14
M	941 – 944	0.00	2.65	0.75	0.00	2.65
N	955 – 958	0.00	9.74	0.24	0.00	9.74
O	1101 – 1104	-0.01	3.88	0.72	0.00	3.89
P	1115 – 1118	0.00	12.25	0.47	0.00	12.25
Q	1261 – 1264	0.00	4.71	0.73	0.00	4.71
R	1275 – 1278	-0.01	12.83	0.30	0.00	12.84
S	1561 – 1564	-0.05	-2.36	0.66	-0.04	3.02
T	1575 – 1578	0.00	9.21	0.98	-0.04	9.20
U	1841 – 1846	-1.11	-1.82	-1.64	-0.22	0.84
V	1852 – 1856	-0.91	7.11	0.98	-0.50	8.09
W	1969 – 1976	-7.48	-2.97	-1.00	-0.99	6.69
X	2370 – 2570	-2.33	-1.35	-0.26	0.36	2.18
Y	2305 – 2565	-0.71	-0.45	-0.28	0.20	0.54
Z	2301 - 2561	-0.36	0.04	-0.18	1.31	2.65

Table 2.10.7-25 P_m Stress Summary (1-Foot Top Corner Drop) – Loading Condition 3 – Drop Orientation = 15.74 Degrees

LOADING CONDITION 3: -40°F Ambient Temperature and No Decay Heat Load

Section	Node to Node	S_X	S_Y	S_Z	S_{XY}	SI
A	177 - 327	-1.39	-1.87	-1.28	-0.03	0.59
B	4 - 104	-1.21	-0.73	-0.46	-0.23	0.84
C	10 – 110	-1.64	-0.38	0.21	-0.39	1.97
D	185 – 335	-3.26	-1.42	-1.42	0.44	2.03
E	18 – 118	-0.58	0.26	1.27	-0.81	2.34
F	143 – 150	-1.85	0.81	0.05	0.55	2.87
G	335 – 340	-3.38	-3.26	-1.26	0.46	2.52
H	346 – 350	-3.02	1.78	0.04	-0.60	4.95
I	621 – 624	-0.01	-7.20	-0.50	0.16	7.20
J	635 – 638	-0.02	3.62	0.82	0.02	3.65
K	841 – 844	-0.01	1.36	0.09	0.00	1.36
L	855 – 858	0.00	2.38	0.12	0.00	2.38
M	941 – 944	-0.01	1.18	0.09	0.00	1.19
N	955 – 958	0.00	2.72	0.15	0.00	2.72
O	1101 – 1104	-0.01	0.45	0.09	0.00	0.45
P	1115 – 1118	0.00	2.10	0.17	0.00	2.10
Q	1261 – 1264	-0.01	-0.83	0.09	0.00	0.92
R	1275 – 1278	0.00	-0.06	0.15	0.00	0.21
S	1561 – 1564	0.02	-2.72	-0.33	-0.11	2.75
T	1575 – 1578	-0.01	-3.59	0.44	0.01	4.03
U	1841 – 1846	0.83	-1.64	2.47	0.35	4.16
V	1852 – 1856	0.57	-3.33	0.81	0.04	4.14
W	1969 – 1976	-1.66	-2.14	-0.87	0.08	1.28
X	2370 – 2570	-2.48	-0.56	-0.45	-0.76	2.45
Y	2305 – 2565	-1.33	-0.61	-0.07	-0.31	1.37
Z	2301 - 2561	-0.40	0.00	0.06	0.00	0.46

Table 2.10.7-26 $P_m + P_b$ Stress Summary (1-Foot Top Corner Drop) – Loading Condition 3 – Drop Orientation = 15.74 Degrees

LOADING CONDITION 3: -40°F Ambient Temperature and No Decay Heat Load

Section	Node to Node	S_X	S_Y	S_Z	S_{XY}	SI
A	177 - 327	-2.74	-2.18	-1.50	-0.45	1.49
B	4 - 104	-1.63	-1.02	-0.98	-0.30	0.86
C	10 – 110	-2.46	-0.46	-0.28	-0.46	2.29
D	185 – 335	-8.25	-1.63	-1.88	0.49	6.69
E	18 – 118	-1.36	0.54	1.16	-0.93	2.90
F	143 – 150	-3.46	1.65	0.06	0.55	5.23
G	335 – 340	-5.83	-5.66	-2.65	0.46	3.56
H	346 – 350	-1.05	8.52	3.89	-0.60	9.65
I	621 – 624	0.09	-7.72	-0.42	0.16	7.82
J	635 – 638	-0.01	5.60	0.90	0.02	5.61
K	841 – 844	0.00	1.42	0.08	0.00	1.42
L	855 – 858	0.00	2.46	0.13	0.00	2.46
M	941 – 944	0.00	1.24	0.08	0.00	1.24
N	955 – 958	0.00	2.82	0.16	0.00	2.82
O	1101 – 1104	0.00	0.48	0.08	0.00	0.48
P	1115 – 1118	0.00	2.18	0.14	0.00	2.18
Q	1261 – 1264	0.00	-0.85	0.07	0.00	0.93
R	1275 – 1278	-0.01	-0.03	0.25	0.00	0.29
S	1561 – 1564	0.06	-3.75	-0.84	-0.11	3.81
T	1575 – 1578	0.01	-3.81	0.33	0.01	4.14
U	1841 – 1846	0.05	-3.84	1.92	0.35	5.79
V	1852 – 1856	0.12	-4.75	0.11	0.04	4.87
W	1969 – 1976	-3.70	-2.35	-1.19	0.08	2.51
X	2370 – 2570	-3.37	-0.56	-0.45	-0.76	3.20
Y	2305 – 2565	-2.73	-0.61	-0.07	-0.31	2.70
Z	2301 - 2561	-1.17	0.00	0.06	0.00	1.24

Table 2.10.7-27 S_n Stress Summary (1-Foot Top Corner Drop) – Loading Condition 3 – Drop Orientation = 15.74 Degrees

LOADING CONDITION 3: -40°F Ambient Temperature and No Decay Heat Load

Section	Node to Node	S_X	S_Y	S_Z	S_{XY}	SI
A	177 - 327	-5.61	-2.23	-4.23	-0.45	3.50
B	4 - 104	0.70	-0.43	1.41	-0.19	1.87
C	10 – 110	0.22	-0.30	2.22	-0.30	2.66
D	185 – 335	-5.90	-1.96	-4.07	0.66	4.16
E	18 – 118	0.17	0.30	1.82	0.01	1.65
F	143 – 150	-4.62	1.98	1.02	0.96	6.87
G	335 – 340	-2.97	-4.43	-0.12	0.04	4.31
H	346 – 350	-5.86	2.75	0.44	-0.62	8.70
I	621 – 624	-0.03	-6.48	-0.36	0.17	6.47
J	635 – 638	-0.00	7.04	0.75	0.04	7.04
K	841 – 844	-0.01	-7.16	-10.21	-0.44	10.23
L	855 – 858	-0.01	-1.30	0.12	0.00	1.42
M	941 – 944	-0.02	-8.21	-9.58	0.00	9.57
N	955 – 958	-0.01	-0.99	0.15	0.00	1.13
O	1101 – 1104	-0.02	-8.92	-9.58	0.00	9.57
P	1115 – 1118	-0.01	-1.58	0.19	0.00	1.77
Q	1261 – 1264	-0.01	-10.13	-9.57	0.00	10.12
R	1275 – 1278	-0.01	-3.63	0.25	0.00	3.88
S	1561 – 1564	0.02	4.32	-4.30	-0.21	8.63
T	1575 – 1578	0.01	-7.53	0.46	0.02	7.99
U	1841 – 1846	0.14	-2.50	3.87	1.36	6.95
V	1852 – 1856	0.15	-7.94	0.29	0.24	8.23
W	1969 – 1976	-0.66	-3.19	-1.16	0.44	2.68
X	2370 – 2570	-2.74	-0.82	-0.66	-0.80	2.50
Y	2305 – 2565	-2.73	-0.82	-0.27	-0.31	2.51
Z	2301 - 2561	-1.17	0.00	-0.14	0.00	1.17

Table 2.10.7-28 P_m Stress Summary (30-Foot Bottom End Drop) – Loading Condition 1

LOADING CONDITION 1: 130°F Ambient Temperature and Maximum Decay Heat Load

Section	Node to Node	S_X	S_Y	S_Z	S_{XY}	SI
A	177 - 327	-2.81	0.86	0.86	0.25	3.70
B	4 - 104	-4.47	1.22	1.22	0.20	5.70
C	10 – 110	-5.23	1.26	1.61	-0.09	6.84
D	185 – 335	-5.81	0.88	0.56	2.15	7.96
E	18 – 118	-3.44	1.18	2.81	-1.27	6.58
F	143 – 150	-3.86	-3.70	1.95	0.98	6.71
G	335 – 340	-0.98	-4.20	3.28	-1.13	7.84
H	346 – 350	-1.69	-2.09	1.96	-0.23	4.15
I	621 – 624	0.03	-8.53	-0.81	0.28	8.58
J	635 – 638	0.00	-1.55	0.20	0.04	1.75
K	841 – 844	-0.03	-8.11	0.44	0.02	8.55
L	855 – 858	0.00	-1.12	0.00	0.00	1.12
M	941 – 944	-0.03	-7.57	0.44	0.00	8.01
N	955 – 958	0.00	-0.58	0.00	0.00	0.58
O	1101 – 1104	-0.03	-6.69	0.44	0.00	7.13
P	1115 – 1118	0.00	0.30	0.00	0.00	0.31
Q	1261 – 1264	-0.03	-5.80	0.47	0.00	6.27
R	1275 – 1278	-0.01	1.18	-0.10	0.00	1.28
S	1561 – 1564	-0.01	-4.94	-0.08	-0.08	4.93
T	1575 – 1578	0.00	2.05	0.26	-0.03	2.05
U	1841 – 1846	-1.11	-2.08	-2.04	-0.27	1.10
V	1852 – 1856	-0.96	1.43	0.61	0.07	2.39
W	1969 – 1976	-0.31	-0.07	0.68	-0.29	1.19
X	2370 – 2570	-0.30	-0.37	0.12	-0.03	0.50
Y	2305 – 2565	-0.18	-0.35	-0.40	-0.03	0.23
Z	2301 - 2561	0.03	0.00	-0.33	0.00	0.35

Table 2.10.7-29 $P_m + P_b$ Stress Summary (30-Foot Bottom End Drop) – Loading Condition 1

LOADING CONDITION 1: 130°F Ambient Temperature and Maximum Decay Heat Load

Section	Node to Node	S_X	S_Y	S_Z	S_{XY}	SI
A	177 - 327	-3.80	0.86	0.86	0.25	4.69
B	4 - 104	-4.84	1.22	1.22	0.20	6.07
C	10 – 110	-5.54	1.26	1.61	-0.09	7.15
D	185 – 335	-13.08	0.88	0.56	2.15	14.61
E	18 – 118	-4.79	1.18	2.81	-1.27	7.87
F	143 – 150	-9.99	-5.56	0.41	0.98	10.60
G	335 – 340	-3.75	-8.88	1.98	-1.13	11.11
H	346 – 350	-4.78	-5.93	-0.12	-0.23	5.86
I	621 – 624	0.15	-10.37	-1.16	0.28	10.54
J	635 – 638	0.01	-2.43	0.07	0.04	2.50
K	841 – 844	-0.05	-8.31	0.27	0.02	8.58
L	855 – 858	0.00	-1.36	-0.24	0.00	1.35
M	941 – 944	-0.05	-7.84	0.21	0.00	8.05
N	955 – 958	0.00	-0.90	-0.31	0.00	0.90
O	1101 – 1104	-0.05	-6.96	0.21	0.00	7.17
P	1115 – 1118	0.00	0.63	0.32	0.00	0.63
Q	1261 – 1264	-0.05	-6.01	0.30	0.00	6.31
R	1275 – 1278	-0.01	1.52	0.15	0.00	1.53
S	1561 – 1564	0.06	-5.15	-0.04	-0.08	5.21
T	1575 – 1578	-0.01	2.92	0.32	-0.03	2.92
U	1841 – 1846	-0.11	-1.72	-2.00	-0.27	1.93
V	1852 – 1856	-0.13	4.34	2.22	0.07	4.47
W	1969 – 1976	-0.75	-1.72	-0.15	-0.29	1.66
X	2370 – 2570	-1.36	-0.37	0.12	-0.03	1.49
Y	2305 – 2565	0.00	-0.35	-0.40	-0.03	0.40
Z	2301 - 2561	0.01	0.00	-0.33	0.00	0.34

Table 2.10.7-30 P_m Stress Summary (30-Foot Bottom End Drop) – Loading Condition 2

LOADING CONDITION 2: -40°F Ambient Temperature and Maximum Decay Heat Load

Section	Node to Node	S_X	S_Y	S_Z	S_{XY}	SI
A	177 - 327	-2.90	-0.61	-0.61	0.27	2.36
B	4 - 104	-4.58	-0.59	-0.57	0.15	4.02
C	10 – 110	-4.67	-0.41	0.50	0.20	5.18
D	185 – 335	-5.31	-0.38	-0.11	1.93	6.26
E	18 – 118	-5.85	0.23	1.56	0.09	7.41
F	143 – 150	-2.63	-5.32	2.26	0.39	7.64
G	335 – 340	-3.57	-5.67	0.67	-0.42	6.41
H	346 – 350	-1.82	-3.00	2.18	-0.45	5.33
I	621 – 624	0.05	-12.18	-1.52	0.32	12.24
J	635 – 638	0.00	-2.83	0.37	0.04	3.19
K	841 – 844	-0.01	-11.75	0.11	0.01	11.86
L	855 – 858	0.00	-2.39	0.01	0.00	2.40
M	941 – 944	-0.01	-11.21	0.10	0.00	11.32
N	955 – 958	-0.01	-1.86	0.00	0.00	1.86
O	1101 – 1104	-0.01	-10.33	0.11	0.00	10.44
P	1115 – 1118	0.00	-0.97	0.00	0.00	0.98
Q	1261 – 1264	-0.01	-9.44	-0.10	0.00	9.44
R	1275 – 1278	-0.02	-0.10	-0.20	0.00	0.18
S	1561 – 1564	0.01	-8.58	-0.82	-0.16	8.60
T	1575 – 1578	0.00	0.77	0.44	-0.02	0.77
U	1841 – 1846	-1.37	-3.46	-3.17	-0.61	2.43
V	1852 – 1856	-1.26	0.57	0.90	0.27	2.20
W	1969 – 1976	-0.42	-0.06	0.76	-0.31	1.36
X	2370 – 2570	-0.29	-0.44	0.14	-0.04	0.60
Y	2305 – 2565	-0.16	-0.40	-0.47	-0.04	0.31
Z	2301 - 2561	0.07	0.00	-0.37	0.00	0.45

Table 2.10.7-31 $P_m + P_b$ Stress Summary (30-Foot Bottom End Drop) – Loading Condition 2

LOADING CONDITION 2: -40°F Ambient Temperature and Maximum Decay Heat Load

Section	Node to Node	S_X	S_Y	S_Z	S_{XY}	SI
A	177 - 327	-4.00	-0.61	-0.61	0.27	3.44
B	4 - 104	-4.81	-0.59	-0.57	0.15	4.24
C	10 – 110	-4.83	-0.41	0.50	0.20	5.34
D	185 – 335	-12.66	-0.38	-0.11	1.93	12.87
E	18 – 118	-8.64	0.23	1.56	0.09	10.20
F	143 – 150	-5.57	-11.51	-0.28	0.39	11.25
G	335 – 340	-6.48	-8.95	-0.32	-0.42	8.70
H	346 – 350	-4.85	-7.40	-0.46	-0.45	7.02
I	621 – 624	0.18	-13.91	-1.67	0.32	14.10
J	635 – 638	0.01	-4.00	0.25	0.04	4.26
K	841 – 844	-0.01	-11.96	-0.11	0.01	11.95
L	855 – 858	0.00	-2.73	-0.36	0.00	2.73
M	941 – 944	-0.01	-11.49	-0.16	0.00	11.48
N	955 – 958	0.00	-2.26	-0.41	0.00	2.26
O	1101 – 1104	-0.01	-10.61	-0.16	0.00	10.59
P	1115 – 1118	0.00	-1.39	-0.42	0.00	1.39
Q	1261 – 1264	0.00	-9.79	-0.39	0.00	9.79
R	1275 – 1278	0.00	-0.77	-0.67	0.00	0.77
S	1561 – 1564	0.10	-8.94	-0.67	-0.16	9.04
T	1575 – 1578	-0.01	1.90	0.46	-0.02	1.91
U	1841 – 1846	-0.09	-3.21	-3.39	-0.61	3.42
V	1852 – 1856	-0.16	4.29	3.11	0.27	4.48
W	1969 – 1976	-0.01	1.50	1.80	-0.31	1.87
X	2370 – 2570	-1.48	-0.44	0.14	-0.04	1.62
Y	2305 – 2565	0.00	-0.40	-0.47	-0.04	0.47
Z	2301 - 2561	0.01	0.00	-0.37	0.00	0.39

Table 2.10.7-32 P_m Stress Summary (30-Foot Bottom End Drop) – Loading Condition 3

LOADING CONDITION 3: -40°F Ambient Temperature and No Decay Heat Load

Section	Node to Node	S_X	S_Y	S_Z	S_{XY}	SI
A	177 - 327	-1.79	1.47	1.47	0.41	3.37
B	4 - 104	-4.27	-1.47	-1.45	0.40	2.91
C	10 – 110	-3.52	-1.43	-1.29	1.50	3.66
D	185 – 335	-2.89	1.55	1.16	2.22	6.28
E	18 – 118	-10.02	-0.60	-2.85	2.62	10.78
F	143 – 150	-1.23	-8.11	0.50	1.39	8.88
G	335 – 340	-3.07	-3.85	0.69	-0.47	4.76
H	346 – 350	0.68	-5.74	-0.06	0.10	6.43
I	621 – 624	0.04	-7.76	-1.05	0.24	7.81
J	635 – 638	0.00	-6.83	-0.06	-0.01	6.83
K	841 – 844	-0.05	-7.34	-0.82	-0.04	7.28
L	855 – 858	0.00	-6.39	0.00	0.00	6.40
M	941 – 944	-0.11	-6.80	-1.78	0.00	6.69
N	955 – 958	0.00	-5.86	0.00	0.00	5.86
O	1101 – 1104	-0.19	-5.91	-3.29	0.00	5.73
P	1115 – 1118	0.00	-4.97	0.00	0.00	4.97
Q	1261 – 1264	-0.27	-5.03	-4.81	0.00	4.76
R	1275 – 1278	0.00	-4.09	0.00	0.00	4.09
S	1561 – 1564	-0.28	-4.17	-5.87	-0.07	5.59
T	1575 – 1578	0.00	-3.23	0.06	0.01	3.29
U	1841 – 1846	0.70	-1.62	-0.89	0.36	2.43
V	1852 – 1856	0.44	-2.22	-0.21	0.13	2.67
W	1969 – 1976	-0.06	-0.96	-0.19	-0.12	0.93
X	2370 – 2570	-0.16	0.02	-0.03	-0.08	0.23
Y	2305 – 2565	-0.02	0.02	0.01	-0.04	0.08
Z	2301 - 2561	-0.01	0.00	0.02	0.00	0.02

Table 2.10.7-33 $P_m + P_b$ Stress Summary (30-Foot Bottom End Drop) – Loading Condition 3

LOADING CONDITION 3: -40°F Ambient Temperature and No Decay Heat Load

Section	Node to Node	S_X	S_Y	S_Z	S_{XY}	SI
A	177 - 327	-3.42	1.47	1.47	0.41	4.96
B	4 - 104	-4.73	-1.47	-1.45	0.40	3.35
C	10 – 110	-4.75	-1.43	-1.29	1.50	4.48
D	185 – 335	-8.83	1.55	1.16	2.22	11.29
E	18 – 118	-20.14	-0.60	-2.85	2.62	20.23
F	143 – 150	0.08	-19.42	-2.13	-1.39	19.70
G	335 – 340	-5.11	-5.41	0.81	-0.47	6.56
H	346 – 350	0.08	-8.13	-0.82	0.10	8.21
I	621 – 624	0.12	-8.99	-1.30	0.24	9.13
J	635 – 638	0.00	-7.03	-0.12	-0.01	7.03
K	841 – 844	-0.01	-7.36	-0.87	-0.04	7.34
L	855 – 858	0.00	-6.39	0.00	0.00	6.40
M	941 – 944	-0.01	-6.80	-1.87	0.00	6.78
N	955 – 958	0.00	-5.86	0.00	0.00	5.86
O	1101 – 1104	-0.01	-5.91	-3.46	0.00	5.90
P	1115 – 1118	0.00	-4.97	0.00	0.00	4.97
Q	1261 – 1264	-0.01	-5.03	-5.05	0.00	5.03
R	1275 – 1278	0.00	-4.09	0.00	0.00	4.09
S	1561 – 1564	0.01	-3.85	-6.08	-0.07	6.10
T	1575 – 1578	0.00	-3.34	0.03	0.01	3.37
U	1841 – 1846	0.06	-4.16	-2.04	0.36	4.29
V	1852 – 1856	0.07	-3.50	-0.65	0.13	3.58
W	1969 – 1976	-0.01	-1.47	-0.29	-0.12	1.48
X	2370 – 2570	-0.59	0.02	-0.03	-0.08	0.63
Y	2305 – 2565	-0.01	0.02	0.01	-0.04	0.08
Z	2301 - 2561	-0.01	0.00	0.02	0.00	0.02

Table 2.10.7-34 P_m Stress Summary (30-Foot Top End Drop) – Loading Condition 1

LOADING CONDITION 1: 130°F Ambient Temperature and Maximum Decay Heat Load

Section	Node to Node	S_X	S_Y	S_Z	S_{XY}	SI
A	177 - 327	-0.06	-0.20	-0.20	0.02	0.14
B	4 - 104	-0.05	1.35	1.34	-0.04	1.41
C	10 – 110	-0.96	1.39	1.70	-0.81	2.91
D	185 – 335	-2.42	-0.20	-0.32	0.76	2.69
E	18 – 118	3.42	1.02	3.52	-2.23	5.06
F	143 – 150	-2.34	2.43	1.38	1.32	5.46
G	335 – 340	-0.11	-1.73	1.65	-0.40	3.47
H	346 – 350	-1.87	1.69	1.73	-0.33	3.64
I	621 – 624	0.00	-4.69	-0.19	0.14	4.70
J	635 – 638	0.00	2.47	0.27	0.03	2.46
K	841 – 844	-0.02	-5.13	0.44	0.02	5.57
L	855 – 858	0.00	2.03	0.00	0.00	2.03
M	941 – 944	-0.03	-5.67	0.44	0.00	6.11
N	955 – 958	0.00	1.49	0.00	0.00	1.50
O	1101 – 1104	-0.03	-6.55	0.44	0.00	7.00
P	1115 – 1118	0.00	0.61	0.00	0.00	0.61
Q	1261 – 1264	-0.03	-7.43	0.47	0.00	7.91
R	1275 – 1278	-0.01	-0.28	-0.10	0.00	0.27
S	1561 – 1564	0.02	-8.29	-0.70	-0.22	8.32
T	1575 – 1578	0.00	-1.13	0.35	-0.04	1.48
U	1841 – 1846	-0.23	-4.69	0.73	0.55	5.48
V	1852 – 1856	-1.43	-1.80	1.55	0.03	3.35
W	1969 – 1976	0.37	-3.95	0.29	-0.20	4.34
X	2370 – 2570	-4.28	-0.22	0.01	-1.02	4.54
Y	2305 – 2565	-3.45	-0.16	-0.21	-0.43	3.40
Z	2301 - 2561	-3.26	0.00	-0.14	0.00	3.26

Table 2.10.7-35 $P_m + P_b$ Stress Summary (30-Foot Top End Drop) – Loading Condition 1

LOADING CONDITION 1: 130°F Ambient Temperature and Maximum Decay Heat Load

Section	Node to Node	S_X	S_Y	S_Z	S_{XY}	SI
A	177 - 327	-0.01	-0.20	-0.20	0.02	0.20
B	4 - 104	-0.21	1.35	1.34	-0.04	1.56
C	10 – 110	-1.71	1.39	1.70	-0.81	3.61
D	185 – 335	-6.70	-0.20	-0.32	0.76	6.67
E	18 – 118	9.55	1.02	3.52	-2.23	9.62
F	143 – 150	-7.67	6.60	1.37	1.32	14.52
G	335 – 340	-1.76	-5.05	0.40	-0.40	5.50
H	346 – 350	-0.18	6.27	4.03	-0.33	6.49
I	621 – 624	0.08	-5.54	-0.31	0.14	5.62
J	635 – 638	0.00	3.41	0.42	0.03	3.42
K	841 – 844	-0.05	-5.34	0.27	0.02	5.60
L	855 – 858	0.00	2.26	0.24	0.00	2.26
M	941 – 944	-0.05	-5.94	0.21	0.00	6.14
N	955 – 958	0.00	1.80	0.30	0.00	1.80
O	1101 – 1104	-0.05	-6.82	0.21	0.00	7.03
P	1115 – 1118	0.00	0.94	0.32	0.00	0.94
Q	1261 – 1264	-0.05	-7.64	0.30	0.00	7.94
R	1275 – 1278	0.00	-0.63	-0.35	0.00	0.63
S	1561 – 1564	0.12	-9.50	-0.89	-0.22	9.64
T	1575 – 1578	0.01	-2.28	0.20	-0.04	2.48
U	1841 – 1846	-0.11	-6.10	0.36	0.55	6.51
V	1852 – 1856	-3.44	-5.84	-0.38	0.03	5.36
W	1969 – 1976	0.02	-4.40	0.51	-0.20	4.92
X	2370 – 2570	-4.84	-0.22	0.01	-1.02	5.07
Y	2305 – 2565	-4.82	-0.16	-0.21	-0.43	4.74
Z	2301 - 2561	-4.79	0.00	-0.14	0.00	4.79

Table 2.10.7-36 P_m Stress Summary (30-Foot Top End Drop) – Loading Condition 2

LOADING CONDITION 2: -40°F Ambient Temperature and Maximum Decay Heat Load

Section	Node to Node	S_X	S_Y	S_Z	S_{XY}	SI
A	177 - 327	-0.15	-1.64	-1.64	0.04	1.50
B	4 - 104	-0.16	-0.49	-0.49	-0.09	0.38
C	10 – 110	-0.36	-0.32	0.56	-0.48	1.38
D	185 – 335	-1.87	-1.43	-0.96	0.51	1.25
E	18 – 118	0.91	0.06	2.21	-0.82	2.66
F	143 – 150	-1.12	0.77	1.69	0.70	3.04
G	335 – 340	-2.64	-3.14	-0.92	0.33	2.38
H	346 – 350	-2.05	0.79	1.95	-0.54	4.10
I	621 – 624	0.02	-8.27	-0.89	0.18	8.30
J	635 – 638	0.00	1.25	0.43	0.04	1.25
K	841 – 844	-0.01	-8.71	0.10	0.01	8.81
L	855 – 858	0.00	0.81	0.00	0.00	0.81
M	941 – 944	-0.01	-9.25	0.10	0.00	9.35
N	955 – 958	-0.01	0.28	0.00	0.00	0.28
O	1101 – 1104	-0.01	-10.13	0.11	0.00	10.24
P	1115 – 1118	0.00	-0.61	0.00	0.00	0.61
Q	1261 – 1264	-0.01	-11.02	-0.10	0.00	11.01
R	1275 – 1278	-0.02	-1.51	-0.20	0.00	1.48
S	1561 – 1564	0.04	-11.87	-1.44	-0.30	11.93
T	1575 – 1578	0.00	-2.35	0.53	-0.03	2.88
U	1841 – 1846	-0.48	-6.05	-0.39	0.20	5.67
V	1852 – 1856	-1.74	-2.62	1.84	0.23	4.52
W	1969 – 1976	0.27	-3.94	0.38	-0.21	4.32
X	2370 – 2570	-4.27	-0.30	0.03	-1.03	4.55
Y	2305 – 2565	-3.43	-0.21	-0.28	-0.44	3.34
Z	2301 - 2561	-3.21	0.00	-0.18	0.00	3.21

Table 2.10.7-37 $P_m + P_b$ Stress Summary (30-Foot Top End Drop) – Loading Condition 2

LOADING CONDITION 2: -40°F Ambient Temperature and Maximum Decay Heat Load

Section	Node to Node	S_X	S_Y	S_Z	S_{XY}	SI
A	177 - 327	-0.02	-1.64	-1.64	0.04	1.62
B	4 - 104	-0.02	-0.49	-0.49	-0.09	0.51
C	10 – 110	-0.67	-0.32	0.56	-0.48	1.56
D	185 – 335	-6.21	-1.43	-0.96	0.51	5.31
E	18 – 118	0.04	0.06	2.21	-0.82	2.99
F	143 – 150	-3.24	0.51	0.66	0.70	4.02
G	335 – 340	-4.44	-5.12	-1.91	0.33	3.35
H	346 – 350	-0.23	6.01	4.87	-0.54	6.34
I	621 – 624	0.11	-9.00	-0.82	0.18	9.12
J	635 – 638	-0.01	2.50	0.56	0.04	2.51
K	841 – 844	-0.01	-8.93	-0.11	0.01	8.92
L	855 – 858	0.00	1.14	0.37	0.00	1.14
M	941 – 944	-0.01	-9.52	-0.16	0.00	9.51
N	955 – 958	0.00	0.67	0.41	0.00	0.67
O	1101 – 1104	-0.01	-10.41	-0.16	0.00	10.40
P	1115 – 1118	0.00	-1.03	-0.42	0.00	1.03
Q	1261 – 1264	0.00	-11.37	-0.39	0.00	11.37
R	1275 – 1278	0.00	-2.17	-0.67	0.00	2.17
S	1561 – 1564	0.17	-13.22	-1.52	-0.30	13.40
T	1575 – 1578	0.02	-3.75	0.43	-0.03	4.18
U	1841 – 1846	-0.08	-7.57	-1.01	0.20	7.50
V	1852 – 1856	-4.13	-7.44	-0.71	0.23	6.74
W	1969 – 1976	0.01	-4.33	0.80	-0.21	5.14
X	2370 – 2570	-4.84	-0.30	0.03	-1.03	5.10
Y	2305 – 2565	-4.82	-0.21	-0.28	-0.44	4.69
Z	2301 - 2561	-4.79	0.00	-0.18	0.00	4.79

Table 2.10.7-38 P_m Stress Summary (30-Foot Side Drop) – Loading Condition 1

LOADING CONDITION 1: 100°F Ambient Temperature and Maximum Decay Heat Load

Section	Node to Node	S_X	S_Y	S_Z	S_{XY}	SI
A	177 - 327	-7.70	-1.71	1.90	-0.46	9.64
B	4 - 104	-6.52	-1.60	0.11	-0.89	6.79
C	10 – 110	-7.99	-0.43	-2.04	0.44	7.61
D	185 – 335	-8.94	-0.19	-3.00	-0.36	8.78
E	18 – 118	-9.09	1.24	-5.45	-0.07	10.32
F	143 – 150	-4.72	0.37	-9.86	-0.80	10.35
G	335 – 340	-5.06	-1.34	-2.30	0.85	4.09
H	346 – 350	-6.40	6.28	-11.46	-0.50	17.76
I	621 – 624	-0.16	5.08	2.22	-0.06	5.23
J	635 – 638	-0.14	14.95	2.52	-0.12	15.08
K	841 – 844	-0.17	18.35	1.15	0.03	18.51
L	855 – 858	-0.04	34.99	1.94	-0.02	35.03
M	941 – 944	-0.19	27.29	0.90	0.03	27.48
N	955 – 958	-0.07	53.54	2.29	0.01	53.61
O	1101 – 1104	-0.21	31.42	0.56	0.00	31.63
P	1115 – 1118	-0.10	65.09	2.67	0.00	65.18
Q	1261 – 1264	-0.17	28.95	1.12	-0.01	29.12
R	1275 – 1278	-0.09	53.03	2.05	0.00	53.13
S	1561 – 1564	-0.17	8.21	2.45	0.12	8.39
T	1575 – 1578	-0.14	24.25	2.83	0.06	24.39
U	1841 – 1846	0.51	0.49	2.13	-0.18	1.81
V	1852 – 1856	4.77	14.30	-1.86	-2.58	16.81
W	1969 – 1976	20.74	3.86	-9.26	-3.37	25.51
X	2370 – 2570	-3.97	-1.82	0.18	1.06	4.59
Y	2305 – 2565	-3.07	-0.06	1.14	0.53	4.29
Z	2301 - 2561	-2.26	0.16	1.36	2.22	5.06

Table 2.10.7-39 $P_m + P_b$ Stress Summary (30-Foot Side Drop) – Loading Condition 1

LOADING CONDITION 1: 100°F Ambient Temperature and Maximum Decay Heat Load

Section	Node to Node	S_X	S_Y	S_Z	S_{XY}	SI
A	177 - 327	-16.88	-3.68	0.56	-3.01	18.10
B	4 - 104	-10.00	-3.37	-3.11	-1.31	7.14
C	10 – 110	-11.24	-0.89	-5.07	0.01	10.36
D	185 – 335	-13.80	-1.54	-5.90	-0.01	12.26
E	18 – 118	-8.66	2.96	-6.08	-0.84	11.75
F	143 – 150	-1.94	7.18	-3.59	-0.80	10.85
G	335 – 340	-9.47	-4.30	-4.96	0.85	5.45
H	346 – 350	-5.16	16.66	-5.20	-0.50	21.87
I	621 – 624	-0.11	6.23	2.33	-0.06	6.34
J	635 – 638	-0.03	19.66	2.20	-0.12	19.69
K	841 – 844	-0.07	19.82	2.32	-0.03	19.88
L	855 – 858	0.04	36.61	1.34	-0.02	36.57
M	941 – 944	-0.11	29.12	2.15	0.03	29.23
N	955 – 958	0.02	56.00	2.10	0.01	55.98
O	1101 – 1104	-0.15	33.42	1.80	0.00	33.57
P	1115 – 1118	0.02	68.25	3.06	0.00	68.23
Q	1261 – 1264	-0.08	30.88	2.38	-0.01	30.96
R	1275 – 1278	0.03	55.93	3.42	0.00	55.91
S	1561 – 1564	-0.15	9.98	3.22	0.12	10.13
T	1575 – 1578	0.01	28.32	4.68	0.06	28.31
U	1841 – 1846	-0.15	0.09	2.90	-0.18	3.15
V	1852 – 1856	10.17	18.66	1.89	-2.58	17.50
W	1969 – 1976	-42.95	-14.16	-10.81	-3.37	32.53
X	2370 – 2570	-11.33	-4.07	1.38	1.72	10.34
Y	2305 – 2565	-2.48	-0.39	1.60	1.55	4.90
Z	2301 - 2561	-1.60	0.12	1.68	8.10	16.29

Table 2.10.7-40 P_m Stress Summary (30-Foot Top Corner Drop) – Loading Condition 1 – Drop Orientation = 15.74 Degrees

LOADING CONDITION 1: 130°F Ambient Temperature and Maximum Decay Heat Load

Section	Node to Node	S_X	S_Y	S_Z	S_{XY}	SI
A	177 - 327	-2.60	-0.76	0.43	-0.13	3.04
B	4 - 104	-2.20	0.78	1.34	-0.33	3.57
C	10 – 110	-3.57	1.21	0.98	-0.64	4.94
D	185 – 335	-5.30	-0.26	-1.30	0.62	5.19
E	18 – 118	0.32	1.40	1.62	-2.19	4.50
F	143 – 150	-3.83	2.48	-1.92	1.02	6.63
G	335 – 340	-1.78	-2.12	0.84	-0.11	2.99
H	346 – 350	-3.93	3.71	-2.10	-0.49	7.70
I	621 – 624	-0.05	-2.87	0.55	0.12	3.43
J	635 – 638	-0.05	7.33	1.09	-0.01	7.38
K	841 – 844	-0.04	6.62	0.63	0.02	6.67
L	855 – 858	-0.01	12.34	0.65	-0.01	12.36
M	941 – 944	-0.05	6.88	0.63	0.00	6.93
N	955 – 958	-0.02	14.31	0.77	0.00	14.33
O	1101 – 1104	-0.06	3.09	0.38	0.00	3.15
P	1115 – 1118	-0.03	11.28	0.97	0.00	11.31
Q	1261 – 1264	-0.05	-3.17	0.63	-0.01	3.80
R	1275 – 1278	-0.02	-0.22	0.77	-0.01	0.99
S	1561 – 1564	0.12	-17.16	-2.01	-0.63	17.32
T	1575 – 1578	-0.05	-18.80	2.21	0.06	21.01
U	1841 – 1846	4.10	-9.86	10.67	0.76	20.57
V	1852 – 1856	2.83	-17.30	3.48	0.29	20.79
W	1969 – 1976	-8.81	-11.00	-5.01	0.27	6.02
X	2370 – 2570	-13.77	-2.99	-1.97	-2.99	12.57
Y	2305 – 2565	-9.19	-3.39	-0.50	-1.53	9.07
Z	2301 - 2561	-2.97	0.00	0.34	0.00	3.31

Table 2.10.7-41 $P_m + P_b$ Stress Summary (30-Foot Top Corner Drop) – Loading Condition 1 – Drop Orientation = 15.74 Degrees

LOADING CONDITION 1: 130°F Ambient Temperature and Maximum Decay Heat Load

Section	Node to Node	S_X	S_Y	S_Z	S_{XY}	SI
A	177 - 327	-5.58	-1.41	-0.01	-0.97	5.79
B	4 - 104	-3.50	0.20	0.27	-0.47	3.84
C	10 – 110	-5.37	1.05	-0.02	-0.78	6.61
D	185 – 335	-11.05	-0.70	-2.26	0.73	10.45
E	18 – 118	6.41	1.97	1.41	-2.44	6.60
F	143 – 150	-8.08	8.77	0.14	1.02	16.97
G	335 – 340	-4.83	-6.32	-1.25	-0.11	5.08
H	346 – 350	-1.88	11.58	2.19	-0.49	13.49
I	621 – 624	0.04	-3.32	0.47	0.12	3.79
J	635 – 638	-0.01	9.80	1.13	-0.01	9.81
K	841 – 844	-0.01	7.03	0.73	0.02	7.04
L	855 – 858	0.02	12.82	0.69	-0.01	12.80
M	941 – 944	-0.01	7.31	0.74	0.00	7.32
N	955 – 958	0.00	14.88	0.80	0.00	14.88
O	1101 – 1104	-0.04	3.33	0.48	0.00	3.37
P	1115 – 1118	0.00	11.76	0.86	0.00	11.76
Q	1261 – 1264	-0.02	-3.19	0.68	-0.01	3.86
R	1275 – 1278	-0.04	-0.11	1.31	-0.01	1.43
S	1561 – 1564	0.33	-22.71	-4.58	-0.63	23.07
T	1575 – 1578	0.02	-19.71	1.68	0.06	21.39
U	1841 – 1846	0.22	-18.32	8.31	0.76	26.66
V	1852 – 1856	0.59	-24.92	-0.15	0.29	25.53
W	1969 – 1976	-19.45	-11.87	-6.68	0.27	12.78
X	2370 – 2570	-14.60	-2.99	-1.97	-2.99	13.35
Y	2305 – 2565	-14.54	-3.39	-0.50	-1.53	14.25
Z	2301 - 2561	-6.27	0.00	0.34	0.00	6.61

Table 2.10.7-42 P_m Stress Summary (30-Foot Top Oblique Drop) – Loading Condition 1 – Drop Orientation = 30 Degrees

LOADING CONDITION 1: 130°F Ambient Temperature and Maximum Decay Heat Load

Section	Node to Node	S_X	S_Y	S_Z	S_{XY}	SI
A	177 - 327	-4.26	-1.09	0.88	-0.24	5.16
B	4 - 104	-3.61	0.18	1.11	-0.52	4.79
C	10 – 110	-5.12	0.86	0.22	-0.40	6.03
D	185 – 335	-6.79	-0.26	-1.89	0.40	6.58
E	18 – 118	-2.29	1.48	-0.22	-1.79	5.19
F	143 – 150	-4.42	2.11	-4.31	0.60	6.64
G	335 – 340	-2.85	-2.09	0.04	0.15	2.92
H	346 – 350	-4.97	4.76	-4.91	-0.53	9.79
I	621 – 624	-0.09	-0.90	1.07	0.08	1.98
J	635 – 638	-0.08	10.12	1.59	-0.04	10.19
K	841 – 844	-0.06	11.68	0.82	0.02	11.74
L	855 – 858	-0.03	22.04	1.08	-0.02	22.07
M	941 – 944	-0.07	14.41	0.82	0.00	14.48
N	955 – 958	-0.04	28.32	1.29	0.00	28.36
O	1101 – 1104	-0.09	11.83	0.40	0.00	11.92
P	1115 – 1118	-0.05	28.16	1.61	0.00	28.22
Q	1261 – 1264	-0.06	5.09	0.81	-0.01	5.16
R	1275 – 1278	-0.04	14.22	1.24	-0.01	14.26
S	1561 – 1564	0.09	-13.96	-1.35	-0.57	14.10
T	1575 – 1578	-0.09	-10.61	3.06	0.05	13.67
U	1841 – 1846	4.53	-8.94	11.08	0.63	20.05
V	1852 – 1856	3.59	-12.06	3.52	-0.21	15.66
W	1969 – 1976	-15.57	-8.28	-7.84	-0.45	7.75
X	2370 – 2570	-13.23	-5.19	-1.47	-3.94	13.37
Y	2305 – 2565	-8.83	-6.21	0.27	-2.93	11.00
Z	2301 - 2561	-2.30	0.00	0.69	0.00	2.99

Table 2.10.7-43 $P_m + P_b$ Stress Summary (30-Foot Top Oblique Drop) – Loading Condition 1 – Drop Orientation = 30 Degrees

LOADING CONDITION 1: 130°F Ambient Temperature and Maximum Decay Heat Load

Section	Node to Node	S_X	S_Y	S_Z	S_{XY}	SI
A	177 - 327	-9.24	-2.17	0.15	-1.63	9.75
B	4 - 104	-5.63	-0.78	-0.65	-0.75	5.10
C	10 – 110	-7.49	0.60	-1.44	-0.63	8.19
D	185 – 335	-12.81	-1.00	-3.48	0.59	11.87
E	18 – 118	2.76	2.42	-0.56	-2.21	5.37
F	143 – 150	-7.08	9.11	-0.89	0.60	16.23
G	335 – 340	-6.56	-6.32	-2.40	0.15	4.23
H	346 – 350	-2.96	14.03	0.32	-0.53	17.03
I	621 – 624	0.00	-0.94	1.03	0.08	1.98
J	635 – 638	-0.02	13.43	1.53	-0.04	13.45
K	841 – 844	-0.01	12.43	1.05	0.02	12.44
L	855 – 858	0.03	22.99	1.13	-0.02	22.96
M	941 – 944	-0.02	15.29	1.05	0.00	15.31
N	955 – 958	0.01	29.53	1.33	0.00	29.52
O	1101 – 1104	-0.07	12.56	0.63	0.00	12.62
P	1115 – 1118	0.01	29.43	1.63	0.00	29.43
Q	1261 – 1264	-0.02	5.54	0.99	-0.01	5.57
R	1275 – 1278	0.00	14.87	1.14	-0.01	14.87
S	1561 – 1564	0.29	-18.93	-3.81	-0.57	19.25
T	1575 – 1578	-0.22	-10.60	3.23	0.05	13.83
U	1841 – 1846	0.24	-17.83	8.54	0.63	26.40
V	1852 – 1856	0.69	-19.48	-0.59	-0.21	20.18
W	1969 – 1976	-34.13	-16.38	-11.80	-0.45	22.34
X	2370 – 2570	-12.73	-5.19	-1.47	-3.94	12.94
Y	2305 – 2565	-12.65	-6.21	0.27	-2.93	14.06
Z	2301 - 2561	-5.33	0.00	0.69	0.00	6.02

Table 2.10.7-44 P_m Stress Summary (30-Foot Top Oblique Drop) – Loading Condition 1 – Drop Orientation = 45 Degrees

LOADING CONDITION 1: 130°F Ambient Temperature and Maximum Decay Heat Load

Section	Node to Node	S_X	S_Y	S_Z	S_{XY}	SI
A	177 - 327	-4.84	-1.17	1.08	-0.28	5.94
B	4 - 104	-4.09	-0.30	0.76	-0.58	4.94
C	10 – 110	-5.48	0.45	-0.39	-0.14	5.94
D	185 – 335	-6.83	-0.22	-2.04	0.17	6.62
E	18 – 118	-3.90	1.30	-1.58	-1.20	5.73
F	143 – 150	-4.16	1.49	-5.44	0.18	6.93
G	335 – 340	-3.21	-1.73	-0.58	0.32	2.70
H	346 – 350	-4.96	4.79	-6.26	-0.48	11.07
I	621 – 624	-0.10	0.75	1.29	0.03	1.39
J	635 – 638	-0.09	10.61	1.71	-0.06	10.69
K	841 – 844	-0.08	13.63	0.87	0.02	13.71
L	855 – 858	-0.03	25.74	1.23	-0.02	25.77
M	941 – 944	-0.09	17.75	0.87	0.00	17.84
N	955 – 958	-0.05	34.21	1.47	0.00	34.25
O	1101 – 1104	-0.12	16.45	0.40	0.00	16.57
P	1115 – 1118	-0.06	36.16	1.82	0.00	36.22
Q	1261 – 1264	-0.08	10.41	0.85	-0.01	10.49
R	1275 – 1278	-0.05	22.61	1.38	-0.01	22.66
S	1561 – 1564	0.05	-9.41	-0.55	-0.45	9.50
T	1575 – 1578	-0.11	-2.53	3.14	0.04	5.67
U	1841 – 1846	4.45	-7.11	10.98	0.40	18.10
V	1852 – 1856	3.78	-5.81	2.67	-0.56	9.66
W	1969 – 1976	-21.29	-4.86	-9.21	-1.60	16.73
X	2370 – 2570	-12.11	-6.71	-0.63	-4.01	13.61
Y	2305 – 2565	-7.72	-7.87	1.25	-3.44	12.49
Z	2301 - 2561	-1.44	0.00	1.29	0.00	2.73

Table 2.10.7-45 $P_m + P_b$ Stress Summary (30-Foot Top Oblique Drop) – Loading Condition 1 – Drop Orientation = 45 Degrees

LOADING CONDITION 1: 130°F Ambient Temperature and Maximum Decay Heat Load

Section	Node to Node	S_X	S_Y	S_Z	S_{XY}	SI
A	177 - 327	-10.54	-2.40	0.25	-1.87	11.19
B	4 - 104	-6.35	-1.40	-1.25	-0.84	5.24
C	10 – 110	-7.90	0.16	-2.28	-0.41	8.10
D	185 – 335	-12.08	-1.06	-3.85	0.39	11.04
E	18 – 118	-0.47	2.37	-1.97	-1.68	5.13
F	143 – 150	-5.18	7.89	-1.53	0.18	13.07
G	335 – 340	-6.82	-5.29	-2.89	0.32	4.00
H	346 – 350	-3.31	13.64	-1.16	-0.48	16.98
I	621 – 624	-0.03	1.02	1.29	0.03	1.32
J	635 – 638	-0.02	14.03	1.59	-0.06	14.05
K	841 – 844	-0.02	14.57	1.31	0.02	14.58
L	855 – 858	0.04	26.88	1.28	-0.02	26.84
M	941 – 944	-0.03	18.87	1.33	0.00	18.90
N	955 – 958	0.01	35.69	1.52	0.00	35.68
O	1101 – 1104	-0.09	17.47	0.84	0.00	17.55
P	1115 – 1118	0.01	37.83	2.00	0.00	37.82
Q	1261 – 1264	-0.03	11.18	1.26	-0.01	11.21
R	1275 – 1278	0.01	23.77	1.78	-0.01	23.76
S	1561 – 1564	0.21	-13.28	-2.79	-0.45	13.52
T	1575 – 1578	-0.24	-3.43	2.82	0.04	6.25
U	1841 – 1846	0.22	-15.21	9.12	0.40	24.33
V	1852 – 1856	0.69	-11.86	-1.35	-0.56	12.60
W	1969 – 1976	-46.39	-19.15	-13.50	-1.60	32.98
X	2370 – 2570	-10.95	-6.71	-0.63	-4.01	12.73
Y	2305 – 2565	-10.90	-7.87	1.25	-3.44	14.40
Z	2301 - 2561	-3.97	0.00	1.29	0.00	5.27

Table 2.10.7-46 P_m Stress Summary (30-Foot Top Oblique Drop) – Loading Condition 1 – Drop Orientation = 60 Degrees

LOADING CONDITION 1: 130°F Ambient Temperature and Maximum Decay Heat Load

Section	Node to Node	S_X	S_Y	S_Z	S_{XY}	SI
A	177 - 327	-5.99	-1.40	1.40	-0.35	7.41
B	4 - 104	-5.07	-0.74	0.58	-0.70	5.76
C	10 – 110	-6.55	0.18	-0.95	0.04	6.73
D	185 – 335	-7.82	-0.22	-2.44	0.00	7.60
E	18 – 118	-5.78	1.34	-2.92	-0.88	7.33
F	143 – 150	-4.52	1.19	-7.13	-0.13	8.32
G	335 – 340	-3.96	-1.68	-1.17	0.51	2.90
H	346 – 350	-5.65	5.49	-8.24	-0.51	13.76
I	621 – 624	-0.12	2.20	1.65	0.01	2.33
J	635 – 638	-0.11	12.50	2.05	-0.08	12.61
K	841 – 844	-0.12	17.17	0.99	0.02	17.28
L	855 – 858	-0.04	32.55	1.53	-0.03	32.59
M	941 – 944	-0.13	23.09	0.98	0.00	23.21
N	955 – 958	-0.06	44.12	1.82	0.00	44.18
O	1101 – 1104	-0.16	22.78	0.40	0.00	22.95
P	1115 – 1118	-0.08	48.26	2.25	0.00	48.34
Q	1261 – 1264	-0.12	16.56	0.97	-0.01	16.68
R	1275 – 1278	-0.07	33.36	1.68	0.00	33.43
S	1561 – 1564	0.01	-6.35	0.06	-0.39	6.43
T	1575 – 1578	-0.15	5.18	3.53	0.03	5.33
U	1841 – 1846	4.88	-6.27	11.92	0.21	18.20
V	1852 – 1856	4.46	-0.13	1.97	-1.03	5.02
W	1969 – 1976	-31.03	-1.79	-12.13	-3.28	29.96
X	2370 – 2570	-12.10	-9.19	0.30	-4.82	15.99
Y	2305 – 2565	-7.40	-10.47	2.41	-4.52	16.11
Z	2301 - 2561	-0.93	0.00	1.95	0.00	2.89

Table 2.10.7-47 $P_m + P_b$ Stress Summary (30-Foot Top Oblique Drop) – Loading Condition 1 – Drop Orientation = 60 Degrees

LOADING CONDITION 1: 130°F Ambient Temperature and Maximum Decay Heat Load

Section	Node to Node	S_X	S_Y	S_Z	S_{XY}	SI
A	177 - 327	-13.09	-2.93	0.36	-2.33	13.95
B	4 - 104	-7.83	-2.11	-1.91	-1.03	6.09
C	10 – 110	-9.34	-0.18	-3.30	-0.29	9.19
D	185 – 335	-13.17	-1.27	-4.69	0.27	11.92
E	18 – 118	-3.18	2.67	-3.41	-1.48	6.55
F	143 – 150	-4.34	8.01	-2.28	-0.13	12.35
G	335 – 340	-7.99	-5.20	-3.70	0.51	4.39
H	346 – 350	-4.07	15.23	-2.54	-0.51	19.32
I	621 – 624	-0.06	2.78	1.69	0.01	2.83
J	635 – 638	-0.02	16.50	1.86	-0.08	16.52
K	841 – 844	-0.04	18.41	1.75	0.02	18.45
L	855 – 858	0.04	34.03	1.59	-0.03	33.98
M	941 – 944	-0.06	24.59	1.79	0.00	24.65
N	955 – 958	0.01	46.06	1.89	0.00	46.05
O	1101 – 1104	-0.12	24.21	1.18	0.00	24.34
P	1115 – 1118	0.01	50.51	2.64	0.00	50.50
Q	1261 – 1264	-0.06	17.74	1.72	-0.01	17.80
R	1275 – 1278	0.02	35.19	2.81	0.00	35.17
S	1561 – 1564	0.16	-9.42	-1.80	-0.39	9.61
T	1575 – 1578	0.01	7.20	4.66	0.03	7.19
U	1841 – 1846	0.24	-14.53	10.39	0.21	24.92
V	1852 – 1856	0.78	-5.40	-2.35	-1.03	6.51
W	1969 – 1976	-66.74	-24.51	-16.52	-3.28	50.48
X	2370 – 2570	7.81	-9.19	0.30	-4.82	19.54
Y	2305 – 2565	-9.99	-10.47	2.41	-4.52	17.16
Z	2301 - 2561	-3.06	0.00	1.95	0.00	5.02

Table 2.10.7-48 P_m Stress Summary (30-Foot Top Corner Drop) – Loading Condition 3 – Drop Orientation = 15.74 Degrees

LOADING CONDITION 3: -40°F Ambient Temperature and No Decay Heat Load

Section	Node to Node	S_X	S_Y	S_Z	S_{XY}	SI
A	177 - 327	-2.69	-2.16	-0.96	-0.11	1.75
B	4 - 104	-2.31	-1.00	-0.44	-0.38	1.97
C	10 – 110	-2.99	-0.45	-0.13	-0.32	2.90
D	185 – 335	-4.76	-1.45	-1.92	0.38	3.40
E	18 – 118	-2.12	0.47	0.35	-0.82	3.06
F	143 – 150	-2.64	0.87	-1.61	0.41	3.61
G	335 – 340	-4.23	-3.49	-1.65	0.60	2.91
H	346 – 350	-4.10	2.84	-1.89	-0.69	7.07
I	621 – 624	-0.03	-6.35	-0.13	0.15	6.32
J	635 – 638	-0.05	6.15	1.25	0.00	6.19
K	841 – 844	-0.01	6.53	0.12	0.00	6.54
L	855 – 858	-0.01	11.68	0.60	-0.01	11.70
M	941 – 944	-0.01	5.68	0.12	0.00	5.69
N	955 – 958	-0.02	13.34	0.74	0.00	13.36
O	1101 – 1104	-0.01	2.07	0.12	0.00	2.08
P	1115 – 1118	-0.02	10.30	0.82	0.00	10.32
Q	1261 – 1264	-0.01	-4.19	0.12	-0.01	4.31
R	1275 – 1278	-0.02	-0.30	0.73	-0.01	1.04
S	1561 – 1564	0.14	-13.57	-2.03	-0.54	13.75
T	1575 – 1578	-0.03	-17.64	2.17	0.06	19.82
U	1841 – 1846	4.75	-8.10	11.71	1.28	19.93
V	1852 – 1856	2.65	-16.36	3.83	0.16	20.19
W	1969 – 1976	-8.10	-10.30	-4.63	0.40	5.74
X	2370 – 2570	-11.88	-2.78	-2.20	-3.78	11.84
Y	2305 – 2565	-6.48	-3.04	-0.36	-1.52	6.69
Z	2301 - 2561	-1.96	0.00	0.27	0.00	2.23

Table 2.10.7-49 $P_m + P_b$ Stress Summary (30-Foot Top Corner Drop) – Loading Condition 3 – Drop Orientation = 15.74 Degrees

LOADING CONDITION 3: -40°F Ambient Temperature and No Decay Heat Load

Section	Node to Node	S_X	S_Y	S_Z	S_{XY}	SI
A	177 - 327	-5.59	-2.81	-1.41	-0.95	4.48
B	4 - 104	-3.32	-1.59	-1.50	-0.52	2.02
C	10 – 110	-4.36	-0.60	-1.13	-0.46	3.87
D	185 – 335	-10.58	-1.90	-2.88	0.49	8.74
E	18 – 118	-2.82	1.04	0.14	-1.07	4.41
F	143 – 150	-3.78	2.86	-0.54	0.41	6.70
G	335 – 340	-7.43	-6.39	-3.49	0.60	4.22
H	346 – 350	-1.93	11.33	3.01	-0.69	13.32
I	621 – 624	0.07	-6.67	-0.03	0.15	6.75
J	635 – 638	-0.02	8.91	1.27	0.00	8.93
K	841 – 844	0.00	6.85	0.12	0.00	6.85
L	855 – 858	0.02	12.10	0.64	-0.01	12.08
M	941 – 944	0.00	5.97	0.12	0.00	5.98
N	955 – 958	0.00	13.85	0.77	0.00	13.84
O	1101 – 1104	0.00	2.22	0.12	0.00	2.22
P	1115 – 1118	0.00	10.69	0.70	0.00	10.69
Q	1261 – 1264	0.00	-4.32	0.06	-0.01	4.39
R	1275 – 1278	-0.04	-0.18	1.24	-0.01	1.42
S	1561 – 1564	0.29	-18.60	-4.46	-0.54	18.92
T	1575 – 1578	0.03	-18.70	1.63	0.06	20.33
U	1841 – 1846	0.33	-17.50	8.96	1.28	26.55
V	1852 – 1856	0.57	-23.23	0.47	0.16	23.80
W	1969 – 1976	-17.92	-10.68	-6.08	0.40	11.86
X	2370 – 2570	-15.16	-2.78	-2.20	-3.78	14.51
Y	2305 – 2565	-13.41	-3.04	-0.36	-1.52	13.27
Z	2301 - 2561	-5.77	0.00	0.27	0.00	6.05

Table 2.10.7-50 P_m Stress Summary (30-Foot Top Oblique Drop) – Loading Condition 3 – Drop Orientation = 30 Degrees

LOADING CONDITION 3: -40°F Ambient Temperature and No Decay Heat Load

Section	Node to Node	S_X	S_Y	S_Z	S_{XY}	SI
A	177 - 327	-4.33	-2.22	-0.25	-0.22	4.10
B	4 - 104	-3.69	-1.26	-0.32	-0.56	3.49
C	10 – 110	-4.65	-0.49	-0.68	-0.14	4.18
D	185 – 335	-6.36	-1.23	-2.39	0.20	5.15
E	18 – 118	-4.26	0.73	-1.25	-0.68	5.17
F	143 – 150	-3.46	0.81	-4.07	0.11	4.88
G	335 – 340	-4.84	-3.20	-1.98	0.72	3.13
H	346 – 350	-5.11	4.06	-4.74	-0.70	9.27
I	621 – 624	-0.07	-3.71	0.52	0.11	4.23
J	635 – 638	-0.08	9.16	1.72	-0.03	9.24
K	841 – 844	0.00	11.15	0.15	0.00	11.15
L	855 – 858	-0.02	20.26	1.00	-0.02	20.29
M	941 – 944	-0.01	11.94	0.15	0.00	11.95
N	955 – 958	-0.04	25.86	1.23	0.00	25.90
O	1101 – 1104	-0.01	9.51	0.15	0.00	9.52
P	1115 – 1118	-0.04	25.43	1.35	0.00	25.47
Q	1261 – 1264	-0.01	2.63	0.15	-0.01	2.63
R	1275 – 1278	-0.03	12.71	1.18	-0.01	12.74
S	1561 – 1564	0.12	-8.97	-1.34	-0.43	9.13
T	1575 – 1578	-0.07	-10.41	3.03	0.07	13.44
U	1841 – 1846	5.46	-6.32	12.54	1.33	19.01
V	1852 – 1856	3.54	-11.76	3.89	-0.36	15.66
W	1969 – 1976	-14.36	-7.79	-7.31	-0.22	7.05
X	2370 – 2570	-11.45	-4.83	-1.71	-4.49	12.01
Y	2305 – 2565	-6.42	-5.66	0.32	-2.77	9.16
Z	2301 - 2561	-1.48	0.00	0.60	0.00	2.08

Table 2.10.7-51 $P_m + P_b$ Stress Summary (30-Foot Top Oblique Drop) – Loading Condition 3 – Drop Orientation = 30 Degrees

LOADING CONDITION 3: -40°F Ambient Temperature and No Decay Heat Load

Section	Node to Node	S_X	S_Y	S_Z	S_{XY}	SI
A	177 - 327	-9.25	-3.30	-0.98	-1.62	8.68
B	4 - 104	-5.49	-2.23	-2.09	–0.79	3.62
C	10 – 110	-6.67	-0.74	-2.33	-0.37	5.98
D	185 – 335	-12.42	-1.96	-3.98	0.39	10.49
E	18 – 118	-4.71	1.67	-1.59	-1.10	6.74
F	143 – 150	-3.60	4.33	-1.45	0.11	7.94
G	335 – 340	-8.67	-6.37	-4.21	0.72	4.66
H	346 – 350	-3.00	13.83	0.98	-0.70	16.89
I	621 – 624	0.03	-3.66	0.63	0.11	4.29
J	635 – 638	-0.02	12.72	1.64	-0.03	12.74
K	841 – 844	0.00	11.73	0.15	0.00	11.72
L	855 – 858	0.03	21.10	1.05	-0.02	21.07
M	941 – 944	0.00	12.57	0.15	0.00	12.57
N	955 – 958	0.01	26.95	1.27	0.00	26.94
O	1101 – 1104	0.00	10.05	0.15	0.00	10.05
P	1115 – 1118	0.01	26.53	1.36	0.00	26.52
Q	1261 – 1264	0.00	2.84	0.09	-0.01	2.84
R	1275 – 1278	0.00	13.28	1.07	-0.01	13.28
S	1561 – 1564	0.23	-13.23	-3.71	-0.43	13.49
T	1575 – 1578	0.03	-10.65	2.81	0.07	13.46
U	1841 – 1846	0.38	-16.54	9.46	1.33	26.11
V	1852 – 1856	0.69	-18.81	-0.05	-0.36	19.51
W	1969 – 1976	-31.55	-14.73	-10.87	-0.22	20.69
X	2370 – 2570	-11.75	-4.83	-1.73	-4.49	12.25
Y	2305 – 2565	-11.67	-5.66	0.32	-2.77	13.08
Z	2301 - 2561	-4.91	0.00	0.60	0.00	5.51

Table 2.10.7-52 P_m Stress Summary (30-Foot Top Oblique Drop) – Loading Condition 3 – Drop Orientation = 45 Degrees

LOADING CONDITION 3: -40°F Ambient Temperature and No Decay Heat Load

Section	Node to Node	S_X	S_Y	S_Z	S_{XY}	SI
A	177 - 327	-4.88	-1.91	0.34	-0.27	5.24
B	4 - 104	-4.15	-1.25	-0.18	-0.60	4.09
C	10 – 110	-5.17	-0.43	-0.98	0.03	4.74
D	185 – 335	-6.55	-0.86	-2.37	0.04	5.69
E	18 – 118	-5.20	0.80	-2.26	-0.47	6.08
F	143 – 150	-3.52	0.63	-5.28	-0.14	5.91
G	335 – 340	-4.52	-2.46	-1.91	0.70	2.83
H	346 – 350	-5.05	4.33	-6.14	-0.59	10.51
I	621 – 624	-0.09	-1.11	0.93	0.06	2.03
J	635 – 638	-0.09	9.98	1.79	-0.05	10.06
K	841 – 844	0.00	12.84	0.16	0.00	12.84
L	855 – 858	-0.03	23.40	1.14	-0.02	23.42
M	941 – 944	-0.01	14.72	0.16	0.00	14.72
N	955 – 958	-0.04	31.03	1.41	0.00	31.07
O	1101 – 1104	-0.01	13.52	0.16	0.00	13.53
P	1115 – 1118	-0.05	32.56	1.53	0.00	32.61
Q	1261 – 1264	-0.01	7.24	0.16	-0.01	7.25
R	1275 – 1278	-0.05	20.28	1.31	-0.01	20.32
S	1561 – 1564	0.10	-4.17	-0.60	-0.31	4.31
T	1575 – 1578	-0.08	-3.11	3.13	0.06	6.24
U	1841 – 1846	5.49	-4.20	12.47	1.16	16.80
V	1852 – 1856	3.83	-6.08	3.03	-0.70	10.00
W	1969 – 1976	-19.66	-4.60	-8.62	-1.29	15.27
X	2370 – 2570	-10.54	-6.24	-0.87	-4.32	12.34
Y	2305 – 2565	-5.75	-7.20	1.21	-3.18	10.95
Z	2301 - 2561	-0.89	0.00	1.16	0.00	2.05

Table 2.10.7-53 $P_m + P_b$ Stress Summary (30-Foot Top Oblique Drop) – Loading Condition 3 – Drop Orientation = 45 Degrees

LOADING CONDITION 3: -40°F Ambient Temperature and No Decay Heat Load

Section	Node to Node	S_X	S_Y	S_Z	S_{XY}	SI
A	177 - 327	-10.54	-3.14	-0.50	-1.86	10.49
B	4 - 104	-6.25	-2.36	-2.19	-0.86	4.26
C	10 – 110	-7.36	-0.72	-2.87	-0.24	6.66
D	185 – 335	-11.82	-1.70	-4.18	0.26	10.13
E	18 – 118	-5.38	1.88	-2.65	-0.95	7.50
F	143 – 150	-2.89	4.74	-1.90	-0.14	7.63
G	335 – 340	-8.20	-5.33	-4.08	0.70	4.28
H	346 – 350	-3.34	13.50	-0.73	-0.59	16.88
I	621 – 624	-0.01	-0.77	1.03	0.06	1.80
J	635 – 638	-0.02	13.56	1.66	-0.05	13.58
K	841 – 844	0.00	13.52	0.16	0.00	13.52
L	855 – 858	0.03	24.41	1.19	-0.02	24.38
M	941 – 944	0.00	15.50	0.16	0.00	15.50
N	955 – 958	0.01	32.36	1.45	0.00	32.36
O	1101 – 1104	0.00	14.26	0.16	0.00	14.27
P	1115 – 1118	0.01	34.01	1.68	0.00	34.00
Q	1261 – 1264	0.00	7.68	0.11	-0.01	7.68
R	1275 – 1278	0.01	21.31	1.67	-0.01	21.30
S	1561 – 1564	0.15	-7.42	-2.94	-0.31	7.60
T	1575 – 1578	-0.20	-3.71	2.91	0.06	6.62
U	1841 – 1846	0.38	-13.80	9.98	1.16	23.87
V	1852 – 1856	0.70	-12.12	-0.93	-0.70	12.90
W	1969 – 1976	-42.93	-17.26	-12.49	-1.29	30.50
X	2370 – 2570	-10.11	-6.24	-0.87	-4.32	12.04
Y	2305 – 2565	-10.06	-7.20	1.21	-3.18	13.33
Z	2301 - 2561	-3.66	0.00	1.16	0.00	4.82

Table 2.10.7-54 P_m Stress Summary (30-Foot Top Oblique Drop) – Loading Condition 3 – Drop Orientation = 60 Degrees

LOADING CONDITION 3: -40°F Ambient Temperature and No Decay Heat Load

Section	Node to Node	S_X	S_Y	S_Z	S_{XY}	SI
A	177 - 327	-6.02	-1.93	0.87	-0.34	6.92
B	4 - 104	-5.11	-1.42	-0.10	-0.72	5.15
C	10 – 110	-6.33	-0.45	-1.37	0.16	5.88
D	185 – 335	-7.62	-0.68	-2.68	-0.09	6.95
E	18 – 118	-6.71	0.98	-3.41	-0.36	7.72
F	143 – 150	-4.07	0.57	-7.02	-0.36	7.62
G	335 – 340	-4.90	-2.20	-2.12	-0.78	3.12
H	346 – 350	-5.72	5.16	-8.16	-0.59	13.35
I	621 – 624	-0.12	0.88	1.39	0.02	1.51
J	635 – 638	-0.11	12.05	2.11	-0.08	12.16
K	841 – 844	0.00	16.05	0.18	0.00	16.05
L	855 – 858	-0.03	29.41	1.42	-0.02	29.45
M	941 – 944	-0.01	19.16	0.18	0.00	19.17
N	955 – 958	-0.05	39.89	1.74	0.00	39.94
O	1101 – 1104	-0.01	18.94	0.18	0.00	18.94
P	1115 – 1118	-0.06	43.40	1.89	0.00	43.47
Q	1261 – 1264	-0.01	12.37	0.18	-0.01	12.37
R	1275 – 1278	-0.06	29.97	1.60	0.00	30.04
S	1561 – 1564	0.08	-0.19	-0.02	-0.22	0.52
T	1575 – 1578	-0.11	3.77	3.54	0.06	3.89
U	1841 – 1846	6.18	-2.71	13.69	1.13	16.54
V	1852 – 1856	4.60	-0.99	2.39	-1.17	6.06
W	1969 – 1976	-28.67	-1.76	-11.37	-2.82	27.50
X	2370 – 2570	-10.60	-8.54	0.02	-4.93	14.63
Y	2305 – 2565	-5.68	-9.61	2.26	-4.14	14.49
Z	2301 - 2561	-0.54	0.00	1.78	0.00	2.32

Table 2.10.7-55 $P_m + P_b$ Stress Summary (30-Foot Top Oblique Drop) – Loading Condition 3 – Drop Orientation = 60 Degrees

LOADING CONDITION 3: -40°F Ambient Temperature and No Decay Heat Load

Section	Node to Node	S_X	S_Y	S_Z	S_{XY}	SI
A	177 - 327	-13.09	-3.46	-0.17	-2.32	13.45
B	4 - 104	-7.76	-2.79	-2.59	-1.05	5.39
C	10 – 110	-8.96	-0.81	-3.72	-0.17	8.16
D	185 – 335	-12.99	-1.72	-4.93	0.18	11.28
E	18 – 118	-6.70	2.32	-3.89	-0.95	9.21
F	143 – 150	-2.70	5.75	-2.54	-0.36	8.49
G	335 – 340	-8.98	-5.23	-4.55	0.78	4.59
H	346 – 350	-4.08	15.14	-2.23	-0.59	19.26
I	621 – 624	-0.04	1.50	1.50	0.02	1.55
J	635 – 638	-0.03	16.16	1.91	-0.08	16.19
K	841 – 844	0.00	16.92	0.19	0.00	16.91
L	855 – 858	0.04	30.73	1.46	-0.02	30.68
M	941 – 944	0.00	20.18	0.18	0.00	20.18
N	955 – 958	0.01	41.63	1.81	0.00	41.62
O	1101 – 1104	0.00	19.96	0.18	0.00	19.96
P	1115 – 1118	0.01	45.38	2.23	0.00	45.37
Q	1261 – 1264	0.00	13.06	0.13	-0.01	13.03
R	1275 – 1278	0.02	31.62	2.62	0.00	31.60
S	1561 – 1564	0.10	-2.70	-2.29	-0.22	2.83
T	1575 – 1578	0.03	5.41	4.51	0.06	5.38
U	1841 – 1846	0.44	-12.84	11.41	1.13	24.34
V	1852 – 1856	0.80	-6.59	-1.97	-1.17	7.75
W	1969 – 1976	-61.79	-22.13	-15.33	-2.82	46.66
X	2370 – 2570	5.18	-8.54	0.02	-4.93	16.90
Y	2305 – 2565	-9.21	-9.61	2.26	-4.14	15.82
Z	2301 - 2561	-2.82	0.00	1.78	0.00	4.60

Table 2.10.7-56 P_m Stress Summary (30-Foot Bottom Corner Drop) – Loading Condition 1 – Drop Orientation = 15.74 Degrees

LOADING CONDITION 1: 130°F Ambient Temperature and Maximum Decay Heat Load

Section	Node to Node	S_X	S_Y	S_Z	S_{XY}	SI
A	177 - 327	-5.04	-7.56	-2.67	0.94	5.20
B	4 - 104	-11.78	-14.59	-4.43	0.67	10.31
C	10 – 110	-10.88	-9.54	-7.98	2.63	5.43
D	185 – 335	-8.96	-6.55	-4.24	1.37	5.35
E	18 – 118	-21.09	-6.96	-12.91	6.23	18.84
F	143 – 150	-3.14	-20.39	-8.86	-5.88	20.87
G	335 – 340	-5.27	-9.88	0.17	0.13	10.06
H	346 – 350	-0.63	-21.20	-3.34	-0.78	20.63
I	621 – 624	0.07	-16.15	-1.45	0.48	16.26
J	635 – 638	-0.04	-23.59	1.64	-0.15	25.24
K	841 – 844	-0.03	-7.74	0.70	0.01	8.44
L	855 – 858	0.01	-12.37	0.76	0.00	13.13
M	941 – 944	-0.05	-1.11	0.63	0.01	1.74
N	955 – 958	-0.01	-0.67	0.84	0.01	1.51
O	1101 – 1104	-0.06	4.72	0.41	0.00	4.78
P	1115 – 1118	-0.03	10.89	0.98	0.01	10.92
Q	1261 – 1264	-0.05	8.86	0.63	0.00	8.91
R	1275 – 1278	-0.02	13.57	0.73	0.00	13.59
S	1561 – 1564	-0.07	-2.08	0.73	-0.04	2.81
T	1575 – 1578	-0.05	9.99	1.19	-0.01	10.04
U	1841 – 1846	-0.91	-1.86	-1.28	-0.32	1.14
V	1852 – 1856	0.64	6.11	-0.02	-0.78	6.24
W	1969 – 1976	6.54	1.21	-2.40	-1.39	9.28
X	2370 – 2570	-1.60	-0.96	0.18	0.32	1.91
Y	2305 – 2565	-1.19	-0.36	-0.01	0.15	1.20
Z	2301 - 2561	-0.72	0.05	0.13	0.73	1.65

Table 2.10.7-57 $P_m + P_b$ Stress Summary (30-Foot Bottom Corner Drop) – Loading Condition 1 – Drop Orientation = 15.74 Degrees

LOADING CONDITION 1: 130°F Ambient Temperature and Maximum Decay Heat Load

Section	Node to Node	S_X	S_Y	S_Z	S_{XY}	SI
A	177 - 327	-5.39	-7.56	-2.67	0.94	5.24
B	4 - 104	-15.50	-14.59	-4.43	0.67	11.42
C	10 – 110	-14.43	-9.54	-7.98	2.63	7.60
D	185 – 335	-18.44	-6.55	-4.24	1.37	14.36
E	18 – 118	-34.78	-6.96	-12.91	6.23	30.48
F	143 – 150	-7.82	-23.43	-11.25	-5.88	19.54
G	335 – 340	-9.77	-13.87	-0.88	0.13	12.99
H	346 – 350	-3.07	-33.67	-8.05	-0.78	30.65
I	621 – 624	0.27	-20.83	-3.90	0.48	21.12
J	635 – 638	-0.10	-24.10	2.07	-0.15	26.17
K	841 – 844	-0.08	-7.29	1.38	0.01	8.67
L	855 – 858	-0.02	-11.43	2.39	0.00	13.82
M	941 – 944	-0.01	-1.10	0.68	0.01	1.78
N	955 – 958	-0.03	-0.39	2.02	0.01	2.40
O	1101 – 1104	-0.04	4.97	0.51	0.00	5.01
P	1115 – 1118	0.00	11.34	0.72	0.01	11.34
Q	1261 – 1264	-0.01	9.30	0.73	0.00	9.32
R	1275 – 1278	0.00	14.14	0.77	0.00	14.14
S	1561 – 1564	0.01	-1.70	1.02	-0.04	2.73
T	1575 – 1578	-0.01	12.18	1.85	-0.01	12.18
U	1841 – 1846	-0.16	-1.64	-0.98	-0.32	1.62
V	1852 – 1856	3.23	10.37	2.78	-0.78	7.68
W	1969 – 1976	-14.90	-6.34	-3.71	-1.39	11.41
X	2370 – 2570	-5.06	-1.70	-0.34	0.54	4.80
Y	2305 – 2565	-0.82	-0.47	0.14	0.48	1.30
Z	2301 - 2561	-0.52	0.04	0.23	2.67	5.38

Table 2.10.7-58 P_m Stress Summary (30-Foot Bottom Oblique Drop) – Loading Condition 1 – Drop Orientation = 30 Degrees

LOADING CONDITION 1: 130°F Ambient Temperature and Maximum Decay Heat Load

Section	Node to Node	S_X	S_Y	S_Z	S_{XY}	SI
A	177 - 327	-4.71	-9.11	-2.31	0.76	6.93
B	4 - 104	-11.36	-24.02	-2.05	4.49	23.40
C	10 – 110	-9.23	-13.86	-7.32	2.84	7.88
D	185 – 335	-7.64	-8.19	-5.65	1.45	3.74
E	18 – 118	-17.97	-9.99	-12.77	5.48	13.56
F	143 – 150	-4.32	-17.17	-10.50	-5.71	17.20
G	335 – 340	-6.62	-8.91	-1.93	0.45	7.07
H	346 – 350	-2.40	-16.98	-7.21	-0.82	14.67
I	621 – 624	0.04	-13.10	-0.77	0.39	13.16
J	635 – 638	-0.08	-16.81	2.03	-0.18	18.84
K	841 – 844	-0.04	-1.80	0.88	0.02	2.67
L	855 – 858	0.00	-1.42	1.19	-0.01	2.60
M	941 – 944	-0.06	6.91	0.81	0.01	6.98
N	955 – 958	-0.02	14.24	1.35	0.01	14.26
O	1101 – 1104	-0.09	13.08	0.45	0.00	13.16
P	1115 – 1118	-0.05	28.16	1.63	0.01	28.21
Q	1261 – 1264	-0.06	16.36	0.81	0.00	16.42
R	1275 – 1278	-0.04	27.63	1.22	0.00	27.67
S	1561 – 1564	-0.10	0.61	1.28	0.00	1.38
T	1575 – 1578	-0.08	14.87	1.75	0.01	14.95
U	1841 – 1846	-0.59	-1.36	-0.44	-0.31	1.04
V	1852 – 1856	1.86	8.94	-0.54	-1.36	9.73
W	1969 – 1976	11.10	2.06	-4.53	-2.07	16.08
X	2370 – 2570	-2.41	-1.29	-0.19	0.56	2.83
Y	2305 – 2565	-1.82	-0.31	0.31	0.27	2.18
Z	2301 - 2561	-1.21	0.09	0.48	1.21	2.75

Table 2.10.7-59 $P_m + P_b$ Stress Summary (30-Foot Bottom Oblique Drop) – Loading Condition 1 – Drop Orientation = 30 Degrees

LOADING CONDITION 1: 130°F Ambient Temperature and Maximum Decay Heat Load

Section	Node to Node	S_X	S_Y	S_Z	S_{XY}	SI
A	177 - 327	-4.80	-9.11	-2.31	0.76	6.93
B	4 - 104	-13.71	-24.02	-2.05	4.49	23.65
C	10 – 110	-6.73	-13.86	-7.32	2.84	9.11
D	185 – 335	-14.58	-8.19	-5.65	1.45	9.24
E	18 – 118	-29.74	-9.99	-12.77	5.48	22.59
F	143 – 150	-6.73	-18.06	-11.46	-5.71	16.09
G	335 – 340	-9.60	-11.15	-1.85	0.45	9.42
H	346 – 350	-5.17	-31.54	-12.91	-0.82	26.42
I	621 – 624	0.22	-16.96	-3.03	0.39	17.19
J	635 – 638	-0.16	-19.06	2.05	-0.18	21.11
K	841 – 844	-0.10	-1.75	1.37	0.02	3.11
L	855 – 858	-0.05	-1.02	2.73	-0.01	3.75
M	941 – 944	-0.02	7.38	0.97	0.01	7.40
N	955 – 958	-0.01	14.64	0.27	0.01	14.65
O	1101 – 1104	-0.06	13.80	0.64	0.00	13.85
P	1115 – 1118	0.01	29.38	1.41	0.01	29.38
Q	1261 – 1264	-0.02	17.25	1.01	0.00	17.27
R	1275 – 1278	0.00	28.83	1.27	0.00	28.83
S	1561 – 1564	-0.03	1.42	1.73	0.00	1.76
T	1575 – 1578	-0.00	17.78	2.81	0.01	17.79
U	1841 – 1846	-0.17	-1.30	0.02	-0.31	1.40
V	1852 – 1856	5.46	13.61	2.78	-1.36	11.06
W	1969 – 1976	-24.08	-9.10	-6.03	-2.07	18.33
X	2370 – 2570	-7.27	-2.52	-0.66	0.92	6.78
Y	2305 – 2565	-1.36	-0.49	0.56	0.82	2.42
Z	2301 - 2561	-0.87	0.07	0.66	4.43	8.91

Table 2.10.7-60 P_m Stress Summary (30-Foot Bottom Oblique Drop) – Loading Condition 1 – Drop Orientation = 45 Degrees

LOADING CONDITION 1: 130°F Ambient Temperature and Maximum Decay Heat Load

Section	Node to Node	S_X	S_Y	S_Z	S_{XY}	SI
A	177 - 327	-3.87	-9.73	-0.29	0.58	9.49
B	4 - 104	-10.17	-27.98	0.97	6.07	30.82
C	10 – 110	-7.65	-16.13	-4.98	2.51	11.83
D	185 – 335	-6.10	-9.77	-4.22	1.14	5.87
E	18 – 118	-14.95	-12.23	-11.27	4.82	10.02
F	143 – 150	-5.61	-14.31	-10.29	-4.78	12.93
G	335 – 340	-8.44	-7.75	-1.86	0.77	7.08
H	346 – 350	-5.80	-13.03	-9.52	-1.62	7.92
I	621 – 624	0.02	-9.59	-0.10	0.32	9.62
J	635 – 638	-0.08	-11.09	2.16	-0.18	13.26
K	841 – 844	-0.07	2.54	0.92	0.02	2.61
L	855 – 858	0.00	5.96	1.37	0.00	5.96
M	941 – 944	-0.08	11.48	0.86	0.01	11.57
N	955 – 958	-0.03	22.46	1.54	0.01	22.49
O	1101 – 1104	-0.11	17.00	0.44	0.00	17.11
P	1115 – 1118	-0.05	36.18	1.85	0.01	36.24
Q	1261 – 1264	-0.09	19.23	0.86	0.00	19.32
R	1275 – 1278	-0.04	33.48	1.39	0.00	33.53
S	1561 – 1564	-0.11	2.57	1.49	0.03	2.68
T	1575 – 1578	-0.09	16.19	1.90	0.02	16.28
U	1841 – 1846	-0.26	-0.77	0.27	-0.25	1.15
V	1852 – 1856	2.48	9.66	-0.85	-1.57	10.84
W	1969 – 1976	12.78	2.37	-5.43	-2.25	18.67
X	2370 – 2570	-2.63	-1.33	0.17	0.65	3.07
Y	2305 – 2565	-2.01	-0.22	0.50	0.32	2.57
Z	2301 - 2561	-1.39	0.10	0.67	1.39	3.15

Table 2.10.7-61 $P_m + P_b$ Stress Summary (30-Foot Bottom Oblique Drop) – Loading Condition 1 – Drop Orientation = 45 Degrees

LOADING CONDITION 1: 130°F Ambient Temperature and Maximum Decay Heat Load

Section	Node to Node	S_X	S_Y	S_Z	S_{XY}	SI
A	177 - 327	-3.95	-9.73	-0.29	0.58	9.49
B	4 - 104	-12.31	-27.98	0.97	6.07	31.03
C	10 – 110	-10.26	-16.13	-4.98	2.51	12.07
D	185 – 335	-11.09	-9.77	-4.22	1.14	7.53
E	18 – 118	-24.07	-12.23	-11.27	4.82	15.27
F	143 – 150	-5.19	-13.85	-8.50	-4.78	12.90
G	335 – 340	-10.88	-8.50	-0.86	0.77	10.25
H	346 – 350	-7.65	-26.92	-15.76	-1.62	19.54
I	621 – 624	0.16	-12.80	-2.60	0.32	12.98
J	635 – 638	-0.17	-13.78	2.91	-0.18	16.69
K	841 – 844	-0.02	2.79	0.64	0.02	2.81
L	855 – 858	0.00	5.78	-0.59	0.00	6.37
M	941 – 944	-0.03	12.26	1.27	0.01	12.29
N	955 – 958	-0.01	23.18	0.33	0.01	23.19
O	1101 – 1104	-0.08	18.00	0.89	0.00	18.08
P	1115 – 1118	0.01	37.75	1.62	0.01	37.75
Q	1261 – 1264	-0.03	20.37	1.31	0.00	20.40
R	1275 – 1278	0.01	34.96	1.45	0.00	34.96
S	1561 – 1564	-0.06	3.56	1.99	0.03	3.63
T	1575 – 1578	0.00	19.18	3.09	0.02	19.18
U	1841 – 1846	-0.15	-0.83	0.78	-0.25	1.69
V	1852 – 1856	6.28	13.89	2.33	-1.57	11.87
W	1969 – 1976	-27.19	-9.73	-6.82	-2.25	20.65
X	2370 – 2570	-7.77	-2.73	-0.80	1.06	7.19
Y	2305 – 2565	-1.55	-0.42	0.79	0.95	2.88
Z	2301 - 2561	-0.99	0.07	0.88	5.05	10.17

Table 2.10.7-62 P_m Stress Summary (30-Foot Bottom Oblique Drop) – Loading Condition 1 – Drop Orientation = 60 Degrees

LOADING CONDITION 1: 130°F Ambient Temperature and Maximum Decay Heat Load

Section	Node to Node	S_X	S_Y	S_Z	S_{XY}	SI
A	177 - 327	-3.61	-11.52	1.18	0.46	12.73
B	4 - 104	-10.12	-35.55	3.96	8.66	42.18
C	10 – 110	-6.86	-20.80	-3.07	2.57	18.19
D	185 – 335	-5.25	-12.67	-3.71	1.14	9.13
E	18 – 118	-13.40	-16.29	-10.75	4.53	9.51
F	143 – 150	-7.49	-12.73	-11.58	-4.70	10.76
G	335 – 340	-11.15	-7.37	-2.40	1.11	9.05
H	346 – 350	-9.69	-10.22	-13.54	-2.47	6.07
I	621 – 624	-0.01	-7.13	0.49	0.29	7.63
J	635 – 638	-0.10	-6.43	2.43	-0.20	8.87
K	841 – 844	-0.10	6.98	1.02	0.02	7.07
L	855 – 858	0.00	14.00	1.69	-0.01	14.00
M	941 – 944	-0.12	17.26	0.97	0.01	17.38
N	955 – 958	-0.04	33.19	1.89	0.02	33.23
O	1101 – 1104	-0.15	22.91	0.46	0.00	23.06
P	1115 – 1118	-0.07	48.40	2.29	0.00	48.47
Q	1261 – 1264	-0.12	24.45	0.97	0.00	24.57
R	1275 – 1278	-0.06	43.35	1.72	0.00	43.40
S	1561 – 1564	-0.14	4.53	1.87	0.06	4.67
T	1575 – 1578	-0.11	19.55	2.29	0.04	19.66
U	1841 – 1846	-0.02	-0.39	0.90	-0.24	1.40
V	1852 – 1856	3.34	11.61	-1.22	-1.97	13.27
W	1969 – 1976	15.96	2.97	-6.92	-2.72	23.43
X	2370 – 2570	-3.19	-1.55	0.18	0.81	3.70
Y	2305 – 2565	-2.45	-0.18	0.74	0.40	3.25
Z	2301 - 2561	-1.74	0.12	0.93	1.72	3.91

Table 2.10.7-63 $P_m + P_b$ Stress Summary (30-Foot Bottom Oblique Drop) – Loading Condition 1 – Drop Orientation = 60 Degrees

LOADING CONDITION 1: 130°F Ambient Temperature and Maximum Decay Heat Load

Section	Node to Node	S_X	S_Y	S_Z	S_{XY}	SI
A	177 - 327	-3.65	-11.52	1.18	0.46	12.73
B	4 - 104	-12.00	-35.55	3.96	8.66	42.36
C	10 – 110	-9.45	-20.80	-3.07	2.57	18.29
D	185 – 335	-8.71	-12.67	-3.71	1.14	9.27
E	18 – 118	-20.92	-16.29	-10.75	4.53	12.94
F	143 – 150	-4.57	-10.25	-6.79	-4.70	10.98
G	335 – 340	-13.00	-6.63	-0.22	1.11	12.98
H	346 – 350	-9.03	5.39	-6.19	-2.47	15.24
I	621 – 624	0.12	-9.80	-2.10	0.29	9.94
J	635 – 638	-0.21	-10.17	3.63	-0.20	13.79
K	841 – 844	-0.03	7.57	1.09	0.02	7.61
L	855 – 858	0.01	14.14	-0.50	-0.01	14.64
M	941 – 944	-0.05	18.43	1.69	0.01	18.48
N	955 – 958	-0.01	34.68	0.68	0.02	34.39
O	1101 – 1104	-0.11	24.31	1.20	0.00	24.41
P	1115 – 1118	0.01	50.52	2.08	0.00	50.51
Q	1261 – 1264	-0.05	25.97	1.72	0.00	26.02
R	1275 – 1278	0.01	45.27	1.80	0.00	45.26
S	1561 – 1564	-0.09	5.83	2.48	0.06	5.92
T	1575 – 1578	0.00	23.03	3.75	0.04	23.02
U	1841 – 1846	-0.16	-0.57	1.51	-0.24	2.18
V	1852 – 1856	7.83	16.07	2.29	-1.97	14.23
W	1969 – 1976	-33.56	-11.61	-8.43	-2.72	25.46
X	2370 – 2570	-9.28	-3.29	-1.03	1.32	8.54
Y	2305 – 2565	-1.92	-0.43	1.09	1.19	3.67
Z	2301 - 2561	-1.24	0.09	1.18	6.28	12.63

2.10.8 Quarter-Scale Model Drop Test Program for the NAC-LWT Cask

2.10.8.1 Introduction

This appendix provides a detailed presentation of the Quarter-Scale Model Drop Test Program, which was carried out for confirmatory support of the analysis and licensing effort for the design qualification of the NAC-LWT cask. The analyses presented elsewhere in this report demonstrate that the NAC-LWT cask design meets all of the requirements for use in the packaging and transportation of radioactive material (10 CFR 71), especially PWR, BWR, and metallic spent-fuel rods. The test results presented in this appendix confirm the analyses and provide additional confidence that the cask design provides for the safe transport of radioactive material. This test program considered the 30-foot (9-meter) Free Drop and the 1-meter (40-in) Puncture events of the 10 CFR 71 Hypothetical Accident Conditions, but the test results also lend credence to the analyses performed for the 10 CFR 71 Normal Conditions of Transport.

2.10.8.2 Purpose

The purpose of the Quarter-Scale Model Drop Test Program was to verify that the NAC-LWT cask design satisfies the Free Drop and the Puncture requirements of 10 CFR 71.73, Hypothetical Accident Conditions; each test simulated a specific load condition. The tests verified the structural adequacy of the NAC-LWT cask packaging in: (1) the performance of its containment function, (2) the performance of the impact limiters, (3) reacting dynamic loadings, and (4) resisting puncture by a pin.

2.10.8.3 Summary

The detailed quarter-scale model of the body of the NAC-LWT cask, which was fabricated for use in this test program, is presented in NAC drawings: 315-40-30, 315-40-31 (sheets 1 through 3), and 315-40-32 (Figure 2.10.8-1 through Figure 2.10.8-3).

The details of the impact limiters, which were fabricated for this test program, are presented in NAC drawings 315-40-33 and 315-40-34 (Figure 2.10.8-4 and Figure 2.10.8-5). The full-scale cask cavity contents weight (4000 lbs) is simulated in the quarter-scale model by the steel cylinder, shown on Drawing 315-40-35 (Figure 2.10.8-6), whose weight is appropriately scaled, $Ws = (4000)/(4)^3 = 62.5$ lbs.

The model of the body of the NAC-LWT cask, which was used in the Drop Test Program, was a quarter-scale duplication of the full-scale cask in all aspects, except as described in subsequent paragraphs of this appendix. The model was fabricated of Type 304 stainless steel inner and

outer shells, upper and lower end forgings, and closure lid; the port cover was Type 17-4PH stainless steel; and the gamma shield was chemical copper lead per ASTM B29. The impact limiters were fabricated of 5052 aluminum honeycomb enclosed in 6061-T6 aluminum alloy shells. The closure lid bolts were SA-453, Grade 660 high strength alloy steel bolting material. A carbon steel tube was used to simulate the fuel basket and payload in the cask cavity.

The quarter-scale model lead gamma shield forms an annulus 1.438 inches thick and 43.75 inches long. The lead was enclosed between the 0.1875 inch thick, 3.344-inch inside diameter inner shell and the 0.28-inch thick, 7.155-inch outer diameter outer shell. The ends of the inner shell include 0.75-inch long by 0.314-inch thick transition regions. The bottom end forging of the quarter-scale model cask was 1.0 inch thick. The bottom also included a 0.75-inch thick, 5.19-inch diameter lead disk enclosed by a 0.875-inch thick end cover. The upper ring forging was 3.5625 inches thick with a machined interior to accept the closure lid. The model closure lid was 5.625 inches in diameter and 2.81 inches thick. The 12 closure lid bolts were 1/4-32 UNEF-2B × 2 1/4 long socket head cap screws, which were selected to provide a tensile stress area equal to 1/(4)2 times that of the full-scale closure bolts. Since the applied impact load on the model is four times that applied to the full-scale cask, the proper bolt stress results. The port cover was a 0.748-inch outer diameter, 0.406-inch inner diameter, piston-type cylinder with an integral 0.25-inch thick, 1.125-inch diameter cover plate. The model impact limiters were quarter-size replicas of the full-scale limiters with full-strength aluminum honeycomb energy absorption material to produce the properly scaled impact loads on the model cask (3500 psi multidirectional and 1200 psi unidirectional crush strengths). The honeycomb sections' pie-shapes, joints, and bonds duplicated those of the full-scale limiters. The aluminum honeycomb of the model limiters was enclosed in 0.062-inch thick aluminum shells with epoxy-bonded joints; the model limiter attachment lugs were 0.062-inch thick aluminum alloy sheet. The model upper impact limiter had an outside diameter of 16.25 inches, a depth of 7.06 inches, an inner cup diameter of 7.22 inches, a cup depth of 3.00 inches, and four 0.75-inch × 1.28-inch trunnion cutouts. The model lower impact limiter had an outside diameter of 15.00 inches, a depth of 7.09 inches, an inner cup diameter of 7.22 inches, and a cup depth of 3.00 inches. The model load was a steel tube 43.75 inches long with a 3.22-inch outside diameter, a 2.00-inch inside diameter, and 0.25-inch thick end plates.

The inner shell, end forgings, and the closure lid establish a model cask cavity of 44.50 inches in length and 3.344 inches in diameter. The weight of the quarter-scale model cask with impact limiters and cavity load was 860 lbs (approximately 6 percent heavier than the design weight).

Three significant differences do exist between the quarter-scale model cask body and the full-scale cask body: (1) the model does not include the neutron shield and expansion tanks; the weight of these tanks and their contents are simulated on the model by segmented steel bars

welded on the exterior surface of the outer shell; (2) the inner and outer shells of the model are Type 304 stainless steel, with a yield strength of S_y = 30 ksi and an ultimate strength of S_u = 75 ksi, while the inner and outer shells of the full-scale cask are Type XM-19 stainless steel with S_y = 55 ksi and S_u = 100 ksi; and (3) the outer shell of the model did not include the transition regions at each end, which are present on the full-scale Type XM-19 stainless steel outer shell. The use of segmented weights to simulate the neutron shield prevents the weights from contributing to the strength of the cask, and conservatively neglects the effect of the neutron shell. The impact limiter attachment lugs were 0.062-inch thick on the impact limiters and 0.037-inch thick on the cask body, while the full-scale lugs are 0.50-inch thick on both components. The quarter-scale model impact limiter joints were riveted and/or epoxyed; whereas, on the full-scale model, the joints are all welded. Some other minor differences do exist between the quarter-scale model and the full-scale cask, but based on the absence of the shield/expansion tanks and the reduced strength of the inner and outer shells, the model is a conservative, fully representative replica of the full-scale cask. The differences, which do exist, are considered in detail in Section 2.10.8.4.

Prior to the start of testing, the model was instrumented with tri-axial accelerometers (one near each end of the cask body) and rosette strain gauges (a set of four, located at 90-degree intervals near the upper end, near the lower end, and at the midpoint of the body), so that a record of the model's response to the various tests could be obtained. The tests were performed at Oak Ridge National Laboratory (ORNL) in Oak Ridge, Tennessee. A detailed description of the test facility can be found in the Drop Test Facility's Information Brochure (Shappert and Box). A description of the test procedures and instrumentation is presented in Section 2.10.8.5 of this report. The test sequence followed at ORNL is summarized as follows:

- Inspect cask model.
- Perform pretest weight and geometry measurements.
- Assemble packaging for the 30-foot End Drop Test (install simulated cavity load, cask closure lid, and port cover, and attach upper impact limiter).
- Pressurize and leak test the cask cavity.
- Perform 30-foot Top End Drop (impact on lid end).
- Observe cask condition and perform leak test.
- Repeat packaging assembly and leak test for each drop.
- Perform 30-foot Top Corner Drop (15.7° from vertical).
- Perform 30-foot Side Drop (cask axis horizontal).
- Perform 30-foot Oblique Drop (cask axis 60° from vertical).
- Perform 40-inch Side Drop on puncture pin (impact at midpoint of side of cask).
- Disassemble cask model and perform final geometry measurement inspection.

This test sequence is summarized in the photographs presented in Figure 2.10.8-7 through Figure 2.10.8-31. The significant results obtained from the LWT Cask Quarter-Scale Drop Test Program are presented in Section 2.10.8.6.

The test program was very successful in confirming the structural adequacy of the NAC-LWT Spent Fuel Shipping Cask for the Hypothetical Accident Condition Free Drop and Puncture events. Based on the pre-test and post-test dimensional measurements, nearly all permanent deformation of the packaging model was limited to the impact limiters, as expected and desired. The only significant deformation of the cask body model occurred in the side puncture test, where local deformation of the outer shell and the lead shielding did occur; as designed, the outer shell was not punctured. This local deformation was fully expected and produced a very slight, local dimple in the inner shell wall (0.05 in) of the model. These local puncture deformations are of no consequence since the containment vessel and its contents are protected.

Because no deformation to the package was observed, except as previously discussed, and the containment vessel sustained essentially no deformation, leakage was not expected and did not occur. As noted in the detailed test results in Section 2.10.8.6, some experimental problems precluded actual "contained" pressure measurements before and after each test; however, leaktightness of the cavity was verified before and after each test. The test results were as expected. The results correlated well with the assumptions made and the analyses performed elsewhere in this report. An accurate detailed analysis of the cask body in the local region of the impact for the side drop puncture test is very difficult, even with state-of-the-art finite element analysis computer programs, but the observed test results confirm the adequacy of the NAC-LWT cask design. The test conservatively did not include the neutron shield shell or the higher strength Type XM-19 stainless steel inner and outer shells. Although the quarter-scaled attachment lugs were significantly undersized through a manufacturing error, the impact limiters remained in position on the cask body and performed their energy absorption function as designed for the entirety of each test. On the basis of the good agreement shown between the test results and those expected (based on analyses), and on the observed physical condition of the test model, it is concluded that this test program has confirmed the adequacy of the NAC-LWT cask design to meet the requirements of the Free Drop (30-ft) and the Puncture (40-in) events specified by 10 CFR 71.73.

2.10.8.4 Description of Quarter-Scale LWT Cask Model

Quarter-scale modeling was achieved by reducing dimensions to precisely one-fourth of the full-scale dimensions. The scaling relations are defined in Table 2.10.8-1. With the exceptions noted below, the quarter-scale model was a duplicate of the full-scale design.

1. Deviations

   The items/components omitted from the quarter-scale model included the neutron shield and expansion tank shells and their contents, the rotation trunnions, and the valve ports. It was determined that omission of these items/components would have either a conservative effect, or no effect, on the test results.

2. Differences

   Some modifications were made to the quarter-scale model to eliminate complex operations, to allow installation of instrumentation, and to meet schedular concerns based on material availability. These modifications included a single external pressure port valve, a single closure lid O-ring (O-ring cross sections and thicknesses do not scale), Type 304 stainless steel inner and outer shells (Type XM19 stainless steel is not commonly available), and lifting trunnions that were not final machined. All of the bolts used in the quarter-scale model - closure lid, port cover, and impact limiter attachment - were chosen with a minimum tensile area equal (as near as practical) to 1/(4)2 = 1/16 of the minimum tensile area of the corresponding full-scale bolt. The cask cavity contents, the fuel basket and payload, were simulated in the quarter-scale model by an appropriately scaled steel cylinder. The weights of the rotation trunnions, the neutron shield and expansion tanks, and the shield fluid were simulated by segments of steel bar welded on the exterior surface of the outer shell. These 4.25-inch × 2.5-inch × 1.0-inch steel bars were spaced along the length of the model body to represent the distribution of the shield/expansion tanks and fluid, but away from the cask midpoint (Puncture Test region). The steel bars were also spaced circumferentially for load distribution and to preclude strengthening the outer shell in that direction.

   In summary, the NAC-LWT cask quarter-scale model that was tested reflects all of the significant structural characteristics of the full-scale cask design, which is defined and analyzed elsewhere in this report. The quarter-scale model weight of 860 lbs, corresponding to a full-scale cask weight of 860 × 43 = 55,040 lbs, provided a 5.8 percent conservative margin over the 52,000-lb cask design weight used in the analyses of this report. With only one impact limiter attached for the top end and top corner drops, the model weight was 840 lbs, providing a 3.4 percent conservative margin.

2.10.8.5 Description of Test Procedures and Instrumentation

The test program for the quarter-scale model consisted of the following five drop tests:

Test No. 1	Vertical top end drop of 30 feet.
Test No. 2	Top corner drop of 30 feet at an angle of 15.7 degrees from the vertical. (At this angle, the center of gravity of the cask is directly over the edge of the cask body, which prohibits rotation of the cask on initial impact.)
Test No. 3	Side drop from a height of 30 feet.
Test No. 4	Bottom oblique drop of 30 feet at an angle of 60 degrees from the vertical.
Test No. 5	A 40-inch drop onto a pin at the mid-point side of the cask.

The tests were performed in this order so as to make the puncture test more severe. All cask drops employed an impact pad located at the ORNL facilities. The impact pad was a 600-metric-ton, reinforced concrete structure (2-inch diameter rebar). The concrete structure is a stepped pyramid arrangement with a large base and a 70-metric-ton armor plate surface (24 inches thick). The massive structure was considered to be unyielding so as to minimize any significant energy absorption by the impact surface.

2.10.8.5.1 Equipment

The ancillary equipment for drop testing the quarter-scale model included the following:

- still and normal speed photography (30 frames/second)
- high speed photography (500 frames/second)
- video recorders
- strain gauge recorders
- computerized drop test timing sequencer (DTTS).

The DTTS is a small computer, which receives a feedback message that stops the sequence leading to the drop of the cask if predetermined messages are not received from each component. When all systems are functional, the computer advances the program to the next step and will automatically fire the release mechanism that drops the cask model. One of the important checks performed by the DTTS is the continuity check of the firing circuits of the explosive release mechanism.

2.10.8.5.2 Instrumentation

The primary data to be used in the assessment of cask integrity is the strain gauge time history data obtained during the cask impact event. Nine rosette strain gauges (each rosette allowed unidirectional strains to be measured in 0/45/90 degree directions) were bonded to the cask. The locations of the strain gauges are shown in Figure 2.10.8-32. The nine rosettes were attached at three longitudinal locations. At each longitudinal location, three rosettes were placed 120 degrees apart around the circumference of the outer surface of the cask model. Such an

arrangement permitted the maximum bending stresses to be determined, as well as, the maximum plastic strains observed during the tests. The strain gauges employed in the test had a rise time of 50 kHz, which would enable the strain gauge to track the high strain rates accompanying the impact. To ensure proper operation of the strain gauges, positive and negative calibrations of the strain gauges were performed prior to the drop. These calibrations are retained with the strain time histories on FM tape.

2.10.8.5.3 Drop Test Sequence

This section describes the test procedures used for each time the cask was dropped. ORNL personnel performed all tasks related to instrumentation and the actual sequence leading up to the drop.

1. Cask Preparation
   - Install the model cask lid using a new cask lid O-ring. The O-ring is inspected for defects prior to installation.
   - Install the port cover on the model cask using a new O-ring for the port cover lid. The O-ring is inspected for defects prior to installation.
   - Verify the lid and port cover seals by pressurizing the cavity to 30 (+5/-0) psig. Observe the cavity pressure over a 10-minute period to ensure leaktightness.
   - Attach limiters to the model cask.
2. Performing the Drop Test
   - Check umbilical cord connection to data recorders.
   - Ensure safety of cask hook assembly prior to lift and correct angle of orientation of the cask.
   - Final check to ascertain if all systems are ready for the drop.
   - Turn on the recorders for the strain gauges.
   - Initiate the 10-second countdown in preparation of the drop.
   - At the 5-second mark, start high speed (500 frames/second) photography and normal speed photography.
   - When the countdown reaches zero, energize the explosive mechanism.

When the explosive mechanism fragments, the nut and bolt assembly restraining the cask in the hook allows the hook to open, which allows the cask to initiate the fall unimpeded.

2.10.8.6 Detailed Test Results

Data obtained from the tests consists of both qualitative information with respect to observations about the cask and the limiter and quantitative data obtained from the recorders. The data for each test to be presented consists of:

- Impact limiter deformation.
- Strain gauge results and stress calculations (for the end drop and side drop only).
- Observations of the cask and attachments.

The strain gauge data is only presented for the end drop and the side drop since the loads developed in those tests are the most severe from an overall structural consideration. The end drop corresponds to the maximum axial loading condition, while the side drop developed the maximum lateral loading on the overall cask body. The puncture test involves larger strains, but only on a localized area at the point of impact. The amount of energy available for the puncture impact is one-ninth of the energy for the 30-foot drop, which limits the amount of the lateral load that can be generated.

2.10.8.6.1 Top End Drop Test

Impact Limiter Deformation Data

Essentially all deformation of the impact limiter occurred at the interface of the cask body outside diameter and the limiter inside diameter (Figure 2.10.8-11 and Figure 2.10.8-12). The cask body moved into the limiter shearing and crushing the aluminum honeycomb at the 7.2-inch diameter to an average depth of 1.2 inches. There was some slight variation of the crush depth around the perimeter of the cask body. This is confirmed by the slight tilt of the cask body after the impact as shown in Figure 2.10.8-10. There was some hoop expansion of the top limiter near the surface of impact, but it was minimal since the limiter shell did not show any signs of tearing Figure 2.10.8-12). The 1.2-inch crush corresponded to an overall crush strain of 33 percent. The soft pad of the 1200 psi crush strength material compressed completely and became solid as expected, since it is designed for the 1-foot drop (Note that the soft pad was changed to 250 psi material since the tests showed that the soft pad is backed up by the harder impact limiter material over its entire diameter). It was also observed that the attachment lugs for the limiter failed; however, once the limiter is engaged in the crushing action, the lugs do not provide additional functionality in the end drop condition.

Strain Gauge Data

Strain gauge time histories for the end drop at the midpoint locations are shown in Figure 2.10.8-33 through Figure 2.10.8-35. The corresponding location on the circumference is shown in Figure 2.10.8-32. The maximum axial strain observed in the test was 560 microstrains. This value is approximately 25 percent larger than the maximums (450 microstrains) recorded on the other two channels, indicating some amount of unequal loading due to variation of the axial stress wave propagation in the cask body. Because of the orientation of the gauges, a positive value in the graphs is associated with a compressive strain. This was as expected. By using elastic properties for the cask body from NUREG/CR-0481, the corresponding axial stress is E (modulus of elasticity) times the strain value, which gives:

$$\sigma = (28.3 \times 10^3)(560 \times 10^{-6})$$

$$= 15.8 \text{ ksi} << \text{yield strength.}$$

Test Observations

As the limiter was driven onto the cask, the test valve used to pressurize the interior was broken off, which prevented the pressure from being measured after the test. A new valve was installed and the cavity was pressurized to 30 psig and was maintained to determine if the cask containment boundary was damaged. There was no measurable pressure loss. The loss of this valve has no implications for the full-scale cask, since the full-scale version does not have this valve.

2.10.8.6.2 Top Corner Drop Test

Impact Limiter Deformation

The corner drop did not produce any significant rotation of the cask about the surface of impact as observed in the high speed photography and by the final upright position of the cask. The final position of the cask after the drop is shown in Figure 2.10.8-15. The crushing of the limiter occurred as in the end drop. The shearing at the outer diameter of the cask is supported by Figure 2.10.8-16. The amount of crush and the distribution of the crush are shown as follows.

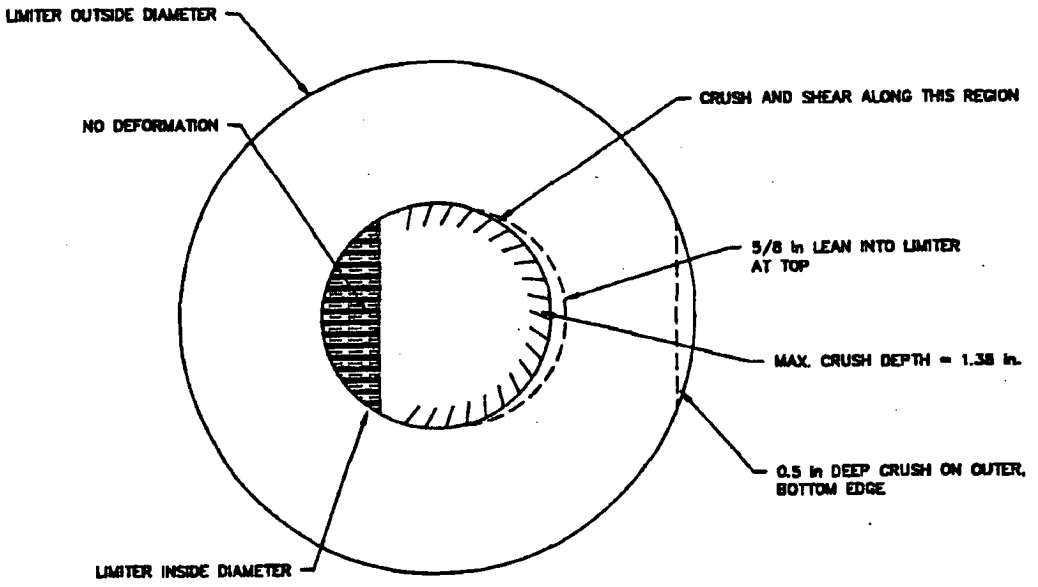

Limiter Deformation for the Top Corner Drop

The maximum amount of crush was determined to be 1.38 inches, which is a strain of 38 percent. It was also observed that the attachment lugs for the limiter failed; however, once the limiter is engaged in the crushing action, the lugs do not provide additional functionality in the corner drop condition.

Test Observations

During the impact event, the coupling connected to the valve used to pressurize the interior was loosened, which prevented the pressure from being measured after the test. The coupling was tightened and the cavity was pressurized to 29.2 psig and was maintained to determine if the cask containment boundary was damaged. There was no measurable pressure loss.

Tethers were attached to the cask to prevent a tip-over after the impact event. In observing the photographic results, the tethers also responded to the fall by vibrating in an oscillatory manner. This additional oscillating load allowed the cask to incur a secondary impact, which would not occur for an untethered cask with an impact limiter attached over each end.

2.10.8.6.3 Side Drop Test

Impact Limiter Deformation

Limiters in the side drop condition were crushed only in regions that are backed by the cask body. The amount of crush and the variation of the crush for the top and bottom limiters for the side drop are described as follows.

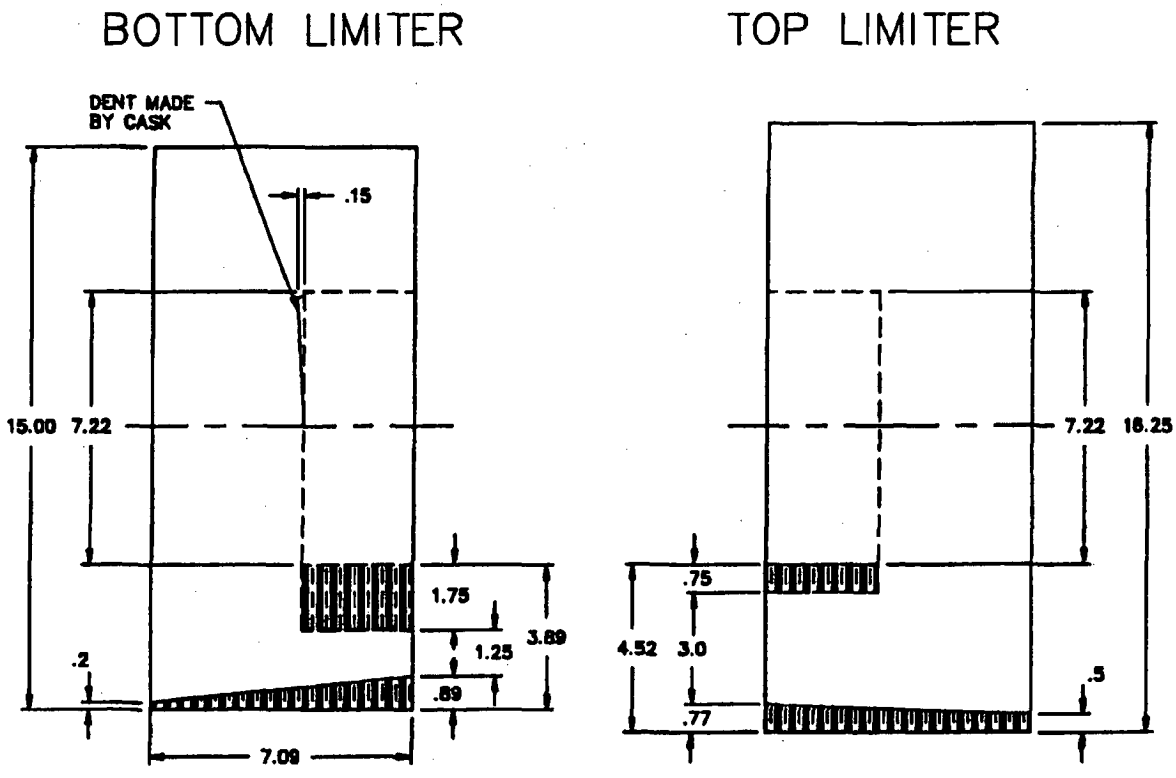

ALL DIMENSIONS ARE IN INCHES
Limiter Deformation for the Side Drop

The uniform crushed surface of the limiters resulting from the side drop can be seen in Figure 2.10.8-19, Figure 2.10.8-20 and Figure 2.10.8-21. Note that the surface is uniform in both the axial direction and the lateral direction. The maximum strain for the side drop was 68 percent for the bottom limiter and 34 percent for the top limiter. The average strains under the backed areas were 30 percent for the top limiter and 59 percent for the bottom limiter. The larger strains correspond to the bottom limiter, since it was significantly smaller than the top limiter.

As shown in the previous sketch, both limiters showed evidence of a small rotation relative to the cask (Figure 2.10.8-17). This accounts for the greater deformation of the circumferential surface along the inner face of the impact limiter and the smaller compression on the outer diameter of the cask. The limiter shell also experienced large deformations that had no effect on the limiter performance.

Strain Gauge Data

Strain gauge time histories for the side drop at the midpoint locations are shown in Figure 2.10.8-36 through Figure 2.10.8-38. The corresponding locations on the circumference are shown in Figure 2.10.8-32. The maximum axial strain observed in the test was 2500 microstrains, which also resulted in a permanent set of 750 microstrains. Due to the manner in which the cask is loaded, the maximum strains occurred at the midpoint. The strains from channels 4 and 5 can be used to estimate the maximum stresses and strains in the side drop test.

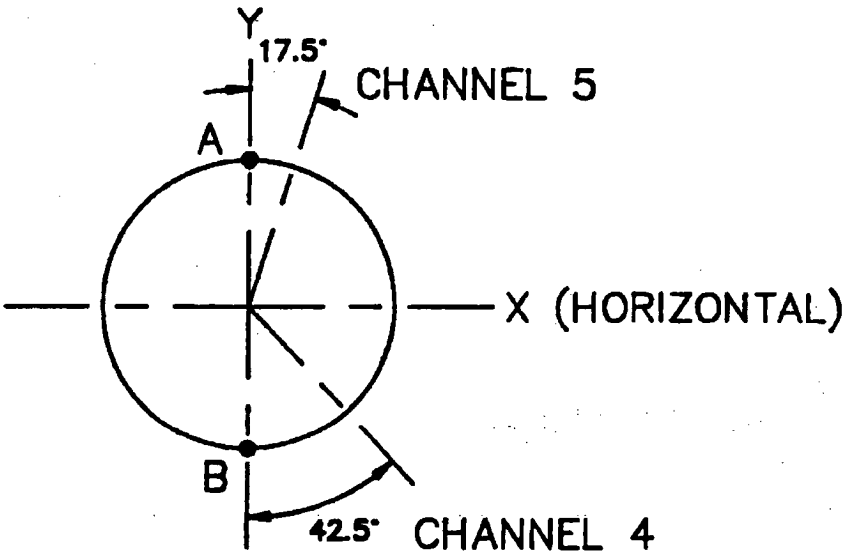

Definition of Channel Orientation for the Side Drop

The maximum strains are expected to occur at points A and B as shown above. Assuming that the cask cross-section remains plane, the values for the maximum strain and plastic strain at

locations A and B can be obtained by factoring the test data by 1/cos(17.5°) and 1/cos(42.5°), respectively.

To estimate the σy and σmax, the stress strain curve for Type 304 stainless steel is required. The static values for Type 304 stainless steel were extracted from NUREG/CR-0481 as:

$E = 28.3 \times 103$ ksi (75°)

$E_T = 370$ ksi

This assumes that the stress strain curve takes the form shown as follows.

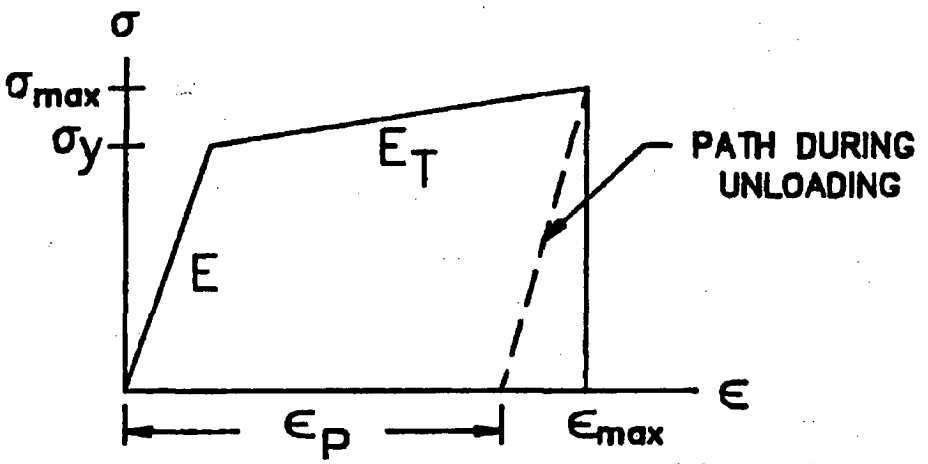

Typical Stress Strain Curve for Type 304 Stainless Steel

The plastic strain recorded from the strain gauge corresponds to εp. The relations for the stress and strain can be written as:

$$\varepsilon_{max} = \frac{\sigma_y}{E} + \varepsilon_p \qquad (1)$$

$$\sigma_{max} = \sigma_y + E_T(\varepsilon_p) \qquad (2)$$

By equation (1)

$$\sigma_y = (\varepsilon_{max} - \varepsilon_p)E \qquad (3)$$

The calculated maximum strains from the strain gauge data are as follows.

	Strain Gauge		Extrapolated			
	εmax	εp	εmax	εp	σY	σmax
Channel	(microstrain)		(microstrain)		(ksi)	(ksi)
4	2200	1000	2984	1356	46.1	46.6
5	2500	750	2621	786	51.9	52.2

Test Observations

In reviewing the high speed photographic results, the side drop actually represents a drop angle that is the most conducive to the slapdown effect. The drop is actually estimated to be 80 degrees rather than 90 degrees. The pressure in the cask was checked prior to the test and afterwards. It was found to be 30.4 psig. This indicates that pressure containment was maintained during the impact.

2.10.8.6.4 Bottom Oblique Drop Test

Impact Limiter Deformation

In the 60-degree oblique drop test, the bottom impact limiter is initially crushed at the corner as shown below. During the deceleration, the cask body also initiates crushing at the inner surface of the limiter. The upper limiter results in a pattern similar to the side drop in which crushing occurs at both the inner surface of the limiter and at the plane of impact. The maximum crush strains for the bottom and top limiters were 60.7 percent and 45 percent, respectively. The strain direction for the 60.7 percent strain is shown as follows.

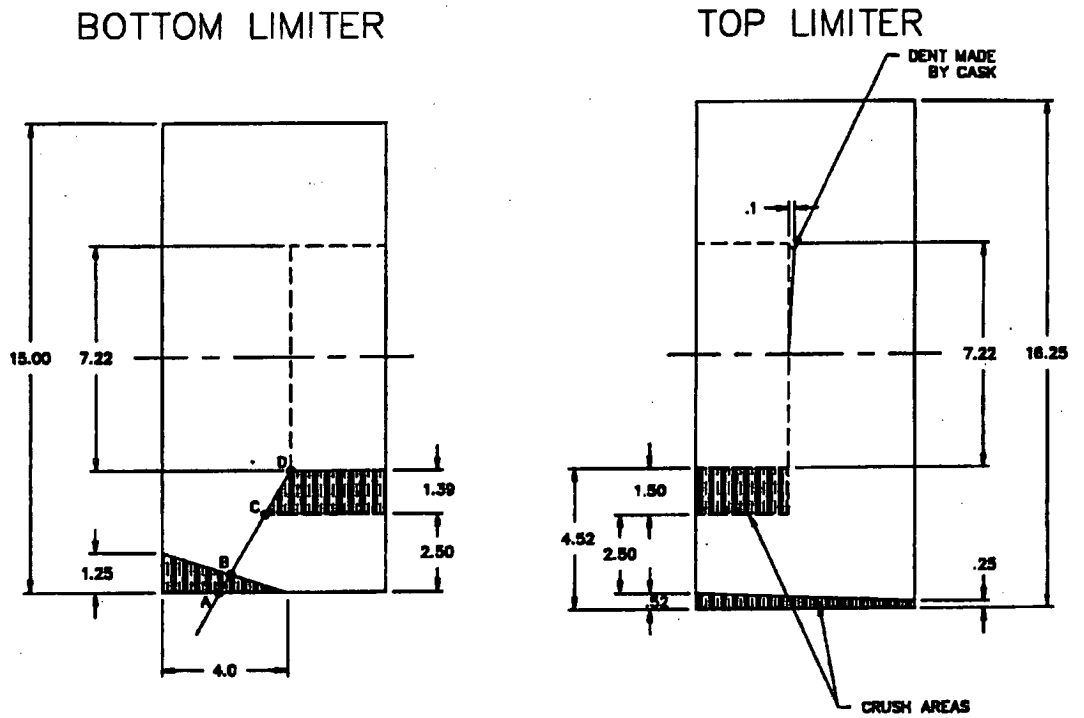

ALL DIMENSIONS ARE IN INCHES
Limiter Deformation for Oblique (60°) Drop

The following equation was used to determine the crush strain for the impact limiter as shown.

$$\text{Crush strain} + \frac{AB + CD}{AD} = 60.7 \text{ percent}$$

where:

CD = 1.39/cos(30) = 1.605 inches

AD = (1.39 + 2.50)/cos(30) = 4.492 inches

AB - AD[sin(30)][sin(30)] = 1.123 inches

Test Observations

The pressure measurement indicated that the cavity pressure did not change as a result of the oblique drop test. Cavity pressure was measured to be 30.2 psig before and after the test.

2.10.8.6.5 One-Meter Puncture Test

As a result of dropping the cask body onto the steel pin, the containment of the cask body was not violated. This was confirmed by the pressure measurements before and after the test. All permanent strain was local to the region of impact of the pin. The resulting shape of the pin impact is shown in Figure 2.10.8-30 and Figure 2.10.8-31. The maximum deformation of the outer shell was 0.5 inch deep and a localized depression of 0.05 inch occurred in the inner shell. Note that the pin puncture impact was directed against the portion of the outer shell that was stressed most severely in the 30-foot drop tests to show that the outer shell retained its puncture capability after the dynamic stress of the 30-foot fall impact.

2.10.8.7 Metrology Results

Prior to the drop tests, the NAC-LWT cask was submitted to the ORNL Plant and Equipment Division to obtain metrology data that would be compared after completion of the drop tests. The cask model was placed on a certified flat surface. The inner diameter was measured in a vertical direction and in a horizontal direction at seven locations starting at the front of the cask cavity and proceeding to the rear of the cavity. The casks' outer diameter measurements were taken at three different locations starting just inside the circumferential welds at either end and in the middle. In addition, external longitudinal measurements were made starting at the open end of the cask and ending at the back end of the external blocks used to simulate the weight of the neutron shield. These measurements, taken before the tests, are given in inches and are shown in Table 2.10.8-2 through Table 2.10.8-4. The same measurements were taken after the last drop test was completed. These values are given in Table 2.10.8-5 through Table 2.10.8-7.

Changes to the inner diameter as a result of the four 30-foot drops onto a solid surface and one 1-meter drop onto a punch can be determined by comparing Table 2.10.8-2 and Table 2.10.8-5. The changes are very small, less than about 0.005 inch at every measured location except in the

cask middle. At the midpoint, some 26 inches from the closure, the changes to the vertical and horizontal diameters were -0.0568 inch and +0.0490 inch, respectively, due to the action of the punch in the 1-meter puncture drop. The change in vertical diameter measurement is equivalent to less than a quarter inch on the full-scale cask.

Changes to the outer diameter measurements as a result of the tests can be determined by comparing Table 2.10.8-3 and Table 2.10.8-6. As before, these dimensions changed little, less than about 0.006 inch at every measured location except in the cask middle. At the midpoint, the vertical change was approximately -0.5 inch, equivalent to 2 inches in a full-scale cask. The change in the horizontal diameter at that location was +0.02 inch, equivalent to less than 0.1 inch in a full-scale cask. These changes were again due to the action of the punch on the outer cask shell in the 1-meter puncture drop.

Changes to the cask length measurements as a result of the tests can be determined by comparing Table 2.10.8-4 and Table 2.10.8-7. With the exception of two data points, all after-drop measurements were within 0.031 (1/32) inch of the beginning data points. This is less than a quarter inch deviation on the full-scale cask. The two exceptions include a 0.14 inch change in length measured at the 180-degree point on the first block set, and at the 270 degree point on the second block set. These exceptions are attributed to error in replicating the exact measuring locations as opposed to a real change in length, since other measurements, even at that block set, showed little or no change.

2.10.8.8 Discussion of Test Results

As previously noted, pre- and post-test measurements showed that nearly all permanent deformation of the packaging model was limited to the impact limiters. The only significant exception to this occurred for the side puncture test, where local deformation of the outer shell and the lead shielding did occur, but the outer shell was not punctured. The local deformation was as expected and produced only a very slight, local dimple in the inner shell wall (0.05 inch).

Before each test, the model closure lid was installed with a new O-ring and with a bolt torque of 44 inch-pounds, which was calculated to produce a bolt tensile stress equal to one-half the yield strength of the bolt material (same as full-scale criteria). This bolt load exceeds the calculated maximum bolt load for the accident conditions. The model cavity was pressurized to 30 psig and held with a gauge reading verifying that leakage was not occurring. After each test, the leaktightness of the cavity was checked. For the side drop, the oblique drop, and the side puncture drop, the pressure gauge provided this verification; for the end drop and the corner drop, verification was provided by repressurizing the cavity and maintaining a gauge reading after repairing the external pressure test valve. The unprotected external pressure test valve was sheared off during the end drop as the model body moved into the upper impact limiter during

the impact. During the corner drop, the valve piping loosened due to shock loading. These occurrences are not a concern in the full-scale cask because the valve ports are protectively recessed in the upper ring forging, where containment is provided by double O-rings in the port covers. Thus, it is concluded that the structural adequacy of the containment vessel is confirmed.

The aluminum honeycomb materials of the model impact limiters were identical in all aspects to those of the full-scale cask. Since the crush area of the limiters and the stress area of the body of the model are reduced by the (scale factor)^2 = 1/16, the impact acceleration is 1/(scale factor) = 4 times that of the full-scale cask and the crush deformation is the (scale factor) = (1/4) times that of the full-scale cask. The measured crush deformations of the model limiters were essentially the same as the values scaled from the full-size impact limiter analyses of this report. Visual observation of the model impact limiter deformations confirmed that for every cask drop orientation, only the "backed" areas of the limiters are effective in absorbing the impact energy. This result supports the "backed" area principle established by previous testing programs and confirms the impact limiter analyses performed elsewhere in this report. As previously described, the model impact limiter attachment lugs were undersized and failed. The four 30-foot drop tests confirmed the analysis results for each cask orientation, which determined that the impact limiters will remain in position on the cask during the impact(s), whether or not there are attachment lugs present; the attachment lugs retain the impact limiters on the cask body until an impact occurs. Thus, it is concluded that the structural and functional adequacy of the NAC-LWT cask impact limiters is confirmed.

The report analyses were confirmed, as the cask body sustained a 30-foot drop test for each of the four drop orientations without incurring any measurable permanent deformation. Since the model did not include the neutron shield and expansion tank shells, the model is conservative. Additionally, the model inner and outer shells are Type 304 stainless steel (S_u = 75 ksi, S_y = 30 ksi), while the full-scale inner and outer shells are Type XM-19 stainless steel (S_u = 100 ksi, S_y = 55 ksi). Therefore, it is concluded that the structural adequacy of the NAC-LWT cask body is confirmed for the 30-foot Free Drop Hypothetical Accident Condition.

Based on visual observation of the model tests; i.e., the side drop and the 60-degree oblique drop, and inspection of the crushed region of the model limiters, no "slapdown"/rebound effects were apparent. This confirms the results of the "slapdown" evaluation analysis found in Section 2.10.4.

The side puncture test was performed last in the testing sequence because some local deformation of the outer shell was expected. Since an accurate, reliable analysis of the local puncture region of the cask body is very difficult, an empirical relationship based on testing of lead-backed shells was used to establish the outer shell thickness. The outer shell of the model cask body incurred significant permanent deformation in a very local region around the point of

impact during the side puncture test. As expected, the outer shell was not penetrated. Based on post-test measurements, a very slight, local deformation (0.05 inch) of the inner shell occurred at the midpoint. Since the full-scale cask will include a well-supported 0.25-inch thick neutron shield tank and the stronger, Type XM-19 stainless steel inner and outer shells, the deformation of the outer shell will be substantially reduced and the deformation of the inner shell will be eliminated. Furthermore, the isolation of the inner shell provided by the lead, as it diffuses the shock of a pin puncture, will be enhanced by the factor of four increase in lead thickness of the full-size cask. It is concluded that the side puncture test has confirmed the adequacy of the puncture protection of the NAC-LWT cask and the design criteria and methodology of this report.

In summary, the detailed results of the Quarter-Scale Model Drop Test Program for the NAC-LWT cask described in this appendix, confirm the analyses found elsewhere in this report and the structural adequacy of the cask design for the Free Drop and Puncture events specified by the Hypothetical Accident Conditions of 10 CFR 71.73.

2.10.8.9 Post-Test Revisions

As discussed in prior paragraphs of this appendix, the impact limiter attachment lugs and bolts (cask and limiter) failed during some of the 30-foot drop tests without any effect on the protection of the cask provided by the impact limiters. The attachment lug thickness on the quarter-scale model impact limiters was 0.062 inch (0.25/4). The actual thickness of the impact limiter attachment lugs on the model cask body was 0.037 inch due to a fabrication error (the lug thickness was designed to be 0.25/4 = 0.062 inch). The model limiter attachment bolts, No. 4-40 NC, were selected to have a cross-sectional area equal to one-fourth that of the full-scale bolts. After the initial drop test (30-foot end drop), the 0.037-inch thick limiter attachment lugs on the model cask body were replaced with 0.125-inch thick lugs and no subsequent failures of those lugs occurred during the ensuing drop tests. Thus, the full-scale impact limiter attachment lug design was revised to include 0.50-inch (0.125 x 4) thick lugs on both the cask body and the impact limiters along with 0.50-inch diameter attachment pins to alleviate concerns about their adequacy.

The purpose of the aluminum impact limiter shell is to provide a sealed container unit for the aluminum honeycomb energy absorbing material since the energy absorption capability of the shell is negligible; a 0.062-inch thickness was selected for the shell of the model impact limiters as the minimum thickness desirable for fabrication. Overlapped and epoxyed joints were used in the model impact limiters, since long-term sealing was not a concern. Because some of the model impact limiters split open at one or more joints during the crushing phase of some of the

drop tests, the full-scale impact limiter design was revised to include 0.125-inch thick aluminum shells with groove-welded joints all around (same as the NLI 1/2 cask.)

Examination of the model impact limiter following the 30-foot top end drop test showed that the 0.38-inch thick layer of lower strength (1,200 psi crush strength) unidirectional honeycomb located at the outer end of the impact limiter was crushed over the full diameter of the model impact limiter. This crushing resulted because the lower strength layer of honeycomb was effectively "backed" by the 3,500 psi crush strength multidirectional honeycomb, which makes up the remainder of the model impact limiter. The 3,500 psi crush strength honeycomb was not crushed over the full model impact limiter diameter; it only crushed over the diameter of the model cask body on the inside of the impact limiter directly under the model cask body. Thus, the calculated maximum design impact force for the 30-foot end drop is not affected by the crushing behavior of the lower strength layer of honeycomb, since that force was calculated based on the "backed" area of the cask body diameter. The purpose of the lower strength layer of honeycomb in the impact limiter is to control the g load applied to the cask during a 1-foot drop. Since the 1,200 psi crush strength of the lower strength honeycomb layer was designed based on the "backed" area of the cask body only, the design crush strength of that honeycomb layer was revised to 250 psi to account for the effective "backed" area of the full diameter of the impact limiter: average $P_{new} = (1200)(D^2_{body} / D^2_{Limiter}) = 250$ psi, where $D_{body} = 7.155$ inches and $D_{Limiter} = 16.25$ inches for the quarter-scale model upper limiter and $D_{Limiter} = 15.00$ inches for the quarter-scale model lower limiter. Thus, the design impact forces for the 1-foot end drops that are used in this report remain unchanged.

Figure 2.10.8-1 Drawing of Quarter-Scale Model

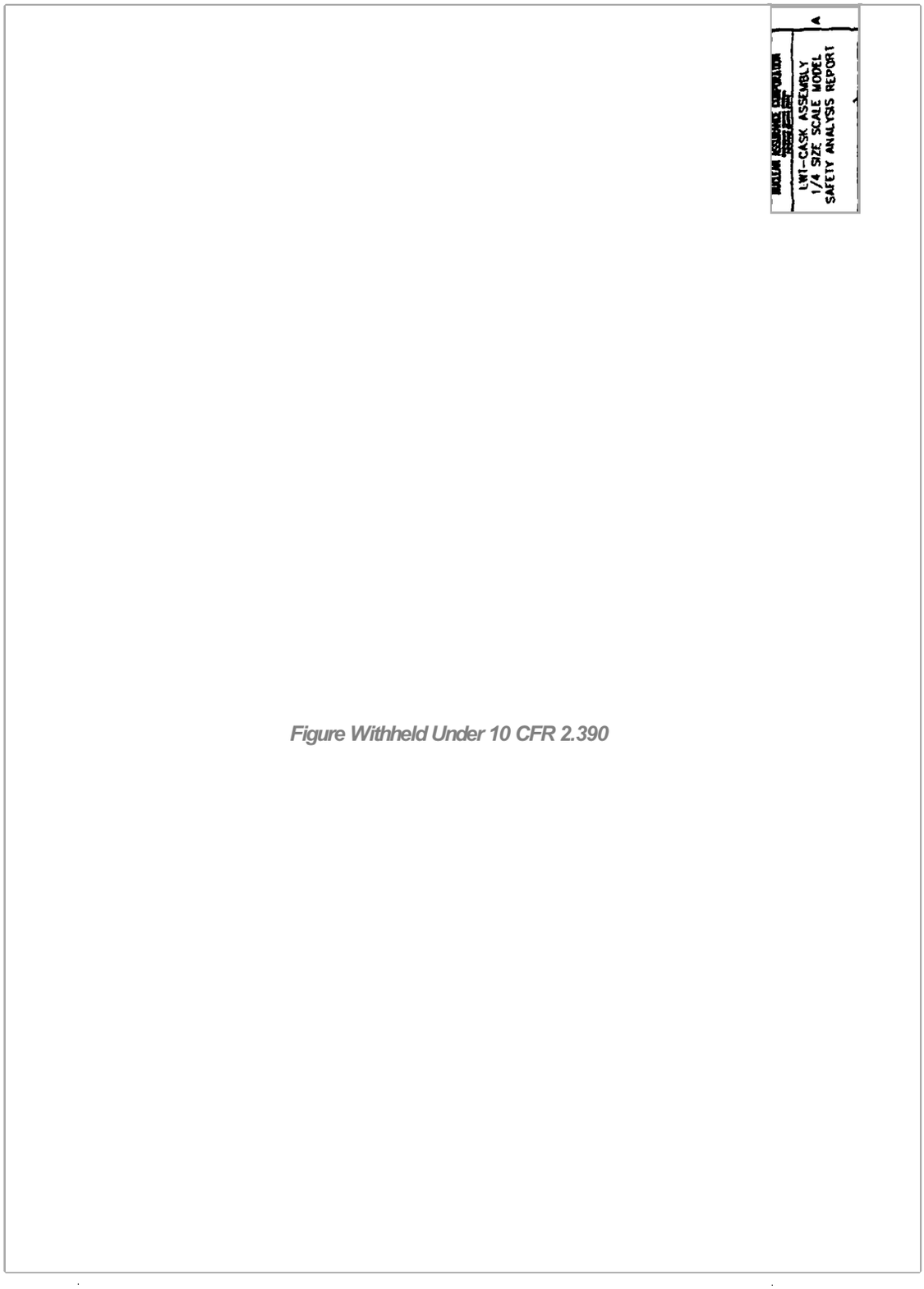

Figure Withheld Under 10 CFR 2.390

Figure 2.10.8-2 Drawing of Model Body

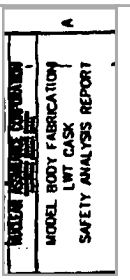

Figure Withheld Under 10 CFR 2.390

Figure 2.10.8-2 Drawing of Model Body(continued)

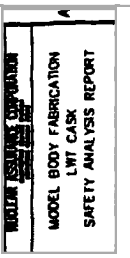

Figure Withheld Under 10 CFR 2.390

Figure 2.10.8-2 Drawing of Model Body (continued)

Figure Withheld Under 10 CFR 2.390

Figure 2.10.8-3 Drawing of Model Lid

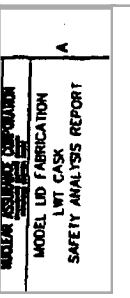

Figure Withheld Under 10 CFR 2.390

Figure 2.10.8-4 Drawing of Model Upper Impact Limiter

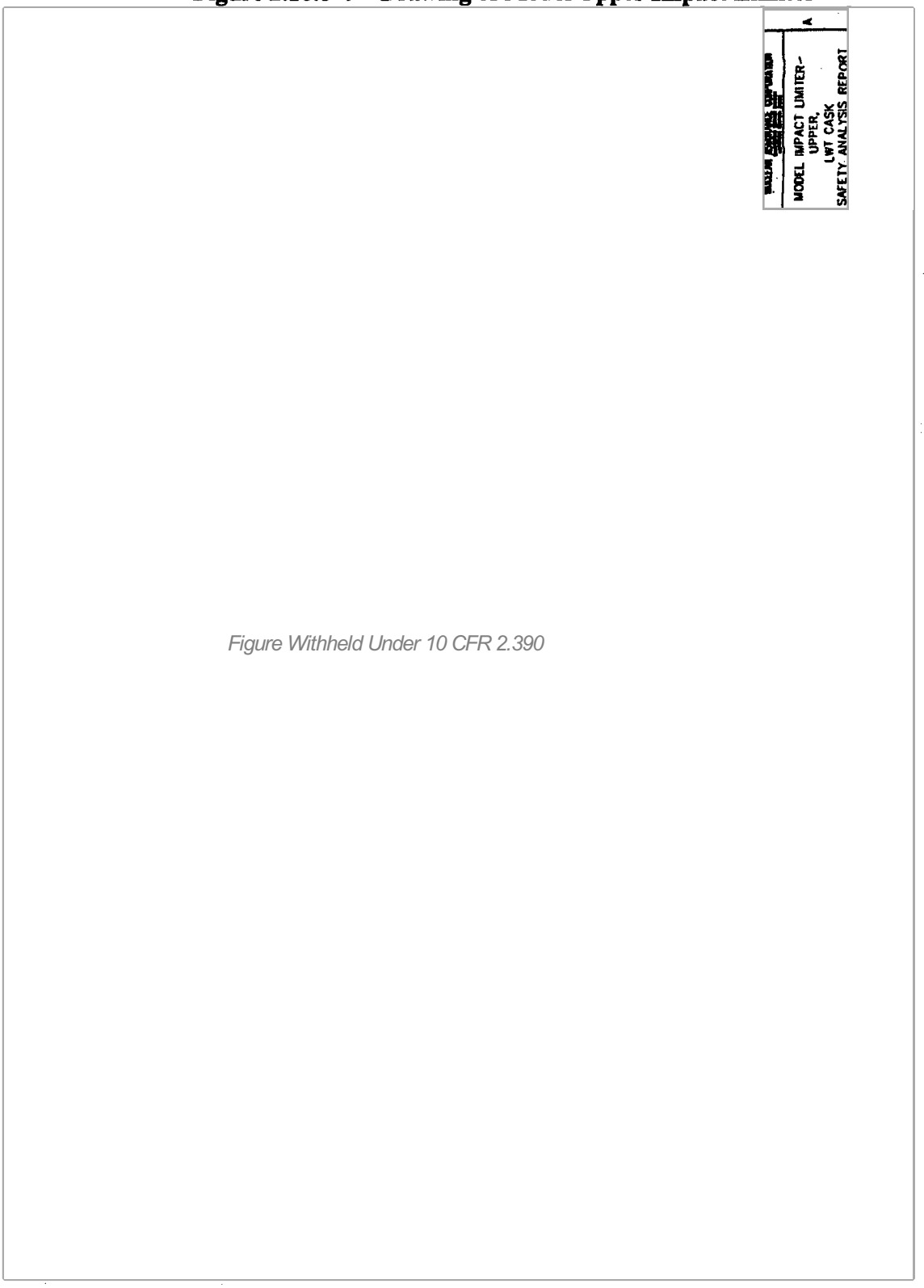

Figure Withheld Under 10 CFR 2.390

Figure 2.10.8-5 Drawing of Model Lower Impact Limiter

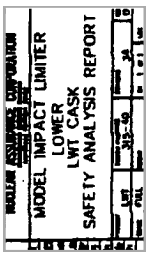

Figure Withheld Under 10 CFR 2.390

Figure 2.10.8-6 Drawing of Model Simulated Cask Contents

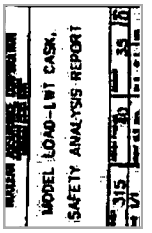

Figure Withheld Under 10 CFR 2.390

Figure 2.10.8-7 Quarter-Scale Model

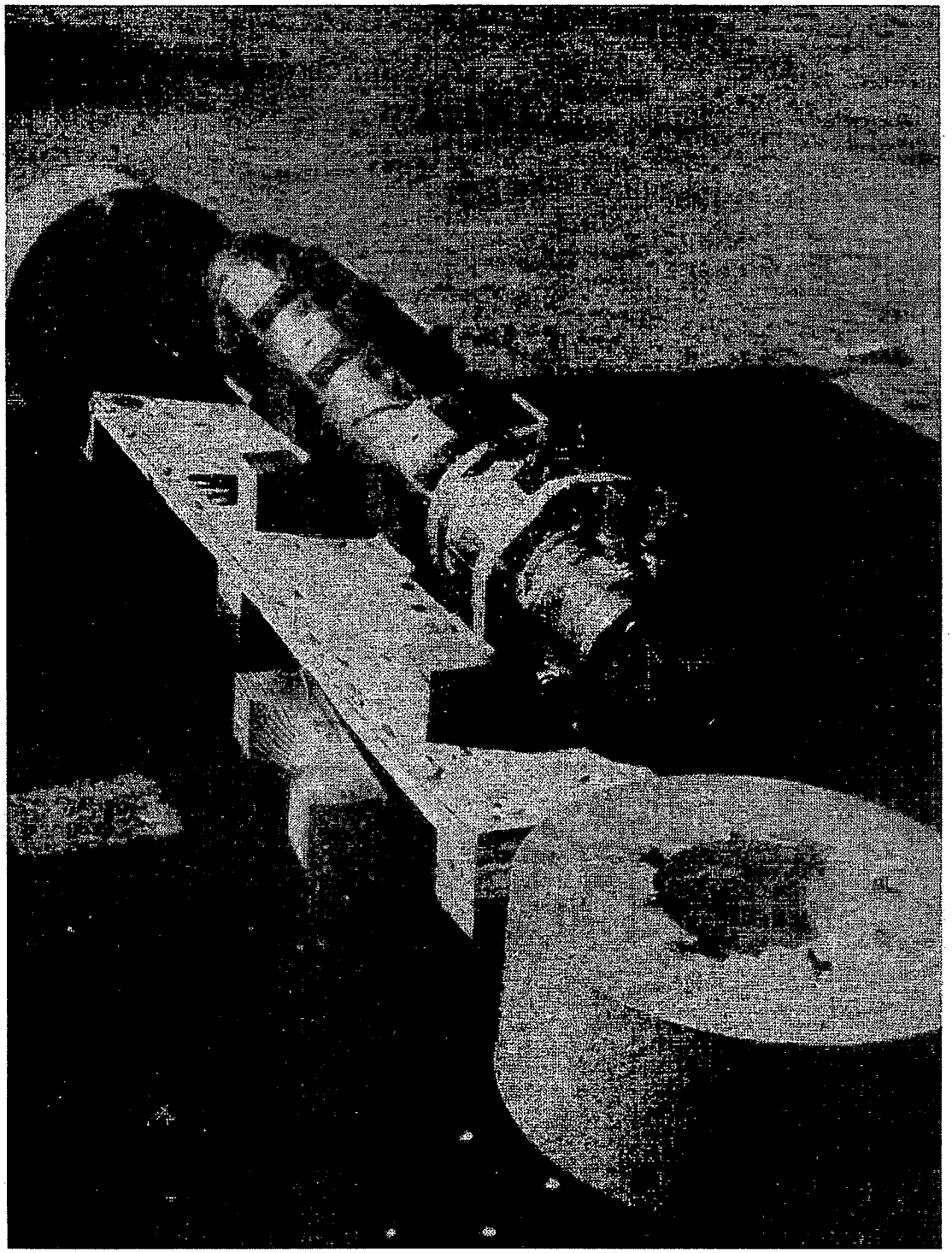

Figure 2.10.8-8 Model Rigged for 30-Foot End Drop

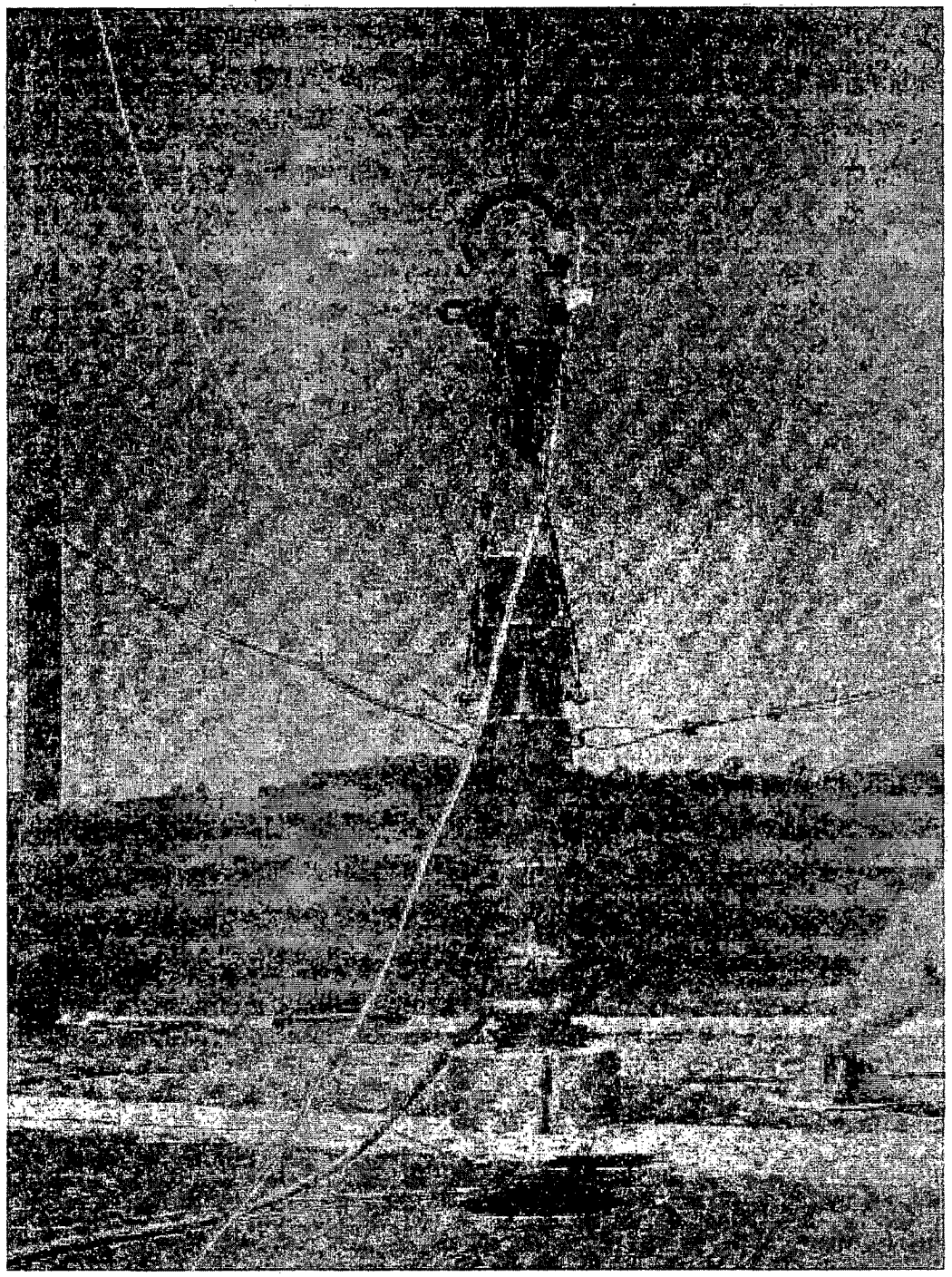

Figure 2.10.8-9 Model Positioned for 30-Foot End Drop

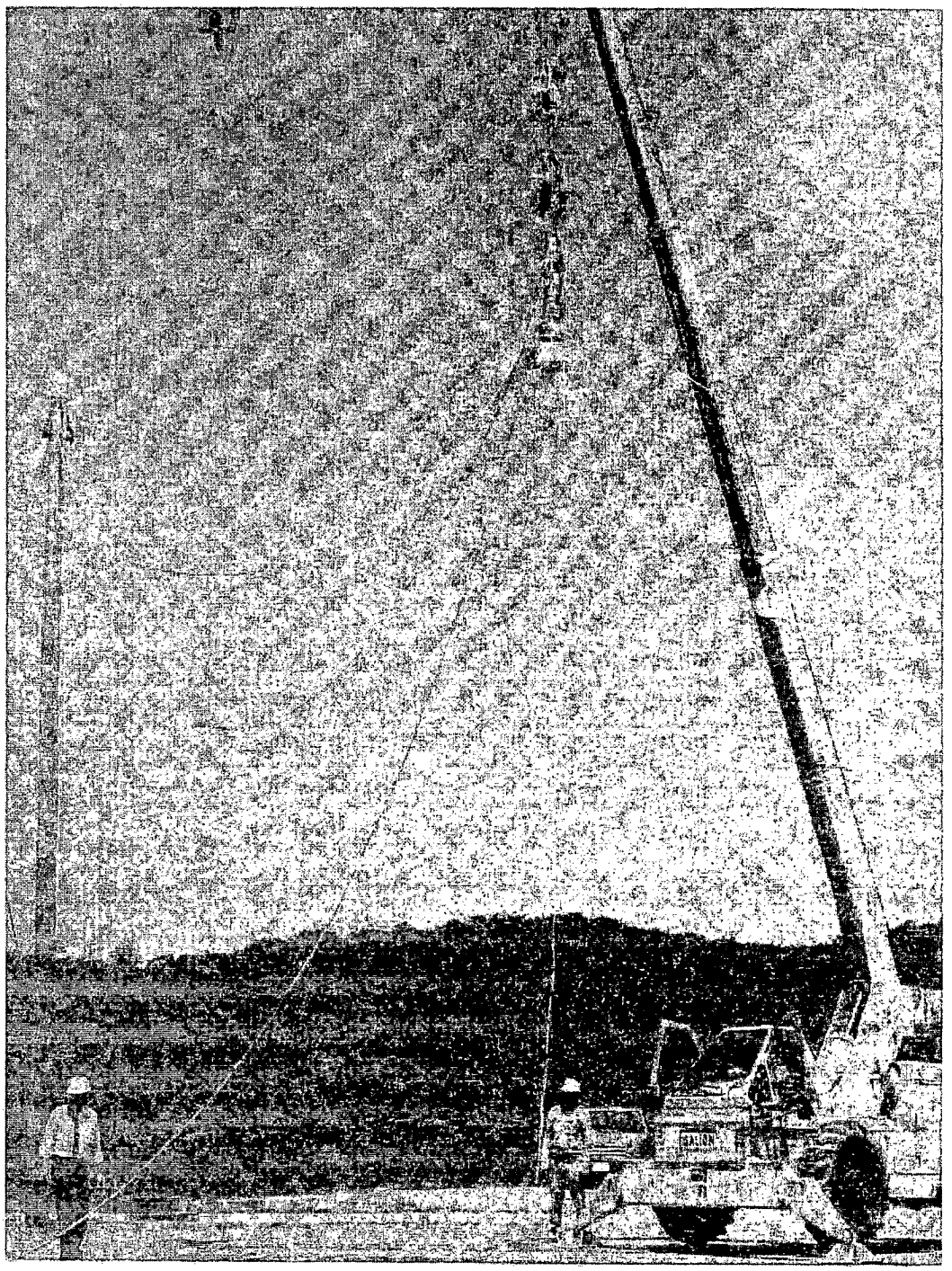

Figure 2.10.8-10 Model Position Following 30-Foot End Drop

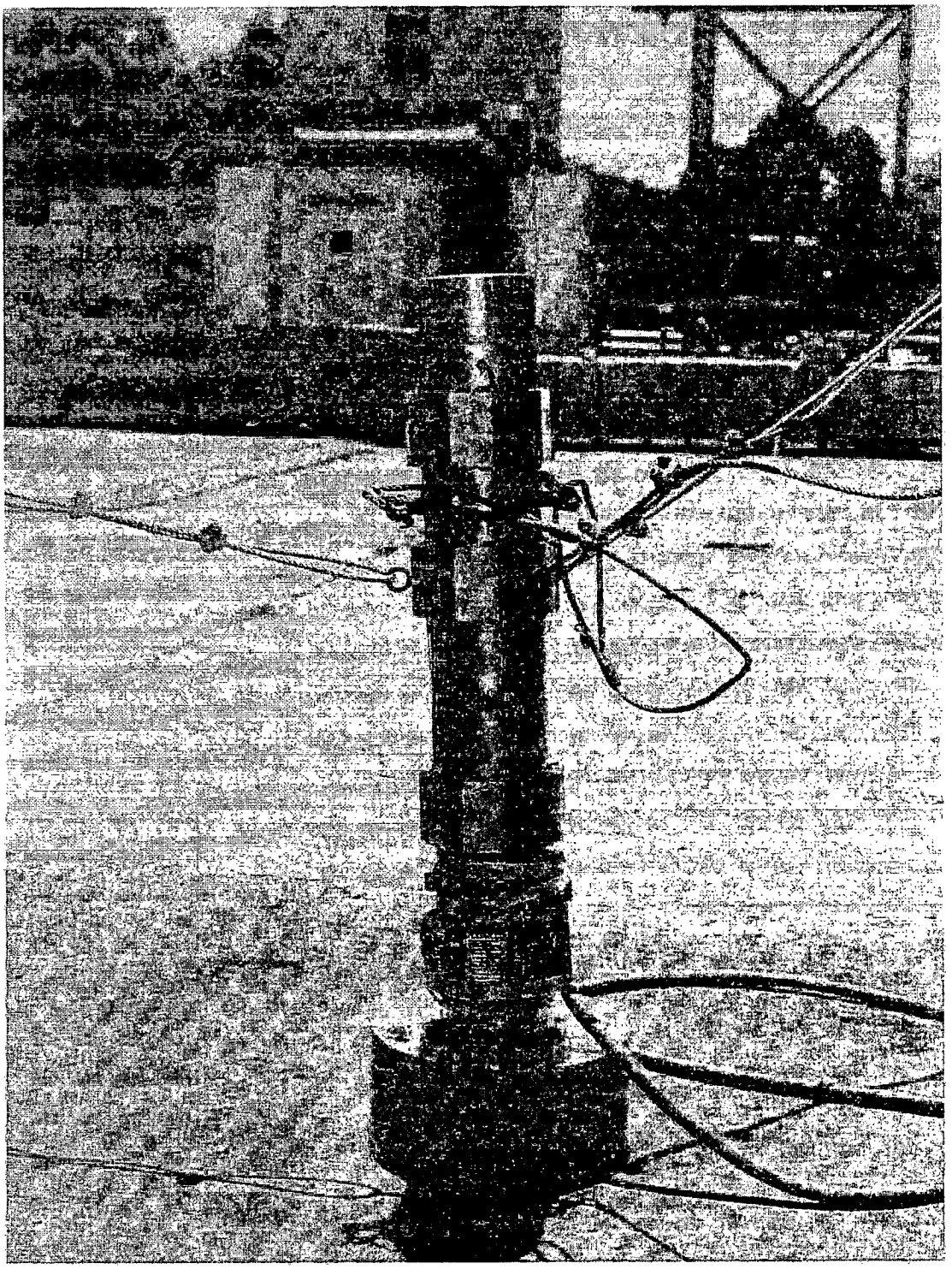

Figure 2.10.8-11 Top End Impact Limiter Following 30-Foot End Drop

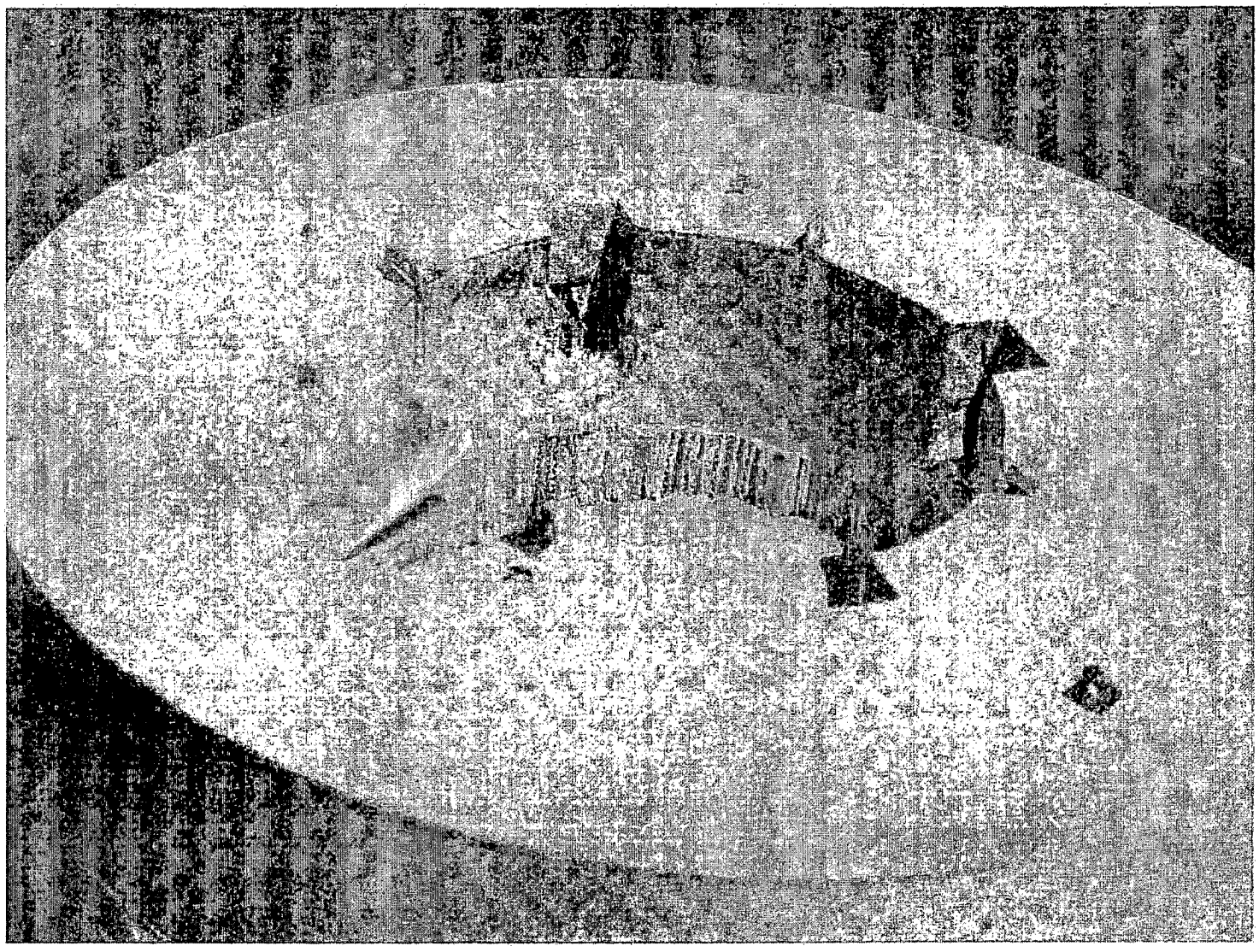

Figure 2.10.8-12 Exterior of Top Impact Limiter Following 30-Foot End Drop

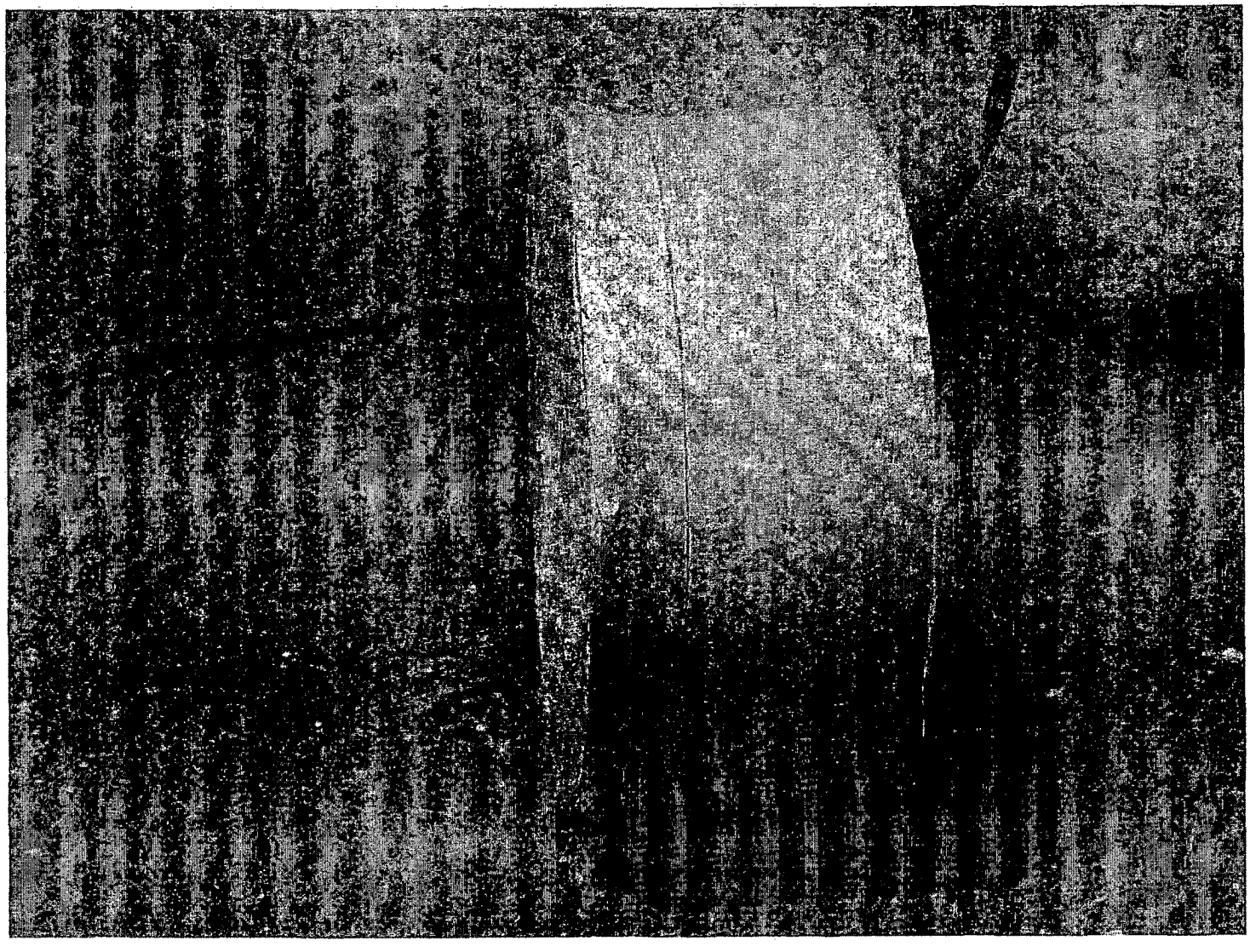

Figure 2.10.8-13 Model Rigged for 30-Foot Corner Drop

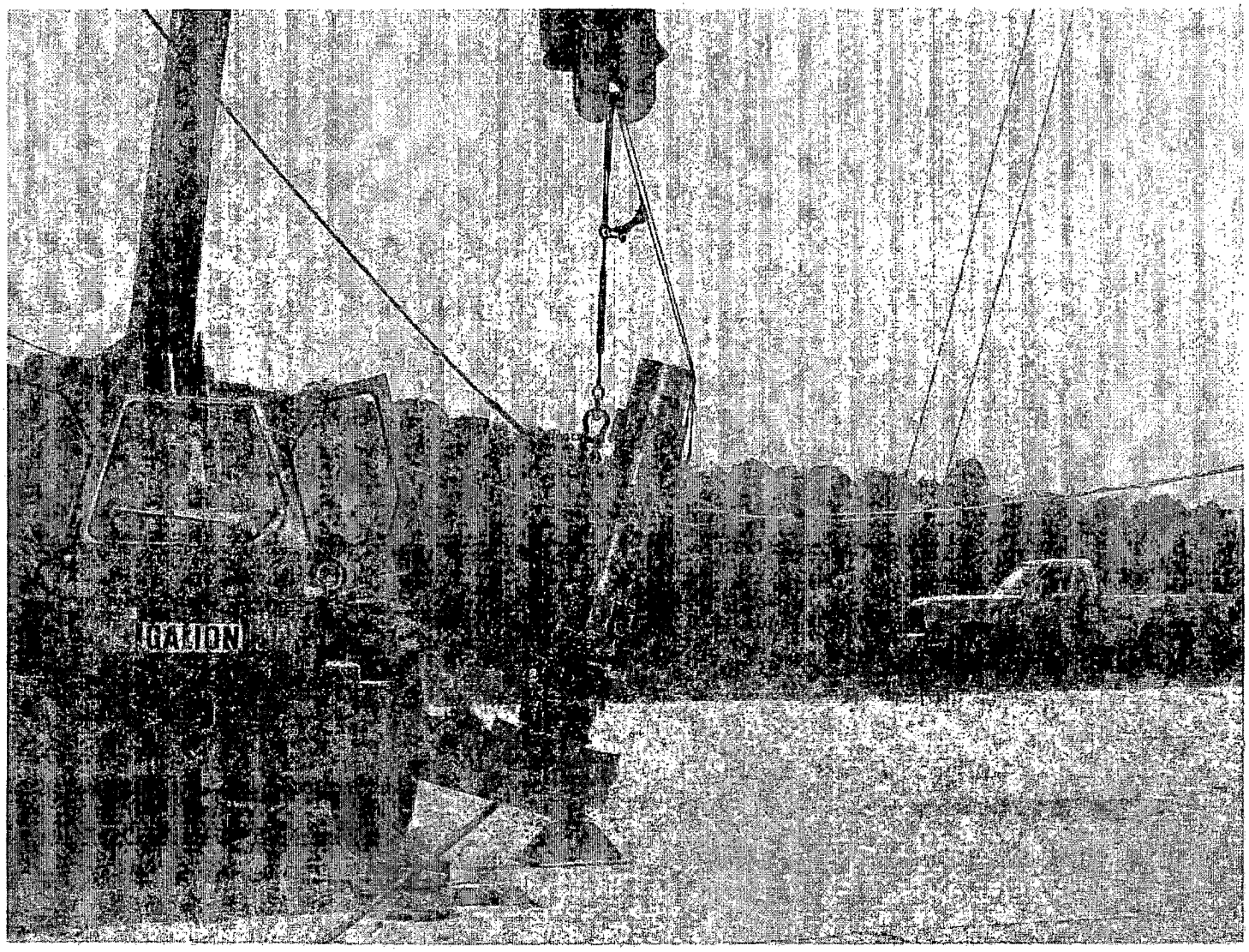

Figure 2.10.8-14 Model Positioned for 30-Foot Corner Drop

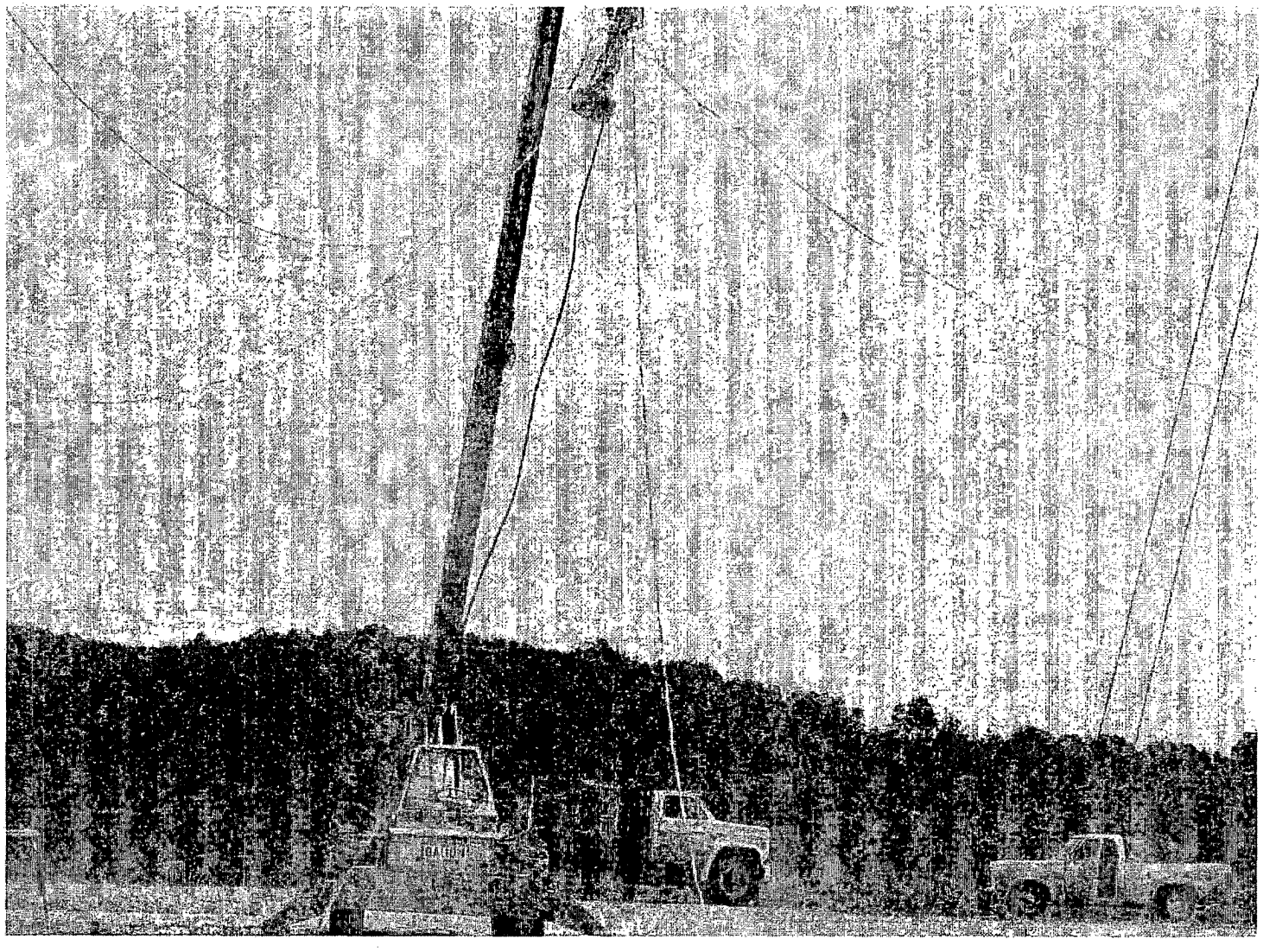

Figure 2.10.8-15 Model Following 30-Foot Corner Drop

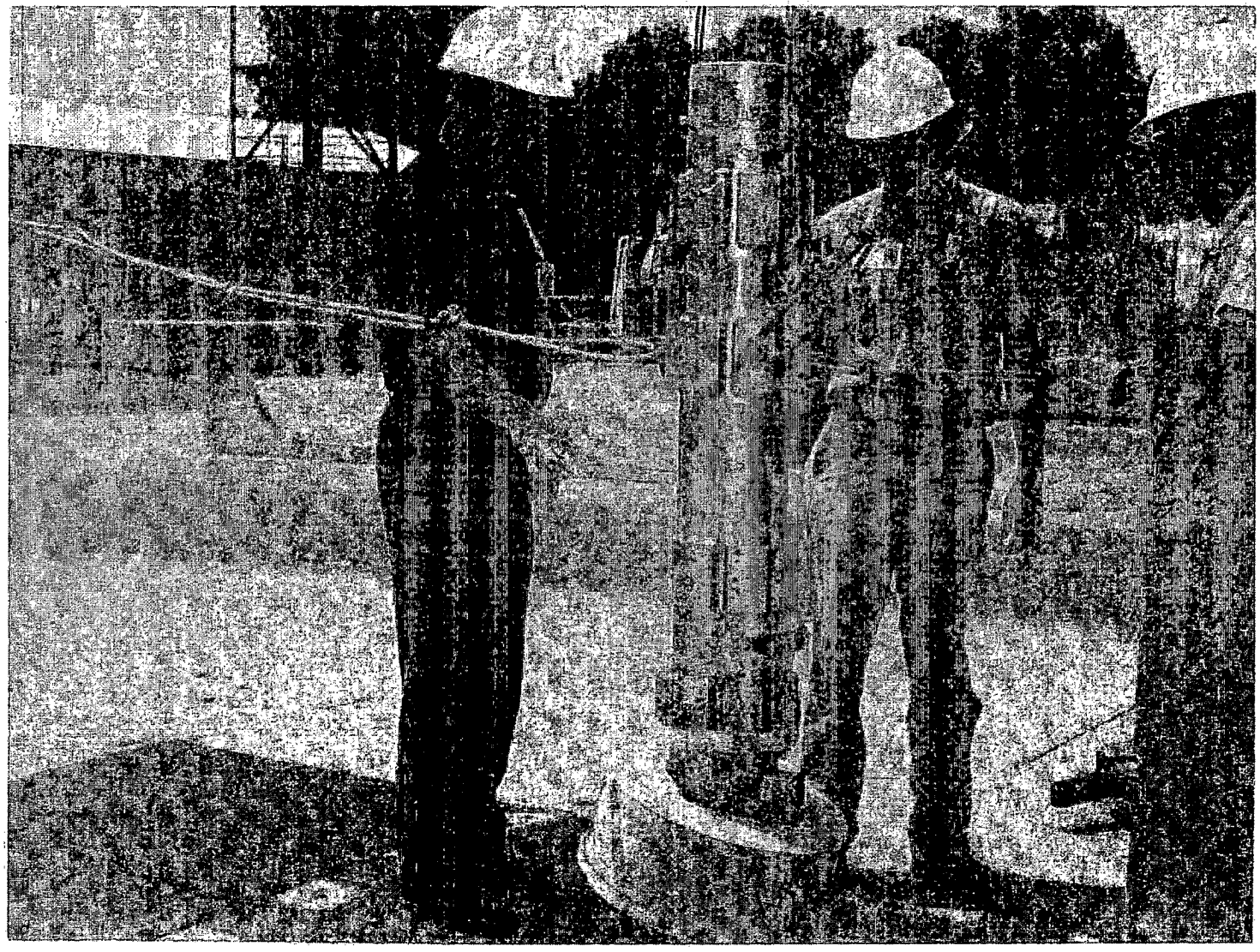

Figure 2.10.8-16 Top Impact Limiter Following 30-Foot Corner Drop

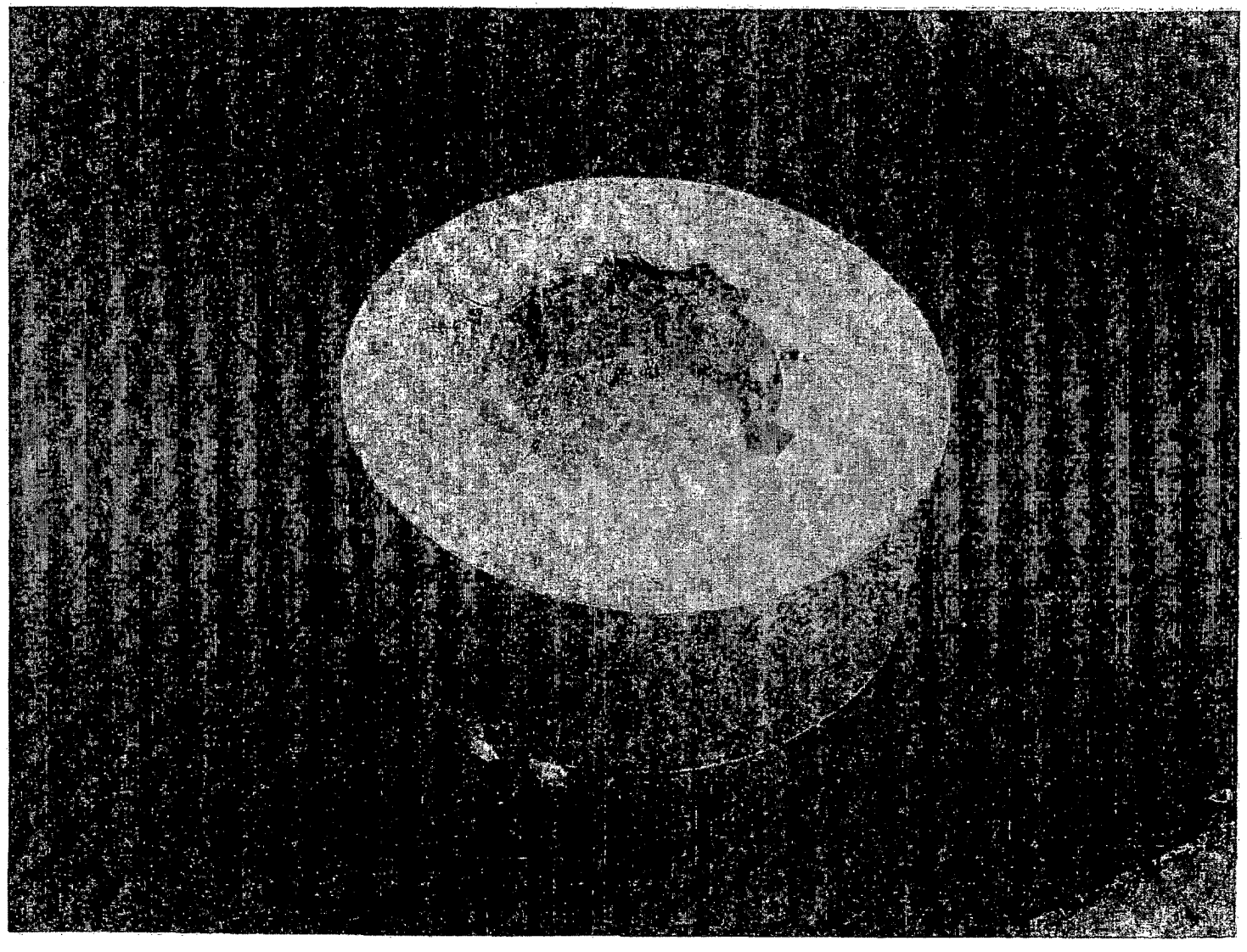

Figure 2.10.8-17 Model Position Following 30-Foot Side Drop – View 1

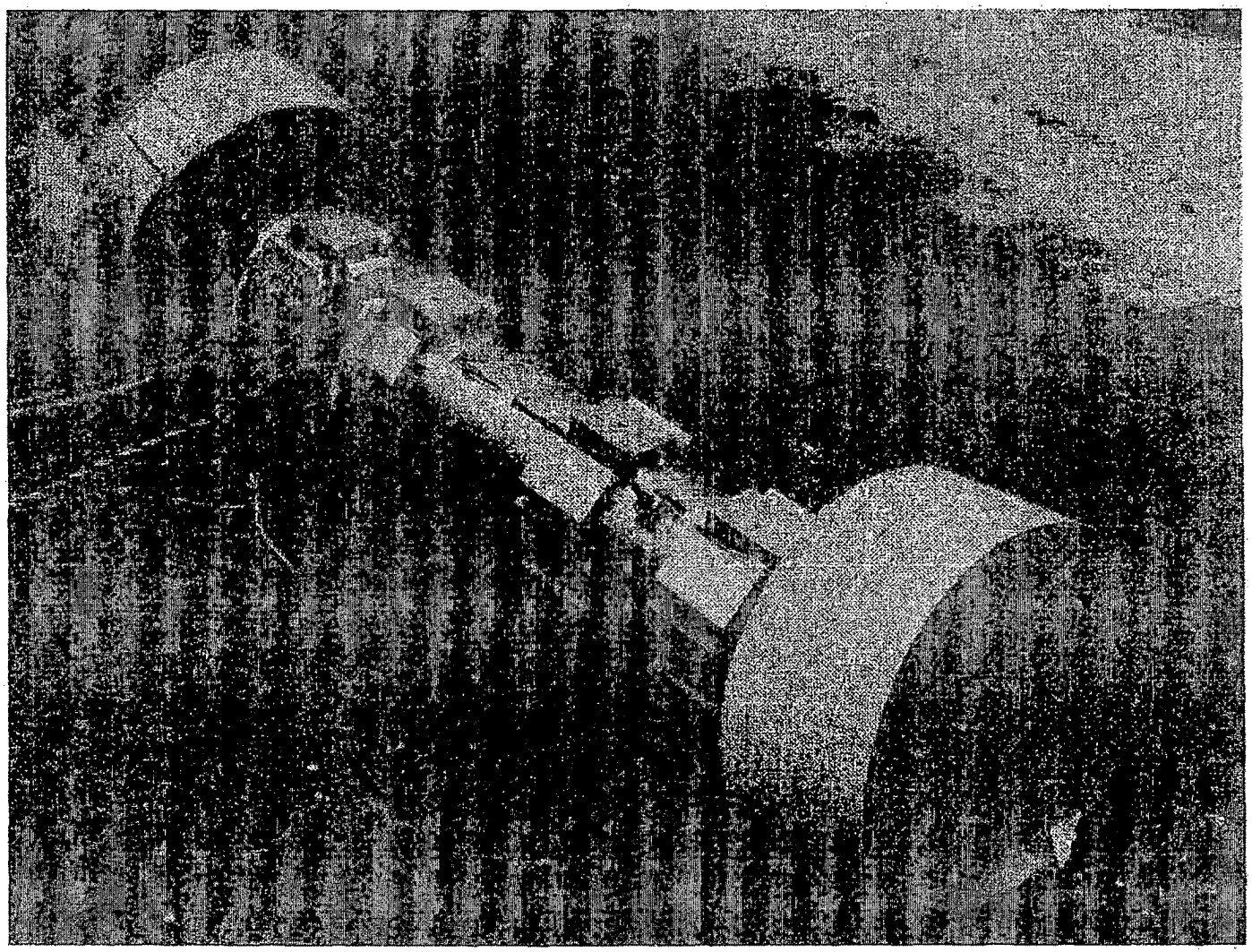

Figure 2.10.8-18 Model Position Following 30-Foot Side Drop – View 2

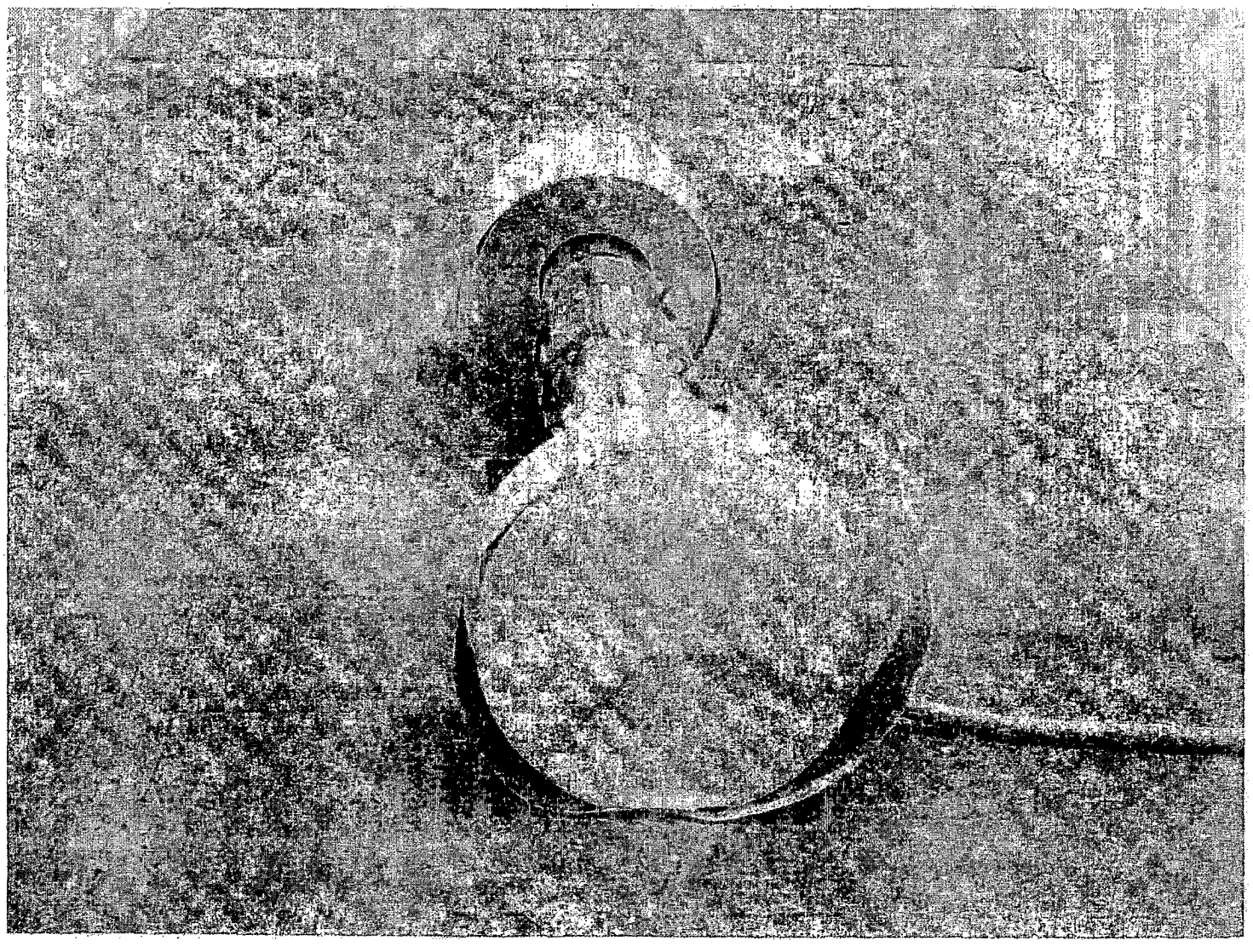

Figure 2.10.8-19 Top Impact Limiter Following 30-Foot Side Drop

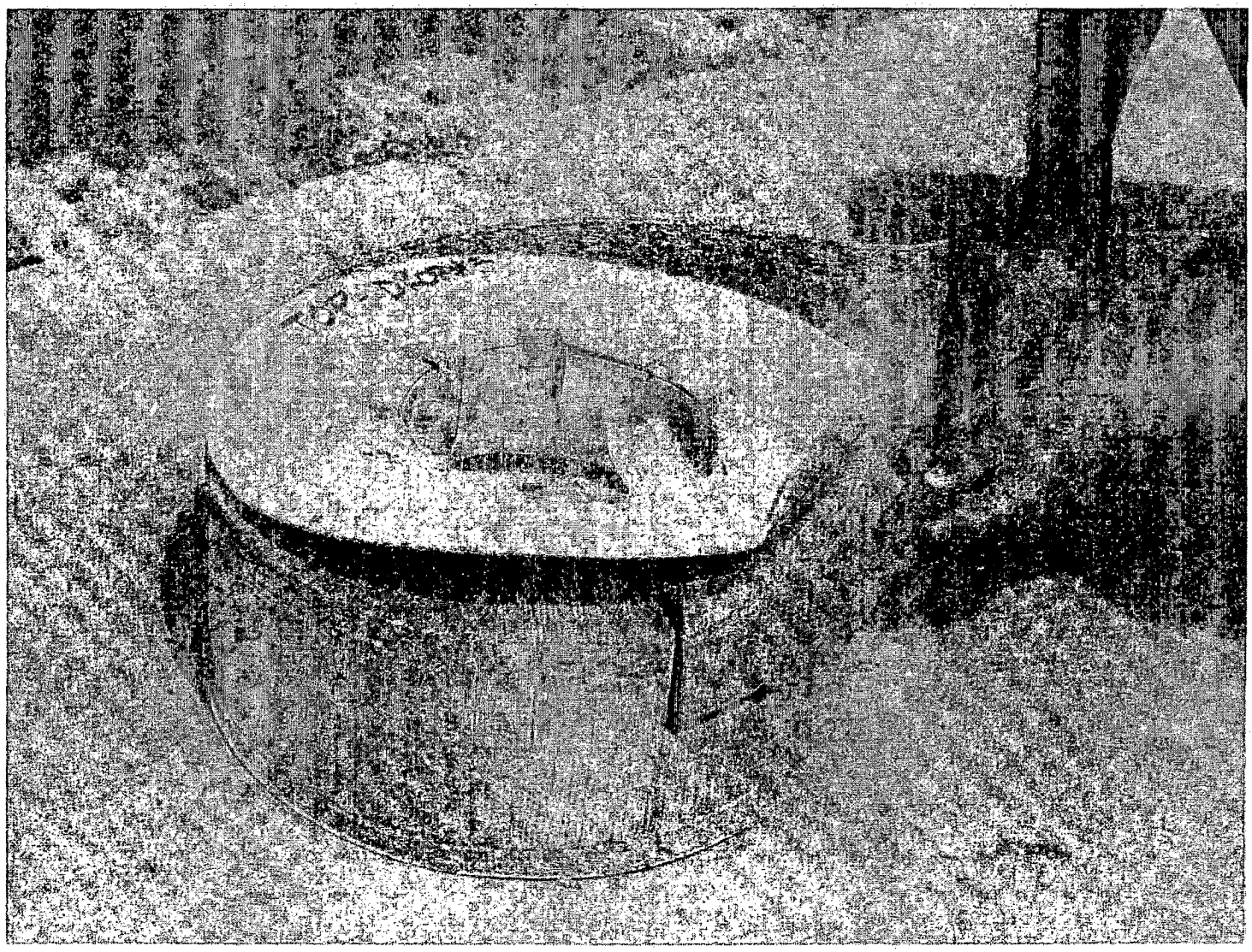

Figure 2.10.8-20 Bottom Impact Limiter Following 30-Foot Side Drop – View 1

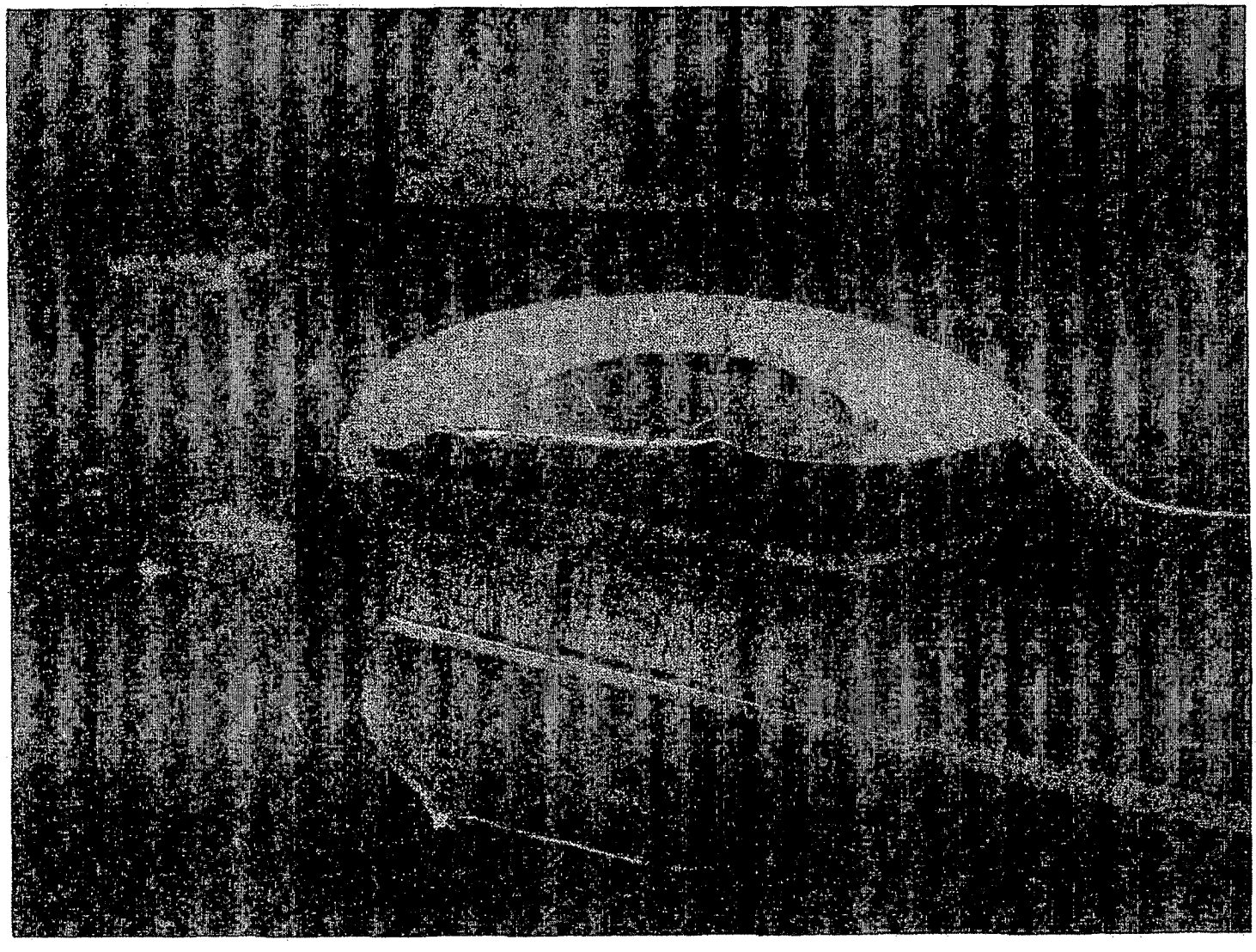

Figure 2.10.8-21 Bottom Impact Limiter Following 30-Foot Side Drop – View 2

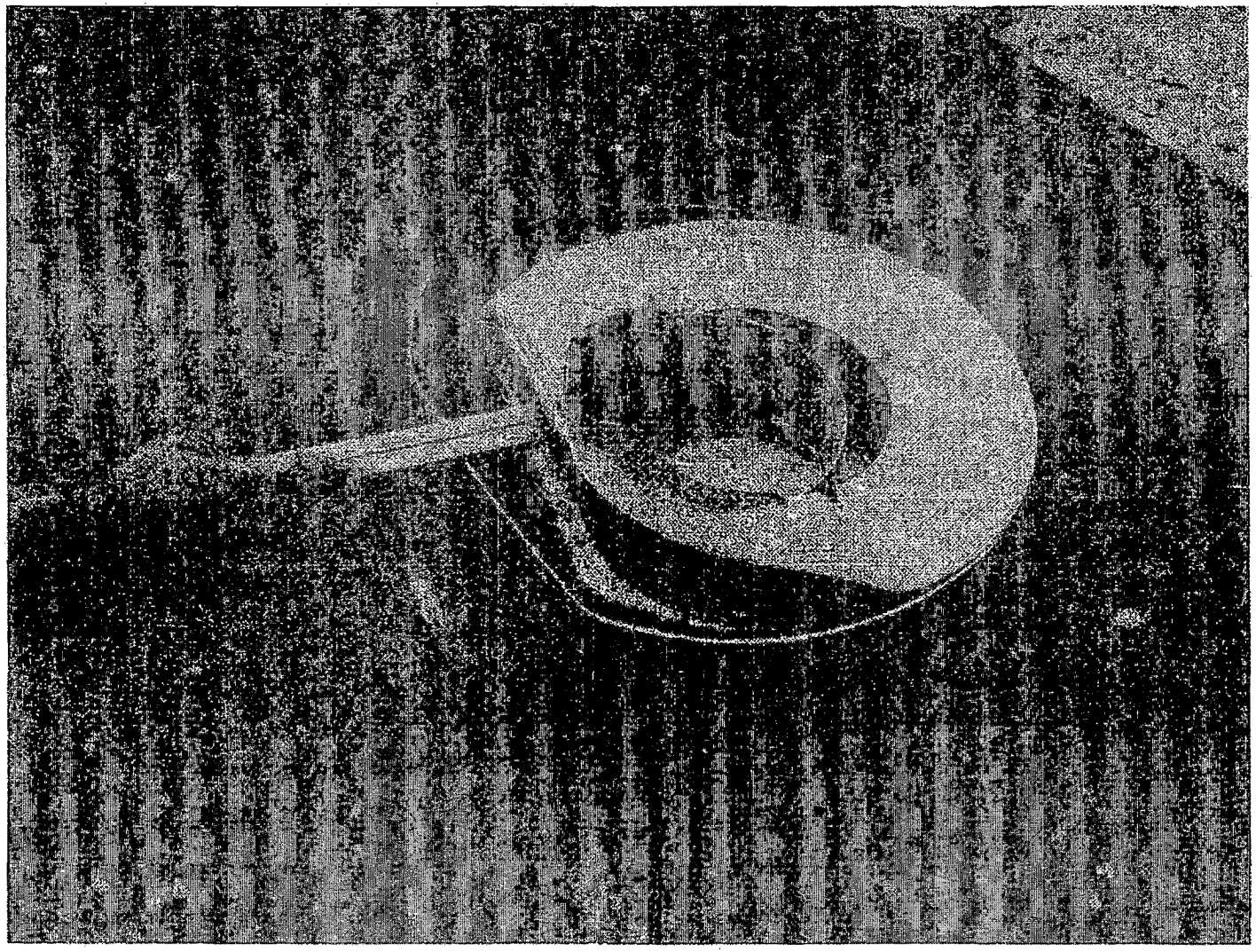

Figure 2.10.8-22 Model Rigged for 30-Foot Oblique Drop

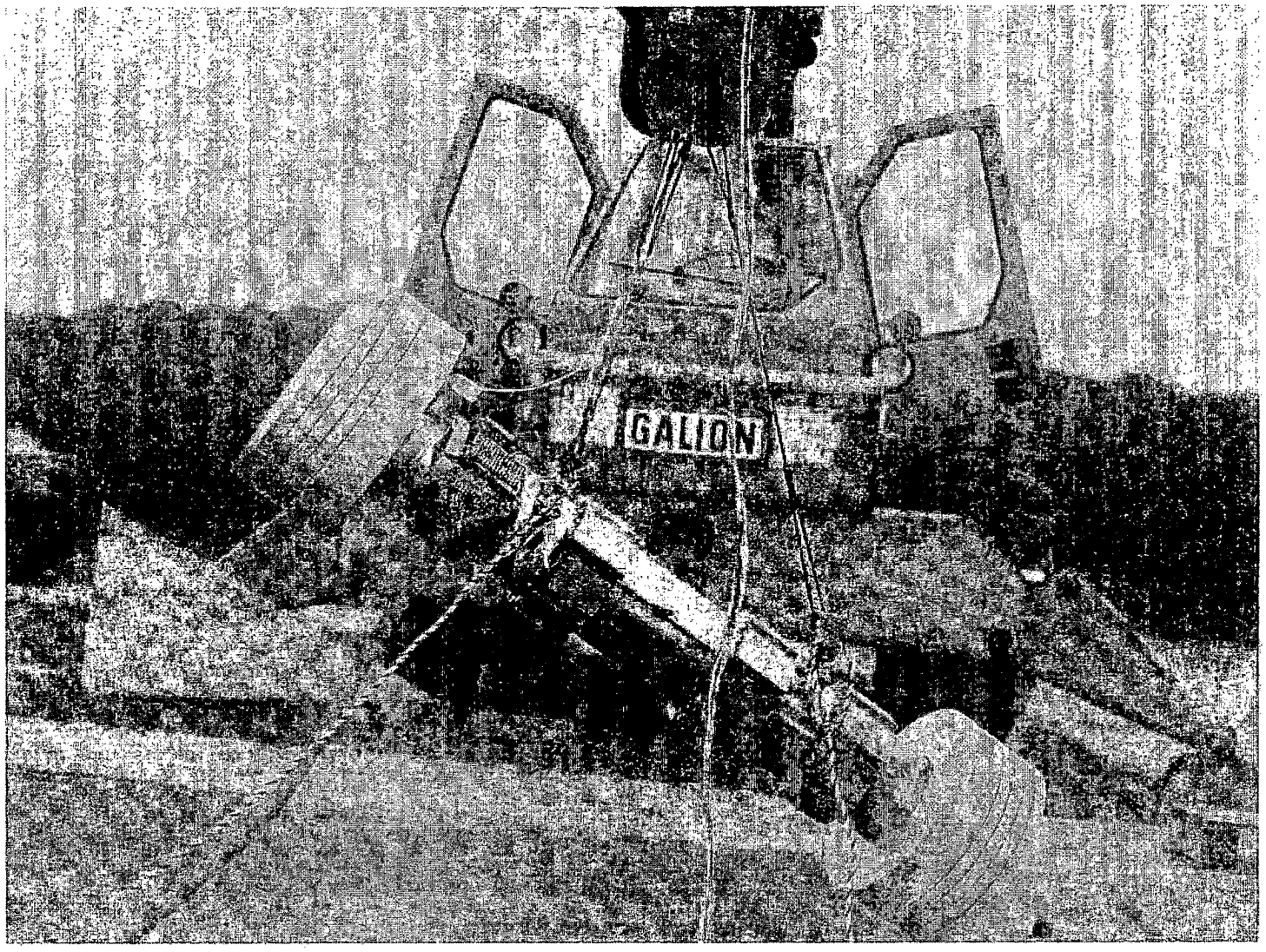

Figure 2.10.8-23 Model Positioned for 30-Foot Oblique Drop

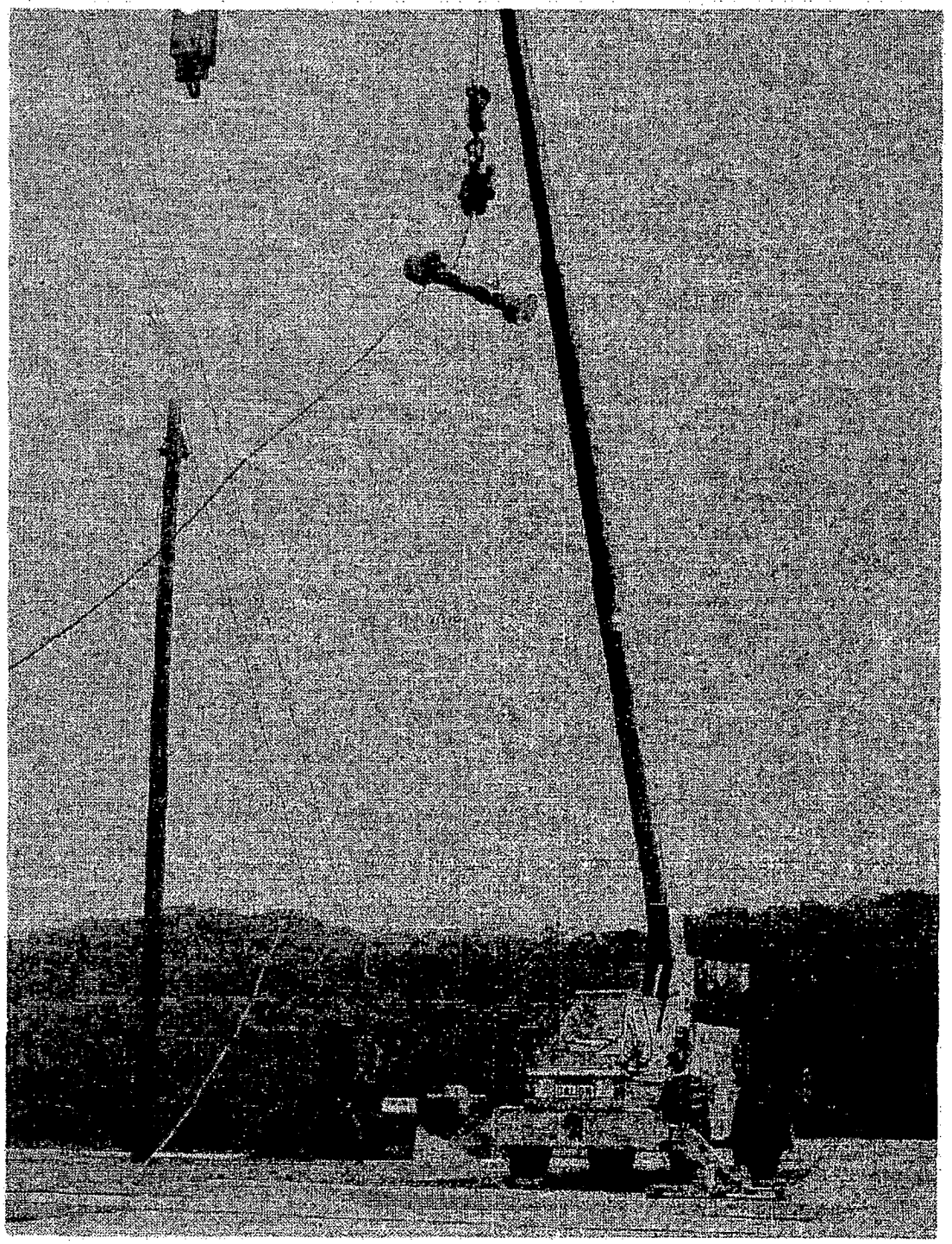

Figure 2.10.8-24 Model Position Following 30-Foot Oblique Drop

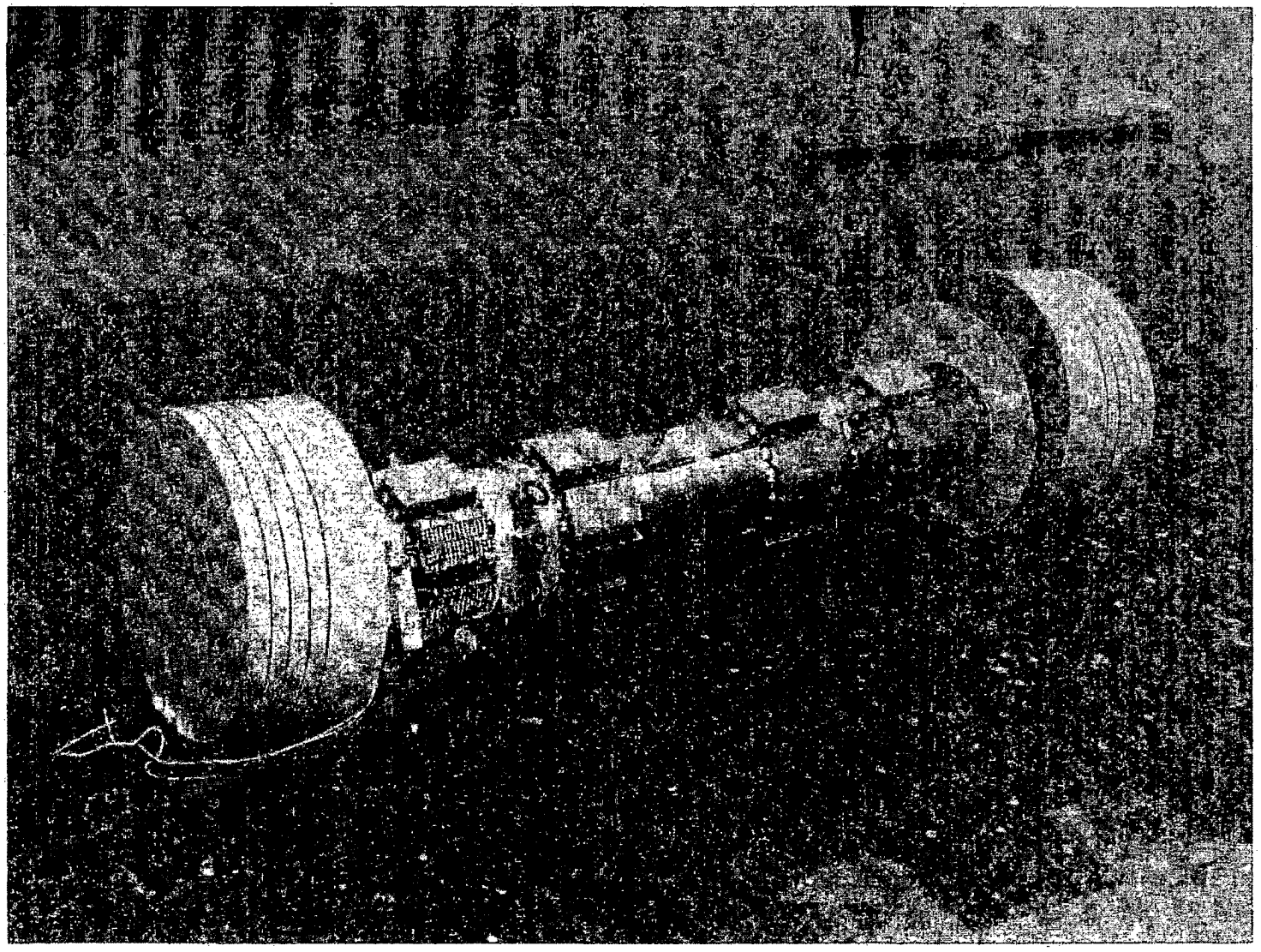

Figure 2.10.8-25 Bottom Impact Limiter Following 30-Foot Oblique Drop

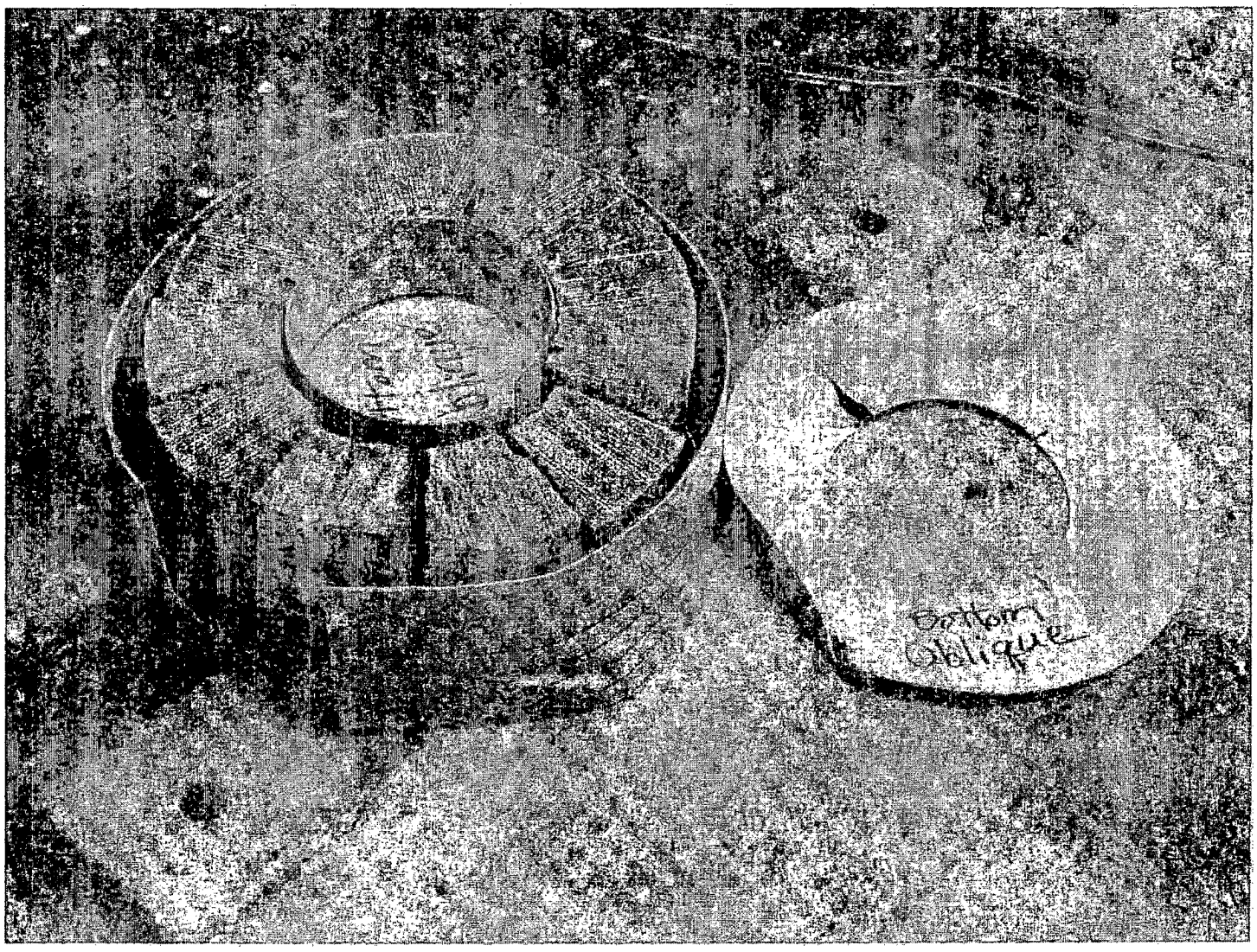

Figure 2.10.8-26 Top Impact Limiter Following 30-Foot Oblique Drop

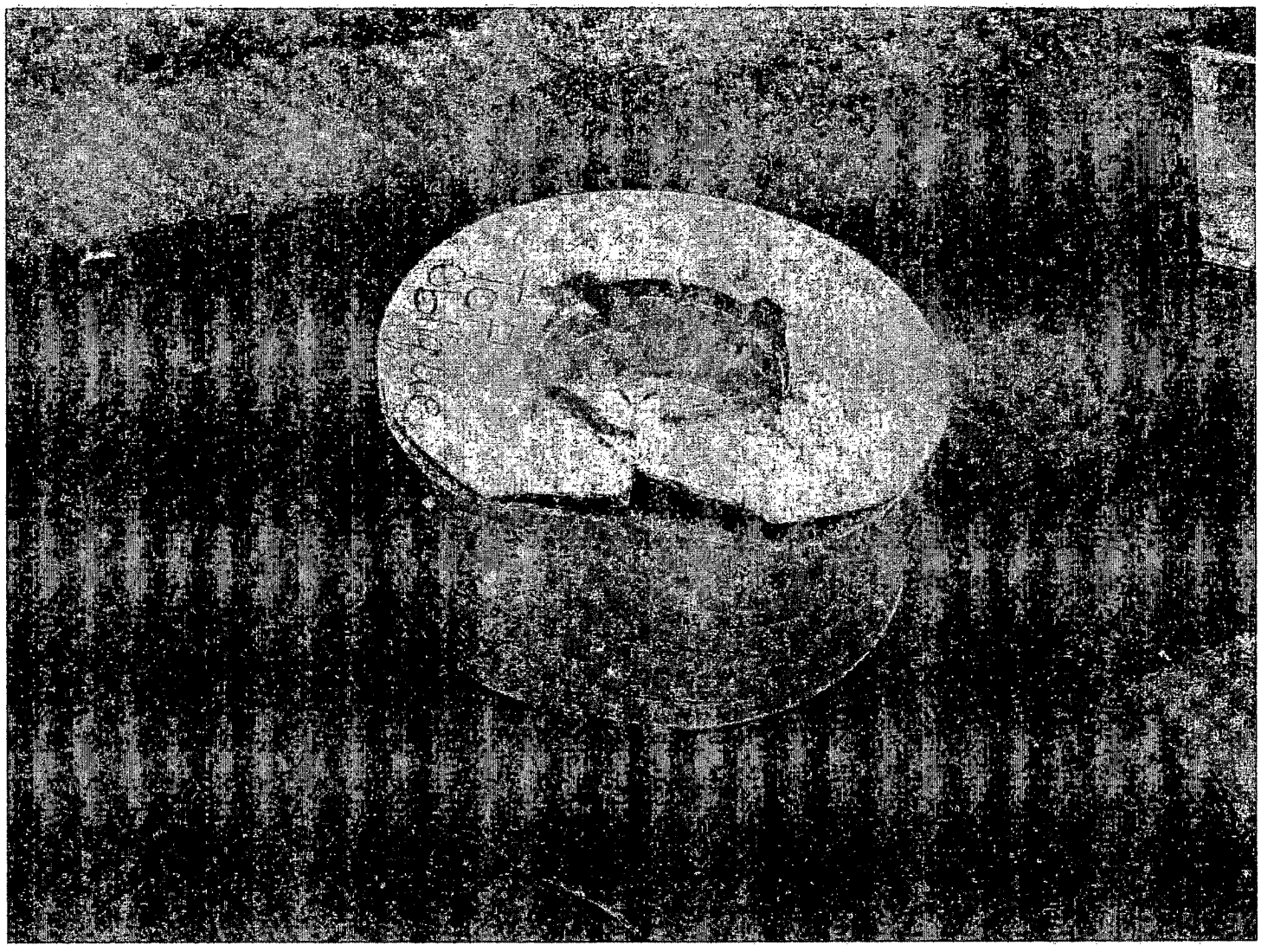

Figure 2.10.8-27 Model Rigged for Midpoint 40-Inch Pin Drop

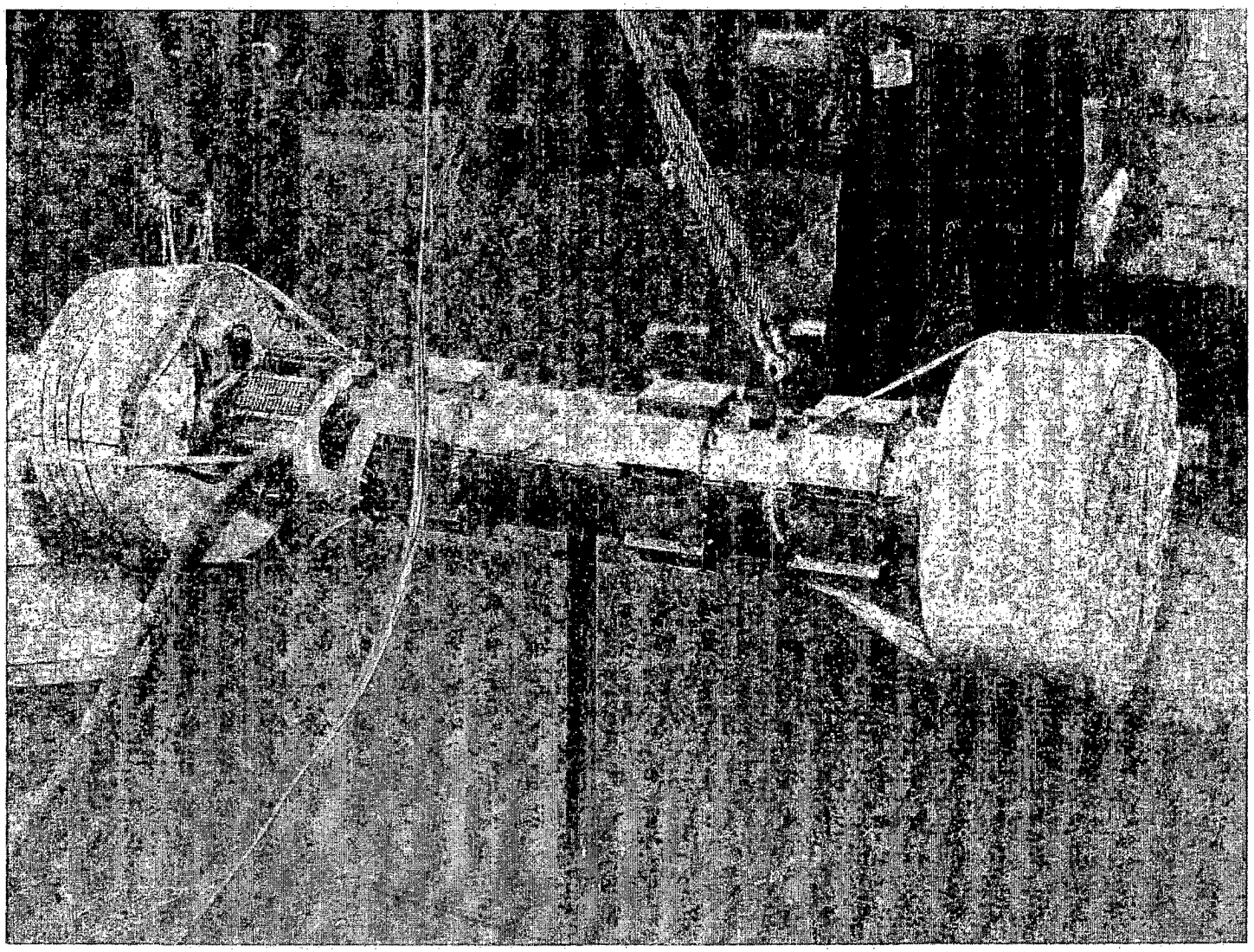

Figure 2.10.8-28 Model Positioned for 40-Inch Pin Drop

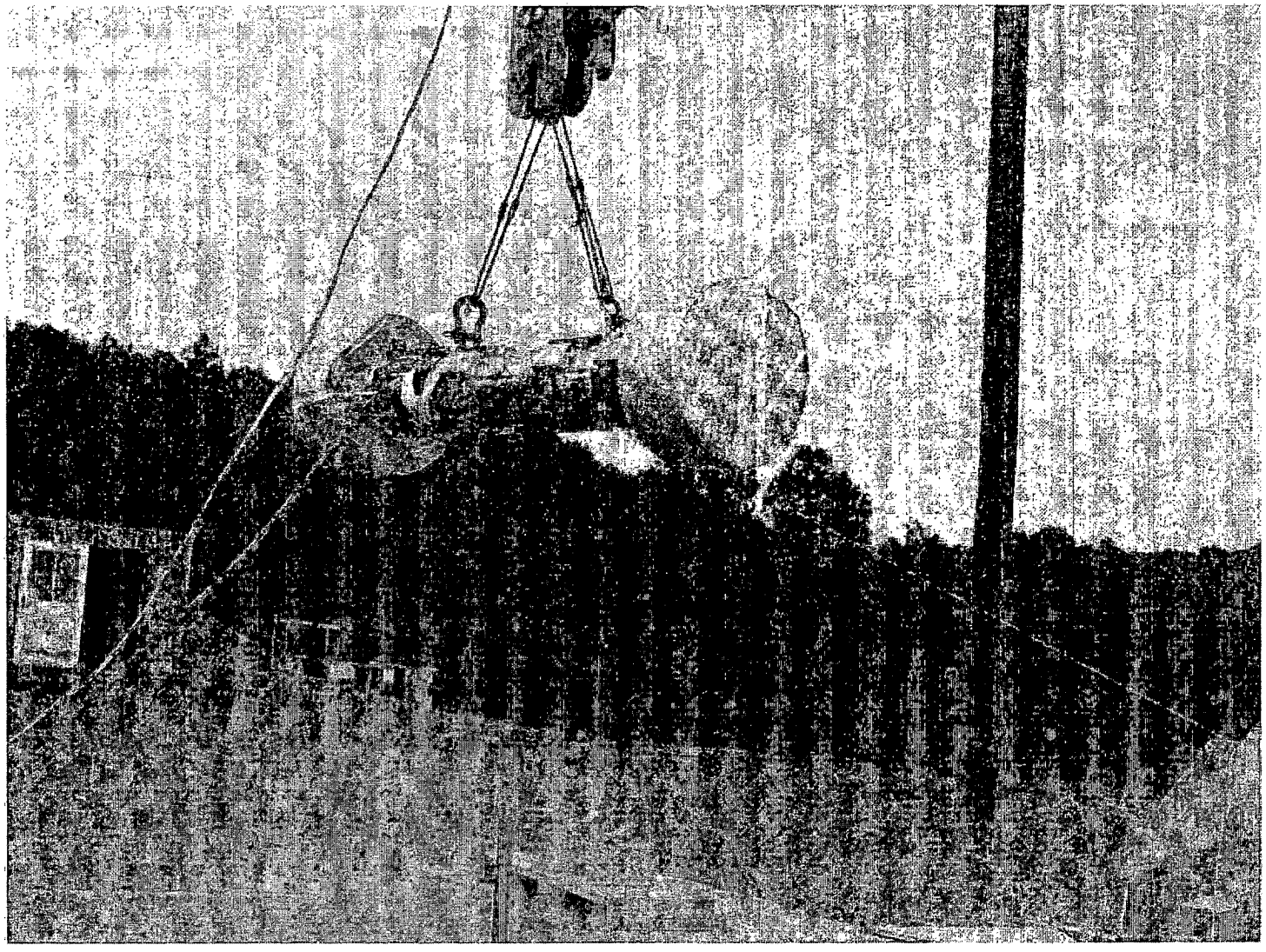

Figure 2.10.8-29 Instant Before Midpoint 40-Inch Pin Drop

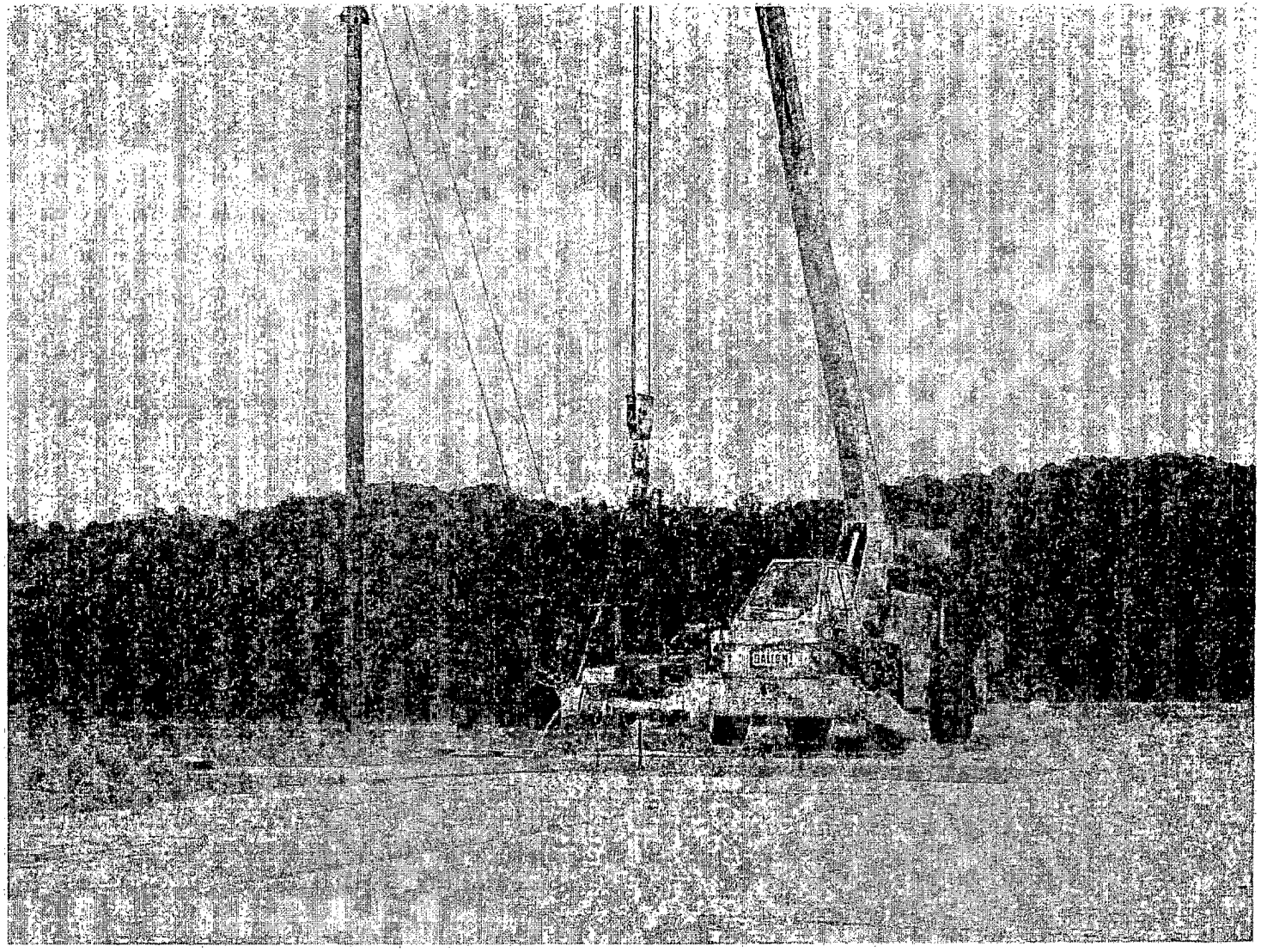

Figure 2.10.8-30 Model Position Following Midpoint 40-Inch Pin Drop

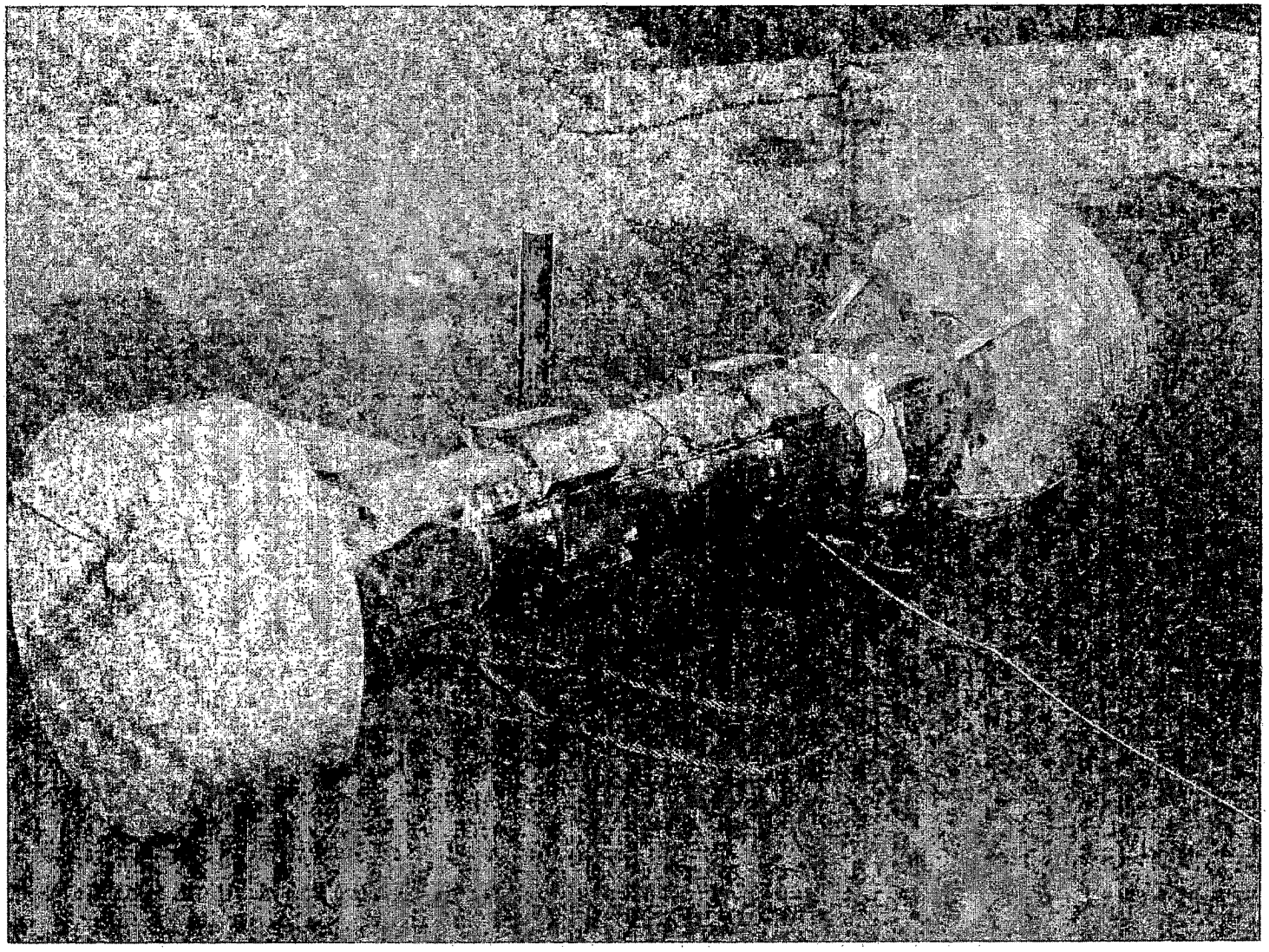

Figure 2.10.8-31 Impact Location – Midpoint 40-Inch Pin Drop

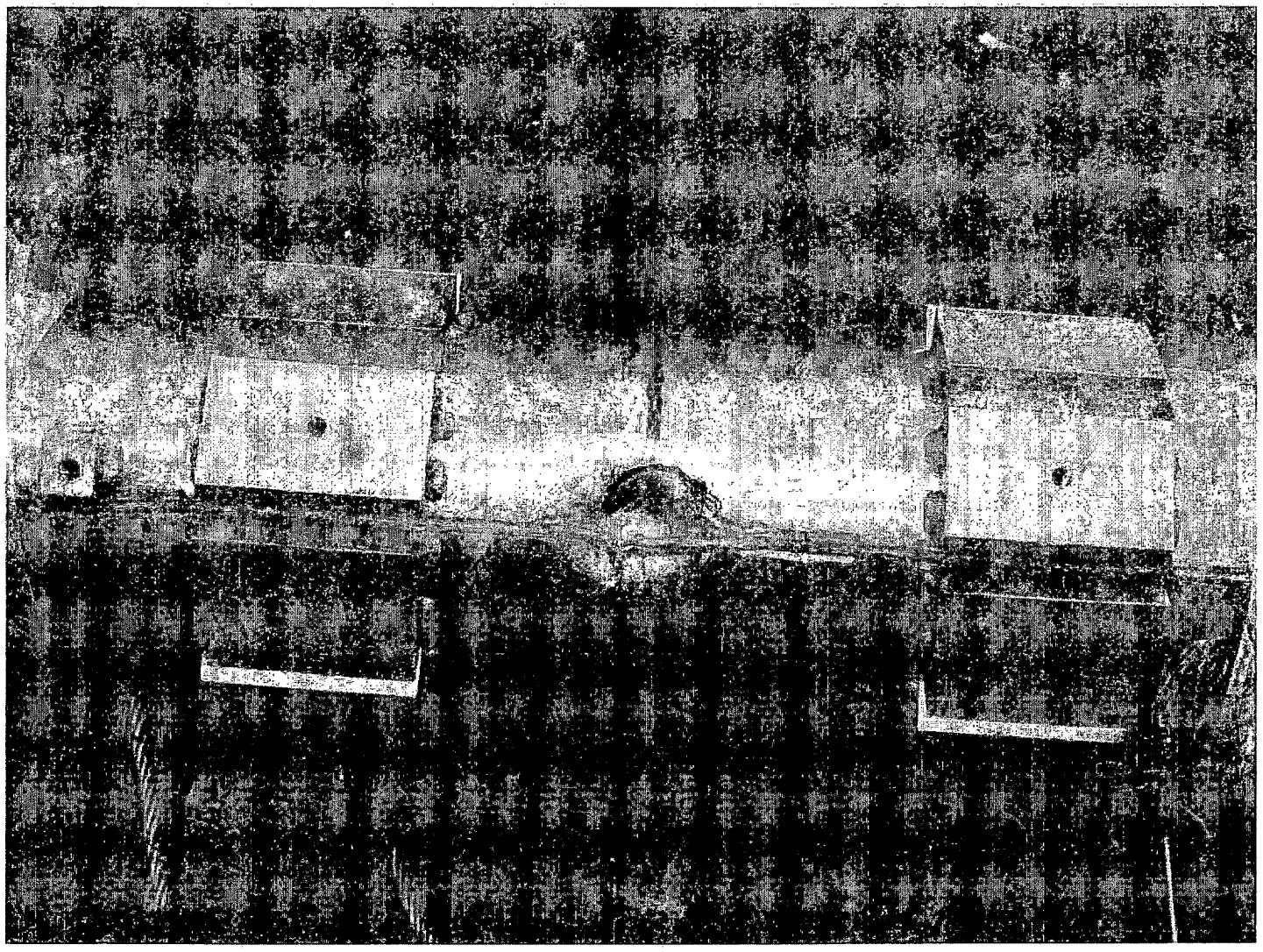

Figure 2.10.8-32 Angular Orientation of Instrumentation

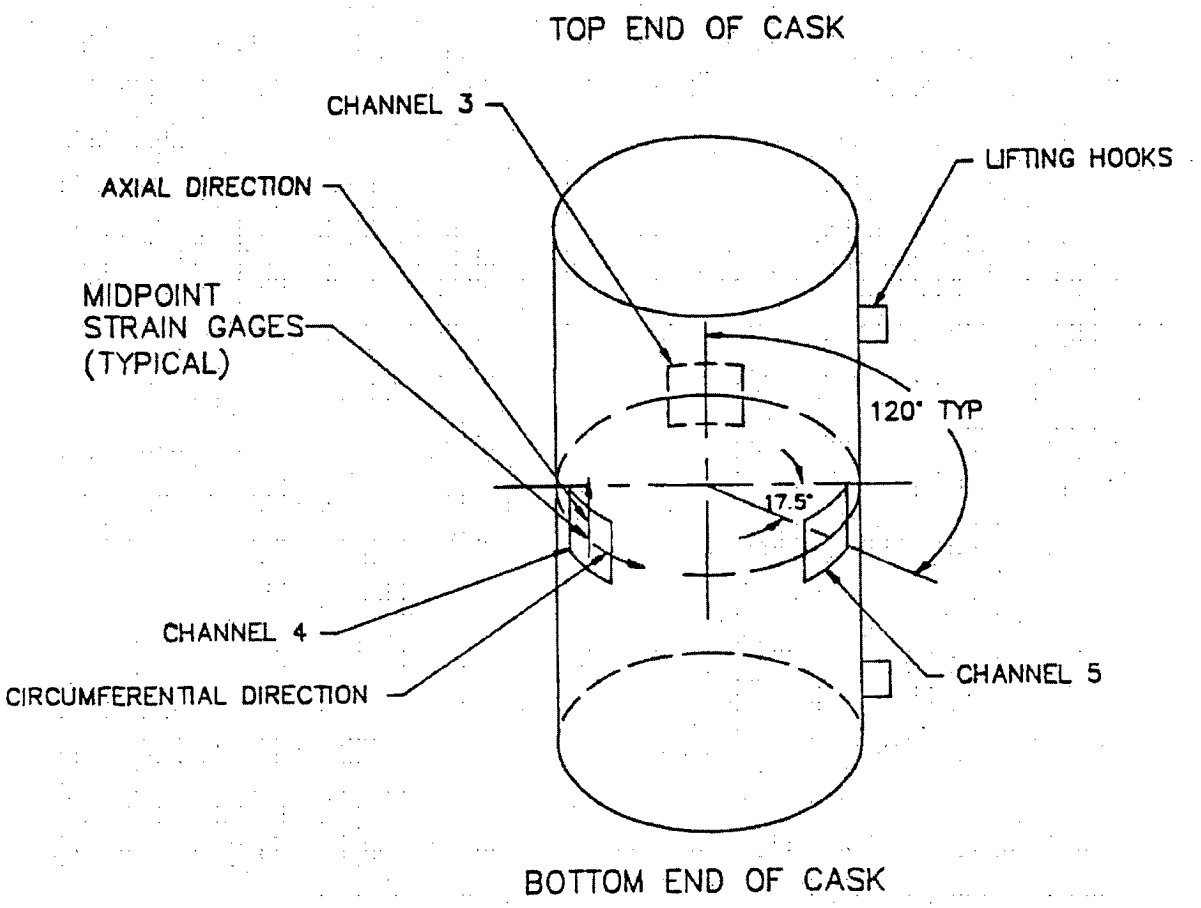

Figure 2.10.8-33 Strain Gauge Time History for Channel 3 – End Drop

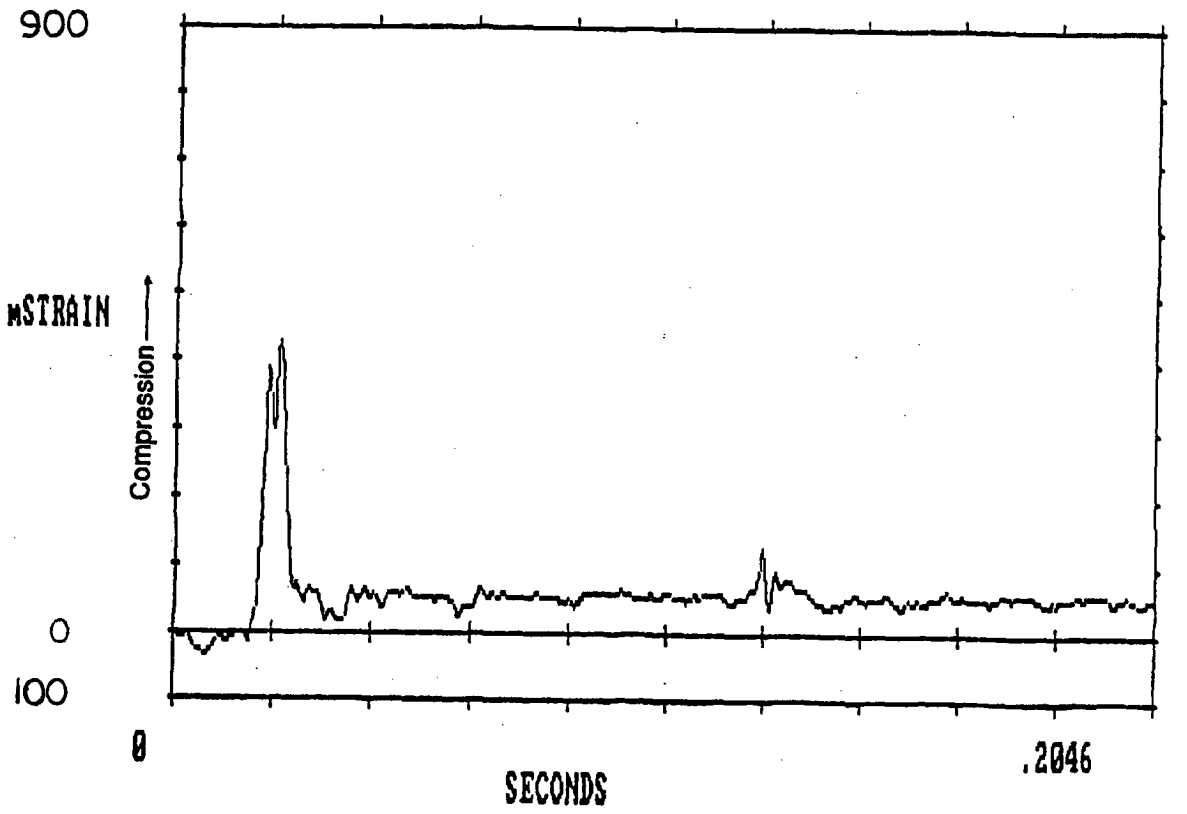

Figure 2.10.8-34 Strain Gauge Time History for Channel 4 – End Drop

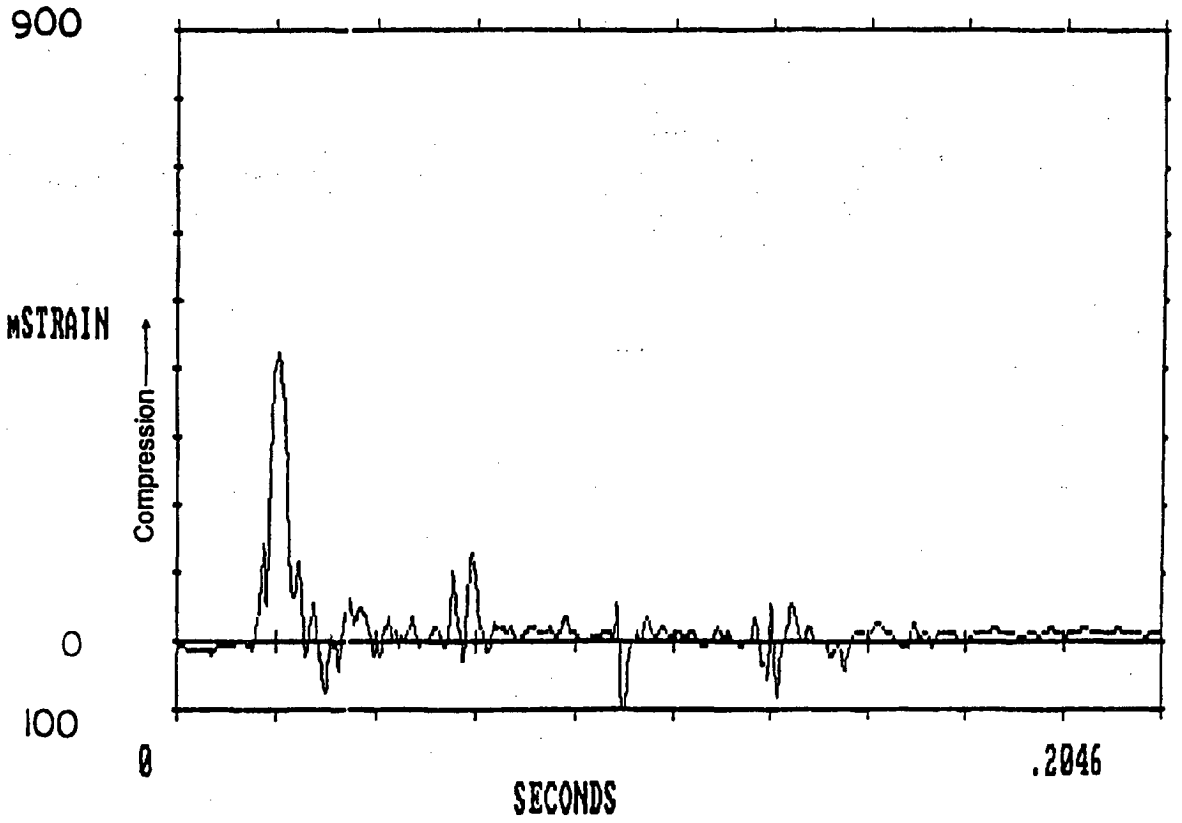

Figure 2.10.8-35 Strain Gauge Time History for Channel 5 – End Drop

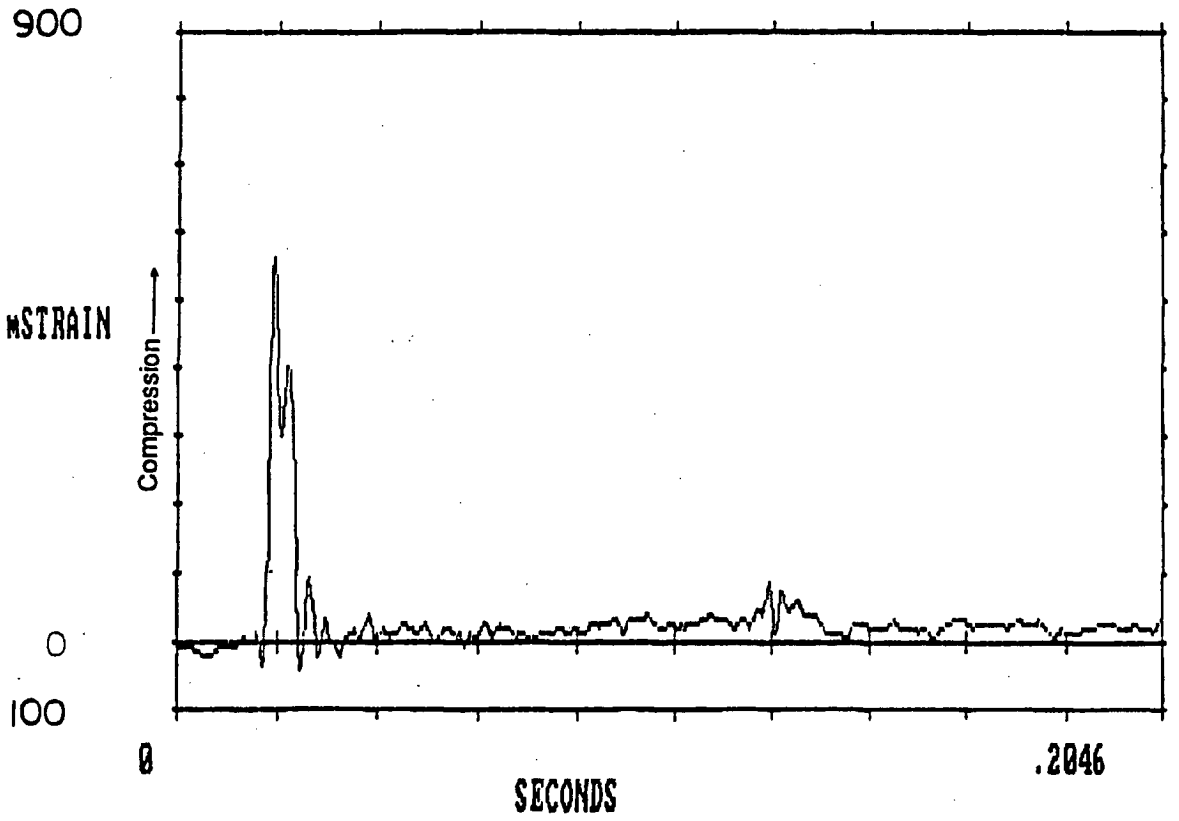

Figure 2.10.8-36 Strain Gauge Time History for Channel 3 – Side Drop

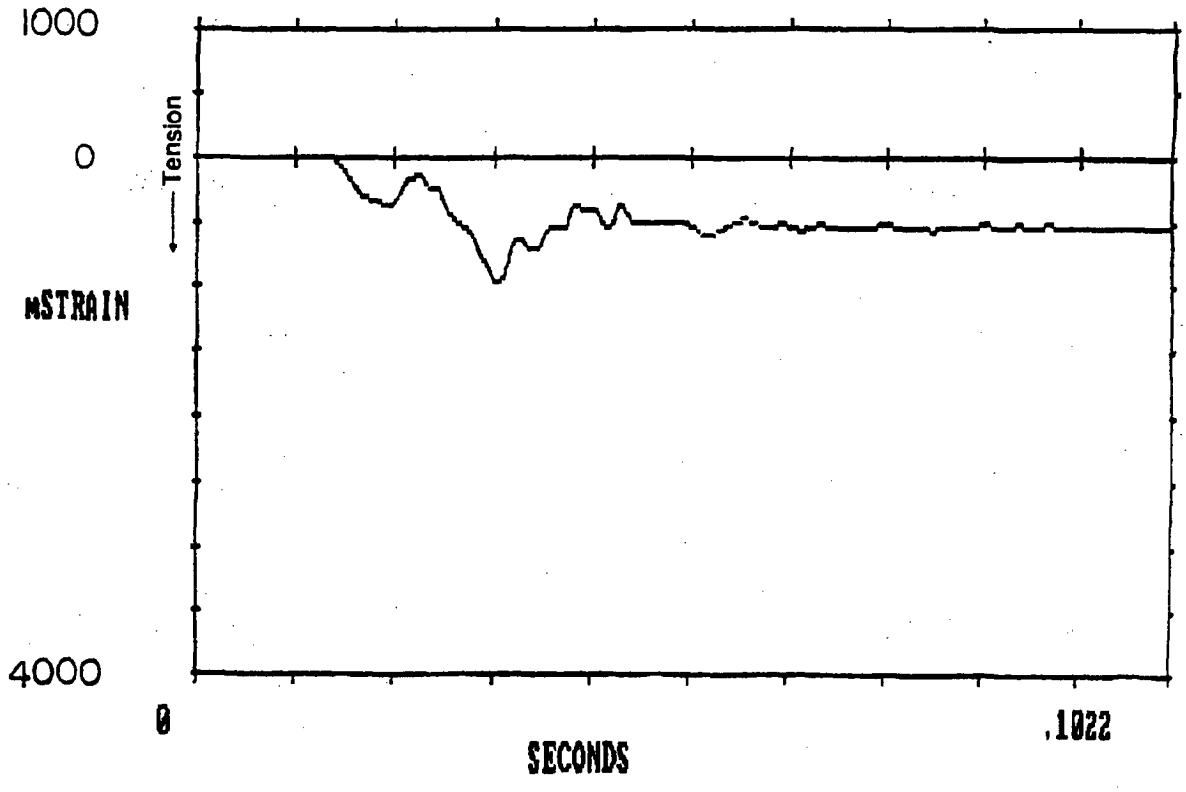

Figure 2.10.8-37 Strain Gauge Time History for Channel 4 – Side Drop

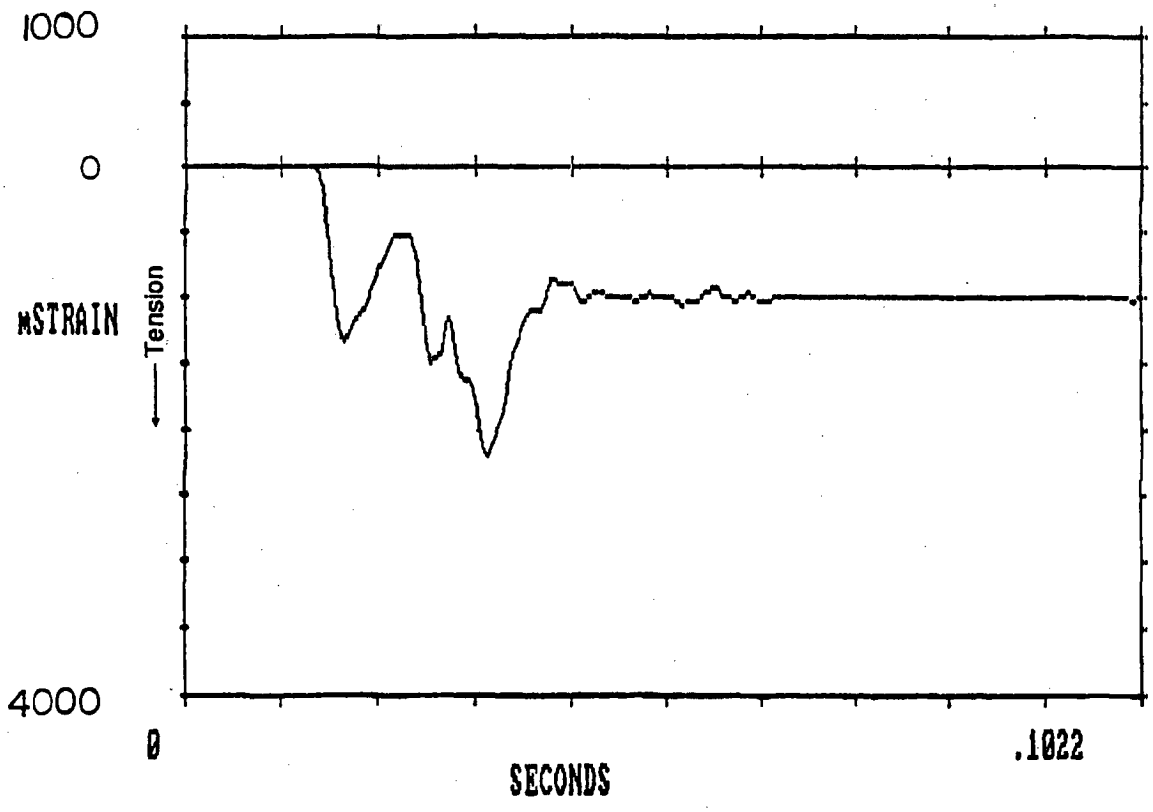

Figure 2.10.8-38 Strain Gauge Time History for Channel 5 – Side Drop

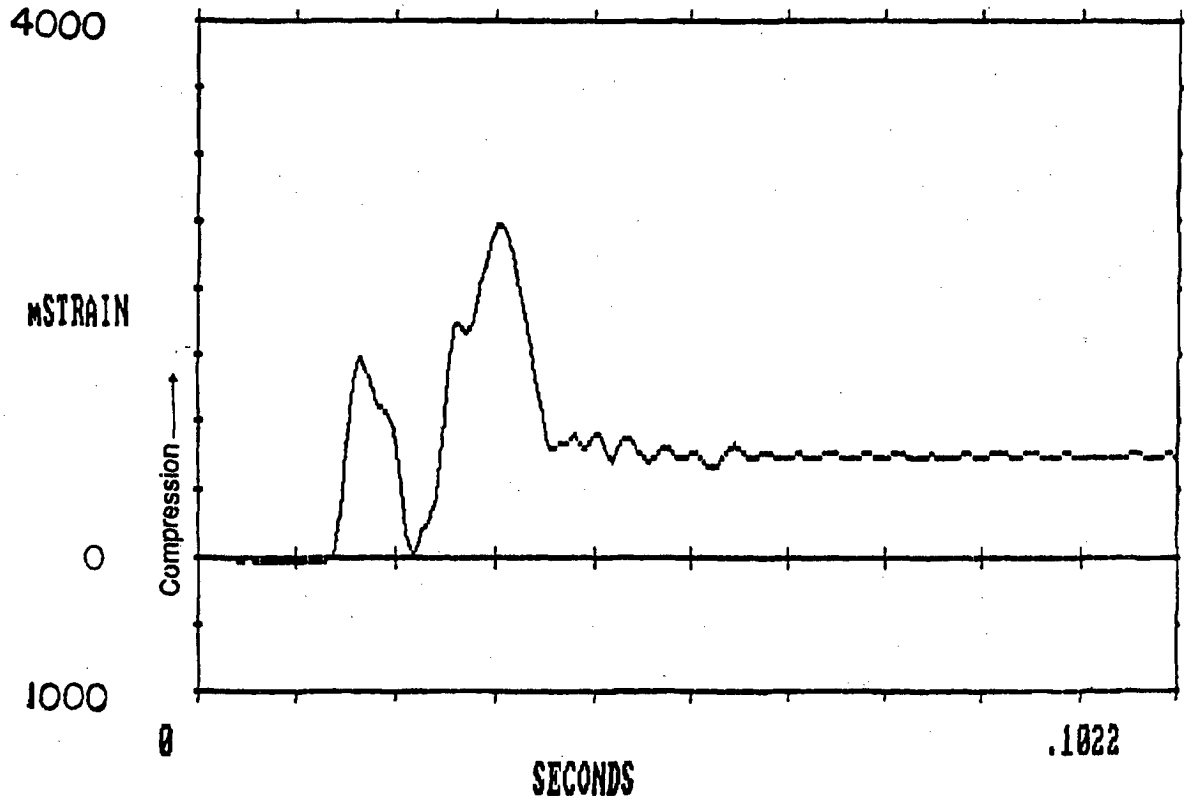

Figure 2.10.8-39 Location of Block Sets[1]

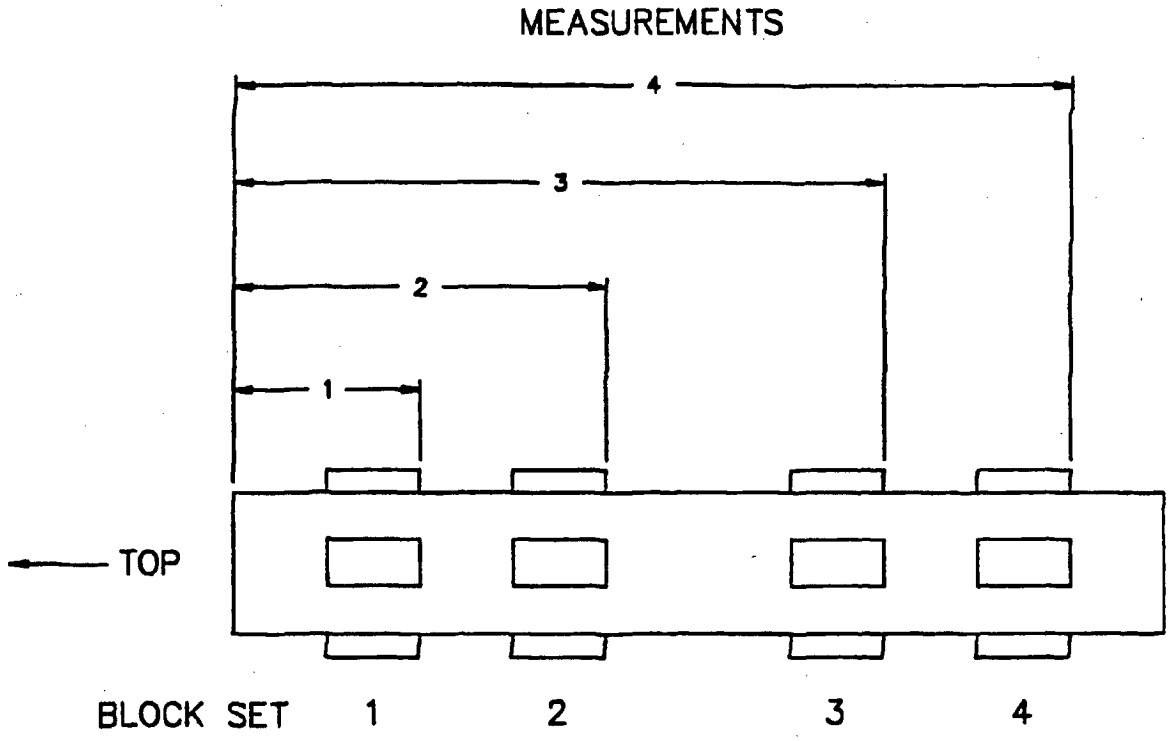

[1] This figure identifies the location of the block sets referred to in Tables 2.10.8-4 and 2.10.8-7.

Table 2.10.8-1 Scaling Relations

For 1/4-Scale Model		
		Law II [1,2]
Weight		1.56%
Velocity		100%
Kinetic Energy		1.56%
Momentum		1.56%
Duration		Scaled (25%)
Deformation		25%
Acceleration		400%
Applied Force	$F_m = \ell_m^2 F_p$	$\pi_{1m} = \ell_m^2 \pi_{1p}$
Mass	$M_m = \ell_m^3 M_p$	
Momentum	$M\theta_m = \ell_m^3 M\theta_p$	

[1] Percentages refer to model as percent of full-scale (1/64 = 1.56%).
[2] LAW II – Does not account for strain-rate effects or gravity.

Table 2.10.8-1 Scaling Relations (continued)

Energy	$E_m = \ell_m^3 E_p$
Velocity	$V_m = V_p$
Applied Acceleration	$N_{Gm} = \frac{N_{Gp}}{\ell_m}$
Duration	$\tau_m = \ell_m \tau_p$
Deformation	$\delta_m = \ell_m \delta_p$
Natural Frequency	$f_m = \frac{1}{\ell_m} f_p$

Table 2.10.8-2 Metrology Results of Inner Diameter Measurements Before Drop

No.	Location	Vertical (in)	Horizontal (in)
1	1 inch from end	3.3443	3.3436
2	13 inches from end	3.3379	3.3513
3	26 inches from end	3.3358	3.3501
4	38 inches from end	3.3390	3.3480
5	At weld joint	3.3153	3.3246
6	At large bore	5.6591	5.6585
7	At middle bore	5.1550	5.1546

Table 2.10.8-3 Metrology Results of Outer Diameter Measurements Before Drop

No.	Location	Vertical (in)	Horizontal (in)
1	Top 1 inch inside weld	7.1378	7.1448
2	Midpoint	7.1449	7.1474
3	Bottom 1 inch inside weld	7.1562	7.1527

Table 2.10.8-4 Metrology Results of External Length Measurements Before Drop*

No.	Location	0°	90°	180°	270°
1	1st block set	11.219	11.234	11.234	11.234
2	2nd block set	20.203	20.203	20.203	20.234
3	3rd block set	34.047	34.094	34.141	34.094
4	4th block set	43.031	43.078	43.125	43.063

* Length measurements are made from the top (closure) end to the back of the steel blocks, welded to the outside of the cask to simulate the weight of the neutron shield. Four measurements were made at each position down the cask starting with a vertical location and proceeding every 90 degrees around the cask periphery (Figure 2.10.8-39).

Table 2.10.8-5 Metrology Results of Inner Diameter Measurements After Drop

No.	Location	Vertical (in)	Horizontal (in)
1	1 inch from end	3.3445	3.3434
2	13 inches from end	3.3369	3.3524
3	26 inches from end	3.2790	3.3991
4	38 inches from end	3.338	3.3523
5	At weld joint	—	—
6	At large bore	5.6590	5.6585
7	At middle bore	5.1548	5.6585

Table 2.10.8-6 Metrology Results of Outer Diameter Measurements After Drop

No.	Location	Vertical (in)	Horizontal (in)
1	Top 1 inch inside weld	7.1400	7.1450
2	Midpoint	6.6600	7.1680
3	Bottom 1 inch inside weld	7.1500	7.1560

Table 2.10.8-7 Metrology Results of External Length Measurements After Drop

No.	Location	0°	90°	180°	270°
1	1st block set	11.219	11.234	11.375	11.234
2	2nd block set	20.188	20.203	20.203	20.375
3	3rd block set	34.016	34.078	34.156	34.125
4	4th block set	43.000	43.063	43.125	43.094

2.10.9 Bolts - Closure Lid (Stress Evaluations)

Bolt stress analysis results for normal and accident conditions are summarized in four tables. Table 2.6.7-35 and Table 2.6.7-36 summarize bolt stresses for hot and cold normal conditions, respectively. Table 2.7.1-60 and Table 2.7.1-61 summarize bolt stresses under hot and cold accident conditions, respectively.

2.10.9.1 Analysis Approach

The bolt stress analyses for normal and accident conditions consider the impact loads, pressure loads, thermal loads and bolt preloads. Each table is preceded with an explicit listing of relevant geometry, mechanical properties and constant loading data (bolt torque, pressure, etc.) taken directly from Sections 2.1, 2.2, 2.3, and the license drawings in Section 1.4.

Impact loads are expressed in g acceleration loads as summarized in Table 2.6.7-33. The "hot" initial condition bolt temperature for normal and accident impact evaluations is taken at 227°F, as summarized in Table 3.4-2. The "cold" initial condition bolt temperature for normal and accident impact evaluations is -20°F, per regulatory requirements. Allowables and properties for the SA-453, Grade 660 bolts are conservatively taken at 300°F and room temperature (70°F) for hot and cold conditions, respectively. Allowable bolt stress is taken as S_y, for normal and accident conditions. For conservatism, external energy absorber reaction forces, which resist separation of the cask lid and body, are completely neglected in all calculations.

An explanatory discussion of bolt stress analytics is found within Section 2.10.9.2. Table 2.10.9-1, which is identical to 2.7.1-60, is fully annotated to "key" to this explanation. An example calculation is included with each note to verify the accuracy of the tabular calculation.

The analysis methodology, allowables and basic assumptions used are consistent with conventional design/analysis codes, such as "AISC Manual of Steel Construction," 8th Edition, and "ASME Boiler and Pressure Vessel Code," Section III, Appendix F, Paragraph F-1335, but this analysis is more conservative. Specifically, this analysis includes stresses associated with preloads. Conventional design/analysis codes consider only externally applied loads and ignore preloads because "the ultimate shear strength of a high-strength bolt is independent of the clamping force. Only the slip resistance and fatigue life are improved by high clamping force" ("AISC Manual of Steel Construction," pages 5-222).

Like the methodology given in the "ASME Boiler and Pressure Vessel Code," Appendix F, Paragraph F-1335, this analysis uses nominal tensile and shear stresses based on the tabulated stress area of the bolts. It should be noted that the elliptic interaction equations of Paragraph F1335.2 of the "ASME Boiler and Pressure Vessel Code" and the approach used here give nearly

identical results when adjustments in loadings are made to account for the differing treatment of preload tension (This method conservatively includes preloads, whereas, the other ignores preloads).

2.10.9.2 Closure Bolt Analyses - Analytics and Assumptions

All numerical examples pertain to the evaluation of the NAC-LWT cask under hypothetical accident conditions (Table 2.10.9-1). The numbering of equations shown below reflects the annotation of values appearing within Table 2.10.9-1.

W_A = weight acting in longitudinal (axial) direction supported by lid bolts, includes payload and lid (a)

= 4000 + 941 lb

= 4941 lb

W_L = weight acting in lateral direction. This amounts to lid weight only (b)

= 941 lb

F_t = bolt thermal load, with example evaluation: (c)

$= A_b \Delta T[E_\ell \alpha_\ell - E_b \alpha_b]$

= 1423 lb

where:

A_b = 6051 in^2 nominal bolt area

ΔT = 157°F thermal differential.

For this illustrative case, the thermal differential, ΔT, is the hot service temperature, 227°F, less the temperature at which the cask bolting was torqued, here taken as room temperature, 70°F. Thus, $\Delta T = 227 - 70 = 157$°F.

E_ℓ = 27.0×10^6 lid modulus

α_ℓ = 9.0×10^{-6} lid expansion coefficient

E_b = 26.7×10^6 bolt modulus

α_b = 8.54×10^{-6} bolt expansion coefficient

Fi = bolt preload calculated from torque relation given in Section 2.1.3.2.2 (d)

$= 12T/(0.08973d) = (12)(260)/[(0.08973)(1.0)]$

$= 34{,}770$ lbs

where:

T = preload torque, ft-lb

d = nominal bolt diameter, in

F_p = bolt pressure load (e)

$= P_p A_p / Nr$

$= 812$ lbs

where:

P_p = internal pressure, 125 psig

$A_p = \pi d_s^2 / 4$

$= 194.8$ in^2, pressure area

d_s = seal diameter

$= 15.75$ inches

N_r = number of bolts

$= 12$

K_b = bolt stiffness (f)

$= A_b E_b / L$

$= 1.903 \times 10^6$ lb/in

where:

$A_b = 0.6051$ in^2

$E_b = 26.7 \times 10^6$ psi

L = (grip length) + 1/2 (nominal diameter)

$= 7.99 + 0.50$

$= 8.49$ inches

K_m = lid stiffness (g)

$= A_L E_\ell / L_g$

$= 2.122 \times 10^7$ lb/in

where:

A_L= an assumed cross-sectional area equal to a thick-walled cylinder with an inner diameter equal to the nominal bolt diameter and an outer diameter equal to three times the nominal bolt diameter (Shigley)

$= \pi/4\ (9d^2 - d2) = 2\pi d^2$

$= 6.28\ in^2$

$E_\ell = 27 \times 10^6$ psi

L_g = grip length

= 7.99 inches

n_g = Impact acceleration based on impact force predictions (Table 2.6.7-33). The (+) mark in the adjoining column denotes a value determined from linear interpolation. (h)

F_A = end impact bolt force (i)

$= P_A/Nr = (296{,}460)/12$

= 24,705 lbs

where:

$P_A = n_g W_A \sin\theta = (60.0)(4941)(1)$

= 296,460 lbs

F_A = oblique impact bolt force

$= P_A[R_L\ (R_L + R_B)/Io]A_b$

= 33,641 lbs

where:

$P_A = n_g W_A \sin\theta = (60.13)(4941)(\cos 5°)$

= 295,972 lbs

A_b = bolt stress area

$= 0.6051\ in^2$

R_L = lid radius

= 11.25 inches

R_B = bolt circle radius

= 8.94 inches

I_o = bolt circle moment of inertia = $\pi R_B^3 t + A_b N_r R_L^2$

= 1209 in^4

t = equivalent ring thickness

= $A_b N_r / (2\pi R_B) = (0.6051)(12)/(17.875\pi)$

= 0.1293 in

The derivation of this relationship for tensile bolt stresses assumes the lid pivots about the outer edge of the lid, point "o". The bolts are approximated as a thin, circular ring with a thickness equivalent to (total bolt area) = (ring area).

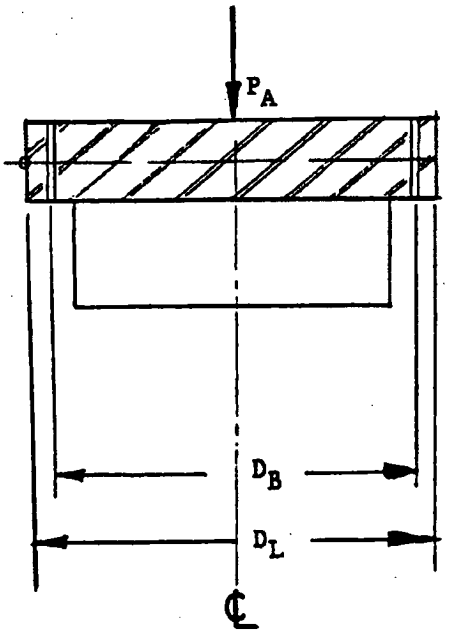

Bolt Circle

$R_B = D_B/2$
$= 8.94$ in

Lid

$R_L = D_L/2$
$= 11.25$ in

Equivalent ring thickness is found as:

$A = \pi D_B t$

or

$T = A/(\pi D_B)$

= 0.1293 in

where:

$A = (12 \text{ bolts})(0.6051 \text{ in/bolt})$; Baumeister, pages 8-10

$= 7.26 \text{ in}^2$

The moment of inertia of the bolt ring about point "o" is:

$$I_o = \pi R_B^3 t + A R_L^2$$

$$= 1209 \text{ in}^4$$

The applied bending moment about point "o" resulting from the impact force, P_A, is:

$$M_o = P_A R_L$$

Thus, the extreme bolt tension stress is found as:

$$f_a = Mc/I$$

$$= [(P_A R_L)(R_L + R_B)]/(\pi R_B^3 t + A R_L^2)$$

or

$$F_A = f_a A_b$$

$$= P_A [R_L (R_L + R_B)/I_o] A_b$$

In this analysis, which sweeps from vertical (end) impacts through side impacts, the two bolt tension relations, equations (i) and (j), must transition from one to the other at some orientation angle. Both conservatively neglect reaction forces from external energy absorbers. This neglect is extraordinarily conservative for near vertical impacts, but becomes more realistic as the package approaches side impact orientations. Specifically, the center of pressure of the external energy absorber reaction force on the lid moves from the center of the lid towards the impacting corner of the package as the impact orientation moves from near vertical to near horizontal.

For conservatism, this transition from an end relation, equation (i), for bolt force to an oblique relation, equation (j), is assumed to occur reasonably close to vertical; hence, only the 0-degree case uses the uniform force assumption.

FL = lateral (shear) bolt load (k)

$= PL/Nr = 4931/12$

$= 411$ lbs

where:

$P_L = n_g W_L \sin\theta = (60.13)(941) \sin 5°$

$= 4931$ lbs

P = total applied external bolt load (1)

$= F_p$ (pressure) + F_A (impact)

$= 812 + 24{,}705$

$= 25{,}517$ lbs

F_b = net bolt tension, considering applied external loads, thermal loads and pretension loads (Shigley) (m)

$= K_b P/(K_b + K_m) + F_i + F_t$

$= 38{,}292$ lbs (at 0°); $Fm < 0$

$= P$; $F_m \geq 0$

where:

P = external load, equation (1)

$= 25{,}517$ lbs

F_t = thermal load, equation (c)

$= 1423$ lbs

F_i = preload, equation (d)

$= 34{,}770$ lbs

K_b = bolt stiffness, equation (f)

$= 1.903 \times 10^6$ lb/in

K_m = lid stiffness, equation (g)

$= 2.112 \times 10^7$ lb/in

F_m = clamping force $= K_m P/(K_b + K_m) - F_i - F_t$

$= -12{,}785$ lbs

f_b = bolt tension stress (n)

$= F_b/A_b = 38{,}292/0.6051$

= 63,282 psi

f_v = bolt nominal shear stress (o)

= F_L/A_b

Principal Stresses (σ_1, σ_2) $= f_b/2 \pm [(fb/2)^2 + f_v^2]^{0.5}$ (p)

$= (59,924)/2 \pm [(59,924/2)^2 + 6752^2]^{0.5}$ (at 90°)

$= 29,962 \pm 30,713$

= -751 psi and 60,675 psi

Stress Intensity (at 90°) (q)

$S_I = \sigma_1 - \sigma_2 = -751 - 60,675$

= 61,427 psi

Margin of Safety (at 90°) (r)

$MS = S_y/S_I - 1 = 81.9/61.427 - 1$

= +0.33

Table 2.10.9-1 NAC-LWT Cask Hot Bolt Analysis Hypothetical Accident Conditions

Nominal Diameter (in):	1.00		
Number of Bolts:	12		
Service Stress, Sy (ksi):	81.9	} at a 300	
Bolt Expansion (in/in):	9E-06	} degree-F	
Bolt Modulus (ksi):	26700	} Service	
Lid Expansion (in/in):	9E-06	} Temperature	
Lid Modulus (ksi):	27000	}	
Stress Area (in2):	0.6051		
Grip Length (in):	7.99		
Maximum Pressure (psi):	50		
Seal Diameter (in):	15.750		
Preload Torque (ft-lbs):	260	at RT	
Nominal Room Temp, RT:	70	deg-F	
Bolt Circle Diameter (in):	17.88		
Lid Diameter (in):	22.50		

Longitudinal Weight (lbs):	4941
Lateral Weight (lbs):	941
Service DT (degrees):	157
[default value =]	230
CALCULATED LOADS & STIFFNESS	
Bolt Thermal Load (lbs):	1423
Bolt Preload (lbs):	34770
Bolt Pressure Load (lbs):	812
Bolt Stiffness (lbs/in):	1.9E+06
Lid Stiffness (lbs/in):	2.1E+07

Angle wrt Vert. (Deg)	Impact Accel. (g)	<**** LOADS (lbs.) Impact Tension	Impact Shear	Bolt Tension Applied	Bolt Tension Net ****	<**** STRESSES (psi) Direct Tension	Direct Shear	Principal Sig-1	Principal Sig-2	Stress Intens. ****	Margin of Safety
0 End	15.80	6506	0	7317	36795	60808	0	0	60808	60808	0.35
5 (+)	14.69	8216	100	9028	36936	61041	166	0	61041	61042	0.34
10 (+)	13.57	7506	185	8318	36877	60944	305	-2	60946	60947	0.34
15.7 Corner	12.30	6650	261	7462	36807	60828	431	-3	60831	60834	0.35
20 (+)	12.99	6858	349	7670	36824	60856	576	-5	60862	60867	0.35
25 (+)	13.80	7025	457	7837	36838	60879	756	-9	60888	60898	0.34
30 (+)	14.61	7106	573	7918	36845	60890	947	-15	60905	60919	0.34
35 (+)	15.42	7093	693	7905	36843	60888	1146	-22	60910	60931	0.34
40 (+)	16.22	6980	818	7792	36834	60873	1352	-30	60903	60933	0.34
45 (+)	17.03	6764	944	7576	36816	60844	1561	-40	60884	60924	0.34
50 (+)	17.84	6440	1072	7252	36790	60800	1771	-52	60851	60903	0.34
55 (+)	18.65	6007	1198	6819	36754	60741	1980	-64	60805	60870	0.35
60 (+)	19.45	5463	1321	6275	36709	60667	2183	-78	60745	60824	0.35
65 (+)	20.26	4809	1440	5621	36656	60578	2380	-93	60671	60765	0.35
70 (+)	21.07	4047	1553	4859	36593	60474	2566	-109	60583	60692	0.35
75 (+)	21.88	3180	1657	3992	36522	60356	2739	-124	60480	60604	0.35
80 (+)	22.68	2212	1752	3024	36442	60225	2895	-139	60364	60503	0.35
85 (+)	23.49	1150	1835	1962	36355	60080	3033	-153	60233	60386	0.36
90 Side	24.30	0	1906	812	36260	59924	3149	-165	60089	60254	0.36

Minimum Margin of Safety: 0.34

2.10.10 Finite Element Stress Results for the 30-Foot Drop Accident Conditions

2.10.10.1 Discussion

The following accident conditions were identified for a detailed finite element stress presentation:

- A 30-foot top end drop (drop orientation = $\phi = 0°$, where ϕ is defined as the impact orientation; that is, the angle between the impact direction and the cask centerline), 130°F ambient temperature, maximum decay heat load.
- A 30-foot top corner drop (drop orientation = $\phi = 15.74°$), 130°F ambient temperature, maximum decay heat load.
- A 30-foot top oblique drop (drop orientation = $\phi = 60°$), 130°F ambient temperature, maximum decay heat load.
- A 30-foot side drop (drop orientation = $\phi = 90°$), 130°F ambient temperature, maximum decay heat load.

The top end ($\phi = 0°$), top corner ($\phi = 15.74°$), top oblique ($\phi = 60°$) and side ($\phi = 90°$) drops envelope all of the drop orientations.

A 1.12-inch outer shell thickness is considered in the finite element analyses for the top end, top corner and top oblique drop conditions. The analyses results are conservative because the current NAC-LWT cask design has a 1.20-inch thick outer shell. The 30-foot side drop analysis considers the 1.20-inch outer shell thickness. The structural stiffness of the neutron shield shell is not considered in the finite element stress analyses.

2.10.10.2 Procedures

The analysis procedures for the above selected events are as follows:

- Perform an ANSYS analysis for each of the individual loadings:
  a. Thermal Hot (130°F)
  b. Maximum Internal Pressure (50 psi)
  c. Bolt Preload (250,000 lbs)[1]
  d. Impact and Inertial Loads/30-Foot Top End Drop (60 g impact load; $\phi = 0°$)
  e. Impact and Inertial Loads/30-Foot Top Corner Drop (60.4 g impact load; $\phi = 15.74°$)

[1] The total bolt preload has been increased to 418,116 lbs (34,843 lb/bolt) to provide the required compression force for the metal O-ring seal. Since the stresses at the locations evaluated in this analysis are less than 0.3 ksi for the bolt preload condition, this change is negligible.

f. Impact and Inertial Loads/30-Foot Top Oblique Drop (44.4 g impact load; $\phi = 60°$)

g. Impact and Inertial Loads/30-Foot Side Drop (49.7 g impact load; $\phi = 90°$)

Note that the fabrication stresses are considered negligible as explained in Section 2.6.11. The puncture analysis is performed using classical hand calculations and, therefore, is not discussed here.

- Tabulate the stress results that are calculated for the 123 selected points on the cask for each load condition. Both the stress components and the principal stresses are included. The 123 selected points are located at the 26 selected sections shown in Figure 2.10.10-1. The stress point locations are tabulated in Table 2.10.10-1. The constraint forces for the 30-foot top end drop ($\phi = 0°$), the 30-foot top corner drop ($\phi = 15.74°$), the 30-foot top oblique drop ($\phi = 60°$), and the 30-foot side drop ($\phi = 90°$) conditions are tabulated in Table 2.10.10-2 through Table 2.10.10-5, respectively.

  For the thin cylinder sections (those selected in the central region of the inner and outer shells), it is only necessary to show the stresses at the inner surface and the outer surface because a linear stress distribution is present for the stress linearization calculations. For thick sections and for thin sections at structural discontinuities, the stresses are presented for several points through the thickness to adequately define the stress distribution for the stress linearization calculations.

- Provide additional stress tables, which show the combined stresses (that is, the primary and the primary plus secondary stress categories) at the same selected points mentioned in step 2. The primary stress is obtained from the stress results induced by all of the primary loads (that is, internal pressure, bolt preload, impact and inertial loads). The primary plus secondary stress is the result of all of the primary loads plus the thermal load.

  As explained in Appendix 2.10.2, the ANSYS STIF12 element (the gap or interface element) is used in the finite element model to accurately represent the fact that no physical bonding exists between the lead and the surrounding stainless steel. The gap (interface) element is nonlinear; that is, the element operates bilinearly and requires an iterative solution process with the stiffness matrix reformulated during each iteration. This implies that the gap element status (being active or not) could change between the load analyses; therefore, it is preferable to calculate the primary stresses using the combined load finite element analysis. The same is true for the primary plus secondary stresses.

- Use the results of the combined stresses obtained in step 3 (the primary stresses) to calculate the primary membrane (P_m) and primary membrane plus primary bending ($P_m + P_b$) stresses, as specified in Regulatory Guide 7.6. The P_m and $P_m + P_b$ stresses will be calculated for 26 selected sections in the cask. The methodology used to calculate the P_m and $P_m + P_b$ stresses at a selected section is explained in detail on pages 5.2.2 through 5.2.12 in the ANSYS Theoretical Manual, Rev. 4.2, "Stress Linearization."

- The P_m and $P_m + P_b$ stresses calculated in step 4 are then compared with the allowable stresses in accordance with the stress requirements specified in Regulatory Guide 7.6.

2.10.10.3 Analysis and Results

A thorough discussion of the NAC-LWT cask finite element model can be found in Section 2.10.2.

Figure 2.10.10-1 presents a sketch of the selected sections in the cask. Each section contains two or more nodal points. The locations for the 123 selected nodal points are given in Table 2.10.10-1.

The stress results, calculated for each individual loading (hot temperature, internal pressure, bolt preload and impact loads) at the 123 nodal points on the cask, are tabulated in Table 2.10.10-6 through Table 2.10.10-14. The combined stresses, classified as the primary, primary plus secondary, P_m and $P_m + P_b$ stress categories, are derived from performing steps 3 and 4 of Section 2.10.10.2 and are tabulated for each drop accident. The stress qualifications of P_m and $P_m + P_b$ are derived from step 5, in accordance with Regulatory Guide 7.6, and are tabulated for each drop accident.

2.10.10.3.1 30-Foot Top End Drop ($\phi = 0°$)

The event scenario is that the cask, equipped with impact limiters, falls through a distance of 30 feet and strikes the unyielding surface on the top end of the package.

The types of loading involved in a top end drop accident include: (1) thermal, (2) internal pressure, (3) closure lid bolt preload, and (4) impact and inertial loads resulting from the end impact. These loadings and the boundary conditions, used in the finite element top end drop analysis, have been discussed in Section 2.7.1.1.2. In addition, the displacement constrained nodes and applied forces used for the 30-foot top end drop are given in Appendix 2.10.2.

The primary, primary plus secondary, P_m, and $P_m + P_b$ stresses induced by the 30-foot top end drop are documented in Table 2.10.10-15 through Table 2.10.10-18. As discussed in Step 3, Section 2.10.10.2, the primary stresses are preferably obtained from the stress results induced by all of the primary loads; that is, internal pressure, bolt preload, impact and inertial loads. The primary stress may also be obtained by algebraically adding the stresses induced by each of the primary loads. A comparison was made of the primary stresses calculated from the combined load method versus the superposition method, which adds the stress results of each separate loading to obtain the primary stresses. The difference is insignificant. The same is true for the primary plus secondary stresses. The stress qualification of P_m and $P_m + P_b$ is presented in Table 2.10.10-19. The P_m and $P_m + P_b$ stress tables, documented in Table 2.10.7-34 and Table 2.10.7-35, are derived based on the primary plus secondary stresses. This provides conservative results

for the P_m and $P_m + P_b$ stresses because the primary plus secondary stresses are larger than the primary stresses.

The hand-calculated method used to evaluate the cask stress for a 30-foot top end drop impact condition is provided in Section 2.10.11.1. The compressive stresses calculated by the finite element method are -3,260 psi and -2,990 psi at the cask midsection in the inner and outer shell, respectively, with an average of -3,125 psi. The hand-calculated stress at the cask midsection is -3,213 psi. The difference is less than three percent.

All margins of safety are positive. Thus, the NAC-LWT cask satisfies the 10 CFR 71 requirements for the end drop accident condition.

2.10.10.3.2 30-Foot Top Corner Drop (ϕ = 15.74°)

The event scenario is that the cask, equipped with impact limiters, falls through a distance of 30 feet and strikes the unyielding surface on the top corner of the package with the package center of gravity directly above the point of impact.

The types of loading involved in a top corner drop accident include: (1) thermal, (2) internal pressure, (3) closure lid bolt preload, and (4) impact and inertial loads resulting from the corner drop impact. These loadings and the boundary conditions, used in the finite element top corner drop analysis, have been discussed in Section 2.7.1.3.2. In addition, the displacement constrained nodes and applied forces used for the 30-foot top corner drop are given in Appendix 2.10.2.

The primary, primary plus secondary, P_m, and $P_m + P_b$ stresses induced by the 30-foot top corner drop are documented in Table 2.10.10-20 through Table 2.10.10-23. The stress qualification of P_m and $P_m + P_b$ is presented in Table 2.10.10-24. An unrealistic stress is induced by the boundary effect because of the displacement restraints at node 2561. Stresses in the region near the restraint are disregarded. As discussed in Section 2.7.1.3.3, the oblique drop condition induces an eccentric (angular) momentum, which causes a rigid body rotation of the cask and a secondary impact onto the unyielding surface. To provide dynamic equilibrium of the cask body in the oblique drop evaluation, displacement restraints are imposed on the finite element model. These restraints cause localized peak stresses in the immediate vicinity of boundary conditions.

This boundary effect attenuates very rapidly at locations slightly away from the boundary region.

To obtain a more realistic stress distribution in the free end of the cask, the method of superposition described in Section 2.7.1.3.3 is used. By this method the stresses for the following nodes and sections have been revised for the tables in Section 2.10.10:

Impact End	Section Cuts[1]	Node Number (S)[2]
Top	A through J	1 through 698
Bottom	S through Z	1481 through 2561

All margins of safety are positive. Thus, the NAC-LWT cask satisfies the 10 CFR 71 requirements for the corner drop accident condition.

2.10.10.3.3 30-Foot Top Oblique Drop (ϕ = 60°)

The event scenario is that the cask, equipped with impact limiters, falls with a drop orientation of 60 degrees from vertical through a distance of 30 feet and strikes the unyielding surface on the top corner of the cask.

The types of loading involved in a top oblique drop accident include: (1) thermal, (2) internal pressure, (3) closure lid bolt preload, and (4) impact and inertial loads resulting from the oblique drop impact. These loadings and the boundary conditions, used in the finite element top oblique drop analysis, have been discussed in Section 2.7.1.3.2. In addition, the displacement constrained nodes and applied forces used for the 30-foot top oblique drop are given in Appendix 2.10.2.

The primary, primary plus secondary, P_m, and $P_m + P_b$ stresses induced by the 30-foot top oblique drop are documented in Table 2.10.10-25 through Table 2.10.10-28. The stress qualification of P_m and $P_m + P_b$ is presented in Table 2.10.10-29. The unrealistic stresses induced by the boundary effect at node 2561 should be disregarded as explained in Section 2.10.10.3.2. For this drop evaluation, the stresses in the vicinity of the free end are revised as described in Section 2.7.1.3.3.

All margins of safety are positive. Thus, the NAC-LWT cask satisfies the 10 CFR 71 requirements for the top oblique drop accident condition.

2.10.10.3.4 30-Foot Side Drop (ϕ = 90°)

The event scenario is that the cask, equipped with impact limiters, falls with a drop orientation of 90 degrees through a distance of 30 feet and strikes the unyielding surface in the horizontal position.

The types of loading involved in a side drop accident include: (1) thermal, (2) internal pressure, (3) closure lid bolt preload, and (4) impact and inertial loads resulting from the side drop impact. These loadings and the boundary conditions, used in the finite element side drop analysis, have been discussed in Section 2.7.1.2. The 30-foot side drop analysis includes a 1.20-inch thick outer shell. Furthermore, the impact g load has been revised to 49.7 g from 52.1 g to reflect the final impact limiter design criteria. Based on improved fabrication techniques, the honeycomb

[1] The section cuts are identified in Figure 2.10.7-1 and their coordinates are listed in Table 2.10.7-1.
[2] The node numbers versus nodal coordinates are specified in Table 2.10.2-1.

crush strength tolerance has been revised to 3,500 psi, +5, -10 percent; thus, the maximum tolerance crush strength of the honeycomb is 3,675 psi. Since the impact load is directly proportional to the honeycomb crush strength, the maximum side impact g-load is (3,675/3,850)(52.1) = 49.7 g. This value has been verified by an RBCUBED program analysis.

The displacement constrained nodes and applied forces used for the 30-foot side drop are given in Appendix 2.10.2.

The finite element stress results are compared with the hand-calculated stress results (Section 2.10.11.2). The finite element method calculates the most critical stress as 68.23 ksi versus 67.24 ksi from the hand-calculated method. The difference is less than 1.5 percent.

The primary, primary plus secondary, P_m, and $P_m + P_b$ stresses induced by the 30-foot side drop are documented in Table 2.10.10-30 through Table 2.10.10-33. In addition, the P_m and $P_m + P_b$ stresses at circular locations 90° and 180° are provided in Table 2.10.10-34 through Table 2.10.10-37. The stresses at circular location 0° are the most critical; therefore, they are the ones used for the stress qualification. Table 2.10.10-38 presents the stress qualification of P_m and $P_m + P_b$.

All margins of safety are positive. Thus, the NAC-LWT cask satisfies the 10 CFR 71 requirements for the side drop accident condition.

2.10.10.4 Conclusion

Based on the finite element stress analysis results for the four critical 30-foot drop conditions selected, the NAC-LWT cask design satisfies the allowable stress criteria specified in Regulatory Guide 7.6.

Figure 2.10.10-1 Stress Point Locations

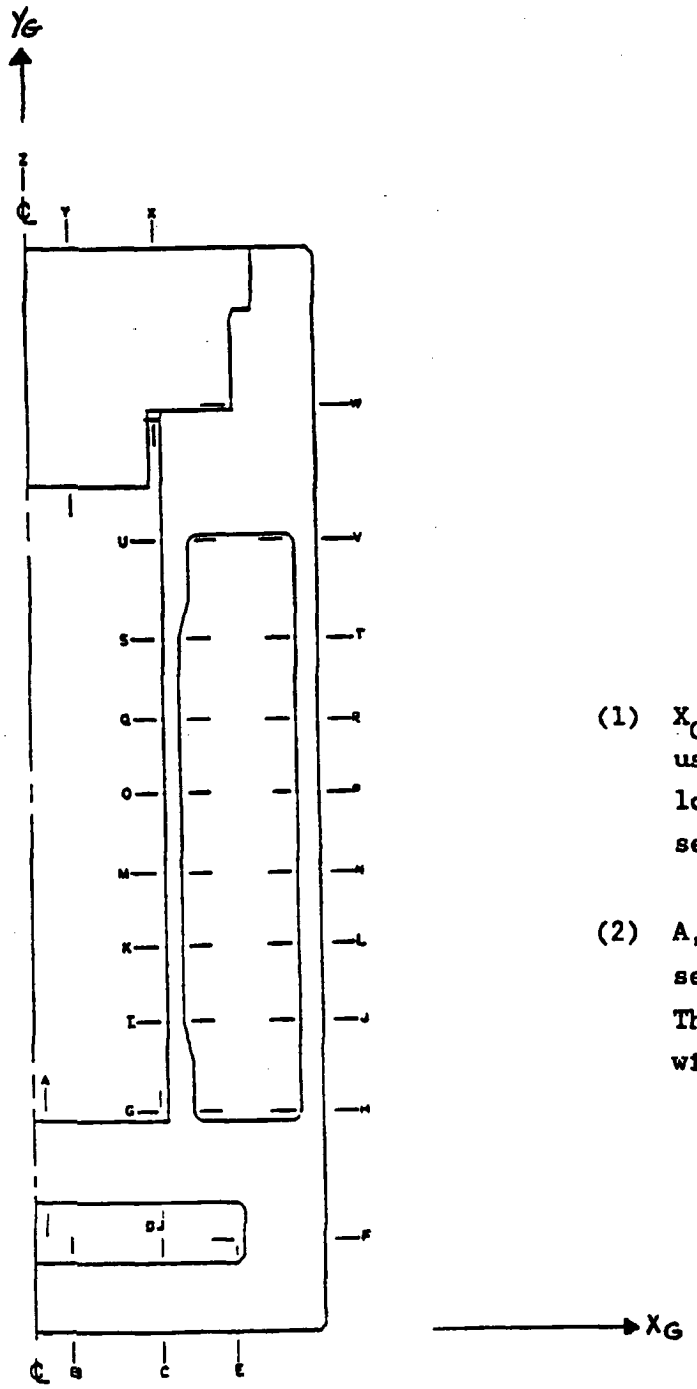

(1) X_G and Y_G are global axes used to measure the location of selected sections.

(2) A, ...Z are selected section designations. There are 26 sections with 52 stress points.

Table 2.10.10-1 Stress Point Locations

Designation	Node No.	Location	
		x	y
A1	327	0.85	10.50
A2	302	0.85	10.25
A3	277	0.85	10.00
A4	252	0.85	9.50
A5	227	0.85	8.50
A6	202	0.85	7.50
A7	177	0.85	6.50
B1	104	2.55	3.50
B2	79	2.55	2.50
B3	54	2.55	1.50
B4	29	2.55	0.50
B5	4	2.55	0.00
C1	110	6.6875	3.50
C2	85	6.6875	2.50
C3	60	6.6875	1.50
C4	35	6.6875	0.50
C5	10	6.6875	0.00
D1	335	6.6875	10.50
D2	310	6.6875	10.25
D3	285	6.6875	10.00
D4	260	6.6875	9.50
D5	235	6.6875	8.50
D6	210	6.6875	7.50
D7	185	6.6875	6.50
E1	118	10.375	3.50
E2	93	10.375	2.50
E3	68	10.375	1.50
E4	43	10.375	0.50
E5	18	10.375	0.00
F1	143	10.375	4.50
F2	144	11.315	4.50

Table 2.10.10-1 Stress Point Locations (continued)

Designation	Node No.	Location	
		x	y
F3	145	12.001	4.50
F4	146	12.688	4.50
F5	147	13.188	4.50
F6	148	13.561	4.50
F7	149	13.934	4.50
F8	150	14.307	4.50
G1	335	6.6875	10.50
G2	336	6.9375	10.50
G3	337	7.1875	10.50
G4	338	7.4375	10.50
G5	339	7.9375	10.50
G6	340	8.4375	10.50
H1	346	12.688	10.50
H2	347	13.188	10.50
H3	348	13.561	10.50
H4	349	13.934	10.50
H5	350	14.307	10.50
I1	621	6.6875	16.50
I2	624	7.4375	16.50
J1	635	13.188	16.50
J2	638	14.307	16.50
K1	841	6.6875	35.50
K2	844	7.4375	35.50
L1	855	13.188	35.50
L2	858	14.307	35.50
M1	941	6.6875	60.50
M2	944	7.4375	60.50
N1	955	13.188	60.50
N2	958	14.307	60.50
O1	1101	6.6875	100.50
O2	1104	7.4375	100.50

Table 2.10.10-1 Stress Point Locations (continued)

Designation	Node No.	Location	
		x	y
P1	1115	13.188	100.50
P2	1118	14.307	100.50
Q1	1261	6.6875	140.50
Q2	1264	7.4375	140.50
R1	1275	13.188	140.50
R2	1278	14.307	1450.50
S1	1561	6.6875	179.50
S2	1564	7.4375	179.50
T1	1575	13.188	179.50
T2	1578	14.307	179.50
U1	1841	6.6875	185.50
U2	1844	8.4375	185.50
V1	1852	12.688	185.50
V2	1856	14.307	185.50
W1	1969	10.315	191.75
W2	1970	11.315	191.75
W3	1971	12.001	191.75
W4	1972	12.688	191.75
W5	1973	13.188	191.75
W6	1974	13.561	191.75
W7	1975	13.934	191.75
W8	1976	14.307	191.75
X1	2370	6.6875	191.75
X2	2390	6.6875	192.75
X3	2410	6.6875	193.75
X4	2430	6.6875	194.75
X5	2450	6.6875	195.75
X6	2470	6.6875	196.75
X7	2490	6.6875	197.75
X8	2510	6.6875	198.25
X9	2530	6.6875	198.75

Table 2.10.10-1 Stress Point Locations (continued)

Designation	Node No.	Location	
		x	y
X10	2550	6.6875	199.25
X11	2570	6.6875	199.75
Y1	2305	3.40	188.50
Y2	2325	3.40	189.75
Y3	2345	3.40	190.75
Y4	2365	3.40	191.75
Y5	2385	3.40	192.75
Y6	2405	3.40	193.75
Y7	2425	3.40	194.75
Y8	2445	3.40	195.75
Y9	2465	3.40	196.75
Y10	2485	3.40	197.75
Y11	2505	3.40	198.25
Y12	2525	3.40	198.75
Y13	2545	3.40	199.25
Y14	2565	3.40	199.75
Z1	2301	0.00	188.50
Z2	2321	0.00	189.75
Z3	2341	0.00	190.75
Z4	2361	0.00	191.75
Z5	2381	0.00	192.75
Z6	2404	0.00	193.75
Z7	2421	0.00	194.75
Z8	2441	0.00	195.75
Z9	2461	0.00	196.75
Z10	2481	0.00	197.75
Z11	2501	0.00	198.25
Z12	2521	0.00	198.75
Z13	2541	0.00	199.25
Z14	2561	0.00	199.75

Table 2.10.10-2 Constraint Forces for the 30-Foot Top End Drop Condition ($\phi = 0°$)

Node	FX	FY	FZ
1	0.722137		
25		-3487.13	
26	0.509030		
51	0.242975		
76	-0.581758		
101	-0.893385		
126	0.417712-001		
151	-0.425787-001		
176	1.21218		
201	0.902732		
226	-0.669590-001		
251	-0.522695		
276	-0.406303		
301	-0.717323		
326	-0.401629		
2301	-9.15600		
2321	-5.97171		
2341	-0.331048		
2361	2.36181		
2381	2.07107		
2401	-0.284169		
2421	-2.24827		
2441	-2.50453		
2461	-0.548714		
2481	1.73193		
2501	2.51800		
2521	3.71850		
2541	3.87877		
2561	4.73436		
3101	0.789074-001		
3176	-0.780999-001		
TOTAL	-0.280365-011	-3487.13	0.000000

Table 2.10.10-3 Constraint Forces for the 30-Foot Top Corner Drop Condition ($\phi = 15.74°$)

Node	FX	FY	FZ
1	-3122.0370	-3760.2436	1159.4410
25	-183131.11		58533.923
2561	50113.502		-44114.872
TOTAL	-136139.64	-3760.2436	15578.492

Table 2.10.10-4 Constraint Forces for the 30-Foot Top Oblique Drop Condition ($\phi = 60°$)

Node	FX	FY	FZ
1	-5429.7002	-2619.1410	3662.7469
2561	151886.32		-134475.85
TOTAL	146456.62	-2619.1410	-130813.10

Table 2.10.10-5 Constraint Forces for the 30-Foot Side Drop Condition ($\phi = 90°$)

Node	FX	FY	FZ
1	4322.1611	1098.7180	-3316.9233
2561	7223.3599		-6394.6917
TOTAL	11545.521	1098.7180	-9711.6149

Table 2.10.10-6 Stress Components – Thermal; 130°F; 1.12-Inch Outer Shell Thickness

Stress Points		Stresses						
Location	Node	S_X	S_Y	S_Z	S_{XY}	S_1	S_2	S_3
A1	327	5.32	0.07	5.30	0.24	5.33	5.30	0.06
A2	302	4.45	0.07	4.45	-0.02	4.45	4.45	0.07
A3	277	3.58	0.01	3.57	-0.10	3.58	3.57	0.01
A4	252	1.85	-0.03	1.85	-0.02	1.85	1.85	-0.03
A5	227	-1.57	-0.05	-1.58	-0.02	-0.05	-1.57	-1.58
A6	202	-4.97	-0.08	-4.98	-0.01	-0.08	-4.97	-4.98
A7	177	-8.41	-0.09	-8.36	0.00	-0.09	-8.36	-8.41
B1	104	0.27	0.03	0.25	0.08	0.30	0.25	0.01
B2	79	1.18	0.05	1.19	0.05	1.19	1.18	0.04
B3	54	2.13	0.09	2.15	0.04	2.15	2.13	0.09
B4	29	3.14	0.05	3.13	0.07	3.14	3.13	0.05
B5	4	4.87	-0.03	4.82	-0.41	4.91	4.82	-0.06
C1	110	0.53	-0.79	0.72	0.22	0.72	0.56	-0.83
C2	85	1.27	-0.64	1.54	0.22	1.54	1.29	-0.66
C3	60	2.09	-0.32	5.52	0.24	2.52	2.11	-0.35
C4	35	3.15	-0.10	3.64	0.08	3.64	3.15	-0.10
C5	10	5.05	-0.02	5.47	-0.12	5.47	5.05	-0.03
D1	335	0.10	-8.29	1.64	-0.89	1.64	0.19	-8.38
D2	310	2.81	-4.74	2.74	-0.98	2.93	2.74	-4.86
D3	285	2.62	-3.03	2.62	-0.87	2.75	2.62	-3.16
D4	260	1.45	-2.10	1.46	-0.80	1.63	1.46	-2.27
D5	235	-0.83	-1.81	-1.23	-0.61	-0.54	-1.23	-2.10
D6	210	-3.47	-1.74	-4.13	0.02	-1.74	-3.47	-4.13
D7	185	-6.52	-1.67	-7.26	0.95	-1.49	-6.70	-7.26
E1	118	3.57	-3.22	2.02	3.56	5.10	2.02	-4.75
E2	93	0.78	0.62	2.50	1.53	2.50	2.24	-0.83
E3	68	0.99	0.23	2.89	1.13	2.89	1.80	-0.58
E4	43	1.03	0.05	3.42	0.54	3.42	1.27	-0.19
E5	18	2.13	0.02	4.88	0.16	4.88	2.14	0.01
F1	143	-9.96	-8.38	-1.96	6.23	-1.96	-2.89	-15.45
F2	144	-8.66	5.37	1.53	3.39	6.15	1.53	-9.44

Table 2.10.10-6 Stress Components – Thermal; 130°F; 1.12-Inch Outer Shell Thickness (continued)

Stress Points		Stresses						
Location	Node	S_X	S_Y	S_Z	S_{XY}	S_1	S_2	S_3
F3	145	-5.57	3.38	1.40	0.44	3.40	1.40	-5.59
F4	146	-2.45	2.61	1.89	-0.26	2.62	1.89	-2.46
F5	147	-1.21	2.14	2.08	-0.40	2.18	2.08	-1.26
F6	148	-0.61	1.92	2.19	-0.38	2.19	1.98	-0.66
F7	149	-0.27	1.83	2.29	-0.24	2.29	1.86	-0.30
F8	150	-0.12	1.98	2.40	-0.14	2.40	1.99	-0.13
G1	335	0.10	-8.29	1.64	-0.89	1.64	0.19	-8.38
G2	336	0.33	-4.60	2.80	0.11	2.80	0.33	-4.60
G3	337	1.57	-1.77	3.93	0.59	3.93	1.67	-1.87
G4	338	2.62	1.52	5.11	-0.04	5.11	2.62	1.52
G5	339	5.97	6.96	7.44	-2.85	9.36	7.44	3.58
G6	340	7.46	1.89	6.59	-3.30	8.99	6.59	0.36
H1	346	-9.25	-3.91	-2.66	0.10	-2.66	-3.90	-9.26
H2	347	-4.69	3.46	0.77	0.32	3.47	0.77	-4.70
H3	348	-2.27	7.91	2.87	-0.15	7.91	2.87	-2.28
H4	349	-0.79	10.55	4.07	-0.31	10.55	4.07	-0.80
H5	350	-0.23	14.21	5.20	-0.27	14.22	5.20	-0.24
I1	621	0.00	3.12	0.38	0.03	3.12	0.38	0.00
I2	624	0.01	1.94	0.19	0.01	1.94	0.19	0.01
J1	635	0.00	10.71	0.23	0.05	10.71	0.23	0.00
J2	638	0.01	8.43	-0.14	0.05	8.43	0.00	-0.14
K1	841	0.00	2.27	-0.21	-0.01	2.27	0.00	-0.21
K2	844	0.00	2.69	0.19	0.01	2.69	0.19	0.00
L1	855	0.00	9.25	-0.36	0.00	9.25	0.00	-0.36
L2	858	0.00	9.78	0.18	0.00	9.78	0.18	0.00
M1	941	0.00	2.21	-0.27	0.00	2.21	0.00	-0.27
M2	944	0.00	2.75	0.25	0.00	2.75	0.25	0.00
N1	955	0.00	9.13	-0.45	0.00	9.13	0.00	-0.45
N2	958	0.00	9.84	0.23	0.00	9.84	0.23	0.00
O1	1101	0.00	2.22	-0.27	0.00	2.22	0.00	-0.27
O2	1104	0.00	2.75	0.25	0.00	2.75	0.25	0.00

Table 2.10.10-6 Stress Components – Thermal; 130°F; 1.12-Inch Outer Shell Thickness (continued)

Stress Points		Stresses						
Location	Node	S_X	S_Y	S_Z	S_{XY}	S_1	S_2	S_3
P1	1115	0.00	9.10	-0.49	0.00	9.10	0.00	-0.49
P2	1118	0.00	9.85	0.24	0.00	9.85	0.24	0.00
Q1	1261	0.00	2.28	-0.18	0.00	2.28	0.00	-0.18
Q2	1264	0.00	2.69	0.22	0.00	2.69	0.22	0.00
R1	1275	0.00	9.15	-0.46	0.00	9.15	0.00	-0.46
R2	1278	-0.01	9.88	0.09	0.00	9.88	0.09	-0.01
S1	1561	0.00	2.12	0.24	0.04	2.12	0.24	0.00
S2	1564	-0.03	2.90	0.56	0.05	2.90	0.56	-0.03
T1	1575	0.00	10.66	0.09	-0.06	10.66	0.09	0.00
T2	1578	0.00	8.45	-0.12	-0.05	8.45	0.00	-0.12
U1	1841	0.02	0.16	-0.54	-0.09	0.21	-0.03	-0.54
U2	1844	0.21	1.24	0.17	-0.07	1.24	0.21	0.17
V1	1852	-5.69	-2.17	-2.44	-1.18	-1.81	-2.44	-6.05
V2	1856	-0.31	12.07	3.55	0.16	12.07	3.55	-0.32
W1	1969	-0.77	-1.85	0.01	-0.81	0.01	-0.34	-2.28
W2	1970	-0.02	-0.76	0.70	-0.68	0.70	0.38	-1.16
W3	1971	-0.11	-0.09	0.96	-0.56	0.96	0.46	-0.65
W4	1972	-0.09	0.54	1.21	-0.48	1.21	0.80	-0.35
W5	1973	-0.07	0.95	1.37	-0.38	1.37	1.07	-0.20
W6	1974	-0.06	1.27	1.52	-0.26	1.52	1.32	-0.11
W7	1975	-0.03	1.55	1.66	-0.13	1.66	1.56	-0.04
W8	1976	0.01	1.81	1.79	-0.07	1.81	1.79	0.01
X1	2370	-1.24	-0.33	-0.33	0.60	-0.03	-0.33	-1.54
X2	2390	-0.33	-0.94	-0.24	0.44	-0.10	-0.24	-1.17
X3	2410	-0.36	-0.54	-0.07	0.06	-0.07	-0.34	-0.56
X4	2430	-0.34	-0.39	0.00	-0.13	0.00	-0.23	-0.50
X5	2450	-0.40	-0.23	0.06	-0.26	0.06	-0.04	-0.60
X6	2470	-0.41	-0.13	0.13	-0.33	0.13	0.08	-0.63
X7	2490	-0.38	-0.06	0.25	-0.34	0.25	0.15	-0.59
X8	2510	-0.34	-0.03	0.34	-0.32	0.34	0.17	-0.54
X9	2530	-0.28	-0.01	0.46	-0.26	0.46	0.15	-0.44

Table 2.10.10-6 Stress Components – Thermal; 130°F; 1.12-Inch Outer Shell Thickness (continued)

Stress Points		Stresses						
Location	Node	S_X	S_Y	S_Z	S_{XY}	S_1	S_2	S_3
X10	2550	-0.22	0.00	0.61	-0.17	0.61	0.09	-0.31
X11	2570	0.62	0.00	1.58	-0.05	1.58	0.62	-0.01
Y1	2305	0.57	-0.03	0.49	-0.04	0.57	0.49	-0.03
Y2	2325	0.02	-0.05	-0.01	0.05	0.05	-0.01	-0.08
Y3	2345	-0.28	-0.11	-0.34	0.05	-0.10	-0.29	-0.34
Y4	2365	-0.55	-0.16	-0.61	0.04	-0.16	-0.56	-0.61
Y5	2385	-0.71	-0.21	-0.78	0.05	-0.20	-0.74	-0.78
Y6	2405	-0.80	-0.25	-0.87	0.04	-0.25	-0.80	-0.87
Y7	2425	-0.78	-0.27	-0.87	0.00	-0.27	-0.78	-0.87
Y8	2445	-0.71	-0.25	-0.80	-0.05	-0.25	-0.72	-0.80
Y9	2465	-0.61	-0.19	-0.67	-0.08	-0.17	-0.63	-0.67
Y10	2485	-0.43	-0.11	-0.44	-0.08	-0.09	-0.44	-0.45
Y11	2505	-0.29	-0.05	-0.29	-0.04	-0.04	-0.29	-0.30
Y12	2525	-0.11	-0.02	-0.11	-0.01	-0.02	-0.11	-0.11
Y13	2545	0.13	0.00	0.11	-0.01	0.13	0.11	0.00
Y14	2565	1.25	0.00	1.15	0.07	1.26	1.15	0.00
Z1	2301	0.51	0.01	0.49	0.00	0.51	0.49	0.01
Z2	2321	0.08	0.03	0.08	0.00	0.08	0.08	0.03
Z3	2341	-0.24	0.07	-0.24	0.00	0.07	-0.24	-0.24
Z4	2361	-0.51	0.09	-0.50	0.00	0.09	-0.50	-0.51
Z5	2381	-0.68	0.11	-0.68	0.00	0.11	-0.68	-0.68
Z6	2401	-0.78	0.11	-0.78	0.00	0.11	-0.78	-0.78
Z7	2421	-0.80	0.11	-0.80	0.00	0.11	-0.80	-0.80
Z8	2441	-0.73	0.10	-0.72	0.00	0.10	-0.72	-0.73
Z9	2461	-0.58	0.09	-0.58	0.00	0.09	-0.58	-0.58
Z10	2481	-0.35	0.07	-0.34	0.00	0.07	-0.34	-0.35
Z11	2501	-0.21	0.05	-0.21	0.00	0.05	-0.21	-0.21
Z12	2521	-0.05	0.03	-0.06	0.00	0.03	-0.05	-0.06
Z13	2541	0.11	0.01	0.10	0.00	0.11	0.10	0.01
Z14	2561	1.06	0.01	1.06	0.00	1.06	1.06	0.01

Table 2.10.10-7 Stress Components – Internal Pressure; 50 psi; 1.12-Inch Outer Shell Thickness

Stress Points		Stresses						
Location	Node	S_X	S_Y	S_Z	S_{XY}	S_1	S_2	S_3
A1	327	-0.11	-0.05	-0.11	0.00	-0.05	-0.11	-0.11
A2	302	-0.09	-0.05	-0.09	0.00	-0.05	-0.09	-0.09
A3	277	-0.07	-0.05	-0.07	0.01	-0.05	-0.07	-0.07
A4	252	-0.04	-0.04	-0.04	0.01	-0.03	-0.04	-0.05
A5	227	0.01	-0.03	0.01	0.01	0.01	0.01	-0.03
A6	202	0.06	-0.01	0.06	0.01	0.06	0.06	-0.01
A7	177	0.12	0.00	0.12	0.00	0.12	0.12	0.00
B1	104	0.01	0.00	0.01	0.00	0.01	0.01	0.00
B2	79	0.01	0.00	0.01	0.00	0.01	0.01	0.00
B3	54	0.00	0.00	0.00	0.00	0.00	0.00	0.00
B4	29	0.00	0.00	0.00	0.00	0.00	0.00	0.00
B5	4	0.00	0.00	0.00	0.00	0.00	0.00	0.00
C1	110	0.01	0.00	0.01	0.00	0.01	0.01	0.00
C2	85	0.01	0.00	0.01	0.00	0.01	0.01	0.00
C3	60	0.00	0.00	0.00	0.00	0.00	0.00	0.00
C4	35	0.00	0.00	0.00	0.00	0.00	0.00	0.00
C5	10	0.00	0.00	0.00	0.00	0.00	0.00	0.00
D1	335	0.24	0.39	0.16	0.11	0.45	0.19	0.16
D2	310	0.05	0.23	0.07	0.08	0.23	0.07	0.02
D3	285	0.02	0.14	0.03	0.06	0.16	0.03	0.00
D4	260	0.00	0.07	0.02	0.04	0.09	0.02	-0.02
D5	235	-0.01	0.03	0.01	0.03	0.04	0.01	-0.02
D6	210	-0.01	0.01	0.02	0.02	0.02	0.02	-0.02
D7	185	-0.02	0.00	0.03	0.01	0.03	0.00	-0.03
E1	118	-0.01	-0.01	0.01	0.00	0.01	0.01	-0.01
E2	93	0.00	0.00	0.00	0.00	0.00	0.00	0.00
E3	68	0.00	0.00	0.00	0.00	0.00	0.00	0.00
E4	43	0.00	0.00	0.00	0.00	0.00	0.00	0.00
E5	18	0.00	0.00	0.00	0.00	0.00	0.00	0.00
F1	143	0.00	-0.02	0.00	0.00	0.00	0.00	-0.02
F2	144	0.00	-0.01	0.00	0.01	0.00	0.00	-0.01

Table 2.10.10-7 Stress Components – Internal Pressure; 50 psi; 1.12-Inch Outer Shell Thickness (continued)

Stress Points		Stresses						
Location	Node	S_X	S_Y	S_Z	S_{XY}	S_1	S_2	S_3
F3	145	0.00	0.00	0.01	0.01	0.01	0.01	-0.01
F4	146	0.00	0.00	0.01	0.01	0.01	0.01	-0.01
F5	147	0.00	0.01	0.01	0.01	0.01	0.01	0.00
F6	148	0.00	0.01	0.01	0.00	0.01	0.01	0.00
F7	149	0.00	0.01	0.01	0.00	0.01	0.01	0.00
F8	150	0.00	0.01	0.01	0.00	0.01	0.01	0.00
G1	335	0.24	0.39	0.16	0.11	0.45	0.19	0.16
G2	336	0.14	0.19	0.08	0.06	0.23	0.10	0.08
G3	337	0.06	0.12	0.04	0.02	0.12	0.05	0.04
G4	338	0.02	0.04	0.01	0.01	0.05	0.01	0.01
G5	339	-0.04	-0.08	-0.04	0.03	-0.02	-0.04	-0.10
G6	340	-0.06	-0.04	-0.04	0.04	-0.01	-0.04	-0.10
H1	346	0.00	0.01	0.00	0.00	0.01	0.00	0.00
H2	347	0.00	0.02	0.00	0.00	0.02	0.00	0.00
H3	348	0.00	0.02	0.00	0.00	0.02	0.00	0.00
H4	349	0.00	0.01	0.00	0.00	0.01	0.00	0.00
H5	350	0.00	0.01	0.00	0.00	0.01	0.00	0.00
I1	621	-0.05	0.08	0.34	-0.01	0.34	0.08	-0.05
I2	624	-0.02	0.16	0.33	0.00	0.33	0.16	-0.02
J1	635	0.00	0.02	0.00	0.00	0.02	0.00	0.00
J2	638	0.00	0.02	0.00	0.00	0.02	0.00	0.00
K1	841	-0.05	0.10	0.36	0.02	0.36	0.10	-0.05
K2	844	-0.01	0.10	0.32	0.02	0.32	0.10	-0.01
L1	855	0.00	0.02	0.00	0.00	0.02	0.00	0.00
L2	858	0.00	0.02	0.00	0.00	0.02	0.00	0.00
M1	941	-0.05	0.10	0.36	0.00	0.36	0.10	-0.05
M2	944	-0.01	0.11	0.32	0.00	0.32	0.10	-0.01
N1	955	0.00	0.02	0.00	0.00	0.02	0.00	0.00
N2	958	0.00	0.02	0.00	0.00	0.02	0.00	0.00
O1	1101	-0.05	0.10	0.36	0.00	0.36	0.10	-0.05
O2	1104	-0.01	0.10	0.32	0.00	0.32	0.10	-0.01

Table 2.10.10-7 Stress Components – Internal Pressure; 50 psi; 1.12-Inch Outer Shell Thickness (continued)

Stress Points		Stresses						
Location	Node	S_X	S_Y	S_Z	S_{XY}	S_1	S_2	S_3
P1	1115	0.00	0.02	0.00	0.00	0.02	0.00	0.00
P2	1118	0.00	0.02	0.00	0.00	0.02	0.00	0.00
Q1	1261	-0.05	0.10	0.36	0.00	0.36	0.10	-0.05
Q2	1264	-0.01	0.10	0.32	0.00	0.32	0.10	-0.01
R1	1275	0.00	0.02	0.00	0.00	0.02	0.00	0.00
R2	1278	0.00	0.02	0.00	0.00	0.02	0.00	0.00
S1	1561	-0.05	0.10	0.35	0.00	0.35	0.10	-0.05
S2	1564	-0.02	0.14	0.32	0.00	0.32	0.14	-0.02
T1	1575	0.00	0.03	0.00	0.00	0.03	0.00	0.00
T2	1578	0.00	0.01	0.00	0.00	0.01	0.00	0.00
U1	1841	-0.05	0.14	0.15	-0.01	0.15	0.14	-0.05
U2	1844	-0.06	0.09	0.11	-0.01	0.11	0.09	-0.06
V1	1852	-0.03	-0.01	0.02	0.01	0.02	-0.01	-0.03
V2	1856	0.00	0.05	0.04	0.00	0.05	0.04	0.00
W1	1969	0.01	0.01	0.01	0.00	0.01	0.01	0.01
W2	1970	0.01	0.00	0.01	0.00	0.01	0.01	0.00
W3	1971	0.00	0.00	0.01	0.00	0.01	0.00	0.00
W4	1972	0.00	0.00	0.01	0.00	0.01	0.00	0.00
W5	1973	0.00	0.00	0.01	0.00	0.01	0.00	0.00
W6	1974	0.00	0.00	0.01	0.00	0.01	0.00	0.00
W7	1975	0.00	-0.01	0.01	0.00	0.01	0.00	-0.01
W8	1976	0.00	-0.01	0.00	0.00	0.00	0.00	-0.01
X1	2370	0.06	0.00	0.03	-0.04	0.08	0.03	-0.02
X2	2390	0.00	0.04	0.02	-0.04	0.06	0.02	-0.03
X3	2410	0.00	0.01	0.01	-0.02	0.03	0.01	-0.02
X4	2430	0.00	0.01	0.01	-0.02	0.02	0.01	-0.01
X5	2450	0.00	0.01	0.01	-0.01	0.02	0.01	-0.01
X6	2470	0.00	0.00	0.01	-0.01	0.01	0.01	-0.01
X7	2490	0.00	0.00	0.01	-0.01	0.01	0.01	-0.01
X8	2510	0.00	0.00	0.01	-0.01	0.01	0.01	0.00
X9	2530	0.00	0.00	0.01	0.00	0.01	0.01	0.00

Table 2.10.10-7 Stress Components – Internal Pressure; 50 psi; 1.12-Inch Outer Shell Thickness (continued)

Stress Points		Stresses						
Location	Node	S_X	S_Y	S_Z	S_{XY}	S_1	S_2	S_3
X10	2550	0.00	0.00	0.01	0.00	0.01	0.00	0.00
X11	2570	0.00	0.00	0.01	0.00	0.01	0.00	0.00
Y1	2305	-0.07	-0.05	-0.07	0.01	-0.05	-0.07	-0.08
Y2	2325	-0.05	-0.05	-0.05	0.00	-0.05	-0.05	-0.06
Y3	2345	-0.04	-0.05	-0.04	0.00	-0.03	-0.04	-0.05
Y4	2365	-0.02	-0.04	-0.02	-0.01	-0.02	-0.02	-0.05
Y5	2385	0.00	-0.04	0.00	-0.01	0.00	0.00	-0.04
Y6	2405	0.00	-0.03	0.00	-0.01	0.01	0.00	-0.04
Y7	2425	0.01	-0.03	0.01	-0.01	0.01	0.01	-0.03
Y8	2445	0.01	-0.02	0.01	-0.01	0.01	0.01	-0.02
Y9	2465	0.01	-0.01	0.01	-0.01	0.01	0.01	-0.02
Y10	2485	0.01	-0.01	0.01	-0.01	0.01	0.01	-0.01
Y11	2505	0.01	0.00	0.01	-0.01	0.01	0.01	-0.01
Y12	2525	0.01	0.00	0.02	-0.01	0.02	0.01	0.00
Y13	2545	0.01	0.00	0.02	0.00	0.02	0.01	0.00
Y14	2565	0.02	0.00	0.02	0.00	0.02	0.02	0.00
Z1	2301	-0.08	-0.05	-0.08	0.00	-0.05	-0.08	-0.08
Z2	2321	-0.05	-0.05	-0.05	0.00	-0.05	-0.05	-0.05
Z3	2341	-0.04	-0.05	-0.04	0.00	-0.04	-0.04	-0.05
Z4	2361	-0.02	-0.05	-0.02	0.00	-0.02	-0.02	-0.05
Z5	2381	-0.01	-0.04	-0.01	0.00	-0.01	-0.01	-0.04
Z6	2401	0.00	-0.04	0.00	0.00	0.00	0.00	-0.04
Z7	2421	0.01	-0.03	0.00	0.00	0.01	0.00	-0.03
Z8	2441	0.01	-0.02	0.01	0.00	0.01	0.01	-0.02
Z9	2461	0.01	-0.02	0.01	0.00	0.01	0.01	-0.02
Z10	2481	0.01	-0.01	0.01	0.00	0.01	0.01	-0.01
Z11	2501	0.02	-0.01	0.02	0.00	0.02	0.02	-0.01
Z12	2521	0.02	0.00	0.02	0.00	0.02	0.02	0.00
Z13	2541	0.02	0.00	0.02	0.00	0.02	0.02	0.00
Z14	2561	0.03	0.00	0.03	0.00	0.03	0.03	0.00

Table 2.10.10-8 Stress Components – Bolt Preload; 1.12-Inch Outer Shell Thickness

Stress Points		Stresses						
Location	Node	S_X	S_Y	S_Z	S_{XY}	S_1	S_2	S_3
A1	327	0.00	0.00	0.00	0.00	0.00	0.00	0.00
A2	302	0.00	0.00	0.00	0.00	0.00	0.00	0.00
A3	277	0.00	0.00	0.00	0.00	0.00	0.00	0.00
A4	252	0.00	0.00	0.00	0.00	0.00	0.00	0.00
A5	227	0.00	0.00	0.00	0.00	0.00	0.00	0.00
A6	202	0.00	0.00	0.00	0.00	0.00	0.00	0.00
A7	177	0.00	0.00	0.00	0.00	0.00	0.00	0.00
B1	104	0.00	0.00	0.00	0.00	0.00	0.00	0.00
B2	79	0.00	0.00	0.00	0.00	0.00	0.00	0.00
B3	54	0.00	0.00	0.00	0.00	0.00	0.00	0.00
B4	29	0.00	0.00	0.00	0.00	0.00	0.00	0.00
B5	4	0.00	0.00	0.00	0.00	0.00	0.00	0.00
C1	110	0.00	0.00	0.00	0.00	0.00	0.00	0.00
C2	85	0.00	0.00	0.00	0.00	0.00	0.00	0.00
C3	60	0.00	0.00	0.00	0.00	0.00	0.00	0.00
C4	35	0.00	0.00	0.00	0.00	0.00	0.00	0.00
C5	10	0.00	0.00	0.00	0.00	0.00	0.00	0.00
D1	335	0.00	0.00	0.00	0.00	0.00	0.00	0.00
D2	310	0.00	0.00	0.00	0.00	0.00	0.00	0.00
D3	285	0.00	0.00	0.00	0.00	0.00	0.00	0.00
D4	260	0.00	0.00	0.00	0.00	0.00	0.00	0.00
D5	235	0.00	0.00	0.00	0.00	0.00	0.00	0.00
D6	210	0.00	0.00	0.00	0.00	0.00	0.00	0.00
D7	185	0.00	0.00	0.00	0.00	0.00	0.00	0.00
E1	118	0.00	0.00	0.00	0.00	0.00	0.00	0.00
E2	93	0.00	0.00	0.00	0.00	0.00	0.00	0.00
E3	68	0.00	0.00	0.00	0.00	0.00	0.00	0.00
E4	43	0.00	0.00	0.00	0.00	0.00	0.00	0.00
E5	18	0.00	0.00	0.00	0.00	0.00	0.00	0.00
F1	143	0.00	0.00	0.00	0.00	0.00	0.00	0.00
F2	144	0.00	0.00	0.00	0.00	0.00	0.00	0.00

Table 2.10.10-8 Stress Components – Bolt Preload; 1.12-Inch Outer Shell Thickness (continued)

Stress Points		Stresses						
Location	Node	S_X	S_Y	S_Z	S_{XY}	S_1	S_2	S_3
F3	145	0.00	0.00	0.00	0.00	0.00	0.00	0.00
F4	146	0.00	0.00	0.00	0.00	0.00	0.00	0.00
F5	147	0.00	0.00	0.00	0.00	0.00	0.00	0.00
F6	148	0.00	0.00	0.00	0.00	0.00	0.00	0.00
F7	149	0.00	0.00	0.00	0.00	0.00	0.00	0.00
F8	150	0.00	0.00	0.00	0.00	0.00	0.00	0.00
G1	335	0.00	0.00	0.00	0.00	0.00	0.00	0.00
G2	336	0.00	0.00	0.00	0.00	0.00	0.00	0.00
G3	337	0.00	0.00	0.00	0.00	0.00	0.00	0.00
G4	338	0.00	0.00	0.00	0.00	0.00	0.00	0.00
G5	339	0.00	0.01	0.00	0.00	0.01	0.00	0.00
G6	340	0.01	0.00	0.00	0.00	0.01	0.00	0.00
H1	346	0.00	0.00	0.00	0.00	0.00	0.00	0.00
H2	347	0.00	0.00	0.00	0.00	0.00	0.00	0.00
H3	348	0.00	0.00	0.00	0.00	0.00	0.00	0.00
H4	349	0.00	0.00	0.00	0.00	0.00	0.00	0.00
H5	350	0.00	0.00	0.00	0.00	0.00	0.00	0.00
I1	621	0.00	0.01	0.00	0.00	0.01	0.00	0.00
I2	624	0.00	0.01	0.00	0.00	0.01	0.00	0.00
J1	635	0.00	0.00	0.00	0.00	0.00	0.00	0.00
J2	638	0.00	0.00	0.00	0.00	0.00	0.00	0.00
K1	841	0.00	0.01	0.00	0.00	0.01	0.00	0.00
K2	844	0.00	0.01	0.00	0.00	0.01	0.00	0.00
L1	855	0.00	0.00	0.00	0.00	0.00	0.00	0.00
L2	858	0.00	0.00	0.00	0.00	0.00	0.00	0.00
M1	941	0.00	0.01	0.00	0.00	0.01	0.00	0.00
M2	944	0.00	0.01	0.00	0.00	0.01	0.00	0.00
N1	955	0.00	0.00	0.00	0.00	0.00	0.00	0.00
N2	958	0.00	0.00	0.00	0.00	0.00	0.00	0.00
O1	1101	0.00	0.01	0.00	0.00	0.01	0.00	0.00
O2	1104	0.00	0.01	0.00	0.00	0.01	0.00	0.00

Table 2.10.10-8 Stress Components – Bolt Preload; 1.12-Inch Outer Shell Thickness (continued)

Stress Points		Stresses						
Location	Node	S_X	S_Y	S_Z	S_{XY}	S_1	S_2	S_3
P1	1115	0.00	0.00	0.00	0.00	0.01	0.00	0.00
P2	1118	0.00	0.00	0.00	0.00	0.01	0.00	0.00
Q1	1261	0.00	0.01	0.00	0.00	0.01	0.00	0.00
Q2	1264	0.00	0.01	0.00	0.00	0.01	0.00	0.00
R1	1275	0.00	0.00	0.00	0.00	0.01	0.00	0.00
R2	1278	0.00	0.00	0.00	0.00	0.01	0.00	0.00
S1	1561	0.00	0.04	0.00	0.00	0.04	0.00	0.00
S2	1564	0.00	-0.02	-0.01	0.00	0.00	-0.01	-0.02
T1	1575	0.00	0.00	-0.01	0.00	0.00	0.00	-0.01
T2	1578	0.00	0.00	-0.01	0.00	0.00	0.00	-0.01
U1	1841	-0.01	-0.30	0.07	0.01	0.07	-0.01	-0.30
U2	1844	-0.07	-0.10	0.09	0.12	0.09	0.03	-0.20
V1	1852	0.10	0.02	0.05	0.01	0.10	0.05	0.02
V2	1856	0.00	-0.05	0.01	0.01	0.01	0.01	-0.05
W1	1969	-0.06	-0.20	0.05	0.18	0.06	0.05	-0.32
W2	1970	-0.01	-0.14	0.07	0.02	0.07	0.00	-0.15
W3	1971	0.00	-0.08	0.08	-0.05	0.08	0.02	-0.10
W4	1972	0.00	-0.03	0.09	-0.05	0.09	0.04	-0.07
W5	1973	0.00	0.01	0.10	-0.05	0.10	0.05	-0.04
W6	1974	0.00	0.04	0.10	-0.04	0.10	0.06	-0.03
W7	1975	0.00	0.07	0.10	-0.02	0.10	0.07	-0.01
W8	1976	0.00	0.09	0.11	-0.01	0.11	0.09	0.00
X1	2370	-0.06	0.00	-0.02	0.13	0.11	-0.02	-0.17
X2	2390	-0.05	-0.21	-0.09	0.10	0.00	-0.09	-0.26
X3	2410	0.06	-0.22	-0.04	-0.01	0.06	-0.04	-0.22
X4	2430	0.03	-0.09	-0.01	-0.06	0.05	-0.01	-0.12
X5	2450	0.01	-0.05	0.00	-0.06	0.05	0.00	-0.08
X6	2470	0.00	-0.01	0.01	-0.04	0.04	0.01	-0.04
X7	2490	0.01	0.00	0.02	-0.02	0.03	0.02	-0.02
X8	2510	0.01	0.00	0.03	-0.02	0.03	0.03	-0.01
X9	2530	0.02	0.00	0.03	-0.01	0.03	0.02	-0.01

Table 2.10.10-8 Stress Components – Bolt Preload; 1.12-Inch Outer Shell Thickness (continued)

Stress Points		Stresses						
Location	Node	S_X	S_Y	S_Z	S_{XY}	S_1	S_2	S_3
X10	2550	0.02	0.00	0.04	-0.01	0.04	0.02	0.00
X11	2570	0.02	0.00	0.04	0.00	0.04	0.02	0.00
Y1	2305	0.02	0.00	0.02	0.00	0.02	0.02	0.00
Y2	2325	0.01	0.00	0.01	0.00	0.01	0.01	0.00
Y3	2345	0.00	-0.01	0.00	0.00	0.00	0.00	-0.01
Y4	2365	-0.01	-0.01	-0.01	0.00	-0.01	-0.01	-0.01
Y5	2385	-0.02	-0.01	-0.02	0.00	-0.01	-0.02	-0.02
Y6	2405	-0.02	-0.01	-0.02	0.00	-0.01	-0.02	-0.02
Y7	2425	-0.01	-0.01	-0.01	0.00	-0.01	-0.01	-0.02
Y8	2445	-0.01	-0.02	0.00	0.00	0.01	0.00	-0.02
Y9	2465	0.02	-0.01	0.01	0.00	0.02	0.01	-0.01
Y10	2485	0.03	-0.01	0.02	0.00	0.03	0.02	-0.01
Y11	2505	0.03	0.00	0.03	-0.01	0.03	0.03	-0.01
Y12	2525	0.04	0.00	0.04	0.00	0.04	0.04	0.00
Y13	2545	0.05	0.00	0.05	0.00	0.05	0.05	0.00
Y14	2565	0.06	0.00	0.06	0.00	0.06	0.06	0.00
Z1	2301	0.02	0.00	0.02	0.00	0.02	0.02	0.00
Z2	2321	0.01	0.00	0.01	0.00	0.01	0.01	0.00
Z3	2341	0.00	0.00	0.00	0.00	0.00	0.00	0.00
Z4	2361	-0.01	0.00	-0.01	0.00	0.01	-0.01	-0.01
Z5	2381	-0.01	0.01	-0.01	0.00	0.01	-0.01	-0.01
Z6	2401	-0.01	0.01	-0.01	0.00	0.01	-0.01	-0.01
Z7	2421	-0.01	0.00	-0.01	0.00	0.00	-0.01	-0.01
Z8	2441	0.00	0.00	0.00	0.00	0.00	0.00	0.00
Z9	2461	0.01	0.00	0.01	0.00	0.01	0.01	0.00
Z10	2481	0.03	0.00	0.03	0.00	0.03	0.03	0.00
Z11	2501	0.03	0.00	0.03	0.00	0.03	0.03	0.00
Z12	2521	0.04	0.00	0.04	0.00	0.04	0.04	0.00
Z13	2541	0.05	0.00	0.05	0.00	0.05	0.05	0.00
Z14	2561	0.06	0.00	0.06	0.00	0.06	0.06	0.00

Table 2.10.10-9 Stress Components – Impact and Inertial Loads; 30-Foot Top End Drop; $\phi = 0°$; 1.12-Inch Outer Shell Thickness

Stress Points		Stresses						
Location	Node	S_X	S_Y	S_Z	S_{XY}	S_1	S_2	S_3
A1	327	0.75	0.01	0.76	0.03	0.76	0.75	0.01
A2	302	0.66	0.01	0.67	-0.01	0.67	0.66	0.01
A3	277	0.58	0.01	0.59	-0.03	0.59	0.58	0.00
A4	252	0.42	-0.01	0.43	-0.02	0.43	0.42	-0.02
A5	227	0.14	-0.04	0.14	-0.03	0.14	0.14	-0.05
A6	202	-0.15	-0.07	-0.15	-0.02	-0.06	-0.15	-0.15
A7	177	-0.48	-0.08	-0.49	-0.01	-0.08	-0.48	-0.49
B1	104	0.31	0.01	0.33	0.00	0.33	0.31	0.01
B2	79	0.04	0.01	0.05	-0.04	0.07	0.05	-0.02
B3	54	-0.21	-0.01	-0.22	-0.05	0.00	-0.21	-0.23
B4	29	-0.47	-0.01	-0.48	-0.04	0.00	-0.47	-0.48
B5	4	-0.61	0.00	-0.63	0.04	0.01	-0.61	-0.63
C1	110	0.02	0.00	0.17	-0.04	0.17	0.06	-0.03
C2	85	-0.09	0.00	-0.02	-0.08	0.05	-0.02	-0.14
C3	60	-0.17	0.00	-0.19	-0.10	0.05	-0.19	-0.22
C4	35	-0.25	0.00	-0.36	-0.06	0.01	-0.27	-0.36
C5	10	-0.31	0.00	-0.46	-0.01	0.00	-0.31	-0.46
D1	335	-0.32	-1.10	-0.01	-0.22	-0.01	-0.25	-1.18
D2	310	0.11	-0.70	0.17	-0.22	0.19	0.15	-0.77
D3	285	0.17	-0.50	0.21	-0.20	0.23	0.21	-0.56
D4	260	0.22	-0.35	0.20	-0.17	0.27	0.20	-0.40
D5	235	0.18	-0.23	0.10	-0.13	0.22	0.10	-0.27
D6	210	0.11	-0.15	-0.02	-0.08	0.13	-0.02	-0.17
D7	185	0.07	-0.12	-0.16	-0.04	0.07	-0.13	-0.16
E1	118	-0.45	-0.42	-0.22	-0.17	-0.22	-0.25	-0.62
E2	93	-0.12	-0.26	-0.15	-0.11	-0.06	-0.15	-0.32
E3	68	-0.06	-0.11	-0.17	-0.06	-0.02	-0.14	-0.18
E4	43	0.00	-0.04	-0.21	-0.02	0.01	-0.05	-0.21
E5	18	0.06	-0.01	-0.23	0.00	0.06	-0.01	-0.23
F1	143	0.03	-0.32	-0.08	-0.16	0.09	-0.08	-0.38
F2	144	-0.03	-0.11	-0.04	-0.19	0.13	-0.04	-0.27

Table 2.10.10-9 Stress Components – Impact and Inertial Loads; 30-Foot Top End Drop; $\phi = 0°$; 1.12-Inch Outer Shell Thickness (continued)

Stress Points		Stresses						
Location	Node	S_X	S_Y	S_Z	S_{XY}	S_1	S_2	S_3
F3	145	-0.07	-0.10	-0.05	-0.21	0.12	-0.05	-0.29
F4	146	-0.04	-0.09	-0.04	-0.17	0.11	-0.04	-0.24
F5	147	-0.02	-0.09	-0.03	-0.14	0.09	-0.03	-0.20
F6	148	-0.01	-0.08	-0.03	-0.10	0.06	-0.03	-0.15
F7	149	-0.01	-0.07	-0.02	-0.05	0.03	-0.02	-0.10
F8	150	0.00	-0.05	-0.01	-0.03	0.02	-0.01	-0.07
G1	335	-0.32	-1.10	-0.01	-0.22	-0.01	-0.25	-1.18
G2	336	-0.23	-0.76	0.10	-0.11	0.10	-0.19	-0.79
G3	337	-0.10	-0.62	0.16	-0.03	0.16	-0.09	-0.62
G4	338	-0.02	-0.53	0.19	0.02	0.19	-0.02	-0.53
G5	339	0.05	-0.27	0.27	0.05	0.27	0.05	-0.27
G6	340	0.15	-0.06	0.34	0.03	0.34	0.16	-0.07
H1	346	0.10	-0.21	0.23	-0.14	0.23	0.15	-0.26
H2	347	0.00	-0.74	0.05	-0.13	0.06	0.03	-0.77
H3	348	0.03	-0.96	0.00	0.00	0.03	0.00	-0.96
H4	349	0.01	-0.84	0.03	0.05	0.03	0.01	-0.84
H5	350	-0.01	-0.78	0.04	0.04	0.04	0.00	-0.78
I1	621	0.00	-1.17	-0.15	0.03	0.00	-0.15	-1.17
I2	624	0.02	-1.64	-0.25	0.03	0.02	-0.25	-1.64
J1	635	0.00	-1.12	0.05	0.00	0.05	0.00	-1.12
J2	638	0.00	-1.16	0.03	0.00	0.03	0.00	-1.16
K1	841	0.00	-1.84	0.00	0.00	0.00	0.00	-1.84
K2	844	0.00	-1.83	0.00	0.00	0.00	0.00	-1.83
L1	855	0.00	-1.57	0.00	0.00	0.00	0.00	-1.57
L2	858	0.00	-1.57	0.00	0.00	0.00	0.00	-1.57
M1	941	0.00	-2.37	0.00	0.00	0.00	0.00	-2.37
M2	944	0.00	-2.37	0.00	0.00	0.00	0.00	-2.37
N1	955	0.00	-2.11	0.00	0.00	0.00	0.00	-2.11
N2	958	0.00	-2.11	0.00	0.00	0.00	0.00	-2.11
O1	1101	0.00	-3.26	0.00	0.00	0.00	0.00	-3.26
O2	1104	0.00	-3.26	0.00	0.00	0.00	0.00	-3.26

Table 2.10.10-9 Stress Components – Impact and Inertial Loads; 30-Foot Top End Drop; $\phi = 0°$; 1.12-Inch Outer Shell Thickness (continued)

Stress Points		Stresses						
Location	Node	S_X	S_Y	S_Z	S_{XY}	S_1	S_2	S_3
P1	1115	0.00	-2.99	0.00	0.00	0.00	0.00	-2.99
P2	1118	0.00	-2.99	0.00	0.00	0.00	0.00	-2.99
Q1	1261	0.00	-4.14	0.00	0.00	0.00	0.00	-4.14
Q2	1264	0.00	-4.14	0.00	0.00	0.00	0.00	-4.14
R1	1275	0.00	-3.88	0.00	0.00	0.00	0.00	-3.88
R2	1278	0.00	-3.88	0.00	0.00	0.00	0.00	-3.88
S1	1561	0.00	-3.75	-0.59	-0.13	0.01	-0.59	-3.76
S2	1564	0.09	-6.30	-1.16	-0.16	0.10	-1.16	-6.31
T1	1575	0.00	-4.40	0.24	-0.01	0.24	0.00	-4.40
T2	1578	0.00	-5.07	0.04	0.00	0.04	0.00	-5.07
U1	1841	0.02	-6.64	2.17	-0.17	2.17	0.03	-6.65
U2	1844	0.83	-3.38	2.99	-0.17	2.99	0.86	-3.40
V1	1852	-1.06	-5.38	0.68	-0.19	0.68	-1.03	-5.40
V2	1856	0.01	-3.42	1.29	-0.04	1.29	0.01	-3.42
W1	1969	1.83	-1.34	0.29	1.37	2.34	0.29	-1.85
W2	1970	1.22	-3.04	-0.21	0.55	1.29	-0.21	-3.11
W3	1971	0.68	-3.78	-0.46	-0.06	0.69	-0.46	-3.79
W4	1972	0.38	-4.48	-0.66	-0.19	0.39	-0.66	-4.50
W5	1973	0.23	-4.98	-0.78	-0.22	0.24	-0.78	-4.99
W6	1974	0.13	-5.36	-0.88	-0.19	0.14	-0.88	-5.37
W7	1975	0.06	-5.77	-0.97	-0.11	0.07	-0.97	-5.77
W8	1976	0.02	-6.21	-1.07	-0.06	0.02	-1.07	-6.21
X1	2370	4.51	1.44	3.44	2.33	5.77	3.44	0.18
X2	2390	0.34	-2.34	0.68	2.04	1.44	0.68	-3.44
X3	2410	0.11	-4.34	-0.20	1.09	0.36	-0.20	-4.59
X4	2430	-0.65	-4.17	-0.57	1.03	-0.37	-0.57	-4.45
X5	2450	-0.68	-4.58	-0.75	1.01	-0.43	-0.75	-4.83
X6	2470	-0.57	-4.60	-0.67	1.01	-0.33	-0.67	-4.84
X7	2490	-0.14	-4.73	-0.46	0.93	0.04	-0.46	-4.91
X8	2510	0.11	-4.75	-0.33	0.82	0.25	-0.33	-4.88
X9	2530	0.43	-4.81	-0.22	0.63	0.51	-0.22	-4.89

Table 2.10.10-9 Stress Components – Impact and Inertial Loads; 30-Foot Top End Drop; $\phi = 0°$; 1.12-Inch Outer Shell Thickness (continued)

Stress Points		Stresses						
Location	Node	S_X	S_Y	S_Z	S_{XY}	S_1	S_2	S_3
X10	2550	0.78	-4.83	-0.11	0.36	0.81	-0.11	-4.86
X11	2570	1.18	-4.84	-0.04	0.20	1.19	-0.04	-4.85
Y1	2305	0.81	-1.90	1.22	0.12	1.22	0.82	-1.91
Y2	2325	0.95	-2.05	1.07	0.51	1.07	1.03	-2.14
Y3	2345	1.15	-2.40	1.08	0.59	1.26	1.08	-2.51
Y4	2365	1.16	-2.72	1.00	0.46	1.21	1.00	-2.77
Y5	2385	0.80	-2.93	0.71	0.31	0.83	0.71	-2.96
Y6	2405	0.26	-3.08	0.32	0.29	0.32	0.29	-3.11
Y7	2425	-0.17	-3.28	-0.05	0.41	-0.05	-0.12	-3.34
Y8	2445	-0.41	-3.58	-0.30	0.55	-0.29	-0.32	-3.68
Y9	2465	-0.50	-3.95	-0.46	0.63	-0.38	-0.46	-4.07
Y10	2485	-0.51	-4.30	-0.57	0.59	-0.42	-0.57	-4.39
Y11	2505	-0.55	-4.53	-0.68	0.53	-0.48	-0.68	-4.60
Y12	2525	-0.60	-4.68	-0.79	0.40	-0.56	-0.79	-4.72
Y13	2545	-0.70	-4.78	-0.96	0.23	-0.68	-0.96	-4.80
Y14	2565	-0.86	-4.82	-1.19	0.04	-0.86	-1.19	-4.82
Z1	2301	1.78	-1.88	1.78	0.00	1.78	1.78	-1.88
Z2	2321	1.26	-2.02	1.26	0.00	1.26	1.26	-2.02
Z3	2341	1.05	-2.32	1.05	0.00	1.05	1.05	-2.32
Z4	2361	0.87	-2.63	0.87	0.00	0.87	0.87	-2.63
Z5	2381	0.63	-2.91	0.63	0.00	0.63	0.63	-2.91
Z6	2401	0.34	-3.18	0.34	0.00	0.34	0.34	-3.18
Z7	2421	0.04	-3.44	0.04	0.00	0.04	0.04	-3.44
Z8	2441	-0.22	-3.74	-0.22	0.00	-0.22	-0.22	-3.74
Z9	2461	-0.45	-4.06	-0.45	0.00	-0.45	-0.45	-4.06
Z10	2481	-0.67	-4.35	-0.67	0.00	-0.67	-0.67	-4.35
Z11	2501	-0.84	-4.53	-0.84	0.00	-0.84	-0.84	-4.53
Z12	2521	-1.03	-4.66	-1.03	0.00	-1.03	-1.03	-4.66
Z13	2541	-1.28	-4.76	-1.28	0.00	-1.28	-1.28	-4.76
Z14	2561	-1.59	-4.80	-1.59	0.00	-1.59	-1.59	-4.80

Table 2.10.10-10 Stress Components – Impact and Inertial Loads; 30-Foot Top Corner Drop; $\phi = 15.74°$; 1.12-Inch Outer Shell Thickness

Stress Points		Stresses						
Location	Node	S_X	S_Y	S_Z	S_{XY}	S_1	S_2	S_3
A1	327	-0.28	0.01	1.55	0.08	1.55	0.03	-0.29
A2	302	-0.53	-0.00	1.36	0.15	1.36	0.04	-0.57
A3	277	-0.70	0.03	1.23	0.34	1.23	0.16	-0.84
A4	252	-1.06	-0.02	0.96	0.46	0.96	0.16	-1.23
A5	227	-1.77	-0.74	0.64	0.30	0.64	-0.66	-1.86
A6	202	-0.03	-1.21	2.68	-1.23	2.68	0.75	-1.99
A7	177	-13.24	-0.82	-3.97	-0.56	-0.79	-3.97	-13.27
B1	104	-3.25	-1.05	-0.84	-0.56	-0.84	-0.91	-3.38
B2	79	-2.44	-0.82	-0.29	-0.26	-0.29	-0.78	-2.48
B3	54	-2.17	-0.44	-0.01	-0.40	-0.01	-0.35	-2.26
B4	29	-1.89	-0.11	0.29	-0.28	-0.29	-0.06	-1.94
B5	4	-1.52	-0.02	-0.48	-0.06	0.48	0.02	-1.52
C1	110	-3.71	-0.27	-1.54	-0.26	-0.25	-1.54	-3.73
C2	85	-3.17	-0.22	-1.10	0.12	-0.22	-1.10	-3.18
C3	60	-2.65	-0.12	-0.73	0.14	-0.11	-0.73	-2.66
C4	35	-2.13	-0.03	-0.32	0.14	-0.02	-0.32	-2.14
C5	10	-1.85	-0.00	-0.08	0.15	0.01	-0.08	-1.86
D1	335	-1.22	-0.13	0.21	-0.30	0.21	-0.05	-1.30
D2	310	-1.40	-0.24	0.02	-0.27	0.02	-0.18	-1.46
D3	285	-1.63	-0.28	-0.13	-0.32	-0.13	-0.21	-1.70
D4	260	-2.03	-0.34	-0.39	-0.41	-0.24	-0.39	-2.13
D5	235	-2.82	-0.41	-0.90	-0.35	-0.36	-0.90	-2.87
D6	210	-3.63	-0.44	-1.46	-0.25	-0.42	-1.46	-3.65
D7	185	-4.41	-0.44	-2.13	0.25	-0.42	-2.13	-4.42
E1	118	-3.12	0.84	-2.09	-0.60	0.93	-2.09	-3.21
E2	93	-3.18	0.28	-2.10	-0.17	0.29	-2.10	-3.19
E3	68	-3.07	0.11	-1.98	0.03	0.11	-1.98	-3.07
E4	43	-3.04	0.03	-1.82	0.09	0.03	-1.82	-3.05
E5	18	-3.12	0.01	-1.74	0.14	0.02	-1.74	-3.13
F1	143	-0.61	3.17	-1.06	-0.82	3.34	-0.78	-1.06
F2	144	-0.72	0.80	-2.33	-0.69	1.07	-0.99	-2.33

Table 2.10.10-10 Stress Components – Impact and Inertial Loads; 30-Foot Top Corner Drop; $\phi = 15.74°$; 1.12-Inch Outer Shell Thickness (continued)

Stress Points		Stresses						
Location	Node	S_X	S_Y	S_Z	S_{XY}	S_1	S_2	S_3
F3	145	-1.06	0.15	-2.95	-0.52	0.35	-1.25	-2.95
F4	146	-1.78	-0.28	-3.58	-0.33	-0.21	-1.85	-3.58
F5	147	-2.25	-0.63	-4.07	-0.24	-0.59	-2.29	-4.07
F6	148	-2.54	-0.95	-4.49	-0.17	-0.93	-2.56	-4.49
F7	149	-2.75	-1.35	-4.92	-0.09	-1.35	-2.75	-4.92
F8	150	-2.85	-1.89	-5.39	-0.04	-1.89	-2.85	-5.39
G1	335	-1.22	-0.13	0.21	-0.30	0.21	-0.05	-1.30
G2	336	-1.01	-0.31	0.01	-0.28	0.01	-0.21	-1.11
G3	337	-1.07	-0.62	-0.25	-0.17	-0.25	-0.56	-1.13
G4	338	-1.37	-0.98	-0.55	0.08	-0.55	-0.96	-1.38
G5	339	-2.17	-1.48	-1.03	0.68	-1.03	-1.06	-2.58
G6	340	-2.96	-0.74	-0.97	0.77	-0.49	-0.97	-3.21
H1	346	-1.61	1.41	-2.58	1.04	1.73	-1.93	-2.58
H2	347	-1.42	4.42	-2.33	0.58	4.48	-1.48	-2.33
H3	348	-2.35	3.00	-3.46	-0.80	3.12	-2.47	-3.46
H4	349	-2.55	-0.63	-4.93	-0.93	-0.25	-2.93	-4.93
H5	350	-2.77	-4.41	-6.40	-0.62	-2.56	-4.61	-6.40
I1	621	-0.06	0.13	0.44	-0.03	0.44	0.13	-0.06
I2	624	-0.01	0.43	0.42	0.04	0.43	0.42	-0.01
J1	635	-0.09	-2.23	0.99	-0.13	2.24	0.99	-0.09
J2	638	-0.01	5.36	0.77	0.05	5.36	0.77	-0.01
K1	841	-0.03	6.09	0.16	-0.01	6.09	0.16	-0.03
K2	844	0.00	6.92	0.41	0.01	6.92	0.41	0.00
L1	855	-0.05	11.83	0.61	-0.04	11.83	0.61	-0.05
L2	858	0.02	12.80	0.69	0.01	12.81	0.69	0.02
M1	941	-0.03	6.32	0.16	0.00	6.32	0.16	-0.03
M2	944	-0.01	7.20	0.41	0.00	7.20	0.41	-0.01
N1	955	-0.05	13.70	0.75	-0.01	13.70	0.75	-0.05
N2	958	0.00	14.87	0.80	0.01	14.87	0.80	0.00
O1	1101	-0.04	2.72	-0.09	0.01	2.72	-0.04	-0.09
O2	1104	-0.03	3.22	0.15	-0.01	3.22	0.15	-0.03

Table 2.10.10-10 Stress Components – Impact and Inertial Loads; 30-Foot Top Corner Drop; $\phi = 15.74°$; 1.12-Inch Outer Shell Thickness (continued)

Stress Points		Stresses						
Location	Node	S_X	S_Y	S_Z	S_{XY}	S_1	S_2	S_3
P1	1115	-0.07	10.77	1.09	0.03	10.78	1.09	-0.07
P2	1118	0.00	11.75	0.86	-0.03	11.75	0.86	0.00
Q1	1261	-0.03	-3.27	0.21	0.02	0.21	-0.03	-3.27
Q2	1264	-0.01	-3.30	0.35	-0.03	0.35	-0.01	-3.30
R1	1275	-0.04	-0.13	1.33	0.06	1.33	-0.01	-0.16
R2	1278	0.00	-0.34	0.24	-0.07	0.24	0.01	-0.36
S1	1561	-0.04	-11.67	0.24	-0.40	0.24	-0.02	-11.68
S2	1564	0.34	-23.09	-4.92	-0.60	0.36	-4.92	-23.11
T1	1575	-0.14	-17.88	2.76	0.15	2.76	-0.14	-17.88
T2	1578	0.02	-19.72	1.70	-0.06	1.70	0.02	-19.72
U1	1841	0.28	-19.99	8.13	-0.19	8.13	0.29	-19.99
U2	1844	3.40	-11.67	9.78	-0.69	9.78	3.43	-11.70
V1	1852	6.10	-10.08	7.23	0.13	7.23	6.10	-10.08
V2	1856	0.59	-23.74	0.54	-0.42	0.60	0.54	-23.75
W1	1969	-19.40	-16.45	-8.37	3.91	-8.37	-13.75	-22.11
W2	1970	-14.06	-8.78	-5.45	1.32	-5.45	-8.47	-14.37
W3	1971	-7.44	-9.92	-4.43	-0.56	-4.43	-7.32	-10.04
W4	1972	-5.36	-10.65	-4.36	-0.73	-4.36	-5.26	-10.75
W5	1973	-4.37	-11.07	-4.37	-0.72	-4.29	-4.37	-11.15
W6	1974	-3.83	-11.20	-4.36	-0.60	-3.78	-4.36	-11.25
W7	1975	-3.57	-11.11	-4.37	-0.36	-3.55	-4.37	-11.13
W8	1976	-3.50	-10.64	-4.31	-0.25	-3.50	-4.31	-10.65
X1	2370	-6.70	-8.14	-1.89	1.84	-1.89	-5.44	-9.39
X2	2390	-5.84	-11.37	-2.73	3.06	-2.73	-4.48	-12.73
X3	2410	-5.21	-12.98	-2.78	3.61	-2.78	-3.79	-14.40
X4	2430	-4.12	-14.33	-2.51	3.72	-2.51	-2.90	-15.55
X5	2450	-3.36	-14.88	-2.09	3.64	-2.09	-2.30	-15.94
X6	2470	-2.49	-15.02	-1.63	3.50	-1.57	-1.63	-15.93
X7	2490	-1.31	-14.92	-1.25	3.23	-0.59	-1.25	-15.65
X8	2510	-0.55	-14.80	-1.14	2.79	-0.03	-1.14	-15.33
X9	2530	0.33	-14.69	-1.14	2.16	0.64	-1.14	-15.00

Table 2.10.10-10 Stress Components – Impact and Inertial Loads; 30-Foot Top Corner Drop; $\phi = 15.74°$; 1.12-Inch Outer Shell Thickness (continued)

Stress Points		Stresses						
Location	Node	S_X	S_Y	S_Z	S_{XY}	S_1	S_2	S_3
X10	2550	1.43	-14.62	-1.27	1.24	1.52	-1.27	-14.72
X11	2570	2.78	-14.60	-1.55	0.73	2.81	-1.55	-14.63
Y1	2305	-0.37	-5.19	1.81	-0.20	1.81	-0.36	-5.20
Y2	2325	-0.64	-5.37	1.53	-0.42	1.53	-0.60	-5.40
Y3	2345	-1.22	-5.61	1.09	-0.49	1.09	-1.16	-5.66
Y4	2365	-2.12	-5.93	0.53	-0.32	0.53	-2.09	-5.96
Y5	2385	-2.85	-6.52	-0.04	0.17	-0.04	-2.84	-6.53
Y6	2405	-3.08	-7.53	-0.47	0.91	-0.47	-2.91	-7.71
Y7	2425	-2.89	-9.01	-0.69	1.79	-0.69	-2.41	-9.50
Y8	2445	-2.65	-10.83	-0.74	2.81	-0.74	-1.78	-11.70
Y9	2465	-3.02	-12.59	-0.74	3.94	-0.74	-1.61	-14.00
Y10	2485	-5.09	-13.75	-1.13	4.77	-1.13	-2.98	-15.86
Y11	2505	-7.13	-14.32	-1.93	4.59	-1.93	-4.89	-16.55
Y12	2525	-8.44	-14.62	-2.95	3.70	-2.95	-6.71	-16.35
Y13	2545	-9.98	-14.55	-4.58	2.23	-4.58	-9.07	-15.46
Y14	2565	-11.04	-14.54	-7.14	0.91	-7.14	-10.82	-14.77
Z1	2301	-0.59	-2.18	2.56	0.14	2.56	-0.58	-2.19
Z2	2321	-1.21	-1.70	2.32	-0.01	2.32	-1.21	-1.70
Z3	2341	-1.56	-1.85	1.74	-0.12	1.74	-1.51	-1.89
Z4	2361	-1.90	-2.04	1.27	-0.33	1.27	-1.63	-2.31
Z5	2381	-2.08	-2.27	0.85	-0.46	0.85	-1.70	-2.65
Z6	2401	-2.04	-2.54	0.46	-0.53	0.46	-1.71	-2.88
Z7	2421	-1.78	-2.88	0.11	-0.56	0.11	-1.54	-3.11
Z8	2441	-1.32	-3.26	-0.20	-0.56	-0.20	-1.17	-3.41
Z9	2461	-0.71	-3.64	-0.50	-0.06	-0.50	-0.71	-3.64
Z10	2481	0.02	-4.03	-0.78	2.71	1.37	-0.78	-5.38
Z11	2501	0.37	-4.21	-1.08	10.55	8.88	-1.08	-12.72
Z12	2521	0.73	-4.37	-1.44	34.89	33.17	-1.44	-36.80
Z13	2541	0.88	-4.93	-2.15	164.65	162.65	-2.15	-166.70
Z14	2561	1.59	-6.27	-4.64	215.93	213.63	-4.64	-218.31

Table 2.10.10-11 Impact and Inertial Loads; 30-Foot Top Oblique Drop; $\phi = 60°$; 1.12-Inch Outer Shell Thickness

Stress Points		Stresses						
Location	Node	S_X	S_Y	S_Z	S_{XY}	S_1	S_2	S_3
A1	327	-2.08	-0.00	2.19	0.12	2.19	0.00	-2.09
A2	302	-2.50	-0.03	1.92	0.37	1.92	0.03	-2.55
A3	277	-2.76	0.04	1.75	0.86	1.75	0.28	-3.00
A4	252	-3.29	-0.02	1.42	1.12	1.42	0.33	-3.64
A5	227	-4.44	-1.67	1.23	0.76	1.23	-1.47	-4.63
A6	202	0.22	-2.72	6.57	-2.85	6.57	1.96	-4.45
A7	177	-30.18	-1.77	-8.38	-1.30	-1.71	-8.38	-30.24
B1	104	-8.22	-2.48	-2.60	-1.31	-2.19	-2.60	-8.51
B2	79	-5.81	-1.94	-0.78	-0.53	-0.78	-1.87	-5.89
B3	54	-4.70	-1.01	0.40	-0.84	0.40	-0.83	-4.89
B4	29	-3.55	-0.23	1.60	-0.59	1.60	-0.13	-3.65
B5	4	-2.40	0.05	2.32	0.06	2.32	0.05	-2.40
C1	110	-8.76	-0.64	-3.94	-0.54	-0.60	-3.94	-8.79
C2	85	-7.28	-0.53	-2.53	0.44	-0.50	-2.53	-7.31
C3	60	-5.90	-0.28	-1.34	0.51	-0.23	-1.34	-5.95
C4	35	-4.52	-0.06	-0.07	0.44	-0.02	-0.07	-4.56
C5	10	-3.76	-0.01	0.70	0.37	0.70	0.03	-3.79
D1	335	-2.25	1.79	0.52	-0.29	1.81	0.52	-2.27
D2	310	-3.50	0.77	-0.27	-0.22	0.76	-0.27	-3.51
D3	285	-4.15	0.30	-0.71	-0.37	0.33	-0.71	-4.18
D4	260	-5.19	-0.13	-1.31	-0.64	-0.05	-1.31	-5.27
D5	235	-6.96	-0.53	-2.31	-0.58	-0.48	-2.31	-7.02
D6	210	-8.72	-0.74	-3.39	-0.44	-0.71	-3.39	-8.75
D7	185	-10.48	-0.80	-4.69	0.67	-0.75	-4.69	-10.53
E1	118	-6.47	2.78	-4.49	-1.08	2.91	-4.49	-6.60
E2	93	-7.24	1.15	-4.64	-0.20	1.16	-4.64	-7.24
E3	68	-7.11	0.47	-4.33	0.18	0.48	-4.33	-7.11
E4	43	-7.15	0.15	-3.87	0.26	0.16	-3.87	-7.15
E5	18	-7.44	0.05	-3.65	0.32	0.06	-3.65	-7.45
F1	143	-1.49	8.06	-2.34	-1.62	8.33	-1.76	-2.34
F2	144	-1.63	2.10	-5.40	-1.26	2.49	-2.02	-5.40

Table 2.10.10-11 Impact and Inertial Loads; 30-Foot Top Oblique Drop; $\phi = 60°$; 1.12-Inch Outer Shell Thickness (continued)

Stress Points		Stresses						
Location	Node	S_X	S_Y	S_Z	S_{XY}	S_1	S_2	S_3
F3	145	-2.35	0.54	-6.82	-0.83	0.77	-2.57	-6.82
F4	146	-4.11	-0.48	-8.33	-0.45	-0.43	-4.16	-8.33
F5	147	-5.25	-1.30	-9.51	-0.30	-1.28	-5.27	-9.51
F6	148	-5.95	-2.08	-10.49	-0.22	-2.06	-5.96	-10.49
F7	149	-6.43	-3.05	-11.52	-0.12	-3.04	-6.43	-11.52
F8	150	-6.70	-4.35	-12.64	-0.04	-4.35	-6.70	-12.64
G1	335	-2.25	1.79	0.52	-0.29	1.81	0.52	-2.27
G2	336	-1.94	0.72	-0.16	-0.44	0.79	-0.16	-2.01
G3	337	-2.33	-0.28	-0.89	-0.35	-0.22	-0.89	-2.39
G4	338	-3.17	-1.29	-1.66	0.15	-1.28	-1.66	-3.18
G5	339	-5.18	-2.97	-2.92	1.50	-2.21	-2.92	-5.94
G6	340	-7.24	-1.62	-2.94	1.76	-1.11	-2.94	-7.75
H1	346	-3.96	3.72	-6.50	2.70	4.57	-4.82	-6.50
H2	347	-3.33	11.79	-5.57	1.61	11.96	-3.50	-5.57
H3	348	-5.58	8.88	-8.13	-1.88	9.12	-5.83	-8.13
H4	349	-6.00	0.12	-11.64	-2.28	0.88	-6.76	-11.64
H5	350	-6.49	-8.86	-15.10	-1.53	-5.74	-9.61	-15.10
I1	621	-0.14	2.53	-1.32	-0.12	2.53	1.32	-0.14
I2	624	-0.06	4.13	1.47	0.04	4.13	1.47	-0.06
J1	635	-0.20	7.38	2.23	-0.29	7.39	2.23	-0.21
J2	638	-0.02	14.80	1.74	0.11	14.80	1.74	-0.02
K1	841	-0.12	15.76	-0.17	-0.07	15.76	-0.12	-0.17
K2	844	-0.03	18.29	1.41	0.07	18.30	1.41	-0.03
L1	855	-0.12	31.01	1.46	-0.14	31.01	1.46	-0.12
L2	858	0.04	34.02	1.59	0.08	34.02	1.59	0.04
M1	941	-0.12	21.41	-0.22	-0.01	21.41	-0.12	-0.22
M2	944	-0.05	24.48	1.44	0.01	24.48	1.44	-0.05
N1	955	-0.13	42.12	1.74	-0.07	42.12	1.74	-0.13
N2	958	0.01	46.04	1.89	0.06	46.04	1.89	0.01
O1	1101	-0.13	21.18	-0.78	0.00	21.18	-0.13	-0.78
O2	1104	-0.11	24.10	0.83	-0.01	24.10	0.83	-0.11

Table 2.10.10-11 Impact and Inertial Loads; 30-Foot Top Oblique Drop; $\phi = 60°$; 1.12-Inch Outer Shell Thickness (continued)

Stress Points		Stresses						
Location	Node	S_X	S_Y	S_Z	S_{XY}	S_1	S_2	S_3
P1	1115	-0.17	45.92	1.85	0.03	45.92	1.85	-0.17
P2	1118	0.01	50.50	2.64	-0.03	50.50	2.64	0.01
Q1	1261	-0.12	15.22	-0.19	0.04	15.22	-0.12	-0.19
Q2	1264	-0.05	17.63	1.38	-0.05	17.63	1.38	-0.05
R1	1275	-0.14	31.45	0.52	0.11	31.45	0.52	-0.14
R2	1278	0.02	35.18	2.79	-0.11	35.18	2.79	0.02
S1	1561	-0.11	-3.35	1.59	-0.18	1.59	-0.10	-3.36
S2	1564	0.17	-9.66	-2.11	-0.41	0.19	-2.11	-9.68
T1	1575	-0.30	3.08	2.37	0.21	3.09	2.37	-0.31
T2	1578	0.01	7.19	4.65	-0.11	7.19	4.65	0.01
U1	1841	0.30	-16.34	10.62	-0.13	10.62	0.30	-16.34
U2	1844	3.93	-7.62	11.06	-0.84	11.06	3.99	-7.68
V1	1852	9.88	1.29	5.59	-2.99	10.82	5.59	0.35
V2	1856	0.78	-7.74	-2.34	0.06	0.78	-2.34	-7.74
W1	1969	-66.69	-41.51	-24.01	-0.65	-24.01	-41.49	-66.71
W2	1970	-48.82	-4.73	-12.06	-3.65	-4.43	-12.06	-49.12
W3	1971	-27.03	-1.84	-8.96	-5.41	-0.73	-8.96	-28.14
W4	1972	-19.48	2.31	-9.40	-4.62	3.25	-9.40	-20.42
W5	1973	-15.85	5.40	-10.14	-3.65	6.01	-10.14	-16.46
W6	1974	-13.87	8.22	-10.72	-2.66	8.53	-10.72	-14.19
W7	1975	-12.85	11.77	-11.35	-1.48	11.86	-11.35	-12.94
W8	1976	-12.54	16.63	-11.84	-0.65	16.64	-11.84	-12.56
X1	2370	-34.36	-16.88	-7.62	1.24	-7.62	-16.79	-34.45
X2	2390	-16.19	-14.00	-1.50	4.84	-1.50	-10.13	-20.06
X3	2410	-12.71	-11.84	0.08	7.40	0.08	-4.86	-19.68
X4	2430	-8.05	-13.16	1.09	7.27	1.09	-2.90	-18.31
X5	2450	-6.21	-12.61	1.72	6.36	1.72	-2.30	-16.53
X6	2470	-5.21	-11.98	1.94	5.21	1.94	-2.38	-14.81
X7	2490	-4.60	-11.11	1.71	4.19	1.71	-2.55	-13.17
X8	2510	-4.03	-10.62	1.43	3.25	1.43	-2.69	-11.95
X9	2530	-3.30	-10.25	0.91	2.35	0.91	-2.58	-10.98

Table 2.10.10-11 Impact and Inertial Loads; 30-Foot Top Oblique Drop; $\phi = 60°$; 1.12-Inch Outer Shell Thickness (continued)

Stress Points		Stresses						
Location	Node	S_X	S_Y	S_Z	S_{XY}	S_1	S_2	S_3
X10	2550	-2.22	-10.08	0.08	1.28	0.08	-2.02	-10.28
X11	2570	-0.71	-10.03	-1.13	0.85	-0.63	-1.13	-10.11
Y1	2305	-0.46	-3.26	2.57	-0.40	2.57	-0.40	-3.32
Y2	2325	-2.95	-3.23	2.89	-0.90	2.89	-2.18	-4.00
Y3	2345	-5.69	-3.25	2.66	-0.90	2.66	-2.96	-5.98
Y4	2365	-8.34	-3.57	2.37	0.16	2.37	-3.56	-8.35
Y5	2385	-9.41	-4.50	2.28	2.00	2.28	-3.79	-10.13
Y6	2405	-8.79	-6.18	2.42	4.01	2.42	-3.27	-11.70
Y7	2425	-7.68	-8.46	2.68	5.92	2.68	-2.14	-14.01
Y8	2445	-7.43	-10.82	3.07	8.05	3.07	-0.89	-17.36
Y9	2465	-9.60	-12.26	3.66	10.53	3.66	-0.31	-21.55
Y10	2485	-16.60	-12.11	3.71	12.23	3.71	-1.92	-26.79
Y11	2505	-22.30	-11.70	2.69	11.42	2.69	-4.42	-29.59
Y12	2525	-25.19	-11.20	1.52	8.79	1.52	-6.96	-29.43
Y13	2545	-27.90	-10.20	-0.77	5.06	-0.77	-8.85	-29.24
Y14	2565	-28.38	-9.99	-5.27	2.37	-5.27	-9.69	-28.68
Z1	2301	-2.89	-0.88	2.35	-0.10	2.35	-0.88	-2.90
Z2	2321	-3.57	-0.45	2.73	-0.22	2.73	-0.44	-3.59
Z3	2341	-4.26	-0.43	2.69	-0.18	2.69	-0.42	-4.27
Z4	2361	-4.90	-0.43	2.68	-0.02	2.68	-0.43	-4.90
Z5	2381	-5.16	-0.47	2.62	0.27	2.62	-0.45	-5.18
Z6	2401	-4.97	-0.58	2.45	0.60	2.45	-0.49	-5.06
Z7	2421	-4.39	-0.75	2.18	0.94	2.18	-0.52	-4.62
Z8	2441	-3.54	-0.96	1.86	1.42	1.86	-0.33	-4.17
Z9	2461	-2.54	-1.17	1.51	3.69	1.90	1.51	-5.61
Z10	2481	-1.50	-1.38	1.18	12.69	11.25	1.18	-14.14
Z11	2501	-1.00	-1.49	0.99	36.68	35.44	0.99	-37.93
Z12	2521	-0.51	-1.56	0.76	110.29	109.25	0.76	-111.32
Z13	2541	-0.23	-1.98	0.30	500.97	499.87	0.30	-502.08
Z14	2561	0.45	-3.06	-1.58	655.17	653.86	-1.58	-656.48

Table 2.10.10-12 Stress Components – Impact and Inertial Loads; 30-Foot Side Drop; $\phi = 90°$; 1.20-Inch Outer Shell Thickness; Circumferential Location = 0°

Stress Points		Stresses						
Location	Node	S_X	S_Y	S_Z	S_{XY}	S_1	S_2	S_3
A1	327	-3.04	-0.01	2.46	0.14	2.46	0.00	-3.04
A2	302	-3.54	-0.04	2.16	0.48	2.16	0.02	-3.60
A3	277	-3.84	0.05	1.98	1.12	1.98	0.35	-4.14
A4	252	-4.45	-0.02	1.63	1.45	1.63	0.41	-4.88
A5	227	-5.79	-2.13	1.52	1.00	1.52	-1.87	-6.05
A6	202	0.36	-3.47	8.55	-3.67	8.55	2.59	-5.69
A7	177	-38.71	-2.24	-10.58	-1.67	-2.17	-10.58	-38.78
B1	104	-10.76	-3.20	-3.51	-1.69	-2.84	-3.51	-11.12
B2	79	-7.52	-2.51	-1.03	-0.67	-1.03	-2.42	-7.61
B3	54	-5.97	-1.30	0.62	-1.06	0.62	-1.07	-6.20
B4	29	-4.36	-0.29	2.29	-0.74	2.29	-0.16	-4.50
B5	4	-2.81	0.06	3.30	0.06	3.30	0.07	-2.81
C1	110	-11.31	-0.82	-5.16	0.68	-0.78	-5.16	-11.35
C2	85	-9.35	-0.68	-3.26	0.60	-0.64	-3.26	-9.39
C3	60	-7.53	-0.36	-1.64	0.71	-0.29	-1.64	-7.60
C4	35	-5.71	-0.08	0.08	0.59	0.08	-0.02	-5.77
C5	10	-4.70	-0.01	1.12	0.48	1.12	0.04	-4.75
D1	335	-2.75	2.83	0.68	-0.27	2.85	0.68	-2.77
D2	310	-4.57	1.33	-0.43	-0.18	1.34	-0.43	-4.57
D3	285	-5.44	0.62	-1.01	-0.38	0.64	-1.01	-5.46
D4	260	-6.80	0.00	-1.78	-0.75	0.09	-1.78	-6.88
D5	235	-9.07	-0.58	-3.03	-0.69	-0.52	-3.03	-9.13
D6	210	-11.31	-0.88	-4.37	-0.53	-0.86	-4.37	-11.34
D7	185	-13.56	-0.97	-5.98	0.89	-0.91	-5.98	-13.63
E1	118	-8.14	3.79	-5.69	-1.31	3.94	-5.69	-8.29
E2	93	-9.28	1.61	-5.92	-0.20	1.61	-5.92	-9.28
E3	68	-9.14	0.66	-5.50	0.26	0.67	-5.50	-9.15
E4	43	-9.22	0.21	-4.89	0.34	0.22	-4.89	-9.23
E5	18	-9.63	0.07	-4.60	0.41	0.09	-4.60	-9.64
F1	143	-1.94	10.55	-2.98	-2.02	10.87	-2.26	-2.98
F2	144	-2.09	2.76	-6.95	-1.54	3.20	-2.53	-6.95

Table 2.10.10-12 Stress Components – Impact and Inertial Loads; 30-Foot Side Drop; $\phi = 90°$; 1.20-Inch Outer Shell Thickness; Circumferential Location = 0° (continued)

Stress Points		Stresses						
Location	Node	S_X	S_Y	S_Z	S_{XY}	S_1	S_2	S_3
F3	145	-3.00	0.75	-8.78	-0.97	0.99	-3.24	-8.78
F4	146	-5.28	-0.58	-10.73	-0.50	-0.53	-5.33	-10.73
F5	147	-6.76	-1.64	-12.26	-0.32	-1.62	-6.78	-12.26
F6	148	-7.67	-2.64	-13.52	-0.23	-2.63	-7.68	-13.52
F7	149	-8.29	-3.90	-14.85	-0.13	-3.90	-8.30	-14.85
F8	150	-8.64	-5.59	-16.31	-0.04	-5.59	-8.64	-16.31
G1	335	-2.75	2.83	0.68	-0.27	2.85	0.68	-2.77
G2	336	-2.39	1.29	-0.25	-0.52	1.36	-0.25	-2.46
G3	337	-2.96	-0.07	-1.22	-0.44	-0.01	-1.22	-3.03
G4	338	-4.08	-1.41	-2.23	0.18	-1.40	-2.23	-4.09
G5	339	-6.71	-3.70	-3.90	1.91	-2.78	-3.90	-7.63
G6	340	-9.42	-2.06	-3.95	2.26	-1.42	-3.95	-10.05
H1	346	-5.16	4.90	-8.50	3.55	6.03	-6.29	-8.50
H2	347	-4.30	15.57	-7.21	2.14	15.80	-4.53	-7.21
H3	348	-7.22	11.92	-10.49	-2.43	12.22	-7.52	-10.49
H4	349	-7.75	0.56	-15.03	-2.97	1.51	-8.70	-15.03
H5	350	-8.37	-11.06	-19.50	-1.99	-7.32	-12.12	-19.50
I1	621	-0.18	3.82	1.77	-0.17	3.83	1.77	-0.18
I2	624	-0.09	6.11	2.02	0.04	6.11	2.02	-0.09
J1	635	-0.26	10.06	2.86	-0.38	10.07	2.86	-0.27
J2	638	-0.03	19.65	2.23	0.14	19.65	2.23	-0.03
K1	841	-0.19	16.70	-0.42	-0.10	16.70	-0.19	-0.42
K2	844	-0.06	19.71	1.97	0.10	19.71	1.97	-0.06
L1	855	-0.14	33.28	2.54	-0.22	33.29	2.54	-0.14
L2	858	0.04	36.59	1.36	0.14	36.60	1.36	0.04
M1	941	-0.18	25.27	-0.76	0.01	25.27	-0.18	-0.76
M2	944	-0.10	29.01	1.80	0.06	29.01	1.80	-0.10
N1	955	-0.16	50.99	2.49	-0.12	50.99	2.49	-0.16
N2	958	0.02	55.99	2.11	0.11	55.99	2.11	0.02
O1	1101	-0.19	29.22	-1.08	0.00	29.22	-0.19	-1.08
O2	1104	-0.14	33.31	1.44	0.01	33.31	1.44	-0.14

Table 2.10.10-12 Stress Components – Impact and Inertial Loads; 30-Foot Side Drop; $\phi = 90°$; 1.20-Inch Outer Shell Thickness; Circumferential Location = 0° (continued)

Stress Points		Stresses						
Location	Node	S_X	S_Y	S_Z	S_{XY}	S_1	S_2	S_3
P1	1115	-0.21	61.81	2.28	0.01	61.81	2.28	-0.21
P2	1118	0.02	68.23	3.05	-0.01	68.23	3.05	0.02
Q1	1261	-0.18	26.83	-0.54	0.03	26.83	-0.18	-0.54
Q2	1264	-0.07	30.77	2.02	-0.04	30.77	2.02	-0.07
R1	1275	-0.19	50.03	0.64	0.12	50.03	0.64	-0.19
R2	1278	0.03	55.92	3.40	-0.12	55.92	3.40	0.03
S1	1561	-0.17	6.33	1.32	0.19	6.34	1.32	-0.17
S2	1564	-0.13	9.95	2.91	0.03	9.95	2.91	-0.13
T1	1575	-0.24	20.03	0.94	0.26	20.03	0.94	-0.25
T2	1578	0.01	28.31	4.66	-0.11	28.31	4.66	0.01
U1	1841	-0.09	-0.34	2.86	0.01	2.86	-0.09	-0.34
U2	1844	0.52	0.75	1.96	-0.38	1.96	1.03	0.24
V1	1852	10.10	10.65	-0.06	-7.17	17.55	3.20	-0.06
V2	1856	0.69	5.00	-6.41	0.52	5.06	0.63	-6.41
W1	1969	-42.89	-26.04	-16.32	-3.90	-16.32	-25.18	-43.75
W2	1970	-32.16	0.28	-8.46	-4.48	0.89	-8.46	-32.77
W3	1971	-18.52	3.25	-6.83	-4.78	4.25	-6.83	-19.52
W4	1972	-13.78	6.93	-7.57	-3.93	7.66	-7.57	-14.50
W5	1973	-11.51	9.51	-8.43	-3.02	9.93	-8.43	-11.94
W6	1974	-10.24	11.82	-9.20	-2.15	12.03	-9.20	-10.45
W7	1975	-9.59	14.59	-10.02	-1.17	14.64	-9.65	-10.02
W8	1976	-9.43	18.26	-10.75	-0.43	18.27	-9.44	-10.75
X1	2370	-20.82	-8.25	-5.44	-0.92	-5.44	-8.19	-20.89
X2	2390	-8.75	-3.95	-0.74	0.91	-0.74	-3.78	-8.91
X3	2410	-6.38	-1.85	0.14	2.51	0.14	-0.74	-7.49
X4	2430	-3.31	-2.19	0.55	2.27	0.55	-0.41	-5.09
X5	2450	-1.90	-1.64	0.72	1.63	0.72	-0.13	-3.41
X6	2470	-1.04	-1.20	0.75	0.97	0.75	-0.15	-2.09
X7	2490	-0.58	-0.65	0.76	0.51	0.76	-0.10	-1.13
X8	2510	-0.32	-0.41	0.81	0.29	0.81	-0.07	-0.66

Table 2.10.10-12 Stress Components – Impact and Inertial Loads; 30-Foot Side Drop; $\phi = 90°$; 1.20-Inch Outer Shell Thickness; Circumferential Location = 0° (continued)

Stress Points		Stresses						
Location	Node	S_X	S_Y	S_Z	S_{XY}	S_1	S_2	S_3
X9	2530	-0.05	-0.19	0.88	0.16	0.88	0.05	-0.29
X10	2550	0.30	-0.06	0.98	0.05	0.98	0.30	-0.07
X11	2570	0.76	-0.01	1.15	0.06	1.15	0.76	-0.02
Y1	2305	-0.12	0.28	0.92	-0.23	0.92	0.38	-0.22
Y2	2325	-1.93	0.19	0.78	-0.67	0.78	0.38	-2.12
Y3	2345	-3.60	0.26	0.80	-0.77	0.80	0.41	-3.75
Y4	2365	-5.05	0.33	0.86	-0.29	0.86	0.35	-5.06
Y5	2385	-5.42	0.26	1.02	0.49	1.02	0.30	-5.46
Y6	2405	-4.76	0.02	1.21	1.13	1.21	0.28	-5.02
Y7	2425	-3.76	-0.26	1.32	1.42	1.32	0.25	-4.27
Y8	2445	-2.87	-0.44	1.33	1.46	1.33	0.24	-3.55
Y9	2465	-2.24	-0.45	1.33	1.38	1.33	0.30	-2.99
Y10	2485	-1.96	-0.30	1.35	1.21	1.35	0.34	-2.59
Y11	2505	-1.96	-0.25	1.35	1.07	1.35	0.27	-2.47
Y12	2525	-1.82	-0.13	1.40	0.78	1.40	0.18	-2.13
Y13	2545	-1.66	-0.01	1.47	0.43	1.47	0.09	-1.76
Y14	2565	-1.36	0.03	1.56	0.19	1.56	0.05	-1.39
Z1	2301	-1.64	0.12	0.74	-0.01	0.74	0.12	-1.64
Z2	2321	-2.03	0.13	0.98	-0.04	0.98	0.13	-2.03
Z3	2341	-2.54	0.20	1.19	-0.04	1.19	0.20	-2.54
Z4	2361	-2.97	0.27	1.39	0.01	1.39	0.27	-2.97
Z5	2381	-3.18	0.31	1.52	0.07	1.52	0.31	-3.19
Z6	2401	-3.12	0.31	1.57	0.15	1.57	0.31	-3.12
Z7	2421	-2.82	0.27	1.56	0.21	1.56	0.28	-2.83
Z8	2441	-2.39	0.21	1.49	0.25	1.49	0.23	-2.42
Z9	2461	-1.93	0.14	1.42	0.36	1.42	0.21	-1.99
Z10	2481	-1.50	0.10	1.36	0.77	1.36	0.41	-1.81
Z11	2501	-1.32	0.05	1.39	1.88	1.39	1.36	-2.63
Z12	2521	-1.16	0.05	1.43	5.35	4.83	1.43	-5.94
Z13	2541	-1.05	0.04	1.49	23.86	23.35	1.49	-24.37
Z14	2561	-1.03	0.03	1.57	31.16	30.66	1.57	-31.66

Table 2.10.10-13 Stress Components – Thermal; 130°F; 1.20-Inch Outer Shell Thickness

Stress Points		Stresses						
Location	Node	S_X	S_Y	S_Z	S_{XY}	S_1	S_2	S_3
A1	327	5.20	0.07	5.19	0.23	5.21	5.19	0.06
A2	302	4.34	0.07	4.34	-0.02	4.34	4.34	0.07
A3	277	3.48	0.01	3.48	-0.10	3.48	3.48	0.01
A4	252	1.77	-0.04	1.77	-0.02	1.77	1.77	-0.04
A5	227	-1.61	-0.06	-1.61	-0.03	-0.06	-1.61	-1.61
A6	202	-4.97	-0.10	-4.98	-0.01	-0.10	-4.97	-4.98
A7	177	-8.36	-0.11	-8.32	0.00	-0.11	-8.32	-8.36
B1	104	0.17	0.03	0.14	0.07	0.20	0.14	0.00
B2	79	1.14	0.05	1.15	0.06	1.15	1.14	0.04
B3	54	2.17	0.10	2.19	0.04	2.19	2.17	0.10
B4	29	3.26	0.05	3.24	0.07	3.26	3.24	0.05
B5	4	5.03	-0.03	4.97	-0.42	5.06	4.97	-0.06
C1	110	0.36	-0.85	0.58	0.23	0.58	0.40	-0.89
C2	85	1.26	-0.69	1.50	0.24	1.50	1.29	-0.72
C3	60	2.13	-0.36	2.55	0.27	2.55	2.16	-0.39
C4	35	3.23	-0.11	3.75	0.10	3.75	3.24	-0.11
C5	10	5.17	-0.02	5.61	-0.11	5.61	5.17	-0.03
D1	335	-0.14	-8.26	1.45	-0.93	1.45	-0.03	-8.37
D2	310	2.59	-4.75	2.56	-1.01	2.72	2.56	-4.89
D3	285	2.42	-3.05	2.46	-0.90	2.57	2.46	-3.19
D4	260	1.31	-2.12	1.35	-0.84	1.51	1.35	-2.32
D5	235	-0.85	-1.84	-1.25	-0.66	-0.52	-1.25	-2.17
D6	210	-3.33	-1.79	-4.06	-0.02	-1.79	-3.33	-4.06
D7	185	-6.26	-1.74	-7.10	0.91	-1.56	-6.44	-7.10
E1	118	3.74	-2.61	2.21	3.55	5.33	2.21	-4.20
E2	93	0.78	0.82	2.56	1.59	2.56	2.39	-0.79
E3	68	0.98	0.29	2.93	1.17	2.93	1.85	-0.58
E4	43	0.97	0.06	3.46	0.55	3.46	1.23	-0.20
E5	18	2.03	0.02	4.91	0.16	4.91	2.04	0.01
F1	143	-9.75	-8.25	-1.88	6.09	-1.88	-2.87	-15.13
F2	144	-8.47	5.17	1.53	3.40	5.97	1.53	-9.27

Table 2.10.10-13 Stress Components – Thermal; 130°F; 1.20-Inch Outer Shell Thickness (continued)

Stress Points		Stresses						
Location	Node	S_X	S_Y	S_Z	S_{XY}	S_1	S_2	S_3
F3	145	-5.46	3.27	1.42	0.59	3.31	1.42	-5.50
F4	146	-2.43	2.55	1.90	-0.12	2.56	1.90	-2.43
F5	147	-1.22	2.11	2.09	-0.28	2.14	2.09	-1.24
F6	148	-0.61	1.87	2.19	-0.29	2.19	1.91	-0.65
F7	149	-0.27	1.76	2.27	-0.19	2.27	1.78	-0.29
F8	150	-0.11	1.87	2.37	-0.12	2.37	1.88	-0.12
G1	335	-0.14	-8.26	1.45	-0.93	1.45	-0.03	-8.37
G2	336	0.15	-4.60	2.62	0.06	2.62	0.15	-4.60
G3	337	1.39	-1.85	3.73	0.55	3.73	1.48	-1.94
G4	338	2.41	1.34	4.88	-0.02	4.88	2.41	1.34
G5	339	5.62	6.62	7.12	-2.70	8.87	7.12	3.37
G6	340	7.01	1.74	6.29	-3.12	8.46	6.29	0.29
H1	346	-9.21	-3.92	-2.76	0.17	-2.76	-3.92	-9.21
H2	347	-4.67	3.43	0.67	0.34	3.44	0.67	-4.68
H3	348	-2.25	7.59	2.68	-0.20	7.59	2.68	-2.26
H4	349	-0.76	10.01	3.82	-0.34	10.02	3.82	-0.77
H5	350	-0.23	13.48	4.89	-0.29	13.48	4.89	-0.23
I1	621	0.00	2.73	0.33	0.03	2.73	0.33	0.00
I2	624	0.01	1.51	0.14	0.01	1.51	0.14	0.01
J1	635	0.00	10.28	0.27	0.05	10.28	0.27	0.00
J2	638	0.01	8.00	-0.11	0.05	8.00	0.01	-0.11
K1	841	0.00	1.87	-0.21	-0.01	1.87	0.00	-0.21
K2	844	0.00	2.29	0.19	0.01	2.29	0.19	0.00
L1	855	0.00	8.82	-0.36	0.00	8.82	0.00	-0.36
L2	858	0.00	9.35	0.18	0.00	9.35	0.18	0.00
M1	941	0.00	1.81	-0.27	0.00	1.81	0.00	-0.27
M2	944	0.00	2.34	0.25	0.00	2.34	0.25	0.00
N1	955	0.00	8.70	-0.45	0.00	8.70	0.00	-0.45
N2	958	0.00	9.41	0.23	0.00	9.41	0.23	0.00
O1	1101	0.00	1.81	-0.27	0.00	1.81	0.00	-0.27
O2	1104	0.00	2.34	0.25	0.00	2.34	0.25	0.00

Table 2.10.10-13 Stress Components – Thermal; 130°F; 1.20-Inch Outer Shell Thickness (continued)

Stress Points		Stresses						
Location	Node	S_X	S_Y	S_Z	S_{XY}	S_1	S_2	S_3
P1	1115	0.00	8.67	-0.49	0.00	8.67	0.00	-0.49
P2	1118	0.00	9.42	0.24	0.00	9.42	0.24	0.00
Q1	1261	0.00	1.87	-0.18	0.00	1.87	0.00	-0.18
Q2	1264	0.00	2.28	0.22	0.00	2.28	0.22	0.00
R1	1275	0.00	8.71	-0.47	0.00	8.71	0.00	-0.47
R2	1278	-0.01	9.46	0.09	0.00	9.46	0.09	-0.01
S1	1561	0.00	1.74	0.20	0.03	1.74	0.20	0.00
S2	1564	-0.03	2.46	0.51	0.05	2.46	0.51	-0.03
T1	1575	0.00	10.28	0.14	-0.06	10.28	0.14	0.00
T2	1578	0.00	7.98	-0.10	-0.05	7.98	0.00	-0.10
U1	1841	0.02	0.16	-0.68	-0.08	0.20	-0.02	-0.68
U2	1844	0.16	1.04	-0.02	-0.08	1.04	0.15	-0.02
V1	1852	-5.61	-2.18	-2.49	-1.23	-1.79	-2.49	-6.00
V2	1856	-0.29	11.50	3.33	0.18	11.50	3.33	-0.29
W1	1969	-0.74	-1.93	0.01	-0.86	0.01	-0.29	-2.38
W2	1970	0.00	-0.82	0.71	-0.72	0.71	0.42	-1.24
W3	1971	-0.10	-0.13	0.97	-0.59	0.97	0.47	-0.71
W4	1972	-0.08	0.52	1.22	-0.52	1.22	0.82	-0.39
W5	1973	-0.07	0.95	1.39	-0.42	1.39	1.10	-0.22
W6	1974	-0.06	1.30	1.54	-0.29	1.54	1.36	-0.12
W7	1975	-0.03	1.61	1.68	-0.15	1.68	1.62	-0.05
W8	1976	0.01	1.88	1.81	-0.07	1.88	1.81	0.01
X1	2370	-1.24	-0.34	-0.33	0.62	-0.03	-0.33	-1.56
X2	2390	-0.31	-0.98	-0.24	0.45	-0.08	-0.24	-1.21
X3	2410	-0.34	-0.56	-0.07	0.06	-0.07	-0.33	-0.58
X4	2430	-0.33	-0.41	0.01	-0.14	0.01	-0.22	-0.51
X5	2450	-0.39	-0.24	0.07	-0.27	0.07	-0.04	-0.60
X6	2470	-0.40	-0.14	0.14	-0.33	0.14	0.09	-0.63
X7	2490	-0.38	-0.06	0.26	-0.34	0.26	0.16	-0.60
X8	2510	-0.33	-0.03	0.35	-0.32	0.35	0.17	-0.54

Table 2.10.10-13 Stress Components – Thermal; 130°F; 1.20-Inch Outer Shell Thickness (continued)

Stress Points		Stresses						
Location	Node	S_X	S_Y	S_Z	S_{XY}	S_1	S_2	S_3
X9	2530	-0.28	-0.01	0.47	-0.27	0.47	0.15	-0.44
X10	2550	-0.22	0.00	0.62	-0.17	0.62	0.09	-0.31
X11	2570	0.62	0.00	1.59	-0.05	1.59	0.63	-0.01
Y1	2305	0.57	-0.03	0.50	-0.04	0.57	0.50	-0.03
Y2	2325	0.03	-0.05	-0.01	0.05	0.05	-0.01	-0.08
Y3	2345	-0.28	-0.11	-0.33	0.05	-0.10	-0.29	-0.33
Y4	2365	-0.55	-0.17	-0.60	0.05	-0.16	-0.55	-0.60
Y5	2385	-0.73	-0.21	-0.78	0.05	-0.21	-0.73	-0.78
Y6	2405	-0.79	-0.25	-0.87	0.04	-0.25	-0.79	-0.87
Y7	2425	-0.77	-0.28	-0.87	0.00	-0.28	-0.77	-0.87
Y8	2445	-0.71	-0.26	-0.79	-0.05	-0.25	-0.71	-0.79
Y9	2465	-0.60	-0.19	-0.66	-0.08	-0.18	-0.62	-0.66
Y10	2485	-0.42	-0.11	-0.44	-0.09	-0.09	-0.44	-0.44
Y11	2505	-0.28	-0.05	-0.28	-0.04	-0.04	-0.28	-0.29
Y12	2525	-0.10	-0.02	-0.10	-0.01	-0.02	-0.10	-0.10
Y13	2545	0.14	0.00	0.12	-0.01	0.14	0.12	0.00
Y14	2565	1.26	0.00	1.16	0.07	1.27	1.16	0.00
Z1	2301	0.51	0.01	0.50	0.00	0.51	0.50	0.01
Z2	2321	0.09	0.03	0.09	0.00	0.09	0.09	0.03
Z3	2341	-0.23	0.07	-0.23	0.00	0.07	-0.23	-0.23
Z4	2361	-0.50	0.09	-0.50	0.00	0.09	-0.50	-0.50
Z5	2381	-0.68	0.10	-0.68	0.00	0.10	-0.68	-0.68
Z6	2401	-0.78	0.10	-0.78	0.00	0.10	-0.78	-0.78
Z7	2421	-0.79	0.10	-0.79	0.00	0.10	-0.79	-0.79
Z8	2441	-0.72	0.10	-0.72	0.00	0.10	-0.72	-0.72
Z9	2461	-0.57	-0.09	-0.57	0.00	0.09	-0.57	-0.57
Z10	2481	-0.34	0.07	-0.33	0.00	0.07	-0.33	-0.34
Z11	2501	-0.20	0.05	-0.20	0.00	0.05	-0.20	-0.20
Z12	2521	-0.04	0.03	-0.05	0.00	0.03	-0.04	-0.05
Z13	2541	0.11	0.01	0.10	0.00	0.11	0.10	0.01
Z14	2561	1.07	0.01	1.07	0.00	1.07	1.07	0.01

Table 2.10.10-14 Stress Components – 50 psi Internal Pressure and Bolt Preload; 1.20-Inch Outer Shell Thickness

Stress Points		Stresses						
Location	Node	S_X	S_Y	S_Z	S_{XY}	S_1	S_2	S_3
A1	327	-0.10	-0.05	-0.11	0.00	-0.05	-0.10	-0.11
A2	302	-0.09	-0.05	-0.09	0.00	-0.05	-0.09	-0.09
A3	277	-0.07	-0.05	-0.07	0.01	-0.05	-0.07	-0.07
A4	252	-0.04	-0.04	-0.04	0.01	-0.03	-0.04	-0.05
A5	227	0.01	-0.03	0.01	0.01	0.01	0.01	-0.03
A6	202	0.06	-0.01	0.06	0.01	0.06	0.06	-0.01
A7	177	0.12	0.00	0.12	0.00	0.12	0.12	0.00
B1	104	0.01	0.00	0.01	0.00	0.01	0.01	0.00
B2	79	0.00	0.00	0.00	0.00	0.00	0.00	0.00
B3	54	0.00	0.00	0.00	0.00	0.00	0.00	0.00
B4	29	0.00	0.00	0.00	0.00	0.00	0.00	0.00
B5	4	0.00	0.00	0.00	0.00	0.00	0.00	0.00
C1	110	0.01	0.00	0.01	0.00	0.01	0.01	0.00
C2	85	0.00	0.00	0.00	0.00	0.00	0.00	0.00
C3	60	0.00	0.00	0.00	0.00	0.00	0.00	0.00
C4	35	0.00	0.00	0.00	0.00	0.00	0.00	0.00
C5	10	0.00	0.00	0.00	0.00	0.00	0.00	0.00
D1	335	0.25	0.39	0.17	0.11	0.45	0.19	0.17
D2	310	0.06	0.23	0.07	0.08	0.27	0.07	0.02
D3	285	0.02	0.14	0.04	0.06	0.16	0.04	0.00
D4	260	0.00	0.07	0.02	0.04	0.09	0.02	-0.02
D5	235	-0.01	0.03	0.01	0.03	0.04	0.01	-0.02
D6	210	-0.01	0.01	0.02	0.02	0.02	0.02	-0.02
D7	185	-0.03	0.00	0.03	0.01	0.03	0.00	-0.03
E1	118	0.01	0.00	0.01	0.00	0.01	0.01	0.00
E2	93	0.00	0.00	0.00	0.00	0.00	0.00	0.00
E3	68	0.00	0.00	0.00	0.00	0.00	0.00	0.00
E4	43	0.00	0.00	0.00	0.00	0.00	0.00	0.00
E5	18	0.00	0.00	0.00	0.00	0.00	0.00	0.00
F1	143	0.00	-0.01	0.00	0.00	0.00	0.00	-0.01
F2	144	0.00	-0.01	0.00	0.00	0.00	0.00	-0.01

Table 2.10.10-14 Stress Components – 50 psi Internal Pressure and Bolt Preload; 1.20-Inch Outer Shell Thickness (continued)

Stress Points		Stresses						
Location	Node	S_X	S_Y	S_Z	S_{XY}	S_1	S_2	S_3
F3	145	0.00	0.00	0.01	0.01	0.01	0.00	-0.01
F4	146	0.00	0.00	0.01	0.01	0.01	0.01	0.00
F5	147	0.00	0.00	0.01	0.00	0.01	0.01	0.00
F6	148	0.00	0.01	0.01	0.00	0.01	0.01	0.00
F7	149	0.00	0.01	0.01	0.00	0.01	0.01	0.00
F8	150	0.00	0.01	0.01	0.00	0.01	0.01	0.00
G1	335	0.25	0.39	0.17	0.11	0.45	0.19	0.17
G2	336	0.14	0.20	0.09	0.06	0.23	0.11	0.09
G3	337	0.06	0.12	0.04	0.02	0.13	0.06	0.04
G4	338	0.02	0.05	0.01	0.01	0.05	0.02	0.01
G5	339	-0.03	-0.07	-0.03	0.03	-0.01	-0.03	-0.09
G6	340	-0.06	-0.04	-0.03	0.04	-0.01	-0.03	-0.09
H1	346	0.00	0.00	0.00	0.00	0.01	0.00	0.00
H2	347	0.00	0.01	0.00	0.00	0.01	0.00	0.00
H3	348	0.00	0.01	0.00	0.00	0.01	0.00	0.00
H4	349	0.00	0.01	0.00	0.00	0.01	0.00	0.00
H5	350	0.00	0.01	0.00	0.00	0.01	0.00	0.00
I1	621	-0.05	0.10	0.35	-0.01	0.35	0.10	-0.05
I2	624	-0.02	0.18	0.33	0.00	0.33	0.18	-0.02
J1	635	0.00	0.01	0.00	0.00	0.01	0.00	0.00
J2	638	0.00	0.01	0.00	0.00	0.01	0.00	0.00
K1	841	-0.05	0.11	0.36	0.02	0.36	0.11	-0.05
K2	844	-0.01	0.10	0.32	0.03	0.32	0.11	-0.01
L1	855	0.00	0.01	0.00	0.00	0.01	0.00	0.00
L2	858	0.00	0.01	0.00	0.00	0.01	0.00	0.00
M1	941	-0.05	0.11	0.36	0.00	0.36	0.11	-0.05
M2	944	-0.01	0.11	0.32	0.00	0.32	0.11	-0.01
N1	955	0.00	0.01	0.00	0.00	0.01	0.00	0.00
N2	958	0.00	0.01	0.00	0.00	0.01	0.00	0.00
O1	1101	-0.05	0.11	0.36	0.00	0.36	0.11	-0.05
O2	1104	-0.01	0.11	0.32	0.00	0.32	0.11	-0.01

Table 2.10.10-14 Stress Components – 50 psi Internal Pressure and Bolt Preload; 1.20-Inch Outer Shell Thickness (continued)

Stress Points		Stresses						
Location	Node	S_X	S_Y	S_Z	S_{XY}	S_1	S_2	S_3
P1	1115	0.00	0.01	0.00	0.00	0.01	0.00	0.00
P2	1118	0.00	0.01	0.00	0.00	0.01	0.00	0.00
Q1	1261	-0.05	0.11	0.36	0.00	0.36	0.11	-0.05
Q2	1264	-0.01	0.11	0.32	0.00	0.32	0.11	-0.01
R1	1275	0.00	0.01	0.00	0.00	0.01	0.00	0.00
R2	1278	0.00	0.01	0.00	0.00	0.01	0.00	0.00
S1	1561	-0.05	0.11	0.35	0.00	0.35	0.11	-0.05
S2	1564	-0.01	0.14	0.32	0.00	0.32	0.14	-0.01
T1	1575	0.00	0.03	0.00	0.00	0.03	0.00	0.00
T2	1578	0.00	0.00	-0.01	0.00	0.00	0.00	-0.01
U1	1841	-0.06	-0.17	0.22	0.01	0.22	-0.06	-0.17
U2	1844	-0.13	-0.01	0.21	0.10	0.21	0.05	-0.19
V1	1852	0.07	0.01	0.07	0.01	0.07	0.07	0.01
V2	1856	0.00	0.00	0.05	0.01	0.05	0.01	0.00
W1	1969	-0.05	-0.19	0.07	0.18	0.07	0.07	-0.31
W2	1970	0.00	-0.14	0.08	0.02	0.08	0.00	-0.14
W3	1971	0.01	-0.08	0.09	-0.05	0.09	0.03	-0.10
W4	1972	0.00	-0.03	0.10	-0.05	0.10	0.04	-0.07
W5	1973	0.00	0.01	0.10	-0.05	0.10	0.05	-0.05
W6	1974	0.00	0.03	0.11	-0.04	0.11	0.06	-0.03
W7	1975	0.00	0.06	0.11	-0.02	0.11	0.07	-0.01
W8	1976	0.00	0.08	0.11	-0.01	0.11	0.08	0.00
X1	2370	0.01	-0.04	-0.01	0.09	0.08	-0.01	-0.10
X2	2390	-0.05	-0.20	-0.08	0.05	-0.03	-0.08	-0.21
X3	2410	0.06	-0.20	-0.03	-0.04	0.07	-0.03	-0.21
X4	2430	0.03	-0.09	0.00	-0.08	0.07	0.00	-0.12
X5	2450	0.01	-0.04	0.01	-0.07	0.06	0.01	-0.09
X6	2470	0.00	-0.01	0.02	-0.05	0.05	0.02	-0.05
X7	2490	0.01	0.00	0.03	-0.03	0.04	0.03	-0.03
X8	2510	0.02	0.00	0.04	-0.02	0.04	0.03	-0.02

Table 2.10.10-14 Stress Components – 50 psi Internal Pressure and Bolt Preload; 1.20-Inch Outer Shell Thickness (continued)

Stress Points		Stresses						
Location	Node	S_X	S_Y	S_Z	S_{XY}	S_1	S_2	S_3
X9	2530	0.02	0.00	0.04	-0.02	0.04	0.03	-0.01
X10	2550	0.02	0.00	0.05	-0.01	0.05	0.03	0.00
X11	2570	0.03	0.00	0.05	0.00	0.05	0.03	0.00
Y1	2305	-0.05	-0.05	-0.05	0.01	-0.04	-0.05	-0.06
Y2	2325	-0.04	-0.05	-0.04	0.00	-0.04	-0.04	-0.05
Y3	2345	-0.03	-0.05	-0.04	0.00	-0.03	-0.04	-0.05
Y4	2365	-0.03	-0.05	-0.03	-0.01	-0.03	-0.03	-0.05
Y5	2385	-0.03	-0.05	-0.03	-0.01	-0.02	-0.03	-0.05
Y6	2405	-0.02	-0.05	-0.02	-0.01	-0.01	-0.02	-0.05
Y7	2425	0.00	-0.04	-0.01	-0.01	0.00	-0.01	-0.04
Y8	2445	0.01	-0.03	0.01	-0.01	0.02	0.01	-0.04
Y9	2465	0.03	-0.02	0.02	-0.02	0.03	0.02	-0.03
Y10	2485	0.04	-0.01	0.04	-0.01	0.04	0.04	-0.02
Y11	2505	0.04	-0.01	0.05	-0.01	0.05	0.05	-0.01
Y12	2525	0.05	0.00	0.06	-0.01	0.06	0.05	-0.01
Y13	2545	0.06	0.00	0.07	-0.01	0.07	0.06	0.00
Y14	2565	0.07	0.00	0.08	0.00	0.08	0.07	0.00
Z1	2301	-0.05	-0.05	-0.05	0.00	-0.05	-0.05	-0.05
Z2	2321	-0.04	-0.05	-0.04	0.00	-0.04	-0.04	-0.05
Z3	2341	-0.04	-0.04	-0.04	0.00	-0.04	-0.04	-0.04
Z4	2361	-0.03	-0.04	-0.03	0.00	-0.03	-0.03	-0.04
Z5	2381	-0.03	-0.04	-0.03	0.00	-0.03	-0.03	-0.04
Z6	2401	-0.02	-0.03	-0.02	0.00	-0.02	-0.02	-0.03
Z7	2421	0.00	-0.03	0.00	0.00	0.00	0.00	-0.03
Z8	2441	0.01	-0.02	0.01	0.00	0.01	0.01	-0.02
Z9	2461	0.02	-0.01	0.02	0.00	0.02	0.02	-0.01
Z10	2481	0.04	-0.01	0.04	0.00	0.04	0.04	-0.01
Z11	2501	0.05	0.00	0.05	0.00	0.05	0.05	0.00
Z12	2521	0.06	0.00	0.06	0.00	0.06	0.06	0.00
Z13	2541	0.08	0.00	0.08	0.00	0.08	0.08	0.00
Z14	2561	0.09	0.00	0.09	0.00	0.09	0.09	0.00

Table 2.10.10-15 Primary Stresses; 30-Foot Top End Drop; $\phi = 0°$; 1.12-Inch Outer Shell Thickness

Stress Points		Stresses						
Location	Node	S_X	S_Y	S_Z	S_{XY}	S_1	S_2	S_3
A1	327	0.64	-0.04	0.65	0.03	0.65	0.64	-0.04
A2	302	0.57	-0.04	0.58	-0.01	0.58	0.57	-0.04
A3	277	0.50	-0.04	0.51	-0.02	0.51	0.50	-0.04
A4	252	0.38	-0.05	0.38	-0.02	0.38	0.38	-0.05
A5	227	0.14	-0.07	0.14	-0.02	0.14	0.14	-0.07
A6	202	-0.09	-0.08	-0.10	-0.02	-0.07	-0.10	-0.10
A7	177	-0.36	-0.09	-0.37	-0.01	-0.09	-0.36	-0.37
B1	104	0.32	0.01	0.34	0.00	0.34	0.32	0.01
B2	79	0.04	0.01	0.05	-0.04	0.07	0.05	-0.02
B3	54	-0.21	-0.01	-0.21	-0.05	0.00	-0.21	-0.22
B4	29	-0.46	-0.01	-0.48	-0.04	-0.01	-0.47	-0.48
B5	4	-0.61	0.00	-0.63	0.04	0.00	-0.61	-0.63
C1	110	0.03	0.00	0.18	-0.04	0.18	0.06	-0.03
C2	85	-0.08	0.00	-0.02	-0.08	0.05	-0.02	-0.13
C3	60	-0.17	0.00	-0.19	-0.10	0.05	-0.19	-0.22
C4	35	-0.25	0.00	-0.36	-0.06	0.01	-0.26	-0.36
C5	10	-0.31	0.00	-0.46	-0.01	0.00	-0.31	-0.46
D1	335	-0.08	-0.71	0.15	-0.12	0.15	-0.06	-0.73
D2	310	0.16	-0.47	0.24	-0.14	0.24	0.19	-0.50
D3	285	0.19	-0.36	0.24	-0.15	0.24	0.23	-0.40
D4	260	0.21	-0.28	0.21	-0.13	0.25	0.21	-0.31
D5	235	0.17	-0.20	0.12	-0.11	0.20	0.12	-0.23
D6	210	0.10	-0.14	0.01	-0.07	0.12	0.01	-0.16
D7	185	0.05	-0.12	-0.13	-0.03	0.05	-0.12	-0.13
E1	118	-0.44	-0.43	-0.22	-0.17	-0.22	-0.27	-0.60
E2	93	-0.12	-0.26	-0.15	-0.11	-0.06	-0.15	-0.32
E3	68	-0.06	-0.11	-0.16	-0.06	-0.02	-0.15	-0.16
E4	43	0.00	-0.04	-0.21	-0.02	0.01	-0.05	-0.21
E5	18	0.06	-0.01	-0.23	0.00	0.06	-0.01	-0.23
F1	143	0.03	-0.33	-0.08	-0.16	0.09	-0.08	-0.39
F2	144	-0.03	-0.12	-0.03	-0.18	0.11	-0.03	-0.26

Table 2.10.10-15 Primary Stresses; 30-Foot Top End Drop; $\phi = 0°$; 1.12-Inch Outer Shell Thickness (continued)

Stress Points		Stresses						
Location	Node	S_X	S_Y	S_Z	S_{XY}	S_1	S_2	S_3
F3	145	-0.07	-0.10	-0.04	-0.20	0.11	-0.04	-0.28
F4	146	-0.04	-0.09	-0.03	-0.17	0.10	-0.03	-0.23
F5	147	-0.02	-0.08	-0.02	-0.13	0.08	-0.02	-0.19
F6	148	-0.01	-0.07	-0.02	-0.09	0.06	-0.02	-0.14
F7	149	-0.01	-0.06	-0.01	-0.05	0.03	-0.01	-0.09
F8	150	0.00	-0.04	0.00	-0.03	0.01	0.00	-0.05
G1	335	-0.08	-0.71	0.15	-0.12	0.15	-0.06	-0.73
G2	336	-0.09	-0.56	0.18	-0.05	0.18	-0.08	-0.57
G3	337	-0.03	-0.51	0.20	-0.01	0.20	-0.03	-0.51
G4	338	0.00	-0.50	0.20	0.03	0.20	0.00	-0.50
G5	339	0.01	-0.36	0.22	0.08	0.22	0.02	-0.37
G6	340	0.08	-0.10	0.29	0.08	0.29	0.11	-0.13
H1	346	0.10	-0.21	0.23	-0.13	0.23	0.15	-0.26
H2	347	0.00	-0.72	0.05	-0.13	0.05	0.02	-0.74
H3	348	0.03	-0.93	0.00	0.00	0.03	0.00	-0.93
H4	349	0.01	-0.82	0.03	0.05	0.03	0.01	-0.83
H5	350	0.00	-0.77	0.04	0.04	0.04	0.00	-0.77
I1	621	-0.05	-1.12	0.32	0.02	0.32	-0.05	-1.12
I2	624	0.02	-1.40	0.22	0.03	0.22	0.02	-1.40
J1	635	0.00	-1.09	0.05	0.00	0.05	0.00	-1.09
J2	638	0.00	-1.13	0.03	0.00	0.03	0.00	-1.13
K1	841	-0.05	-1.68	0.47	0.03	0.47	-0.05	-1.68
K2	844	0.00	-1.69	0.42	0.02	0.42	0.00	-1.69
L1	855	0.00	-1.55	0.00	0.00	0.00	0.00	-1.55
L2	858	0.00	-1.55	0.00	0.00	0.00	0.00	-1.55
M1	941	-0.05	-2.22	0.47	0.00	0.47	-0.05	-2.22
M2	944	0.00	-2.22	0.42	0.00	0.42	0.00	-2.22
N1	955	0.00	-2.09	0.00	0.00	0.00	0.00	-2.09
N2	958	0.00	-2.09	0.00	0.00	0.00	0.00	-2.09
O1	1101	-0.05	-3.11	0.47	0.00	0.47	-0.05	-3.11
O2	1104	0.00	-3.11	0.42	0.00	0.42	0.00	-3.11

Table 2.10.10-15 Primary Stresses; 30-Foot Top End Drop; $\phi = 0°$; 1.12-Inch Outer Shell Thickness (continued)

Stress Points		Stresses						
Location	Node	S_X	S_Y	S_Z	S_{XY}	S_1	S_2	S_3
P1	1115	0.00	-2.97	0.00	0.00	0.00	0.00	-2.97
P2	1118	0.00	-2.97	0.00	0.00	0.00	0.00	-2.97
Q1	1261	-0.05	-3.99	0.47	0.00	0.47	-0.05	-3.99
Q2	1264	0.00	-3.99	0.42	0.00	0.42	0.00	-3.99
R1	1275	0.00	-3.85	0.00	0.00	0.00	0.00	-3.85
R2	1278	0.00	-3.86	0.00	0.00	0.00	0.00	-3.86
S1	1561	-0.05	-3.64	-0.12	-0.13	-0.04	-0.12	-3.64
S2	1564	0.09	-6.12	-0.72	-0.16	0.09	-0.72	-6.12
T1	1575	0.00	-4.36	0.24	-0.01	0.24	0.00	-4.36
T2	1578	0.00	-5.06	0.04	-0.01	0.04	0.00	-5.06
U1	1841	-0.05	-6.77	2.41	-0.16	2.41	-0.04	-6.78
U2	1844	0.71	-3.39	3.21	-0.07	3.21	0.71	-3.39
V1	1852	-1.00	-5.38	0.75	-0.18	0.75	-0.99	-5.38
V2	1856	0.02	-3.40	1.35	-0.03	1.35	0.02	-3.40
W1	1969	1.88	-1.46	0.39	1.51	2.46	0.39	-2.04
W2	1970	1.30	-3.17	-0.12	0.55	1.36	-0.12	-3.24
W3	1971	0.71	-3.85	-0.36	-0.11	0.71	-0.36	-3.85
W4	1972	0.39	-4.51	-0.56	-0.25	0.40	-0.56	-4.52
W5	1973	0.23	-4.97	-0.69	-0.27	0.24	-0.69	-4.99
W6	1974	0.13	-5.33	-0.78	-0.23	0.14	-0.78	-5.34
W7	1975	0.06	-5.71	-0.87	-0.13	0.07	-0.87	-5.72
W8	1976	0.02	-6.14	-0.97	-0.07	0.02	-0.97	-6.14
X1	2370	4.33	1.35	3.33	2.45	5.71	3.33	-0.02
X2	2390	0.30	-2.59	0.57	2.12	1.42	0.57	-3.71
X3	2410	0.19	-4.58	-0.24	1.04	0.41	-0.24	-4.80
X4	2430	-0.61	-4.28	-0.57	0.94	-0.38	-0.57	-4.50
X5	2450	-0.67	-4.63	-0.74	0.93	-0.47	-0.74	-4.83
X6	2470	-0.57	-4.61	-0.64	0.95	-0.35	-0.64	-4.82
X7	2490	-0.12	-4.73	-0.43	0.89	0.04	-0.43	-4.90
X8	2510	0.14	-4.75	-0.29	0.79	0.26	-0.29	-4.87
X9	2530	0.46	-4.81	-0.17	0.61	0.53	-0.17	-4.88

Table 2.10.10-15 Primary Stresses; 30-Foot Top End Drop; $\phi = 0°$; 1.12-Inch Outer Shell Thickness (continued)

Stress Points		Stresses						
Location	Node	S_X	S_Y	S_Z	S_{XY}	S_1	S_2	S_3
X10	2550	0.81	-4.83	-0.05	0.35	0.84	-0.05	-4.85
X11	2570	1.22	-4.84	0.02	0.20	1.22	0.02	-4.85
Y1	2305	0.76	-1.95	1.17	0.12	1.17	0.77	-1.95
Y2	2325	0.90	-2.10	1.01	0.50	1.01	0.98	-2.19
Y3	2345	1.10	-2.45	1.03	0.58	1.19	1.03	-2.54
Y4	2365	1.10	-2.76	0.94	0.46	1.15	0.94	-2.82
Y5	2385	0.75	-2.97	0.66	0.31	0.77	0.66	-3.00
Y6	2405	0.23	-3.13	0.28	0.29	0.28	0.25	-3.15
Y7	2425	-0.18	-3.32	-0.06	0.40	-0.06	-0.13	-3.38
Y8	2445	-0.40	-3.62	-0.30	0.54	-0.30	-0.31	-3.70
Y9	2465	-0.47	-3.98	-0.43	0.61	-0.37	-0.43	-4.08
Y10	2485	-0.47	-4.32	-0.53	0.57	-0.39	-0.53	-4.40
Y11	2505	-0.50	-4.54	-0.62	0.51	-0.44	-0.62	-4.60
Y12	2525	-0.54	-4.68	-0.72	0.39	-0.50	-0.72	-4.72
Y13	2545	-0.62	-4.78	-0.87	0.22	-0.61	-0.87	-4.80
Y14	2565	-0.77	-4.82	-1.09	0.04	-0.77	-1.09	-4.82
Z1	2301	1.72	-1.93	1.72	0.00	1.72	1.72	-1.93
Z2	2321	1.21	-2.07	1.21	0.00	1.21	1.21	-2.07
Z3	2341	1.00	-2.36	1.00	0.00	1.00	1.00	-2.36
Z4	2361	0.82	-2.66	0.82	0.00	0.82	0.82	-2.66
Z5	2381	0.59	-2.94	0.59	0.00	0.59	0.59	-2.94
Z6	2401	0.31	-3.20	0.31	0.00	0.31	0.31	-3.20
Z7	2421	0.03	-3.46	0.03	0.00	0.03	0.03	-3.46
Z8	2441	-0.22	-3.75	-0.22	0.00	-0.22	-0.22	-3.75
Z9	2461	-0.42	-4.07	-0.42	0.00	-0.42	-0.42	-4.07
Z10	2481	-0.62	-4.35	-0.62	0.00	-0.62	-0.62	-4.35
Z11	2501	-0.78	-4.54	-0.78	0.00	-0.78	-0.78	-4.54
Z12	2521	-0.96	-4.66	-0.96	0.00	-0.96	-0.96	-4.66
Z13	2541	-1.19	-4.76	-1.19	0.00	-1.19	-1.19	-4.76
Z14	2561	-1.49	-4.80	-1.49	0.00	-1.49	-1.49	-4.80

Table 2.10.10-16 Primary Plus Secondary Stresses; 30-Foot Top End Drop; $\phi = 0°$; 1.12-Inch Outer Shell Thickness

Stress Points		Stresses						
Location	Node	S_X	S_Y	S_Z	S_{XY}	S_1	S_2	S_3
A1	327	2.83	-0.01	2.82	0.13	2.84	2.82	-0.01
A2	302	2.43	-0.01	2.43	-0.01	2.43	2.43	-0.01
A3	277	2.04	-0.03	2.04	-0.06	2.04	2.04	-0.03
A4	252	1.26	-0.04	1.27	-0.01	1.27	1.26	-0.04
A5	227	-0.24	-0.06	-0.24	-0.03	-0.05	-0.24	-0.25
A6	202	-1.68	-0.09	-1.68	-0.03	-0.09	-1.68	-1.68
A7	177	-3.11	-0.10	-3.12	0.00	-0.10	-3.11	-3.12
B1	104	-4.55	-0.21	-4.57	-0.25	-0.20	-4.56	-4.57
B2	79	-1.30	-0.14	-1.30	0.16	-0.12	-1.30	-1.32
B3	54	2.04	0.03	2.06	0.16	2.06	2.05	0.02
B4	29	5.50	0.04	5.49	0.18	5.51	5.49	0.04
B5	4	8.51	-0.05	8.41	-0.71	8.57	8.41	-0.11
C1	110	-2.98	-1.71	-3.67	0.33	-1.63	-3.07	-3.67
C2	85	-0.30	-1.44	-0.61	0.94	0.23	-0.61	-1.97
C3	60	1.84	-0.83	2.30	1.20	2.31	2.30	-1.29
C4	35	4.12	-0.27	5.36	0.67	5.36	4.22	-0.37
C5	10	6.86	-0.07	8.31	0.08	8.31	6.86	-0.07
D1	335	-1.76	-6.70	-0.25	-1.20	-0.25	-1.48	-6.98
D2	310	0.59	-4.20	0.79	-1.20	0.87	0.79	-4.49
D3	285	0.75	-2.97	0.96	-1.11	1.05	0.96	-3.28
D4	260	0.61	-2.27	0.69	-1.01	0.93	0.69	-2.59
D5	235	0.03	-2.00	-0.16	-0.85	0.34	-0.16	-2.31
D6	210	-0.71	-1.98	-1.10	-0.50	-0.54	-1.10	-2.15
D7	185	-1.58	-2.00	-2.14	-0.11	-1.55	-2.03	-2.14
E1	118	8.44	9.55	5.26	4.18	13.22	5.26	4.77
E2	93	0.81	5.31	3.04	2.95	6.77	3.04	-0.65
E3	68	0.07	1.54	2.88	1.97	2.90	2.88	-1.30
E4	43	-1.46	0.42	3.42	0.94	3.42	0.81	-1.85
E5	18	-1.68	0.15	4.84	0.35	4.84	0.22	-1.75
F1	143	-7.67	6.79	1.34	2.96	7.37	1.34	-8.26
F2	144	-4.89	5.03	1.29	2.40	5.58	1.29	-5.44

Table 2.10.10-16 Primary Plus Secondary Stresses; 30-Foot Top End Drop; $\phi = 0°$; 1.12-Inch Outer Shell Thickness (continued)

Stress Points		Stresses						
Location	Node	S_X	S_Y	S_Z	S_{XY}	S_1	S_2	S_3
F3	145	-1.64	2.90	1.49	1.57	3.40	1.49	-2.13
F4	146	-0.56	1.59	1.48	0.95	1.95	1.48	-0.92
F5	147	-0.23	0.80	1.42	0.65	1.42	1.11	-0.55
F6	148	-0.11	0.25	1.36	0.44	1.36	0.54	-0.40
F7	149	-0.04	-0.29	1.30	0.23	1.30	0.10	-0.43
F8	150	0.00	-0.83	1.23	0.12	1.23	0.02	-0.85
G1	335	-1.76	-6.70	-0.25	-1.20	-0.25	-1.48	-6.98
G2	336	-1.24	-4.36	0.63	-0.45	0.63	-1.17	-4.43
G3	337	-0.40	-3.09	1.26	0.05	1.26	-0.40	-3.09
G4	338	-0.04	-1.87	1.72	0.13	1.72	-0.03	-1.88
G5	339	0.56	0.61	2.52	-0.54	2.52	1.12	0.04
G6	340	0.66	-0.58	2.19	-0.86	2.19	1.09	-1.02
H1	346	-4.63	-1.72	-0.36	-1.06	-0.36	-1.38	-4.97
H2	347	-2.72	-1.01	0.62	-0.74	0.62	-0.73	-2.99
H3	348	-1.24	1.65	2.03	-0.03	2.03	1.66	-1.24
H4	349	-0.52	4.14	3.03	0.07	4.14	3.03	-0.52
H5	350	-0.18	6.96	3.92	0.05	6.96	3.92	-0.18
I1	621	-0.06	-3.85	-0.07	0.10	-0.05	-0.07	-3.85
I2	624	0.08	-5.60	-0.33	0.12	0.08	-0.33	-5.60
J1	635	-0.01	3.34	0.36	0.03	3.34	0.36	-0.01
J2	638	0.01	1.52	0.09	0.02	1.52	0.09	0.01
K1	841	-0.05	-5.34	0.26	0.02	0.26	-0.05	-5.34
K2	844	0.00	-4.93	0.61	0.03	0.61	0.00	-4.93
L1	855	0.00	1.67	-0.37	0.00	1.67	0.00	-0.37
L2	858	0.00	2.21	0.18	0.00	2.21	0.18	0.00
M1	941	-0.05	-5.94	0.20	0.00	0.20	-0.05	-5.94
M2	944	0.00	-5.41	0.67	0.00	0.67	0.00	-5.41
N1	955	0.00	1.03	-0.45	0.00	1.03	0.00	-0.45
N2	958	0.00	1.73	0.23	0.00	1.73	0.23	0.00
O1	1101	-0.05	-6.82	0.21	0.00	0.21	-0.05	-6.82
O2	1104	0.00	-6.29	0.68	0.00	0.68	0.00	-6.29

Table 2.10.10-16 Primary Plus Secondary Stresses; 30-Foot Top End Drop; $\phi = 0°$; 1.12-Inch Outer Shell Thickness (continued)

Stress Points		Stresses						
Location	Node	S_X	S_Y	S_Z	S_{XY}	S_1	S_2	S_3
P1	1115	0.00	0.11	-0.49	0.00	0.11	0.00	-0.49
P2	1118	0.00	0.86	0.24	0.00	0.86	0.24	0.00
Q1	1261	-0.05	-7.65	0.29	0.00	0.29	-0.05	-7.65
Q2	1264	0.00	-7.24	0.64	0.00	0.64	0.00	-7.24
R1	1275	0.00	-0.73	-0.46	0.00	0.00	-0.46	-0.73
R2	1278	-0.01	0.00	0.09	0.00	0.09	0.00	-0.01
S1	1561	-0.06	-7.10	-0.52	-0.16	-0.05	-0.52	-7.11
S2	1564	0.12	-9.61	-0.92	-0.20	0.13	-0.92	-9.61
T1	1575	-0.01	-0.04	0.42	-0.03	0.42	0.02	-0.06
T2	1578	0.01	-2.33	0.16	-0.03	0.16	0.01	-2.33
U1	1841	-0.11	-6.70	0.01	-0.10	0.01	-0.11	-6.70
U2	1844	-0.07	-5.11	0.73	-0.20	0.73	-0.06	-5.12
V1	1852	-3.44	-6.09	-0.58	-0.03	-0.58	-3.44	-6.09
V2	1856	-0.13	2.31	3.33	-0.04	3.33	2.31	-0.13
W1	1969	1.02	-3.29	0.10	0.75	1.15	0.10	-3.41
W2	1970	0.69	-3.78	0.17	0.02	0.69	0.17	-3.78
W3	1971	0.34	-3.90	0.24	-0.48	0.39	0.24	-3.95
W4	1972	0.16	-4.04	0.31	-0.54	0.31	0.23	-4.11
W5	1973	0.08	-4.14	0.36	-0.49	0.36	0.13	-4.19
W6	1974	0.03	-4.19	0.43	-0.37	0.43	0.07	-4.22
W7	1975	0.01	-4.27	0.50	-0.21	0.50	0.02	-4.28
W8	1976	0.02	-4.39	0.55	-0.11	0.55	0.02	-4.40
X1	2370	3.53	1.78	3.46	3.07	5.84	3.46	-0.53
X2	2390	-0.35	-3.06	0.36	2.67	1.29	0.36	-4.70
X3	2410	-0.15	-5.23	-0.35	1.21	0.12	-0.35	-5.50
X4	2430	-0.98	-4.64	-0.58	0.88	-0.58	-0.79	-4.84
X5	2450	-1.05	-4.91	-0.69	0.70	-0.69	-0.93	-5.03
X6	2470	-0.97	-4.74	-0.52	0.65	-0.52	-0.86	-4.85
X7	2490	-0.49	-4.81	-0.18	0.57	-0.18	-0.42	-4.88
X8	2510	-0.20	-4.77	0.05	0.47	0.05	-0.15	-4.82
X9	2530	0.18	-4.83	0.28	0.35	0.28	0.20	-4.86

Table 2.10.10-16 Primary Plus Secondary Stresses; 30-Foot Top End Drop; $\phi = 0°$; 1.12-Inch Outer Shell Thickness (continued)

Stress Points		Stresses						
Location	Node	S_X	S_Y	S_Z	S_{XY}	S_1	S_2	S_3
X10	2550	0.59	-4.83	0.54	0.19	0.60	0.54	-4.84
X11	2570	1.84	-4.84	1.60	0.15	1.84	1.60	-4.85
Y1	2305	1.30	-1.98	1.65	0.10	1.65	1.30	-1.98
Y2	2325	0.94	-2.16	1.03	0.57	1.04	1.03	-2.26
Y3	2345	0.88	-2.57	0.75	0.64	1.00	0.75	-2.69
Y4	2365	0.64	-2.94	0.41	0.49	0.70	0.41	-3.01
Y5	2385	0.09	-3.18	-0.05	0.33	0.12	-0.05	-3.21
Y6	2405	-0.54	-3.36	-0.55	0.31	-0.51	-0.55	-3.39
Y7	2425	-0.96	-3.56	-0.92	0.39	-0.90	-0.92	-3.62
Y8	2445	-1.12	-3.84	-1.09	0.49	-1.03	-1.09	-3.93
Y9	2465	-1.09	-4.15	-1.10	0.55	-1.00	-1.10	-4.24
Y10	2485	-0.91	-4.41	-0.98	0.50	-0.84	-0.98	-4.48
Y11	2505	-0.80	-4.58	-0.92	0.49	-0.74	-0.92	-4.64
Y12	2525	-0.66	-4.70	-0.85	0.39	-0.62	-0.85	-4.73
Y13	2545	-0.51	-4.78	-0.79	0.22	-0.49	-0.79	-4.80
Y14	2565	0.46	-4.82	0.03	0.11	0.46	0.03	-4.82
Z1	2301	2.24	-1.92	2.24	0.00	2.24	2.24	-1.92
Z2	2321	1.32	-2.04	1.32	0.00	1.32	1.32	-2.04
Z3	2341	0.80	-2.31	0.80	0.00	0.80	0.80	-2.31
Z4	2361	0.36	-2.59	0.36	0.00	0.36	0.36	-2.59
Z5	2381	-0.04	-2.85	-0.04	0.00	-0.04	-0.04	-2.85
Z6	2401	-0.43	-3.10	-0.43	0.00	-0.43	-0.43	-3.10
Z7	2421	-0.75	-3.36	-0.75	0.00	-0.75	-0.75	-3.36
Z8	2441	-0.93	-3.65	-0.93	0.00	-0.93	-0.93	-3.65
Z9	2461	-1.00	-3.98	-1.00	0.00	-1.00	-1.00	-3.98
Z10	2481	-0.98	-4.28	-0.98	0.00	-0.98	-0.98	-4.28
Z11	2501	-1.01	-4.49	-1.01	0.00	-1.01	-1.01	-4.49
Z12	2521	-1.04	-4.63	-1.04	0.00	-1.04	-1.04	-4.63
Z13	2541	-1.12	-4.74	-1.12	0.00	-1.12	-1.12	-4.74
Z14	2561	-0.46	-4.79	-0.46	0.00	-0.46	-0.46	-4.79

Table 2.10.10-17 Primary Membrane (P_m) Stresses; 30-Foot Top End Drop; $\phi = 0°$; 1.12-Inch Outer Shell Thickness

		Stresses* (ksi)							
Section	Node to Node	S_x	S_y	S_z	S_{xy}	S_1	S_2	S_3	SI
A	327 – 177	0.14	-0.07	0.14	-0.01	0.14	0.14	-0.07	0.21
B	104 – 4	-0.14	0.00	-0.14	-0.03	0.01	-0.14	-0.15	0.16
C	110 – 10	-0.14	0.00	-0.14	-0.07	0.03	-0.14	-0.17	0.21
D	335 – 185	0.14	-0.24	0.10	-0.10	0.16	0.10	-0.26	0.42
E	118 – 18	-0.11	-0.18	-0.18	-0.08	-0.06	-0.18	-0.22	0.17
F	143 – 150	-0.03	-0.11	-0.03	-0.14	0.08	-0.03	-0.22	0.30
G	335 – 340	-0.01	-0.42	0.21	0.02	0.21	-0.01	-0.42	0.63
H	346 – 350	0.02	-0.72	0.06	-0.04	0.06	0.03	-0.73	0.79
I	621 – 624	-0.02	-1.25	0.27	0.03	0.27	-0.02	-1.25	1.52
J	635 – 638	0.00	-1.11	0.04	0.00	0.04	0.00	-1.11	1.15
K	841 – 844	-0.02	-1.69	0.44	0.02	0.44	-0.02	-1.69	2.13
L	855 – 858	0.00	-1.55	0.00	0.00	0.00	0.00	-1.55	1.55
M	941 – 944	-0.02	-2.22	0.45	0.00	0.45	-0.02	-2.22	2.67
N	955 – 958	0.00	-2.09	0.00	0.00	0.00	0.00	-2.09	2.09
O	1101 – 1104	-0.02	-3.11	0.45	0.00	0.45	-0.02	-3.11	3.55
P	1115 – 1118	0.00	-2.97	0.00	0.00	0.00	0.00	-2.97	2.97
Q	1261 – 1264	-0.02	-3.99	0.45	0.00	0.45	-0.02	-3.99	4.44
R	1275 – 1278	0.00	-3.85	0.00	0.00	0.00	0.00	-3.85	3.85
S	1561 – 1564	0.01	-4.85	-0.41	-0.18	0.02	-0.41	-4.85	4.88
T	1575 – 1578	0.00	-4.72	0.14	-0.01	0.14	0.00	-4.72	4.85
U	1841 – 1846	0.79	-3.15	3.22	0.85	3.22	0.97	-3.32	6.54
V	1852 – 1856	-0.37	-4.23	1.11	0.05	0.00	-0.37	-4.23	5.34
W	1969 – 1976	0.73	-4.16	-0.40	0.14	0.74	-0.40	-4.17	4.90
X	2370 – 2570	0.16	-4.04	-0.13	1.06	0.41	-0.13	-4.29	4.71
Y	2305 – 2565	0.20	-3.31	0.20	0.43	0.25	0.20	-3.36	3.61
Z	2301 – 2561	0.20	-3.33	0.20	0.00	0.20	0.00	-3.33	3.52

* Stresses are taken at 0 degrees (under the load) at each section.

Table 2.10.10-18 Primary Membrane Plus Primary Bending ($P_m + P_b$) Stresses; 30-Foot Top End Drop; $\phi = 0°$; 1.12-Inch Outer Shell Thickness

		Stresses* (ksi)							
Section	Node to Node	S_x	S_y	S_z	S_{xy}	S_1	S_2	S_3	SI
A	327 – 177	0.63	-0.04	0.63	-0.01	0.63	0.63	-0.04	0.67
B	104 – 4	-0.60	-0.01	-0.62	-0.03	-0.01	-0.60	-0.62	0.61
C	110 – 10	-0.30	0.00	-0.45	-0.06	0.01	-0.31	-0.45	0.46
D	335 – 185	0.19	-0.43	0.29	-0.16	0.29	0.23	-0.46	0.75
E	118 – 18	-0.31	-0.39	-0.16	-0.16	-0.16	-0.19	-0.51	0.35
F	143 – 150	0.03	-0.22	-0.06	-0.14	0.09	-0.06	-0.28	0.38
G	335 – 340	-0.08	-0.68	0.16	0.02	0.16	-0.08	-0.68	0.83
H	346 – 350	0.00	-0.97	-0.02	-0.04	0.00	-0.02	-0.97	0.96
I	621 – 624	0.02	-1.39	0.22	0.03	0.22	0.02	-1.39	1.61
J	635 – 638	0.00	-1.13	0.03	0.00	0.03	0.00	-1.13	1.16
K	841 – 844	-0.05	-1.68	0.47	0.02	0.47	-0.05	-1.68	2.15
L	855 – 858	0.00	-1.55	0.00	0.00	0.00	0.00	-1.55	-1.55
M	941 – 944	-0.05	-2.22	0.47	0.00	0.47	-0.05	-2.22	2.69
N	955 – 958	0.00	-2.09	0.00	0.00	0.00	0.00	-2.09	2.09
O	1101 – 1104	-0.05	-3.11	0.47	0.00	0.47	-0.05	-3.11	3.58
P	1115 – 1118	0.00	-2.97	0.00	0.00	0.00	0.00	-2.97	2.97
Q	1261 – 1264	-0.05	-3.99	0.47	0.00	0.47	-0.05	-3.99	4.46
R	1275 – 1278	0.00	-3.85	0.00	0.00	0.00	0.00	-3.85	3.85
S	1561 – 1564	0.09	-6.05	-0.70	-0.18	0.09	-0.70	-6.06	6.15
T	1575 – 1578	0.00	-5.06	0.04	-0.01	0.04	0.00	-5.06	5.09
U	1841 – 1846	-0.05	-5.53	2.76	0.85	2.76	0.08	-5.66	8.42
V	1852 – 1856	-1.00	-4.81	0.90	0.05	0.90	-1.00	-4.81	5.71
W	1969 – 1976	0.02	-6.20	-1.04	0.14	0.03	-1.04	-6.20	6.23
X	2370 – 2570	-0.23	-5.65	-0.77	0.34	-0.21	-0.77	-5.67	5.46
Y	2305 – 2565	-0.87	-4.81	-1.00	0.44	-0.82	-1.00	-4.86	4.04
Z	2301 – 2561	-1.22	-4.89	-1.22	0.00	-1.22	-1.22	-4.89	3.67

* Stresses are taken at 0 degrees (under the load) at each section.

Table 2.10.10-19 Primary Membrane (P_m) and Primary Membrane Plus Primary Bending ($P_m + P_b$) Stress Qualification; 30-Foot Top End Drop; $\phi = 0°$; 1.12-Inch Outer Shell Thickness

Section	Node to Node	Max. Temp. (°F)	P_m Stresses (ksi)			$P_m + P_b$ Stresses (ksi)		
			Allow. * 0.7 S_u	Calc.	MS	Allow. * 1.0 S_u	Calc.	MS
A	327 – 177	222	48.93	0.21	+Large	69.90	0.67	+Large
B	104 – 4	215	49.18	0.16	+Large	70.25	0.61	+Large
C	110 – 10	212	49.28	0.21	+Large	70.40	0.46	+Large
D	335 – 185	221	48.96	0.42	+Large	69.95	0.75	+Large
E	118 – 18	208	49.42	0.17	+Large	70.60	0.35	+Large
F	143 – 150	209	49.38	0.30	+Large	70.55	0.38	+Large
G	335 – 340	221	48.96	0.63	+Large	69.95	0.83	+Large
H	346 – 350	212	49.28	0.79	+Large	70.40	0.96	+Large
I	621 – 624	222	48.93	1.52	+Large	69.90	1.61	+Large
J	635 – 638	199	49.73	1.15	+Large	71.04	1.16	+Large
K	841 – 844	232	68.49	2.13	+Large	97.84	2.15	+Large
L	855 – 858	204	69.50	1.55	+Large	99.29	1.55	+Large
M	941 – 944	247	67.94	2.67	+Large	97.06	2.69	+Large
N	955 – 958	211	69.25	2.09	+Large	98.93	2.09	+Large
O	1101 – 1104	255	67.65	3.55	+Large	96.64	3.58	+Large
P	1115 – 1118	216	69.07	2.97	+Large	98.67	2.97	+Large
Q	1261 – 1264	251	67.80	4.44	+Large	96.85	4.46	+Large
R	1275 – 1278	216	69.07	3.85	+Large	98.67	3.85	+Large
S	1561 – 1564	217	49.10	4.88	+Large	70.15	6.15	+Large
T	1575 – 1578	197	49.78	4.85	+Large	71.12	5.09	+Large
U	1841 – 1846	212	49.28	6.54	+Large	70.40	8.42	+Large
V	1852 – 1856	205	49.52	5.34	+Large	70.75	5.71	+Large
W	1969 – 1976	198	49.76	4.90	+Large	71.08	6.23	+Large
X	2370 – 2570	201	49.66	4.71	+Large	70.95	5.46	+Large
Y	2305 – 2565	205	49.52	3.61	+Large	70.75	4.04	+Large
Z	2301 – 2561	204	49.56	3.52	+Large	70.80	3.67	+Large

* Allowable stresses for sections "K" through "R" are taken from Type XM-19 stainless steel; all others are from Type 304 stainless steel.

Table 2.10.10-20 Primary Stresses; 30-Foot Top Corner Drop; $\phi = 15.74°$; 1.12-Inch Outer Shell Thickness

Stress Points		Stresses						
Location	Node	S_X	S_Y	S_Z	S_{XY}	S_1	S_2	S_3
A1	327	-0.42	-0.06	1.41	0.07	1.41	-0.04	-0.43
A2	302	-0.64	-0.07	1.25	0.15	1.25	-0.03	-0.68
A3	277	-0.81	-0.04	1.13	0.35	1.13	0.10	-0.94
A4	252	-1.11	-0.07	0.89	0.46	0.89	0.10	-1.29
A5	227	-1.77	-0.78	0.64	0.31	0.64	-0.69	-1.86
A6	202	0.05	-1.23	2.74	-1.23	2.74	0.80	-1.97
A7	177	-13.08	-0.83	-3.81	-0.56	-0.80	-3.81	-13.11
B1	104	-3.24	-1.05	-0.83	-0.56	-0.83	-0.91	-3.37
B2	79	-2.44	-0.82	-0.29	-0.26	-0.29	-0.78	-2.48
B3	54	-2.17	-0.44	0.00	-0.40	0.00	-0.35	-2.26
B4	29	-1.89	-0.11	0.29	-0.28	0.29	-0.06	-1.93
B5	4	-1.52	0.02	0.48	0.06	0.48	0.02	-1.52
C1	110	-3.70	-0.27	-1.52	-0.26	-0.25	-1.52	-3.72
C2	85	-3.16	-0.22	-1.10	0.12	-0.22	-1.10	-3.17
C3	60	-2.65	-0.12	-0.73	0.14	-0.11	-0.73	-2.66
C4	35	-2.13	-0.03	-0.32	0.14	-0.02	-0.32	-2.14
C5	10	-1.85	-0.00	-0.08	0.15	0.01	-0.08	-1.86
D1	335	-0.90	0.38	0.43	-0.17	0.43	0.40	-0.93
D2	310	-1.33	0.06	0.12	-0.17	0.12	0.08	-1.35
D3	285	-1.60	-0.10	-0.09	-0.25	-0.06	-0.09	-1.65
D4	260	-2.04	-0.25	-0.38	-0.36	-0.17	-0.38	-2.11
D5	235	-2.83	-0.38	-0.88	-0.32	-0.33	-0.88	-2.87
D6	210	-3.64	-0.43	-1.43	-0.24	-0.41	-1.43	-3.66
D7	185	-4.44	-0.44	-2.09	0.27	-0.42	-2.09	-4.45
E1	118	-3.11	0.83	-2.09	-0.60	0.92	-2.09	-3.20
E2	93	-3.18	0.28	-2.10	-0.17	0.29	-2.10	-3.19
E3	68	-3.07	0.11	-1.97	0.03	0.11	-1.97	-3.07
E4	43	-3.04	0.03	-1.82	0.09	0.03	-1.82	-3.05
E5	18	-3.12	0.01	-1.74	0.14	0.02	-1.74	-3.13
F1	143	-0.61	3.16	-1.06	-0.82	3.33	-0.78	-1.06
F2	144	-0.72	0.79	-2.32	-0.68	1.05	-0.98	-2.32

Table 2.10.10-20 Primary Stresses; 30-Foot Top Corner Drop; $\phi = 15.74°$; 1.12-Inch Outer Shell Thickness (continued)

Stress Points		Stresses						
Location	Node	S_X	S_Y	S_Z	S_{XY}	S_1	S_2	S_3
F3	145	-1.06	0.15	-2.94	-0.51	0.34	-1.25	-2.94
F4	146	-1.78	-0.28	-3.57	-0.33	-0.21	-1.85	-3.57
F5	147	-2.25	-0.62	-4.06	-0.23	-0.58	-2.28	-4.06
F6	148	-2.54	-0.94	-4.48	-0.16	-0.92	-2.56	-4.48
F7	149	-2.75	-1.34	-4.91	-0.09	-1.34	-2.75	-4.91
F8	150	-2.85	-1.88	-5.38	-0.04	-1.88	-2.85	-5.38
G1	335	-0.90	0.38	0.43	-0.17	0.43	0.40	-0.93
G2	336	-0.83	-0.05	0.12	-0.20	0.12	-0.01	-0.88
G3	337	-0.99	-0.48	-0.20	-0.15	-0.20	-0.44	-1.02
G4	338	-1.34	-0.93	-0.54	0.09	-0.54	-0.91	-1.36
G5	339	-2.21	-1.59	-1.09	0.71	-1.09	-1.12	-2.68
G6	340	-3.05	-0.79	-1.04	0.84	-0.51	-1.04	-3.32
H1	346	-1.61	1.42	-2.58	1.05	1.74	-1.93	-2.58
H2	347	-1.42	4.44	-2.33	0.58	4.50	-1.48	-2.33
H3	348	-2.35	3.03	-3.46	-0.80	3.15	-2.47	-3.46
H4	349	-2.55	-0.61	-4.93	-0.93	-0.23	-2.92	-4.93
H5	350	-2.76	-4.40	-6.40	-0.62	-2.55	-4.60	-6.40
I1	621	-0.12	0.21	1.01	-0.04	1.01	0.21	-0.13
I2	624	-0.02	0.72	0.99	0.04	0.99	0.72	-0.02
J1	635	-0.09	2.27	0.99	-0.13	2.27	0.99	-0.09
J2	638	-0.01	5.39	0.77	0.05	5.39	0.77	-0.01
K1	841	-0.08	6.20	0.52	0.00	6.20	0.52	-0.08
K2	844	-0.01	7.03	0.73	0.03	7.03	0.73	-0.01
L1	855	-0.05	11.85	0.61	-0.04	11.85	0.61	-0.05
L2	858	0.02	12.82	0.69	0.01	12.82	0.69	0.02
M1	941	-0.08	6.43	0.52	0.00	6.43	0.52	-0.08
M2	944	-0.02	7.31	0.74	0.00	7.31	0.74	-0.02
N1	955	-0.05	13.71	0.75	-0.01	13.71	0.75	-0.05
N2	958	0.00	14.88	0.80	0.01	14.88	0.80	0.00
O1	1101	-0.09	2.83	0.28	0.01	2.83	0.28	-0.09
O2	1104	-0.04	3.33	0.48	-0.01	3.33	0.48	-0.04

Table 2.10.10-20 Primary Stresses; 30-Foot Top Corner Drop; $\phi = 15.74°$; 1.12-Inch Outer Shell Thickness (continued)

Stress Points		Stresses						
Location	Node	S_X	S_Y	S_Z	S_{XY}	S_1	S_2	S_3
P1	1115	-0.07	10.79	1.09	0.03	10.79	1.09	-0.07
P2	1118	0.00	11.76	0.86	-0.03	11.76	0.86	0.00
Q1	1261	-0.08	-3.16	0.58	0.02	0.58	-0.08	-3.16
Q2	1264	-0.02	-3.19	0.67	-0.03	0.67	-0.02	-3.19
R1	1275	-0.04	-0.11	1.33	0.06	1.33	0.00	-0.15
R2	1278	0.00	-0.33	0.24	-0.07	0.24	0.01	-0.34
S1	1561	-0.09	-11.56	0.60	-0.40	0.60	-0.07	-11.57
S2	1564	0.33	-22.95	-4.59	-0.60	0.34	-4.59	-22.97
T1	1575	-0.14	-17.85	2.76	0.15	2.76	-0.14	-17.85
T2	1578	0.02	-19.72	1.69	-0.06	1.69	0.02	-19.72
U1	1841	0.23	-20.15	8.35	-0.18	8.35	0.23	-20.15
U2	1844	3.27	-11.67	9.99	-0.59	9.99	3.29	-11.69
V1	1852	6.17	-10.07	7.30	0.15	7.30	6.17	-10.07
V2	1856	0.60	-23.74	0.58	-0.41	0.60	0.58	-23.75
W1	1969	-19.47	-16.62	-8.31	4.08	-8.31	-13.72	-22.37
W2	1970	-14.06	-8.92	-5.38	1.34	-5.38	-8.59	-14.39
W3	1971	-7.43	-10.00	-4.34	-0.60	-4.34	-7.29	-10.13
W4	1972	-5.37	-10.68	-4.26	-0.78	-4.26	-5.25	-10.79
W5	1973	-4.37	-11.06	-4.27	-0.77	-4.27	-4.28	-11.15
W6	1974	-3.83	-11.17	-4.26	-0.63	-3.78	-4.26	-11.22
W7	1975	-3.57	-11.06	-4.26	-0.38	-3.55	-4.26	-11.08
W8	1976	-3.50	-10.56	-4.20	-0.26	-3.49	-4.20	-10.57
X1	2370	-6.70	-8.27	-1.94	1.91	-1.94	-5.42	-9.55
X2	2390	-5.86	-11.62	-2.81	3.08	-2.81	-4.52	-12.96
X3	2410	-5.16	-13.15	-2.80	3.56	-2.80	-3.81	-14.51
X4	2430	-4.08	-14.42	-2.50	3.65	-2.50	-2.93	-15.58
X5	2450	-3.35	-14.91	-2.08	3.57	-2.08	-2.34	-15.93
X6	2470	-2.48	-15.03	-1.61	3.45	-1.59	-1.61	-15.92
X7	2490	-1.30	-14.93	-1.22	3.20	-0.59	-1.22	-15.64
X8	2510	-0.54	-14.80	-1.11	2.76	-0.02	-1.11	-15.32
X9	2530	0.35	-14.70	-1.10	2.14	0.65	-1.10	-15.00

Table 2.10.10-20 Primary Stresses; 30-Foot Top Corner Drop; $\phi = 15.74°$; 1.12-Inch Outer Shell Thickness (continued)

Stress Points		Stresses						
Location	Node	S_X	S_Y	S_Z	S_{XY}	S_1	S_2	S_3
X10	2550	1.45	-14.62	-1.22	1.23	1.54	-1.22	-14.71
X11	2570	2.80	-14.60	-1.49	0.73	2.83	-1.49	-14.63
Y1	2305	-0.42	-5.24	1.76	-0.19	1.76	-0.41	-5.25
Y2	2325	-0.68	-5.42	1.49	-0.43	1.49	-0.64	-5.46
Y3	2345	-1.25	-5.66	1.05	-0.50	1.05	-1.20	-5.72
Y4	2365	-2.15	-5.98	0.49	-0.32	0.49	-2.12	-6.01
Y5	2385	-2.88	-6.57	-0.07	0.16	-0.07	-2.87	-6.58
Y6	2405	-3.10	-7.58	-0.49	0.90	-0.49	-2.93	-7.75
Y7	2425	-2.89	-9.05	-0.70	1.78	-0.70	-2.42	-9.53
Y8	2445	-2.63	-10.87	-0.74	2.79	-0.74	-1.78	-11.73
Y9	2465	-3.00	-12.61	-0.72	3.93	-0.72	-1.60	-14.01
Y10	2485	-5.06	-13.76	-1.09	4.76	-1.09	-2.96	-15.86
Y11	2505	-7.08	-14.33	-1.89	4.58	-1.89	-4.87	-16.55
Y12	2525	-8.39	-14.62	-2.89	3.69	-2.89	-6.68	-16.33
Y13	2545	-9.92	-14.55	-4.51	2.23	-4.51	-9.02	-15.45
Y14	2565	-10.96	-14.54	-7.06	0.92	-7.06	-10.74	-14.76
Z1	2301	-0.64	-2.23	2.51	0.14	2.51	-0.63	-2.24
Z2	2321	-1.26	-1.75	2.27	-0.01	2.27	-1.26	-1.75
Z3	2341	-1.60	-1.89	1.70	-0.12	1.70	-1.55	-1.94
Z4	2361	-1.94	-2.08	1.24	-0.33	1.24	-1.67	-2.35
Z5	2381	-2.11	-2.30	0.82	-0.46	0.82	-1.73	-2.68
Z6	2401	-2.06	-2.57	0.44	-0.53	0.44	-1.73	-2.90
Z7	2421	-1.78	-2.90	0.10	-0.56	0.10	-1.55	-3.14
Z8	2441	-1.31	-3.28	-0.19	-0.56	-0.19	-1.17	-3.43
Z9	2461	-0.68	-3.66	-0.48	-0.06	-0.48	-0.68	-3.66
Z10	2481	0.06	-4.04	-0.74	2.70	1.40	-0.74	-5.38
Z11	2501	0.42	-4.21	-1.03	10.55	8.90	-1.03	-12.70
Z12	2521	0.79	-4.37	-1.38	34.89	33.20	-1.38	-36.77
Z13	2541	0.96	-4.93	-2.08	164.70	162.74	-2.08	-166.71
Z14	2561	1.68	-6.27	-4.55	215.90	213.64	-4.55	-218.23

Table 2.10.10-21 Primary Plus Secondary Stresses; 30-Foot Top Corner Drop; $\phi = 15.74°$; 1.12-Inch Outer Shell Thickness

Stress Points		Stresses						
Location	Node	S_X	S_Y	S_Z	S_{XY}	S_1	S_2	S_3
A1	327	3.42	-0.01	5.22	0.24	5.22	3.44	-0.02
A2	302	2.59	-0.02	4.48	0.14	4.48	2.60	-0.02
A3	277	1.84	-0.02	3.76	0.28	3.76	1.88	-0.06
A4	252	0.32	-0.07	2.34	0.46	2.34	0.63	-0.38
A5	227	-2.67	-0.79	-0.26	0.30	-0.26	-0.74	-2.72
A6	202	-3.13	-1.27	-0.44	-1.24	-0.44	-0.65	-3.75
A7	177	-18.51	-0.87	-9.22	-0.55	-0.86	-9.22	-18.53
B1	104	-7.90	-1.25	-5.54	-0.77	-1.16	-5.54	-7.99
B2	79	-3.37	-0.95	-1.22	-0.05	-0.95	-1.22	-3.37
B3	54	0.72	-0.37	2.93	-0.18	2.93	0.75	-0.40
B4	29	4.97	-0.04	7.15	-0.05	7.15	4.97	-0.04
B5	4	8.98	-0.04	10.88	-0.81	10.88	9.06	-0.11
C1	110	-6.50	-2.21	-5.07	0.17	-2.21	-5.07	-6.51
C2	85	-2.96	-1.85	-1.17	1.19	-1.09	-1.17	-3.72
C3	60	0.00	-1.04	2.53	1.49	2.53	1.06	-2.09
C4	35	3.18	-0.32	6.46	0.88	6.43	3.39	-0.53
C5	10	6.81	-0.08	10.28	0.20	10.28	6.82	-0.08
D1	335	-2.58	-8.16	0.52	-1.53	0.52	-2.19	-8.55
D2	310	-0.06	-5.12	1.49	-1.53	1.49	0.36	-5.55
D3	285	-0.26	-3.64	1.42	-1.48	1.42	0.29	-4.19
D4	260	-1.22	-2.88	0.53	-1.49	0.53	-0.34	-3.76
D5	235	-3.25	-2.73	-1.56	-1.26	-1.56	-1.70	-4.27
D6	210	-5.53	-2.80	-3.84	-0.66	-2.65	-3.84	-5.68
D7	185	-8.08	-2.83	-6.38	0.49	-2.79	-6.38	-8.13
E1	118	6.73	9.65	3.96	4.79	13.20	3.96	3.18
E2	93	-2.02	5.95	1.84	3.32	7.15	1.84	-3.22
E3	68	-2.62	1.81	1.95	2.38	2.85	1.95	-3.66
E4	43	-4.14	0.50	2.85	1.21	2.85	0.79	-4.43
E5	18	-4.14	0.18	4.80	0.53	4.80	0.24	-4.20
F1	143	-11.30	7.34	-0.30	4.21	8.25	-0.30	-12.21
F2	144	-8.23	7.49	-0.54	2.95	8.03	-0.54	-8.76

Table 2.10.10-21 Primary Plus Secondary Stresses: 30-Foot Top Corner Drop; φ = 15.74°; 1.12-Inch Outer Shell Thickness (continued)

Stress Points		Stresses						
Location	Node	S_X	S_Y	S_Z	S_{XY}	S_1	S_2	S_3
F3	145	-4.38	4.14	-0.98	1.40	4.36	-0.98	-4.61
F4	146	-3.09	2.20	-1.48	0.72	2.29	-1.48	-3.18
F5	147	-2.86	0.93	-1.98	0.43	0.98	-1.98	-2.91
F6	148	-2.84	-0.01	-2.42	0.26	0.01	-2.42	-2.87
F7	149	-2.86	-0.98	-2.89	0.12	-0.98	-2.87	-2.89
F8	150	-2.89	-2.03	-3.40	0.07	-2.02	-2.89	-3.40
G1	335	-2.58	-8.16	0.52	-1.53	0.52	-2.19	-8.55
G2	336	-1.89	-5.26	1.42	-0.57	1.42	-1.80	-5.35
G3	337	-0.89	-3.59	2.06	0.09	2.06	-0.88	-3.59
G4	338	-0.58	-1.82	2.55	0.18	2.55	-0.56	-1.85
G5	339	0.17	1.53	3.49	-0.78	3.49	1.89	-0.18
G6	340	-0.17	-0.68	2.89	-1.10	2.89	0.71	-1.56
H1	346	-9.23	-1.35	-4.06	0.20	-1.34	-4.06	-9.24
H2	347	-5.60	5.29	-1.56	0.10	5.29	-1.56	-5.60
H3	348	-4.33	8.04	-0.61	-0.90	8.11	-0.61	-4.39
H4	349	-3.31	7.51	-0.76	-1.02	7.60	-0.76	-3.40
H5	350	-3.01	7.55	-1.02	-0.70	7.60	-1.02	-3.06
I1	621	-0.13	-1.54	0.74	0.05	0.74	-0.13	-1.54
I2	624	0.04	-2.86	0.50	0.14	0.50	0.05	-2.86
J1	635	-0.10	9.96	1.38	-0.08	9.96	1.38	-0.10
J2	638	0.00	10.60	0.79	0.08	10.60	0.79	0.00
K1	841	-0.08	8.51	0.42	0.00	8.51	0.42	-0.08
K2	844	0.00	9.75	1.02	0.04	9.75	1.02	0.00
L1	855	-0.05	21.09	0.25	-0.04	21.09	0.25	-0.05
L2	858	0.02	22.60	0.87	0.01	22.60	0.87	0.02
M1	941	-0.08	8.68	0.36	0.00	8.68	0.36	-0.08
M2	944	-0.01	10.09	1.08	-0.01	10.09	1.08	-0.01
N1	955	-0.06	22.85	0.30	-0.01	22.85	0.30	-0.06
N2	958	0.00	24.72	1.03	0.01	24.72	1.03	0.00
O1	1101	-0.09	5.08	0.12	0.01	5.08	0.12	-0.09
O2	1104	-0.03	6.11	0.83	-0.01	6.11	0.83	-0.03

Table 2.10.10-21 Primary Plus Secondary Stresses; 30-Foot Top Corner Drop; $\phi = 15.74°$; 1.12-Inch Outer Shell Thickness (continued)

Stress Points		Stresses						
Location	Node	S_X	S_Y	S_Z	S_{XY}	S_1	S_2	S_3
P1	1115	-0.07	19.90	0.61	0.03	19.90	0.61	-0.07
P2	1118	0.00	21.62	1.10	-0.03	21.62	1.10	0.00
Q1	1261	-0.08	-0.85	0.50	0.02	0.50	-0.08	-0.85
Q2	1264	-0.01	-0.47	0.99	-0.04	0.99	0.00	-0.47
R1	1275	-0.04	9.04	0.87	0.06	9.04	0.87	-0.04
R2	1278	-0.02	9.55	0.34	-0.07	9.56	0.34	-0.02
S1	1561	-0.09	-9.44	0.96	-0.36	0.96	-0.07	-9.46
S2	1564	0.31	-20.02	-3.92	-0.54	0.32	-3.92	-20.03
T1	1575	-0.14	-7.19	2.84	0.09	2.84	-0.14	-7.19
T2	1578	0.03	-11.27	1.57	-0.12	1.57	0.03	-11.27
U1	1841	0.24	-19.96	7.82	-0.27	7.82	0.25	-19.96
U2	1844	3.47	-10.45	10.15	-0.66	10.15	3.50	-10.48
V1	1852	0.48	-12.25	4.85	-1.04	4.85	0.56	-12.33
V2	1856	0.28	-11.67	4.13	-0.25	4.13	0.29	-11.68
W1	1969	-20.24	-18.47	-8.30	3.27	-8.30	-15.97	-22.74
W2	1970	-14.08	-9.68	-4.67	0.66	-4.67	-9.58	-14.18
W3	1971	-7.53	-10.09	-3.38	-1.16	-3.38	-7.09	-10.54
W4	1972	-5.45	-10.14	-3.05	-1.26	-3.05	-5.13	-10.46
W5	1973	-4.44	-10.11	-2.89	-1.15	-2.89	-4.22	-10.33
W6	1974	-3.89	-9.90	-2.74	-0.89	-2.74	-3.76	-10.03
W7	1975	-3.60	-9.50	-2.60	-0.52	-2.60	-3.56	-9.55
W8	1976	-3.49	-8.75	-2.42	-0.33	-2.42	-3.47	-8.77
X1	2370	-7.94	-8.60	-2.27	2.51	-2.27	-5.74	-10.80
X2	2390	-6.18	-12.56	-3.05	3.52	-3.05	-4.62	-14.12
X3	2410	-5.53	-13.69	-2.88	3.62	-2.88	-4.15	-15.07
X4	2430	-4.43	-14.82	-2.50	3.51	-2.50	-3.35	-15.90
X5	2450	-3.75	-15.15	-2.02	3.31	-2.02	-2.86	-16.04
X6	2470	-2.89	-15.16	-1.48	3.13	-1.48	-2.14	-15.91
X7	2490	-1.68	-14.99	-0.97	2.86	-0.97	-1.09	-15.58
X8	2510	-0.87	-14.83	-0.77	2.45	-0.46	-0.77	-15.25
X9	2530	0.07	-14.71	-0.64	1.88	0.30	-0.64	-14.95

Table 2.10.10-21 Primary Plus Secondary Stresses; 30-Foot Top Corner Drop; $\phi = 15.74°$; 1.12-Inch Outer Shell Thickness (continued)

Stress Points		Stresses						
Location	Node	S_X	S_Y	S_Z	S_{XY}	S_1	S_2	S_3
X10	2550	1.23	-14.63	-0.61	1.06	1.30	-0.61	-14.70
X11	2570	3.42	-14.60	0.09	0.68	3.45	0.09	-14.63
Y1	2305	0.15	-5.27	2.25	-0.22	2.25	0.16	-5.28
Y2	2325	-0.66	-5.47	1.48	-0.37	1.48	-0.63	-5.50
Y3	2345	-1.53	-5.77	0.72	-0.45	0.72	-1.49	-5.82
Y4	2365	-2.70	-6.15	-0.11	-0.28	-0.11	-2.68	-6.17
Y5	2385	-3.61	-6.78	-0.86	0.21	-0.86	-3.60	-6.79
Y6	2405	-3.90	-7.83	-1.36	0.94	-1.36	-3.69	-8.04
Y7	2425	-3.67	-9.32	-1.57	1.78	-1.57	-3.16	-9.84
Y8	2445	-3.35	-11.12	-1.54	2.75	-1.54	-2.48	-11.99
Y9	2465	-3.61	-12.80	-1.39	3.85	-1.39	-2.21	-14.20
Y10	2485	-5.49	-13.87	-1.53	4.67	-1.53	-3.40	-15.96
Y11	2505	-7.38	-14.38	-2.17	4.54	-2.17	-5.14	-16.61
Y12	2525	-8.50	-14.64	-2.99	3.68	-2.99	-6.78	-16.36
Y13	2545	-9.79	-14.55	-4.41	2.22	-4.41	-8.91	-15.43
Y14	2565	-9.71	-14.54	-5.90	0.98	-5.90	-9.52	-14.73
Z1	2301	-0.13	-2.21	3.00	0.14	3.00	-0.12	-2.22
Z2	2321	-1.17	-1.71	2.35	-0.01	2.35	-1.17	-1.71
Z3	2341	-1.84	-1.83	1.47	-0.12	1.47	-1.71	-1.95
Z4	2361	-2.44	-1.99	0.73	-0.33	0.73	-1.82	-2.62
Z5	2381	-2.79	-2.20	0.14	-0.46	0.14	-1.95	-3.04
Z6	2401	-2.84	-2.47	-0.34	-0.53	-0.34	-2.10	-3.21
Z7	2421	-2.58	-2.80	-0.69	-0.56	-0.69	-2.12	-3.26
Z8	2441	-2.04	-3.18	-0.92	-0.56	-0.92	-1.81	-3.41
Z9	2461	-1.26	-3.57	-1.05	-0.06	-1.05	-1.26	-3.57
Z10	2481	-0.29	-3.97	-1.08	2.70	1.14	-1.08	-5.40
Z11	2501	0.21	-4.16	-1.23	10.55	8.80	-1.23	-12.75
Z12	2521	0.74	-4.34	-1.43	34.89	33.18	-1.43	-36.78
Z13	2541	1.06	-4.92	-1.98	164.70	162.80	-1.98	-166.66
Z14	2561	2.74	-6.25	-3.49	215.90	214.19	-3.49	-217.70

Table 2.10.10-22 Primary Membrane (Pm) Stresses; 30-Foot Top Corner Drop; $\phi = 15.74°$; 1.12-Inch Outer Shell Thickness

		Stresses* (ksi)							
Section	Node to Node	S_x	S_y	S_z	S_{xy}	S_1	S_2	S_3	SI
A	177 – 327	-2.41	-0.63	0.76	-0.16	0.76	-0.62	-2.42	3.18
B	4 – 104	-2.29	-0.53	-0.10	-0.32	-0.10	-0.47	-2.34	2.25
C	10 – 110	-2.77	-0.14	-0.81	0.08	-0.14	-0.81	-2.77	2.64
D	185 – 335	-2.81	-0.30	-0.89	-0.22	-0.28	-0.89	-2.83	2.56
E	18 – 118	-3.11	0.23	-1.97	-0.10	0.24	-1.97	-3.11	3.35
F	143 – 150	-1.59	0.02	-3.28	-0.40	0.11	-1.68	-3.28	3.39
G	335 – 340	-1.68	-0.85	-0.56	0.30	-0.56	-0.75	-1.78	1.22
H	346 – 350	-2.09	1.37	-3.72	-0.20	1.39	-2.10	-3.72	5.11
I	621 – 624	-0.07	0.46	0.99	0.01	0.99	0.46	-0.07	1.07
J	635 – 638	-0.05	3.86	0.87	-0.04	3.86	0.87	-0.05	3.90
K	841 – 844	-0.04	6.62	0.63	0.02	6.62	0.63	-0.04	6.67
L	855 – 858	-0.01	12.34	0.65	-0.01	12.34	0.65	-0.01	12.36
M	941 – 944	-0.05	6.88	0.63	0.00	6.88	0.63	-0.05	6.93
N	955 – 958	-0.02	14.31	0.77	0.00	14.31	0.77	-0.02	14.33
O	1101 – 1104	-0.06	3.09	0.38	0.00	3.09	0.38	-0.06	3.15
P	1115 – 1118	-0.03	11.28	0.97	0.00	11.28	0.97	-0.03	11.31
Q	1261 – 1264	-0.05	-3.17	0.63	-0.01	0.63	-0.05	-3.17	3.80
R	1275 – 1278	-0.02	-0.22	0.77	-0.01	0.77	-0.02	-0.22	0.99
S	1561 – 1564	0.12	-17.16	-2.01	-0.63	0.14	-2.01	-17.18	17.32
T	1575 – 1578	-0.05	-18.80	2.21	0.06	2.21	-0.05	-18.80	21.01
U	1841 – 1846	4.10	-9.86	10.67	0.76	10.67	4.14	-9.90	20.57
V	1822 – 1856	2.83	-17.30	3.49	0.29	3.49	2.84	-17.31	20.79
W	1969 – 1976	-8.82	-11.00	-5.01	0.27	-5.01	-8.78	-11.03	6.02
X	2370 – 2570	-2.99	-13.78	-1.98	2.99	-1.98	-2.22	-14.56	12.58
Y	2305 – 2565	-3.39	-9.19	-0.50	1.53	-0.50	-3.02	-9.57	9.07
Z	2301 – 2561	-1.04	-2.97	0.34	14.17	12.20	0.34	-16.21	28.42

* Stresses are taken at 0 degrees (under the load) at each section.

Table 2.10.10-23 Primary Membrane Plus Primary Bending ($P_m + P_b$) Stresses; 30-Foot Top Corner Drop; $\phi = 15.74°$; 1.12-Inch Outer Shell Thickness

		Stresses* (ksi)							
Section	Node to Node	S_x	S_y	S_z	S_{xy}	S_1	S_2	S_3	SI
A	177 – 327	-4.96	-1.25	0.80	-1.00	0.80	-1.00	-5.21	6.01
B	4 – 104	-3.88	-1.12	-1.63	-0.46	-1.05	-1.63	-3.96	2.91
C	10 – 110	-4.00	-0.29	-2.11	-0.05	-0.29	-2.11	-4.00	3.71
D	185 – 335	-4.37	-0.93	-1.67	-0.16	-0.92	-1.67	-4.38	3.46
E	18 – 118	-3.16	0.60	-2.16	-0.43	0.65	-2.16	-3.21	3.86
F	143 – 150	-0.61	2.16	-1.24	-0.40	2.21	-0.67	-1.24	3.46
G	335 – 340	-3.20	-2.08	-1.48	0.30	-1.48	-2.00	-3.28	1.80
H	346 – 350	-1.70	4.56	-1.74	-0.20	4.56	-1.71	-1.74	6.30
I	621 – 624	-0.02	0.71	0.98	0.01	0.98	0.71	-0.02	1.00
J	635 – 638	-0.01	5.39	0.76	-0.04	5.39	0.76	-0.01	5.40
K	841 – 844	-0.01	7.03	0.73	0.02	7.03	0.73	-0.01	7.04
L	855 – 858	0.02	12.82	0.69	-0.01	12.82	0.69	0.02	12.80
M	941 – 944	-0.01	7.31	0.74	0.00	7.31	0.74	-0.01	7.32
N	955 – 958	0.00	14.88	0.80	0.00	14.88	0.80	0.00	14.88
O	1101 – 1104	-0.04	3.33	0.48	0.00	3.33	0.48	-0.04	3.37
P	1115 – 1118	0.00	11.76	0.86	0.00	11.76	0.86	0.00	11.76
Q	1261 – 1264	-0.02	-3.19	0.68	-0.01	0.68	-0.02	-3.19	3.86
R	1275 – 1278	-0.04	-0.11	1.31	-0.01	1.31	-0.04	-0.11	1.43
S	1561 – 1564	0.33	-22.71	-4.58	-0.63	0.35	-4.58	-22.72	-23.07
T	1575 – 1578	0.02	-19.71	1.68	0.06	1.68	0.02	-19.71	21.39
U	1841 – 1846	0.23	-18.32	8.31	0.76	8.31	0.26	-18.35	26.66
V	1822 – 1856	0.59	-24.92	-0.15	0.29	0.60	-0.15	-24.93	25.53
W	1969 – 1976	-19.47	-11.87	-6.68	0.27	-6.68	-11.86	-19.48	12.80
X	2370 – 2570	1.23	-16.09	-1.01	2.42	1.56	-1.01	-16.42	17.98
Y	2305 – 2565	-7.29	-15.03	-3.15	4.26	-3.15	-5.40	-16.91	13.77
Z	2301 – 2561	0.12	-4.66	-2.02	53.49	51.27	-2.02	-55.81	107.10

* Stresses are taken at 0 degrees (under the load) at each section.

Table 2.10.10-24 Primary Membrane (P_m) and Primary Membrane Plus Primary Bending ($P_m + P_b$) Stresses; 30-Foot Top Corner Drop; $\phi = 15.74°$; 1.12-Inch Outer Shell Thickness

Section	Node to Node	Max. Temp. (°F)	P_m Stresses (ksi)			$P_m + P_b$ Stresses (ksi)		
			Allow. * 0.7 S_u	Calc.	MS	Allow. * 1.0 S_u	Calc.	MS
A	327 – 177	222	48.93	3.18	+Large	69.90	6.01	+Large
B	104 – 4	215	49.18	2.25	+Large	70.25	2.91	+Large
C	110 – 10	212	49.28	2.64	+Large	70.40	3.71	+Large
D	335 – 185	221	48.96	2.56	+Large	69.95	3.46	+Large
E	118 – 18	208	49.42	3.35	+Large	70.60	3.86	+Large
F	143 – 150	209	49.38	3.39	+Large	70.55	3.46	+Large
G	335 – 340	221	48.96	1.22	+Large	69.95	1.80	+Large
H	346 – 350	212	49.28	5.11	+Large	70.40	6.30	+Large
I	621 – 624	222	48.93	1.07	+Large	69.90	1.00	+Large
J	635 – 638	199	49.73	3.90	+Large	71.04	5.40	+Large
K	841 – 844	232	68.49	6.67	+Large	97.84	7.04	+Large
L	855 – 858	204	69.50	12.36	+Large	99.29	12.80	+Large
M	941 – 944	247	67.94	6.93	+Large	97.06	7.32	+Large
N	955 – 958	211	69.25	14.33	+3.83	98.93	14.88	+Large
O	1101 – 1104	255	67.65	3.15	+Large	96.64	3.37	+Large
P	1115 – 1118	216	69.07	11.31	+Large	98.67	11.76	+Large
Q	1261 – 1264	251	67.80	3.80	+Large	96.85	3.86	+Large
R	1275 – 1278	216	69.07	0.99	+Large	98.67	1.43	+Large
S	1561 – 1564	217	49.10	17.32	+1.83	70.15	23.07	+2.04
T	1575 – 1578	197	49.78	21.01	+1.37	71.12	21.39	+2.32
U	1841 – 1846	212	49.28	20.57	+1.40	70.40	26.66	+1.64
V	1852 – 1856	205	49.52	20.79	+1.38	70.75	25.53	+1.77
W	1969 – 1976	198	49.76	6.02	+Large	71.08	12.80	+Large
X	2370 – 2570	201	49.66	12.58	+2.95	70.95	17.98	+2.95
Y	2305 – 2565	205	49.52	9.07	+Large	70.75	13.77	+Large
Z	2301 – 2561	204	49.56	28.42	+0.74	70.80	107.10**	**

* Allowable stresses for sections "K" through "R" are taken from Type XM-19 stainless steel; all others are from Type 304 stainless steel.

** This stress is induced by the boundary effect from the displacement restraints at node 2561 and, therefore, is disregarded.

Table 2.10.10-25 Primary Stresses; 30-Foot Top Oblique Drop; $\phi = 60°$; 1.12-Inch Outer Shell Thickness

Stress Points		Stresses						
Location	Node	S_X	S_Y	S_Z	S_{XY}	S_1	S_2	S_3
A1	327	-2.20	-0.06	2.06	0.11	2.06	-0.06	-2.20
A2	302	-2.59	-0.08	1.82	0.38	1.82	-0.03	-2.65
A3	277	-2.85	-0.01	1.67	0.87	1.67	0.24	-3.09
A4	252	-3.34	-0.06	1.37	1.12	1.37	0.28	-3.68
A5	227	-4.43	-1.70	1.24	0.78	1.24	-1.49	-4.63
A6	202	0.29	-2.73	6.63	-2.85	6.63	2.01	-4.44
A7	177	-30.04	-1.78	-8.24	-1.29	-1.72	-8.24	-30.10
B1	104	-8.21	-2.48	-2.59	-1.31	-2.19	-2.59	-8.50
B2	79	-5.81	-1.94	-0.78	-0.53	-0.78	-1.87	-5.89
B3	54	-4.70	-1.01	0.41	-0.84	0.41	-0.83	-4.89
B4	29	-3.55	-0.23	1.60	-0.59	1.60	-0.13	-3.65
B5	4	-2.40	0.05	2.32	0.06	2.32	0.05	-2.40
C1	110	-8.75	-0.64	-3.92	-0.53	-0.60	-3.92	-8.78
C2	85	-7.28	-0.53	-2.53	0.44	-0.50	-2.53	-7.30
C3	60	-5.90	-0.28	-1.34	0.51	-0.23	-1.34	-5.95
C4	35	-4.52	-0.06	-0.07	0.44	-0.02	-0.07	-4.56
C5	10	-3.76	-0.01	0.70	0.37	0.70	0.03	-3.79
D1	335	-1.97	2.24	0.71	-0.18	2.25	0.71	-1.97
D2	310	-3.44	1.04	-0.18	-0.13	1.05	-0.18	-3.44
D3	285	-4.13	0.45	-0.66	-0.30	0.47	-0.66	-4.15
D4	260	-5.19	-0.04	-1.29	-0.61	0.03	-1.29	-5.26
D5	235	-6.97	-0.50	-2.29	-0.55	-0.45	-2.29	-7.02
D6	210	-8.74	-0.73	-3.37	-0.43	-0.71	-3.37	-8.77
D7	185	-10.51	-0.80	-4.66	0.69	-0.75	-4.66	-10.56
E1	118	-6.47	2.78	-4.48	-1.08	2.90	-4.48	-6.60
E2	93	-7.24	1.15	-4.64	-0.20	1.16	-4.64	-7.24
E3	68	-7.11	0.47	-4.32	0.18	0.48	-4.32	-7.11
E4	43	-7.15	0.14	-3.87	0.26	0.15	-3.87	-7.15
E5	18	-7.44	0.05	-3.65	0.32	0.06	-3.65	-7.45
F1	143	-1.49	8.05	-2.34	-1.62	8.32	-1.76	-2.34
F2	144	-1.63	2.09	-5.40	-1.25	2.47	-2.01	-5.40

Table 2.10.10-25 Primary Stresses; 30-Foot Top Oblique Drop; $\phi = 60°$; 1.12-Inch Outer Shell Thickness (continued)

Stress Points		Stresses						
Location	Node	S_X	S_Y	S_Z	S_{XY}	S_1	S_2	S_3
F3	145	-2.35	0.54	-6.82	-0.83	0.76	-2.57	-6.82
F4	146	-4.11	-0.48	-8.33	-0.44	-0.43	-4.16	-8.33
F5	147	-5.25	-1.29	-9.50	-0.30	-1.27	-5.27	-9.50
F6	148	-5.95	-2.06	-10.49	-0.20	-2.05	-5.96	-10.49
F7	149	-6.43	-3.04	-11.51	-0.12	-3.03	-6.43	-11.51
F8	150	-6.70	-4.34	-12.63	-0.04	-4.34	-6.70	-12.63
G1	335	-1.97	2.24	0.71	-0.18	2.25	0.71	-1.97
G2	336	-1.78	0.94	-0.07	-0.38	0.99	-0.07	-1.83
G3	337	-2.26	-0.15	-0.84	-0.32	-0.10	-0.84	-2.31
G4	338	-3.15	-1.24	-1.65	0.16	-1.23	-1.65	-3.16
G5	339	-5.22	-3.05	-2.97	1.53	-2.27	-2.97	-6.01
G6	340	-7.31	-1.66	-2.98	1.81	-1.13	-2.98	-7.84
H1	346	-3.96	3.73	-6.50	2.70	4.58	-4.82	-6.50
H2	347	-3.33	11.81	-5.57	1.61	11.98	-3.50	-5.57
H3	348	-5.58	8.90	-8.13	-1.88	9.14	-5.83	-8.13
H4	349	-6.00	0.14	-11.64	-2.28	0.89	-6.76	-11.64
H5	350	-6.49	-8.86	-15.10	-1.53	-5.74	-9.60	-15.10
I1	621	-0.20	2.62	1.76	-0.13	2.63	1.76	-0.20
I2	624	-0.08	4.36	1.90	0.04	4.36	1.90	-0.08
J1	635	-0.20	7.40	2.23	-0.29	7.41	2.23	-0.21
J2	638	-0.02	14.82	1.74	0.11	14.82	1.74	-0.02
K1	841	-0.17	15.88	0.19	-0.05	15.88	0.19	-0.17
K2	844	-0.04	18.40	1.73	0.09	18.40	1.73	-0.04
L1	855	-0.12	31.03	1.46	-0.14	31.03	1.46	-0.12
L2	858	0.04	34.03	1.59	0.08	34.03	1.59	0.04
M1	941	-0.17	21.52	0.15	-0.01	21.52	0.15	-0.17
M2	944	-0.06	24.59	1.76	0.01	24.59	1.76	-0.06
N1	955	-0.13	42.13	1.74	-0.07	42.13	1.74	-0.13
N2	958	0.01	46.06	1.89	0.06	46.06	1.89	0.01
O1	1101	-0.18	21.29	-0.41	0.00	21.29	-0.18	-0.41
O2	1104	-0.12	24.21	1.16	-0.01	24.21	1.16	-0.12

Table 2.10.10-25 Primary Stresses; 30-Foot Top Oblique Drop; $\phi = 60°$; 1.12-Inch Outer Shell Thickness (continued)

Stress Points		Stresses						
Location	Node	S_X	S_Y	S_Z	S_{XY}	S_1	S_2	S_3
P1	1115	-0.17	45.94	1.85	0.03	45.94	1.85	-0.17
P2	1118	0.01	50.51	2.64	-0.03	50.51	2.64	0.01
Q1	1261	-0.17	15.33	0.18	0.04	15.33	0.18	-0.17
Q2	1264	-0.06	17.74	1.70	-0.05	17.74	1.70	-0.06
R1	1275	-0.14	31.46	0.52	0.11	31.46	0.52	-0.14
R2	1278	0.02	35.19	2.79	-0.11	35.19	2.79	0.02
S1	1561	-0.16	-3.23	1.96	-0.18	1.96	-0.15	-3.25
S2	1564	0.16	-9.52	-1.78	-0.41	0.17	-1.78	-9.54
T1	1575	-0.30	3.10	2.37	0.21	3.12	2.37	-0.31
T2	1578	0.01	7.20	4.64	-0.12	7.20	4.64	0.01
U1	1841	0.24	-16.50	10.84	-0.13	10.84	0.24	-16.50
U2	1844	3.80	-7.62	11.27	-0.74	11.27	3.85	-7.67
V1	1852	9.95	1.30	5.66	-2.98	10.88	5.66	0.37
V2	1856	0.78	-7.73	-2.30	0.06	0.78	-2.30	-7.73
W1	1969	-66.76	-41.68	-23.95	-0.48	-23.95	-41.67	-66.77
W2	1970	-48.81	-4.87	-11.98	-3.63	-4.57	-11.98	-49.11
W3	1971	-27.02	-1.92	-8.87	-5.46	-0.78	-8.87	-28.15
W4	1972	-19.49	2.28	-9.31	-4.67	3.24	-9.31	-20.45
W5	1973	-15.85	5.41	-10.04	-3.70	6.03	-10.04	-16.48
W6	1974	-13.88	8.25	-10.62	-2.69	8.57	-10.62	-14.20
W7	1975	-12.85	11.83	-11.25	-1.50	11.92	-11.25	-12.94
W8	1976	-12.54	16.71	-11.73	-0.67	16.73	-11.73	-12.56
X1	2370	-34.36	-17.01	-7.66	1.31	-7.66	-16.91	-34.46
X2	2390	-16.21	-14.25	-1.58	4.86	-1.58	-10.27	-20.19
X3	2410	-12.66	-12.01	0.06	7.35	0.06	-4.98	-19.69
X4	2430	-8.01	-13.25	1.10	7.19	1.10	-2.98	-18.29
X5	2450	-6.21	-12.65	1.73	6.28	1.73	-2.37	-16.49
X6	2470	-5.20	-11.99	1.96	5.16	1.96	-2.42	-14.77
X7	2490	-4.59	-11.11	1.74	4.16	1.74	-2.56	-13.14
X8	2510	-4.01	-10.62	1.46	3.23	1.46	-2.70	-11.93
X9	2530	-3.28	-10.25	0.95	2.34	0.95	-2.57	-10.96

Table 2.10.10-25 Primary Stresses; 30-Foot Top Oblique Drop; $\phi = 60°$; 1.12-Inch Outer Shell Thickness (continued)

Stress Points		Stresses						
Location	Node	S_X	S_Y	S_Z	S_{XY}	S_1	S_2	S_3
X10	2550	-2.20	-10.08	0.13	1.27	0.13	-2.00	-10.28
X11	2570	-0.68	-10.03	-1.07	0.85	-0.61	-1.07	-10.11
Y1	2305	-0.50	-3.31	2.52	-0.39	2.52	-0.45	-3.37
Y2	2325	-2.99	-3.28	2.85	-0.90	2.85	-2.22	-4.05
Y3	2345	-5.73	-3.30	2.62	-0.90	2.62	-3.00	-6.02
Y4	2365	-8.38	-3.62	2.34	0.15	2.34	-3.61	-8.38
Y5	2385	-9.44	-4.55	2.25	2.00	2.25	-3.84	-10.15
Y6	2405	-8.81	-6.23	2.40	4.00	2.40	-3.31	-11.73
Y7	2425	-7.68	-8.50	2.67	5.91	2.67	-2.17	-14.02
Y8	2445	-7.41	-10.86	3.08	8.04	3.08	-0.91	-17.36
Y9	2465	-9.57	-12.29	3.68	10.52	3.68	-0.32	-21.54
Y10	2485	-16.57	-12.12	3.75	12.22	3.75	-1.92	-26.77
Y11	2505	-22.26	-11.71	2.74	11.40	2.74	-4.42	-29.55
Y12	2525	-25.13	-11.21	1.58	8.78	1.58	-6.96	-29.38
Y13	2545	-27.83	-10.20	-0.70	5.06	-0.70	-8.85	-29.18
Y14	2565	-28.31	-9.99	-5.19	2.37	-5.19	-9.69	-28.61
Z1	2301	-2.94	-0.93	2.30	-0.10	2.30	-0.92	-2.95
Z2	2321	-3.62	-0.50	2.68	-0.22	2.68	-0.48	-3.63
Z3	2341	-4.30	-0.47	2.65	-0.18	2.65	-0.46	-4.31
Z4	2361	-4.93	-0.47	2.65	-0.02	2.65	-0.47	-4.93
Z5	2381	-5.19	-0.50	2.59	0.27	2.59	-0.49	-5.21
Z6	2401	-4.99	-0.61	2.43	0.60	2.43	-0.53	-5.07
Z7	2421	-4.39	-0.77	2.17	0.94	2.17	-0.54	-4.62
Z8	2441	-3.53	-0.98	1.86	1.42	1.86	-0.34	-4.17
Z9	2461	-2.52	-1.18	1.53	3.69	1.90	1.53	-5.60
Z10	2481	-1.46	-1.39	1.23	12.69	11.26	1.23	-14.12
Z11	2501	-0.95	-1.49	1.04	36.69	35.47	1.04	-37.91
Z12	2521	-0.45	-1.56	0.83	110.30	109.30	0.83	-111.31
Z13	2541	-0.15	-1.98	0.37	501.00	499.93	0.37	-502.07
Z14	2561	0.54	-3.06	-1.49	655.20	653.94	-1.49	-656.46

Table 2.10.10-26 Primary Plus Secondary Stresses; 30-Foot Top Oblique Drop; $\phi = 60°$; 1.12-Inch Outer Shell Thickness

Stress Points		Stresses						
Location	Node	S_X	S_Y	S_Z	S_{XY}	S_1	S_2	S_3
A1	327	2.64	0.00	6.89	0.33	6.89	2.68	-0.04
A2	302	1.46	-0.02	5.87	0.35	5.87	1.54	-0.10
A3	277	0.42	0.00	4.93	0.78	4.93	1.02	-0.59
A4	252	-1.64	-0.09	3.07	1.10	3.07	0.48	-2.22
A5	227	-5.82	-1.74	-0.16	0.76	-0.16	-1.61	-5.95
A6	202	-4.15	-2.81	2.18	-2.86	2.18	-0.54	-6.42
A7	177	-37.54	-1.86	-15.71	-1.29	-1.81	-15.71	-37.58
B1	104	-9.88	-2.53	-4.29	-1.34	-2.30	-4.29	-10.12
B2	79	-5.43	-1.96	-0.38	-0.41	-0.38	-1.91	-5.47
B3	54	-2.19	-0.92	2.95	-0.73	2.95	-0.59	-2.52
B4	29	1.17	-0.17	6.32	-0.45	6.32	1.31	-0.31
B5	4	4.86	0.01	9.51	-0.54	9.51	4.92	-0.05
C1	110	-9.58	-1.93	-4.90	-0.23	-1.93	-4.90	-9.59
C2	85	-6.38	-1.59	-1.59	1.00	-1.39	-1.59	-6.58
C3	60	-3.50	-0.86	1.56	1.20	1.56	-0.39	-3.97
C4	35	-0.39	-0.25	4.95	0.78	4.95	0.47	-1.10
C5	10	2.90	-0.05	8.29	0.32	8.29	2.94	-0.08
D1	335	-2.70	-6.38	1.69	-1.30	1.69	-2.29	-6.80
D2	310	-1.28	-4.02	2.00	-1.30	2.00	-0.76	-4.54
D3	285	-2.05	-2.87	1.50	-1.36	1.50	-1.04	-3.88
D4	260	-4.03	-2.42	-0.06	-1.58	-0.06	-1.45	-5.00
D5	235	-7.68	-2.59	-3.37	-1.34	-2.26	-3.37	-8.01
D6	210	-11.62	-2.80	-6.92	-0.60	-2.76	-6.92	-11.66
D7	185	-15.97	-2.84	-10.91	1.36	-2.70	-10.91	-16.11
E1	118	-0.29	4.45	-0.74	3.28	6.13	-0.74	-1.97
E2	93	-6.29	3.85	-1.48	2.17	4.29	-1.48	-6.73
E3	68	-6.30	1.31	-0.92	1.84	1.73	-0.92	-6.72
E4	43	-6.93	0.36	0.16	1.05	0.51	0.16	-7.08
E5	18	-6.51	0.13	2.03	0.57	2.03	0.17	-6.56
F1	143	-11.90	4.29	-3.27	4.25	5.33	-3.27	-12.95
F2	144	-9.99	8.00	-3.72	2.34	8.30	-3.72	-10.29

Table 2.10.10-26 Primary Plus Secondary Stresses; 30-Foot Top Oblique Drop; $\phi = 60°$; 1.12-Inch Outer Shell Thickness (continued)

Stress Points		Stresses						
Location	Node	S_X	S_Y	S_Z	S_{XY}	S_1	S_2	S_3
F3	145	-7.16	4.19	-5.14	0.29	4.20	-5.14	-7.17
F4	146	-6.18	2.12	-6.30	-0.12	2.12	-6.18	-6.30
F5	147	-6.27	0.67	-7.35	-0.22	0.68	-6.28	-7.35
F6	148	-6.47	-0.50	-8.28	-0.24	-0.49	-6.48	-8.28
F7	149	-6.65	-1.76	-9.26	-0.16	-1.75	-6.65	-9.26
F8	150	-6.78	-3.18	-10.34	-0.07	-3.18	-6.78	-10.34
G1	335	-2.70	-6.38	1.69	-1.30	1.69	-2.29	-6.80
G2	336	-2.08	-4.03	2.13	-0.48	2.13	-1.97	-4.14
G3	337	-1.32	-2.54	2.44	0.13	2.44	-1.31	-2.55
G4	338	-1.29	-0.71	2.70	0.17	2.70	-0.66	-1.34
G5	339	-0.66	2.43	3.40	-0.80	3.40	2.63	-0.85
G6	340	-1.66	-0.49	2.60	-0.95	2.60	0.04	-2.20
H1	346	-12.85	0.12	-8.85	2.49	0.58	-8.85	-13.31
H2	347	-7.96	14.36	-4.84	1.64	14.48	-4.84	-8.08
H3	348	-7.80	15.74	-5.31	-2.05	15.92	-5.31	-7.98
H4	349	-6.78	9.73	-7.57	-2.53	10.11	-7.16	-7.57
H5	350	-6.73	4.45	-9.87	-1.75	4.72	-7.00	-9.87
I1	621	-0.20	3.73	1.87	-0.08	3.73	1.87	-0.20
I2	624	-0.05	3.97	1.81	0.09	3.98	1.81	-0.05
J1	635	-0.21	17.01	2.55	-0.24	17.02	2.55	-0.21
J2	638	-0.01	22.00	1.68	0.15	22.00	1.68	-0.01
K1	841	-0.17	18.19	0.09	-0.05	18.19	0.09	-0.17
K2	844	-0.03	21.13	2.02	0.10	21.13	2.02	-0.03
L1	855	-0.12	40.27	1.10	-0.14	40.27	1.10	-0.12
L2	858	0.05	43.81	1.77	0.08	43.81	1.77	0.05
M1	941	-0.17	23.77	-0.02	-0.02	23.77	-0.02	-0.17
M2	944	-0.05	27.37	2.11	0.01	27.37	2.11	-0.05
N1	955	-0.13	51.27	1.29	-0.06	51.27	1.29	-0.13
N2	958	0.01	55.90	2.12	0.06	55.90	2.12	0.01
O1	1101	-0.18	23.55	-0.57	0.00	23.55	-0.18	-0.57
O2	1104	-0.11	26.99	1.51	-0.01	26.99	1.51	-0.11

Table 2.10.10-26 Primary Plus Secondary Stresses; 30-Foot Top Oblique Drop; $\phi = 60°$; 1.12-Inch Outer Shell Thickness (continued)

Stress Points		Stresses						
Location	Node	S_X	S_Y	S_Z	S_{XY}	S_1	S_2	S_3
P1	1115	-0.17	55.04	1.36	0.03	55.04	1.36	-0.17
P2	1118	0.01	60.36	2.88	-0.03	60.36	2.88	0.01
Q1	1261	-0.17	17.64	0.10	0.03	17.64	0.10	-0.17
Q2	1264	-0.05	20.46	2.02	-0.06	20.46	2.02	-0.05
R1	1275	-0.14	40.61	0.06	0.11	40.61	0.06	-0.14
R2	1278	0.01	45.07	2.88	-0.11	45.07	2.88	0.01
S1	1561	-0.16	-1.12	2.31	-0.14	2.31	-0.14	-1.14
S2	1564	0.14	-6.58	-1.11	-0.36	0.15	-1.11	-6.60
T1	1575	-0.30	13.77	2.45	0.15	13.77	2.45	-0.30
T2	1578	0.02	15.65	4.52	-0.17	15.65	4.52	0.02
U1	1841	0.26	-16.32	10.30	-0.22	10.30	0.26	-16.32
U2	1844	4.00	-6.40	11.44	-0.71	11.44	4.07	-6.46
V1	1852	4.26	-0.87	3.22	-4.16	6.58	3.22	-3.20
V2	1856	0.46	4.34	1.25	0.22	4.35	1.25	0.45
W1	1969	-67.53	-43.53	-23.94	-1.29	-23.94	-43.46	-67.60
W2	1970	-48.84	-5.63	-11.28	-4.31	-5.20	-11.28	-49.27
W3	1971	-27.13	-2.01	-7.91	-6.01	-0.64	-7.91	-28.49
W4	1972	-19.57	2.81	-8.10	-5.16	3.95	-8.10	-20.70
W5	1973	-15.93	6.35	-8.66	-4.08	7.08	-8.66	-16.65
W6	1974	-13.94	9.52	-9.09	-2.95	9.88	-9.09	-14.31
W7	1975	-12.89	13.38	-9.59	-1.63	13.48	-9.59	-12.99
W8	1976	-12.53	18.52	-9.94	-0.73	18.54	-9.94	-12.55
X1	2370	-35.61	-17.34	-7.99	1.91	-7.99	-17.14	-35.81
X2	2390	-16.54	-15.19	-1.82	5.30	-1.82	-10.52	-21.21
X3	2410	-13.03	-12.55	-0.02	7.41	-0.02	-5.37	-20.21
X4	2430	-8.36	-13.64	1.09	7.06	1.09	-3.46	-18.54
X5	2450	-6.61	-12.88	1.79	6.02	1.79	-2.95	-16.54
X6	2470	-5.61	-12.12	2.09	4.84	2.09	-3.04	-14.70
X7	2490	-4.97	-11.18	1.99	3.82	1.99	-3.15	-13.00
X8	2510	-4.35	-10.65	1.81	2.91	1.81	-3.21	-11.79
X9	2530	-3.57	-10.27	1.40	2.07	1.40	-2.98	-10.86

Table 2.10.10-26 Primary Plus Secondary Stresses; 30-Foot Top Oblique Drop; $\phi = 60°$; 1.12-Inch Outer Shell Thickness (continued)

Stress Points		Stresses						
Location	Node	S_X	S_Y	S_Z	S_{XY}	S_1	S_2	S_3
X10	2550	-2.42	-10.09	0.74	1.10	0.74	-2.27	-10.24
X11	2570	-0.06	-10.03	0.51	0.80	0.51	0.00	-10.09
Y1	2305	0.06	-3.34	3.01	-0.43	3.01	0.12	-3.40
Y2	2325	-2.97	-3.33	2.84	-0.85	2.84	-2.28	-4.02
Y3	2345	-6.01	-3.41	2.29	-0.85	2.29	-3.16	-6.26
Y4	2365	-8.93	-3.78	1.73	0.20	1.73	-3.77	-8.94
Y5	2385	-10.17	-4.76	1.46	2.04	1.46	-4.07	-10.86
Y6	2405	-9.61	-6.48	1.53	4.04	1.53	-3.71	-12.38
Y7	2425	-8.47	-8.77	1.79	5.91	1.79	-2.71	-14.53
Y8	2445	-8.13	-11.11	2.28	7.99	2.28	-1.49	-17.75
Y9	2465	-10.18	-12.47	3.01	10.44	3.01	-0.82	-21.83
Y10	2485	-17.00	-12.23	3.30	12.13	3.30	-2.25	-26.98
Y11	2505	-22.55	-11.76	2.45	11.37	2.45	-4.57	-29.74
Y12	2525	-25.24	-11.22	1.47	8.77	1.47	-7.00	-29.46
Y13	2545	-27.70	-10.20	-0.60	5.05	-0.60	-8.85	-29.05
Y14	2565	-27.05	-9.99	-4.04	2.44	-4.04	-9.65	-27.39
Z1	2301	-2.44	-0.91	2.79	-0.10	2.79	-0.91	-2.44
Z2	2321	-3.53	-0.47	2.76	-0.22	2.76	-0.45	-3.55
Z3	2341	-4.54	-0.40	2.41	-0.18	2.41	-0.40	-4.55
Z4	2361	-5.44	-0.38	2.14	-0.02	2.14	-0.38	-5.44
Z5	2381	-5.87	-0.40	1.91	0.27	1.91	-0.39	-5.89
Z6	2401	-5.78	-0.50	1.65	0.60	1.65	-0.43	-5.84
Z7	2421	-5.19	-0.67	1.38	0.94	1.38	-0.48	-5.38
Z8	2441	-4.25	-0.88	1.14	1.42	1.14	-0.36	-4.78
Z9	2461	-3.10	-1.09	0.96	3.69	1.73	0.96	-5.92
Z10	2481	-1.81	-1.32	0.89	12.69	11.13	0.89	-14.26
Z11	2501	-1.16	-1.44	0.84	36.69	35.39	0.84	-37.99
Z12	2521	-0.50	-1.53	0.77	110.30	109.28	0.77	-111.32
Z13	2541	-0.05	-1.97	0.47	501.00	499.99	0.47	-502.01
Z14	2561	1.60	-3.05	-0.43	655.20	654.48	-0.43	-655.93

Table 2.10.10-27 Primary Membrane (P_m) Stresses; 30-Foot Top Oblique Drop; $\phi = 60°$; 1.12-Inch Outer Shell Thickness

		Stresses* (ksi)							
Section	Node to Node	S_x	S_y	S_z	S_{xy}	S_1	S_2	S_3	SI
A	177 – 327	-5.92	-1.35	1.52	-0.36	1.52	-1.32	-5.94	7.47
B	4 – 104	-5.10	-1.24	0.03	-0.70	0.03	-1.12	-5.23	5.26
C	10 – 110	-6.24	-0.33	-1.63	0.32	-0.32	-1.63	-6.26	5.94
D	185 – 335	-6.88	-0.24	-2.29	-0.32	-0.22	-2.29	-6.89	6.67
E	18 – 118	-7.09	0.89	-4.29	-0.08	0.90	-4.29	-7.09	7.98
F	143 – 150	-3.67	0.25	-7.65	-0.67	0.36	-3.78	-7.65	8.01
G	335 – 340	-3.93	-1.19	-1.70	0.67	-1.04	-1.70	-4.08	3.04
H	346 – 350	-4.95	4.60	-8.86	-0.40	4.62	-4.97	-8.86	13.48
I	621 – 624	-0.13	3.47	1.82	-0.04	3.47	1.82	-0.13	3.61
J	635 – 638	-0.11	11.18	1.97	-0.09	11.18	1.97	-0.11	11.29
K	841 – 844	-0.12	17.17	0.99	0.02	17.17	0.99	-0.012	17.28
L	855 – 858	-0.04	32.55	1.53	-0.03	32.55	1.53	-0.04	32.59
M	941 – 944	-0.13	23.09	0.98	0.00	23.09	0.98	-0.13	23.21
N	955 – 958	-0.06	44.12	1.82	0.00	44.12	1.82	-0.06	44.18
O	1101 – 1104	-0.16	22.78	0.40	0.00	22.78	0.40	-0.16	22.95
P	1115 – 1118	-0.08	48.26	2.25	0.00	48.26	2.25	-0.08	48.34
Q	1261 – 1264	-0.12	16.56	0.97	-0.01	16.56	0.97	-0.12	16.68
R	1275 – 1278	-0.07	33.36	1.68	0.00	33.36	1.68	-0.07	33.43
S	1561 – 1564	0.01	-6.35	0.06	-0.39	0.06	0.04	-6.38	6.43
T	1575 – 1578	-0.15	5.18	3.53	0.03	5.18	3.53	-0.15	5.33
U	1841 – 1846	4.88	-3.27	11.92	0.21	11.92	4.89	-6.28	18.20
V	1852 – 1856	4.46	-0.13	1.97	-1.03	4.68	1.97	-0.34	5.02
W	1969 – 1976	-31.03	-1.79	-12.13	-3.28	-1.43	-12.13	-31.40	29.97
X	2370 – 2570	-9.19	-12.12	0.30	4.82	0.30	-5.62	-15.69	15.99
Y	2305 – 2565	-10.47	-7.40	2.41	4.52	2.41	-4.17	-13.71	16.11
Z	2301 – 2561	-3.33	-0.93	1.95	45.03	42.91	1.95	-47.18	90.09

* Stresses are taken at 0 degrees (under the load) at each section.

Table 2.10.10-28 Primary Membrane Plus Primary Bending ($P_m + P_b$) Stresses; 30-Foot Top Oblique Drop; $\phi = 60°$; 1.12-Inch Outer Shell Thickness

		Stresses* (ksi)							
Section	Node to Node	S_x	S_y	S_z	S_{xy}	S_1	S_2	S_3	SI
A	177 – 327	-12.85	-2.87	0.67	-2.34	0.67	-2.35	-13.37	14.04
B	4 – 104	-7.97	-2.62	-2.64	-1.03	-2.43	-2.64	-8.16	5.74
C	10 – 110	-8.82	-0.69	-4.10	-0.01	-0.69	-4.10	-8.82	8.13
D	185 – 335	-10.62	-1.35	-4.47	-0.07	-1.35	-4.47	-10.63	9.27
E	18 – 118	-6.83	2.15	-4.77	-0.71	2.21	-4.77	-6.88	9.09
F	143 – 150	-1.49	5.48	-2.80	-0.67	5.55	-1.56	-2.80	8.35
G	335 – 340	-7.37	-3.58	-3.78	0.67	-3.47	-3.78	-7.48	4.01
H	346 – 350	-4.00	12.55	-4.04	-0.40	12.56	-4.01	-4.04	16.60
I	621 – 624	-0.08	4.31	1.89	-0.04	4.31	1.89	-0.08	4.39
J	635 – 638	-0.02	14.82	1.72	-0.09	14.82	1.72	-0.02	14.84
K	841 – 844	-0.04	18.41	1.75	0.02	18.41	1.75	-0.04	18.45
L	855 – 858	0.04	34.03	1.59	-0.03	34.03	1.59	0.04	33.98
M	941 – 944	-0.06	24.59	1.79	0.00	24.59	1.79	-0.06	24.65
N	955 – 958	0.01	46.06	1.89	0.00	46.06	1.89	0.01	46.05
O	1101 – 1104	-0.12	24.21	1.18	0.00	24.21	1.18	-0.12	24.34
P	1115 – 1118	0.01	50.51	2.64	0.00	50.51	2.64	0.01	50.50
Q	1261 – 1264	-0.06	17.74	1.72	-0.01	17.74	1.72	-0.06	17.80
R	1275 – 1278	0.02	35.19	2.81	0.00	35.19	2.81	0.02	35.17
S	1561 – 1564	0.16	-9.42	-1.80	-0.39	0.17	-1.80	-9.44	9.61
T	1575 – 1578	0.01	7.20	4.66	0.03	7.20	4.66	0.01	7.19
U	1841 – 1846	0.24	-14.53	10.39	0.21	10.39	0.24	-14.54	24.92
V	1852 – 1856	0.78	-5.40	-2.35	-1.03	0.94	-2.35	-5.57	6.51
W	1969 – 1976	-66.76	-24.50	-16.52	-3.28	-16.52	-24.25	-67.01	50.49
X	2370 – 2570	-20.23	-14.00	-1.74	6.55	-1.74	-9.86	-24.37	22.63
Y	2305 – 2565	-21.21	-13.13	1.72	11.16	1.72	-5.31	-29.04	30.75
Z	2301 – 2561	-1.37	-1.67	0.72	166.60	165.08	0.72	-168.12	333.20

* Stresses are taken at 0 degrees (under the load) at each section.

Table 2.10.10-29 Primary Membrane (P_m) and Primary Membrane Plus Primary Bending ($P_m + P_b$) Stresses; 30-Foot Top Oblique Drop; $\phi = 60°$; 1.12-Inch Outer Shell Thickness

			P_m Stresses (ksi)			$P_m + P_b$ Stresses (ksi)		
Section	Node to Node	Max. Temp. (°F)	Allow.[1] 0.7 S_u	Calc.	MS	Allow.[1] 1.0 S_u	Calc.	MS
A	327 – 177	222	48.93	7.47	+Large	69.90	14.04	+3.97
B	104 – 4	215	49.18	5.26	+Large	70.25	5.74	+Large
C	110 – 10	212	49.28	5.94	+Large	70.40	8.13	+Large
D	335 – 185	221	48.96	6.67	+Large	69.95	9.27	+Large
E	118 – 18	208	49.42	7.98	+Large	70.60	9.09	+Large
F	143 – 150	209	49.38	8.01	+Large	70.55	8.35	+Large
G	335 – 340	221	48.96	3.04	+Large	69.95	4.01	+Large
H	346 – 350	212	49.28	13.48	+2.66	70.40	16.60	+3.24
I	621 – 624	222	48.93	3.61	+Large	69.90	4.39	+Large
J	635 – 638	199	49.73	11.29	+3.40	71.04	14.84	+3.79
K	841 – 844	232	68.49	17.28	+2.96	97.84	18.45	+Large
L	855 – 858	204	69.50	32.59	+1.13	99.29	33.98	+1.92
M	941 – 944	247	67.94	23.21	+1.93	97.06	24.65	+2.94
N	955 – 958	211	69.25	44.18	+0.57	98.93	46.05	+1.15
O	1101 – 1104	255	67.65	22.95	+1.95	96.64	24.34	+2.97
P	1115 – 1118	216	69.07	48.34	+0.43	98.67	50.50	+0.95
Q	1261 – 1264	251	67.80	16.68	+3.06	96.85	17.80	+Large
R	1275 – 1278	216	69.07	33.43	+1.07	98.67	35.17	+1.81
S	1561 – 1564	217	49.10	6.43	+Large	70.15	9.61	+Large
T	1575 – 1578	197	49.78	5.33	+Large	71.12	7.19	+Large
U	1841 – 1846	212	49.28	18.20	+1.71	70.40	24.92	+1.83
V	1852 – 1856	205	49.52	5.02	+Large	70.75	6.51	+Large
W	1969 – 1976	198	49.76	29.97	+0.66	71.08	50.49	+0.41
X	2370 – 2570	201	49.66	15.99	+2.11	70.95	22.63	+2.14
Y	2305 – 2565	205	49.52	16.11	+2.07	70.75	30.75	+1.30
Z	2301 – 2561	204	49.56	90.09[2]	[2]	70.80	333.202	[2]

[1] Allowable stresses for sections "K" through "R" are taken from Type XM-19 stainless steel; all others are from Type 304 stainless steel.

[2] This stress is induced by the boundary effect from the displacement restraints at node 2561 and, therefore, is disregarded.

Table 2.10.10-30 Primary Stresses; 30-Foot Side Drop; $\phi = 90°$; 1.20-Inch Outer Shell Thickness; Circumferential Location = 0°

Stress Points		Stresses (ksi)						
Location	Node	S_X	S_Y	S_Z	S_{XY}	S_1	S_2	S_3
A1	327	-3.14	-0.06	2.35	0.13	2.35	-0.05	-3.15
A2	302	-3.62	-0.09	2.07	0.49	2.07	-0.03	-3.69
A3	277	-3.91	0.01	1.91	1.13	1.91	0.31	-4.21
A4	252	-4.49	-0.06	1.58	1.45	1.58	0.37	-4.92
A5	227	-5.78	-2.16	1.53	1.01	1.53	-1.89	-6.05
A6	202	0.42	-3.48	8.60	-3.67	8.60	2.62	-5.68
A7	177	-38.59	-2.25	-10.46	-1.66	-2.17	-10.46	-38.67
B1	104	-10.75	-3.20	-3.50	-1.69	-2.84	-3.50	-11.11
B2	79	-7.52	-2.51	-1.03	-0.67	-1.03	-2.42	-7.61
B3	54	-5.97	-1.30	0.63	-1.06	0.63	-1.07	-6.20
B4	29	-4.36	-0.29	2.29	-0.74	2.29	-0.16	-4.49
B5	4	-2.81	0.06	3.30	0.06	3.30	0.07	-2.81
C1	110	-11.30	-0.82	-5.15	-0.67	-0.78	-5.15	-11.34
C2	85	-9.35	-0.68	-3.26	0.60	-0.64	-3.26	-9.39
C3	60	-7.53	-0.36	-1.64	0.71	-0.29	-1.64	-7.60
C4	35	-5.71	-0.08	0.08	0.59	0.08	-0.02	-5.77
C5	10	-4.70	-0.01	1.12	0.48	1.12	0.04	-4.75
D1	335	-2.50	3.23	0.85	-0.17	3.23	0.85	-2.51
D2	310	-4.51	1.57	-0.35	-0.10	1.57	-0.35	-4.51
D3	285	-5.42	0.75	-0.97	-0.32	0.77	-0.97	-5.43
D4	260	-6.80	0.08	-1.76	-0.72	0.15	-1.76	-6.87
D5	235	-9.08	-0.55	-3.01	-0.66	-0.50	-3.01	-9.13
D6	210	-11.33	-0.88	-4.35	-0.52	-0.85	-4.35	-11.35
D7	185	-13.59	-0.97	-5.95	0.90	-0.90	-5.95	-13.65
E1	118	-8.14	3.79	-5.68	-1.31	3.93	-5.68	-8.28
E2	93	-9.28	1.61	-5.92	-0.20	1.61	-5.92	-9.28
E3	68	-9.14	0.66	-5.50	0.26	0.66	-5.50	-9.15
E4	43	-9.22	0.20	-4.89	0.34	0.22	-4.89	-9.23
E5	18	-9.63	0.07	-4.60	0.41	0.09	-4.60	-9.64
F1	143	-1.94	10.54	-2.98	-2.02	10.86	-2.26	-2.98
F2	144	-2.09	2.75	-6.95	-1.53	3.19	-2.53	-6.95

Table 2.10.10-30 Primary Stresses; 30-Foot Side Drop; $\phi = 90°$; 1.20-Inch Outer Shell Thickness; Circumferential Location = 0° (continued)

Stress Points		Stresses (ksi)						
Location	Node	S_X	S_Y	S_Z	S_{XY}	S_1	S_2	S_3
F3	145	-3.00	0.75	-8.78	-0.97	0.98	-3.23	-8.78
F4	146	-5.28	-0.58	-10.73	-0.49	-0.53	-5.33	-10.73
F5	147	-6.76	-1.63	-12.25	-0.32	-1.61	-6.78	-12.25
F6	148	-7.67	-2.63	-13.52	-0.22	-2.62	-7.68	-13.52
F7	149	-8.29	-3.89	-14.85	-0.13	-3.89	-8.30	-14.85
F8	150	-8.64	-5.58	-16.30	-0.04	-5.58	-8.64	-16.30
G1	335	-2.50	3.23	0.85	-0.17	3.23	0.85	-2.51
G2	336	-2.25	1.48	-0.17	-0.46	1.54	-0.17	-2.30
G3	337	-2.90	0.05	-1.18	-0.41	0.11	-1.18	-2.95
G4	338	-4.06	-1.36	-2.22	0.19	-1.35	-2.22	-4.07
G5	339	-6.74	-3.77	-3.94	1.93	-2.82	-3.94	-7.69
G6	340	-9.47	-2.10	-3.99	2.30	-1.44	-3.99	-10.13
H1	346	-5.16	4.91	-8.50	3.55	6.03	-6.29	-8.50
H2	347	-4.30	15.58	-7.21	2.14	15.81	-4.52	-7.21
H3	348	-7.22	11.93	-10.49	-2.43	12.24	-7.52	-10.49
H4	349	-7.75	0.57	-15.03	-2.97	1.52	-8.70	-15.03
H5	350	-8.37	-11.06	-19.50	-1.99	-7.31	-12.11	-19.50
I1	621	-0.23	3.92	2.12	-0.18	3.93	2.12	-0.24
I2	624	-0.11	6.29	2.35	0.04	6.29	2.35	-0.11
J1	635	-0.26	10.07	2.86	-0.38	10.09	2.86	-0.27
J2	638	-0.03	19.66	2.23	0.14	19.66	2.23	-0.03
K1	841	-0.23	16.81	-0.06	-0.08	16.81	-0.06	-0.24
K2	844	-0.07	19.81	2.28	0.11	19.81	2.28	-0.07
L1	855	-0.14	33.30	2.54	-0.22	33.30	2.54	-0.14
L2	858	0.04	36.61	1.36	0.14	36.61	1.36	0.04
M1	941	-0.23	25.38	-0.40	0.01	25.38	-0.23	-0.40
M2	944	-0.11	29.12	2.12	0.06	29.12	2.12	-0.11
N1	955	-0.16	51.01	2.49	-0.12	51.01	2.49	-0.16
N2	958	0.02	56.00	2.11	0.11	56.00	2.11	0.02
O1	1101	-0.24	29.33	-0.72	0.00	29.33	-0.24	-0.72
O2	1104	-0.15	33.42	1.76	0.01	33.42	1.76	-0.15

Table 2.10.10-30 Primary Stresses; 30-Foot Side Drop; $\phi = 90°$; 1.20-Inch Outer Shell Thickness; Circumferential Location = 0° continued)

Stress Points		Stresses (ksi)						
Location	Node	S_X	S_Y	S_Z	S_{XY}	S_1	S_2	S_3
P1	1115	-0.21	61.83	2.28	0.01	61.83	2.28	-0.21
P2	1118	0.02	68.25	3.05	-0.01	68.25	3.05	0.02
Q1	1261	-0.23	26.93	-0.18	0.03	26.93	-0.18	-0.23
Q2	1264	-0.08	30.88	2.34	-0.04	30.88	2.34	-0.08
R1	1275	-0.19	50.04	0.64	0.12	50.04	0.64	-0.19
R2	1278	0.03	55.93	3.40	-0.12	55.93	3.40	0.03
S1	1561	-0.22	6.45	1.68	0.19	6.45	1.68	-0.22
S2	15.64	-0.15	10.08	3.23	0.03	10.08	3.23	-0.15
T1	1575	-0.24	20.06	0.94	0.25	20.06	0.94	-0.25
T2	1578	0.01	28.31	4.65	-0.11	28.31	4.65	0.01
U1	1841	-0.15	-0.51	3.08	0.02	3.08	-0.15	-0.51
U2	1844	0.39	0.74	2.17	-0.27	2.17	0.89	0.24
V1	1852	10.17	10.66	0.01	-7.15	17.57	3.26	0.01
V2	1856	0.69	5.00	-6.36	0.52	5.06	0.63	-6.36
W1	1969	-42.95	-26.22	-16.25	-3.73	-16.25	-25.43	-43.74
W2	1970	-32.16	0.14	-8.38	-4.46	0.75	-8.38	-32.76
W3	1971	-18.51	3.17	-6.74	-4.82	4.19	-6.74	-19.54
W4	1972	-13.78	6.90	-7.47	-3.98	7.64	-7.47	-14.52
W5	1973	-11.52	9.51	-8.33	-3.07	9.95	-8.33	-11.96
W6	1974	-10.25	11.85	-9.09	-2.18	12.07	-9.09	-10.46
W7	1975	-9.60	14.64	-9.91	-1.19	14.70	-9.65	-9.91
W8	1976	-9.43	18.35	-10.64	-0.44	18.35	-9.44	-10.64
X1	2370	-20.80	-8.29	-5.45	-0.83	-5.45	-8.24	-20.86
X2	2390	-8.80	-4.14	-0.82	0.96	-0.82	-3.95	-8.99
X3	2410	-6.31	-2.06	0.11	2.47	0.11	-0.93	-7.44
X4	2430	-3.28	-2.28	0.55	2.20	0.55	-0.53	-5.04
X5	2450	-1.90	-1.68	0.73	1.56	0.73	-0.22	-3.35
X6	2470	-1.04	-1.21	0.77	0.92	0.77	-0.20	-2.05
X7	2490	-0.57	-0.66	0.79	0.48	0.79	-0.13	-1.09
X8	25.10	-0.30	-0.41	0.84	0.27	0.84	-0.08	-0.63

Table 2.10.10-30 Primary Stresses; 30-Foot Side Drop; $\phi = 90°$; 1.20-Inch Outer Shell Thickness; Circumferential Location = 0° ° (continued)

Stress Points		Stresses (ksi)						
Location	Node	S_X	S_Y	S_Z	S_{XY}	S_1	S_2	S_3
X9	2530	-0.03	-0.19	0.92	0.14	0.92	0.05	-0.27
X10	2550	0.32	-0.06	1.03	0.05	1.03	0.33	-0.07
X11	2570	0.78	-0.01	1.20	0.06	1.20	0.79	-0.02
Y1	2305	-0.17	0.22	0.87	-0.22	0.87	0.32	-0.26
Y2	2325	-1.97	0.14	0.73	-0.67	0.73	0.33	-2.16
Y3	2345	-3.64	0.20	0.77	-0.78	0.77	0.35	-3.79
Y4	2365	-5.08	0.28	0.82	-0.30	0.82	0.30	-5.09
Y5	2385	-5.44	0.21	0.99	0.49	0.99	0.25	-5.48
Y6	2405	-4.78	-0.02	1.19	1.13	1.19	0.23	-5.03
Y7	2425	-3.77	-0.30	1.31	1.41	1.31	0.21	-4.27
Y8	2445	-2.86	-0.47	1.34	1.44	1.34	0.21	-3.54
Y9	2465	-2.22	-0.47	1.35	1.37	1.35	0.27	-2.97
Y10	2485	-1.92	-0.31	1.39	1.20	1.39	0.33	-2.56
Y11	2505	-1.92	-0.25	1.39	1.06	1.39	0.26	-2.43
Y12	2525	-1.77	-0.14	1.45	0.77	1.45	0.17	-2.08
Y13	2545	-1.59	-0.02	1.54	0.42	1.54	0.09	-1.70
Y14	2565	-1.29	0.03	1.64	0.19	1.64	0.05	-1.32
Z1	2301	-1.69	0.08	0.69	-0.01	0.69	0.08	-1.69
Z2	2321	-2.07	0.08	0.94	-0.04	0.94	0.08	-2.07
Z3	2341	-2.58	0.16	1.15	-0.04	1.15	0.16	-2.58
Z4	2361	-3.01	0.23	1.36	0.01	1.36	0.23	-3.01
Z5	2381	-3.21	0.27	1.50	0.07	1.50	0.27	-3.21
Z6	2401	-3.13	0.28	1.56	0.15	1.56	0.28	-3.14
Z7	2421	-2.83	0.24	1.55	0.21	1.55	0.26	-2.84
Z8	2441	-2.38	0.19	1.50	0.25	1.50	0.21	-2.41
Z9	2461	-1.90	0.13	1.45	0.36	1.45	0.19	-1.97
Z10	2481	-1.46	0.09	1.40	0.77	1.40	0.40	-1.77
Z11	2501	-1.26	0.05	1.44	1.88	1.44	1.38	-2.60
Z12	2521	-1.09	0.05	1.49	5.35	4.85	1.49	-5.90
Z13	25541	-0.98	0.04	1.56	23.86	23.39	1.56	-24.33
Z14	2561	-0.94	0.03	1.65	31.16	30.70	1.65	-31.61

Table 2.10.10-31 Primary Plus Secondary Stresses; 30-Foot Side Drop; $\phi = 90°$; 1.20-Inch Outer Shell Thickness; Circumferential Location = 0°

Stress Points		Stresses (ksi)						
Location	Node	S_X	S_Y	S_Z	S_{XY}	S_1	S_2	S_3
A1	327	2.06	0.01	7.54	0.36	7.54	2.12	-0.05
A2	302	0.72	-0.02	6.42	0.46	6.42	0.94	-0.25
A3	277	-0.43	0.02	5.39	1.03	5.39	0.84	-1.26
A4	252	-2.72	-0.10	3.35	1.43	3.35	0.53	-3.35
A5	227	-7.39	-2.22	-0.09	0.99	-0.09	-2.04	-7.57
A6	202	-4.55	-3.58	3.62	-3.68	3.62	-0.36	-7.77
A7	177	-46.95	-2.35	-18.78	-1.66	-2.29	-18.78	-47.01
B1	104	-10.58	-3.17	-3.36	-1.61	-2.83	-3.36	-10.92
B2	79	-6.38	-2.46	0.13	-0.61	0.13	-2.37	-6.47
B3	54	-3.80	-1.20	2.82	-1.02	2.82	-0.85	-4.15
B4	29	-1.11	-0.24	5.53	-0.67	5.53	0.12	-1.47
B5	4	2.21	0.04	8.26	-0.36	8.26	2.27	-0.02
C1	110	-10.94	-1.68	-4.57	-0.45	-1.66	-4.57	-10.96
C2	85	-8.09	-1.37	-1.76	0.84	-1.26	-1.76	-8.19
C3	60	-5.40	-0.71	0.91	0.98	0.91	-0.52	-5.60
C4	35	-2.47	-0.19	3.83	0.69	3.83	0.00	-2.67
C5	10	0.47	-0.03	6.73	0.37	6.73	0.66	-0.23
D1	335	-2.64	-5.04	2.30	-1.10	2.30	-2.21	-5.46
D2	310	-1.93	-3.18	2.20	-1.11	2.20	-1.28	-3.83
D3	285	-3.00	-2.29	1.48	-1.22	1.48	-1.37	-3.91
D4	260	-5.49	-2.04	-0.41	-1.56	-0.41	-1.44	-6.09
D5	235	-9.93	-2.39	-4.27	-1.32	-2.16	-4.27	-10.16
D6	210	-14.66	-2.67	-8.41	-0.53	-2.64	-8.41	-14.68
D7	185	-19.85	-2.71	-13.05	1.81	-2.52	-13.05	-20.04
E1	118	-4.40	1.18	-3.47	2.24	1.97	-3.47	-5.19
E2	93	-8.50	2.43	-3.36	1.39	2.60	-3.36	-8.67
E3	68	-8.16	0.95	-2.56	1.43	1.17	-2.56	-8.38
E4	43	-8.25	0.27	-1.43	0.90	0.36	-1.43	-8.34
E5	18	-7.60	0.09	0.31	0.57	0.31	0.13	-7.64
F1	143	-11.69	2.29	-4.86	4.07	3.39	-4.86	-12.78
F2	144	-10.56	7.92	-5.42	1.87	8.10	-5.42	-10.75

Table 2.10.10-31 Primary Plus Secondary Stresses; 30-Foot Side Drop; $\phi = 90°$; 1.20-Inch Outer Shell Thickness; Circumferential Location = 0° ° (continued)

Stress Points		Stresses (ksi)						
Location	Node	S_X	S_Y	S_Z	S_{XY}	S_1	S_2	S_3
F3	145	-8.46	4.02	-7.35	-0.38	4.03	-7.35	-8.47
F4	146	-7.71	1.98	-8.83	-0.61	2.01	-7.75	-8.83
F5	147	-7.98	0.48	-10.16	-0.60	0.52	-8.02	-10.16
F6	148	-8.29	-0.76	-11.33	-0.52	-0.72	-8.32	-11.33
F7	149	-8.56	-2.13	-12.57	-0.32	-2.12	-8.58	-12.57
F8	150	-8.75	-3.71	-13.93	-0.15	-3.71	-8.76	-13.93
G1	335	-2.64	-5.04	2.30	-1.10	2.30	-2.21	-5.46
G2	336	-2.09	-3.12	2.45	-0.40	2.45	-1.96	-3.26
G3	337	-1.51	-1.80	2.55	0.14	2.55	-1.45	-1.86
G4	338	-1.65	-0.02	2.66	0.16	2.66	-0.01	-1.67
G5	339	-1.12	2.85	3.18	-0.77	3.18	3.00	-1.26
G6	340	-2.46	-0.36	2.31	-0.82	2.31	-0.08	-2.74
H1	346	-14.37	0.98	-11.25	3.72	1.84	-11.25	-15.22
H2	347	-8.97	19.01	-6.54	2.47	19.23	-6.54	-9.18
H3	348	-9.47	19.52	-7.82	-2.63	19.76	-7.82	-9.71
H4	349	-8.50	10.58	-11.21	-3.30	11.14	-9.06	-11.21
H5	350	-8.60	2.42	-14.61	-2.28	2.87	-9.05	-14.61
I1	621	-0.23	6.65	2.45	-0.15	6.65	2.45	-0.23
I2	624	-0.10	7.80	2.49	0.06	7.80	2.49	-0.10
J1	635	-0.26	20.36	3.12	-0.33	20.36	3.12	-0.26
J2	638	-0.02	27.66	2.12	0.18	27.66	2.12	-0.02
K1	841	-0.23	18.68	-0.27	-0.09	18.68	-0.24	-0.27
K2	844	-0.07	22.10	2.48	0.12	22.10	2.48	-0.07
L1	855	-0.14	42.12	2.18	-0.21	42.12	2.18	-0.14
L2	858	0.04	45.96	1.54	0.14	45.96	1.54	0.04
M1	941	-0.23	27.19	-0.67	0.01	27.19	-0.23	-0.67
M2	944	-0.11	31.46	2.37	0.06	31.46	2.37	-0.11
N1	955	-0.16	59.71	2.04	-0.12	59.71	2.04	-0.16
N2	9.58	0.02	64.41	2.34	0.11	65.41	2.34	0.02
O1	1101	-0.24	31.14	-0.98	0.00	31.14	-0.24	-0.98
O2	1104	-0.15	35.76	2.01	0.01	35.76	2.01	-0.15

Table 2.10.10-31 Primary Plus Secondary Stresses; 30-Foot Side Drop; $\phi = 90°$; 1.20-Inch Outer Shell Thickness; Circumferential Location = 0° (continued)

Stress Points		Stresses (ksi)						
Location	Node	S_X	S_Y	S_Z	S_{XY}	S_1	S_2	S_3
P1	1115	-0.22	70.50	1.79	0.01	70.50	1.79	-0.22
P2	1118	0.02	77.67	3.29	-0.01	77.67	3.29	0.02
Q1	1261	-0.23	28.81	-0.36	0.02	28.81	-0.23	-0.36
Q2	1264	-0.08	33.16	2.56	-0.04	33.16	2.56	-0.08
R1	1275	-0.18	58.75	0.17	0.12	58.75	0.17	-0.18
R2	1278	0.01	65.39	3.49	-0.11	65.39	3.49	0.01
S1	1561	-0.22	8.19	1.88	0.23	8.20	1.88	-0.22
S2	1564	-0.17	12.54	3.74	0.08	12.54	3.74	-0.17
T1	1575	-0.24	30.33	1.07	0.19	30.33	1.07	-0.25
T2	1578	0.01	36.29	4.55	-0.16	36.29	4.55	0.01
U1	1841	-0.13	-0.35	2.40	-0.07	2.40	-0.11	-0.37
U2	1844	0.55	1.78	2.15	-0.36	2.15	1.87	0.45
V1	1852	4.57	8.47	-2.48	-8.39	15.13	-2.09	-2.48
V2	1856	0.41	16.50	-3.03	0.70	16.53	0.38	-3.03
W1	1969	-43.69	-28.15	-16.24	-4.59	-16.24	-26.90	-44.95
W2	1970	-32.16	-0.68	-7.68	-5.18	0.15	-7.68	-32.99
W3	1971	-18.61	3.03	-5.77	-5.41	4.31	-5.77	-19.89
W4	1972	-13.86	7.42	-6.25	-4.51	8.33	-6.25	-14.78
W5	1973	-11.59	10.46	-6.94	-3.49	11.00	-6.94	-12.13
W6	1974	-10.31	13.15	-7.55	-2.47	13.41	-7.55	-10.57
W7	1975	-9.63	16.25	-8.23	-1.33	16.32	-8.23	-9.70
W8	1976	-9.42	20.23	-8.83	-0.51	20.24	-8.83	-9.43
X1	2370	-22.05	-8.63	-5.78	-0.21	-5.78	-8.63	-22.05
X2	2390	-9.10	-5.13	-1.06	1.41	-1.06	-4.68	-9.55
X3	2410	-6.66	-2.62	0.05	2.53	0.05	-1.40	-7.87
X4	2430	-3.61	-2.69	0.56	2.06	0.56	-1.04	-5.26
X5	2450	-2.29	-1.91	0.80	1.29	0.80	-0.80	-3.41
X6	2470	-1.44	-1.34	0.91	0.59	0.91	-0.81	-1.98
X7	2490	-0.94	-0.72	1.05	0.14	1.05	-0.65	-1.01
X8	2510	-0.63	-0.44	1.19	-0.05	1.19	-0.43	-0.65

Table 2.10.10-31 Primary Plus Secondary Stresses; 30-Foot Side Drop; $\phi = 90°$; 1.20-Inch Outer Shell Thickness; Circumferential Location = 0°° (continued)

Stress Points		Stresses (ksi)						
Location	Node	S_X	S_Y	S_Z	S_{XY}	S_1	S_2	S_3
X9	2530	-0.31	-0.20	1.38	-0.13	1.38	-0.12	-0.40
X10	2550	0.10	-0.07	1.64	-0.12	1.64	0.17	-0.13
X11	2570	1.40	-0.02	2.79	0.01	2.79	1.40	-0.02
Y1	2305	0.40	0.20	1.37	-0.25	1.37	0.57	0.03
Y2	2325	-1.94	0.08	0.73	-0.62	0.73	0.26	-2.11
Y3	2345	-3.92	0.09	0.43	-0.73	0.43	0.22	-4.04
Y4	2365	-5.62	0.12	0.22	-0.25	0.22	0.13	-5.64
Y5	2385	-6.17	0.00	0.21	0.54	0.21	0.04	-6.21
Y6	2405	-5.57	-0.28	0.33	1.16	0.33	-0.03	-5.82
Y7	2425	-4.54	-0.57	0.44	1.41	0.44	-0.12	-4.99
Y8	2445	-3.56	-0.73	0.55	1.40	0.55	-0.16	-4.13
Y9	2465	-2.82	-0.66	0.69	1.29	0.69	-0.07	-3.42
Y10	2485	-2.34	-0.42	0.96	1.11	0.96	0.09	-2.85
Y11	2505	-2.20	-0.31	1.12	1.02	1.12	0.14	-2.64
Y12	2525	-1.87	-0.15	1.36	0.76	1.36	0.14	-2.16
Y13	2545	-1.45	-0.02	1.65	0.41	1.65	0.09	-1.56
Y14	2565	-0.03	0.03	2.81	0.26	2.81	0.26	-0.26
Z1	2301	-1.18	0.09	1.19	-0.01	1.19	0.09	-1.18
Z2	2321	-1.98	0.11	1.02	-0.04	1.02	0.11	-1.98
Z3	2341	-2.81	0.22	0.92	-0.04	0.92	0.22	-2.81
Z4	2361	-3.51	0.32	0.86	0.01	0.86	0.32	-3.51
Z5	2381	-3.89	0.37	0.82	0.07	0.82	0.37	-3.89
Z6	2401	-3.91	0.38	0.78	0.15	0.78	0.38	-3.91
Z7	2421	-3.62	0.35	0.76	0.21	0.76	0.36	-3.63
Z8	2441	-3.10	0.29	0.78	0.25	0.78	0.31	-3.12
Z9	2461	-2.47	0.22	0.88	0.36	0.88	0.27	-2.52
Z10	2481	-1.80	0.16	1.07	0.77	1.07	0.42	-2.06
Z11	2501	-1.46	0.09	1.25	1.88	1.35	1.25	-2.72
Z12	2521	-1.14	0.07	1.45	5.35	4.85	1.45	-5.91
Z13	2541	-0.86	0.05	1.67	23.86	23.45	1.67	-24.27
Z14	2561	0.13	0.05	2.73	31.16	31.25	2.73	-31.07

Table 2.10.10-32 Primary Membrane (P_m) Stresses; 30-Foot Side Drop; $\phi = 90°$; 1.20-Inch Outer Shell Thickness; Circumferential Location = 0°

		Stresses* (ksi)							
Section	Node to Node	S_x	S_y	S_z	S_{xy}	S_1	S_2	S_3	SI
A	177 – 327	-7.70	-1.71	1.90	-0.46	1.90	-1.67	-7.73	9.64
B	4 – 104	-6.52	-1.60	0.11	-0.89	0.11	-1.45	-6.68	6.79
C	10 – 110	-7.99	-0.43	-2.04	0.44	-0.41	-2.04	-8.02	7.61
D	185 – 335	-8.94	-0.19	-3.00	-0.36	-0.18	-3.00	-8.96	8.78
E	18 – 118	-9.09	1.24	-5.45	-0.07	1.24	-5.45	-9.09	10.32
F	143 – 150	-4.72	0.37	-9.86	-0.80	0.49	-4.85	-9.86	10.35
G	335 – 340	-5.06	-1.34	-2.30	0.85	-1.16	-2.30	-5.25	4.09
H	346 – 350	-6.40	6.28	-11.46	-0.50	6.30	-6.42	-11.46	17.76
I	621 – 624	-0.16	5.08	2.22	-0.06	5.08	2.22	-0.16	5.23
J	635 – 638	-0.14	14.95	2.52	-0.12	14.95	2.52	-0.14	15.08
K	841 – 844	-0.17	18.35	1.15	0.03	18.35	1.15	-0.17	18.51
L	855 – 858	-0.04	34.99	1.94	-0.02	34.99	1.94	-0.04	35.03
M	941 – 944	-0.19	27.29	0.90	0.03	27.29	0.90	-0.19	27.48
N	955 – 958	-0.07	53.54	2.29	0.01	53.54	2.29	-0.07	53.61
O	1101 – 1104	-0.21	31.42	0.56	0.00	31.42	0.56	-0.21	31.63
P	1115 – 1118	-0.10	65.09	2.67	0.00	65.09	2.67	-0.10	65.18
Q	1261 – 1264	-0.17	28.95	1.12	-0.01	28.95	1.12	-0.17	29.12
R	1275 – 1278	-0.09	53.03	2.05	0.00	53.03	2.05	-0.09	53.13
S	1561 – 1564	-0.17	8.21	2.45	0.12	8.22	2.45	-0.17	8.39
T	1575 – 1578	-0.14	24.25	2.83	0.06	24.25	2.83	-0.14	24.39
U	1841 – 1846	0.51	0.49	2.13	-0.18	2.13	0.68	0.32	1.81
V	1852 – 1856	4.77	14.30	-1.86	-2.58	14.95	4.11	-1.86	16.81
W	1969 – 1976	20.74	3.86	-9.26	-3.37	4.32	-9.26	-21.20	25.51
X	2370 –2570	-3.97	-1.82	0.18	1.06	0.18	-1.38	-4.40	4.59
Y	2305 – 2565	-3.07	-0.06	1.14	0.53	1.14	0.03	-3.16	4.29
Z	2301 – 2561	-2.26	0.16	1.36	2.22	1.48	1.36	-3.58	5.06

* Stresses are taken at 0 degrees (under the load) at each section.

Table 2.10.10-33 Primary Membrane Plus Primary Bending ($P_m + P_b$) Stresses; 30-Foot Side Drop; $\phi = 90°$; 1.20-Inch Outer Shell Thickness; Circumferential Location = 0°

		Stresses* (ksi)							
Section	Node to Node	S_x	S_y	S_z	S_{xy}	S_1	S_2	S_3	SI
A	177 – 327	-16.88	-3.68	0.56	-3.01	0.56	-3.03	-17.54	18.10
B	4 – 104	-10.00	-3.37	-3.11	-1.31	-3.11	-3.12	-10.25	7.14
C	10 – 110	-11.24	-0.89	-5.07	0.01	-0.89	-5.07	-11.24	10.36
D	185 – 335	-13.80	-1.54	-5.90	-0.01	-1.54	-5.90	-13.80	12.26
E	18 – 118	-8.66	2.96	-6.08	-0.84	3.03	-6.08	-8.73	11.75
F	143 – 150	-1.94	7.18	-3.59	-0.80	7.25	-2.01	-3.59	10.85
G	335 – 340	-9.47	-4.30	-4.96	0.85	-4.16	-4.96	-9.61	5.45
H	346 – 350	-5.16	16.66	-5.20	-0.50	16.67	-5.17	-5.20	21.87
I	621 – 624	-0.11	6.23	2.33	-0.06	6.23	2.33	-0.11	6.34
J	635 – 638	-0.03	19.66	2.20	-0.12	19.66	2.20	-0.03	19.69
K	841 – 844	-0.07	19.82	2.32	0.03	19.82	2.32	-0.07	19.88
L	855 – 858	0.04	36.61	1.34	-0.02	36.61	1.34	0.04	36.57
M	941 – 944	-0.11	29.12	2.15	0.03	29.12	2.15	-0.11	29.23
N	955 – 958	0.02	56.00	2.10	0.01	56.00	2.10	0.02	55.98
O	1101 – 1104	-0.15	33.42	1.80	0.00	33.42	1.80	-0.15	33.57
P	1115 – 1118	0.02	68.25	3.06	0.00	68.25	3.06	0.02	68.23
Q	1261 – 1264	-0.08	30.88	2.38	-0.01	30.88	2.38	-0.08	30.96
R	1275 – 1278	0.03	55.93	3.42	0.00	55.93	3.42	0.03	55.91
S	1561 – 1564	-0.15	9.98	3.22	0.12	9.98	3.22	-0.15	10.13
T	1575 – 1578	0.01	28.32	4.68	0.06	28.32	4.68	0.01	28.31
U	1841 – 1846	-0.15	0.09	2.90	-0.18	2.90	0.19	-0.24	3.15
V	1852 – 1856	10.17	18.66	1.89	-2.58	19.39	9.45	1.89	17.50
W	1969 – 1976	-42.95	-14.16	-10.81	-3.37	-10.81	-13.77	-43.34	32.53
X	2370 – 2570	-11.33	-4.07	-1.38	1.72	-1.38	-3.68	-11.72	10.34
Y	2305 – 2565	-2.48	-0.39	1.60	1.55	1.60	0.43	-3.30	4.90
Z	2301 – 2561	-1.60	0.12	1.68	8.10	7.40	1.68	-8.88	16.29

* Stresses are taken at 0 degrees (under the load) at each section.

Table 2.10.10-34 Primary Membrane (P_m) Stresses; 30-Foot Side Drop; $\phi = 90°$; 1.20-Inch Outer Shell Thickness; Circumferential Location = 90°

		Stresses* (ksi)									
Section	Node to Node	S_x	S_y	S_z	S_{xy}	S_{yz}	S_{xz}	S_1	S_2	S_3	SI
A	177 – 327	1.27	-0.03	-4.99	0.02	-2.03	-0.91	1.50	0.56	-5.81	7.32
B	4 – 104	1.13	-0.01	-4.30	0.04	1.07	-0.94	1.30	0.21	-4.69	5.99
C	10 – 110	0.76	0.00	-3.08	0.07	0.23	-2.17	1.74	0.01	-4.07	5.81
D	185 – 335	0.76	0.42	-3.12	0.09	-1.46	-2.31	2.17	0.43	-4.53	6.70
E	18 – 118	0.25	0.18	-1.51	0.05	-1.33	-2.17	2.08	0.15	-3.31	5.39
F	143 – 150	-0.06	0.11	-0.92	0.03	-3.30	0.23	2.94	-0.05	-3.76	6.70
G	335 – 340	0.90	0.62	-2.01	0.18	-1.63	-2.46	2.79	0.54	-3.82	6.62
H	346 – 350	-0.03	0.06	-0.41	0.01	-11.67	-5.75	12.83	-0.02	-13.19	26.02
I	621 – 624	-0.08	0.38	0.35	-0.09	-5.88	-0.06	6.24	-0.07	-5.51	11.75
J	635 – 638	0.00	0.30	0.03	0.00	-15.87	-0.06	16.03	0.00	-15.70	31.73
K	841 – 844	-0.01	-0.08	0.55	0.03	-3.80	-0.01	4.05	-0.01	-3.58	7.63
L	855 – 858	-0.01	0.23	-0.03	0.00	-12.09	-0.03	12.19	-0.01	-11.99	24.18
M	941 – 944	-0.01	0.05	0.54	0.00	-1.33	0.01	1.65	-0.01	-1.06	2.71
N	955 – 958	0.00	0.10	-0.01	0.00	-8.08	-0.01	8.12	0.00	-8.03	16.16
O	1101 - 1104	-0.01	0.06	0.54	0.00	-0.22	0.01	0.63	-0.01	-0.03	0.66
P	1115 – 1118	0.00	0.13	0.02	0.00	0.20	-0.01	0.28	0.00	-0.13	0.42
Q	1261 – 1264	-0.01	0.05	0.54	0.00	1.83	0.00	2.15	-0.01	-1.56	3.70
R	1275 – 1278	0.02	-0.28	0.07	-0.01	8.05	-0.01	7.95	0.02	-8.16	16.11
S	1561 – 1564	-0.04	-0.20	0.26	0.03	6.00	-0.06	6.04	-0.04	-5.98	12.02
T	1575 – 1578	0.01	-2.23	0.26	0.03	15.08	0.00	14.14	0.01	-16.11	30.26
U	1841 – 1846	-0.99	0.32	-1.39	0.10	2.40	0.24	2.03	-0.99	-3.10	5.13
V	1852 – 1856	-0.30	-2.02	0.51	0.15	11.13	-5.20	11.70	-0.50	-13.01	24.71
W	1969 – 1976	3.42	-1.82	-1.43	0.61	3.63	-0.54	3.50	2.01	-5.34	8.84
X	2370 – 2570	1.47	0.99	-1.44	-0.59	0.31	-0.61	2.00	0.60	-1.58	3.58
Y	2305 – 2565	1.32	0.21	-2.02	-0.24	-0.05	-0.33	1.40	0.17	-2.06	3.45
Z	2301 –2561	1.36	0.16	-2.25	0.00	-2.45	0.00	1.69	1.36	-3.78	5.47

* Stresses are taken at 0 degrees (under the load) of each section.

Table 2.10.10-35 Primary Membrane Plus Primary Bending ($P_m + P_b$) Stresses; 30-Foot Side Drop; $\phi = 90°$; 1.20-Inch Outer Shell Thickness; Circumferential Location = 90°

		Stresses* (ksi)									
Section	Node to Node	S_x	S_y	S_z	S_{xy}	S_{yz}	S_{xz}	S_1	S_2	S_3	SI
A	177 – 327	1.36	-0.05	-4.68	0.01	-1.81	-1.81	2.01	0.34	-5.72	7.73
B	4 – 104	1.56	-0.03	-4.19	0.00	1.14	-1.73	2.08	0.17	-4.92	7.00
C	10 – 110	0.79	-0.01	-3.02	0.06	0.38	-3.22	2.63	0.01	-4.89	7.52
D	185 – 335	1.41	1.07	-2.39	0.32	-2.90	-4.10	5.01	0.88	-5.81	10.82
E	18 – 118	0.56	0.41	-1.48	0.11	-2.93	-2.24	3.38	0.40	-4.28	7.66
F	143 – 150	0.01	0.47	-1.63	0.03	-3.30	0.23	2.89	0.02	-4.06	6.95
G	335 – 340	2.47	1.30	-2.16	0.18	-1.63	-2.46	3.83	1.43	-3.64	7.46
H	346 – 350	0.06	0.40	-0.45	0.01	-11.67	-5.75	12.96	0.12	-13.07	26.03
I	621 – 624	-0.07	0.88	0.78	-0.09	-5.88	-0.06	6.70	-0.07	-5.05	11.75
J	635 – 638	0.00	0.53	0.18	0.00	-15.87	-0.06	16.22	0.00	-15.51	31.73
K	841 – 844	-0.05	0.12	1.16	0.03	-3.80	-0.01	4.48	-0.05	-3.20	7.68
L	855 – 858	-0.01	0.08	-0.45	0.00	-12.09	-0.03	11.91	-0.01	-12.28	24.19
M	941 – 944	-0.05	0.24	1.25	0.00	-1.33	0.01	2.17	-0.05	-0.68	2.85
N	955 – 958	0.00	0.18	0.23	0.00	-8.08	-0.01	8.28	0.00	-7.88	16.16
O	1101 – 1104	-0.05	0.24	1.24	0.00	-0.22	0.01	1.28	0.20	-0.05	1.33
P	1115 – 1118	0.00	0.06	-0.29	0.00	0.20	-0.01	0.15	0.00	-0.38	0.54
Q	1261 – 1264	-0.05	0.24	1.25	0.00	1.83	0.00	2.65	-0.05	-1.16	3.81
R	1275 – 1278	0.02	0.11	1.33	-0.01	8.05	-0.01	8.80	0.02	-7.35	16.16
S	1561 – 1564	-0.03	-0.38	0.05	0.03	6.00	-0.06	5.84	-0.03	-6.18	12.02
T	1575 – 1578	0.01	-2.93	-0.46	0.03	15.08	0.00	13.43	0.01	-16.82	30.26
U	1841 – 1846	-0.11	0.72	-1.31	0.10	2.40	0.24	2.33	-0.12	-2.91	5.25
V	1852 – 1856	-0.03	-1.96	0.67	0.15	11.13	-5.20	11.83	-0.26	-12.89	24.72
W	1969 – 1976	9.68	2.99	-0.85	0.61	3.63	-0.54	9.74	5.17	-3.09	12.83
X	2370 – 2570	3.65	2.27	-2.21	-0.89	0.89	-1.63	4.59	1.84	-2.72	7.31
Y	2305 – 2565	1.21	0.23	-2.54	0.06	0.00	-0.55	1.30	0.22	-2.62	3.91
Z	2301 – 2561	1.67	0.12	-1.61	0.00	-9.29	0.00	8.58	1.67	-10.08	18.66

* Stresses are taken at 0 degrees (under the load) of each section.

Table 2.10.10-36 Primary Membrane (P_m) Stresses; 30-Foot Side Drop; $\phi = 90°$; 1.20-Inch Outer Shell Thickness; Circumferential Location = 180°

		Stresses* (ksi)									
Section	Node to Node	S_x	S_y	S_z	S_{xy}	S_{yz}	S_{xz}	S_1	S_2	S_3	SI
A	177 – 327	-2.36	1.64	0.62	0.45	0.00	0.00	1.69	0.62	-2.41	4.10
B	4 – 104	-2.77	1.44	2.05	0.76	0.00	0.00	2.05	1.58	-2.91	4.96
C	10 – 110	-1.99	0.44	2.92	-0.68	0.00	0.00	2.92	0.62	-2.16	5.09
D	185 – 335	-1.86	0.13	3.49	0.27	0.00	0.00	3.49	0.17	-1.90	5.39
E	18 – 118	-0.99	-1.22	3.41	-0.43	0.00	0.00	3.41	-0.66	-1.55	4.96
F	143 – 150	-0.70	-1.20	4.44	0.21	0.00	0.00	4.44	-0.63	-1.27	5.71
G	335 – 340	-4.22	-0.41	1.36	-0.02	0.00	0.00	1.36	-0.41	-4.22	5.58
H	346 – 350	-5.62	-7.07	2.37	-2.99	0.00	0.00	2.37	-3.27	-9.42	11.79
I	621 – 624	-0.01	-5.43	-0.64	0.13	0.00	0.00	-0.01	-0.64	-5.43	5.42
J	635 – 638	0.15	-16.16	-3.10	0.11	0.00	0.00	0.15	-3.10	-16.16	16.32
K	841 – 844	-0.07	-18.02	-0.15	0.03	0.00	0.00	-0.07	-0.15	-18.02	17.95
L	855 – 858	0.06	-35.26	-1.88	0.03	0.00	0.00	0.06	-1.88	-35.26	35.32
M	941 – 944	-0.05	-27.22	0.12	-0.03	0.00	0.00	0.12	-0.05	-27.22	27.34
N	955 – 958	0.07	-53.61	-2.26	0.00	0.00	0.00	0.07	-2.26	-53.61	53.68
O	1101 – 1104	-0.02	-31.36	0.46	0.00	0.00	0.00	0.46	-0.02	-31.36	31.82
P	1115 – 1118	0.09	-65.21	-2.71	0.00	0.00	0.00	0.09	-2.71	-65.21	65.30
Q	1261 – 1264	-0.06	-28.88	-0.10	0.00	0.00	0.00	-0.06	-0.10	-28.88	28.81
R	1275 – 1278	0.06	-52.34	-2.20	0.02	0.00	0.00	0.06	-2.20	-52.34	52.40
S	1561 – 1564	0.00	-7.47	-0.83	-0.17	0.00	0.00	0.00	-0.83	-7.47	7.47
T	1575 – 1578	0.11	-19.27	-3.16	-0.09	0.00	0.00	0.11	-3.16	-19.27	19.39
U	1841 – 1846	0.98	-1.06	2.15	0.05	0.00	0.00	2.15	0.98	-1.06	3.22
V	1852 – 1856	-4.17	-9.23	0.78	2.62	0.00	0.00	0.78	-3.06	-10.34	11.12
W	1969 – 1976	-2.02	-0.11	0.97	0.07	0.00	0.00	0.97	-0.11	-2.02	3.00
X	2370 – 2570	-1.53	-1.48	0.89	0.20	0.00	0.00	0.89	-1.30	-1.71	2.60
Y	2305 – 2565	-1.52	0.04	1.21	-0.07	0.00	0.00	1.21	0.04	-1.52	2.73
Z	2301 – 2561	-2.26	0.16	1.36	-2.22	0.00	0.00	1.48	1.36	-3.58	5.06

* Stresses are taken at 0 degrees (under the load) of each section.

Table 2.10.10-37 Primary Membrane Plus Primary Bending ($P_m + P_b$) Stresses; 30-Foot Side Drop; $\phi = 90°$; 1.20-Inch Outer Shell Thickness; Circumferential Location = 180°

		Stresses* (ksi)									
Section	Node to Node	S_x	S_y	S_z	S_{xy}	S_{yz}	S_{xz}	S_1	S_2	S_3	SI
A	177 – 327	-10.98	-0.42	-0.59	-2.11	0.00	0.00	-0.02	-0.59	-11.39	11.37
B	4 – 104	-5.81	-0.09	-0.01	0.78	0.00	0.00	0.01	-0.01	-5.91	5.92
C	10 – 110	-3.97	0.010	1.26	-0.62	0.00	0.00	1.26	0.11	-4.07	5.33
D	185 – 335	-6.48	-1.22	0.47	0.03	0.00	0.00	0.47	-1.21	-6.48	6.96
E	18 – 118	-2.52	-2.83	3.24	-0.77	0.00	0.00	3.24	-1.88	-3.46	6.70
F	143 – 150	0.81	-4.81	4.46	0.21	0.00	0.00	4.46	0.82	-4.82	9.27
G	335 – 340	-7.62	-0.86	1.22	-0.02	0.00	0.00	1.22	-0.86	-7.62	8.84
H	346 – 350	-12.20	-16.96	-2.69	-2.99	0.00	0.00	-2.69	-10.76	-18.40	15.71
I	621 – 624	0.03	-6.68	-1.18	0.13	0.00	0.00	0.04	-1.18	-6.68	6.72
J	635 – 638	0.00	-19.78	-4.04	0.11	0.00	0.00	0.00	-4.04	-19.78	19.79
K	841 – 844	-0.07	-18.98	0.27	0.03	0.00	0.00	0.27	-0.07	-18.98	19.25
L	855 – 858	-0.05	-37.16	-2.24	0.03	0.00	0.00	-0.05	-2.24	-37.16	37.11
M	941 – 944	-0.02	-28.54	0.67	-0.03	0.00	0.00	0.67	-0.02	-28.54	29.21
N	955 – 958	-0.02	-56.22	-2.56	0.00	0.00	0.00	-0.02	-2.56	-56.22	56.19
O	1101 – 1104	0.02	-32.86	1.01	0.00	0.00	0.00	1.01	0.02	-32.86	33.88
P	1115 – 1118	-0.01	-68.24	-2.47	0.00	0.00	0.00	-0.01	-2.47	-68.24	68.23
Q	1261 – 1264	-0.05	-30.30	0.44	0.00	0.00	0.00	0.44	-0.05	-30.30	30.74
R	1275 – 1278	0.01	-54.47	-1.05	0.02	0.00	0.00	0.01	-1.05	-54.47	54.48
S	1561 – 1564	0.07	-8.63	-0.90	-0.17	0.00	0.00	0.08	-0.90	-8.63	8.71
T	1575 – 1578	-0.01	-22.01	-3.35	-0.09	0.00	0.00	-0.01	-3.35	-22.01	22.00
U	1841 – 1846	0.02	-3.55	1.48	0.05	0.00	0.00	1.48	0.02	-3.55	5.03
V	1852 – 1856	-8.45	-16.56	-3.18	2.62	0.00	0.00	-3.18	-7.67	-17.33	14.15
W	1969 – 1976	-6.29	-1.31	0.67	0.07	0.00	0.00	0.67	-1.30	-6.29	6.96
X	2370 – 2570	-4.58	-3.65	0.14	0.63	0.00	0.00	0.14	-3.33	-4.90	5.04
Y	2305 – 2565	-2.72	0.03	0.92	-0.17	0.00	0.00	0.92	0.04	-2.73	3.65
Z	2301 – 2561	-1.60	0.12	1.68	-8.10	0.00	0.00	7.40	1.68	-8.88	16.28

* Stresses are taken at 0 degrees (under the load) of each section.

Table 2.10.10-38 Primary Membrane (P_m) and Primary Membrane Plus Primary Bending ($P_m + P_b$) Stress Qualification; 30-Foot Side Drop; $\phi = 90°$; 1.20-Inch Outer Shell Thickness; Circumferential Location = 0°

			P_m Stresses (ksi)			$P_m + P_b$ Stresses (ksi)		
Section	Node to Node	Max. Temp. (°F)	Allow. * 0.7 S_u	Calc.	MS	Allow. * 1.0 S_u	Calc.	MS
A	177 – 327	222	48.93	9.64	+Large	69.90	18.10	+2.86
B	4 – 104	215	49.18	6.79	+Large	70.25	7.14	+Large
C	10 – 110	212	49.28	7.61	+Large	70.40	10.35	+Large
D	185 – 335	221	48.96	8.78	+Large	69.95	12.26	+Large
E	18 – 118	208	49.42	10.32	+3.79	70.60	11.75	+Large
F	143 – 150	209	49.38	10.35	+3.77	70.55	10.85	+Large
G	335 – 340	221	48.96	4.09	+Large	69.95	5.45	+Large
H	346 – 350	212	49.28	17.76	+1.77	70.40	21.87	+2.22
I	621 – 624	222	48.93	5.23	+Large	69.90	6.34	+Large
J	635 – 638	199	49.73	15.08	+2.30	71.04	19.69	+2.61
K	841 – 844	232	68.49	18.51	+2.70	97.84	19.88	+3.92
L	855 – 858	204	69.50	35.03	+0.98	99.29	36.57	+1.72
M	941 – 944	247	67.94	27.48	+1.47	97.06	29.23	+2.32
N	955 – 958	211	69.25	53.61	+0.29	98.93	55.98	+0.77
O	1101 – 1104	255	67.65	31.63	+1.14	96.64	33.57	+1.88
P	1115 – 1118	216	69.07	65.18	+0.06	98.67	68.23	+0.45
Q	1261 – 1264	251	67.79	29.12	+0.30	96.85	30.96	+2.13
R	1275 – 1278	216	69.07	53.13	+0.30	98.67	55.91	+0.76
S	1561 – 1564	217	49.10	8.39	+Large	70.15	1013	+Large
T	1575 – 1578	197	49.78	24.39	+1.04	71.12	28.31	+1.51
U	1841 – 1846	212	49.28	1.81	+Large	70.40	3.15	+Large
V	1852 – 1856	205	49.53	16.81	+1.95	70.75	17.50	+3.04
W	1969 – 1976	198	49.76	25.51	+0.95	71.08	32.53	+1.19
X	2370 – 2570	201	49.66	4.59	+Large	70.95	10.34	+Large
Y	2305 – 2565	205	49.53	4.29	+Large	70.75	4.90	+Large
Z	2301 – 2561	204	49.56	5.06	+Large	70.80	16.29	+3.35

* Allowable stresses for sections "K" through "R" are taken from Type XM-19 stainless steel; all others are from Type 304 stainless steel.

2.10.11 Hand Calculation for the 30-Foot Drop Accident Conditions

2.10.11.1 Top End Drop

The hand-calculation method is used to evaluate the stresses for a 30-foot top end drop condition. Only the stress at the midsection of the cask is evaluated. The hand-calculated stress results can be used to verify the accuracy of the finite element calculations and vice versa.

The NAC-LWT cask is considered as a hollow, circular cylinder, which contains the inner, lead and outer shells, and is subjected to a 30-foot top end impact as shown in Figure 2.10.11-1. A free body diagram (shown below) is provided for the portion of the cask above section "P-P," which is located 100.5 inches from the cask bottom.

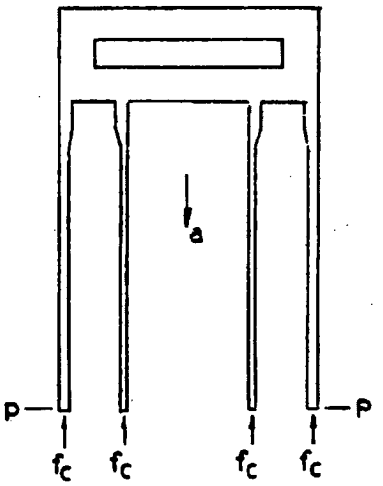

The axial (compressive) stresses developed in the cask at section "P-P" are calculated by using the following formula:

$$f_c = \frac{W}{A}$$

where:

W = cask weight above sections "O-O" and "P-P," but not including the weight of the lead shell (Figure 2.10.11-1)

= 5,440 lbs

A = cross-sectional areas of the stainless steel inner and outer shells

$= \pi(14.30752 - 13.18752 + 7.43752 - 6.68752)$

$= 130.03\ in^2$

W is obtained from the following calculations. Table 2.10.11-1 presents the geometric dimensions of the cask.

$W = W_9 + W_8 + W_7 + W'_6 + W'_4$ (W'_4 through W_9 are the weights of components 4 through 9 as shown in Figure 2.10.2-5.)

where:

$W_9 = \pi \times 10.375^2 \times 3 \times 0.41$

$= 416$ lbs

$W_8 + W_7 = (\pi \times 14.3075^2 \times 10.5 - \pi \times 10.3752 \times 3)(0.288)$

$= 1{,}653$ lbs

$W'_6 = \pi (14.307^2 - 13.1875^2)(100.5 - 10.5)(0.288)$

$= 2{,}508$ lbs

$W'_4 = \pi (7.4375^2 - 6.6875^2)(100.5 - 10.5)(0.288)$

$= 863$ lbs

The compressive stress at the midpoint (±) of the cask resulting from its mass is:

$$f_c = \frac{-5440}{130.03} = -41.84 \text{ psi}$$

This compressive stress results from a 1 g cask weight load. To account for a 30-foot top end drop condition, multiply this result by 76.8 g. The 76.8 g is derived from the multiplication of 60 g (Table 2.6.7-34) by the factor 48,000/37,519, where 48,000 lbs is the cask body design weight and 37,519 lbs is the model weight.

$f_c = 76.8 (-41.84) = -3{,}213$ psi

The compressive stresses[1] at sections "O-O" and "P-P" calculated by the finite element method are -3,260 psi and -2,990 psi, respectively, with an average of -3,125 psi. The difference between the hand calculation and the finite element stresses is 3 percent, which compares favorably as expected.

2.10.11.2 Side Drop

The hand-calculation method is used to evaluate the stresses for the 30-foot side drop condition. The hand-calculated stress results can be used to verify the accuracy of the finite element

[1] Table 2.10.10-4 documents the compressive stresses, SY, for sections "O-O" and "P-P."

calculations and vice versa. Because of the limitation of the hand-calculation method, only the stress results at the most critical region (the central portion of the cask outer shell) are evaluated.

The cask structure is considered as a hollow, circular, cross-sectional beam that is simply supported at each end of the cask centerline and is subject to internal pressure and impact and inertial loads. The classical beam theory method is used to calculate the bending stress resulting from impact and inertial loads for a 30-foot side drop condition:

$$\sigma_b = \frac{M_c}{I_{eff}}$$

where:

σ_b = bending stress

M = bending moment in the cask

C = radial distance between the cask centerline and the selected point (location) in the cask

I_{eff} = effective moment of inertia of the cask

The geometric dimensions of the cask are:

Inner Shell (I.S.)	r_i	=	inner radius = 6.6875 inches
	r_o	=	outer radius = 7.4375 inches
	E_s	=	Young's modulus (stainless steel)
		=	27.3×10^6 psi at 250°F
Lead	r_i	=	inner radius = 7.4375 in
	r_o	=	outer radius = 13.133 in
	E_L	=	Young's modulus (lead)
		=	2.0×10^6 psi at 250°F
Outer Shell (O.S.)	r_i	=	inner radius = 13.188 in
	r_o	=	outer radius = 14.387 in
	E_s	=	Young's modulus (stainless steel)
		=	27.3×10^6 psi at 250°F

The effective bending rigidity, $(EI)_{eff}$, of the cask is:

$$(EI)_{eff} = (EI)_{I.S.} + (EI)_{Lead} + (EI)_{O.S.}$$

$$\frac{\pi}{4}[(7.4375^4 - 6.6875^4)(27.3 \times 10^6)$$

$$+ (13.1334 - 7.43754)(2.0 \times 10^6)$$

$+(14.3874 - 13.1884)(27.3 \times 10^6]$

$= 3.347 \times 10^{11}$ lb-in^2

The effective moment of inertia for the cask is:

$$I_{eff} = \frac{(EI)_{eff}}{E_s} = \frac{3.347 \times 10^{11}}{27.3 \times 10^6} = 12{,}259 \text{ in}^4$$

The bending moments induced in the cask as a result of the 30-foot side drop condition are calculated by considering the following:

The cask weight without content (48,000 pounds), which is assumed to be uniformly distributed over the entire cask length of 199.75 inches.

The content weight (4000 pounds), which is uniformly distributed over the entire cask cavity length of 178 inches.

Impact loads (totaling 52,000 pounds), which are assumed to be uniformly distributed over the 12 inches at each end of the cask.

2.10.11.2.1 Case A

The bending moments at locations "J," "L," "N," "P," "R" and "T" in the cask are a result of the cask weight due to a 1 g load.[1]

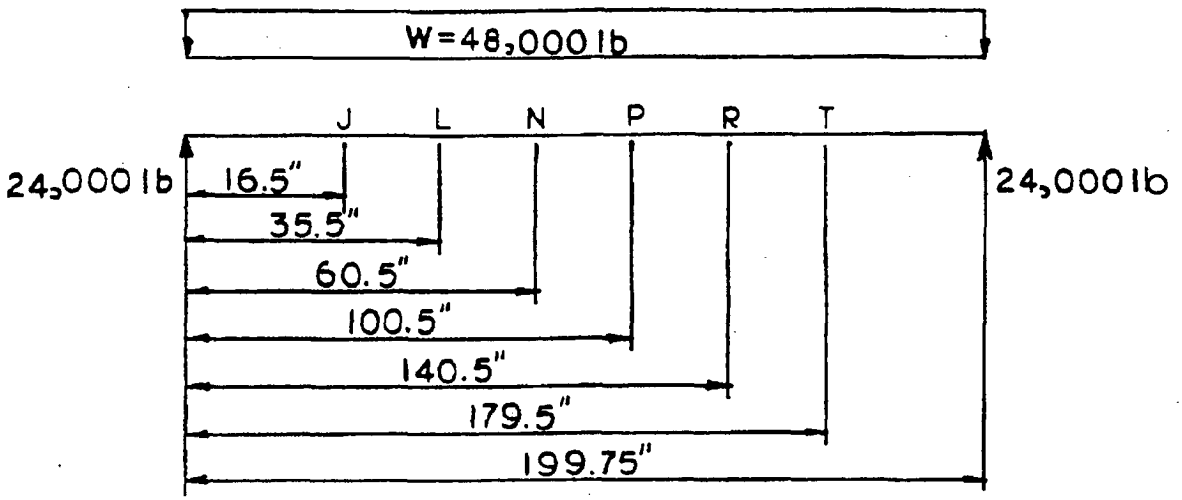

w = cask weight/total cask length $\frac{48{,}000}{199.75} = 240.30$ lb / in

[1] The g load factor for the 30-foot side drop condition is 49.7 g.

$$M_J = 24{,}000\ (16.5) - \frac{w(16.5^2)}{2} = 363{,}289\ \text{in} - \text{lb}$$

$$M_L = 24{,}000\ (33.5) - \frac{w(33.5^2)}{2} = 669{,}161\ \text{in} - \text{lb}$$

$$M_N = 24{,}000\ (60.5) - \frac{w(60.5^2)}{2} = 1{,}012{,}220\ \text{in} - \text{lb}$$

$$M_P = 24{,}000\ (100.5) - \frac{w}{2}(100.5^2) = 1{,}198{,}453\ \text{in} - \text{lb}$$

$$M_R = 24{,}000\ (140.5) - \frac{w(140.5^2)}{2} = 1{,}000{,}205\ \text{in} - \text{lb}$$

$$M_T = 24{,}000\ (179.5) - \frac{w(179.5^2)}{2} = 436{,}731\ \text{in} - \text{lb}$$

2.10.11.2.2 Case B

The bending moments at locations "J," "L," "N", "P," "R" and "T" are a result of the impact and content load due to a 1 g load.[1]

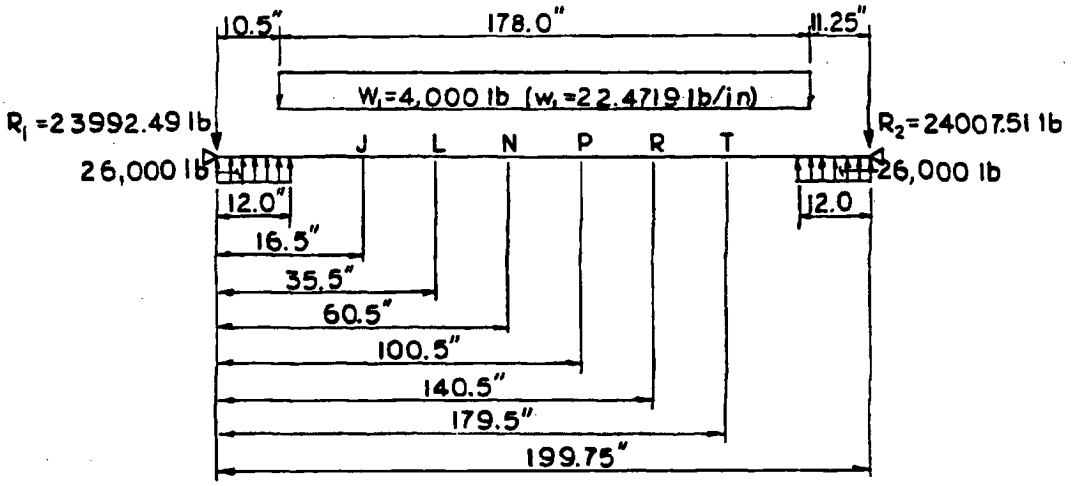

w_1 = content weight/cask cavity length = $\frac{4000}{178} = 22{,}472\ \text{lb/in}$

R_1 = reaction force at cask left end resulting from the impact and content loads

[1] The g load factor for the 30-foot side drop condition is 49.7 g.

$$M_J = 26{,}000\ (10.5) - 23{,}992.49\ (16.5) - \left(\frac{22.472}{2}\right)(6^2) = -123{,}281\ \text{in}-\text{lb}$$

$$M_L = 26{,}000\ (29.5) - 23{,}992.49\ (35.5) - \frac{w_1}{2}(25^2) = -91{,}756\ \text{in}-\text{lb}$$

$$M_N = 26{,}000\ (54.5) - R_1\ (60.5) - \frac{w_1}{2}\ (50^2) = -62{,}636\ \text{in}-\text{lb}$$

$$M_P = 26{,}000\ (94.5) - R_1\ (100.5) - \frac{w_1}{2}\ (90^2) = -45{,}256\ \text{in}-\text{lb}$$

$$M_R = 26{,}000\ (134.5) - R_1\ (140.5) - \frac{w_1}{2}\ (130^2) = -63{,}832\ \text{in}-\text{lb}$$

$$M_T = 26{,}000\ (173.5) - R_1\ (179.5 - \frac{w_1}{2}\ (169^2) = -116{,}562\ \text{in}-\text{lb}$$

The bending stresses in the cask are calculated by adding the bending moments resulting from cases A and B and by using the classical beam theory method:

$$\sigma_b = \frac{M_J C_i}{I_{eff}}$$

where:

M_J = summation of bending moments at location "J" as a result of Case A and Case B and so forth

C_i = radial distance between the cask centerline and the selected point

I_{eff} = 12,259 in^4

Table 2.10.11-2 gives the bending stresses in the cask, at different locations in the inner and outer shell regions, obtained by the above-mentioned hand-calculation method. Table 2.10.11-2 also provides the comparison of the hand-calculated and finite element stress results. At the midsection of the outer shell (location "P2" in Table 2.10.11-2), the bending stresses are 67,236 psi by the hand-calculation method and 68,230 psi by the finite element method. The difference in the stress results is less than 1.5 percent between these two methods. The stress comparison between these two methods is also provided for other locations, denoted as "K" through "O" and "Q" through "R". The average difference in the stress results between these two methods is acceptable.

In conclusion, the comparison is extremely favorable and indicates the following results:

- The finite element model was accurately constructed; the use of higher aspect ratio elements in the central portion of the finite element model does produce accurate stresses in the shells.
- The inertial weight of the cask was adequately represented in the finite element model analysis.

Figure 2.10.11-1 Mathematical Model of NAC-LWT Cask (30-Foot Top End Impact)

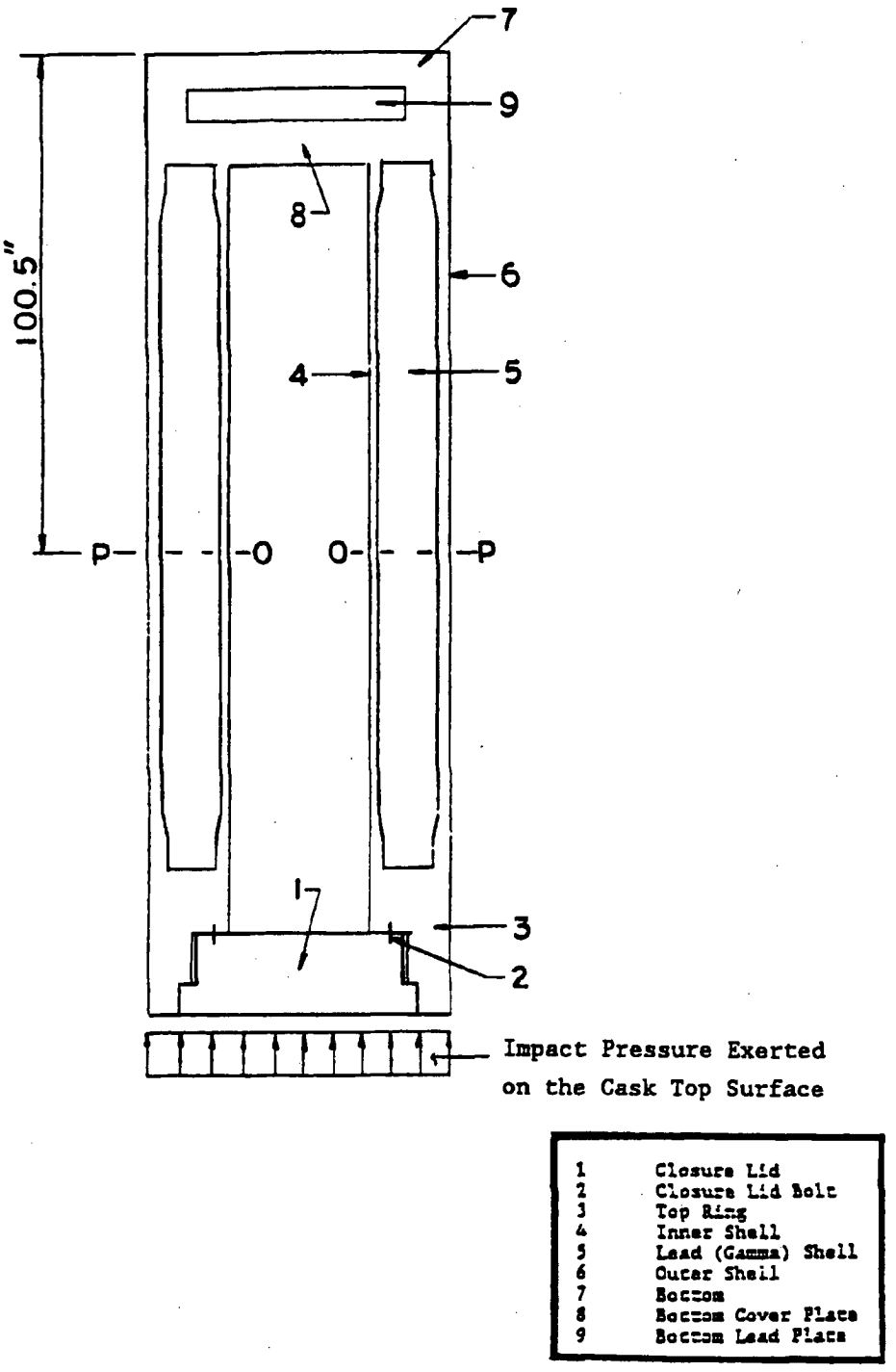

Table 2.10.11-1 Geometric Dimensions of the Cask

	Dimensions
Inner Shell (I.S.)	r_i = inner radius = 6.6875 in.
	r_o = outer radius = 7.4375 in.
	ρ_s = density for stainless steel = 0.288 lb/in^3
Outer Shell (O.S.)	r_i = inner radius = 13.1875 in.
	r_o = outer radius = 14.3075 in.
	ρ_s = density for stainless steel = 0.288 lb/in^3
Lead	ρ_L = density for lead = 0.41 lb/in^3

Table 2.10.11-2 Comparison of the Hand-Calculated and Finite Element Results

Location	C_i	Moments (in-lb)		σ_b (1 g)	Hand-Calculated	Finite[1] Element
		Case A	Case B		σ_b (49.7 g)	σ_b (49.7 g)
I1	6.6875	363,289	-123.281	130.90	6,504	3,820
I2	7.4375	363,289	-123.281	145.91	7,234	6,110
J1	13.188	363,289	-123.281	258.20	12,827	10,060
J2	14.387	363,289	-123.281	281.67	13,993	19,650
K1	6.6875	669,161	-91,756	314.98	15,648	16,700
K2	7.4375	669,161	-91,756	350.31	17,403	19,710
L1	13.188	669,161	-91,756	621.16	30,859	33,280
L2	14.387	669,161	-91,756	677.63	33,664	36,590
M1	6.6875	1,012,220	-62,636	518.01	25,735	25,270
M2	7.4375	1,012,220	-62,636	576.11	28,621	29,010
N1	13.188	1,012,220	-62,636	1021.54	50,750	50,990
N2	14.387	1,012,220	-62,636	1114.42	55,364	55,990
O1	6.6875	1,198,453	-45,256	629.09	31,253	29,220
O2	7.4375	1,198,453	-45,256	699.64	34,758	33,310
P1	13.188	1,198,453	-45,256	1240.58	61,632	61,810
P2	14.387	1,198,453	-45,256	1353.38	67,236	68,230
Q1	6.6875	1,000,205	-63,832	510.81	25,377	26,830
Q2	7.4375	1,000,205	-63,832	568.09	28,223	30,770
R1	13.188	1,000,205	-63,832	1007.33	50,044	50,030
R2	14.387	1,000,205	-63,832	1098.91	54,594	55,920
S1	6.6875	436,731	-116,562	174.65	8,677	6,330
S2	7.4375	436,731	-116,562	194.25	9,650	9,950
T1	13.188	436,731	-116,562	344.43	17,111	20,030
T2	14.387	436,731	-116,562	375.75	18,667	28,310

[1] The finite element stress values are taken from the SY stress category in Table 2.10.10-38.

2.10.12 Impact Limiter Force-Deflection Curves and Data

2.10.12.1 Potential Energy and Cask Drop Motion

The Code of Federal Regulations, 10 CFR 71, states that analyses must show that a licensed spent-fuel shipping cask is capable of sustaining a normal condition test (a 1-foot free drop) followed by a hypothetical accident test (a 30-foot free drop). This has conservatively been interpreted to mean, impact limiters must be designed to absorb or dissipate no less than the potential energy of the cask if dropped, in any orientation, from 31 feet onto an unyielding surface. When at rest on the unyielding surface (a datum surface), the cask has zero potential energy.

The distance through which the cask free falls is measured from the nearest point on the cask (either impact limiter) to the unyielding surface. This assures that center of gravity will translate a minimum of 31 feet before an impact limiter contacts the unyielding surface. Additionally, it is assumed that the cask will always seek a stable orientation after contacting the unyielding surface on both impact limiters. After an end drop, for example, the cask is assumed to tip over and reach a stable horizontal orientation.

Potential energy is calculated by multiplying the weight of the cask by the height to which the center of gravity of the cask was raised. The design weight of the cask, contents and impact limiters is 52,000 lbs. For these analyses, the NAC-LWT cask is assumed to be symmetric about the three major axes; therefore, the center of gravity is at the midpoint of the longitudinal centerline of the cask. The center of gravity is a datum point at which all the mass (weight) is located.

2.10.12.1.1 Translational Motion - Side Drop

Figure 2.10.12-1 shows the cask in the horizontal or side drop position. When released in this orientation from 31 feet (372 inches), the cask has 1.934×10^7 inch-pounds of potential energy. As shown by the heavy dashed lines in Figure 2.10.12-1, the cask translates vertically on an unyielding surface. The deceleration forces created when crushing the impact limiters opposes the translational motion of the cask. Impact limiter crushing continues until all the potential energy from the cask is absorbed; thereby, decelerating the cask to rest. Both impact limiters crush simultaneously in a side drop; therefore, once at rest, the cask is in a stable orientation.

In a side drop, the cask experiences only vertical, translational motion. Ignoring the energy stored elastically in the impact limiter during deceleration, the dissipated energy equals the initial potential energy of the cask. During the side drop, both impact limiters engage in

simultaneously decelerating the cask; therefore, each impact limiter absorbs the "energy absorbed by the first limiter" (El) as shown in Table 2.10.12-1.

2.10.12.1.2 Translational and End-Rotational Motion - End Drop

Figure 2.10.12-2 shows the cask in the end drop position. End drops are drop angles that range between 0 degrees (end drop) and 15 degrees (corner drop) and characteristically show translational and end-rotational motion. As in a side drop, a cask in the end drop position translates vertically through 31 feet and decelerates on the unyielding surface. Deceleration forces acting on the bottom of the cask are symmetric and uniform; therefore, the cask remains upright during deceleration and after the cask has come to rest. The energy absorbed by the single impact limiter while decelerating the cask (El, Table 2.10.12-1), equals the initial potential energy of the cask; however, the center of gravity is approximately 116.4 inches above the unyielding datum surface. The cask is metastable when resting on the crushed impact limiter. The cask has 6.04×10^6 inch-pounds more potential energy (EP) after the cask has come to rest. It has been assumed that the cask will seek a stable state, and a force is applied to the cask causing it to rotate on its end (crushed limiter). By tipping over, the cask will reach a stable orientation. The potential energy will be absorbed by the second impact limiter, as if the cask were in a side drop.

2.10.12.1.3 Translational, End-Rotational, Mid-Point Rotational Motion - Oblique Drops

Figure 2.10.12-3 shows the cask in an oblique drop orientation. Oblique drops are drop angles that range between 15 degrees (corner drop) and 90 degrees (side drop). The cask translates vertically after it is released, to the unyielding surface. The impact limiter, which contacts the unyielding surface first, decelerates the lower end of the cask, and brings its velocity to zero. Energy absorbed by the first limiter (El) decelerates the lower end of the cask to rest. The cask is now able to rotate or pivot on the stopped lower end. However, the energy absorbed by the first impact limiter is less than the initial energy of the cask, leaving the energy remaining (ER) to be absorbed by the second impact limiter.

Simultaneously during deceleration of the first or lower end of the cask, two other actions are taking place. First, the upper or free end of the cask rotates around the stopped end of the cask and continues to accelerate due to gravity. Second, a component of the deceleration force causes a torque perpendicular to the longitudinal axis of the cask, resulting in the cask beginning to rotate around the center of gravity. Both "actions" increase the energy to be absorbed by the second impact limiter.

During deceleration of the lower end of the cask, the upper end continues to accelerate while translating vertically because no deceleration force is applied to it. Newton's first law, "Every body persists in its state of rest or of uniform motion in a straight line unless it is compelled to

change that state by forces impressed on it..." (Resnick, page 75) requires the upper end to continue to translate vertically and continue to be accelerated by gravity until the second impact limiter contacts the unyielding surface. However, because the cask body is rigid, when the lower end of the cask stops, the upper end of the cask continues translating and the cask begins to pivot on the crushed impact limiter. This continues until the second impact limiter contacts the unyielding surface and significant deceleration forces are generated.

The second action, occurring while the lower end of the cask is decelerating, is a vector component of the deceleration force that causes the cask to rotate around its center of gravity. The deceleration force is always perpendicular to the unyielding surface. Depending on the cask angle, the deceleration force can be vectorially broken down into a force parallel to the longitudinal axis of the cask and a component perpendicular to the cask longitudinal axis. The perpendicular force component acts at a distance of approximately half the cask length. A torque, equivalent to the perpendicular force multiplied by half the cask length, attempts to spin the cask around the center of gravity. The "spin" or rotational velocity can also be thought of as rotational kinetic energy that must be absorbed by the second impact limiter. A detailed explanation of the torque and rotational kinetic energy is presented in Appendix 2.10.4.

Finally, the third component of energy that must be absorbed by the second impact limiter is the energy stored elastically in the first impact limiter. The elastically stored energy causes a force perpendicular to the unyielding surface to augment the rotational velocity of the cask and "lift" the first impact limiter, which is at rest.

Oblique drops have four distinct quantities of energy that need to be absorbed to bring the cask to rest in a stable, horizontal orientation.

- Potential energy absorbed by the impact limiter to strike the unyielding surface first (EI), which brings the translational velocity of the lower end of the cask to zero. The remaining potential energy (ER), also needs to be absorbed.
- Potential energy (EP), of the center of gravity, which results from its height above the unyielding surface.
- Rotational kinetic energy given to the cask as a result of the deceleration force and elastically stored energy (ES) from the impact that brings the lower end of the cask to rest.

2.10.12.2 Potential to Kinetic Energy Conversion

Just before the release, the cask is at rest and at a given drop angle. The uniform gravitational force constantly acts on the cask and when released, accelerates the cask at a constant rate. Gravitational acceleration (g) equals 32.2 ft/sec^2. No other forces act on the cask as it falls; therefore, no additional energy is supplied to the cask that must be dissipated by the impact limiters. Uniform forces acting on the cask mean the drop angle will not change while the cask

is falling. Since energy can not be created or destroyed, the initial potential energy of the cask is converted to kinetic energy. To calculate the velocity at the time the impact limiter contacts the unyielding surface, energy conversion is used in the following way:

$$PE = KE$$

or

$$mgh = \frac{1}{2}mv^2$$

Solving for v:

$$v = (2gh)^{0.5}$$

The initial velocity (at the time crushing begins) is a constant and is only a function of drop height. For a drop height of 31 feet, the velocity of the cask at the time an impact limiter contacts the unyielding surface is 44.7 feet/second.

The correlation between potential energy and kinetic energy is the foundation on which the computer program RBCUBED is based. Translational velocity (translational kinetic energy), which the cask gained while free falling or while pivoting on end (oblique drop), is directly attributable to the initial potential energy of the cask. Rotational velocity (rotational kinetic energy) is created during an oblique drop while decelerating the lower end of the cask; elastically stored energy is a small, calculable quantity of energy. When it is shown that the total energy absorbed is at least equal to the initial potential energy, the rotational kinetic energy and the stored energy of the cask, then the cask is at rest.

2.10.12.3 Deceleration Forces and Energy Absorption Calculation

The following quotation describes how an aluminum honeycomb impact limiter works: "...the kinetic energy of a body in motion is equal to the work it can do in being brought to rest..." (Resnick, page 75). The source of kinetic energy in a cask was established in Section 2.10.12.2. Work done by crush force is the magnitude of that force multiplied by the distance (deformation) through which the crush occurs. The units of work are in inch-pounds.

The NAC-LWT cask impact limiters are right cylindrical aluminum shells filled with aluminum honeycomb. Aluminum honeycomb is used to dissipate the kinetic energy of the cask. "Honeycomb" describes cells created when multiple corrugated thin aluminum sheets are bonded together. The honeycomb cells are designed to crush when a nominal force per unit area is applied to the honeycomb. Honeycomb is anisotropic. Honeycomb shows nominal crush strength in the plane, parallel with the corrugations and a greatly reduced crush strength perpendicular to the corrugations. Aluminum honeycomb is manufactured in batch blocks and

tested to ensure that the crush strength is within specified tolerances. Wedges of tested honeycomb are bonded together giving the impact limiter isotropic crush strength for all drop angles between 0 degrees (end drop) and 90 degrees (side drop). A thin aluminum exterior skin is bonded and seal welded to the honeycomb to prevent cosmetic and contamination damage to each impact limiter.

The aluminum honeycomb crushes because it is trapped between the cask and the unyielding surface. The initial energy (PE) of the cask will have an equivalent amount of kinetic energy (KE) just before the impact limiter contacts the unyielding surface. When the limiter contacts the unyielding surface, it immediately comes to rest; however, the cask continues to move into the impact limiter until it is opposed by a force vector. To explain the work done in stopping the cask, an illustrative example of the end drop is presented:

The cask is assumed to have been dropped 8.8 inches; PE = KE = 456,000 inch-pounds; cask velocity when the limiter contacts the unyielding surface is 6.9 feet/second (82.5 in/sec).

The cask is a rigid structure and each end has an area of approximately 651 square inches. Nominal crush strength of the honeycomb material is 3,500 psi. The cask is rigid and isolates ("backs") the honeycomb material that effectively stops the cask from that which does not. The force required to crush the backed honeycomb is 2.28×10^6 pounds. When the backed honeycomb crushes 0.1 inch, 228,000 inch-pounds of work is performed:

$$W = (F)(d)$$

where:

$F = 2.28 \times 10^6$ lbs

$d = 0.1$ in

Using the definition of work and Newton's second law, F = ma, yields the following derivation:

$$W = \frac{1}{2}mv^2 - \frac{1}{2}mv_o^2$$

where:

W = work performed on a particle, in-lb (Work performed on the cask by the honeycomb is negative.)

m = mass of the cask weight of the cask divided by the gravitational constant 32.2 ft/sec^2, lbf*sec^2/ft

v = velocity of the cask after the work is performed, ft/sec

v_o = initial velocity of the cask, ft/sec

Solving for the velocity after an incremental amount of work has been performed:

$$v = \sqrt{\frac{2W}{m} + v_o^2}$$

Substituting for W, m, v_o and adjusting for correct units, the cask velocity after the first crush increment is 4.91 feet/second. Repeating this analysis for another 0.1-inch increment, shows that the cask velocity diminishes to 0.76 feet/second, and after another fraction of a crush increment, the cask is stopped.

In summary, the force (a vector quantity) that is created by crushing the honeycomb opposes the velocity of the cask, which is also a vector quantity. Crushing an incremental amount of honeycomb is a finite quantity of work performed on the cask, decreasing its velocity and kinetic energy. Once the kinetic energy is completely dissipated, the cask velocity equals zero.

RBCUBED, the impact limiter computer program used to design the aluminum honeycomb impact limiters, functions in exactly the same way as the illustrative example. Cask geometry and weight, drop angle, crush increment, honeycomb crush strengths, honeycomb lock-up stroke and honeycomb geometry are input to the program. The computer calculates an initial velocity (as the limiter touches the unyielding surface), a backed area engaged in crushing, a crush force, the energy absorbed for a crush increment, the elapsed crush time and the cask velocity at the end of the crush increment. The computation cycle is repeated until all the kinetic energy is absorbed and the end of the cask is stopped.

RBCUBED calculates the energy dissipation necessary to stop the translational motion of the end of the cask that first contacts the unyielding surface (both limiters in the side drop). In Table 2.10.12-1, the energy dissipated while reducing the translational velocity of the first end to contact the unyielding surface is the energy absorbed by the first limiter (El). If El is less than the initial kinetic energy of the cask, the difference is reported by RBCUBED as "remaining energy," and shown in Table 2.10.12-1 as energy remaining after first impact (ER).

In oblique drops, at the instant the translational velocity of the first end to contact the unyielding surface is zero, the cask is in position 2 in Figure 2.10.12-3 (Rotation of the cask around its mid-point is addressed in Appendix 2.10.4). The center of gravity of the cask has a calculable potential energy, which is the energy that increases the velocity of the cask as it pivots on the crushed ("first") impact limiter. In Table 2.10.12-1, the potential energy, which equals the velocity gain as the cask pivots on end, is the potential energy of cask after first impact (EP).

The aluminum honeycomb dissipates energy while crushing, but elastically stores a small amount of the total energy dissipated. The quantity of elastically stored energy was determined by quasi-static testing of the scale model impact limiters (Section 2.10.12.5). The quantity of stored energy ranged between 5.3 percent (side drop) to 9.7 percent (end drop) of the total energy dissipated by the limiters tested. As stated above, once all the kinetic energy (El) has been

absorbed, the stored energy is released. The force, which the stored energy creates, tends to augment the torque attempting to cause the cask to spin around the center of gravity. This analysis has conservatively ignored the cask spinning and elected to absorb the energy in the second impact limiter. In Table 2.10.12-1, the elastically stored energy is the energy stored in the first limiter and absorbed in the second limiter while in the side drop orientation (ES).

In summary, lower end translational velocity is reduced to zero by absorbing an amount of energy (El). The cask will pivot over and absorb the remaining potential energy (ER), the potential energy due to rotation to a horizontal orientation (EP) and the elastically stored energy (ES) all in the second limiter in the side drop orientation. Table 2.10.12-1 shows that the four components of energy are absorbed by both impact limiters for drop angles from 0 degrees to 90 degrees.

2.10.12.4 RBCUBED Calculated Force-Deflection Graphs

Figure 2.10.12-4 through Figure 2.10.12-17 show the deceleration force as a function of crush depth, calculated using RBCUBED for the full-scale cask. Each graph is for either the top or bottom limiter, showing the plus and minus tolerance energy absorption profile. Graphs for the top end (0°), oblique (60°) and side (90°) are broken into simple geometric shapes to facilitate checking of the energy absorbed and maximum force. Quasi-static tests substantiate RBCUBED calculated values for the quarter-scale model limiters, as described in Section 2.10.12.5.

2.10.12.5 Quarter-Scale Model Quasi-Static Force-Deflection Tests

Quasi-static force-deflection tests were performed on quarter-scale model impact limiters used in drop testing a model earlier at Oak Ridge National Laboratories. Limiter samples were selected for a particular quasi-static test based on the limiter having no damage for test orientation. Three limiter orientations - 0 degrees, 15 degrees, 90 degrees - were tested. While each limiter tested was being compressed, two calibrated linear variable differential transformers (LVDT) mechanically attached to test fixtures provided data to an X - Y recorder, which plotted crush force as the impact limiter deformed. Deformation of the limiter proceeded well into honeycomb lock-up. As the force on the limiter decreased after the limiter locked up, force and deflection continued to be monitored, revealing the amount of elastically stored energy. Based on the results of the quasi-static tests, the energy absorption capacity of each limiter is presented in Figure 2.10.12-18 through Figure 2.10.12-20. The static force for each data point is multiplied by 1.196, a static to dynamic scaling factor, enabling comparison with RBCUBED computed values. The scaling factor is an average value established by manufacturers' tests. Figure 2.10.12-18 through Figure 2.10.12-20 show for comparison, the dynamically scaled forces and

RBCUBED computed values. These figures also clearly show the energy absorption capacity of each limiter and the potential energy absorption margins.

Figure 2.10.12-18 through Figure 2.10.12-20 also show the maximum deceleration forces that occur for each of the drop angles. RBCUBED calculated force values are higher in all cases except the end drop. Closer examination of the crushed impact limiter, quasi-statically tested in the end drop orientation, revealed a shearing previously unaccounted for, causing 10 percent higher forces than calculated by RBCUBED. The shearing and shear force generation occurs simultaneously with crushing, and is a small force compared with the crush force. Figure 2.10.12-21 shows a cross section of the crushed impact limiter, with the shear plane clearly visible. Table 2.10.12-2 compares the average maximum/peak forces and g-loads calculated using RBCUBED with corresponding values from each of the quasi-static tests. Force margins are also shown in Table 2.10.12-2 along with stress (structural) margins assuring that structural margins are satisfactory.

Figure 2.10.12-1 Side Drop (θ = 90°)

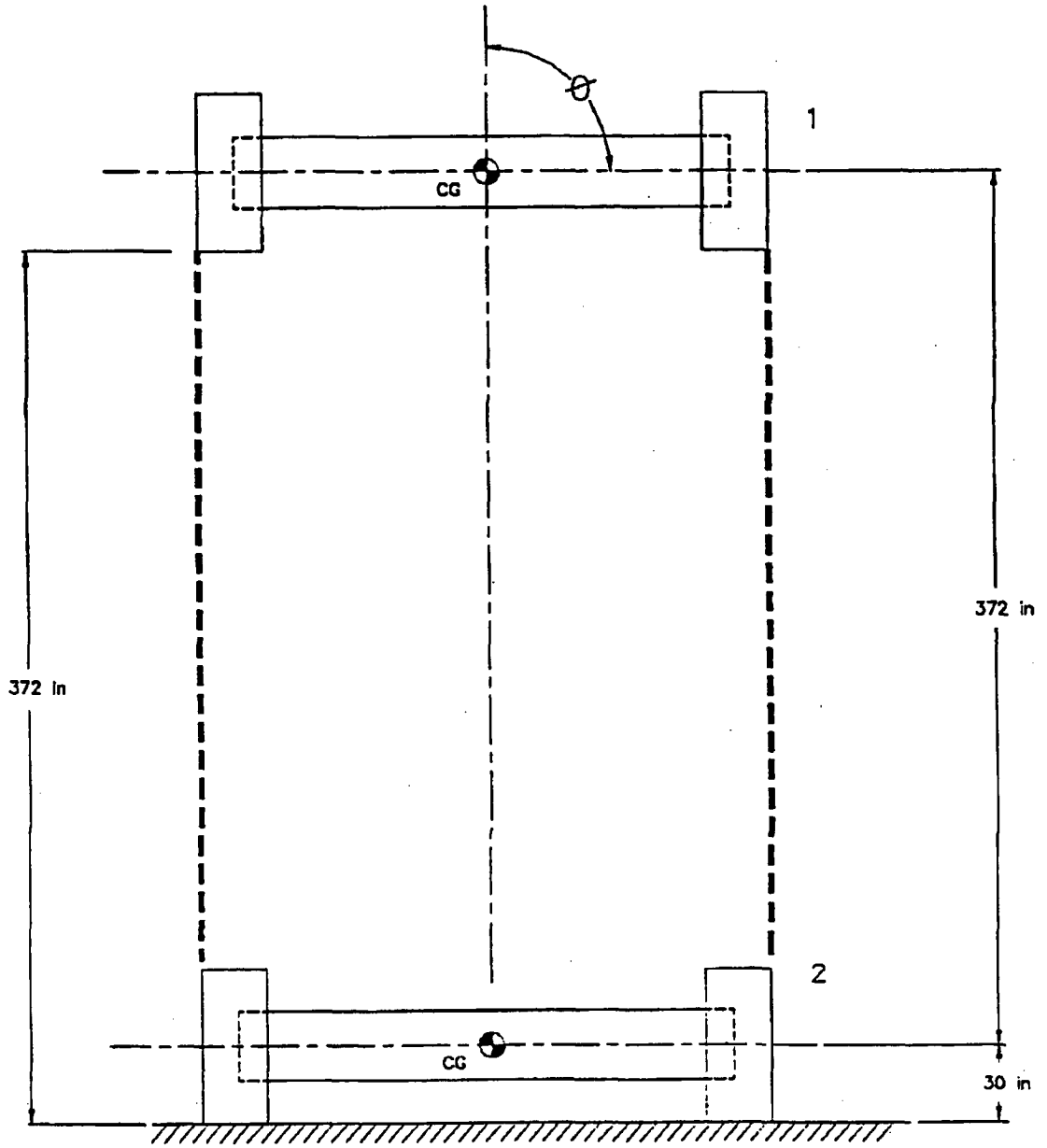

Figure 2.10.12-2 End Drop ($0° \leq \theta < 15°$)

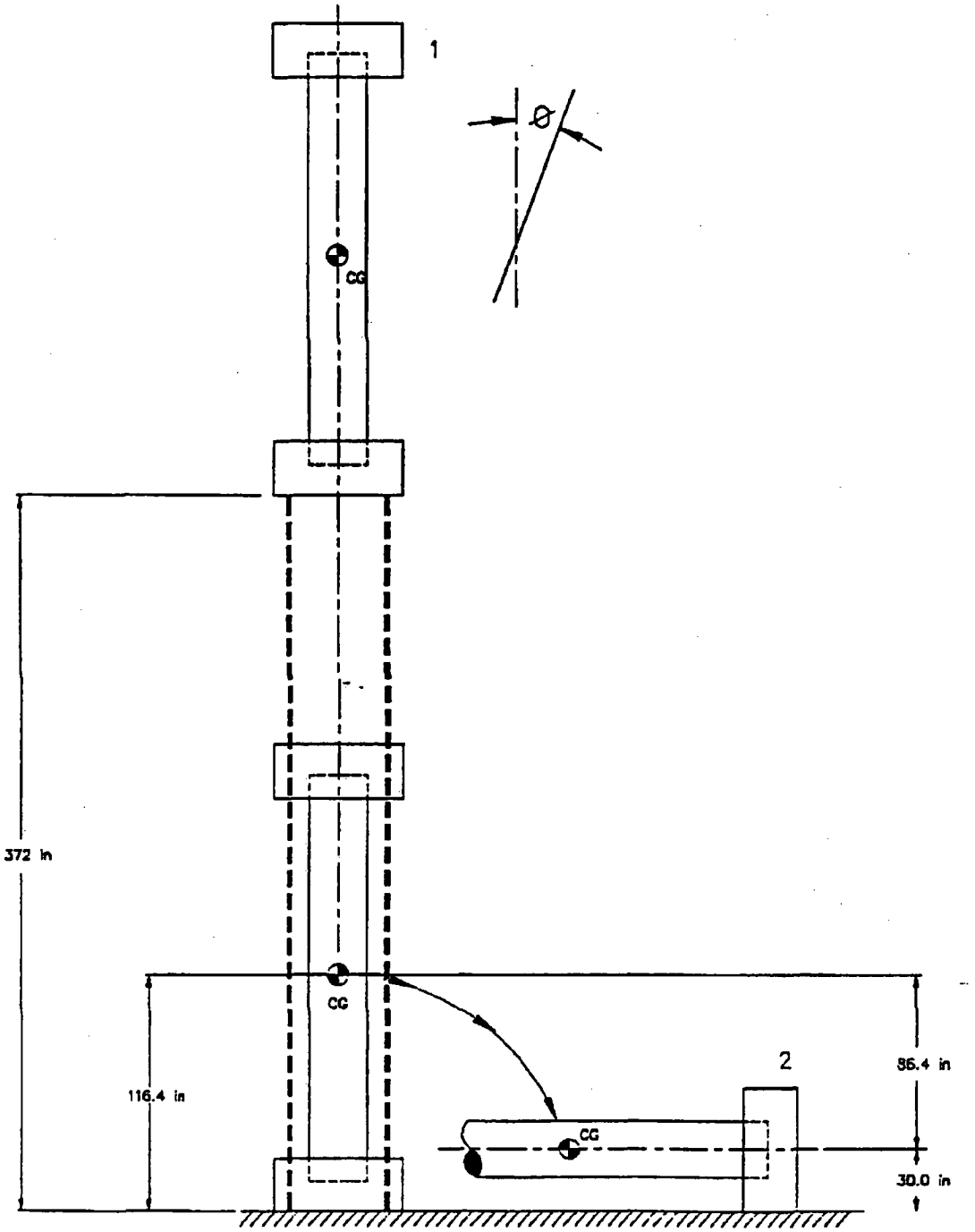

Figure 2.10.12-3 Oblique Drop ($15° \leq \theta < 90°$)

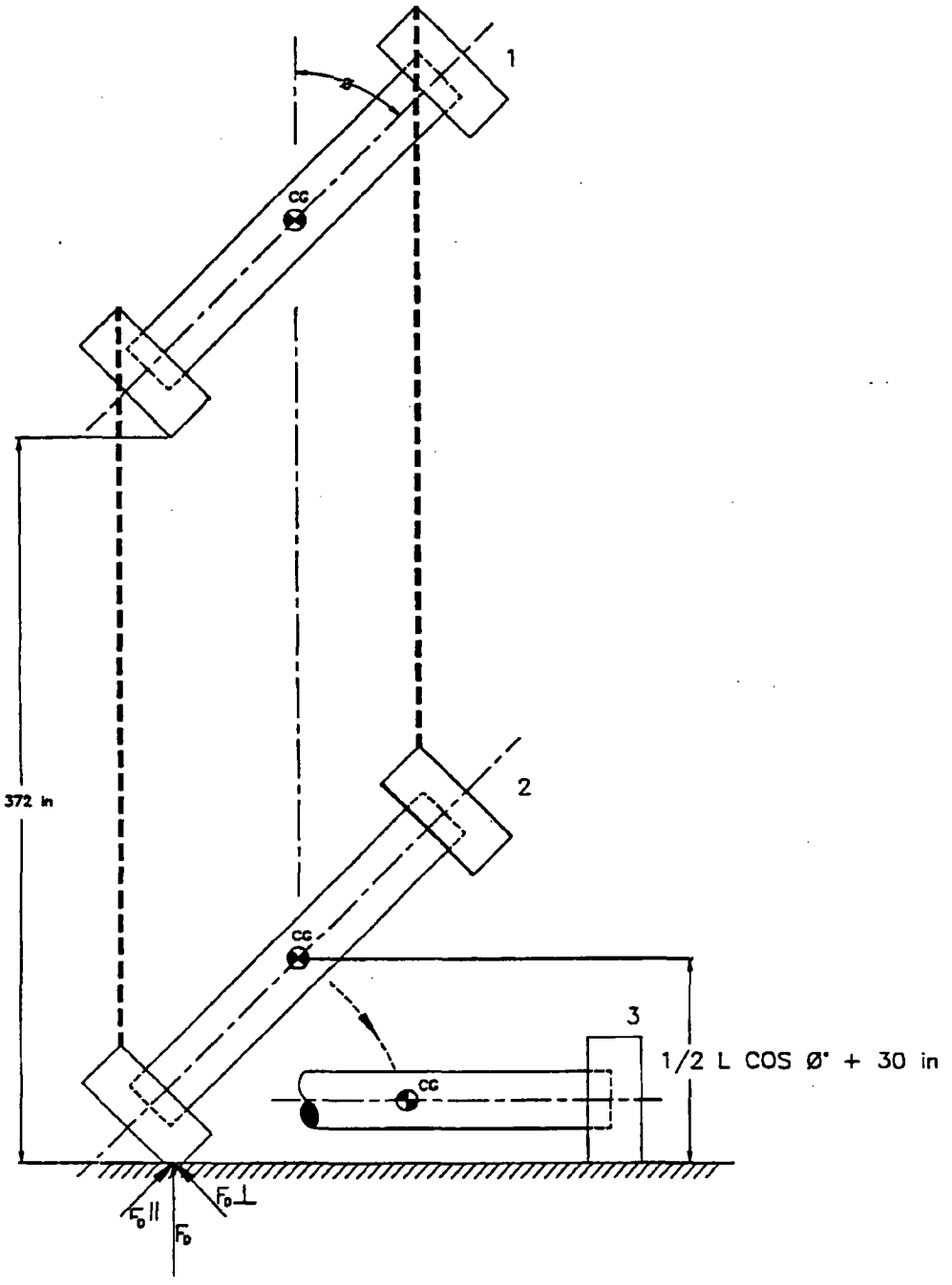

Figure 2.10.12-4 Force-Deflection Graph (0-Degree, Top End Drop)

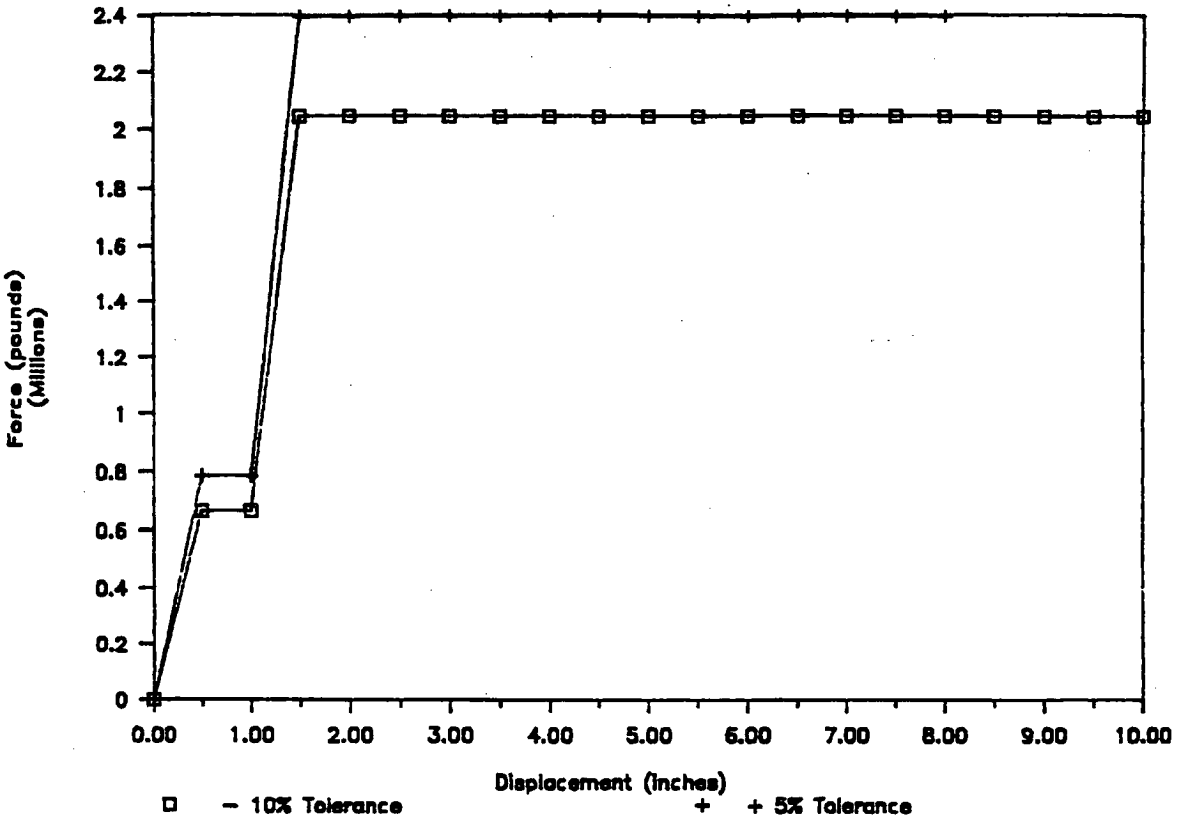

Figure 2.10.12-5 Force-Deflection Graph (0-Degree, Bottom End Drop)

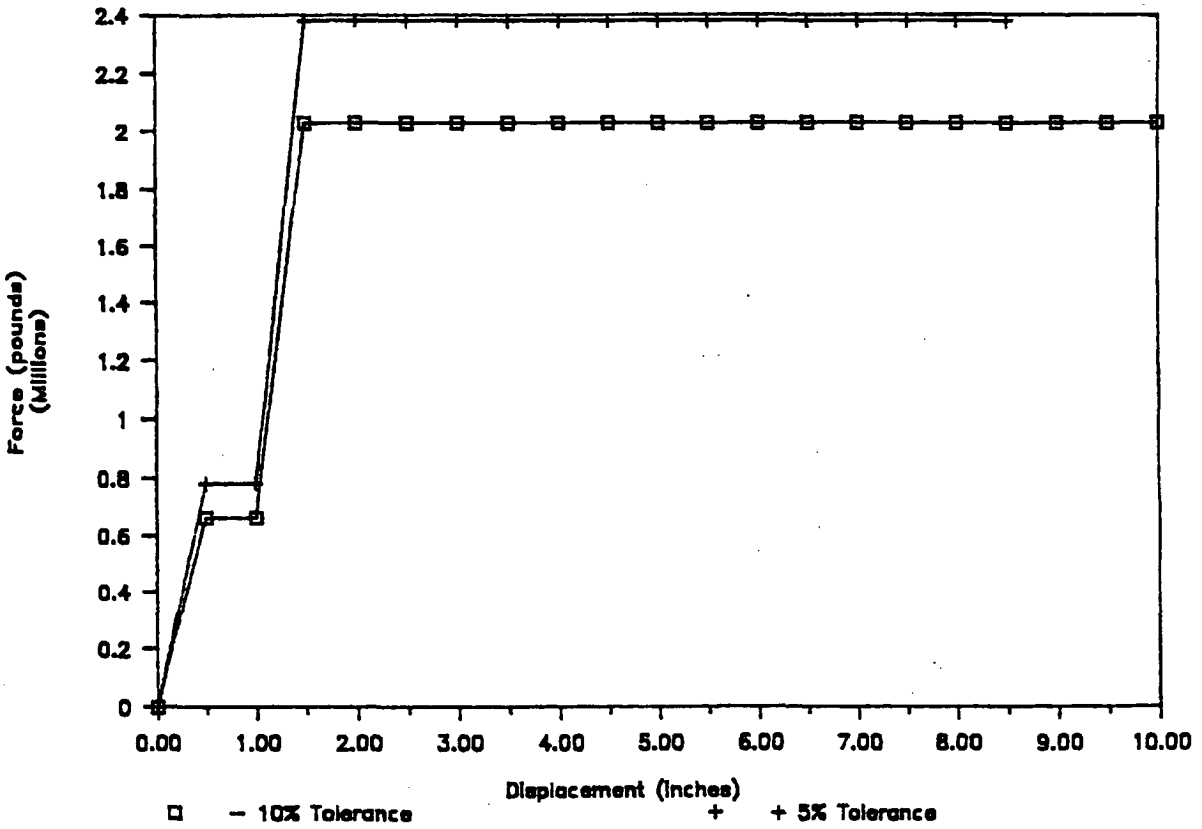

Figure 2.10.12-6 Force-Deflection Graph (15.74-Degree, Top Corner Drop)

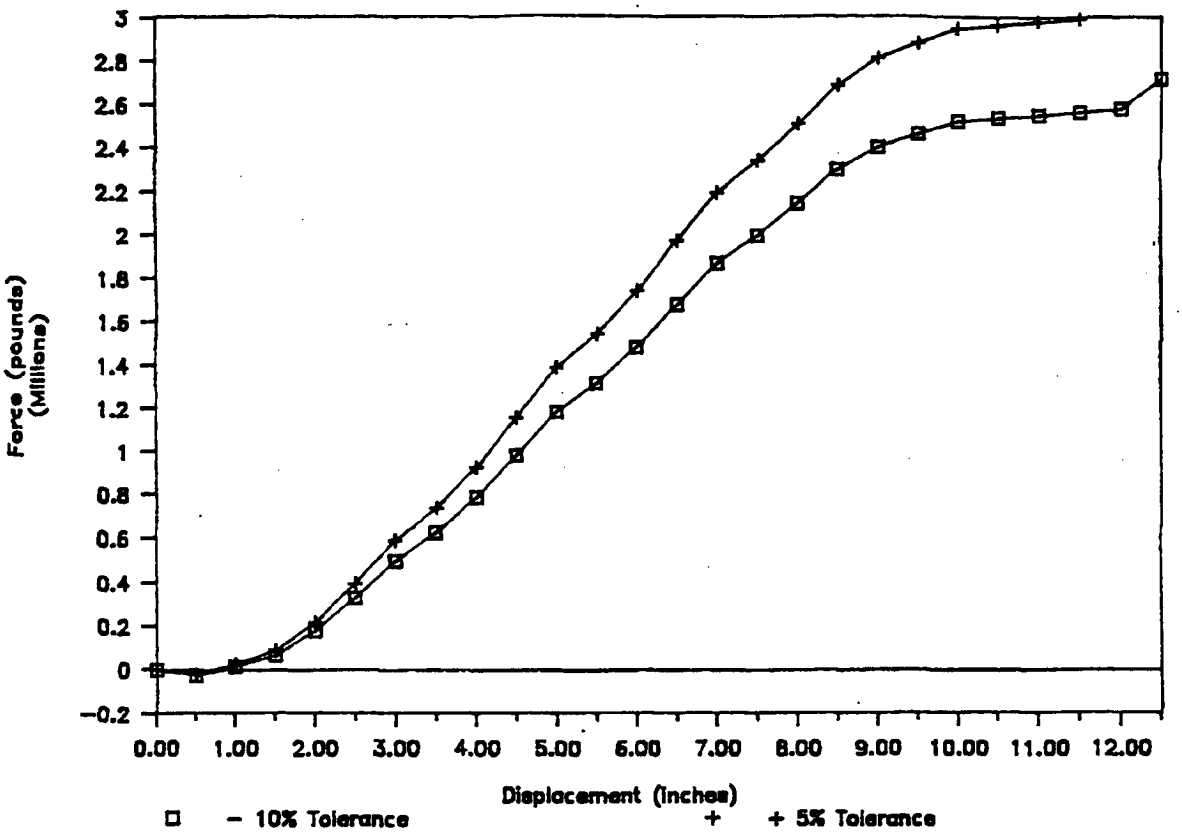

Figure 2.10.12-7 Force-Deflection Graph (14.5-Degree, Bottom Corner Drop)

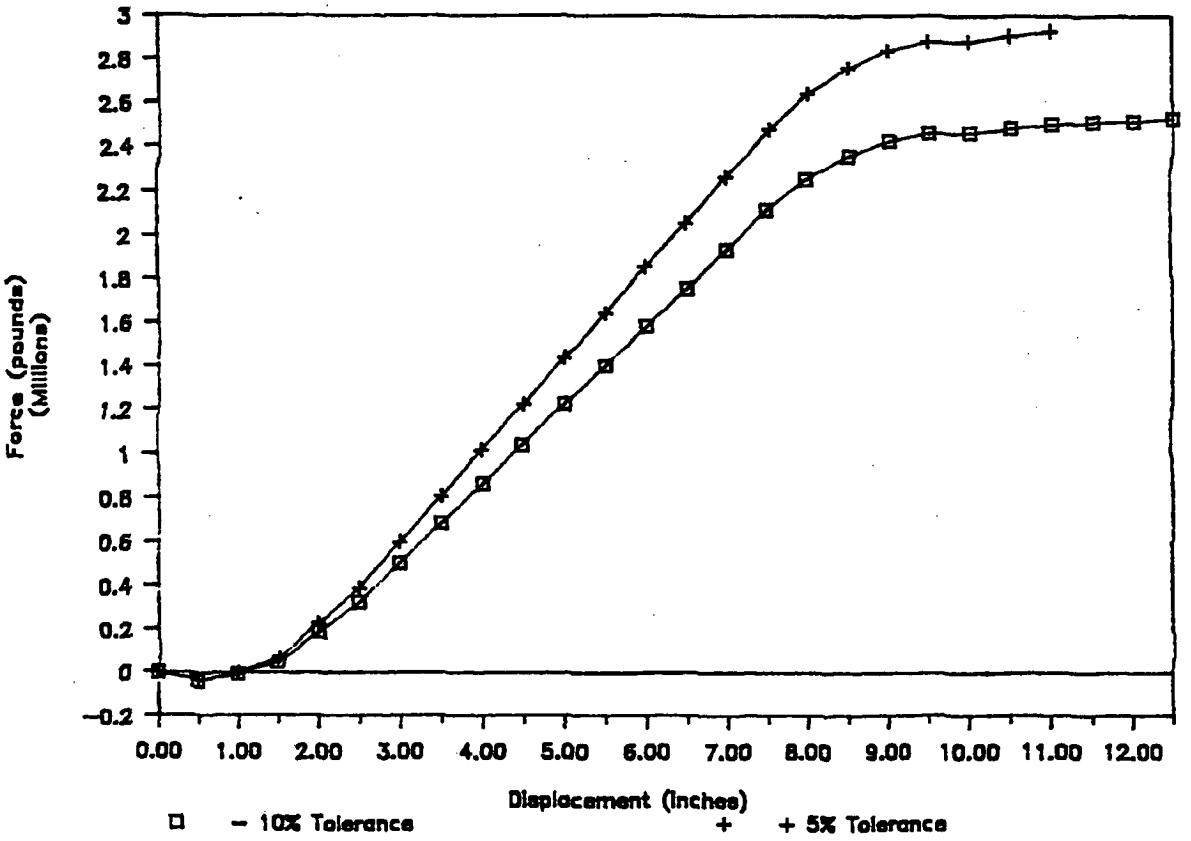

Figure 2.10.12-8 Force-Deflection Graph (30-Degree, Top Oblique Drop)

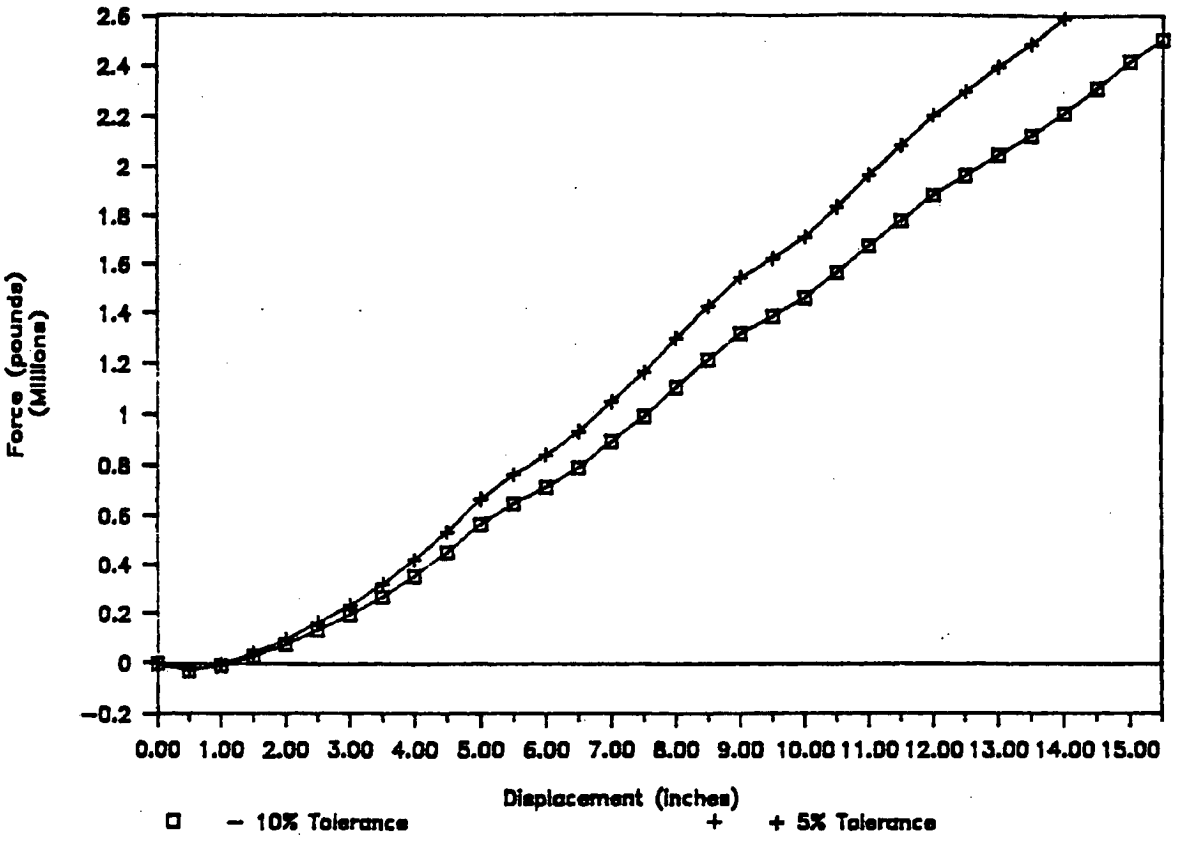

Figure 2.10.12-9 Force-Deflection Graph (30-Degree, Bottom Oblique Drop)

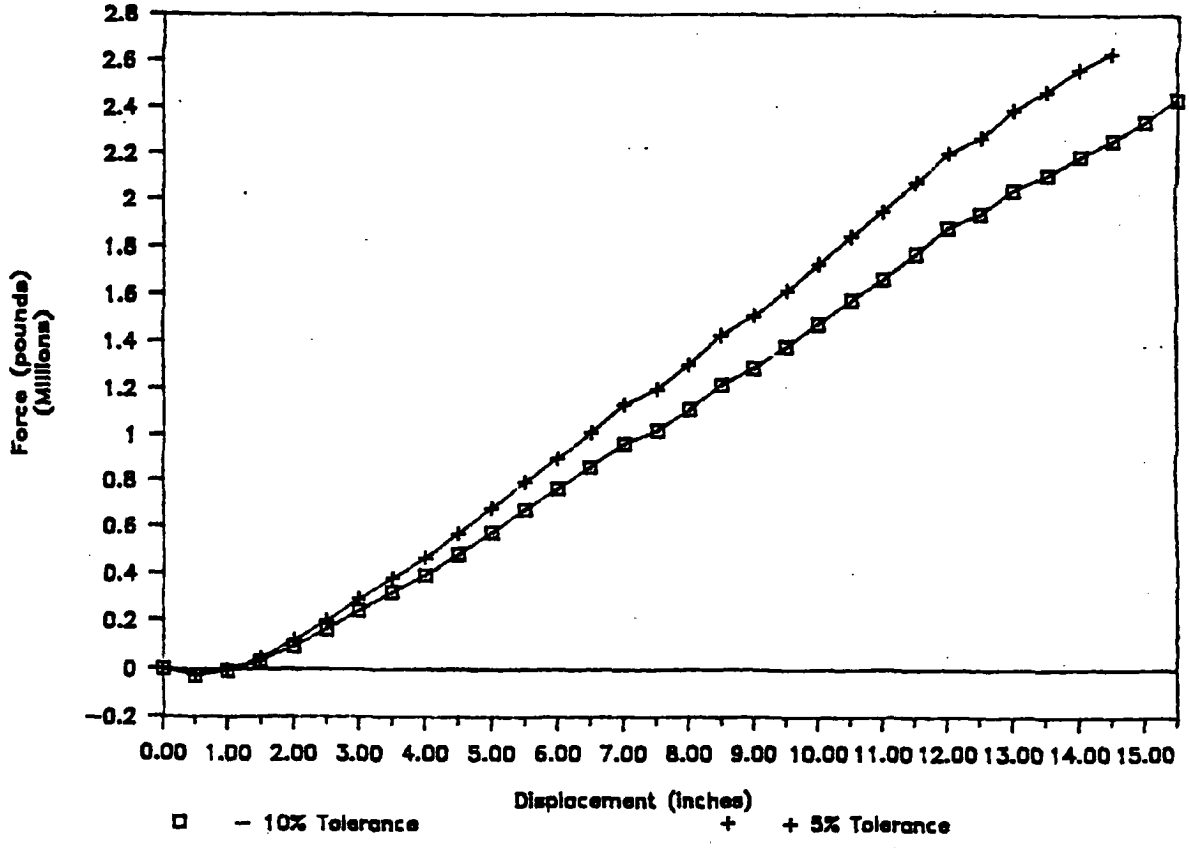

Figure 2.10.12-10 Force-Deflection Graph (45-Degree, Top Oblique Drop)

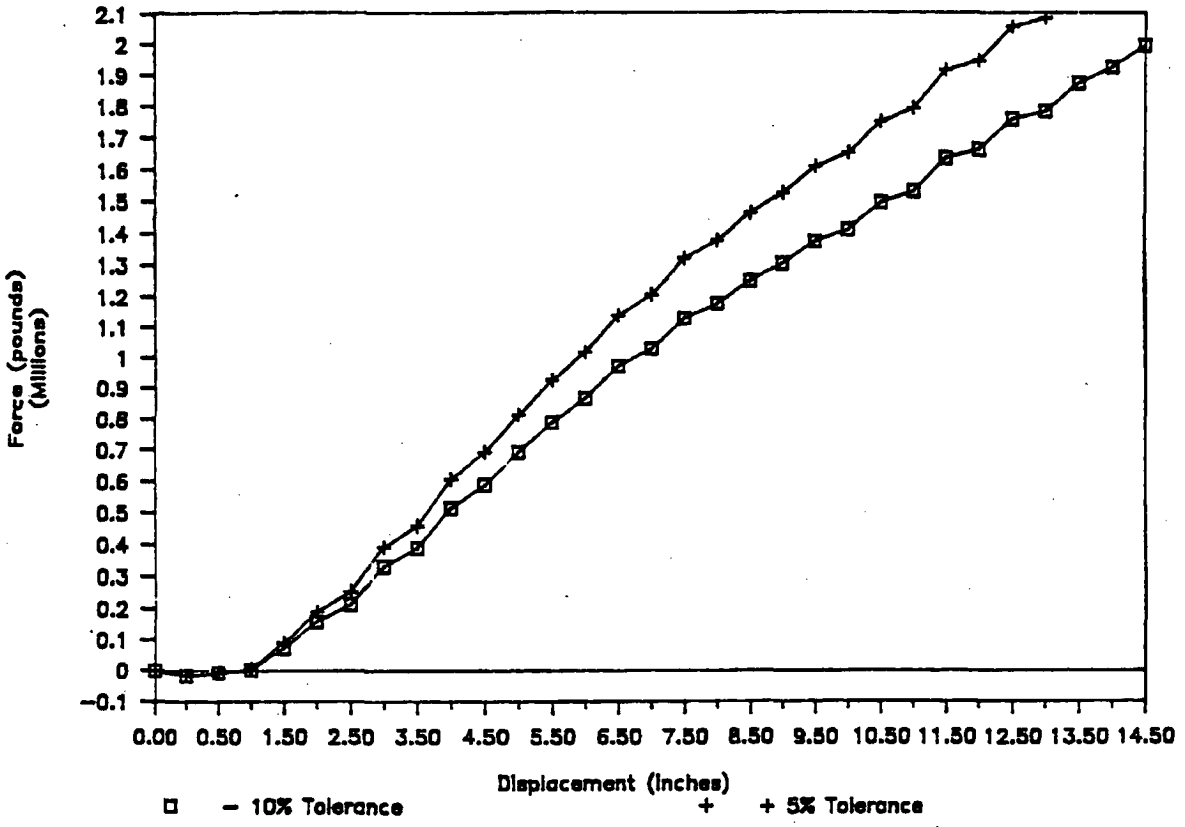

Figure 2.10.12-11 Force-Deflection Graph (45-Degree, Bottom Oblique Drop)

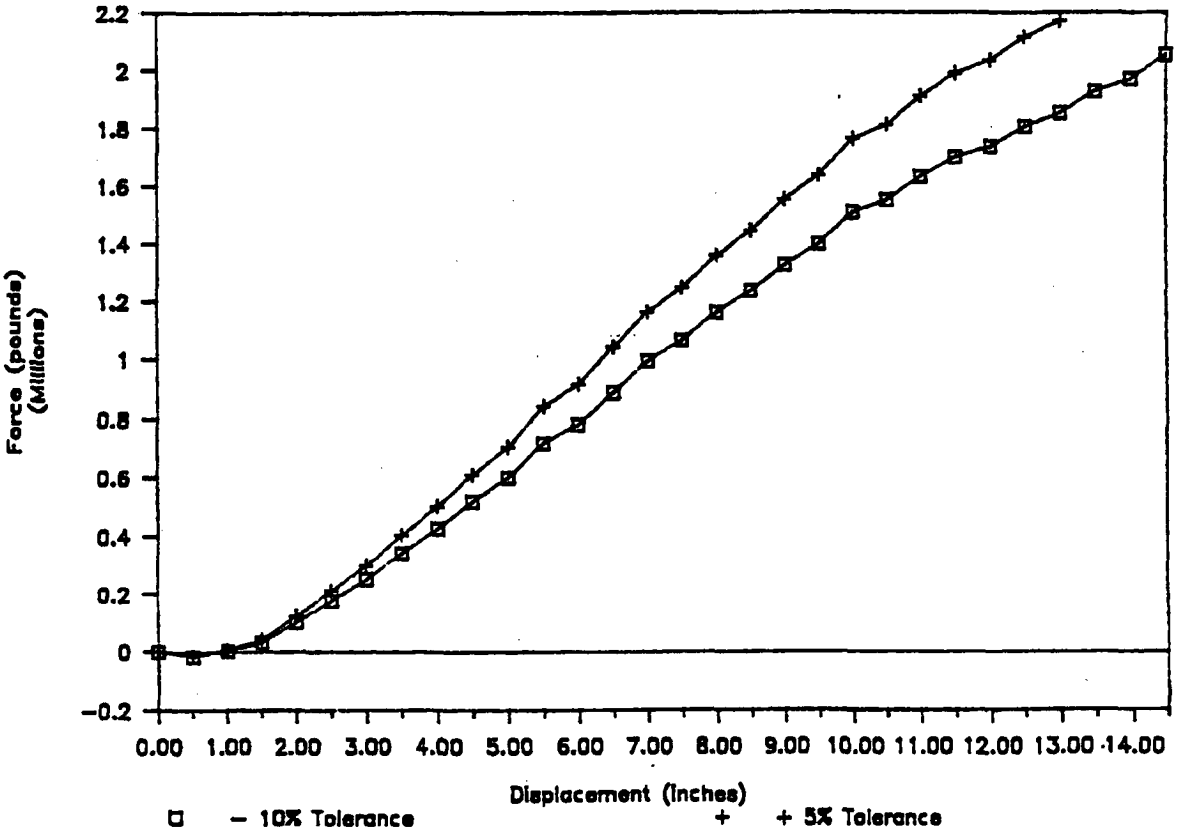

Figure 2.10.12-12 Force-Deflection Graph (60-Degree, Top Oblique Drop)

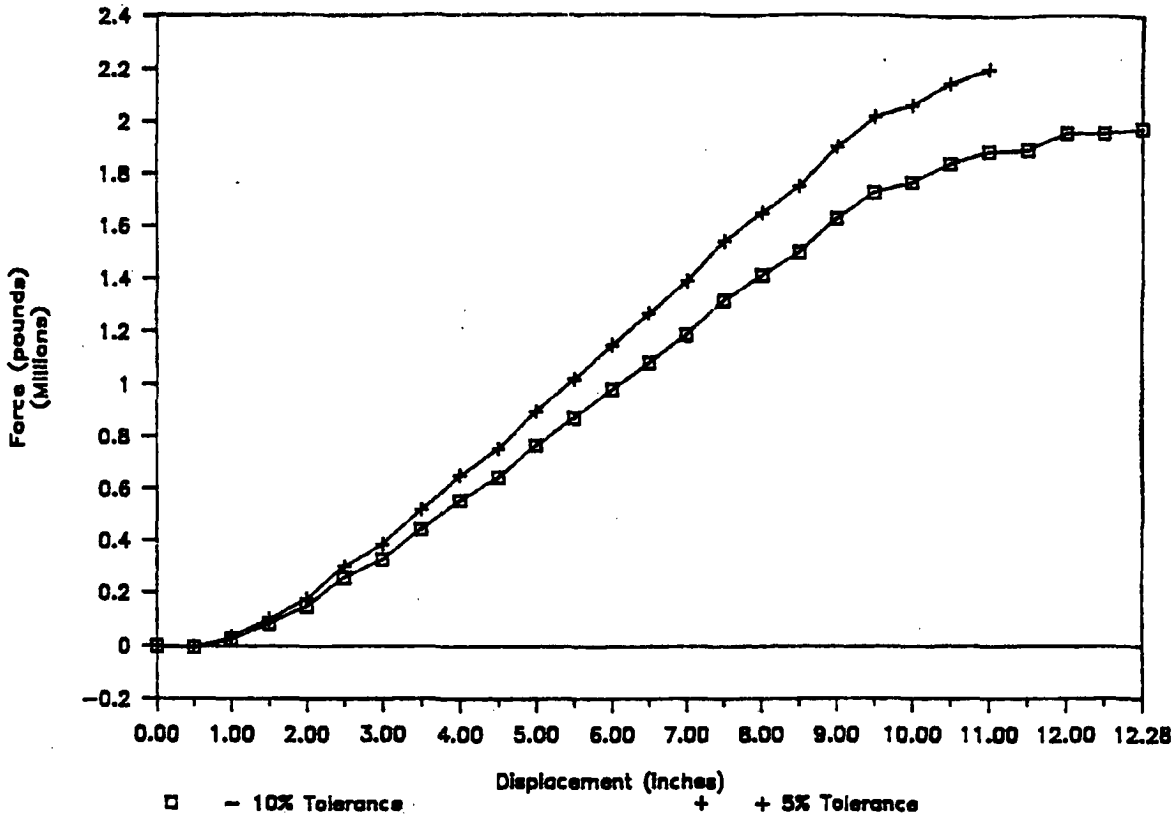

Figure 2.10.12-13 Force-Deflection Graph (60-Degree, Bottom Oblique Drop)

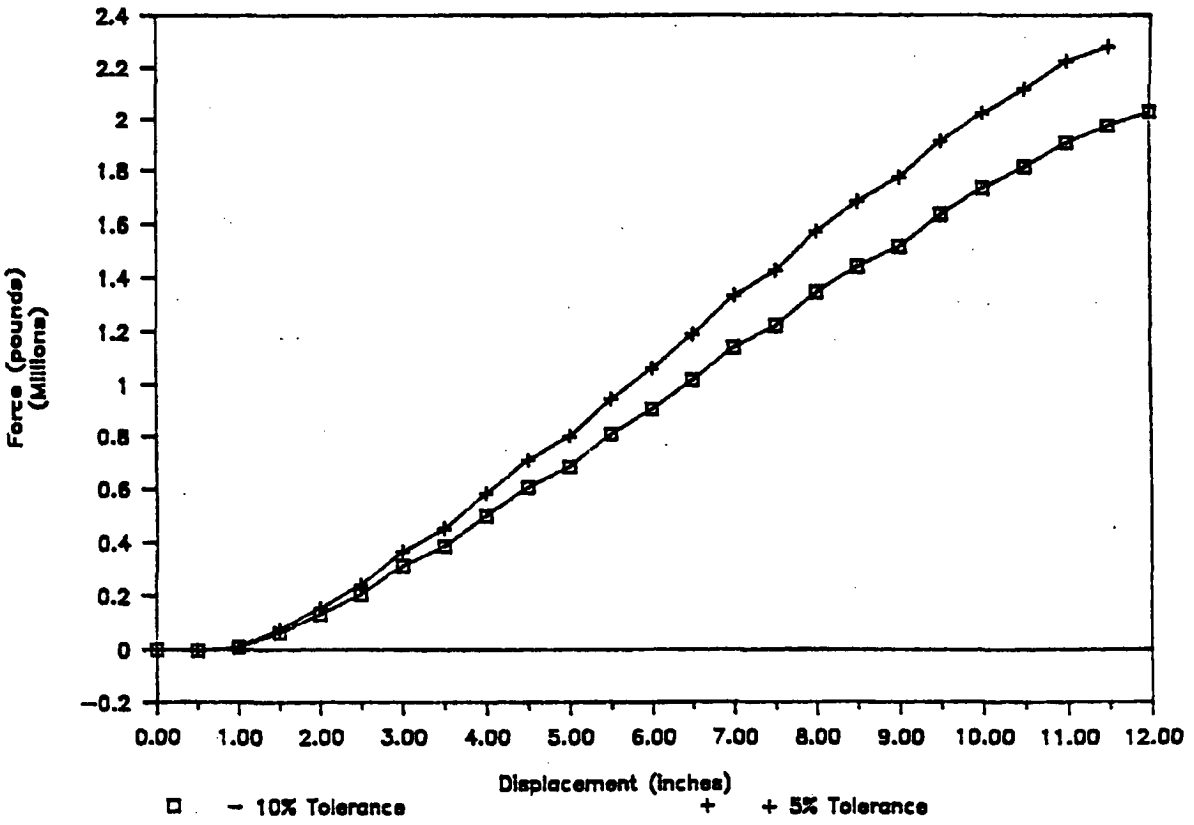

Figure 2.10.12-14 Force-Deflection Graph (75-Degree, Top Oblique Drop)

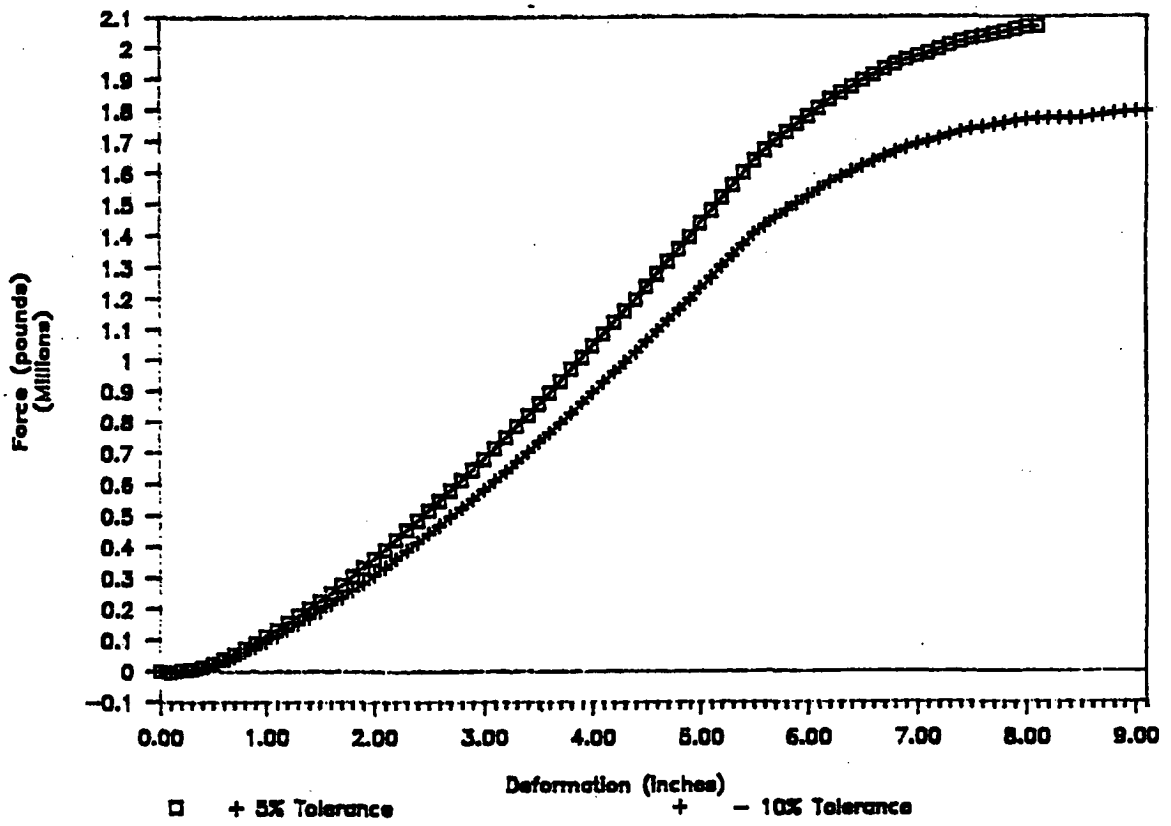

Figure 2.10.12-15 Force-Deflection Graph (75-Degree, Bottom Oblique Drop)

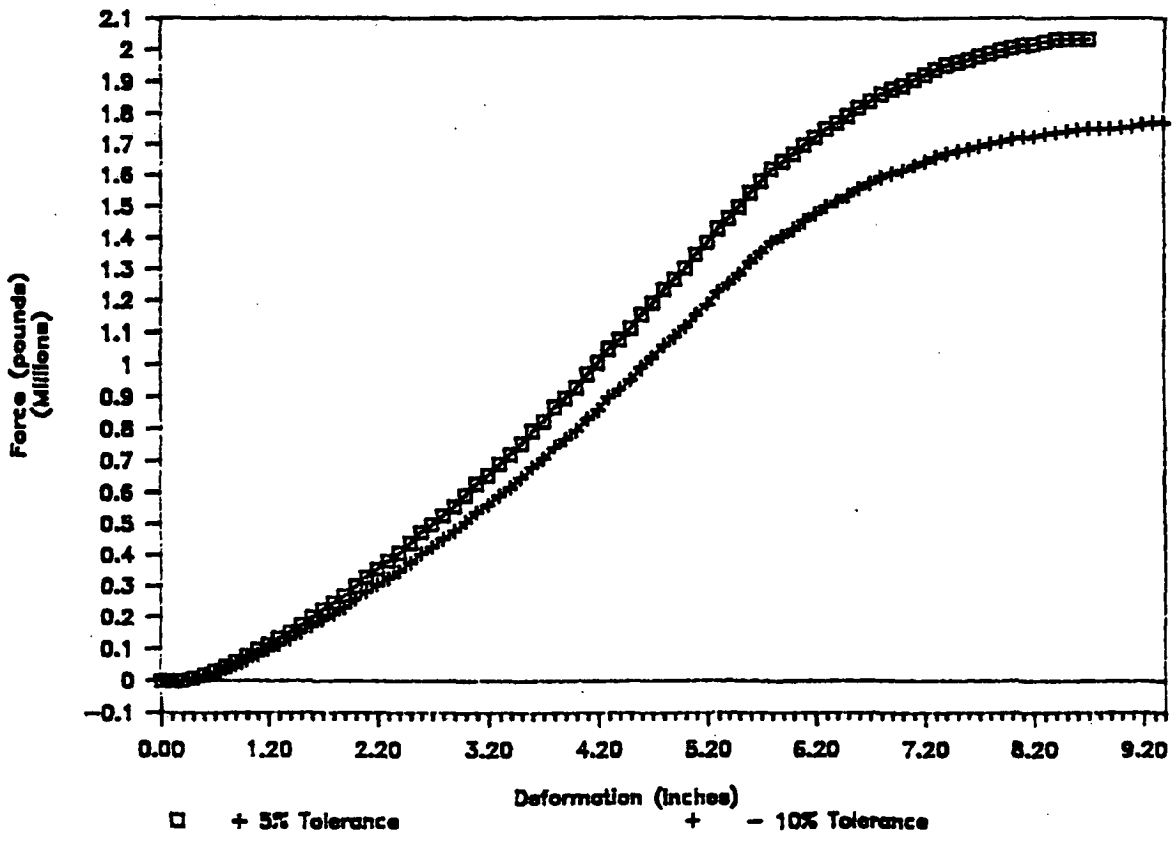

Figure 2.10.12-16 Force-Deflection Graph (90-Degree, Top Side Drop)

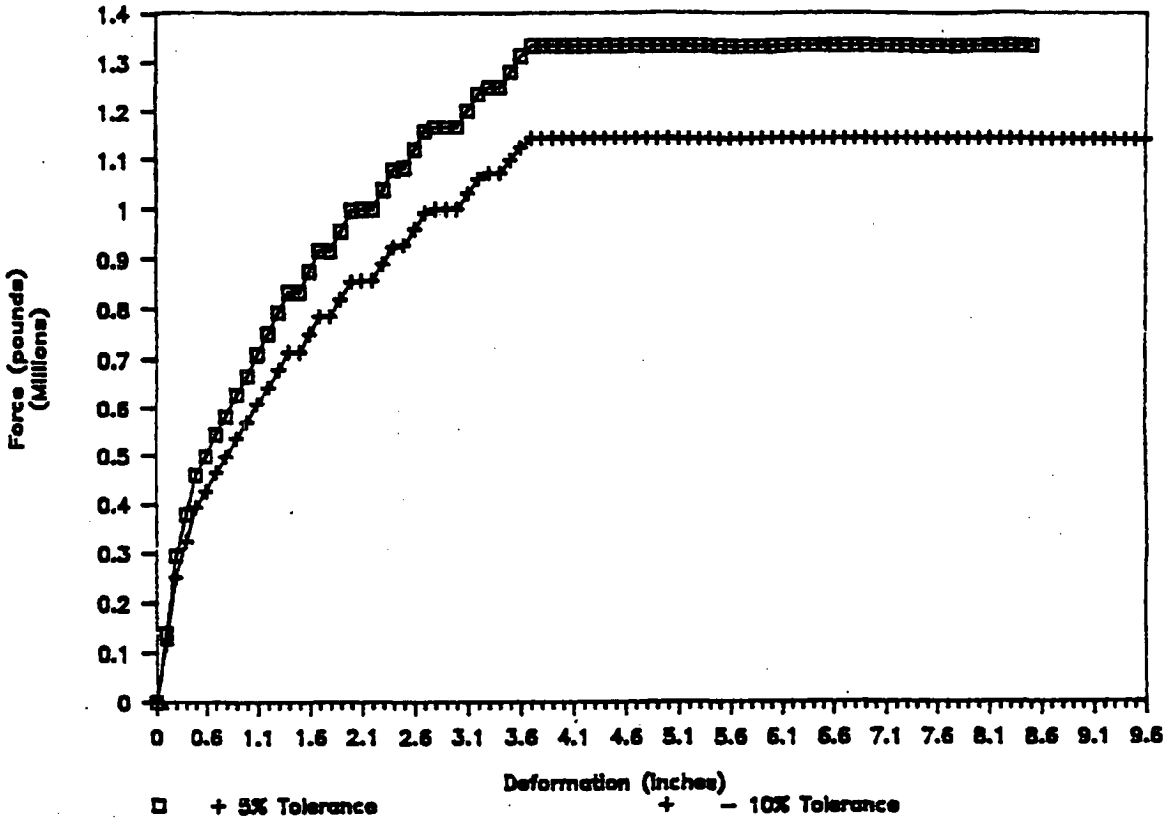

Figure 2.10.12-17 Force-Deflection Graph (90-Degree, Bottom Side Drop)

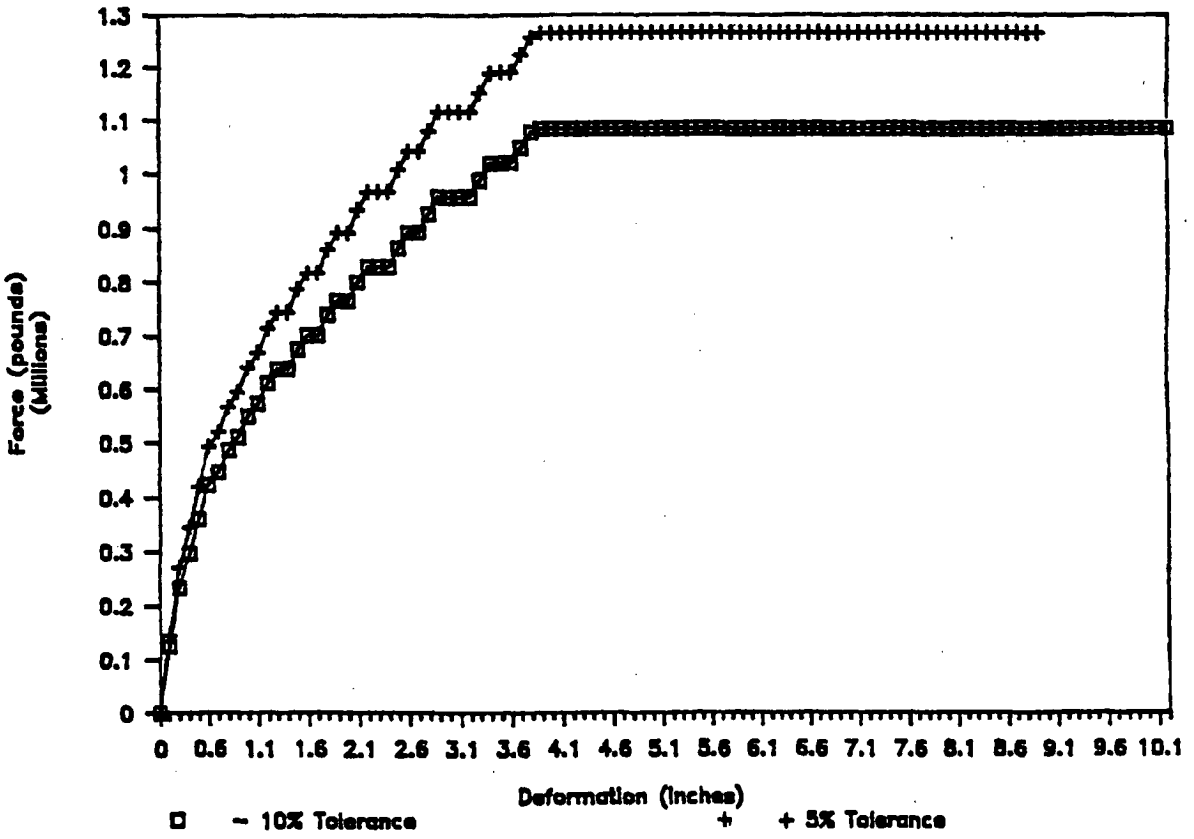

Figure 2.10.12-18 Force-Deflection Curve (0-Degree Impact, Drop Tested Limiter)

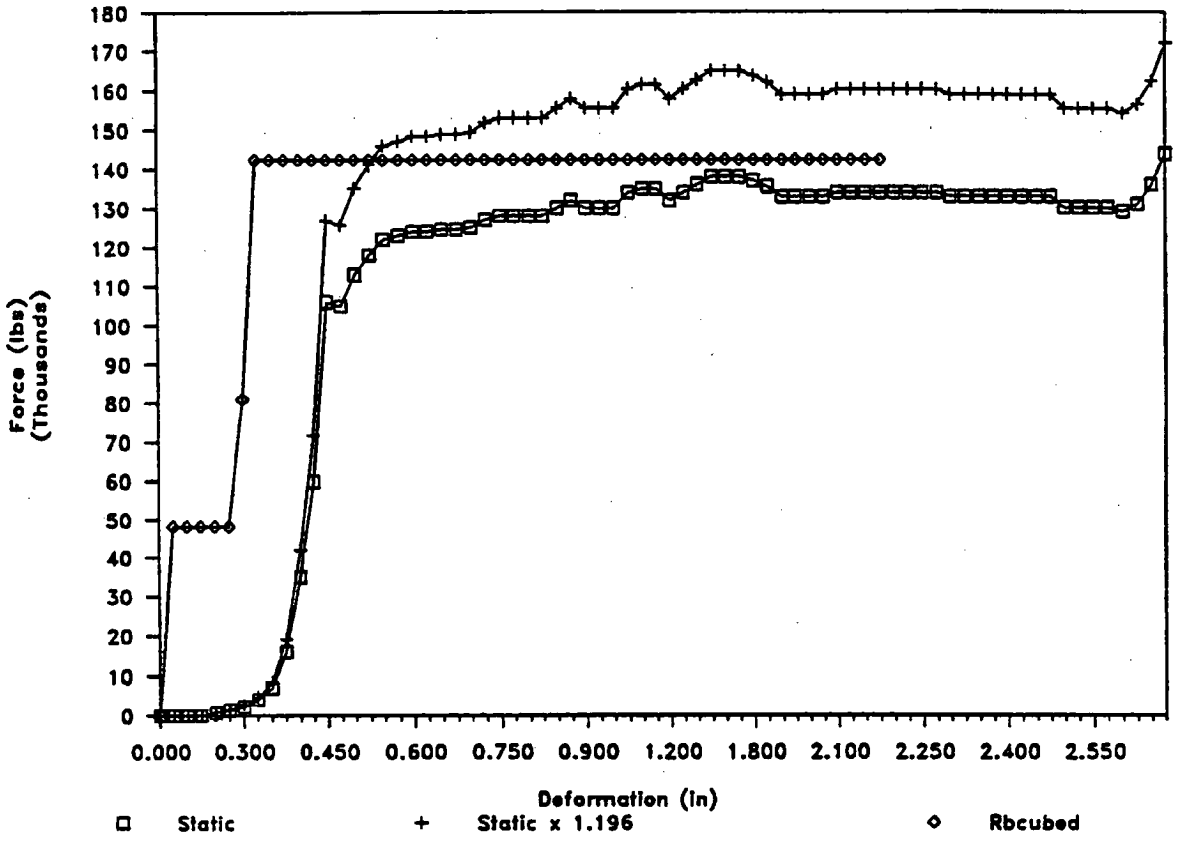

Figure 2.10.12-19 Force-Deflection Curve (14-Degree Impact, Drop Tested Limiter)

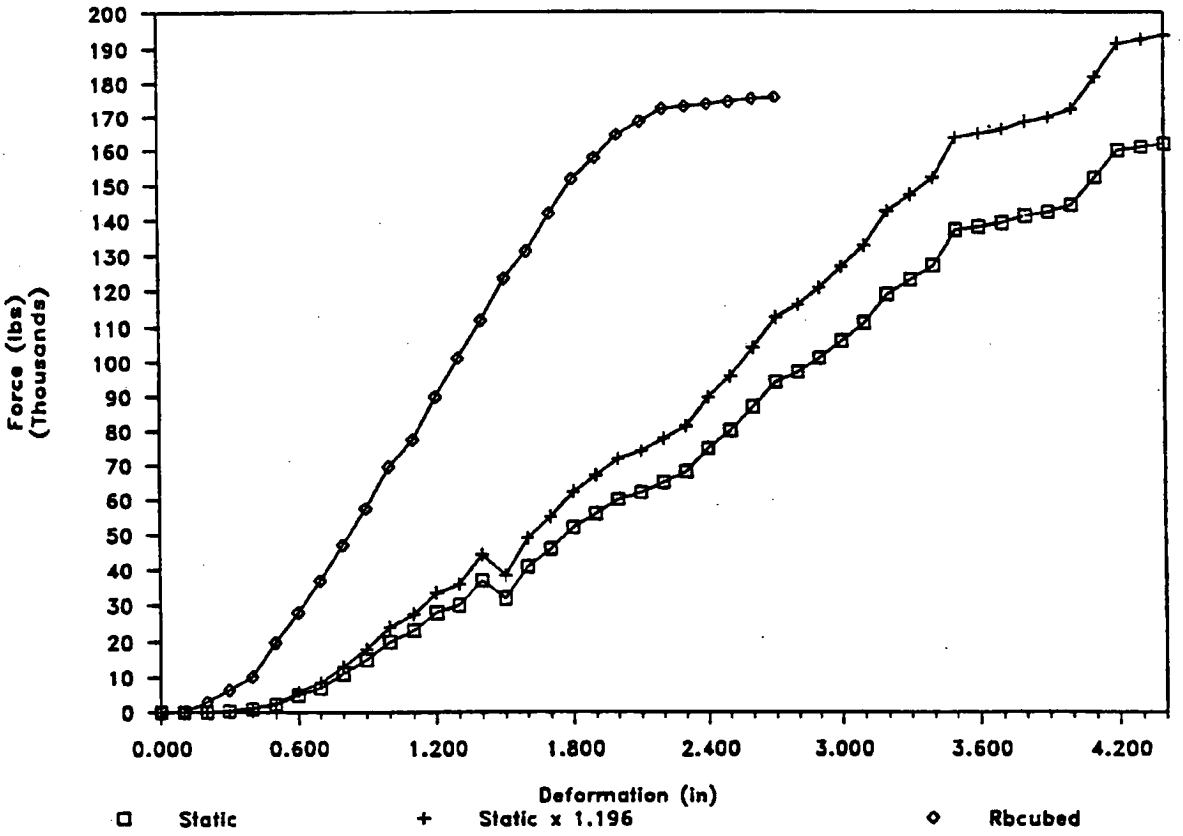

Figure 2.10.12-20 Force-Deflection Curve (90-Degree Impact, Drop Tested Limiter)

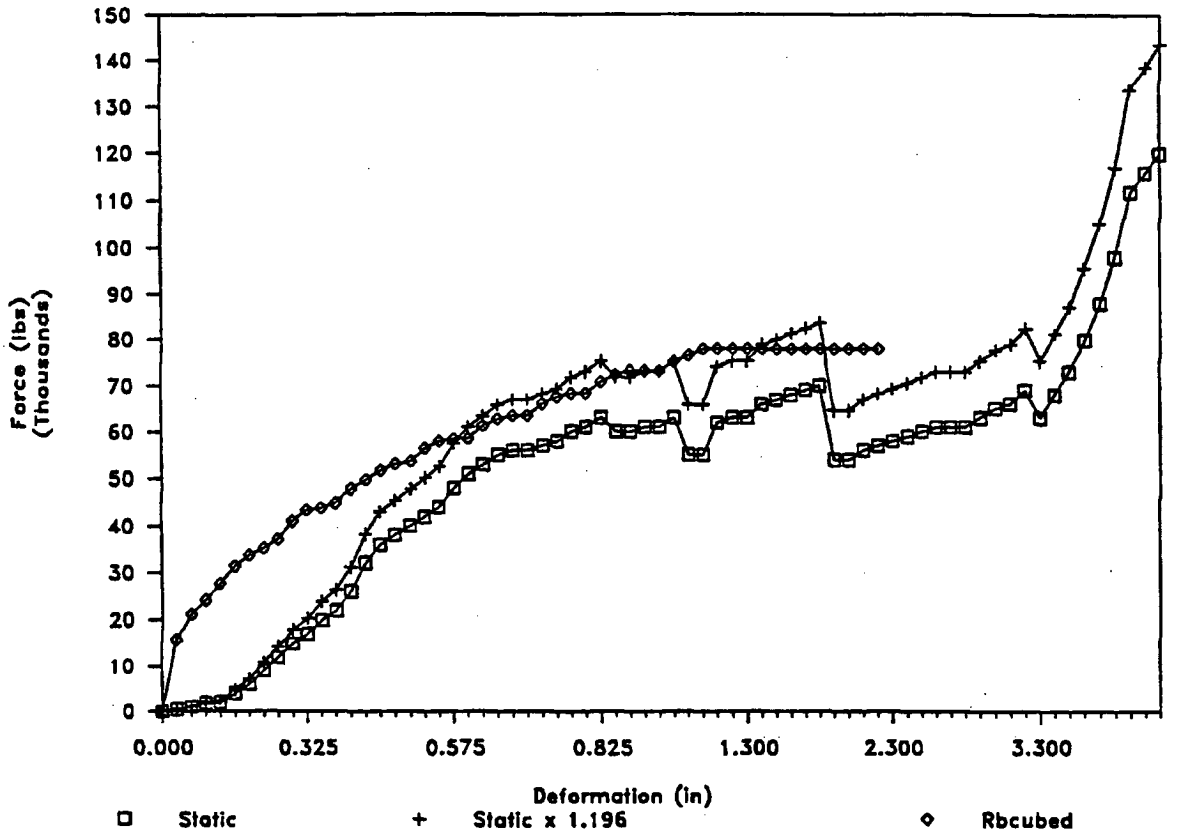

Figure 2.10.12-21 End Drop Impact Limiter Cross Section

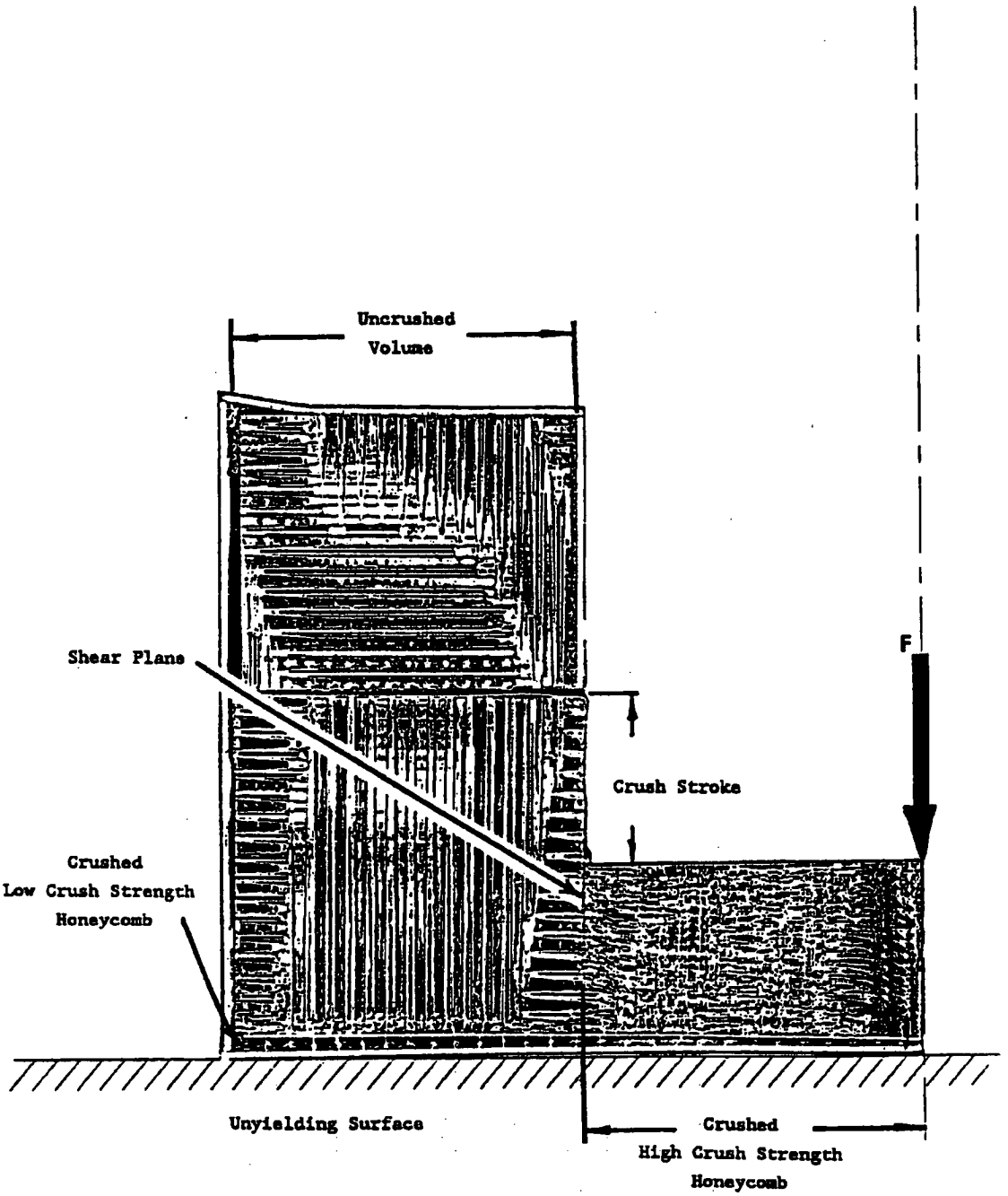

Table 2.10.12-1 Determination of Maximum Energy Remaining for Secondary Impact – Full-Scale Impact Limiter

DROP ANGLE (degrees)	0	15	30	45	60	75	90
EI Energy absorbed by first limiter (in-lb)	1.93×10^7	1.88×10^7	1.74×10^7	1.52×10^7	1.23×10^7	1.03×10^7	9.67×10^6
ER Energy remaining after first impact (in-lb)	0.00	5.40×10^5	1.94×10^6	4.14×10^6	7.04×10^6	9.02×10^6	9.67×10^6
EP Potential energy of cask after first impact (in-lb)	6.04×10^6 [1]	4.97×10^6	4.40×10^6	3.45×10^6	2.21×10^6	7.68×10^5	0.00
ES Energy stored in first limiter; absorbed in second limiter in side drop orientation (in-lb)	1.87×10^6 (9.7%)	1.24×10^6 (6.6%)	1.04×10^6 (6.0%)[2]	8.66×10^5 (5.7%)[2]	6.77×10^5 (5.5%)[2]	5.56×10^5 (5.4%)[2]	5.13×10^5 (5.3%)
E2 Secondary impact total of ER + EP + ES (in-lb)	7.91×10^6	6.75×10^6	7.38×10^6	8.46×10^6	9.93×10^6	1.03×10^7	1.02×10^7
Emax – Side Drop Maximum energy absorption capability of impact limiter in side drop orientation (in-lb)	1.49×10^7	1.49×10^7	1.49×10^7	1.49×10^7	1.49×10^7	1.49×10^7	1.49×10^7
Energy Absorption Margin	88.32%	120.71%	101.79%	76.20%	50.10%	44.04%	46.33%

[1] Assumes tip-over of cask onto the second impact limiter.
[2] Interpolated values.

Table 2.10.12-2 Determination of Extreme Force During Cask Deceleration (First Limiter) – Quarter-Scale Impact Limiter

DROP ANGLE (degrees)	0	15	90
RBCUBED Average Maximum or Peak Force	142,340	175,710	78,070
Equivalent g Load	177.9	219.6	97.6
STATIC TEST – DROP-TESTED LIMITERS Dynamic Average Maximum or Peak Force	158,382	169,000	74,152
Equivalent g Load	198.0	211.3	92.7
FORCE MARGIN	-11.27%	3.82%	5.02%
CALCULATED STRESS MARGIN	200.00%	1.00%	6.00%
REVISED STRESS MARGIN*	188.73%	4.82%	11.02%

* Approximate stress margin, which includes the effect of impact limiter testing. Quarter-scale cask model weight = 800 lbs

2.10.13 Structural Evaluation of Failed Fuel Cans and Liners (Baskets)

This evaluation documents the thermal and structural adequacy of the failed fuel cans (FFCs) and liners (baskets) for a three-hole basket and a six-hole basket to be used for the transport of failed fuel and failed fuel filters in the NAC-LWT spent fuel shipping cask. The maximum normal operating temperature is calculated to be 214°F for the FFC in the six-hole basket, and 229°F for the FFC in the three-hole basket. Each FFC in the six-hole basket has been designed to contain a single failed fuel rod. Each FFC in the three-hole basket has been evaluated for up to three failed fuel rods per FFC (up to nine failed fuel rods per cask) or up to ten failed fuel filters (up to 30 failed fuel filters per cask). The conservatively calculated minimum margin of safety for any component is +0.24. The FFCs and liners are structurally adequate to satisfy all regulatory requirements.

2.10.13.1 Discussion

Nuclear Assurance Corporation has designed an FFC and three-hole basket that will permit up to nine encapsulated failed metallic fuel rods or up to 30 encapsulated failed fuel filters to be shipped in the NAC-LWT cask. A six-hole basket containing six smaller diameter FFCs has been evaluated based on a capacity of six failed fuel rods per cask. With either basket, the FFC is a sealed, dry aluminum canister. Up to three failed metallic fuel rods or up to ten failed fuel filters are placed in each FFC when the three-hole basket is used. Only one failed metallic fuel rod may be placed in each FFC if the six-hole basket is used.

Each metallic fuel rod is assumed to weigh 125 lbs (actual weight is 53 kg or 117 lbs) and is approximately 124 inches long. Each failed fuel filter is assumed to weigh 12 pounds and is approximately 11 inches long. The failed fuel rods have a maximum decay heat load of 5 watts per rod, resulting in a maximum decay heat load of 30 watts for the six-hole basket, and 45 watts for the three-hole basket. Each FFC containing up to 10 failed fuel filters is limited to the amount of fuel in a single metallic fuel rod resulting in a maximum decay heat load of 5 watts, or a total of 15 watts for the three-hole basket.

2.10.13.2 Method of Analysis

Thermal analyses were performed using the one-dimensional SCOPE computer program to determine the maximum normal operating temperature of the FFC and liner. A total decay heat load of 30 watts was used for the six-hole basket, and 45 watts for the three-hole basket. The maximum FFC temperature was 214°F for the six-hole basket, and 229°F for the three-hole

basket. A temperature of 250°F was conservatively used to determine the material properties of the FFCs and liners. The SCOPE inputs and outputs are provided in Section 3.6.

Classical stress analysis methods are used to evaluate the FFCs for buckling during the end impact and for bending during a side impact. The tubes in the liners are also analyzed for bending during a side impact. The impact loadings include the g-factors determined in Section 2.6.7.4. The calculated stresses in the FFCs and the liners are conservatively compared to the material yield strength to demonstrate that containment is maintained by the FFCs and that no permanent deformation of the FFCs or the liners occurs.

2.10.13.3 Input Geometry & Data

1. Total Heat Load = 30 Watts (For 6 Metallic Fuel Rods).
   = 45 Watts (For 9 Metallic Fuel Rods).
   = 15 Watts (For 30 Failed Fuel Filters).

2. Metallic Fuel Rod Weight = 125 lbs/Rod.
   Failed Fuel and Filter Weight = 12 lbs/Filter.

3. NAC-LWT Cask Geometry: (Ref. Section 1.4)

Inner Shell (Cavity) I.D.	= 13.375 inches
Inner Shell Thickness	= 0.75 inch
Lead Shell Thickness	= 5.75 inches
Outer Shell Thickness	= 1.20 inches
Neutron Shield Thickness	= 5.00 inches
Neutron Shield Shell Thickness	= 0.24 inch

4. Free Drop Impact G-Loads: (Ref. Table 2.6.7-33 and Table 2.6.7-34)

Normal Operation[1]	
1-Foot Side Drop	24.3 g
Accident[1]	
30-Foot Top End Drop	48.3 g
30-Foot Bottom End Drop	48.1 g
30-Foot Side Drop	49.7 g
30-Foot Corner Drop	60.4 g

[1] Ref. 10 CFR 71 and Regulatory Guide 7.8.

2.10.13.4 Mechanical Properties of Materials

1. 6061-T6 Aluminum Alloy (Ref. MIL-HDBK-5E)

	$(S_u)_{70}$ = 42 ksi (70°F)	$(S_y)_{70}$ = 35 ksi (70°F)	(page 3-222)
At 250°F:	$(S_u)_{250}$ = 0.86	$(S_u)_{70}$ = 36.1 ksi	(page 3-227)
	$(S_y)_{250}$ = 0.88	$(S_y)_{70}$ = 30.8 ksi	(page 3-228)

2. 6063-T832 Aluminum Alloy (Ref. ASME B210)

	$(S_u)_{70}$ = 40 ksi	$(S_y)_{70}$ = 35 ksi	(page 194)
At 250°F:	$(S_u)_{250}$ = 0.86[1]	$(S_u)_{70}$ = 34.4 ksi	
	$(S_y)_{250}$ = 0.88[1]	$(S_y)_{70}$ = 30.8 ksi	

3. 6061-T6511 Aluminum Alloy (Ref. MIL-HDBK-5E)

	$(S_u)_{70}$ = 38 ksi	$(S_y)_{70}$ = 35 ksi	(page 3-225)
At 250°F:	$(S_u)_{250}$ = 0.86[1]	$(S_u)_{70}$ = 32.7 ksi	
	$(S_y)_{250}$ = 0.88[1]	$(S_y)_{70}$ = 30.8 ksi	

2.10.13.5 Thermal Evaluation

The SCOPE thermal analysis computer program is used to evaluate the NAC-LWT cask containing the six-hole basket with six 2.75-inch inner diameter (I.D.) FFCs loaded with one metallic fuel rod each, for a total heat load of 30 watts. The maximum temperature for the FFC is 214°F. A similar analysis for the three-hole basket with three 4.00-inch I.D. FFCs loaded with three metallic fuel rods each for a total heat load of 45 watts, resulted in a maximum temperature of 229°F for the FFCs. This is the bounding maximum thermal case for the three-hole basket.

2.10.13.6 Structural Evaluation

The FFCs are evaluated to demonstrate that containment of the failed fuel rod or the failed fuel filters is maintained for all loading conditions. The maximum stress occurs in the shells of the FFCs for the 30-foot side drop load case. Buckling of the shells is evaluated for the 30-foot end drop load case.

[1] The strength variation with temperature is assumed to be the same as that for 6061-T6 Aluminum Alloy.

The liners (baskets) for the failed fuel cans are evaluated to demonstrate that rupture (ultimate failure) does not occur for any loading condition. The maximum stress occurs in the housing (tube) of the liners for the 30-foot side drop load case.

The drawings referenced in these evaluations are included as Figure 2.10.13-1 through Figure 2.10.13-5.

2.10.13.6.1 Failed Fuel Can - 2.75-Inch Inner Diameter

Shell – Bending

Ref. Dwg. 340-108-D2 (Figure 2.10.13-4)

Loading (temperature conservatively assumed - 250°F)

30-Foot Side Drop Acceleration = 49.7 g

Support Spacing = 33.66 inches (Ref. Dwg. 315-40-12)

Weight: Fuel = 125 lbs/124 inches = 1.008 lb/in

Shell = $(\pi/4)[(3.0)^2 - (2.75)^2](1)(0.10)$ = 0.113 lb/in

Total = 1.121 lb/in

Conservatively, assume the shell is simply supported at the support disks; then, the moment during impact is:

$M = (1/8)(1.121)(33.66)^2 (49.7) = 7{,}890$ in-lb

Shell Properties:

$I/C = 0.7791$ in^3

Material Properties: (ASTM B221 Type 6061-T6)

$(S_y)250 = 30.8$ ksi

Stresses:

$S_b = 7890/0.7791 = 10{,}127$ psi

$MS = [(S_y)_{250}/S_b] - 1 = +2.04$

Shell – Buckling

Estimated Weight of Can Assembly = 20 lbs

The maximum axial acceleration is for the corner drop

Top End Drop Deceleration = 48.3 g

Maximum axial acceleration [cos(15.74°)](60.4) = 58.2 g

The compressive stress in the shell due to its weight during impact is:

$$S_c = \frac{(20)(58.2)}{[\pi/4][(3.0)^2 - (2.75)^2]} = 1{,}031 \text{ psi}$$

The margin of safety on yield is:

$$\text{M.S.} = \frac{30.8}{1.03} - 1 = \underline{\text{Large}}$$

The buckling of the cylindrical shell under the action of uniform axial compression may be evaluated using equation 11-1 on page 458 of Theory of Elastic Stability by Timoshenko and Gere.

$$S_{cr} = \frac{Et}{r[3(1 - \upsilon^2)]^{0.5}}$$

$$= 267 \text{ ksi}$$

where:

$E = (0.97)(10.IE03) = 9.8E03$ ksi at 250°F

$t = 0.125$ in

$r = 2.81$ inches, env. radius for all tubes in assembly

$\nu = 0.33$

The margin of safety on buckling is:

$MS = S_{cr}/S_c - 1 = +\underline{\text{Large}}$

Conclusion

The stress in the cylindrical shell caused by a corner drop with an axial component of 58.2 g deceleration is much lower than the yield stress and the critical buckling stress.

2.10.13.6.2 Liner - Failed Fuel Can - 2.75 Inner Diameter

Housing – Bending

Ref. Dwg. 315-040-43 (Figure 2.10.13-2)

Loading (temperature conservatively assumed - 250°F)

30-Foot Side Drop Deceleration = 49.7 g
Support Spacing = 33.66 inches

Weight: Fuel	= 125 lbs/124 inches	= 1.008 lb/in
Aluminum Shell	= $[\pi/4][(3)^2 - (2.75)^2](1)(0.10)$	= 0.113 lb/in
Housing	= $[\pi/4][(3.75)^2 - (3.5)^2](1)(0.10)$	= 0.142 lb/in
	Total	= 1.263 lb/in

Conservatively, assume the housing is simply supported at the support disks; then, the moment during impact is:

$M = (1/8)(1.263)\ (33.66)^2\ (49.7) = 8{,}890$ in-lb

Housing Properties:

$I/C = (\pi)(d_o^4 - d_i^4)/32d_o$

$= (\pi)\ [3.75)^4 - (3.5)^4]/(32)(3.75) = 1.2485$ in^3

Material Properties: (ASTM B210 Type 6063-T832)

$(S_y)_{250} = 30.8$ ksi

Stresses:

S_b = 8,890/1.2485 = 7121 psi

MS = $[(S_y)_{250}/S_b] - 1 = +3.32$

Weld Between Bulkhead and Tubes

Peak Deceleration = 60.0 g (Ref. Table 2.6.7-34, 30-Foot End Drop)

Ref. Dwg. 315-040-43 (Figure 2.10.13-2)

Weight of 1 Bulkhead = $(\pi/4)[(13)^2 - (6)(2.75)^2](1/4)(0.1)$

= 2.4 lbs

Weight of U-Bolts = 1.6 lbs

Total = 4.0 lbs

Inertial load of bulkhead on welds: P_{act} = (4)(60) = 240 lbs

Total length of weld per bulkhead: L_w = (4)(6) + (2)(3) = 30 inches

Size of fillet = 1/8 in

Assume F_u of aluminum weld: = 4,000 psi

Allowable shear stress = (0.3)(4,000) – 1,200 psi

(Ref. AISC Manual of Steel Construction, 8th Ed., Section 1.5.3)

Working capacity of welds $= P_{cap}$

$= (0.707)(1/8)(30)(1200)$

$= 3,180$ lbs

M.S. $= [P_{cap} / P_{act}] - 1 = 3,180/240 - 1 - +$Large

The other accident drop conditions are:

30-Foot Top End Drop $a = 48.3$ g

30-Foot Bottom End Drop $a = 48.1$ g

30-Foot Top Corner Drop $a = 60.4$ g

Compared to a 30-foot side drop accident condition, with a = 49.7 g, the above accident conditions are less critical. Therefore, neither rupture nor yielding of the liner housing will occur.

2.10.13.6.3 Failed Fuel Rod Can - 4.00 Inner Diameter (3 Failed Fuel Rod Loading)

Shell – Bending

Ref. Dwg. 340-108-Dl (Figure 2.10.13-3)

Loading (Temperature conservatively assumed - 250°F)

30-Foot Side Drop Acceleration	= 49.7 g
Support Spacing	= 50.37 inches
Weight: Fuel = (125 lbs/124 inches)(3)	= 3.024 lb/in
Shell = $[\pi/4][(4.25)^2 - (4.0)2](1)(0.10)$	= 0.162 lb/in
Total	= 3.186 lb/in

Conservatively, assume the shell is simply supported at the support disks at four locations with the maximum spacing of 50.37 inches. The moment during impact, by Case 36 of the AISC steel manual, is:

$M = (0.100)(3.186)(50.37)2(49.7) = 40,174$ in-lb

Shell Properties:

$I/C = (\pi)[(4.25)4 - (4)4]/(32)(4.25) = 1.623$ in^3

Material Properties: (ASTM B210 Type 6061 T6)

$(S_y)_{250} = 30.8$ ksi

Stresses:

S_b = 40,174/1.623 = 24,753 psi

M.S. = $[(S_y)_{250}/S_b]$ - 1 = +0.24

2.10.13.6.4 Liner - 3 Element NAC-LWT Cask (3 Failed Fuel Rods/Can)

Tube - Bending

Ref. Dwg. 315-040-12 (Figure 2.10.13-1)

Loading

30-Foot Side Drop Acceleration		= 49.7 g
Support Spacing		= 50.37 in
Weight:	Fuel = (125 lb/124 in)(3)	= 3.024 lb/in
	Shell = $[\pi/4][(4.25)^2 - (4.0)^2$ (l)(0.10)	= 0.162 lb/in
	Tube = $[\pi/4][(5.625)^2 - (5.375)2(1)(0.1)$	= 0.216 lb/in
	Total	= 3.402 lb/in

Conservatively, assume the tube is simply supported at the support disks; then, the moment during impact is:

M = $(1/8)(3.402)(50.37)^2$ (49.7) = 53,622 in-lb

Tube Properties:

I/C = $(\pi)[(5.625)^4 - (5.375)^4]/(32)(5.625) = 2.9053$ in^3

Material Properties: (ASTM B210 Type 6061-T6)

$(S_y)_{250}$ = 30.8 ksi

Stresses:

S_b = 53,622/2.9053 = 18,457 psi

M.S. = $[(S_y)_{250}/S_b]$ - 1 = +0.67

Weld Between Bulkhead and Tubes

Ref. Dwg. 315-40-12 (Figure 2.10.13-1)

Peak Deceleration = 60.0g (30-Foot End Drop)

Weight of Bulkhead $= [\pi/4][(13)^2 - (3)(5.625)^2](1/4)(0.1)$
$= 1.5$ lbs

Weight of U-Bolts $= 1.5$ lbs

Total $= 3.0$ lbs

Inertial load of bulkhead on welds: $P = (3.0)(60) = 180$ lbs

Total length of weld per bulkhead: $L_w = (3)(3.0) = 9.0$ in min

Size of fillet $= 3/32$ in

Working capacity of welds: $P_{cap} = (0.707)(3/32)(9.0)(1200)$
$= 716$ lbs

M.S. $= [P_{cap}/P_{act}] - 1 = 716/180 - 1 = +2.98$

2.10.13.6.5 Failed Fuel Rod Can - 4.00 Inner Diameter (Ten Failed Fuel Filter Elements/Can)

Shell - Bending

Ref. Dwg 340-108-Dl, (Figure 2.10.13-3)

Ref. Dwg 491-042, (Figure 2.10.13-5)

Loading

30-Foot Side Drop Acceleration $= 49.7$ g

Support Spacing $= 50.37$ inches

Weight: Fuel $= 12$ lbs/11.2 inches $= 1.071$ lb/in

(Assumed to be effectively a distributed load; actual loading will occur near the ends of each failed fuel filter element)

Shell $= \frac{\pi}{4}\left((4.25)^2 - (4.0)^2\right)(1)(0.10) = \underline{0.162 \text{ lb/in}}$

Total $= 1.233$ lb/in

Conservatively, assume the shell is simply supported at the support disks; then, the moment during impact is:

$$M = \frac{1}{8}(1.233)(50.37)^2(49.7)$$

$= 19{,}435$ in-lb

Shell Properties: (4.00 I.D., t = 0.125 in)

I/C = [π][(4.25)4 - (4)4]/[(32)(4.25)]

= 1.623 in^3

Material Properties: (ASTM B221 Type 6061 T6)

$(S_y)_{250}$ = 30.8 ksi

Stresses:

S_b = 19,435/1.623 = 11,974 psi

M.S. = $[(S_y)_{250}/S_b]$ - 1 = +1.57

2.10.13.6.6 Liner - 3 Element (Ten Failed Fuel Filter Elements/Can)

Tube - Bending

Ref. Dwg 315-040-12, (Figure 2.10.13-1)

Ref. Dwg 491-042, (Figure 2.10.13-5)

Loading

30-Foot Side Drop Acceleration = 49.7 g

Support Spacing = 50.37 inches

Weight: Fuel = 12 lbs/11.2 inches = 1.071 lb/in

Shell $= \frac{\pi}{4}\left((4.25)^2 - (4.0)^2\right)(1)(0.10)$ = 0.162 lb/in

Tube $= \frac{\pi}{4}\left((5.625)^2 - (5.375)^2\right)(1)(0.1)$ = 0.216 lb/in

Total = 1.449 lb/in

Conservatively assume the tube is simply supported at the support disks; then, the moment during impact is:

$$M = \frac{1}{8}(1.449)(50.37)^2)(49.7)\,8$$

= 22,839 in-lb

Tube Properties:

I/C = [π][(5.625)4 - (5.375)4]/[(32)(5.625)]

= 2.9053 in^3

(The FFC is conservatively not considered to provide any bending strength for this analysis.)

Material Properties: (ASTM B210 Type 6061-T6)

$(S_y)_{250}$ = 30.8 ksi

Stresses:

S_b = 22,839/2.9053 = 7861 psi

M.S. = $[(S_y)_{250} / S_b] - 1$ = +2.91

2.10.13.7 Results and Conclusion

The maximum normal operating temperature of the failed fuel cans and the liner (basket) is calculated to be 211°F. The structural evaluation conservatively uses material properties at 250°F.

The calculated margins of safety are:

1. Failed Fuel Can - 2.75 Inner Diameter

Shell – Bending	+2.04
Shell – Buckling	+Large

2. Liner - Failed Fuel Can - 2.75 Inner Diameter

Housing – Bending	+3.32
Weld - Bulkhead/Tube	+Large

3. Failed Fuel Rod Can - 4.00 Inner Diameter (3 Failed Fuel Rod Loading)

Shell – Bending	+0.24

4. Liner - 3-Element (3 Failed Fuel Rods/Can)

Tube – Bending	+0.67
Weld - Bulkhead/Tube	+2.98

5. Failed Fuel Rod Can - 4.00 Inner Diameter (10 Failed Fuel Filter Elements/Can)

Shell – Bending	+1.57

6. Liner - 3-Element (10 Failed Fuel Filter Elements/Can)

Tube - Bending	+ 2.91

No permanent deformation occurs in the failed fuel cans or the liners for the critical loading conditions. Containment of the failed metallic fuel rods and failed fuel filters is maintained and the liner structure remains intact; therefore, structural adequacy is ensured.

2.10.13.8 Failed Fuel Shipment Component Drawings

The drawings referenced in Section 2.10.13.6 in support of analyses associated with the transport of failed fuel rods or filters containing severely failed fuel are provided in this section.

- NAC Drawing: 340-108-D1, Failed Fuel Rod Can - 4.00 I.D., Fuel Rod Containerization
- NAC Drawing: 340-108-D2, Failed Fuel Rod Can - 2.75 I.D., Fuel Rod Containerization
- NAC Drawing: 315-40-12, LWT Cask Metal Fuel Basket Assembly Safety Analysis Report
- NAC Drawing: 315-040-43, Liner - Failed Fuel Can, 2.75 I.D., LWT Cask, Safety Analysis Report
- NAC Drawing: 491-042, Failed Fuel Filter

Figure 2.10.13-1 LWT Cask, Metal Fuel Basket Assembly Safety Analysis Report, NAC Drawing No. 315-40-12

Figure Withheld Under 10 CFR 2.390

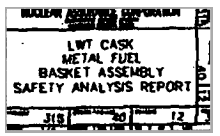

Figure 2.10.13-2 Liner-Failed Fuel Can, 2.75 I.D., LWT Cask, Safety Analysis Report, NAC Drawing No. 315-040-43

Figure Withheld Under 10 CFR 2.390

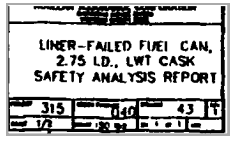

Figure 2.10.13-3 Failed Fuel Rod Can – 4.00 I.D., Fuel Rod Containerization, NAC Drawing No. 340-108-D1

Figure Withheld Under 10 CFR 2.390

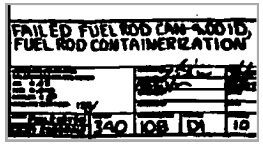

Figure 2.10.13-4 Failed Fuel Rod Can – 2.75 I.D., Fuel Rod Containerization, NAC Drawing No. 340-108-D2

Figure Withheld Under 10 CFR 2.390

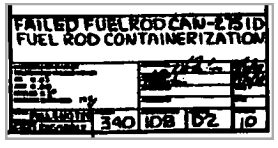

Figure 2.10.13-5 Failed Fuel Filter, NAC Drawing No. 491-042

Figure Withheld Under 10 CFR 2.390

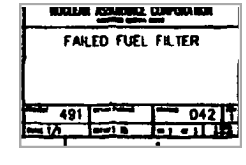

2.10.14 Structural Evaluation of the NAC-LWT Cask Body with TPBAR Contents

This section presents a structural evaluation of the NAC-LWT cask system with TPBAR contents under normal conditions of transport and hypothetical accident conditions. The NAC-LWT cask system with TPBARs is comprised of four primary components: NAC-LWT cask body, TPBAR basket, basket spacers, and TPBAR contents. The NAC-LWT cask system is structurally evaluated for two TPBAR content conditions: up to 300 production TPBARs loaded into an open (i.e., unsealed) consolidation canister; and up to 55 segmented TPBARs loaded into a welded closed waste container.

The NAC-LWT cask system containing TPBAR contents is required to have the Alternate B port covers installed and tested on the vent and drain ports to assure a leaktight containment boundary during transport. Section 2.10.15 presents the structural evaluation of the Alternate B port cover. Sections 2.6.12.10 and 2.7.7.12 present the structural evaluation for the TPBAR basket and basket spacers for the transport of the TPBAR content conditions under normal conditions of transport and hypothetical accident conditions, respectively.

2.10.14.1 Normal Conditions of Transport for Cask Body with TPBAR Contents

This section provides the cask body structural evaluation for normal conditions of transport. The following sections discuss the governing conditions of hot, cold, and drop conditions for normal transport.

2.10.14.1.1 Hot and Cold Conditions

Hot and cold conditions, as defined in 10CFR 71.71 (c) (1) and (2), are evaluated as part of the normal conditions of transport for a 1-foot free-drop evaluation (see Section 2.10.14.1.2). Since the 1-foot drop evaluations include the inertial loads and a bounding thermal load, the 1-foot drop evaluation bounds the evaluation for hot and cold conditions.

2.10.14.1.2 Free Drop (1 Foot)

The normal conditions drop orientations considered are: side drop, top-end drop, bottom-end drop, top-end CG-over-corner drop, and bottom-end CG-over-corner drop. Corner drops are defined as the CG of the cask over the impact limiter corner (15.74° from vertical).

Finite Element Model Description

A three-dimensional half-symmetry model of the LWT cask body is constructed using ANSYS solid elements (SOLID45). The finite element model contains the top and bottom forgings, cask sidewalls, lead shielding, cask lid and bolts. The cask shells are modeled using SA-240 Type

XM-19 stainless steel material properties. The cask top and bottom forgings and cask lid are modeled using SA182 Type 304 stainless steel forging material properties. The model is shown in Figure 2.10.14-1 through Figure 2.10.14-3.

The neutron shield tank and water inside the neutron shield tanks are represented with ANSYS MASS21 elements (approximately 5,600 lbs for entire cask, 2,000 lbs for tanks, and 3,600 lbs for the water). For the end drops, the MASS21 elements are applied around the outer circumference (0°–180°) of the LWT cask. For the side and corner drops, the MASS21 elements are applied to the lower half of the outer circumference (0°–90°) of the outer shell. As a modeling convenience, a small hole is modeled in the center of the lid and bottom of the cask. Symmetry boundary conditions are applied to the plane of symmetry of the cask body model. The lid bolts are modeled using beam elements (BEAM4). The preload of 35,000 lbs per bolt is modeled by applying an initial strain to the beam elements. The applied strain is 0.00273 in/in.

The lead is considered a soft material when compared with the stainless steel shells. To simulate the interface between lead and the stainless steel shells, a small gap of 0.015 inch is modeled using ANSYS CONTAC52 gap elements. Gap elements are also modeled between the lid and top forging and between the cask and the impact limiters. The interface between the cask and impact limiters simulates the pressure applied by the impact limiters during drop conditions. The gap stiffness is modeled as a cosine distribution from a maximum value of 1.0×10^6 lb/in at the line of impact to a value of 1.31×10^5 lb/in at an angle of 82.5° from the line of impact. A minimal value of 100 lb/in is used from 90° to 180°.

Inertia loads of 25 g for side drop and 20 g for the end and corner drops are used in the cask body evaluation for normal conditions. For all drop cases, a conservative internal pressure of 300 psig is applied on the cask cavity and lid interior surfaces in the outward normal direction. The pressure bounds the MNOP of 289 psig for normal conditions of transport (Section 3.4.4.4). The weight of the contents (basket, consolidation canister, and TPBARs) is also applied as a concentrated pressure loading over a single row of elements (7.5°) for side and corner drops. For end drops, the contents weight is applied to either the cask lid or bottom forging as appropriate. For other drop orientations, pressure is applied on the appropriate surface, depending on the drop angle.

To calculate the thermal stresses in the cask, the temperature results from the design basis PWR fuel configuration are used to derive a conservative temperature gradient for the calculation of thermal stresses. The heat load for the design basis PWR fuel of 2.5 kW is greater than the heat load for the TPBAR configuration (< 0.7 kW) and, therefore, the analysis is conservative. A temperature of 227°F is applied to the cask lid and top forging regions. At the axial center of the inner and outer shells, a temperature of 274°F and 229°F is applied, respectively. For the bottom of the cask and interface with the inner and outer shells, a temperature of 239°F is used. Using

these temperatures as input, a thermal conduction solution is obtained using the finite element model described in this section, with the exception that the ANSYS SOLID45 structural elements are replaced with the equivalent SOLID70 thermal elements. Once calculated, the temperatures from the thermal conduction solution are applied as a boundary condition to the cask body structural model to calculate thermal stresses.

Finite Element Analysis Result Summary

The most crucial sections for each cask component are shown in Figure 2.10.14-4. Table 2.10.14-1 shows the material designation at each section location. The maximum P_m, $P_m + P_b$, and P+Q stresses for each component are reported in Table 2.10.14-2 through 2.10.14-16 for the different drop orientations. Allowable stresses are conservatively reported at a temperature of 250°F. Margins of Safety greater than +10 are reported as "+Large."

The minimum margin of safety is +0.13, which occurs at section 2 for the condition of P_m stress for 1-foot side-drop conditions. This section is located at the axial center of the cask outer shell. The minimum margins of safety for each stress category for 1-foot drop conditions are as follows.

Stress Category	Section	Drop Orientation	Stress Intensity, ksi	Stress Allowable, ksi	Margin of Safety
P_m	2	Side	28.57	32.3	+0.13
$P_m + P_b$	2	Side	32.87	48.45	+0.47
P+Q	18	Side	31.3	60.0	+0.93

2.10.14.2 Hypothetical Accident Conditions for Cask Body with TPBAR Contents

This section provides the cask body structural evaluation for hypothetical accident conditions. The following sections discuss drop conditions and inner shell buckling.

2.10.14.2.1 Free Drop (30-Foot)

The hypothetical accident conditions drop orientations considered are: side drop, top-end drop, bottom-end drop, top-end CG-over-corner drop, and bottom-end CG-over-corner drop. Corner drops are defined as the CG of the cask over the impact limiter corner (15.74° from vertical).

Finite Element Model Description

The finite element model is described in Section 2.10.14.1.2. For accident conditions, an acceleration of 60 g is applied to all drop orientations. The temperature-dependent material properties presented in Section 2.3 are used in the analysis.

Finite Element Analysis Result Summary

The most critical sections for each cask component are shown in Figure 2.10.14-4. Table 2.10.14-1 shows the material at each section location. The maximum P_m and $P_m + P_b$ stresses for each component are reported in Tables 2.10.14-17 through 2.10.14-26 for different drop conditions. Allowable stresses are reported at a temperature of 250°F. Margins of Safety greater than +10.0 are reported as "+Large."

The minimum margin of safety is +0.02, which occurs at section 2 for the condition of P_m stress, for 30-foot drop conditions. This section is located at the axial center of the cask outer shell. The minimum Margins of Safety for each stress category for 30-foot drop conditions are as follows.

Stress Category	Section	Drop Orientation	Stress Intensity, Ksi	Stress Allowable, ksi	Margin of Safety
P_m	2	Side	66.5	67.83	+0.02
P_m+P_b	2	Side	74.14	96.9	+0.31

2.10.14.2.2 Fire Accident

A finite element analysis is performed using the three-dimensional model as described in Section 2.10.14.1.2 for the evaluation of the fire accident conditions. The maximum calculated internal pressure for the fire accident is 337 psig (Section 3.5.4.4). A bounding internal pressure of 600 psig is conservatively used in combination with the inertial load in the model. The maximum P_m and P_m+P_b stresses for each cask component are presented in Table 2.10.14-27 and Table 2.10.14-28. The minimum Margin of Safety is +7.38 and +8.32 for the P_m and P_m+P_b stresses, respectively.

2.10.14.3 Inner Shell Buckling

Section 2.10.6 presents a buckling evaluation of the cask inner shell per ASME Code Case N-284 for the design basis cask configuration. The evaluation presented in Section 2.10.6 bounds the TPBAR contents based on the following.

- The maximum weight of the TPBAR contents of 1,000 lbs envelops the weight of the design basis contents, which would reduce the compressive stresses in the cask shells due to less inertia loading for the drop conditions.
- The cask internal pressure for the TPBAR contents is significantly higher than the cask internal pressure for the design basis contents. The increase in the pressure would increase the tensile stresses in the shell that provide a stiffening of the inner shell and, consequently, reduce the compressive stresses associated with buckling.

The interaction summary presented in Table 2.10.6-10, associated with the design basis weight and the design basis pressure, is bounding for the TPBAR content conditions. Therefore, it is

concluded that the cask inner shell will not buckle with the TPBAR contents in the NAC-LWT cask.

2.10.14.4 NAC-LWT Cask Closure Lid and Bolts

The NAC-LWT cask closure lid is bolted to the cask body top forging with twelve 1-8 UNC bolts fabricated from SA-453, Grade 660 high-alloy steel. The threaded portion of the bolt engages the cask body a minimum of 1.875 inches. From Section 2.1.3.2.2, the torque on the cask lid bolts is 260 ± 20 ft-lb and the bolt preload is specified as 34,843 lbs. For the LWT cask configured to ship TPBARs, the maximum internal pressure of 600 psig is conservatively used in the closure lid evaluation. This pressure bounds the maximum pressure during the fire accident contained in Section 3.5.4.4. To ensure that the seal is not unloaded during accident conditions, the preload is calculated to account for the weight of the lid, internal weight of the cask contents, force resulting from internal pressure, force resulting from compression of the TFE O-ring, and force resulting from compression of the metallic O-ring. The load resulting from the weight of the LWT cask contents is

$$F_2 = W_c a = 1{,}800 \times 60g = 108{,}000 \text{ lbs}$$

where:

W_c = 1,800 lbs (bounding weight of TPBAR basket and contents)

a = 60 g (maximum accident acceleration)

The load resulting from accident pressure (fire accident) is:

$$F_{ip} = P_{ip} A = 600 \times 171.36 = 102{,}816 \text{ lbs}$$

where:

P_{ip} = 600 psig (accident internal pressure)

$$A = \frac{\pi}{4} \times 14.771^2 = 171.36 \text{ in}^2$$

The total required bolt preload force (12 bolts) is:

$$FT = F_1 + F_2 + F_{tr} + F_{mr} + F_{ip}$$

$$= 56{,}460 + 108{,}000 + 2{,}474 + 79{,}470 + 102{,}816 = 349{,}220 \text{ lbs}$$

where:

F_{tr} = 2,474 lbs, TFE O-ring load (Section 2.1.3.2.2)

F_{mr} = 79,470 lbs, Metallic O-ring load (Section 2.1.3.2.2)

F_1 = 56,460 lbs, Lid load (Section 2.1.3.2.2)

The required bolt preload per bolt is:

$$F_{bolt} = \frac{F_T}{12} = \frac{349{,}220}{12} = 29{,}102 \text{ lbs} \qquad < 34{,}843 \text{ lbs} \quad \text{(Section 2.1.3.2.2)}$$

Since the bolt preload presented in Section 2.1.3.2.2 of the NAC-LWT is bounding, no further analysis of the LWT lid bolts is required.

The preload applied to the cask lid bolts is due to the load applied to the lid. The load applied to the lid for the design basis weight and pressure for the PWR fuel bounds the load applied to the lid for the TPBAR contents. Therefore, the stresses in the cask lid due to the design basis weight and pressure also bound the stresses in the cask lid due to the TPBAR content weight and pressure.

2.10.14.5 Conclusion

Based on the evaluations presented in Sections 2.10.14.1 through 2.10.14.4, the NAC-LWT cask with TPBAR contents satisfies the requirements of 10 CFR 71 for the normal conditions of transport and for hypothetical accidents.

Figure 2.10.14-1 ANSYS Finite Element Model of the Cask Body

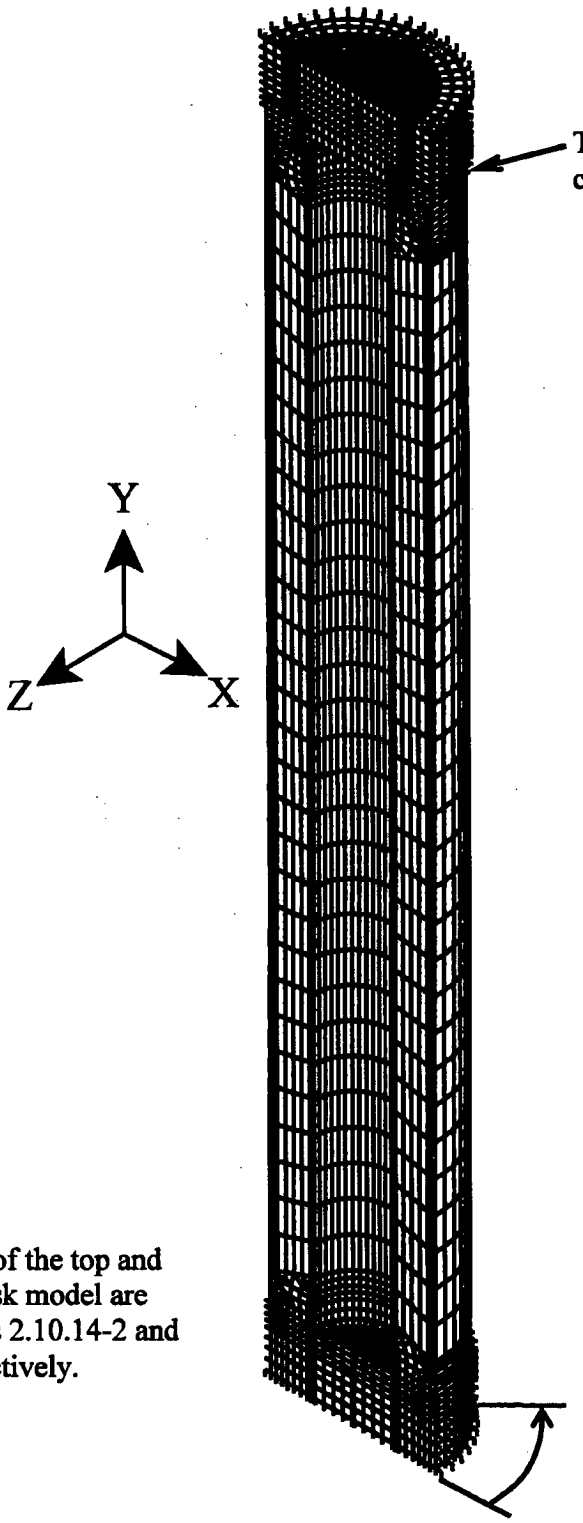

Note:
A detailed view of the top and bottom of the cask model are shown in Figures 2.10.14-2 and 2.10.14-3, respectively.

Figure 2.10.14-2 Detailed View of the Cask Body Finite Element Model Top

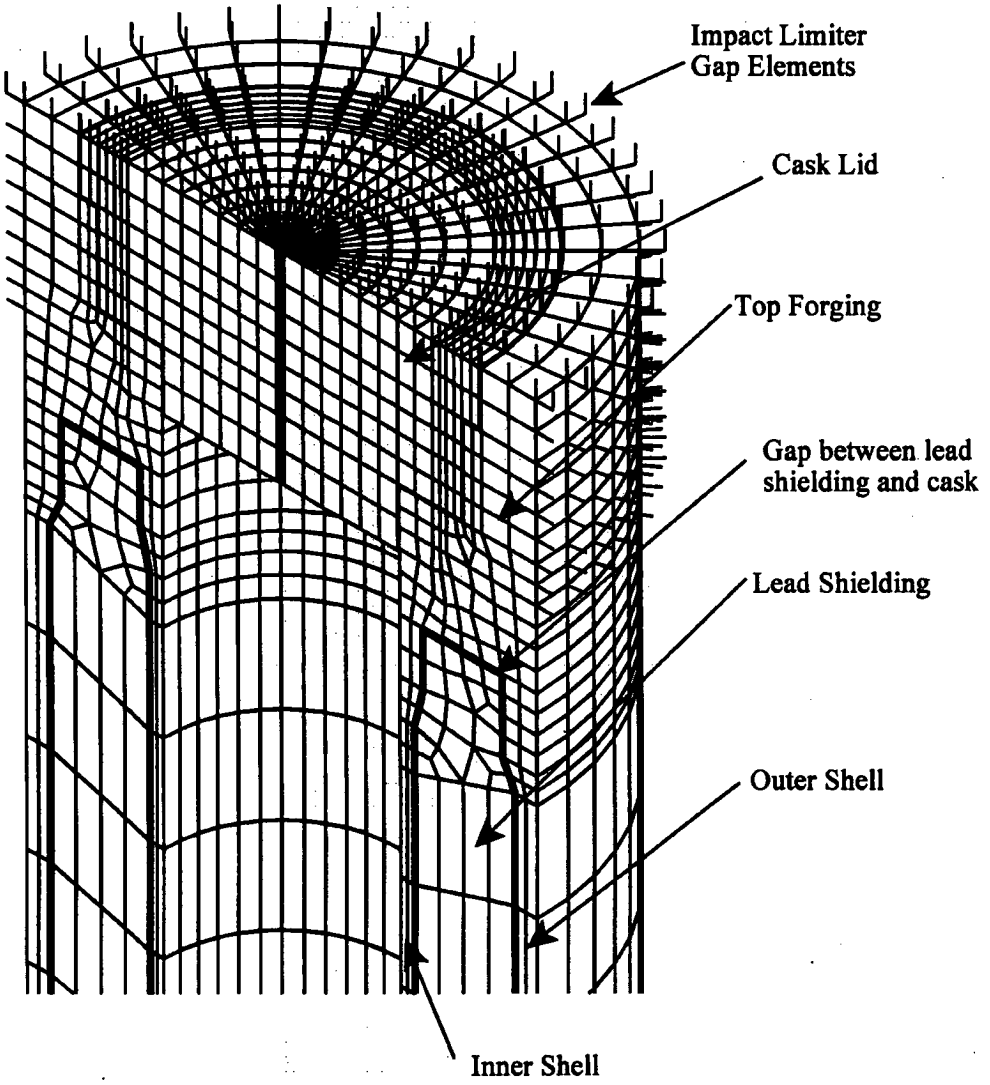

Figure 2.10.14-3 Detailed View of the Cask Body Finite Element Model Bottom

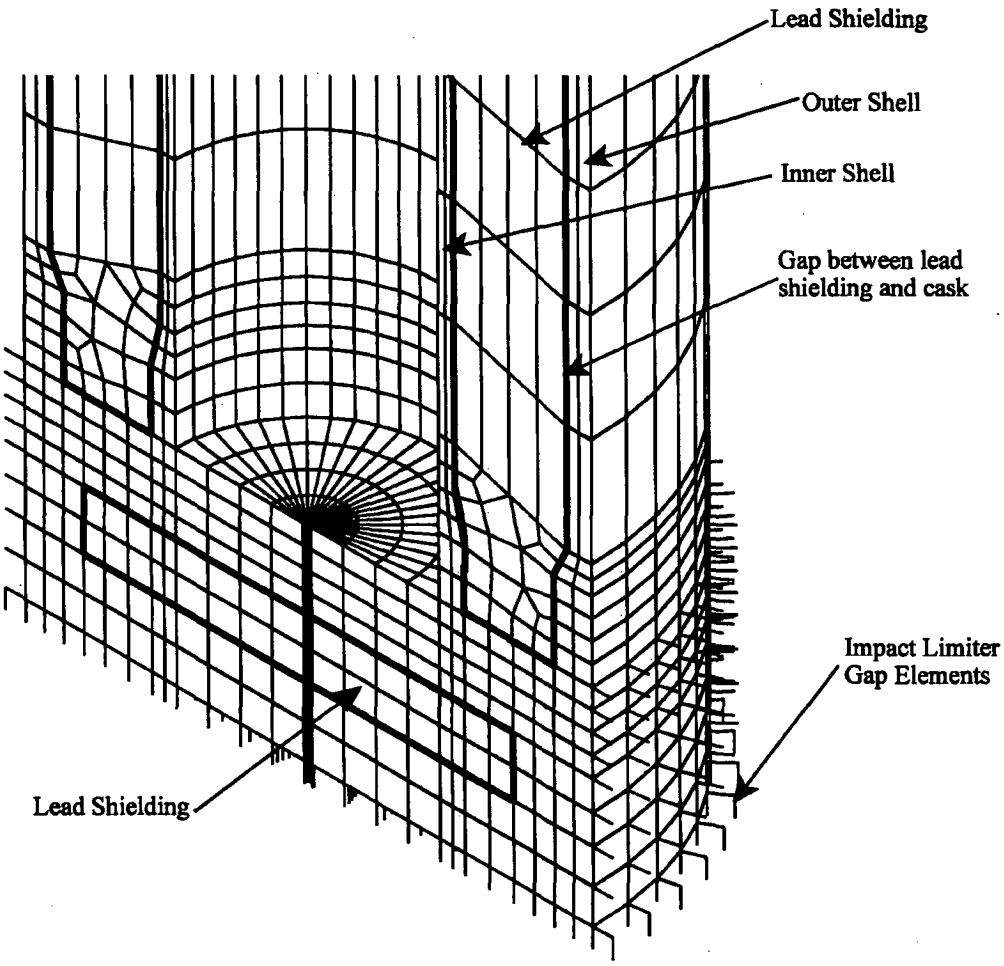

Figure 2.10.14-4 Location of Sections of the NAC-LWT Cask Body Model

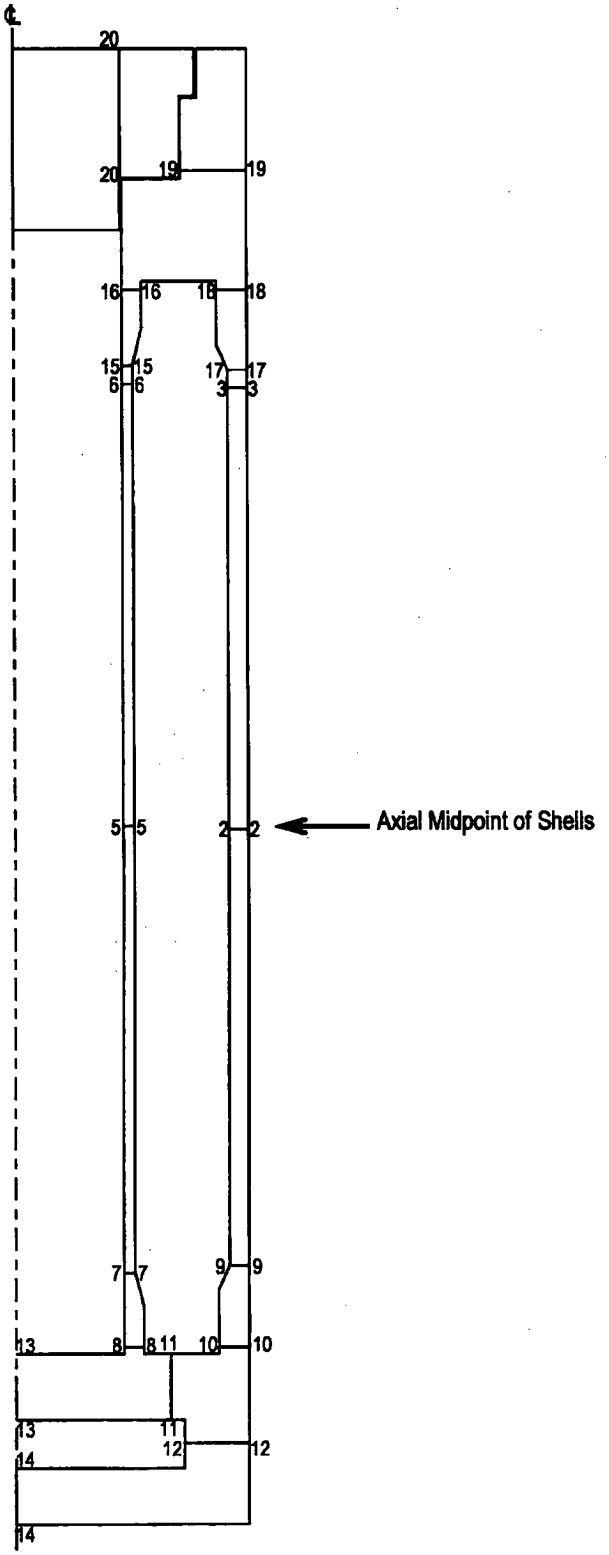

Table 2.10.14-1 Material Designations for Sections

Location	Material	Sections[1]
Outer Shell	SA240 Type XM-19	1-3
Inner Shell	SA240 Type XM-19	4-6
Bottom Forging	SA182 Type 304	7-14
Top Forging	SA182 Type 304	15-19
Lid	SA182 Type 304	20

[1] Sections are shown on Figure 2.10.14-4

Table 2.10.14-2 1-Foot Side Drop with Internal Pressure, P_m Stresses, ksi

Sec[1]	Location (deg)[2]	S_x[3]	S_y[3]	S_z[3]	S_{xy}[3]	S_{yz}[3]	S_{xz}[3]	Stress Intensity	Stress Allow.	MS
1	75	0.03	0.28	2.66	0.08	-6.74	-0.03	13.69	32.30	1.36
2	0	-0.14	1.71	28.41	-0.18	-0.01	0.00	28.57	32.30	0.13
3	67.5	0.04	0.39	3.97	0.05	6.06	0.00	12.64	32.30	1.56
4	97.5	-0.21	2.30	1.31	0.10	-4.21	0.01	8.48	32.30	2.81
5	180	-0.17	2.54	-16.05	0.18	0.00	0.00	18.61	32.30	0.74
6	97.5	-0.22	2.26	1.16	0.10	4.14	-0.01	8.36	32.30	2.86
7	112.5	-0.25	1.92	1.95	0.01	-5.75	-0.01	11.50	20.00	0.74
8	180	-1.99	1.79	6.11	0.06	-0.30	-1.98	9.04	20.00	1.21
9	67.5	0.02	-0.43	2.97	-0.34	-6.56	0.06	13.57	20.00	0.47
10	0	1.78	-4.55	1.05	0.74	-0.43	3.56	9.81	20.00	1.04
11	0	-4.87	-4.05	-0.46	0.11	0.06	0.28	4.45	20.00	3.49
12	0	-0.02	-1.51	-0.31	0.12	0.03	-0.54	1.92	20.00	9.42
13	90	-0.73	-3.26	-0.41	-0.08	0.36	0.04	2.94	20.00	5.80
14	0	-0.26	0.85	-0.41	0.00	-0.18	-0.33	1.56	20.00	+Large
15	112.5	-0.26	1.58	1.55	-0.03	5.90	0.00	11.81	20.00	0.69
16	127.5	-0.18	0.66	1.86	0.03	4.05	0.06	8.18	20.00	1.44
17	67.5	0.04	0.22	3.39	-0.30	6.07	-0.05	12.56	20.00	0.59
18	60	0.04	-0.27	2.57	0.05	4.11	-0.18	8.70	20.00	1.30
19	0	-2.82	-3.44	-1.15	0.41	0.06	1.74	4.04	20.00	3.95
20	105	0.12	-0.10	-0.78	-0.14	0.08	-0.43	1.30	20.00	+Large

Notes:
1. See Figure 2.10.14-4 for locations of sections.
2. The location specifies the angle at which the maximum stress intensity occurs. See Figure 2.10.14-1 for definition of angular location.
3. Stress components correspond to a cylindrical coordinate system.

Table 2.10.14-3 Side Drop with Internal Pressure, $P_m + P_b$ Stresses, ksi

Sec[1]	Location (deg)[2]	S_x[3]	S_y[3]	S_z[3]	S_{xy}[3]	S_{yz}[3]	S_{xz}[3]	Stress Intensity	Stress Allow.	MS
1	67.5	0.06	1.96	3.85	0.10	-7.45	-0.02	15.03	48.45	2.22
2	180	-0.06	5.49	-27.35	0.40	-0.01	0.00	32.87	48.45	0.47
3	67.5	0.07	2.32	4.74	0.08	6.85	-0.01	13.91	48.45	2.48
4	105	-0.38	-2.18	-0.40	0.07	-4.49	0.00	9.17	48.45	4.28
5	180	-0.10	3.68	-16.56	0.25	0.00	0.00	20.25	48.45	1.39
6	105	-0.10	6.74	2.59	0.03	3.79	-0.01	9.08	48.45	4.34
7	120	-0.31	-2.74	-0.38	-0.08	-6.52	-0.03	13.25	30.00	1.26
8	180	-3.38	1.06	11.77	0.00	0.00	-2.00	15.66	30.00	0.92
9	60	-0.07	0.46	3.44	-0.65	-7.78	0.24	15.90	30.00	0.89
10	0	4.60	-8.34	-11.23	0.64	-0.03	3.96	17.74	30.00	0.69
11	0	-8.51	-6.19	-0.09	0.09	0.09	0.82	8.59	30.00	2.49
12	0	0.19	-1.60	0.64	0.08	-0.06	-0.26	2.37	30.00	+Large
13	90	-1.43	-4.34	-0.43	-0.03	0.22	0.02	3.93	30.00	6.63
14	0	0.16	1.78	-1.80	0.02	-0.64	-0.30	3.84	30.00	6.81
15	120	-0.31	-3.50	-0.84	-0.15	6.59	0.01	13.45	30.00	1.23
16	180	-1.05	2.38	12.50	0.23	0.12	2.22	14.27	30.00	1.10
17	60	-0.08	1.62	4.85	-0.61	7.18	-0.31	14.78	30.00	1.03
18	37.5	-0.28	-0.47	6.66	0.12	5.17	-1.38	12.88	30.00	1.33
19	0	-1.16	-0.70	2.61	0.02	0.20	1.43	4.74	30.00	5.33
20	15	-2.43	-1.21	-1.48	0.08	-0.17	1.79	3.73	30.00	7.04

Notes:
1. See Figure 2.10.14-4 for locations of sections.
2. The location specifies the angle at which the maximum stress intensity occurs. See Figure 2.10.14-1 for definition of angular location.
3. Stress components correspond to a cylindrical coordinate system.

Table 2.10.14-4 1-Foot Side Drop with Internal Pressure, P + Q Stresses, ksi

Sec[1]	Location (deg)[2]	S_x[3]	S_y[3]	S_z[3]	S_{xy}[3]	S_{yz}[3]	S_{xz}[3]	Stress Intensity	Stress Allow.	MS
1	0	-0.55	15.41	23.96	-1.59	-0.42	0.12	24.70	96.90	2.92
2	0	-0.71	19.69	44.57	-1.80	-0.01	0.00	45.44	96.90	1.13
3	0	-0.54	13.83	26.27	-1.43	0.36	-0.13	26.97	96.90	2.59
4	105	-0.36	-2.17	3.28	0.07	-4.50	0.01	10.53	96.90	8.20
5	0	-0.18	6.18	23.65	-0.50	0.00	0.00	23.86	96.90	3.06
6	105	-0.38	-2.53	2.98	0.06	4.39	0.01	10.37	96.90	8.34
7	127.5	-0.28	-1.89	5.19	-0.29	-6.44	-0.03	14.72	60.00	3.08
8	180	-3.32	7.25	20.14	0.56	-0.01	-3.12	24.31	60.00	1.47
9	60	-0.93	8.89	16.68	-0.64	-7.74	1.26	22.56	60.00	1.66
10	0	0.34	6.19	26.82	0.50	-0.65	3.58	27.50	60.00	1.18
11	180	4.69	4.56	-9.20	0.03	-0.55	-3.99	16.06	60.00	2.74
12	180	-9.18	5.30	19.13	0.72	-0.15	1.68	28.54	60.00	1.10
13	90	-5.07	-10.02	0.47	-0.13	0.49	0.28	10.56	60.00	4.68
14	0	13.71	21.20	-4.61	-0.29	-0.83	-0.40	25.89	60.00	1.32
15	120	-0.32	-3.25	1.66	-0.15	6.60	0.17	14.09	60.00	3.26
16	180	-6.25	-4.80	8.34	-0.53	0.72	5.04	17.92	60.00	2.35
17	52.5	-0.81	9.24	19.43	-0.69	6.98	-1.50	24.02	60.00	1.50
18	0	-10.55	1.90	17.33	-1.49	-0.70	-6.67	31.10	60.00	0.93
19	0	-4.67	-5.23	-4.44	0.73	-0.11	2.00	4.31	60.00	+Large
20	45	-0.64	0.39	-1.81	0.39	-0.15	-3.41	7.01	60.00	7.56

Notes:
1. See Figure 2.10.14-4 for locations of sections.
2. The location specifies the angle at which the maximum stress intensity occurs. See Figure 2.10.14-1 for definition of angular location.
3. Stress components correspond to a cylindrical coordinate system.

Table 2.10.14-5 1-Foot Top-End Drop with Normal Internal Pressure, P_m Stresses, ksi

Sec[1]	S_x^2	S_y^2	S_z^2	S_{xy}^2	S_{yz}^2	S_{xz}^2	Stress Intensity	Stress Allow.	MS
1	0.00	-0.01	0.02	0.00	0.00	0.00	0.03	32.30	+Large
2	0.00	0.00	-0.42	0.00	0.00	0.00	0.42	32.30	+Large
3	0.00	-0.05	-0.95	0.00	0.00	0.00	0.96	32.30	+Large
4	-0.13	2.65	0.80	-0.18	0.00	0.00	2.81	32.30	+Large
5	-0.13	2.66	0.36	-0.18	0.00	0.00	2.82	32.30	+Large
6	-0.13	2.69	-0.15	-0.19	0.00	0.00	2.85	32.30	+Large
7	-0.14	2.75	0.82	-0.19	0.00	-0.05	2.92	20.00	5.85
8	-0.18	0.63	0.50	-0.05	0.01	0.14	0.84	20.00	+Large
9	0.00	-0.01	0.04	0.00	0.00	0.00	0.05	20.00	+Large
10	0.00	0.01	0.04	0.00	0.00	0.00	0.04	20.00	+Large
11	-0.04	0.01	-0.02	0.00	0.00	0.02	0.06	20.00	+Large
12	0.00	0.02	0.01	0.00	0.00	0.02	0.04	20.00	+Large
13	0.02	0.02	-0.21	0.00	0.00	0.03	0.24	20.00	+Large
14	0.04	0.05	-0.02	0.00	0.00	0.01	0.07	20.00	+Large
15	-0.15	2.63	-0.25	-0.18	0.01	0.04	2.91	20.00	5.87
16	-2.27	-1.66	-1.13	-0.24	0.10	0.88	2.16	20.00	8.26
17	0.02	0.35	-0.94	0.00	0.00	0.02	1.29	20.00	+Large
18	-2.14	0.67	-1.27	0.34	0.14	-0.50	3.12	20.00	5.41
19	-0.25	0.73	-1.44	0.10	-0.06	0.34	2.27	20.00	7.81
20	-0.27	-0.52	-2.01	-0.01	-0.01	0.31	1.85	20.00	9.81

Notes: 1. See Figure 2.10.14-4 for locations of sections.

2. Stress components correspond to a cylindrical coordinate system.

Table 2.10.14-6 1-Foot Top-End Drop with Internal Pressure, $P_m + P_b$ Stresses, ksi

Sec[1]	S_x[2]	S_y[2]	S_z[2]	S_{xy}[2]	S_{yz}[2]	S_{xz}[2]	Stress Intensity	Stress Allow.	MS
1	0.00	-0.01	0.03	0.00	0.00	0.00	0.03	48.45	+Large
2	0.00	0.00	-0.42	0.00	0.00	0.00	0.43	48.45	+Large
3	0.00	-0.11	-1.10	0.01	0.00	0.00	1.10	48.45	+Large
4	-0.21	2.84	0.84	-0.20	0.00	0.00	3.07	48.45	+Large
5	-0.20	2.85	0.39	-0.20	0.00	0.00	3.07	48.45	+Large
6	-0.21	2.94	-0.09	-0.21	0.01	0.01	3.18	48.45	+Large
7	-0.20	2.80	0.36	-0.20	0.00	-0.05	3.02	30.00	8.93
8	-0.33	0.92	1.28	-0.08	0.01	0.16	1.65	30.00	+Large
9	0.00	0.00	0.06	0.00	0.00	0.01	0.06	30.00	+Large
10	0.00	0.01	0.04	0.00	0.00	0.00	0.04	30.00	+Large
11	-0.06	0.02	-0.04	0.00	0.00	0.00	0.08	30.00	+Large
12	-0.01	0.02	0.00	0.00	0.00	0.02	0.05	30.00	+Large
13	0.33	0.48	-0.15	-0.01	0.00	0.03	0.63	30.00	+Large
14	0.08	0.13	-0.02	0.00	0.00	0.01	0.16	30.00	+Large
15	-0.19	2.70	-0.94	-0.19	0.01	0.05	3.65	30.00	7.22
16	-3.18	-3.36	-4.31	0.43	-0.36	1.53	3.42	30.00	7.77
17	0.00	0.22	-1.23	-0.02	0.01	0.02	1.45	30.00	+Large
18	-3.50	-0.35	-3.43	-0.47	-0.39	-1.04	4.34	30.00	5.91
19	-0.49	0.68	-1.77	0.14	-0.13	0.47	2.64	30.00	+Large
20	0.13	-0.14	-1.72	0.00	-0.01	1.83	4.10	30.00	6.32

[1] See Figure 2.10.14-4 for locations of sections.
[2] Stress components correspond to a cylindrical coordinate system.

Table 2.10.14-7 1-Foot Top-End Drop with Internal Pressure, P + Q Stresses, ksi

Sec[1]	S_x[2]	S_y[2]	S_z[2]	S_{xy}[2]	S_{yz}[2]	S_{xz}[2]	Stress Intensity	Stress Allow.	MS
1	-0.52	12.95	15.18	-1.32	0.04	0.04	15.83	96.90	5.12
2	-0.64	15.83	13.76	-1.49	0.00	0.00	16.74	96.90	4.79
3	-0.52	10.70	13.97	-1.14	-0.10	-0.08	14.61	96.90	5.63
4	-0.20	3.10	4.88	0.00	-0.21	0.02	5.10	96.90	+Large
5	-0.20	2.83	3.76	-0.20	0.00	0.00	3.97	96.90	+Large
6	-0.21	3.31	4.56	0.02	0.48	-0.01	4.93	96.90	+Large
7	-0.28	5.22	5.61	-0.18	-1.18	-0.12	6.91	60.00	7.68
8	-0.81	6.85	8.05	-0.38	-0.88	-0.76	9.45	60.00	5.35
9	-0.51	7.65	14.92	-0.65	0.20	0.33	15.50	60.00	2.87
10	2.39	4.05	20.04	1.25	-0.57	2.66	19.10	60.00	2.14
11	-2.18	-14.93	-8.39	2.15	0.03	-3.63	15.09	60.00	2.98
12	-11.68	-3.17	20.44	0.95	0.25	0.86	32.27	60.00	0.86
13	-12.94	-27.36	-3.27	2.41	1.70	0.18	24.72	60.00	1.43
14	14.78	25.68	0.00	0.43	2.99	0.07	26.38	60.00	1.27
15	-0.51	6.64	6.70	-0.24	1.89	0.26	9.09	60.00	5.60
16	-2.24	-10.97	2.01	-0.21	3.30	0.34	14.59	60.00	3.11
17	-1.28	7.78	13.30	-0.79	0.05	-1.06	14.80	60.00	3.05
18	-13.49	2.32	3.59	1.97	1.52	-5.23	20.64	60.00	1.91
19	-0.33	-21.42	-6.90	1.77	2.11	-0.54	21.71	60.00	1.76
20	-4.38	-1.14	-3.50	-0.08	-0.46	6.65	13.37	60.00	3.49

[1] See Figure 2.10.14-4 for locations of sections.
[2] Stress components correspond to a cylindrical coordinate system.

Table 2.10.14-8 1-Foot Top-Corner Drop with Internal Pressure, P_m Stresses, ksi

Sec[1]	Location (deg)[2]	S_x[3]	S_y[3]	S_z[3]	S_{xy}[3]	S_{yz}[3]	S_{xz}[3]	Stress Intensity	Stress Allow.	MS
1	180	0.00	0.10	-1.84	0.00	-0.03	-0.01	1.95	32.30	+Large
2	180	-0.03	-0.13	-3.67	0.00	0.02	0.00	3.65	32.30	7.85
3	0	0.02	0.11	-2.83	0.00	0.07	0.00	2.94	32.30	9.99
4	90	-0.14	2.66	0.59	0.04	-0.87	0.01	3.12	32.30	9.35
5	180	-0.15	2.63	-2.37	0.17	0.01	0.00	5.01	32.30	5.45
6	0	-0.14	2.80	-2.49	-0.22	0.05	0.00	5.31	32.30	5.08
7	120	-0.17	2.54	1.01	0.03	-1.26	-0.02	3.42	20.00	4.85
8	180	-0.75	1.14	2.00	0.05	-0.09	-0.55	2.97	20.00	5.73
9	60	0.00	-0.06	0.42	-0.04	-0.95	-0.01	1.96	20.00	9.20
10	0	0.10	-0.78	-0.21	0.09	-0.07	0.72	1.58	20.00	+Large
11	180	0.18	0.23	0.19	-0.01	0.04	-0.42	0.85	20.00	+Large
12	0	0.00	-0.23	-0.17	0.02	0.02	-0.19	0.43	20.00	+Large
13	82.5	-0.04	-0.25	0.00	0.02	0.07	0.00	0.30	20.00	+Large
14	90	0.03	-0.30	0.00	-0.01	0.08	-0.01	0.36	20.00	+Large
15	0	-0.13	2.29	-3.27	-0.17	0.05	-0.05	5.57	20.00	2.59
16	180	-2.14	-1.54	0.38	-0.23	0.09	0.87	3.12	20.00	5.41
17	0	0.03	0.55	-3.01	-0.03	0.07	0.07	3.57	20.00	4.60
18	0	-2.92	0.34	-3.47	-0.43	-0.12	-0.68	4.35	20.00	3.60
19	0	-1.02	-0.31	-3.45	0.01	0.12	0.47	3.24	20.00	5.17
20	0	-0.56	-0.65	-2.69	0.03	0.04	0.38	2.27	20.00	7.81

[1] See Figure 2.10.14-4 for locations of sections.
[2] The location specifies the angle at which the maximum stress intensity occurs. See Figure 2.10.14-1 for definition of angular location.
[3] Stress components correspond to a cylindrical coordinate system.

Table 2.10.14-9 1-Foot Top-Corner Drop with Internal Pressure, $P_m + P_b$ Stresses, ksi

Sec[1]	Location (deg)[2]	S_x[3]	S_y[3]	S_z[3]	S_{xy}[3]	S_{yz}[3]	S_{xz}[3]	Stress Intensity	Stress Allow.	MS
1	52.5	0.02	0.75	0.68	0.02	-1.19	-0.01	2.38	48.45	+Large
2	180	-0.02	1.88	-3.16	0.14	0.02	0.00	5.06	48.45	8.58
3	0	0.03	0.19	-2.96	-0.01	0.07	0.00	3.15	48.45	+Large
4	180	-0.21	5.36	1.54	0.29	-0.06	0.00	5.60	48.45	7.65
5	180	-0.22	2.93	-2.17	0.19	0.01	0.00	5.11	48.45	8.48
6	0	-0.04	3.07	-2.44	-0.23	0.04	-0.01	5.53	48.45	7.76
7	180	-0.30	4.86	3.07	0.23	-0.18	-0.03	5.20	30.00	4.77
8	180	-1.05	0.29	3.37	-0.02	0.08	-0.57	4.56	30.00	5.58
9	45	-0.02	0.29	0.44	-0.12	-1.30	0.03	2.62	30.00	+Large
10	0	0.63	-1.09	-2.46	0.08	0.07	0.74	3.44	30.00	7.72
11	180	0.85	0.60	0.02	-0.01	0.05	-0.55	1.37	30.00	+Large
12	180	0.06	0.13	0.24	0.00	0.01	-0.25	0.54	30.00	+Large
13	90	-0.13	-0.39	0.03	-0.02	0.10	0.01	0.47	30.00	+Large
14	105	-0.05	-0.48	0.02	-0.13	0.07	0.00	0.56	30.00	+Large
15	15	-0.16	2.38	-3.36	-0.02	0.29	-0.04	5.77	30.00	4.20
16	7.5	-1.53	-2.80	-6.23	0.11	-0.21	0.48	4.81	30.00	5.24
17	0	-0.03	0.52	-3.23	-0.03	0.06	-0.02	3.75	30.00	7.00
18	0	-4.71	-0.82	-5.65	-0.61	-0.44	-1.37	6.00	30.00	4.00
19	7.5	-0.55	-0.93	-4.50	0.09	0.07	0.29	4.02	30.00	6.46
20	15	0.53	-0.15	-1.96	0.03	0.01	1.82	4.41	30.00	5.80

[1] See Figure 2.10.14-4 for locations of sections.
[2] The location specifies the angle at which the maximum stress intensity occurs. See Figure 2.10.14-1 for definition of angular location.
[3] Stress components correspond to a cylindrical coordinate system.

Table 2.10.14-10 1-Foot Top-Corner Drop with Internal Pressure, P + Q Stresses, ksi

Sec[1]	Location (deg)[2]	S_x[3]	S_y[3]	S_z[3]	S_{xy}[3]	S_{yz}[3]	S_{xz}[3]	Stress Intensity	Stress Allow.	MS
1	0	-0.61	13.84	16.03	-1.45	0.00	0.09	16.78	96.90	4.77
2	0	-0.68	17.69	17.49	-1.62	0.02	0.00	18.65	96.90	4.20
3	180	-0.58	10.62	13.95	1.13	0.13	-0.09	14.65	96.90	5.61
4	180	-0.20	5.24	5.22	0.28	-0.07	0.01	5.52	96.90	+Large
5	0	-0.08	3.13	6.51	-0.23	0.01	0.00	6.61	96.90	+Large
6	180	-0.23	2.64	5.39	0.20	0.04	0.00	5.63	96.90	+Large
7	180	-0.31	5.20	7.56	0.25	-0.19	0.00	7.90	60.00	6.59
8	180	-1.00	6.47	11.74	0.54	0.07	-1.69	13.22	60.00	3.54
9	30	-0.89	8.92	13.67	-0.16	-1.38	1.06	15.09	60.00	2.98
10	0	0.94	6.46	15.53	-0.24	-0.04	1.11	14.77	60.00	3.06
11	7.5	5.44	-0.93	-7.47	0.03	-0.02	-3.90	15.09	60.00	2.98
12	180	-9.30	4.39	18.60	0.70	-0.13	1.85	28.18	60.00	1.13
13	75	7.18	10.40	-0.43	-0.01	0.04	-0.03	10.83	60.00	4.54
14	0	13.27	19.46	-2.77	-0.31	-0.19	-0.14	22.25	60.00	1.70
15	180	-0.25	3.87	8.31	0.26	0.03	0.26	8.59	60.00	5.98
16	165	-2.03	-4.30	7.35	-0.10	0.25	0.62	11.71	60.00	4.12
17	180	-1.17	7.04	14.41	0.73	0.03	-1.36	15.88	60.00	2.78
18	180	-12.10	2.59	6.12	1.79	1.42	-4.91	21.15	60.00	1.84
19	0	-1.40	0.01	-4.32	0.09	-0.01	0.22	4.36	60.00	+Large
20	15	1.69	0.13	-2.70	0.02	0.00	3.18	7.73	60.00	6.76

[1] See Figure 2.10.14-4 for locations of sections.
[2] The location specifies the angle at which the maximum stress intensity occurs. See Figure 2.10.14-1 for definition of angular location.
[3] Stress components correspond to a cylindrical coordinate system.

Table 2.10.14-11 1-Foot Bottom-End Drop with Internal Pressure, P_m Stresses, ksi

Sec[1]	S_x[2]	S_y[2]	S_z[2]	S_{xy}[2]	S_{yz}[2]	S_{xz}[2]	Stress Intensity	Stress Allow.	MS
1	0.01	0.08	-1.34	0.00	0.00	-0.01	1.42	32.30	+Large
2	0.00	0.00	-0.78	0.00	0.00	0.00	0.78	32.30	+Large
3	0.00	0.02	-0.34	0.00	0.00	0.00	0.36	32.30	+Large
4	-0.13	2.69	-0.49	-0.18	0.00	0.00	3.19	32.30	9.13
5	-0.13	2.66	0.00	-0.18	0.00	0.00	2.82	32.30	+Large
6	-0.13	2.67	0.43	-0.18	0.00	0.00	2.82	32.30	+Large
7	-0.12	2.58	-0.57	-0.18	0.00	0.00	3.16	20.00	5.33
8	0.07	1.33	-0.38	-0.01	-0.01	0.04	1.71	20.00	+Large
9	0.01	0.09	-1.30	-0.01	0.00	-0.03	1.39	20.00	+Large
10	0.09	0.29	-0.98	0.01	0.00	-0.08	1.28	20.00	+Large
11	0.62	0.06	-3.56	-0.04	-0.22	0.14	4.20	20.00	3.76
12	-0.35	0.34	-1.66	0.04	0.03	-0.17	2.03	20.00	8.85
13	0.69	0.93	-0.79	0.02	0.00	-0.13	1.73	20.00	+Large
14	-0.40	-0.68	-4.05	0.02	-0.05	-0.60	3.85	20.00	4.19
15	-0.14	2.68	0.45	-0.18	0.00	0.03	2.84	20.00	6.04
16	-0.08	1.08	0.29	-0.08	0.00	-0.06	1.18	20.00	+Large
17	0.00	0.02	-0.29	0.00	0.00	0.01	0.32	20.00	+Large
18	0.00	0.06	-0.18	0.00	0.00	0.02	0.25	20.00	+Large
19	-0.04	0.22	-0.22	0.00	0.00	0.03	0.45	20.00	+Large
20	-0.15	0.08	-0.90	0.00	0.00	-0.25	1.06	20.00	+Large

[1] See Figure 2.10.14-4 for locations of sections.
[2] Stress components correspond to a cylindrical coordinate system.

Table 2.10.14-12 1-Foot Bottom-End Drop with Internal Pressure, $P_m + P_b$ Stresses, ksi

Sec[1]	S_x[2]	S_y[2]	S_z[2]	S_{xy}[2]	S_{yz}[2]	S_{xz}[2]	Stress Intensity	Stress Allow.	MS
1	0.01	0.12	-1.35	-0.01	0.00	-0.01	1.47	48.45	+Large
2	0.00	0.01	-0.78	0.00	0.00	0.00	0.79	48.45	+Large
3	0.00	0.02	-0.34	0.00	0.00	0.00	0.36	48.45	+Large
4	-0.20	2.92	-0.45	-0.20	0.00	0.00	3.38	48.45	+Large
5	-0.20	2.85	0.03	-0.20	0.00	0.00	3.07	48.45	+Large
6	-0.21	2.85	0.47	-0.20	0.00	0.00	3.09	48.45	+Large
7	-0.19	2.75	-0.71	-0.19	0.00	0.00	3.47	30.00	7.65
8	-0.08	1.45	-0.52	0.10	-0.01	0.01	1.98	30.00	+Large
9	0.03	0.11	-1.36	-0.01	-0.01	-0.07	1.47	30.00	+Large
10	0.07	0.21	-1.16	-0.03	-0.03	-0.06	1.38	30.00	+Large
11	-0.32	-1.37	-7.60	-0.07	-0.62	0.23	7.37	30.00	3.07
12	-0.63	-0.07	-3.13	0.04	0.03	-0.26	3.09	30.00	8.71
13	1.89	2.83	-0.47	0.01	-0.01	-0.11	3.31	30.00	8.06
14	1.41	3.02	-2.90	0.00	0.05	-0.70	6.03	30.00	3.98
15	-0.20	2.77	0.13	-0.19	0.00	0.03	2.99	30.00	9.03
16	-0.18	1.29	0.63	-0.10	-0.01	-0.06	1.49	30.00	+Large
17	0.01	0.02	-0.31	0.00	0.00	0.02	0.34	30.00	+Large
18	0.01	0.07	-0.18	0.00	0.00	0.02	0.26	30.00	+Large
19	-0.06	0.22	-0.45	0.00	0.01	0.02	0.67	30.00	+Large
20	-0.31	0.33	-0.88	0.01	0.00	-1.66	3.37	30.00	7.90

[1] See Figure 2.10.14-4 for locations of sections.
[2] Stress components correspond to a cylindrical coordinate system.

Table 2.10.14-13 1-Foot Bottom-End Drop with Internal Pressure, P + Q Stresses, ksi

Sec[1]	S_x[2]	S_y[2]	S_z[2]	S_{xy}[2]	S_{yz}[2]	S_{xz}[2]	Stress Intensity	Stress Allow.	MS
1	-0.51	12.99	13.84	-1.32	0.03	0.04	14.48	96.90	5.69
2	-0.64	15.83	13.40	-1.49	0.00	0.00	16.74	96.90	4.79
3	-0.53	10.82	14.75	-1.15	-0.10	-0.07	15.40	96.90	5.29
4	-0.16	3.34	3.35	-0.07	-0.56	-0.01	4.06	96.90	+Large
5	-0.20	2.83	3.40	-0.20	0.00	0.00	3.61	96.90	+Large
6	-0.21	3.26	5.02	0.02	0.46	-0.01	5.34	96.90	+Large
7	-0.28	5.08	4.11	-0.19	-1.24	-0.08	6.22	60.00	8.65
8	-0.61	7.94	8.34	-0.39	-0.92	-0.87	9.81	60.00	5.12
9	-0.52	7.71	13.65	-0.66	0.20	0.36	14.24	60.00	3.21
10	2.70	4.55	19.44	1.26	-0.54	2.56	18.13	60.00	2.31
11	1.52	0.70	-16.74	-0.02	-1.30	-1.91	18.76	60.00	2.20
12	-12.30	-3.34	17.50	0.96	0.22	0.72	29.94	60.00	1.00
13	-13.81	-28.99	-4.35	2.43	1.73	0.00	25.26	60.00	1.38
14	11.85	19.76	-7.14	0.45	1.90	-0.81	27.22	60.00	1.20
15	-0.46	6.38	6.77	-0.23	1.81	0.24	8.88	60.00	5.76
16	-1.29	-7.82	1.82	-0.45	3.42	0.31	11.86	60.00	4.06
17	-1.31	7.38	13.67	-0.76	0.05	-1.07	15.20	60.00	2.95
18	-10.04	2.68	6.68	1.51	1.13	-4.19	19.03	60.00	2.15
19	-0.21	-22.47	-6.98	1.67	2.23	-0.70	22.88	60.00	1.62
20	-5.62	-2.02	-2.52	-0.04	-0.44	5.39	11.25	60.00	4.33

[1] See Figure 2.10.14-4 for locations of sections.
[2] Stress components correspond to a cylindrical coordinate system.

Table 2.10.14-14 1-Foot Bottom-Corner Drop with Internal Pressure, P_m Stresses, ksi

Sec[1]	Location (deg)[2]	S_x[3]	S_y[3]	S_z[3]	S_{xy}[3]	S_{yz}[3]	S_{xz}[3]	Stress Intensity	Stress Allow.	MS
1	0	0.03	0.29	-3.53	-0.01	-0.09	-0.02	3.83	32.30	7.43
2	180	-0.03	-0.13	-3.65	0.00	-0.02	0.00	3.62	32.30	7.92
3	180	0.00	0.13	-2.21	0.01	0.03	0.01	2.34	32.30	+Large
4	0	-0.14	2.80	-2.63	-0.21	-0.05	0.00	5.44	32.30	4.94
5	180	-0.15	2.63	-2.35	0.17	-0.01	0.00	4.99	32.30	5.47
6	82.5	-0.14	2.69	0.54	0.04	0.82	0.00	3.11	32.30	9.39
7	0	-0.11	2.28	-3.40	-0.17	-0.05	0.08	5.70	20.00	2.51
8	7.5	0.17	0.97	-2.24	-0.02	-0.04	0.23	3.23	20.00	5.19
9	0	0.02	0.09	-3.75	0.00	-0.08	-0.07	3.84	20.00	4.21
10	0	0.50	-0.14	-2.88	0.07	-0.06	0.08	3.39	20.00	4.90
11	0	-0.04	-0.24	-4.08	0.05	0.26	0.53	4.22	20.00	3.74
12	0	-0.96	-0.25	-3.79	0.03	-0.07	-0.25	3.56	20.00	4.62
13	180	0.12	0.71	-0.73	0.01	0.00	-0.24	1.51	20.00	+Large
14	180	-0.38	-0.52	-3.79	-0.02	0.06	-0.75	3.73	20.00	4.36
15	112.5	-0.16	2.56	0.76	0.04	1.25	0.01	3.36	20.00	4.95
16	165	-0.16	1.58	1.85	-0.01	0.53	0.46	2.59	20.00	6.72
17	180	0.00	0.16	-1.95	-0.01	0.02	0.05	2.12	20.00	8.43
18	180	-0.01	0.04	-1.25	0.00	0.01	0.08	1.29	20.00	+Large
19	180	-0.09	0.20	-0.32	0.02	-0.03	0.17	0.61	20.00	+Large
20	82.5	0.02	-0.38	-0.99	0.10	0.02	-0.16	1.08	20.00	+Large

[1] See Figure 2.10.14-4 for locations of sections.
[2] The location specifies the angle at which the maximum stress intensity occurs. See Figure 2.10.14-1 for definition of angular location.
[3] Stress components correspond to a cylindrical coordinate system.

Table 2.10.14-15 1-Foot Bottom-Corner Drop with Internal Pressure, $P_m + P_b$ Stresses, ksi

Sec[1]	Location (deg)[2]	S_x[3]	S_y[3]	S_z[3]	S_{xy}[3]	S_{yz}[3]	S_{xz}[3]	Stress Intensity	Stress Allow.	MS
1	0	0.04	0.39	-3.44	-0.02	-0.08	0.00	3.84	48.45	+Large
2	180	-0.02	1.88	-3.13	0.14	-0.03	0.00	5.03	48.45	8.63
3	180	0.01	0.38	-2.18	0.02	0.04	0.00	2.56	48.45	+Large
4	0	-0.05	3.09	-2.58	-0.23	-0.04	0.01	5.69	48.45	7.51
5	180	-0.22	2.87	-2.17	0.19	-0.01	0.00	5.06	48.45	8.58
6	180	-0.21	5.48	1.33	0.30	0.06	0.00	5.72	48.45	7.47
7	0	-0.03	2.32	-3.59	-0.17	-0.03	0.08	5.92	30.00	4.07
8	7.5	0.41	0.83	-2.60	-0.03	0.02	0.22	3.45	30.00	7.70
9	0	0.09	0.04	-3.99	0.00	-0.11	-0.22	4.11	30.00	6.30
10	0	0.50	-0.74	-4.57	0.03	-0.07	0.18	5.08	30.00	4.91
11	0	-0.70	-1.66	-8.28	0.10	0.70	0.77	7.82	30.00	2.84
12	0	-0.96	-0.45	-4.83	-0.01	-0.06	-0.34	4.41	30.00	5.80
13	7.5	1.23	2.32	-0.47	0.06	0.00	-0.02	2.79	30.00	9.75
14	7.5	1.46	2.91	-2.86	0.01	-0.01	-0.44	5.81	30.00	4.16
15	180	-0.28	4.86	3.14	0.23	0.18	-0.02	5.19	30.00	4.78
16	180	-0.09	1.16	4.05	0.13	-0.08	0.62	4.34	30.00	5.91
17	37.5	-0.01	0.54	0.81	-0.14	1.21	-0.06	2.45	30.00	+Large
18	22.5	-0.07	0.01	1.28	0.02	1.01	-0.28	2.46	30.00	+Large
19	180	-0.21	0.31	-0.27	0.05	-0.08	0.25	0.83	30.00	+Large
20	45	-0.23	0.33	-0.87	0.11	-0.03	-1.67	3.41	30.00	7.80

[1] Figure 2.10.14-4 for locations of sections.
[2] The location specifies the angle at which the maximum stress intensity occurs. See Figure 2.10.14-1 for definition of angular location.
[3] Stress components correspond to a cylindrical coordinate system.

Table 2.10.14-16 1-Foot Bottom-Corner Drop with Internal Pressure, P + Q Stresses, ksi

Sec[1]	Location (deg)[2]	S_x[3]	S_y[3]	S_z[3]	S_{xy}[3]	S_{yz}[3]	S_{xz}[3]	Stress Intensity	Stress Allow.	MS
1	180	-0.62	12.07	14.85	1.27	-0.13	0.07	15.60	96.90	5.21
2	0	-0.68	17.69	17.35	-1.62	-0.02	0.00	18.65	96.90	4.20
3	0	-0.57	12.42	16.02	-1.31	-0.01	-0.10	16.72	96.90	4.80
4	180	-0.08	2.46	5.51	0.17	-0.04	0.00	5.60	96.90	+Large
5	0	-0.09	3.16	6.42	-0.23	-0.01	0.00	6.52	96.90	+Large
6	180	-0.22	5.33	5.05	0.30	0.06	0.00	5.59	96.90	+Large
7	180	-0.22	3.33	6.15	0.24	-0.04	-0.04	6.39	60.00	8.39
8	0	0.29	4.73	-5.70	-0.27	-0.09	-0.99	10.61	60.00	4.66
9	180	-1.36	7.51	13.74	0.81	0.02	1.25	15.38	60.00	2.90
10	180	1.51	7.41	13.95	0.36	-0.24	0.37	12.49	60.00	3.80
11	0	1.43	0.66	-17.49	0.04	1.40	-1.33	19.21	60.00	2.12
12	180	-9.62	4.51	17.43	0.73	-0.17	2.15	27.43	60.00	1.19
13	7.5	8.54	12.54	-0.89	0.03	0.00	-0.04	13.43	60.00	3.47
14	0	11.05	15.72	-8.54	-0.22	-0.32	-0.43	24.29	60.00	1.47
15	127.5	-0.23	4.70	7.10	0.00	1.04	0.17	7.72	60.00	6.77
16	180	-5.29	-6.02	-0.11	-0.63	0.52	3.45	9.07	60.00	5.62
17	30	-0.79	8.41	14.78	-0.16	1.26	-1.19	15.99	60.00	2.75
18	0	-10.18	2.24	9.24	-1.50	-0.97	-4.88	21.99	60.00	1.73
19	165	-0.10	1.23	-1.27	-0.02	-0.02	-0.22	2.54	60.00	+Large
20	75	-0.96	0.43	-1.89	0.03	-0.01	-3.39	6.84	60.00	7.77

[1] See Figure 2.10.14-4 for locations of sections.
[2] The location specifies the angle at which the maximum stress intensity occurs. See Figure 2.10.14-1 for definition of angular location.
[3] Stress components correspond to a cylindrical coordinate system.

Table 2.10.14-17 30-Foot Side Drop with Internal Pressure, P_m Stresses, ksi

Sec[1]	Location (deg)[2]	S_x[3]	S_y[3]	S_z[3]	S_{xy}[3]	S_{yz}[3]	S_{xz}[3]	Stress Intensity	Stress Allow.	MS
1	75	0.04	0.89	5.89	0.11	-15.69	-0.04	31.78	67.83	1.13
2	0	-0.30	4.10	66.15	-0.43	-0.03	0.00	66.50	67.83	0.02
3	75	0.08	0.97	6.23	0.07	14.38	0.01	29.24	67.83	1.32
4	97.5	-0.31	1.59	1.21	0.02	-9.10	0.02	18.20	67.83	2.73
5	180	-0.12	2.40	-36.71	0.12	-0.01	0.00	39.12	67.83	0.73
6	97.5	-0.31	1.50	0.66	-0.02	9.07	-0.01	18.16	67.83	2.74
7	112.5	-0.37	0.56	2.52	-0.23	-12.30	-0.04	24.67	48.00	0.95
8	180	-3.13	3.13	10.63	0.08	-0.56	-3.64	15.61	48.00	2.07
9	75	0.02	-0.55	5.28	-0.81	-15.37	0.09	31.32	48.00	0.53
10	0	4.62	-9.90	3.03	1.72	-0.95	7.57	21.90	48.00	1.19
11	0	-11.37	-9.00	-0.92	0.29	0.10	0.26	10.50	48.00	3.57
12	0	-0.01	-3.58	-0.50	0.28	0.02	-1.20	4.59	48.00	9.46
13	90	-1.53	-7.84	-0.72	-0.20	0.73	0.06	7.28	48.00	5.59
14	127.5	0.31	-0.09	-0.05	-1.20	0.67	0.35	2.83	48.00	+Large
15	112.5	-0.29	-0.22	1.50	-0.43	12.67	0.02	25.41	48.00	0.89
16	120	-0.16	-0.93	1.93	-0.02	8.29	-0.07	16.83	48.00	1.85
17	75	0.05	0.84	5.35	-0.73	14.28	-0.05	28.95	48.00	0.66
18	67.5	0.05	-0.15	4.57	0.03	9.72	-0.32	20.02	48.00	1.40
19	0	-6.41	-8.47	-2.13	1.01	0.16	3.99	9.76	48.00	3.92
20	15	-2.56	-0.62	-1.27	0.41	-0.29	0.45	2.32	48.00	+Large

[1] See Figure 2.10.14-4 for locations of sections.
[2] The location specifies the angle at which the maximum stress intensity occurs. See Figure 2.10.14-1 for definition of angular location.
[3] Stress components correspond to a cylindrical coordinate system.

Table 2.10.14-18 30-Foot Side Drop with Internal Pressure, $P_m + P_b$ Stresses, ksi

Sec[1]	Location (deg)[2]	S_x[3]	S_y[3]	S_z[3]	S_{xy}[3]	S_{yz}[3]	S_{xz}[3]	Stress Intensity	Stress Allow.	MS
1	75	0.07	3.30	6.47	0.19	-17.17	-0.04	34.49	96.90	1.81
2	180	-0.09	8.89	-65.21	0.65	-0.03	0.00	74.14	96.90	0.31
3	75	0.13	3.98	7.54	0.14	15.84	0.00	31.88	96.90	2.04
4	97.5	-0.50	-6.43	-1.73	0.03	-9.93	0.01	20.41	96.90	3.75
5	0	-0.26	3.65	40.86	-0.45	-0.01	0.00	41.17	96.90	1.35
6	97.5	-0.46	-6.87	-2.30	-0.02	9.80	0.01	20.13	96.90	3.81
7	112.5	-0.37	-6.53	-2.00	-0.19	-13.83	-0.04	28.04	68.50	1.44
8	180	-5.70	2.96	22.06	0.07	-0.15	-3.64	28.71	68.50	1.39
9	67.5	-0.15	0.45	6.24	-1.51	-17.91	0.42	36.41	68.50	0.88
10	0	10.64	-18.81	-23.45	1.44	-0.18	8.60	38.28	68.50	0.79
11	0	-19.75	-13.55	-0.19	0.25	0.16	1.39	19.77	68.50	2.46
12	0	0.45	-3.78	1.86	0.18	-0.19	-0.51	5.83	68.50	+Large
13	90	-2.66	-9.71	-0.67	-0.11	0.43	0.01	9.08	68.50	6.54
14	0	0.61	3.47	-1.97	0.02	-0.65	-0.53	5.69	68.50	+Large
15	112.5	-0.33	-7.35	-2.50	-0.44	13.99	0.02	28.41	68.50	1.41
16	127.5	-0.11	-2.45	-0.26	0.04	12.99	0.54	26.10	68.50	1.62
17	67.5	-0.07	2.89	8.46	-1.40	16.45	-0.51	33.50	68.50	1.04
18	52.5	-0.37	-0.58	10.45	0.23	12.54	-1.93	27.69	68.50	1.47
19	22.5	-0.91	-4.63	6.48	0.55	0.46	1.91	11.68	68.50	4.86
20	15	-5.76	-2.35	-2.16	0.25	-0.35	2.61	6.40	68.50	9.70

[1] See Figure 2.10.14-4 for locations of sections.
[2] The location specifies the angle at which the maximum stress intensity occurs. See Figure 2.10.14-1 for definition of angular location.
[3] Stress components correspond to a cylindrical coordinate system.

Table 2.10.14-19 30-Foot Top-End Drop with Internal Pressure, P_m Stresses, ksi

Sec[1]	S_x[2]	S_y[2]	S_z[2]	S_{xy}[2]	S_{yz}[2]	S_{xz}[2]	Stress Intensity	Stress Allow.	MS
1	0.00	0.00	-0.16	0.00	0.00	0.00	0.16	67.83	+Large
2	0.00	0.00	-1.49	0.00	0.00	0.00	1.50	67.83	+Large
3	0.02	-0.11	-3.07	0.01	0.00	-0.01	3.08	67.83	+Large
4	-0.13	2.65	0.60	-0.18	0.00	0.00	2.81	67.83	+Large
5	-0.13	2.66	-0.71	-0.18	0.00	0.00	3.39	67.83	+Large
6	-0.12	2.76	-2.20	-0.19	0.01	0.00	4.97	67.83	+Large
7	-0.14	2.74	0.68	-0.19	0.00	-0.04	2.90	48.00	+Large
8	-0.18	0.67	0.42	0.06	-0.01	0.13	0.89	48.00	+Large
9	0.00	0.01	-0.09	0.00	0.00	0.00	0.09	48.00	+Large
10	0.00	0.02	-0.04	0.00	0.00	-0.01	0.07	48.00	+Large
11	-0.02	0.03	-0.03	0.00	0.00	0.00	0.07	48.00	+Large
12	-0.01	0.01	-0.01	0.00	0.00	-0.01	0.03	48.00	+Large
13	0.04	0.06	-0.22	0.00	0.00	0.02	0.28	48.00	+Large
14	0.01	0.01	-0.02	0.00	0.00	0.00	0.03	48.00	+Large
15	-0.17	2.42	-2.51	0.01	0.08	0.05	4.94	48.00	8.72
16	-6.61	-6.94	-4.45	-0.87	0.30	2.74	6.31	48.00	6.61
17	0.05	1.10	-3.01	0.00	0.05	0.07	4.11	48.00	+Large
18	-6.44	1.95	-3.98	1.02	0.41	-1.48	9.35	48.00	4.13
19	-0.66	1.84	-3.89	0.26	-0.17	0.99	6.04	48.00	6.95
20	-1.11	-1.22	-4.78	-0.08	-0.11	1.01	4.23	48.00	+Large

[1] See Figure 2.10.14-4 for locations of sections.
[2] Stress components correspond to a cylindrical coordinate system.

Table 2.10.14-20 30-Foot Top-End Drop with Internal Pressure, $P_m + P_b$ Stresses, ksi

Sec[1]	S_x[2]	S_y[2]	S_z[2]	S_{xy}[2]	S_{yz}[2]	S_{xz}[2]	Stress Intensity	Stress Allow.	MS
1	0.00	0.00	-0.16	0.00	0.00	0.00	0.16	96.90	+Large
2	0.00	0.01	-1.50	0.00	0.00	0.00	1.51	96.90	+Large
3	0.02	-0.30	-3.47	0.02	0.01	0.00	3.49	96.90	+Large
4	-0.21	2.84	0.64	-0.20	0.00	0.00	3.07	96.90	+Large
5	-0.20	2.84	-0.68	-0.20	0.00	0.00	3.53	96.90	+Large
6	-0.22	3.12	-2.13	-0.22	0.01	0.01	5.26	96.90	+Large
7	-0.20	2.78	0.25	-0.19	0.00	-0.04	3.01	68.50	+Large
8	-0.33	0.94	1.15	-0.08	0.01	0.16	1.52	68.50	+Large
9	0.00	0.01	-0.09	0.00	0.00	0.00	0.10	68.50	+Large
10	0.00	0.02	-0.07	0.00	0.00	-0.01	0.09	68.50	+Large
11	-0.04	0.01	-0.07	0.00	0.00	-0.03	0.10	68.50	+Large
12	-0.01	0.01	-0.02	0.00	0.00	-0.01	0.04	68.50	+Large
13	0.27	0.40	-0.17	-0.01	0.00	0.03	0.57	68.50	+Large
14	0.02	0.02	-0.03	0.00	0.00	0.01	0.05	68.50	+Large
15	-0.18	2.46	-3.79	-0.17	0.01	0.06	6.25	68.50	9.96
16	-9.52	-11.56	-13.10	1.37	-1.07	4.69	10.62	68.50	5.45
17	0.00	0.75	-3.79	-0.06	0.02	0.06	4.54	68.50	+Large
18	-10.51	-1.13	-10.56	-1.41	-1.16	-3.09	13.02	68.50	4.26
19	-1.35	1.80	-4.42	0.40	-0.31	1.41	6.85	68.50	9.00
20	0.31	-0.29	-3.55	0.00	-0.02	3.23	7.52	68.50	8.11

[1] See Figure 2.10.14-4 for locations of sections.
[2] Stress components correspond to a cylindrical coordinate system.

Table 2.10.14-21 30-Foot Top-Corner Drop with Internal Pressure, P_m Stresses, ksi

Sec[1]	Location (deg)[2]	S_x[3]	S_y[3]	S_z[3]	S_{xy}[3]	S_{yz}[3]	S_{xz}[3]	Stress Intensity	Stress Allow.	MS
1	67.5	0.02	0.20	0.80	0.04	-2.72	-0.02	5.48	67.83	+Large
2	180	-0.04	-0.28	-10.37	0.00	0.04	0.00	10.33	67.83	5.57
3	52.5	0.07	0.30	-5.70	0.02	3.53	0.00	9.26	67.83	6.33
4	120	-0.19	2.32	-0.33	-0.06	-1.41	0.00	3.87	67.83	+Large
5	180	-0.08	2.48	-6.10	0.14	0.02	0.00	8.59	67.83	6.90
6	0	-0.17	2.59	-5.85	-0.24	0.04	0.02	8.46	67.83	7.02
7	120	-0.19	1.96	-0.08	0.00	-2.50	0.03	5.40	48.00	7.89
8	180	-1.22	1.17	2.55	0.05	-0.18	-1.09	4.37	48.00	9.98
9	60	0.01	-0.12	0.86	-0.14	-2.70	0.00	5.50	48.00	7.73
10	0	0.44	-1.90	-0.39	0.26	-0.20	1.58	3.77	48.00	+Large
11	0	-1.54	-1.53	-0.01	0.05	-0.02	-0.23	1.63	48.00	+Large
12	0	0.03	-0.75	-0.27	0.07	0.01	-0.48	1.16	48.00	+Large
13	90	-0.17	-1.05	-0.06	-0.03	0.10	0.00	1.01	48.00	+Large
14	97.5	0.11	-0.49	-0.02	-0.10	0.11	-0.01	0.66	48.00	+Large
15	0	-0.22	1.61	-6.24	-0.20	-0.02	-0.04	7.88	48.00	5.09
16	180	-6.31	-7.41	-1.56	-0.90	0.29	2.61	7.97	48.00	5.02
17	30	0.08	1.49	-7.98	-0.13	2.34	0.18	10.58	48.00	3.54
18	0	-7.62	0.50	-10.26	-1.09	-0.25	-1.78	11.84	48.00	3.05
19	0	-2.63	-1.19	-8.95	0.04	0.32	1.43	8.09	48.00	4.93
20	0	-1.82	-1.55	-6.33	0.14	0.20	1.14	5.25	48.00	8.14

[1] See Figure 2.10.14-4 for locations of sections.
[2] The location specifies the angle at which the maximum stress intensity occurs. See Figure 2.10.14-1 for definition of angular location.
[3] Stress components correspond to a cylindrical coordinate system.

Table 2.10.14-22 30-Foot Top-Corner Drop with Internal Pressure, $P_m + P_b$ Stresses, ksi

Sec[1]	Location (deg)[2]	S_x[3]	S_y[3]	S_z[3]	S_{xy}[3]	S_{yz}[3]	S_{xz}[3]	Stress Intensity	Stress Allow.	MS
1	60	0.04	1.44	1.37	0.04	-3.16	-0.02	6.33	96.90	+Large
2	180	-0.03	3.04	-9.78	0.22	0.04	0.00	12.83	96.90	6.55
3	60	0.04	0.53	-4.64	0.05	4.17	0.01	9.82	96.90	8.87
4	180	-0.16	6.38	0.28	0.33	-0.14	-0.02	6.58	96.90	+Large
5	180	-0.12	7.50	-4.28	0.48	0.02	0.00	11.80	96.90	7.21
6	0	-0.27	4.85	-5.03	-0.40	0.01	0.04	9.91	96.90	8.78
7	127.5	-0.25	-0.78	-1.40	-0.07	-3.30	0.01	6.64	68.50	9.32
8	180	-1.96	0.27	5.70	-0.03	0.07	-1.09	7.97	68.50	7.59
9	52.5	-0.03	0.56	0.96	-0.30	-3.42	0.05	6.88	68.50	8.96
10	0	1.66	-3.19	-5.62	0.24	0.03	1.68	8.03	68.50	7.53
11	180	1.34	1.11	0.01	-0.01	0.08	-0.94	2.30	68.50	+Large
12	0	-0.10	-0.60	-0.13	0.09	0.02	-0.67	1.36	68.50	+Large
13	105	-0.03	-0.98	-0.06	-0.26	0.03	0.01	1.09	68.50	+Large
14	105	0.08	-0.63	-0.01	-0.23	0.09	0.00	0.86	68.50	+Large
15	15	-0.02	2.92	-6.20	0.08	-0.25	-0.03	9.13	68.50	6.50
16	0	-9.28	-10.03	-13.27	1.18	-0.98	4.68	10.55	68.50	5.49
17	45	0.17	1.62	-6.23	-0.33	3.87	0.37	11.06	68.50	5.19
18	0	-12.28	-2.39	-15.48	-1.58	-1.06	-3.57	15.87	68.50	3.32
19	7.5	-1.31	-2.99	-12.42	0.24	0.21	0.86	11.28	68.50	5.07
20	15	1.26	-0.32	-4.05	0.08	0.04	3.14	8.23	68.50	7.32

[1] See Figure 2.10.14-4 for locations of sections.
[2] The location specifies the angle at which the maximum stress intensity occurs. See Figure 2.10.14-1 for definition of angular location.
[3] Stress components correspond to a cylindrical coordinate system.

Table 2.10.14-23 30-Foot Bottom-End Drop with Internal Pressure, P_m Stresses, ksi

Sec[1]	S_x[2]	S_y[2]	S_z[2]	S_{xy}[2]	S_{yz}[2]	S_{xz}[2]	Stress Intensity	Stress Allow.	MS
1	0.02	0.24	-4.22	-0.01	-0.01	-0.02	4.46	67.83	+Large
2	0.00	0.00	-2.55	0.00	0.00	0.00	2.55	67.83	+Large
3	0.00	0.09	-1.21	0.00	0.00	0.01	1.30	67.83	+Large
4	-0.12	2.77	-3.26	-0.18	-0.01	0.00	6.04	67.83	+Large
5	-0.13	2.66	-1.79	-0.18	0.00	0.00	4.47	67.83	+Large
6	-0.13	2.68	-0.49	-0.18	0.00	0.00	3.19	67.83	+Large
7	-0.10	2.23	-3.48	-0.15	0.00	0.10	5.72	48.00	7.39
8	0.80	2.85	-2.23	-0.01	-0.02	-0.17	5.09	48.00	8.43
9	0.03	0.34	-4.10	-0.03	-0.01	-0.08	4.45	48.00	9.79
10	0.34	1.15	-3.10	0.03	-0.01	-0.29	4.27	48.00	+Large
11	2.86	1.32	-7.84	-0.10	-0.48	0.34	10.75	48.00	+Large
12	-1.00	0.93	-5.08	0.12	0.10	-0.67	6.13	48.00	6.83
13	2.20	2.97	-1.94	0.05	0.01	-0.46	4.96	48.00	8.68
14	-1.32	-2.22	-11.77	0.07	-0.15	-1.74	11.02	48.00	3.36
15	-0.13	2.58	-0.39	-0.18	0.00	0.00	2.98	48.00	+Large
16	-0.08	1.10	-0.16	-0.08	0.00	-0.09	1.33	48.00	+Large
17	0.00	0.10	-1.08	0.00	0.00	0.03	1.18	48.00	+Large
18	-0.01	0.07	-0.68	0.00	0.00	0.06	0.76	48.00	+Large
19	-0.05	0.22	-0.32	0.00	0.00	0.06	0.56	48.00	+Large
20	-0.18	0.05	-0.93	0.00	0.00	-0.20	1.03	48.00	+Large

[1] See Figure 2.10.14-4 for locations of sections.
[2] Stress components correspond to a cylindrical coordinate system.

Table 2.10.14-24 30-Foot Bottom-End Drop with Internal Pressure, $P_m + P_b$ Stresses, ksi

Sec[1]	S_x[2]	S_y[2]	S_z[2]	S_{xy}[2]	S_{yz}[2]	S_{xz}[2]	Stress Intensity	Stress Allow.	MS
1	0.02	0.36	-4.25	-0.02	-0.01	-0.04	4.61	96.90	+Large
2	0.00	0.01	-2.55	0.00	0.00	0.00	2.56	96.90	+Large
3	0.00	0.08	-1.26	0.00	0.00	0.01	1.34	96.90	+Large
4	-0.20	3.09	-3.22	-0.21	-0.01	-0.01	6.33	96.90	+Large
5	-0.20	2.84	-1.76	-0.20	0.00	0.00	4.62	96.90	+Large
6	-0.21	2.87	-0.46	-0.20	0.00	0.00	3.35	96.90	+Large
7	-0.01	1.77	-4.01	-0.12	-0.01	0.10	5.79	68.50	+Large
8	0.68	2.56	-4.53	0.12	-0.02	-0.29	7.12	68.50	8.62
9	0.10	0.42	-4.24	-0.03	-0.02	-0.24	4.68	68.50	+Large
10	0.64	1.84	-2.82	0.01	-0.04	-0.35	4.69	68.50	+Large
11	2.16	-1.09	-16.04	-0.20	-1.32	0.68	18.38	68.50	2.73
12	-1.81	-0.19	-9.08	0.10	0.11	-1.00	9.03	68.50	6.59
13	6.29	9.44	-0.86	0.02	-0.04	-0.38	10.32	68.50	5.64
14	4.12	8.84	-8.49	0.01	0.15	-2.03	17.65	68.50	2.88
15	-0.19	2.69	-0.63	-0.19	0.00	0.00	3.33	68.50	+Large
16	-0.19	1.32	0.18	-0.10	-0.01	-0.09	1.54	68.50	+Large
17	0.01	0.06	-1.24	0.00	0.00	0.09	1.30	68.50	+Large
18	0.01	0.07	-0.73	0.00	0.01	0.07	0.80	68.50	+Large
19	-0.08	0.24	-0.49	0.00	0.01	0.06	0.74	68.50	+Large
20	-0.36	0.25	-0.89	0.01	0.00	-1.65	3.34	68.50	+Large

[1] See Figure 2.10.14-4 for locations of sections.
[2] Stress components correspond to a cylindrical coordinate system.

Table 2.10.14-25 30-Foot Bottom-Corner Drop with Internal Pressure, P_m Stresses, ksi

Sec[1]	Location (deg)[2]	S_x[3]	S_y[3]	S_z[3]	S_{xy}[3]	S_{yz}[3]	S_{xz}[3]	Stress Intensity	Stress Allow.	MS
1	0	-0.04	1.75	-10.25	-0.18	-0.35	-0.03	12.04	67.83	4.63
2	180	-0.04	-0.28	-10.82	0.00	-0.05	0.00	10.78	67.83	5.29
3	180	-0.01	0.31	-5.34	0.01	0.09	0.03	5.66	67.83	+Large
4	0	-0.17	2.59	-6.85	-0.23	-0.03	-0.02	9.46	67.83	6.17
5	180	-0.08	2.48	-6.68	0.14	-0.02	0.00	9.17	67.83	6.40
6	142.5	-0.18	2.20	-1.87	-0.20	1.02	0.03	4.57	67.83	+Large
7	0	-0.16	1.50	-7.19	-0.19	0.02	0.15	8.71	48.00	4.51
8	15	0.95	2.55	-4.19	-0.02	0.02	-0.09	6.74	48.00	6.12
9	0	0.13	0.48	-11.26	0.00	-0.34	-0.18	11.76	48.00	3.08
10	0	1.33	-0.73	-9.11	0.22	-0.24	0.19	10.47	48.00	3.58
11	0	1.26	0.32	-8.62	0.15	0.51	0.82	10.09	48.00	3.76
12	0	-2.47	-1.01	-10.59	0.09	-0.23	-1.08	9.73	48.00	3.93
13	180	0.74	2.35	-1.83	0.03	-0.01	-0.80	4.41	48.00	9.88
14	180	-1.31	-1.79	-11.13	-0.07	0.15	-2.16	10.74	48.00	3.47
15	112.5	-0.18	1.91	-1.13	0.04	2.48	-0.07	5.83	48.00	7.23
16	127.5	-0.06	0.49	-0.50	0.07	2.06	-0.26	4.26	48.00	+Large
17	180	0.01	0.40	-4.57	-0.01	0.08	0.14	4.97	48.00	8.66
18	60	0.02	0.09	0.45	0.02	1.74	0.07	3.50	48.00	+Large
19	0	-1.44	-1.46	-0.82	0.18	0.05	0.74	1.66	48.00	+Large
20	97.5	0.07	-0.46	-1.01	-0.13	0.00	-0.15	1.15	48.00	+Large

[1] See Figure 2.10.14-4 for locations of sections.
[2] The location specifies the angle at which the maximum stress intensity occurs. See Figure 2.10.14-1 for definition of angular location.
[3] Stress components correspond to a cylindrical coordinate system.

Table 2.10.14-26 30-Foot Bottom-Corner Drop with Internal Pressure, $P_m + P_b$ Stresses, ksi

Sec[1]	Location (deg)[2]	S_x[3]	S_y[3]	S_z[3]	S_{xy}[3]	S_{yz}[3]	S_{xz}[3]	Stress Intensity	Stress Allow.	MS
1	15	-0.01	1.27	-10.61	0.02	-1.51	-0.06	12.27	96.90	6.90
2	180	-0.03	3.04	-10.21	0.22	-0.05	0.00	13.27	96.90	6.30
3	180	0.01	0.82	-5.25	0.05	0.11	0.01	6.08	96.90	+Large
4	0	-0.26	4.74	-6.06	-0.38	-0.01	-0.03	10.83	96.90	7.95
5	180	-0.12	7.49	-4.87	0.48	-0.02	0.00	12.39	96.90	6.82
6	180	-0.17	6.47	-0.89	0.35	0.13	0.03	7.38	96.90	+Large
7	37.5	0.01	1.65	-7.51	0.03	-0.35	0.19	9.20	68.50	6.45
8	0	0.63	2.19	-7.06	-0.18	0.06	-0.14	9.27	68.50	6.39
9	52.5	0.22	0.18	-8.01	-0.42	-4.78	-0.44	12.63	68.50	4.42
10	0	1.30	-2.45	-14.17	0.11	-0.25	0.46	15.51	68.50	3.42
11	0	1.99	-1.54	-16.99	0.28	1.42	1.39	19.35	68.50	2.54
12	0	-2.54	-1.43	-12.80	0.00	-0.22	-1.52	11.59	68.50	4.91
13	7.5	4.62	8.13	-0.86	0.17	-0.01	-0.10	9.00	68.50	6.61
14	7.5	4.26	8.58	-8.38	0.03	0.00	-1.33	17.10	68.50	3.01
15	127.5	-0.25	-1.48	-2.34	-0.11	3.37	-0.04	6.79	68.50	9.09
16	142.5	-0.17	0.45	-0.67	0.06	4.05	0.17	8.19	68.50	7.36
17	52.5	-0.04	1.06	0.90	-0.28	3.14	-0.03	6.31	68.50	9.86
18	37.5	-0.10	0.08	1.60	0.06	2.68	-0.36	5.63	68.50	+Large
19	0	-0.66	-0.19	1.04	-0.02	0.15	0.74	2.28	68.50	+Large
20	45	-0.20	0.21	-0.85	0.23	-0.06	-1.66	3.42	68.50	+Large

[1] See Figure 2.10.14-4 for locations of sections.
[2] The location specifies the angle at which the maximum stress intensity occurs. See Figure 2.10.14-1 for definition of angular location.
[3] Stress components correspond to a cylindrical coordinate system.

Table 2.10.14-27 Accident Internal Pressure with Inertia Load, P_m Stresses, ksi

Sec[1]	Location (deg)[2]	S_x[3]	S_y[3]	S_z[3]	S_{xy}[3]	S_{yz}[3]	S_{xz}[3]	Stress Intensity	Stress Allow.	MS
1	0	0.01	0.07	-1.22	0.00	0.00	-0.01	1.29	67.83	+Large
2	30	0.00	0.00	-0.67	0.00	0.00	0.00	0.67	67.83	+Large
3	180	0.00	0.00	-0.23	0.00	0.00	0.00	0.23	67.83	+Large
4	0	-0.26	5.34	0.37	-0.37	0.00	0.00	5.65	67.83	+Large
5	0	-0.26	5.33	0.86	-0.37	0.00	0.00	5.63	67.83	+Large
6	0	-0.26	5.32	1.29	-0.37	0.00	0.00	5.63	67.83	+Large
7	0	-0.26	5.33	0.29	-0.36	-0.01	-0.04	5.64	48.00	7.51
8	97.5	-0.16	2.06	0.30	-0.01	-0.07	0.16	2.27	48.00	+Large
9	0	0.01	0.08	-1.19	-0.01	0.00	-0.02	1.27	48.00	+Large
10	7.5	0.09	0.31	-0.90	0.01	0.00	-0.07	1.22	48.00	+Large
11	180	0.58	0.06	-3.57	-0.04	-0.22	0.16	4.18	48.00	+Large
12	180	-0.35	0.37	-1.64	0.05	0.03	-0.15	2.03	48.00	+Large
13	180	0.71	0.95	-0.99	0.02	0.01	-0.10	1.95	48.00	+Large
14	0	-0.36	-0.63	-4.17	0.02	-0.06	-0.61	4.00	48.00	+Large
15	0	-0.27	5.41	1.31	-0.37	0.00	0.06	5.73	48.00	7.38
16	0	-0.17	2.25	0.80	-0.16	0.00	-0.09	2.45	48.00	+Large
17	157.5	0.00	0.05	-0.19	0.00	0.00	0.00	0.24	48.00	+Large
18	180	0.01	0.20	-0.11	0.01	0.00	0.04	0.33	48.00	+Large
19	105	-0.03	0.20	-0.20	0.00	0.00	0.04	0.41	48.00	+Large
20	105	-0.15	0.13	-0.88	0.00	0.00	-0.33	1.14	48.00	+Large

[1] See Figure 2.10.14-4 for locations of sections.
[2] The location specifies the angle at which the maximum stress intensity occurs. See Figure 2.10.14-1 for definition of angular location.
[3] Stress components correspond to a cylindrical coordinate system.

Table 2.10.14-28 Accident Internal Pressure with Inertia Load, $P_m + P_b$ Stresses, ksi

Sec[1]	Location (deg)[2]	S_x[3]	S_y[3]	S_z[3]	S_{xy}[3]	S_{yz}[3]	S_{xz}[3]	Stress Intensity	Stress Allow.	MS
1	0	0.01	0.11	-1.23	0.00	0.00	-0.01	1.34	96.90	+Large
2	0	0.00	0.01	-0.66	0.00	0.00	0.00	0.67	96.90	+Large
3	0	0.00	-0.01	-0.24	0.00	0.00	0.00	0.24	96.90	+Large
4	0	-0.41	5.76	0.46	-0.41	0.00	0.00	6.22	96.90	+Large
5	0	-0.41	5.69	0.93	-0.40	0.00	0.00	6.15	96.90	+Large
6	0	-0.41	5.69	1.38	-0.40	0.00	0.00	6.16	96.90	+Large
7	0	-0.39	5.55	-0.31	-0.39	-0.01	-0.05	6.01	68.50	+Large
8	105	-0.47	2.39	0.87	0.00	-0.09	0.19	2.89	68.50	+Large
9	0	0.03	0.11	-1.22	-0.01	-0.01	-0.06	1.33	68.50	+Large
10	0	0.07	0.22	-1.09	-0.03	-0.03	-0.06	1.33	68.50	+Large
11	180	-0.34	-1.37	-7.60	-0.07	-0.62	0.27	7.35	68.50	8.32
12	180	-0.63	-0.04	-3.13	0.04	0.03	-0.22	3.11	68.50	+Large
13	172.5	1.58	2.37	-0.74	0.01	-0.01	-0.09	3.11	68.50	+Large
14	7.5	1.42	3.06	-2.98	0.00	0.05	-0.71	6.15	68.50	+Large
15	0	-0.39	5.57	0.65	-0.39	0.00	0.06	6.02	68.50	+Large
16	0	-0.36	2.64	1.34	-0.20	-0.01	-0.09	3.03	68.50	+Large
17	150	0.00	0.03	-0.22	0.00	0.00	0.00	0.26	68.50	+Large
18	0	0.03	0.17	-0.26	-0.01	0.00	0.05	0.44	68.50	+Large
19	105	-0.05	0.22	-0.33	0.00	0.01	0.03	0.55	68.50	+Large
20	45	-0.25	0.42	-0.89	0.01	0.00	-1.68	3.42	68.50	+Large

[1] See Figure 2.10.14-4 for locations of sections.
[2] The location specifies the angle at which the maximum stress intensity occurs. See Figure 2.10.14-1 for definition of angular location.
[3] Stress components correspond to a cylindrical coordinate system.

2.10.15 NAC-LWT Alternate B Port Cover

The Alternate B port cover has two face seals on the inner end of the port cover. The primary containment seal is provided by an inner metal face seal located in a groove on the face (towards the inner edge) of the barrel of the port cover body. The metal face seal is used to maintain a leaktight containment boundary per the requirements of ANSI N14.5-1997. The secondary (test annulus) face seal is a single Viton® O-ring located in a groove on the face (towards the outer edge) of the barrel of the port cover body. The Alternate B port cover is fabricated from Type XM-19 stainless steel and is fastened to the cask top forging using high-strength SB-637 Grade N07718 bolts (⅜-16 UNC).

2.10.15.1 Alternate B Port Cover Bolt Analysis

2.10.15.1.1 Port Cover Bolt Preload

The Alternate B port cover uses a metallic O-ring for containment and Viton® O-ring face seal for leakage rate testing. The metallic O-ring requires a 1,725 lb/in sealing force and the Viton® O-ring requires a sealing force of 120 lb/in (based on manufacturers' data).

The force required to compress the metallic O-ring seal is:

$$P1 = Y2 \times C = 1{,}898 \times (\pi \times 1.86) = 11{,}090 \text{ lbs}$$

where:

$Y2 = Km \times Kd \times Y1 = 1 \times 1.1 \times 1{,}725 = 1{,}898$ lb/in

$C = \pi \times d$, Circumference of the O-ring

d = 1.86 inches, The average diameter of the seal groove

Km= 1.0, Material Factor

Kd = 1.1, Diameter Factor

Y1 = 1,725 lbs, Ideal compressive load

The load due to internal pressure is:

$$P2 = P \times \frac{\pi \times d}{4} = 600 \times \frac{\pi \times 1.86^2}{4} = 1{,}630 \text{ lbs}$$

where:

P = 600 psig, which bounds the maximum pressure in the LWT cask during the fire accident (Section 3.5.4.4)

The force due to the port cover weight is:

$P3 = W_{pc} \times 60g = 600$ lbs

where:

W_{pc} = 10 lbs, The approximate weight of the port cover

The force required to compress the Viton® O-ring is:

$P4 = 120 \times \pi \times dp = 955$ lbs

where:

d_p = 2.534 in, diameter of the Viton® seal

The required bolt preload per bolt is:

$$F = \frac{P1+P2+P3+P4}{3} = \frac{11{,}090+1{,}630+600+955}{3} = 4{,}758 \text{ lb/bolt}$$

Therefore, the required bolt torque is:

$T = 0.2Fd = 0.2 \times 4758 \times 0.281 = 267$ in-lb

where:

d = 0.281 in, the mean bolt diameter

The recommended torque is 285 ± 15 in-lb, which corresponds to a maximum bolt preload of 5,340 lbs.

The port cover is attached to the cask body with three bolts. The bolts are threaded into the SA182 Type-304 stainless steel top forging of the cask using Helicoils. The tensile stress in the bolt when the maximum bolt preload is applied is:

$$S = \frac{P}{A} = \frac{5{,}340}{0.06158} = 86.7 \text{ ksi}$$

where:

P = 5,340 lbs, the bolt preload

$A = \pi d^2/4$, bolt cross-sectional area

d = 0.28 in, the bolt shank diameter

The margin of safety is:

$$MS = \frac{S_y}{S} - 1 = \frac{142.35}{86.7} - 1 = +0.64$$

where:

S_y = 142.35 ksi, yield strength of SB-637, Grade N07718 @ 250°F

The tensile stress in the ⅜-16UNC bolt is:

$$S = \frac{P}{A_t} = \frac{5{,}340}{0.074} = 72.2 \text{ ksi}$$

where:

P = 5,340 lbs, the bolt preload

$$A_t = 3.1416\left(\frac{Es_{min}}{2} - \frac{0.16238}{n}\right)^2 = 3.1416\left(\frac{0.3266}{2} - \frac{0.16238}{16}\right)^2 = 0.074 \text{ in}^2$$

= 0.074 in^2, tensile area of the bolt

For the ⅜-16UNC bolts (Machinery's Handbook)

n	16, number of threads per inch
D	0.375 in, bolt diameter
Kn_{max}	0.321 in, maximum minor diameter of internal thread
Es_{min}	0.3266 in, minimum major diameter of external thread
En_{max}	0.3429 in, maximum pitch diameter of internal thread
Ds_{min}	0.3595 in, minimum major diameter of external thread
Le	0.75 in, thread engagement

The margin of safety is:

$$MS = \frac{S_y}{S} - 1 = \frac{142.35}{72.2} - 1 = +0.97 \text{ @ } 250°F$$

where:

S_y = 142.35 ksi, yield strength of SB-637, Grade N07718 @250°F

The shear stress in the bolt thread is:

$$\tau = \frac{P}{A_s} = \frac{5{,}340}{0.348} = 15.3 \text{ ksi}$$

where:

P = 5,340 lbs, the bolt preload

$$A_s = 3.1416nL_eKn_{max}\left[\frac{1}{2n} + 0.57735(Es_{min} - Kn_{max})\right]$$

$= 0.348$ in^2, shear area of the bolt threads

The margin of safety is:

$$MS = \frac{0.6S_m}{t} - 1 = \frac{0.6 \times 47.5}{15.3} - 1 = +0.86$$

where:

S_m = 47.5 ksi, stress intensity of SB-637, Grade N07718 @250°F

Conservatively ignoring the strength of the Helicoil, the shear stress of the threads in the top forging is:

$$S = \frac{5{,}340}{0.461} = 11.6\,\text{ksi}$$

where:

P = 5,340 lbs, the bolt preload

$$A_n = 3.1416nL_eDs_{min}\left[\frac{1}{2n} + 0.57735(Ds_{min} - En_{max})\right]$$

$= 0.461$ in^2, shear area of the bolt threads

The margin of safety is:

$$MS = \frac{0.6S_m}{S} - 1 = \frac{0.6 \times 20.0}{11.6} - 1 = +0.03$$

where:

S_m = 20.0 ksi, stress intensity of Type 304 stainless steel @ 250°F

2.10.15.1.2 Port Cover Bolt Thermal Stress Evaluation

Thermal stresses generated in the port cover are due to the difference in thermal expansion of the port cover bolts and adjacent components.

Cold

During the cold condition (–40°F), the port cover will contract at a faster rate than the port cover bolt. The change in length due to thermal expansion/contraction for the components is calculated using the following equation.

$$\Delta L = \Delta T \alpha L$$

At –40°F, the changes in length of the port cover and port cover bolt due to a temperature differential of -110°F (-40 - 70) are as follows.

Component	Material	Coefficient of Thermal Expansion, α (in/in-°F)	Component Length, L (in)	Change in Length, ΔL (in)
Port Cover	SA-479 Type XM-19	8.16×10^{-6}	1.0	-9.0×10^{-4}
Bolt	SB-637 Grade N07718	7.05×10^{-6}	1.0	-7.8×10^{-4}

The net change in bolt length is:

$$\Delta L = (-9.0 \times 10\text{-}4) - (-7.8 \times 10\text{-}4) = -0.0001 \text{ in}$$

The bolt strain associated with this change in length is 0.0001 (0.0001/1.0). Since the port cover contracts more than the bolts, no additional load is applied to the port cover bolts during a –40°F condition.

To maintain the seal in the cold condition, the bolt strain must be less than the strain due to the bolt preload. From Section 2.10.15.1.1, the bolt preload (F) is 5,340 lbs. The strain associated with the preload is:

$$\varepsilon = \frac{F}{AE} = \frac{5{,}340}{0.0616 \times 29.6 \times 10^6} = 0.00293$$

where:

$E = 29.6 \times 10^{-6}$ psi, modulus of elasticity for SB-637 Grade N07718 @-40°F

$A = \frac{\pi d^2}{4} = 0.0616 \text{ in}^2$, bolt cross-sectional area

$d = 0.28$ in, diameter of the bolt

Since the preload strain is significantly larger than the strain due to cold conditions, the seal is maintained.

Fire Accident

For the fire accident, a peak temperature of 845°F (Section 2.7.2.4.3) is used for the evaluation of the thermal stress in the port cover bolts. At 845°F, the changes in length of the port cover and port cover bolt due to a temperature differential of 775°F (845 – 70) are as follows.

Component	Material	Coefficient of Thermal Expansion, σ (in/in-°F)	Component Length, L (in)	Change in Length, ΔL (in)
Port Cover	SA-479 Type XM-19	9.26×10^{-6}	1.0	7.18×10^{-3}
Bolt	SB-637 Grade N07718	7.92×10^{-6}	1.0	6.14×10^{-3}

The net change in length of the port cover bolt is:

$$\Delta L_{bolt} = (7.18 \times 10^{-3}) - (6.14 \times 10^{-3}) = 1.0 \times 10^{-3} \text{ in}$$

The change in length of the bolt results in a uniform strain of:

$$\varepsilon b = \frac{\Delta L}{L} = \frac{1.0 \times 10^{-3}}{1.0} = 0.0010 \text{ in/in}$$

where:

L = bolt length (shank) = 1.0 in

The thermal stress in the bolt is:

$$S = \varepsilon_b E = 0.0010 \times (25.7 \times 10^6) = 25{,}700 \text{ psi} = 25.7 \text{ ksi}$$

where:

E = 25.7×10^{-6} psi, modulus of elasticity for SB-637 Grade N07718 @845°F

Combining the thermal stress and preload stress (Section 2.10.15.1.1), the total stress in the bolt is:

S = 25.7 + 86.7 = 112.4 ksi

The margin of safety is:

$$MS = \frac{S_y}{S} - 1 = \frac{132.7}{112.4} - 1 = +0.18 \text{ @ } 845°F$$

where:

S_y = 132.7 ksi, the yield strength of SB-637 Grade N077/8@845°F

To determine the sealing capacity of the metallic seal during the fire accident, the thermal expansion of each component is calculated. The following gives the thermal expansion of each component.

Component	Length for Expansion, L (in)	Average Temperature (°F)	Change in Temperature, ΔT (°F)	Coefficient of Thermal Expansion, α (in/in-F)	Change in Length, ΔL (in)
Cask	2.255 (3.255-1.0)	640	570	9.59×10^{-6}	0.01233
Bolt	1.000	826	756	7.90×10^{-6}	0.00597
Port Cover	3.255 (3.63-0.375)	659	589	9.10×10^{-6}	0.01745

The displacement that tends to lift the port cover off the seals is:

$$\Delta L_{seal} = 0.01233 + 0.00597 - 0.01745$$

$$= 0.00085 \text{ in}$$

This corresponds to a strain in the bolt shank of 0.00085. Since the preload strain is 0.00293 inch and is larger than the strain due to fire accident conditions, the seal is maintained.

2.10.15.1.3 Port Cover Bolt Side-Drop Evaluation

The governing cask drop orientation that would result in reducing the force applied to the metal face seal is the side-drop condition. The side-drop condition is evaluated with the cask body in the orientation, which results in the inertia load of the port cover reducing the force applied to the port cover metal face seal.

A three-dimensional ANSYS finite element model representing one-sixth of the port cover is used to evaluate the LWT port cover during side-drop conditions (see Figure 2.10.15-1). The model is constructed using ANSYS SOLID45, CONTAC52, and BEAM4 elements. CONTAC52 elements are used to model the sealing surface of the port cover to evaluate the sealing force. Beam (BEAM4) elements are used to model the port cover bolts. An initial strain is specified in the BEAM4 elements to generate the initial preload force. Since the bolts are located at a symmetry plane in the model, the applied strain is based on one-half of the total bolt force.

Symmetry boundary conditions are applied to the model on the 0° and 60° surfaces. To prevent axial motion of the port cover, the lower node of the bolt is restrained axially. The CONTAC52 elements on the sealing surface represent the interface with the cask body. The following presents the results for the side-drop analyses for the SB-637 Grade N07718 port cover bolts.

Load Case	Seal Force (lb)	Load per Bolt (lb)	Bolt Stress (psi)	MS
Preload only	2,679	5,357	86,388	0.65
Preload + Normal Pressure	2,759	5,365	86,516	0.65
Preload + Normal Pressure + 60 g	2,501	5,377	86,698	0.64
Preload + Accident Pressure	2,172	4,762	76,788	0.85

Where the reported seal force is one-sixth of the actual port cover seal force. The material allowables during normal conditions are at 250°F; for accident conditions, allowables are at 850°F.

The required force to compress the seals is 12,045 lbs (11,090 + 955) as shown in Section 2.10.15.1.1. For a one-sixth model, the force is 2,008 lbs (12,045/6). Since the sealing forces presented above are greater than 2,008 lbs, the seal is maintained.

2.10.15.1.4 Penetration Evaluation

Using the methodology presented in Section 2.6.10.5, a finite element analysis of the port cover is performed for the penetration event for the normal conditions of transport. The finite element model described in Section 2.10.15.1.3 (Figure 2.10.15-1) is used.

The equivalent dynamic loading, from Ugural and Fenster, is calculated using the following relation.

$$P_{dyn} = W (1+ (1 + 2h / \delta st)^{1/2})$$

where:

P_{dyn} = dynamic load resulting from weight (W) free falling a height (h), lb

W = weight, 13 lbs

h = drop height, 40 inches

δ_{st} = static deflection resulting from weight (W) on plate, inches

The dynamic loading is calculated to be 6,799 lbs, resulting from the 13-lb, 1.25-inch diameter projectile dropped through a distance of 40 inches onto the port cover. The sealing surface bearing stress is calculated to be 2.61 ksi, which results in a margin of safety of +8.0 compared with yield strength of the upper forging. The dynamic load on the port cover is applied as a bearing load, which will pass through the port cover body to the top forging. Also, the dynamic load increases the compressive force on the inner end O-ring, trapped in an O-ring groove at the bottom of the port cover body. Thus, the primary seal is not affected.

2.10.15.1.5 Puncture Evaluation

The puncture accident follows the 30-foot drop that the cask must sustain. The impact limiters remain attached subsequent to the 30-foot free drop, as shown in Section 2.6.7.4. It is concluded in Section 2.7.1.6 that the hypothetical crush accident does not apply to the NAC-LWT cask. Therefore, the impact limiters are attached to the cask prior to the cask dropping onto the mild steel pin. The port covers are located near the top of the cask, underneath the impact limiter.

When the top impact limiter strikes the mild steel pin, it will support the top end of the cask, while the bottom of the cask continues to translate, then begins to rotate about the mild steel pin as a pivot point, until the bottom impact limiter contacts the unyielding surface. During the time in which the cask is rotating about the pin-impact limiter contact, the maximum force, which can be applied to the port cover surface, is limited by the crush strength of the impact limiter material. The force is calculated from the product of the crush strength of the impact limiter (3,500 psi) and the common area of contact between the impact limiter and the port cover (12.3 in^2). The maximum load applied to the port cover by the impact limiter is:

$$P_b = 3{,}500 \times 12.3$$

$$= 43{,}050 \text{ lbs}$$

The stress in the Alternate B port cover at the cask body interface is:

$$\frac{P_b}{A_s} = \frac{43{,}050}{A_s} \text{ psi}$$

$$= 43{,}050/2.07 \text{ psi}$$

$$= 20.8 \text{ ksi}$$

where:

A_s = Total concentric ring bearing area at inner face of port cover = 2.07 in^2

The maximum port cover temperature is less than 250°F. For the Alternate B port cover, the margin of safety is:

$$MS = \frac{2.4 \times S_m}{20.8} - 1 = +2.7$$

where:

S_m = 32.3 ksi @ 250°F

The controlling stress in the port cover has a significant margin for the pin puncture event. Therefore, the bolt preload and the Alternate B port cover will maintain the necessary load on the metal face seal to maintain containment.

Figure 2.10.15-1 Alternate B Port Cover Finite Element Model

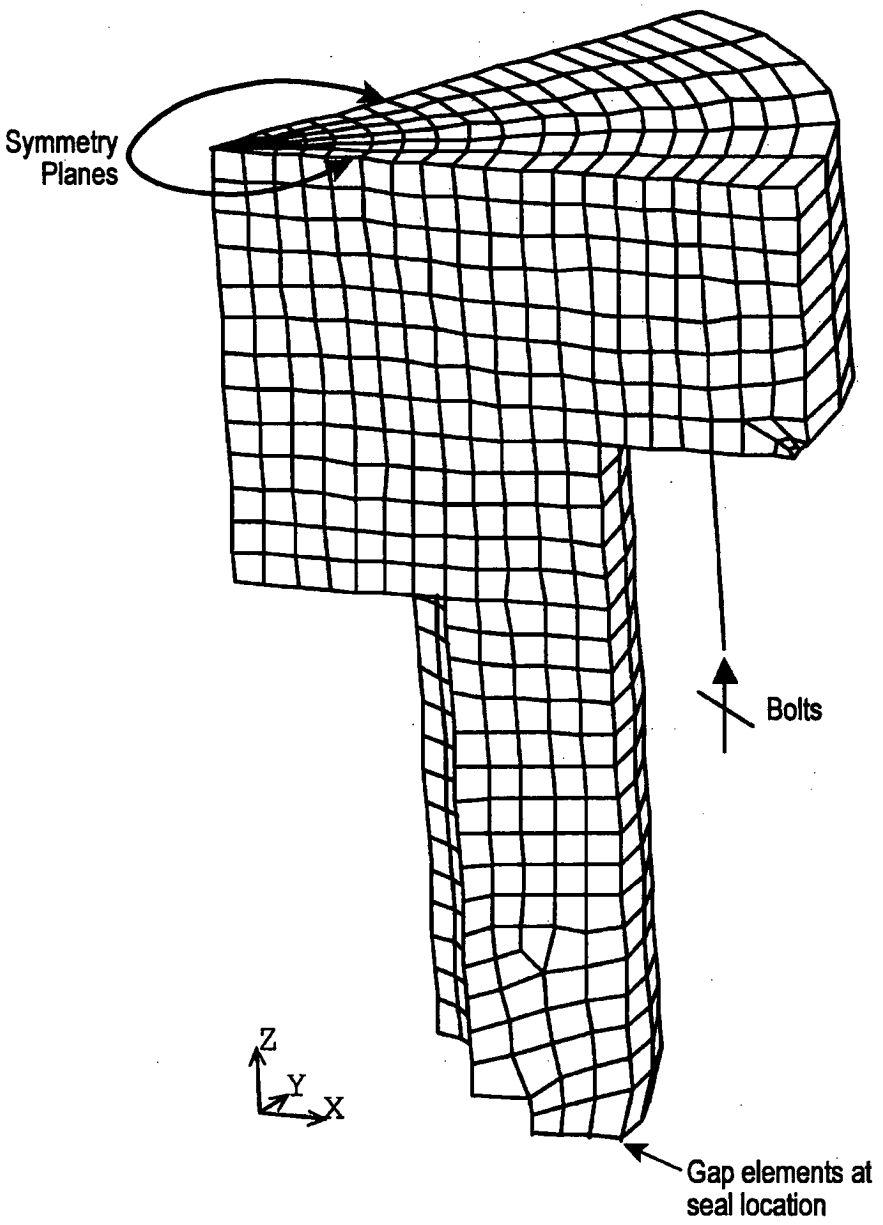

Table of Contents

List of Figures

List of Figures (continued)

List of Tables

List of Tables (continued)

3 THERMAL EVALUATION

3.1 Discussion

This chapter summarizes the thermal analyses, which are performed to demonstrate fulfillment of the thermal capability requirements established in 10 CFR 71.

The NAC-LWT cask is designed to safely contain irradiated nuclear fuel and other radioactive materials under a variety of normal transport conditions (as described in 10 CFR 71.71) and accident conditions (as described in 10 CFR 71.73). In order to verify the adequacy of the design, detailed analyses of a reference design PWR shipment are performed considering extreme normal transport and hypothetical accident conditions. The NAC-LWT cask is designed to transport one intact PWR fuel assembly; up to 2 intact BWR fuel assemblies; up to 25 individual PWR or BWR rods (including up to 14 fuel rods classified as damaged); up to 42 MTR and DIDO fuel elements; up to 140 TRIGA fuel elements or 560 TRIGA fuel rod clusters; up to 300 TPBARs (of which two can be prefailed), up to 55 segmented TPBARs; or up to 700 PULSTAR fuel elements (intact or damaged); and metallic fuel. The PULSTAR fuel will be loaded in the 28 MTR basket and consist of intact fuel assemblies, intact fuel rods loaded in fuel rod inserts or fuel cans, or intact or damaged fuel and nonfuel components or fuel assemblies loaded in fuel cans. High burnup PWR/BWR fuel rods may be placed in a rod holder or in a fuel assembly lattice. Damaged PWR/BWR fuel rods must be placed in a rod holder.

An intact PWR fuel assembly with a maximum decay heat load of 2.5 kW is used in a majority of the thermal analyses. The failed fuel basket analysis in Section 3.6 uses a decay heat load of 30 Watts. The 42 MTR fuel assembly basket in Section 3.4.1.3 uses a decay heat load of 1.26 kW. A decay heat load of 1.05 kW is conservatively used for the TRIGA fuel basket analysis and a decay heat load of 0.693 kW is used for the TPBAR basket analysis. The maximum heat load for the PULSTAR fuel is 0.840 kW per cask. As long as the decay heat load is within the design limit of 2.5 kW, any of the fuel types and other radioactive material that the NAC-LWT cask is analyzed to carry are bounded by the cask body thermal analyses of the design basis PWR assembly.

The primary heat rejection design criteria for the NAC-LWT cask are that:

1. Components important to safety shall not be subjected to temperatures outside their safe operating ranges.

2. Thermally induced stresses in the cask containment (in combination with pressure and various load condition stresses) shall not cause degradation of the cask containment capability.

The first criterion is fulfilled by thermal analysis results, which show that components important to safety are maintained within their safe operating ranges. In the event that the temperatures of the components important to safety fall outside the safe operating ranges, it is assumed that the component has failed. Temperatures of components important to safety may not fall outside the safe operating range during normal transport conditions. There are three important safety components that are subject to this thermal criterion – the tetrafluoroethylene (TFE), Viton®, and metallic O-ring seals; the lead gamma shield; and the 56 % ethylene glycol and water neutron shield.

An additional thermal consideration is associated with the liquid neutron shield tank – the reduction in neutron shielding capability caused by thermal contraction. An expansion tank is provided to ensure that the neutron shield tank remains full despite worst case contraction of the liquid in the tank during cooling. The method used by the expansion tank to keep the neutron shield tank full is described in Section 2.6.7.7.1.

The second criterion is fulfilled by the structural analysis of Chapter 2, which shows that combined load stresses (including thermally induced stresses) are less than the limits stated in Section 2.1.2.

The thermal analyses were performed for a 0.25-inch thick neutron shield tank shell, while the actual fabricated thickness is only 0.24 inch (6mm). The shell thickness difference of 0.01 inch equates to only a 0.009°F ΔT; therefore, the analyses reported in this chapter are valid.

3.2 Thermal Properties of Materials

The transfer of heat within the NAC-LWT cask is accomplished by conduction, convection and radiation. The thermal analysis of the cask requires that thermal conductivities and emissivities of the materials of construction be provided. The coefficients used to describe natural convective heat transfer in the air gaps, liquid shield tank, and from the cask surface are also provided. Thermal properties have been tabulated for the materials that form the major heat transfer pathways. Materials for small components, such as valves and trunnions, are not included in the thermal property tabulation. In addition, typical thermal values for materials of similar composition do not deviate from one another significantly. This allows the use of the same properties for A356.0-T61 and 6061-T6 aluminum alloys. The thermal properties of materials for the NAC-LWT cask are presented in Table 3.2-1 through Table 3.2-8. Specific heat and density of the thermal insulator are used in the hypothetical fire accident case. Conservatively, these values are assumed to be those of air.

Thermal expansion and contraction have been taken into account in the radial lead gamma shield. A 0.0541-inch gap is calculated for the radial lead region. This is based on the lead and the surrounding stainless steel being heated from 70°F to 620°F and then cooled to 250°F (conservatively less than the maximum temperature of this region under normal transport conditions). This represents the possible formation of a gap after the lead pour during fabrication. The lead gamma shield at the bottom of the cask is machined rather than poured; therefore, no gaps are created from thermal expansion or contraction during fabrication.

3.2.1 Conductive Properties

The values for the thermal conductivities of the major component materials of the NAC-LWT cask are shown in Table 3.2-1 through Table 3.2-8. The thermal conductivity of the thermal insulator, BISCO FPC and Fiberfrax Ceramic Fiber Paper, are shown in Table 3.2-6 and Table 3.2-8, respectively.

To evaluate the maximum fuel rod clad temperature that is found in the cask, it is necessary to describe in the HEATING5 (Turner) model a means of heat transfer within the fuel assembly. This is accomplished by use of an effective thermal conductivity for the fuel assembly. This value is determined using a method that has been developed for evaluating effective thermal conductivities following damage to a core from an accident (Cook). This method is based on the thermal conductivities of the fuel and the air in an assembly and conservatively does not take into account convection or radiation.

3.2.2 Radiative Properties

Radiation heat transfer during the normal transport conditions is accounted for by the effective heat transfer coefficient, h_r, used for describing radiation heat transfer in the HEATING5 computer code. This value is calculated for the heat transfer from the stainless steel surface of the cask to the air surrounding the cask. Radiation heat transfer is also accounted for in the cask during the fire accident. The thermal effects of the fire accident are evaluated using the SCOPE computer code (Bucholz). This computer code takes into account radiative heat transfer between components in the cask and between the cask and the environment.

The HEATING5 effective radiative heat transfer coefficient, h_r, is calculated as follows:

$$h_r = \sigma F$$

where:

σ = the Stefan-Boltzman constant = 0.1714×10^{-8} Btu/hr-ft^2 -°R^4

F = the gray body shape factor for the surfaces involved.

According to the Principles of Heat Transfer (Kreith), the gray body shape factor, F, is calculated as:

$$F = \frac{1}{\frac{P_1}{E_1} + \frac{A_1 P_2}{A_2 E_2} + 1}$$

where:

A_1 and A_2 are the areas of the two surfaces,

E_1 and E_2 are the emissivities of the two surfaces, and

P_1 and P_2 are the reflectivities of the two surfaces.

HEATING5 equates the areas A_1 and A_2 (using the smaller area) and since $P + E = 1$, the equation can be rewritten:

$$F = \frac{1}{\frac{1}{E_1} + \frac{1}{E_2} - 1}$$

Thus, the radiative heat transfer coefficient, h_r, is calculated as:

$$h_r = \frac{\sigma}{\frac{1}{E_1} + \frac{1}{E_2} - 1}$$

In the HEATING5 analysis, only radiation from the surface of the cask to the environment is considered. The radiative heat transfer coefficient is evaluated for this case. The value for the emissivity of stainless steel is found in Table 3.2-1. A value of 1.0 is used for the emissivity of the environment.

$$h_r = \frac{\sigma}{\frac{1}{E_1} + \frac{1}{E_2} - 1}$$

$$= \frac{0.1714 \times 10^{-8}}{\frac{1}{1.0} + \frac{1}{0.35} - 1}$$

$= 6.0 \times 10^{-10}$ Btu/hr-ft^2 -°R^4

$= 4.166 \times 10^{-12}$ Btu/hr-in^2 -°R^4

3.2.3 Convective Properties

Heat transfer by convection is also evaluated for the NAC-LWT cask. This means of heat transfer is evaluated only where its effect is of significant importance. These locations include the liquid neutron shield tank, its associated expansion tank, the air gap between the fuel assembly and the basket wall, the air gap between the basket and the cask body, and the cask surface to the environment.

The effects of convection in these locations are accounted for in the HEATING5 analysis in different ways. In the liquid regions, the conduction and convection coefficients are combined into a single term called the effective thermal conductivity (k_e). The equation for k_e (Bucholz) is:

$$k_e = 0.135\, k_c \left[\frac{Pr^2\, Gr}{1.36 + Pr}\right]^{0.278}, \qquad 10^3 < \left[\frac{Pr^2\, Gr}{1.36 + Pr}\right]^{0.278} < 10^8$$

where:

k_c = thermal conductivity of ethylene glycol mixture

Pr = Prandtl number = $\frac{c_p \mu}{k_c}$

$$Gr = g\beta \frac{\rho^2}{\mu^2} (r2 - r1)^3 \Delta T$$

where:

g = gravitational constant, ft/hr^2

β = volumetric expansion coefficient, °F^{-1}

ρ = density, lbm/ft^3

μ = dynamic viscosity, lbm/hr-ft

$r_2 - r_1$ = radial thickness of the region, ft

Solving for the effective conductivity using thermal properties for the ethylene glycol and water solution found in Table 3.2-5 results in a k_e for the neutron shield tank of 0.7785 Btu/hr-in-°F and a k_e for the expansion thank of 0.3573 Btu/hr-in-°F.

A similar approach is used to evaluate convective heat transfer in the air gaps. An overall heat transfer coefficient that takes into account conduction and convection is obtained. Note that this coefficient has the units of a convection heat transfer coefficient and, therefore, the heat transfer in the air gaps may be described in terms of the HEATING5 convection heat transfer coefficient, h_c. The formula for vertical free convection comes from Principles of Heat Transfer (Krieth) for enclosed air spaces.

$$\frac{Ub}{k} = 0.0317\ Gr^{0.37}$$

where:

U = overall heat transfer coefficient, Btu/hr-in^2 -°F

b = radial thickness of the region, in

k = thermal conductivity of air, Btu/hr-in -°F

$$Gr = \text{Grashof number} = g\beta \frac{\rho^2}{\mu^2} L^3 \Delta T$$

where:

all values in the Grashof number are as described previously with L being the vertical length of the air gap region.

This formula yields an h_c for the gap between the fuel assembly and the inner basket wall of $0.21\ \Delta T^{0.37}$ Btu/hr-in^2-°F and an h_c for the gap between the basket and the cask body of $0.88\ \Delta T^{0.37}$ Btu/hr-in^2-°F.

The formula used to describe the convection coefficient, h_c, for the surface of the cask to the environment is dependent upon the surface orientation. For flat surfaces, h_c was calculated from the formula for vertical flat surfaces from Principles of Heat Transfer (Krieth):

$$h_c = 0.13\ k\ (Gr\ Pr)^{0.33}\ /L$$

where:

k = conductivity of air

Pr = Prandtl number as defined previously

Gr = Grashof number as defined previously

This results in a convection coefficient for vertical flat surfaces of $0.00128\ \Delta T^{0.33}$.

According to Principles of Heat Transfer (Krieth), the convection coefficient for horizontal cylindrical surfaces for $10^9 < Gr < 10^{12}$ is $0.00125\ \Delta T^{0.33}$.

A combined convective and radiative heat transfer between the cask surface and the ambient can be incorporated for the fire transient analysis by modifying the convection coefficient as follows:

$$Q_t = q_r + q_c$$

where q_r is specified as shown for the radiation heat transfer and q_c, which is the heat transfer by convection, is expressed as

$$q_c = h_c A(T_i - T_j)$$

where:

h_c = film coefficient (Btu/hr - in^2 - °F).

Radiation heat transfer for the pre-fire and post-fire conditions between two nodes, i (hotter node) and j (colder node), is accounted for in the fire transient analysis by the expression:

$$q_r = \sigma \varepsilon A F\left(T_i^4 - T_j^4\right)$$

$$q_r = \sigma \varepsilon A F(T_i^2 + T_j^2)(T_i + T_j)(T_i - T_j)\ .$$

where:

σ = Stefan-Boltzman constant = 1.19 x 10^{-11} Btu/hr-in^2-°R^4

ε = emissivity

A = surface area

F = shape factor for the surfaces

T_i = absolute temperature of surface

T_j = absolute temperature of ambient.

By combining both expressions,

$$Q_t = (\sigma\varepsilon F(T_i^2 + T_j^2)(T_i+T_j) + h_c)A(T_i - T_j)$$

or

$$Q_t = h_{eff}A(T_i - T_j)$$

where:

$h_{eff} = \sigma\varepsilon F(T_i^2 + T_j^2)(T_i+T_j) + h_c$

= the effective convection coefficient

The effective convection coefficient used for the cask surface (h_{eff}) now includes the radiation heat transfer. The form factor (F) is taken to be unity. The convective heat transfer coefficient (h_c) is $0.00125\Delta T^{0.33}$ for pre-fire and post-fire conditions and 0.02446 Btu/hr-in^2-°F during the fire.

Table 3.2-1 Thermal Properties of Type 304 Stainless Steel

Property (units)/Temperature (°F)	70	212	392	572	752	932	1112
Density (lbm/in^3)	--	0.2888	0.2872	0.2855	0.2839	0.2822	0.2805
Conductivity (Btu/hr-in-°F)	0.7143	0.7800	0.8592	0.9333	1.0042	1.0717	1.1375
Specific Heat (Btu/lbm-°F)	0.1141	0.1207	0.1272	0.1320	0.1356	0.1385	0.1412
Emissivity	0.35 (77°F)						

Reference: Nuclear Systems Materials Handbook

Table 3.2-2 Thermal Properties of 6061-T6 Aluminum Alloy

Property (units) / Temperature (°F)	200	300	400	500	600
Density (lbm/in^3) [2]	0.098	0.098	0.098	0.098	0.098
Conductivity (Btu/hr-in-°F) [1]	8.25	8.38	8.49	8.49	8.49
Specific Heat (Btu/lbm-°F) [2]	0.23				
Emissivity [3]	0.22				

Reference:

1 ASME Boiler and Pressure Vessel Code, Section II Part D –Properties, Table TCD, 1995 Edition with 1997 addendum, American Society of Mechanical Engineers, New York, NY.

2 "Metallic Material And Element For Aerospace Vehicle Structures", MIL-HDBK-5H, 1998, Figure 3.6.2.0.

3 Bucholz, J.A., Scoping Design Analyses for Optimized Shipping Casks Containing 1-, 2-, 3-, 5-, 7-, or 10- Year-old PWR Spent Fuel, Oak Ridge National Laboratory, ORNL/CSD/TM-149, 1983.

Table 3.2-3 Thermal Properties of Dry Air

Property (units) /Temperature (°F)	0	100	200	300	400	500	600	700
Conductivity (Btu/hr-in-°F)	0.00111	0.00128	0.00145	0.00161	0.00177	0.00193	0.00208	0.00223
Prandtl Number	0.73	0.72	0.72	0.71	0.689	0.683	0.685	0.690
$g\beta\rho^2/\mu^2$ (1/°F-in^3)	2430	1020	492	257	149	92.0	61.3	40.7

Reference: Kreith.

Table 3.2-4 Thermal Properties of Chemical Copper Lead

Property (units)/Temperature (°F)	68	209	400	499	581	630
Conductivity (Btu/hr-in-°F)	1.6651	1.6308	1.5260	1.4111	1.2096	1.0079

Reference: Edwards.

Table 3.2-5 Thermal Properties of 56 Percent Ethylene Glycol Solution

Property (units)/Temperature (°F)	-50[1]	0[1]	50	100	150	200	250	300
Density (lbm/in^3)	0.0401	0.0396	0.0391	0.0385	0.0378	0.0370	0.0362	0.0353
Conductivity (Btu/hr-in-°F)	0.0194	0.0191	0.0188	0.0185	0.0182	0.0179	0.0177	0.0174
Specific Heat (Btu/lbm-°F)	0.694	0.718	0.742	0.766	0.800	0.826	0.852	0.878
Dynamic Viscosity (lbm/hr-in)	57.735	5.854	1.468	0.5832	0.3008	0.1828	0.1228	0.0714
Coefficient of Thermal Expansion (in/in/°F)	0.000361	(200°F)						

[1] Values below 50°F are extrapolated.

References:

1. Cragoe
2. Bates
3. "Coefficient of Cubical Expansion for Glycol, Water and Glycol-Water Solutions."

Table 3.2-6 Thermal Properties of BISCO FPC (Fireblock Silicone Foam)

Temperature (°F)	100	176	500	700	1051
K (BTU/hr – in - °F)	4.375E-3[1]	7.222E-3[2]	6.250E-3[3]	6.389E-3[3]	9.653E-3[3]

References:

1. BISCO Products Data, "FPC (Fireblock Silicone Foam," BISCO Products, Inc., Park Ridge, IL, February 1988.
2. Letter from Rogers Corporation, BISCO Materials Unit, dated February 2, 1999 from Daniel J. Kubrick.
3. Holometrix Micromet test report NCN-2, dated May 2000.

Table 3.2-7 Thermal Properties of Helium

Property (units) / Temperature (°F)		200	400	600	800
Conductivity (Btu/hr-in-°F)		.00808	.00942	.01075	.01150
Density (lbm/in^3)		.48322 E-05	.37037E-05	.30093E-05	.25231E-05
Specific Heat (Btu/ lbm-°F)			1.24		

Reference:
Kreith

Table 3.2-8 Fiberfrax Ceramic Fiber Paper, Grades 550, 880, and 970

Property	Units
Thermal Conductivity	
500°F	0.40 Btu in/hr/ft²/°F
1000°F	0.79 Btu in/hr/ft²/°F
2000°F	1.29 Btu in/hr/ft²/°F
Temperature Use Limit	≥ 2300°F

Reference:
UNIFRAX Product Specifications, Fiberfrax® Ceramic Fiber Paper, C-1423, Unifrax Corporation, Niagara Falls, NY, June 1996.

3.3 Technical Specifications of Components

There are three components important to safety that must be maintained within their safe operating temperature ranges - the TFE, metallic and Viton® O-ring seals, the lead gamma shield, and the 56 percent ethylene glycol and water neutron shield.

The safe operating ranges for the O-rings, lead gamma shield, and liquid neutron shield are as follows:

Component	Safe Operating Range
TFE O-ring	-40°F to +735°F[1]
Metallic O-ring	-40°F to +800°F
Viton® O-ring	-40°F to +550°F[2]
Lead gamma shield	-40°F to +600°F
Liquid neutron shield	-40°F to +350°F

The safe operating range of the O-rings ensures that the cask cavity contents are contained within the cask and are not released to the atmosphere because of thermal failure of the O-rings. The safe operating range of the lead gamma shield ensures that the gamma shield does not melt and, therefore, maintains full gamma shielding capability. The analyses of Sections 3.4.2 and 3.1.1 show that the temperatures of the O-rings are maintained within the safe operating range during normal transport and hypothetical accident conditions. To preclude localized lead temperatures from exceeding their safe operating range, a thermal insulator is used to shield the lead from the high temperatures that are found during the 10 CFR 71 hypothetical fire accident. A 1/8-inch layer of the material is located at the cask outer wall above the neutron shield, around the outer corners of the radial lead shield, and around the sides and the bottom of the lead disk in the cask bottom.

The maximum safe operating temperature of the 56-percent ethylene glycol and water neutron shield ensures that the neutron shield does not boil and, therefore, provides full neutron shielding capability. An expansion tank is also provided to ensure that the neutron shield remains full at the minimum safe operating temperature. The analyses of Sections 3.4.2 and 3.4.3 show that the temperature of the liquid neutron shield remains within its safe operating range during normal transport conditions. The neutron shield is lost during the hypothetical accident, removing the necessity for it to remain within its safe operating range (See Section 5.4 for a discussion of the effect of a loss of the neutron shield on the cask dose rates).

---

1 Verified through testing (Certified Test Report D9-3362-1, Applied Technical Services, Inc., Marietta, GA, February 8, 1989).

2 Verified through testing (Certified Test Report 43939-01, Wyle Laboratories, Inc., Huntsville, AL, February 21, 2000).

3.4 Thermal Evaluation for Normal Conditions of Transport

The temperatures of each of the components of the NAC LWT cask must be evaluated during normal transport conditions. The NAC-LWT cask must prevent components from exceeding their allowable temperatures by rejecting sufficient decay heat to the environment when the design basis, 2-year cooled, Westinghouse 15 × 15 fuel assembly is being transported. Since the neutron shield may be empty when metallic fuel is being transported, cask temperatures are also evaluated for this configuration. Components important to safety, identified in Section 3.3, must be maintained within their safe operating ranges. Also, the thermally induced stresses, in combination with pressure and mechanical load stresses, must be maintained below allowable stress levels.

3.4.1 Thermal Model

The temperatures of the NAC-LWT cask are evaluated for normal transport conditions. The cask is analyzed for two different cases referred to as the Heat Case and the Cold Case.

The Heat Case consists of an ambient temperature of 130°F, still air, and direct solar heating of 737 Btu/ft^2 on the vertical flat surfaces and 1,475 Btu/ft^2 on the curved surfaces for a period of 12 out of every 24 hours.

The Cold Case uses an ambient temperature of –40°F, still air, and shade (no solar heat load). This case requires no thermal analysis when a 0.0 kW decay heat load is considered because a uniform cask temperature of –40°F results. The more limiting decay heat load, from a thermal stress standpoint, is the design fuel assembly maximum decay heat load of 2.5 kW.

3.4.1.1 PWR Analytical Model

The temperatures of the NAC-LWT cask were evaluated using the HEATING5 computer code (Turner). The model used to evaluate the temperature distribution is shown in Figure 3.4-1. The model consists of the fuel basket section and the cask body.

The fuel basket section consists of several regions. These are the active fuel region, the non-power producing portion of the fuel region, the end-fittings, the spacer, an air region above the upper end-fitting, an air gap surrounding the fuel region, and an aluminum annulus (the basket wall) surrounding the gap. The fuel region is modeled as a cylinder 9.5 inches in diameter. (This diameter is actually an effective diameter for an 8.426-inch square fuel assembly.) The active fuel region is broken up into six regions of varying heat generation to closely approximate the axial power distribution shown in Figure 3.4-2. The effective diameter of the air gap is determined based on the 8.875-inch square cavity area minus the 8.426-inch

square fuel assembly area. The effective diameter of the aluminum annulus is obtained by taking the area of the basket and subtracting the area of the cavity. The cask cavity is modeled axially with an active fuel length of 144 inches, 6 inches on either side of the active fuel length as the non-power producing portion of the fuel region, a 4-inch end-fitting on the top and a 3-inch endfitting on the bottom, a 7-inch spacer at the bottom and an 8-inch air gap at the top.

The cask body is modeled based on the nominal dimensions of the license drawings in Section 1.4 with the exception of the radial lead region. The method used to obtain the dimensions of the lead region is described in Section 3.2. Because the calculation of the gap is conservative, the effect of the thermal insulator can be ignored during normal transport conditions. The resulting temperatures will still be conservative.

For ease of designing the analytical model, some of the methods of heat transfer within the NAC-LWT cask are not modeled. The effect of this simplification is an additional conservative small overestimation of overall temperatures within the cask. The heat generated by the fuel rods is transferred within the fuel assembly by conduction and to the air gap surrounding the assembly by convection. Conduction is the only axial means of heat transfer from the fuel assembly to the stainless steel at the top and bottom of the fuel basket. Heat is conducted through the aluminum surrounding the fuel assembly and then transferred by means of convection through the air gap between the fuel basket and the cask body. Heat is then conducted through the inner stainless steel wall, the air gap assumed in the lead region, the lead itself, and the outside stainless steel wall. In the liquid neutron shield, heat is transferred by both convection and conduction. It is then conducted through the stainless steel to the surface of the cask where it is transferred to the environment by means of convection and radiation. The solar heat load is evaluated using a steady-state HEATING5 analysis based on one-half of the maximum hourly solar heat load. The factor of one-half is based on the maximum insolance being applied to all cask surfaces for a period of 12 out of every 24 hours. For this report, this steady-state value for the solar heat load is referred to as full insolation.

3.4.1.2 Metallic Fuel Analytical Model

A HEATING5 computer analysis is performed for the NAC-LWT cask containing metallic fuel. When loaded with this fuel, the neutron shield tank (which is not required for neutron shielding of metallic fuel) is empty. This configuration reduces the heat transfer through the neutron shield region requiring further evaluation. The analysis is performed on the NAC-LWT cask containing the design basis metallic fuel producing 540 watts of decay heat.

This thermal analysis shows that the design basis PWR is the more limiting fuel. The results of the metallic fuel thermal analysis are presented in Table 3.4-1 and show that the temperatures are

lower at all locations (except the neutron shield region) than the corresponding temperatures for the design basis PWR fuel presented in Table 3.4-2.

3.4.1.3 MTR Fuel Analytical Models

Heat transfer analysis of the NAC-LWT containing MTR fuel is performed using two separate two-dimensional planar finite element models and the general purpose ANSYS computer code. The first model represents the entire cask and uses a nominal, effective thermal conductivity to represent the fuel element in each basket location. This cask model is used to determine the maximum temperatures throughout the cask, including the temperature of the fuel element side plates. The second model represents the detailed construction of the fuel element itself. The detailed fuel model uses the results from the cask model to specify the boundary condition temperature of the fuel element side plate. This model is used to determine the maximum fuel temperature for each case. Note that the loose fuel plate configuration in the MTR canister is bounded by the assembled fuel element because the stacked loose plates have a much greater contact area for heat transfer to the basket walls. Therefore, the loose fuel plate configuration is not evaluated. Two transport conditions are evaluated:

Condition 1:

The NAC-LWT is supported in an ISO container with solar insolance applied on the surface of the ISO container, and the NAC-LWT is considered to be insulated from the environment (only for normal conditions of transport steady state conditions). The gas inside the ISO container is air. The cavity of the NAC-LWT is backfilled with helium as required by operational procedures.

Condition 2:

The NAC-LWT is not located in an ISO container and solar insolance is applied to the NAC-LWT cask surface. For the purpose of performing the thermal analyses, the cavity of the NAC-LWT is considered to be filled with air.

Of these two conditions, Condition 2 (air in cavity case) produces the higher temperatures as shown in Table 3.4-6. Therefore, the detailed fuel model is used to evaluate Condition 2 only. For each of the two conditions listed above, two different fuel configurations are considered for evaluation for steady-state normal transport conditions.

(1) Uniform design basis heat load of 30 watts per MTR fuel assembly:

This configuration consists of seven MTR fuel elements with design basis heat loads (30 watts per element) corresponding to a total MTR package contents heat load of 1.26 kilowatts (42 fuel elements).

(2) MTR fuel with variable decay heat:

As described in Section 5.3.4, MTR fuel may also be shipped in a variable decay heat configuration. In this case, a basket module may be loaded with only three elements, each having a maximum decay heat of 70 watts, or with three elements with maximum decay heats of 120 watts, 70 watts, and 20 watts. The total decay heat load for the basket must not exceed 210 watts. The same detailed heat transfer model described in Section 3.4.1.3.1 is also used for this analysis.

The fuel decay heat is modeled using uniform volumetric heat generation terms defined by administrative controls from Section 7.1.5. The administrative controls define bounding basket loading configurations that:

- Limit the combined basket heat load to 210 watts per basket module.
- Exclude MTR elements having decay heat loads in excess of 120 watts.
- Require MTR elements having decay heat loads between 120 watts and 70 watts to be loaded into the center basket module position.
- Require MTR elements with decay heat loads between 30 watts and 70 watts to be loaded in the center in-line row of the basket module.
- Limit decay heat loads of MTR elements placed in peripheral basket tubes, not on the center line, to a 30-watt decay heat load (per element).

These constraints result in two bounding loading configurations of MTR fuel elements. Assuming that individual elements have maximum decay heats of 70 watts and 120 watts, the two bounding configurations are:

1. Three 70-watt fuel elements
2. One 120-watt fuel element, one 70-watt fuel element, and one 20-watt fuel element

These combinations are depicted in Figure 3.5-7. Of these two configurations, the second configuration will produce the highest temperatures, as the center assembly contains a 120-watt MTR fuel element. This is the fuel configuration, which is analyzed for the variable decay heat loading. The thermally limiting configuration is also depicted in Figure 3.4-4, which conservatively bounds any fuel loading configuration permitted by the operating procedure presented in Section 7.1.5.

3.4.1.3.1 MTR Fuel Thermal Model of the NAC-LWT (Transported in an ISO Container)

For Condition 1, the detailed fuel model is not used because this condition is bounded by Condition 2, as shown in Section 3.4.1.3.2. Thermal analyses of the NAC-LWT cask for Condition 1 are performed using a half-symmetry, cross-sectional model of the cask in an ISO container positioned along the container centerline. Heat transfer to the environment is limited to surface convection and radiation on both horizontal and vertical surfaces of the ISO container with an emissivity of 0.36. Solar insolance is applied to the vertical surfaces and the top horizontal surface of the ISO container. Heat transfer from the cask to the ISO container is modeled as conduction, convection and radiation. Convective and conductive heat transfer are modeled in the liquid neutron shield, while heat transfer in the cask cavity is limited to conduction and radiation. Axial heat transfer is conservatively ignored in the model. The MTR fuel elements are represented in the model with homogenized fuel elements. The conductive heat flow path from the cask through the saddle support to the bottom surface of the ISO container is conservatively ignored.

Thermal conductivity for 6061-T6 aluminum alloy is based on ASME Code, Section II, Part D, Table TCD. The finite element model for the uniform 30 watts per MTR fuel element is shown in Figure 3.4-3, while the finite element model for the variable decay heat of 120 watts, 70 watts and 20 watts is shown in Figure 3.4-4. For the basket slots, which are empty for the variable decay heat, only conduction through the cavity gas is modeled. In each of these fuel models, the fuel is considered to rest on the surface of each basket slot. The details of this modeling are shown in Figure 3.4-6. While the MTR fuel assemblies are considered to rest on the surface of the basket, the basket is conservatively modeled as being in the center of the cask cavity. Conduction (through helium) and radiation (using emissivity of stainless steel for both surfaces) are modeled from the inner shell of the cask to the basket.

The heat transfer analysis model represents the cask cavity free space using the conductivity of helium. (see Table 3.2-7). The properties for the remaining materials are contained in Table 3.2-1 through Table 3.2-6.

The air space between the NAC-LWT cask and the ISO container is modeled using air with an effective conductivity. This effective conductivity (Incropera) is:

$$\frac{k_{eff}}{k} = 0.386\left(\frac{Pr}{0.861+Pr}\right)^{1/4}\left(Ra_c^*\right)^{1/4}$$

$$Ra_c^* = \frac{[\ln(D_0/D_i)]^4}{L^3 (D_i^{-3/5} + D_0^{-3/5})^5} Ra_L$$

$$Ra_L = \frac{g\beta(T_i - T_o)L^3}{\alpha\nu}$$

where:

Pr = Prandtl number (Krieth)

ν = kinematic viscosity (Krieth)

α = thermal diffusivity (Krieth)

β = $1/T_f$

T_f = $(T_i+T_o)/2$

T_i = inner surface temperature

T_o = outer surface temperature

D_i = inner diameter (cask surface)

D_o = outer diameter (height of the ISO container)

L = $(D_o - D_i)/2$

The effective conductivity for the neutron shield and expansion tank as well as the convection from the surface of the ISO container to an ambient temperature of 100°F are presented in Section 3.2.3.

Decay heat for the different MTR package configurations is conservatively enveloped for the heat transfer analysis. Each fuel element of the maximum capacity MTR package configuration, 42 elements, is modeled with a heat generation of 30 watts. Total MTR package contents heat load is 1.26 kilowatts, approximately half of the NAC-LWT cask maximum decay heat load of 2.5 kilowatts. The decay heat is modeled as uniformly generated within the homogenized fuel regions.

The Condition 1 models of the NAC-LWT cask with uniform and variable decay heat MTR fuel element loadings are shown in Figure 3.4-3 and Figure 3.4-4, respectively.

3.4.1.3.2 MTR Fuel Thermal Model of the NAC-LWT (Transported via Truck Trailer)

Thermal analyses of the NAC-LWT cask for Condition 2 are performed using two separate models. The first is a half-symmetry cross-sectional model of the cask in which the outer surface of the expansion tank is the boundary of the model. This model is used to determine the temperatures throughout the cask up to and including the maximum fuel element side plate temperatures. The second is a half-symmetry cross-sectional model of the fuel element. This model is used to determine the maximum fuel temperature within the element for the worst-case fuel plate dimensions. The worst case dimensions are based on the limiting design dimensions combined with the limiting manufacturing tolerances that result in the maximum resistance to heat transfer from the fuel to the side plates.

Cask Model

The modeling of the normal steady state condition of the NAC-LWT from the center of the cask to the outer surface of the expansion tank is identical to the model described in Section 3.4.1.3.1 with the following exceptions:

1. The gas in the NAC-LWT cask cavity is considered to be air.
2. The MTR basket is shifted downward towards the inner shell leaving a minimum gap of 0.07 inch between the outer diameter of the basket end plate and the cask inner shell surface. This is an effective representation of the normal condition of transport (i.e. cask horizontal).
3. The solar insolance and convection to the ambient temperature of 100°F is applied to the outer shell of the expansion tank.

The Condition 2 models of the NAC-LWT cask with uniform and with variable decay heat MTR fuel element loadings are shown in Figure 3.5-6 and Figure 3.5-7, respectively. These same models are used to calculate both normal and accident condition temperatures for the cask.

Fuel Element Model

The fuel element model includes the side plate, the fuel, cladding, and the air between the plates and surrounding the side plate. The total element heat load is uniformly distributed throughout the fuel. Based on symmetry, only one-half of the fuel element assembly is modeled. Figure 3.4-13 shows the model for both the minimum 10-plate and maximum 23-plate cases. These two configurations bound fuel elements with any intermediate number of plates. The boundary condition for this model is the applied side plate temperature at the lower right corner of the model. This assumes that the basket is oriented such that only the ends of the element side plates are in contact with the basket. The lateral surfaces of the side plates are assumed to be adiabatic, which results in a conservative calculation of the maximum temperature of the fuel.

	K, BTU/hr-in-°F		
Temperature, °F	Aluminum	UO_2	Fuel Matrix 75% UO_2
100	8.08	0.42	2.33
200	8.25	0.37	2.34
300	8.38	0.33	2.35
400	8.49	0.30	2.35

The worst-case fuel effective thermal conductivity occurs for the maximum UO_2 percentage of 75% and corresponds to the LEU fuel plates.

The fuel in the center of each fuel plate is a matrix of aluminum and uranium or aluminum and uranium oxide (UO_2) combined in various ratios. The effective thermal conductivity is calculated using a mass-weighted average of the conductivity of the individual materials. The fuel plates are modeled using worst-case dimensions as shown:

1. Fuel plate thickness = 0.045 inch (< 0.05 inch)
2. Cladding thickness = 0.008 inch (< 0.015 inch)

A sensitivity analysis shows that variation of the active fuel width within the fuel plate has a negligible effect. A constant value of 6.6 cm is used in the analysis. This corresponds to the worst case for reactivity considerations. Note that the case of the loose fuel plates in the MTR canister is bounded by that of the assembled fuel element and, therefore, is not evaluated.

3.4.1.3.3 MTR Fuel Heat Transfer Analyses Results

The thermal analysis is performed to demonstrate that the temperature of the MTR fuel is maintained within acceptable limits. A conservative temperature of 400°F is established as the maximum allowable MTR fuel cladding temperature for normal conditions of transport. The aluminum retains its capability to function as a mechanical component in this temperature range, and it is not close to the 1,220°F melting temperature of aluminum (Table 6.4.1, pg. 6-60, Marks' Standard Handbook for Mechanical Engineers). The material properties presented in MIL-HDBK-5F indicate that 6061-T6 aluminum alloy retains over 40% of its room temperature yield and ultimate strengths at a long-term temperature of 400°F.

Maximum temperatures for package components with the NAC-LWT configured for MTR fuel are summarized in Table 3.4-6. The reported temperatures are lower at all locations than the corresponding temperatures for the design basis PWR fuel presented in Table 3.4-2. Temperatures of the MTR fuel element cladding are maintained below 400°F for both the design basis uniform decay heat loading and the variable heat loading.

3.4.1.4 PWR Rod

Heat transfer of the NAC-LWT containing 25 PWR rods with a total heat load of 1.41 kW configured in the PWR/BWR aluminum basket in the NAC-LWT cask enclosed in an International Shipping Organization (ISO) container was evaluated using ANSYS. The model presented in Figure 3.4-3 was revised to include the PWR/BWR aluminum basket and 25 PWR rods. Results from this evaluation are summarized in Table 3.4-7.

These results show that the temperatures are lower at all locations (except the neutron shield region) than the corresponding temperatures for the design basis PWR fuel presented in Table 3.4-2. Similar to the discussion presented in Section 3.4.1.3.3 for the MTR heat transfer analysis, temperature results from the two dimensional heat transfer analysis are conservative based on the imposed limitations of the model and can be used to evaluate acceptability of component temperatures outside the modeled section. Temperature of components in the lid closure region is less than the hottest basket temperature which is directly influenced by the decay heat of the fuel. It is concluded that the temperature of the safety related O-ring seals is within the allowable range of temperature of -40°F to +735°F. The maximum temperature of the lead gamma shield in the base of the LWT cask is less than the cask inner shell and much lower than the maximum of +600°F.

3.4.1.5 Thermal Evaluation for TRIGA Fuel

The thermal evaluation for TRIGA fuel is performed using classical analysis employing a thermal resistance model. The TRIGA fuel is transported in a basket assembly consisting of 5 modules - a base module, a top module, and three intermediate modules. During transport all 5 modules must be installed in the cask. The three intermediate modules are interchangeable, but the top and base modules are not. Each module contains 7 cells, and each open cell holds up to 4 TRIGA fuel elements. The top module is sized to accept fuel follower control elements, which are longer than the typical element. The center cell of each module is blocked with an 11-gage stainless steel plate so that fuel cannot be loaded in the center cell. The thermal evaluation conservatively assumes that the center cell also contains 4 fuel elements, so although only 120 fuel elements may be loaded into the cask, the thermal evaluation assumes 140 elements. Consequently, the total heat load in the thermal evaluation is conservatively considered to be 1.05 kW (7.5 watt/fuel element × 140 = 1.05 kW).

TRIGA fuel elements may be transported directly in a basket module cell, in a screened failed fuel can, or in a sealed failed fuel can. The fuel cans fit in either a top or base module cell. The screened failed fuel cans hold up to four (4) TRIGA fuel elements, while the sealed failed fuel can holds up to two (2) damaged elements or equivalent fuel debris.

As described in Section 1.2.3.1, TRIGA fuel elements with minor cladding defects are loaded into screened failed fuel cans (screened cans). The screened can precludes gross particulate material from escaping the cell. The screened failed fuel cans are provided in two lengths. The screened failed fuel can is a square tube of 14-gage, Type 304 stainless steel, that holds four fuel elements. It is provided with a closure lid and an end plate that is screened to allow water draining.

TRIGA fuel debris and damaged fuel elements, which do not have structural integrity, are loaded into sealed failed fuel cans (sealed cans). The sealed cans are used to containerize the TRIGA fuel debris. The cans are provided in two lengths. The shorter can may be used in the base or top basket modules. The longer can may only be used in the top module. The cans are vacuum dried and leak tested prior to loading into a TRIGA fuel basket.

The TRIGA fuel thermal evaluation determines the maximum fuel cladding temperatures based on the maximum basket temperatures determined for the design basis heat load MTR thermal analysis presented in Section 3.4.1.3.1. An intermediate basket module with the shortest TRIGA fuel, which provides the highest heat load density, is used to obtain a bounding evaluation. Based on the maximum basket temperature and heat load density, the maximum fuel cladding temperatures are determined using a thermal resistance model.

The cross-section of the TRIGA and MTR fuel baskets are identical. As shown in Section 1.2.3 and Table 1.2-4, the maximum decay heat load for MTR fuel is 1.26 kW per cask. The maximum decay heat load for TRIGA fuel is 1.05 kW per cask. Therefore, it is conservative to use the maximum basket temperature for MTR fuel as a boundary condition for the thermal resistance model for TRIGA fuel.

Since the total decay heat load for MTR fuel bounds that for TRIGA fuel, the temperatures for cask components for the MTR fuel also bound those for the TRIGA fuel. The cask body temperatures for the MTR fuel are shown in Table 3.4-6.

3.4.1.5.1 TRIGA Model Description

The heat generated from the TRIGA fuel in the basket is transferred to the basket module by thermal conduction and radiation, and then transferred to the cask inner shell from the basket surface by the same heat transfer modes. The heat is finally transferred through the cask and International Shipping Organization (ISO) container to ambient. The thermal resistance model and thermal analysis of TRIGA fuel considers the regions inside a single basket opening of the TRIGA fuel basket. This analysis bounds transport in the cask without an ISO container.

The thermal resistance model is shown in Figure 3.4-5. The maximum temperature of the basket (T_{basket}) is taken from the MTR design basis heat loading thermal analysis. The temperatures for

the TRIGA fuel are determined by stepping through each of the resistors in the thermal circuit, from the basket to the fuel cladding. All temperatures calculated are maximums, based on the basket temperature. Each successive maximum temperature calculated is then applied uniformly over the next surface in the resistance model. Fuel may be shipped directly in a basket cell, in a screened failed fuel can, or in a sealed failed fuel can. Since the model assumes the presence of the can, the model is conservative for configurations in which a can is not used.

The gas in the cask cavity is considered to be air in the thermal resistance model. Thermal conductivities of air and stainless steel are obtained from "Fundamentals of Heat and Mass Transfer" (Incropera). Emissivities of stainless steel (basket) and aluminum (fuel clad) are obtained from the Nuclear Systems Material Handbook and from "Scoping Design Analyses for Optimized Shipping Casks Containing 1-, 2-, 3-, 5-, or 10-Year-Old PWR Spent Fuel" (Bucholz), respectively.

Assuming the maximum temperature of the basket (T_{basket}) occurs at all inside surfaces of the webs forming the central cell in the basket module, the temperature of the can (T_{can}) is then determined by considering heat conduction and radiation between the can surface and the inside surface of the basket central cell. Convection in the gap between these surfaces is conservatively ignored.

The heat transfer rate across the gap per unit length (q_{gap}) between the can surface and the inside surface of the basket central cell wall can be represented as follows:

$$q_{gap} = q_{cond} + q_{rad}$$

$$q_{gap} = \frac{A(k_{cond})(T1-T2)}{L_{gap}} + \frac{A(\sigma(\sigma)(^4 - T2^4)}{\left(\frac{1}{\varepsilon_1} + \frac{1}{\varepsilon_2} - 1\right)}$$

where:

q_{gap} = 7.5 watt × 4/14 = 2.14 watt = 7.302 Btu/hr

A = Can surface area = 3.33 × 4 = 13.32 inch^2

K_{cond} = Air conductivity @ 260°F (400°K) = 1.628 × 10^{-3} Btu/hr-in-°F

L_{gap} = Gap size between can and basket = (3.44-3.33)/2 = 0.055 inch

T1 = temperature at can surface (T_{can})

T2 = temperature at inside surface of the basket central cell (T_{basket}) = 267°F

σ = 1.19 × 10^{-11} Btu/hr-in^2-°R

ε_1 = emissivity of web of basket central cell (stainless steel) = 0.36

ε_2 = emissivity of can (stainless steel) = 0.36

The temperature at the can (T_{can}) is calculated to be 287°F.

The maximum temperature of the can (T_{can}) is then applied to all can surfaces for determining the cladding temperature of the fuel. It is assumed that there are four (4) fuel elements inside the can surrounded by air. In the equivalent resistor analogy, the fuel elements do not contact each other, neglecting heat conduction between fuel elements. For a specific fuel element, an assumed circular region equivalent to 1/4 of the area inside the can, is developed to contain a fuel element, which results in a uniform air gap. The fuel cladding temperature is determined using the formula representing a hollow cylinder. Note that convective heat transfer in the gap between the fuel clad and the can is conservatively ignored.

Heat transfer rate per unit length of the basket (Q_{leng}) can be represented as:

$$Q_{leng} = q_{cond} + q_{rad}$$

$$Q_{leng} = \frac{2\pi\pi(_{cond})(T1 - T2)}{\ln\left(\frac{r_2}{r_1}\right)} + \frac{\sigma(2\pi r_1)(T1^4 - T2^4)}{\left(\frac{1}{\varepsilon_1}\right) + \left(\frac{1-\varepsilon_2}{\varepsilon_2}\right)\left(\frac{r_1}{r_2}\right)}$$

where:

r_1 = fuel cladding outer radius = 0.675 inch

r_2 = radius of equivalent circular region representing ¼ of the area inside a can
= 0.93 inch

K_{cond} = Air conductivity @ 260°F (400°K) = 1.628×10^{-3} Btu/hr-in-°F

σ = 1.19×10^{-11} Btu/hr-in^2-°R

ε_1 = emissivity of fuel cladding (aluminum) = 0.22

ε_2 = emissivity of the can (stainless steel) = 0.36

T1 = fuel cladding temperature (T_{clad})

T2 = can temperature (T_{can}) = 287°F

The fuel cladding temperature (T_{clad}) is solved to be 326°F.

3.4.1.5.2 TRIGA Fuel Thermal Evaluation Results

Using the model described above, and the assumed boundary condition of 267°F for the maximum basket temperature (from Table 3.4-6), the maximum normal transport conditions temperature of the TRIGA fuel is determined as shown in Table 3.4-8.

A conservative temperature of 400°F is established as the maximum allowable temperature for aluminum-clad TRIGA fuel, as described in Section 3.4.1.3.3 for MTR fuel. Stainless steel clad TRIGA fuel is allowed a significantly higher cladding temperature, since the melting temperature of stainless steel is 2,600°F (Mark's) and stainless steel retains its capability to function as a mechanical component at temperatures up to the 800°F range. Therefore, the temperatures calculated for the TRIGA fuel cladding are acceptable.

3.4.1.6 TRIGA Fuel Cluster Rods

The TRIGA fuel cluster rods are 0.542 inches OD with 0.016-inch thick Incoloy 800 cladding. Each rod is inserted into a 6061-T6 aluminum tube (0.75 inch OD, 0.62 inch ID) that is part of the fuel rod insert. Up to sixteen rods and a fuel rod insert are placed into a single cell of the seven cell basket. This TRIGA basket has the same cross sectional dimensions and basket material as the MTR basket presented in Section 3.4.1.3. The thermal evaluation for the TRIGA fuel cluster rods is performed using two-dimensional planar finite element analyses and the general purpose ANSYS computer code. Two transport conditions are evaluated:

Condition 1:

The NAC-LWT is supported in an ISO container with solar insolance applied on the surface of the ISO container, and the NAC-LWT is considered to be insulated from the environment (only for the normal conditions of transport steady state conditions). The gas inside the ISO container is air. The cavity of the NAC-LWT is actually backfilled with helium as required by operational procedures.

Condition 2:

The NAC-LWT is not located in an ISO container and solar insolation is applied to the NAC-LWT cask surface.

For the purpose of performing these thermal analyses, the cavity of the NAC-LWT is considered to be filled with air.

For each of the two conditions listed above, only a single fuel configuration is evaluated: 16 rods in a fuel rod insert in each of the seven cells comprising a basket section. This corresponds to a total heat load of 210 watts for each basket section (30 watts per cell of a basket section which

corresponds to 30/16 or 1.875 watts per rod). Therefore, the heat load in the cask cavity corresponding to five basket sections is 5 times 210 watts or 1.05 kW.

Since the finite element model corresponds to a one inch axial length, the heat generation applied to each rod in the model was 1.875 watts divided by the length of the rod or 22 inches. Although the aluminum inserts will conduct heat in the axial direction, this was conservatively ignored.

3.4.1.6.1 Condition 1 Analysis of TRIGA Fuel Cluster Rods

Thermal analyses of the NAC-LWT cask for Condition 1 are performed using a half symmetry cross sectional model of the cask in an ISO container positioned along the container centerline. The model employed for the ISO container, cask body and the seven-celled basket is the same finite element model used in Section 3.4.1.3.1 for the MTR fuel thermal model (Condition 1). The similarity in modeling includes the finite element mesh and the material properties for conduction, convection and radiation. The 16 rods and fuel rod inserts are modeled in each of the seven cells, as shown in Figure 3.4-7. Figure 3.4-8 and Figure 3.4-9 show details of the fuel region model. The TRIGA fuel cluster rods were conservatively modeled in the center of the aluminum fuel tube, and the fuel rod inserts were modeled without any contact with the sides of the basket. The 0.13 inch aluminum shell, which surrounds the TRIGA fuel cluster, provides a heat transfer path from the rods to the basket surface. This aluminum shell was conservatively not considered in the analysis. The space between the aluminum tubes and the stainless steel basket surface was modeled with the cavity gas, and the modes of heat transfer from fuel rod insert to the basket surface included conduction through the gas and radiation from the surface of the insert to the basket surface.

3.4.1.6.2 Condition 2 Analysis of TRIGA Fuel Cluster Rods

Thermal analyses of the NAC-LWT cask for Condition 2 are performed using a half symmetry cross sectional model of the cask in which the outer surface of the expansion tank is the boundary of the model. The modeling of the normal steady state conditions of the NAC-LWT from the center of the cask to the outer surface of the expansion tank is identical to the model described in Section 3.4.1.3.1 with the following exceptions:

1. The gas in the NAC-LWT cask cavity is considered to be air.
2. The solar insolance and convection to the ambient temperature of 100°F is applied to the outer shell of the expansion tank.

3.4.1.6.3 TRIGA Fuel Cluster Rods Heat Transfer Results

The thermal analysis is performed to demonstrate that the temperature of the TRIGA fuel cluster rod is maintained within acceptable limits. A conservative temperature of 800°F is established as

the maximum allowable TRIGA fuel cladding temperature for normal conditions of transport. For aluminum 6061-T6 aluminum alloy, the allowable temperature is considered to be 400°F.

Temperatures for package components with the NAC-LWT configured for the TRIGA fuel are summarized in Table 3.4-9. In this table, the maximum fuel clad temperature is 295°F, which is significantly below the 800°F value. For the aluminum, the maximum reported temperature is 292°F, which is also well below the 400°F limit.

3.4.1.7 High Burnup PWR or BWR Rods in a Rod Holder

The high burnup rods may be either BWR rods or PWR rods. The decay heat for the PWR is 2.3 kW with a corresponding peaking factor of 1.1 and for the BWR the decay heat per rod is 2.1 kW with a peaking factor of 1.22. The thermal evaluation employs a two-dimensional planar model to ensure that the peaking factor is conservatively included and the heat load applied to the finite element model is the total heat load factored by the peaking factor. The bounding product of the heat load and the peaking factor corresponds to the BWR. The evaluation of the BWR rod is considered to bound the temperatures corresponding to the PWR rod configuration. All of the fuel rods are considered to be intact for this evaluation. The evaluation of damaged fuel rods is provided in Section 3.4.1.11.

The rod holder for the high burnup rod transport can accommodate two configurations: a 4×4 matrix of pin tubes containing 16 rods and a 5×5 matrix of pin tubes containing 25 rods. Since the decay heat per rod is considered to be the same, the maximum heat load is bounded by the 25-rod configuration. For the 4×4 matrix of pin tubes, an additional stainless steel insert, .31-inch thick, is placed in the can weldment. This permits the can weldment to be employed for the 16-rod transport or the 25-rod transport configuration. For the can weldment, the aluminum basket and the remainder of the cask, the additional insert has a negligible affect on their temperatures. Therefore, the bounding configuration is the 25-rod configuration, since it produces 56% more heat load in the cask basket than the 16-rod configuration. The bounding configuration for the clad temperatures and the pin tubes supporting the fuel rods is also the 25-rod configuration due to the 56% additional heat load. While the additional insert increases the thermal resistance, this is significantly offset by the additional 56% additional decay heat.

Heat transfer analysis of the NAC-LWT containing high burnup rods is performed using two-dimensional planar finite element analyses and the general purpose ANSYS computer code. Two transport conditions are evaluated:

Condition 1:

The NAC-LWT is supported in an ISO container with solar insolance applied on the surface of the ISO container, and the NAC-LWT is considered to be insulated from the environment (only for normal conditions of transport steady state conditions). The gas inside the ISO container is air.

The cavity of the NAC-LWT is backfilled with helium as required by operational procedures.

Condition 2:

The NAC-LWT is not located in an ISO container and solar insolance is applied to the NAC-LWT cask surface.

For the purpose of performing the thermal analyses, the cavity of the NAC-LWT is considered to be filled with air.

3.4.1.7.1 High Burnup PWR and BWR Fuel Rods Thermal Model of the NAC-LWT (Transported in an ISO Container)

Thermal analyses of the NAC-LWT cask for Condition 1 are performed using a half-symmetry, cross-sectional model of the cask in an ISO container. Heat transfer to the environment is limited to surface convection and radiation on both horizontal and vertical surfaces of the ISO container with an emissivity of 0.36. Solar insolance is applied to the vertical surfaces and the top horizontal surface. Heat transfer from the cask to the ISO container is modeled as conduction, convection and radiation. Convective and conductive heat transfer are modeled in the liquid neutron shield, while heat transfer in the cask cavity is limited to conduction and radiation. Axial heat transfer is conservatively ignored in the model.

Bounding configuration of BWR fuels used in analyses is based on U.S. Department of Energy, Office of Civilian Radioactive Waste Management, "Characteristics of Spent Fuel, High-Level Waste, and Other Radioactive Wastes Which May Require Long -Term Isolation," Appendix 2A, December 1987. Thermal properties of UO_2 and zirconium alloy cladding are from 1) Hagrman, D.L., Reymann, G.A., "Matpro-Version 11, A Handbook of Material Properties for Use in the Analysis of Light Water Reactor Rod Behavior," Idaho Falls, ID, EG&G Idaho, Inc., 1997; 2) Rust, J.H., "Nuclear Power Plant Engineering," Atlanta, GA, S.W., Holland Company, 1979. Thermal conductivity for 6061-T651 aluminum alloy is based on ASME Code, Section II, Part D, Table TCD.

The finite element model for the condition 1 is shown in Figure 3.4-10. The fuel cladding and the inner surface of the pin tube are considered to be in point-to-point contact. The outer surface

of the fuel cladding only contacts the pin tube in one point in the model. The pin tubes are conservatively considered separated and a gap of 0.0005 inch between pin tubes is modeled. This condition neglects any pin tube contact due to dead weight loading of the contents. One of the can weldment sides is modeled in contact with the aluminum insert. For the other three sides, a gap 0.042/0.084/0.042 inch between the aluminum insert and the tube of the can weldment is modeled. The details of this modeling are shown in Figure 3.4-11. Likewise, only one surface between the PWR aluminum insert and the PWR basket is considered to be in contact.

Conduction (through helium) and radiation (using emissivity of stainless steel for both surfaces) are modeled from the inner shell of the cask to the basket.

The heat transfer analysis model uses conduction in the remaining volume of the cask cavity. The conductivity of this material corresponds to helium. (see Table 3.2-7). The properties for the remaining materials are contained in Table 3.2-1 through Table 3.2-8.

The air space between the NAC-LWT cask and the ISO container is modeled using air with an effective conductivity. This effective conductivity (Incropera) is:

$$\frac{k_{eff}}{k} = 0.386\left(\frac{Pr}{0.861+Pr}\right)^{1/4}\left(Ra_c^*\right)^{1/4}$$

$$Ra_c^* = \frac{[\ln(D_0/D_i]^4}{L^3\left(D_i^{-3/5}+D_0^{-3/5}\right)^5}\,Ra_L$$

$$Ra_L = \frac{g\beta(T_i-T_o)L^3}{\alpha\nu}$$

where:

Pr = Prandtl number (Krieth)

ν = kinematic viscosity (Krieth)

α = thermal diffusivity (Krieth)

β = $1/T_f$

T_f = $(T_i+T_o)/2$

T_i = inner surface temperature

T_o = outer surface temperature

D_i = inner diameter (cask surface)

D_o = outer diameter (height of the ISO container)

$L = (D_o - D_i)/2$

3.4.1.7.2 High Burnup PWR and BWR Fuel Rods Thermal Model of the NAC-LWT (Transported via Truck Trailer)

Thermal analyses of the NAC-LWT cask for Condition 2 are performed using a half-symmetry planar cross-sectional model of the cask in which the inner surface of the inner shell is the boundary of the model. The maximum temperature of 274°F (PWR design basis fuel with 2.5 kW heat load and a peaking factor of 1.2 under normal transport condition [Table 3.4-2]) is applied to the boundary of the model. The modeling of the normal steady state condition of the NAC-LWT from the center of the cask to the inner surface of the inner shell is identical to the model described in Section 3.4.1.7.1 with the following exceptions:

1. The gas in the NAC-LWT cask cavity is considered to be air.
2. The constant temperature of 274°F is applied to the outer surface of the model, which corresponds to the inner surface of the cask inner shell. This temperature corresponds to the condition, which imposes solar insolance and convection/radiation boundary at the outer shell of the expansion tank. This is also described in Section 3.4.1.1.

The Condition 2 model of the NAC-LWT cask with high burnup PWR and BWR fuel rods is shown in Figure 3.4-12. This model is also used to calculate both normal and accident condition temperatures for the cask.

3.4.1.7.3 High Burnup PWR and BWR Fuel Rods Heat Transfer Analyses Results

The thermal analysis is performed to demonstrate that the component temperature of NAC-LWT cask loaded with high burnup PWR and BWR rods is maintained within acceptable limits.

Maximum temperatures for package components with the NAC-LWT configured for high burnup PWR and BWR rods are summarized in Table 3.4-10. As shown in Table 3.4-10, component temperatures are all maintained within their allowable temperatures.

3.4.1.8 Thermal Evaluation for DIDO Fuel

3.4.1.8.1 Analytical Models for the DIDO Fuel Contents

Heat transfer analysis of the NAC-LWT containing DIDO fuel is performed using a two-dimensional planar finite element analysis and the general purpose ANSYS computer code. Two transport conditions are evaluated:

Condition 1:

The NAC-LWT is supported in an ISO container with solar insolance on the surface of the ISO container, and the NAC-LWT is considered to be insulated from the environment (only for the normal conditions of transport steady state conditions). The gas inside the ISO container is air. The cavity of the NAC-LWT is backfilled with helium as required by operational procedures.

Condition 2:

The NAC-LWT is not located in an ISO container and solar insolation is applied to the NAC-LWT cask surface. For the purpose of performing the thermal analysis, the cavity of the NAC-LWT is considered to be filled with air.

A single fuel configuration is considered for this evaluation. Each DIDO fuel assembly is limited to having a heat load of 25 W per assembly. The total contents of the NAC-LWT for the DIDO fuel are limited to having six basket modules and each module is limited to having seven DIDO fuel assemblies. This limits the heat load of a basket module to 175 W, and a total NAC-LWT heat load of 1.05 kW. The 1.05 kW total heat load is enveloped by the 1.26 kW total heat load for the NAC-LWT MTR fuel contents contained in Section 3.4.1.3. Since the NAC-LWT cask ambient conditions are the same for the DIDO fuel as for the MTR fuel, the maximum temperature of all cask body components for the DIDO contents are enveloped by the maximum temperatures for the MTR fuel contents. Therefore, the cask inner shell temperature for the MTR fuel contents bounds the maximum cask inner shell temperature for the DIDO fuel contents. The maximum cask inner shell temperature is used as the boundary condition for the finite element model for the DIDO thermal evaluation. For Condition 1 and Condition 2, the maximum inner shell temperatures are 214°F and 181°F, respectively. These values correspond to the design basis heat load values obtained from Table 3.4-6.

Two finite element models are used in the evaluation of the DIDO fuel basket and the DIDO fuel assemblies.

The evaluation of the maximum basket component temperatures for these conditions is performed using a finite element model, which is shown in Figure 3.4-14. This model is used to evaluate both conditions. This model corresponds to the 4.01-inch inside diameter stainless steel tubes, the 1/2-inch thick plates, the 3/4-inch × 3/8-inch aluminum bars (thermal shunts) and the 0.19-inch thick aluminum sheet (heat transfer shell) on the outside of the tubes. The SOLID70, eight-noded brick element is used to represent stainless steel components, the heat transfer shell and the cavity gas between the surfaces of the circular plates and the heat transfer shell and the

inner shell of the cask body. To account for the axial conductance of the thermal shunts, they are modeled as conduction elements using an area corresponding to the dimensions of the aluminum bars. Radiation is conservatively neglected from the outer surface of the heat transfer shell and the inner surface of the cask inner shell. The center tube is assumed not to be in contact with any of the six outer tubes. During transport, the NAC-LWT is in a horizontal position in which the basket modules are in contact with the inner shell of the cask. To represent the contact of the basket module with the cask inner shell, the inner shell temperature was applied to two nodes of the circular plates and the remaining nodes corresponding to the inner surface of the inner shell of the cask body. The 25 W per assembly heat load is represented by applying the heat flux along a concentrated area at the inner tube surface, which would correspond to the contact of the fuel assembly with the 4.01-inch inside diameter stainless steel tube.

For Condition 1, the elements representing the cavity gas between the basket and the inner shell correspond to helium, whereas for Condition 2, these elements use properties for air.

To determine the maximum temperature for the fuel, a separate detailed model of a DIDO fuel assembly is constructed. This model is shown in Figure 3.4-15, which consists of four circular cylinders in contact at a corresponding single point to be transported in the horizontal position. Each cylinder is comprised of a layer of fuel of 0.64 mm (0.025 in.) thickness between two aluminum shells, each being 0.46 mm (0.018 in.) thick. The boundary condition of this model is the maximum basket temperature determined from the detailed basket model and the volumetric heat generation corresponding to 25 W per assembly.

3.4.1.8.2 DIDO Fuel Heat Transfer Analyses Results

The thermal analysis is performed to demonstrate that the temperature of the DIDO fuel is maintained within acceptable limits. A conservative temperature of 400°F is established as the maximum allowable DIDO fuel cladding temperature for normal conditions of transport. The aluminum retains it capability to function as a mechanical component in this temperature range and it is not close to the 1,220°F melting temperature of aluminum (Table 6.4.1, p. 6-60, Marks' Mechanical Handbook for Mechanical Engineers). The material properties presented in MIL-HDBK-5F indicate that 2000 series aluminum retains over 40% of its room temperature yield and ultimate strengths at a long-term temperature of 300°F.

Maximum temperatures for package components with the NAC-LWT configured for DIDO fuel are summarized in Table 3.4-12. The reported temperatures are lower at all locations than the corresponding temperatures for the design basis PWR fuel presented in Table 3.4-2. The DIDO fuel assembly cladding temperatures are maintained below 400°F.

3.4.1.9 Thermal Evaluation for General Atomics IFM

The heat generated from the General Atomics IFM in the Fuel Handling Unit (FHU) is transferred to the basket by thermal conduction and radiation, and is then transferred to the cask inner shell from the basket surface by the same heat transfer modes. The heat is finally transferred through the cask and International Shipping Organization (ISO) container to ambient. The thermal resistance model and thermal analysis of General Atomics IFM consider a single FHU of the fuel. The maximum temperature from the resistor model corresponds to the FHU's stainless steel shell, while the minimum temperature corresponds to the inner surface of the transport cask inner shell. The fuel is actually stored in two FHUs, but the evaluation conservatively considers the total heat load of 13 W to be placed into a container at the center of the cask cavity. The evaluation does not consider the reduction in thermal resistance due to the contact of the FHU with the basket or of the basket with the inner shell of the transport cask. Additional conservatism is included by ignoring heat transfer by radiation across any of the gaps in the system. To ensure that a bounding temperature for the basket is calculated, air properties are used in the analysis for the gas in the cavity. Also, conservatism is included by using the inner shell temperature corresponding to the 1.26 kW condition for the cask body as opposed to 13 W. This analysis, therefore, bounds transport in the cask with and without an ISO container.

A thermal evaluation of the top module is performed by considering a heat load of 13 W in the center of the basket with only one 6.0-inch diameter top module tube. This is conservative because it maximizes the gap between the tube and the cask inner shell. Air is used as the cavity gas as an additional conservatism. The maximum temperature is computed using the resistor analogy.

For concentric cylinders, the thermal resistance (R) for the heat flow through the cylinders is taken from Krieth as:

$$R = \frac{\ln\left(\frac{r_2}{r_1}\right)}{2\pi K L}$$

where:

r_2 = outer radius of cylinder (inch)

r_1 = inner radius of cylinder (inch)

K = thermal conductivity (BTU/hr/in/°F)

The effective resistance from the secondary enclosure can be expressed as to the cask inner shell:

$$R_T = R_1 + R_2 + R_3 + \frac{1}{\frac{1}{R_4} + \frac{1}{R_5}}$$

where:

R_1 = resistor of the outer canister

R_2 = resistor of the gap between outer canister and the basket shell

R_3 = resistor basket shell

R_4 = resistor of the air from the basket shell to inner shell surface (outside of the basket disks)

R_5 = resistor of stainless steel disks supporting the basket shell in series with the air gap between the basket disks and the inner shell

The maximum temperature of the secondary enclosure can be determined by the following equation:

$$T_i = R_t Q + T_{cask}$$

where:

Q = total heat load

T_{cask} = temperature of cask inner shell

The following parameters will be used for this evaluation:

Q = 13 Watts

L = 37.0 inches – length of shortest secondary fuel closure

r_1 = 2.255 inches – minimum inner radius of secondary closure

r_2 = 2.375 inches – minimum outer radius of secondary closure

r_3 = 2.75 inches – inner radius of module fuel cell

r_4 = 3.00 inches – outer radius of module fuel cell

r_5 = 6.688 inches – inner radius of LWT

r_6 = 6.6325 inches – outer radius of the basket disks

K_{ss} = 0.7143 Btu/hr/in/F at 70°F for stainless steel

K_{air} = 0.00161 Btu/hr/in/F at 300°F for air

From Table 3.4-6, the maximum temperature of the LWT inner shell for a 1.26 kW heat load is 214°F, with 100°F ambient temperature with solar insolance. This is used as a bounding temperature for the cask inner shell (T_{cask}) for this evaluation.

$$R_{eff} = \frac{1}{\frac{1}{R_4} + \frac{1}{R_5}} \qquad R_4 = \frac{\ln(6.688/3.0)}{2\pi(0.00161)(37.0-2)}$$

$$R_4 = 2.264$$

$$R_5 = \frac{\ln(6.8125/3.0)}{2\pi(0.7143)(2)} + \frac{\ln(6.688/6.6325)}{2\pi(0.00161)(2)}$$

(Stainless steel disk in series with the air between the basket disk and the inner shell)

$$R_5 = 0.503$$

$$R_{eff} = \frac{1}{\frac{1}{R_4} + \frac{1}{R_5}}$$

$$R_{eff} = 0.412$$

$$R_T = R_1 + R_2 + R_3 + R_{eff}$$

$$R_T = \frac{\ln(2.375/2.255)}{2\pi(0.7143)(37.0)} + \frac{\ln(2.75/2.375)}{2\pi(0.00161)(37.0)} + \frac{\ln(3.0/2.75)}{2\pi(0.7143)(37.0)} + 0.412$$

$$R_T = 0.0003 + 0.392 + 0.0005 + .412 = 0.805$$

The maximum temperature of the secondary enclosure (T_i) is:

$$T_i = 0.805(13 \times 3.415) + 214 = 250^\circ F$$

The maximum temperature of the basket is conservatively considered to be the same as the temperature of the secondary enclosure (250°F). Temperatures of individual components are summarized in Table 3.4-13.

The maximum content temperature for the GA IFM shipment is considered to be bounded by the TRIGA maximum fuel cladding temperature of 326°F contained in Table 3.4-8, which corresponds to a bounding heat load of 1.05 kW (as compared to the approximately 13 watts for the GA IFM).

A conservative temperature of 800°F is established as the maximum allowable temperature for the stainless steel basket and the contents, which is comprised of the steel-clad TRIGA fuel and the HTGR pellets. The steel cladding of the TRIGA fuel is actually an inconel alloy. Mil HDBK-5G (1 November 1994), Section 6.3.2, identifies that alloys of inconel are used for parts

requiring strength for temperatures exceeding 1,000°F, which significantly exceeds 800°F. The HTGR pellets were designed for operational exposure to reactor core temperatures exceeding 1,000°F, which also exceeds 800°F. Therefore, the maximum temperatures for the contents for the GA IFM are acceptable.

3.4.1.10 High Burnup PWR or BWR Fuel Rods in a Fuel Assembly Lattice

The NAC-LWT cask may transport up to 25 intact high burnup PWR or BWR fuel rods that are in a fuel assembly lattice. The decay heat for the PWR rods is 2.3 kW with a corresponding peaking factor of 1.1, and the decay heat for the BWR rods is 2.1 kW with a corresponding peaking factor of 1.22.

The thermal evaluation employs two-dimensional planar half-symmetry models of the fuel lattice with 25 fuel rods, fuel channel (for BWR fuel), PWR insert (for BWR fuel), fuel basket, and the gas inside the cask cavity. The model extends to the inner surface of the cask inner shell. The model for a 7 × 7 BWR fuel lattice with 25 fuel rods is shown in Figure 3.4-16. BWR arrays of 7 × 7, 8 × 8, 9 × 9, and 10 × 10 are analyzed. PWR arrays of 14 × 14, 15 × 15, 16 × 16, and 7 × 17 are analyzed. The BWR model includes a fuel channel and insert, which are absent from the PWR model.

To determine the worst-case fuel rod arrangement, the 25 fuel rods are analyzed in five different arrangements:

1. Centered (top and bottom) in the two-dimensional model (as shown in Figure 3.4-16).
2. Centered horizontally and concentrated at the bottom of the lattice cross-section.
3. Spread out horizontally and concentrated at the bottom of the lattice cross-section.
4. Centered horizontally and concentrated at the top of the lattice cross-section.
5. Spread out horizontally and concentrated at the top of the lattice cross-section.

For the even numbered fuel arrays (i.e., 8 × 8, 10 × 10, 14 × 14, and 16 × 16), only 24 fuel rods are modeled due to the use of the half-symmetry models. For these cases, a higher heat generation rate is applied at each fuel rod so that the total heat load of 2.3 kW for PWR and 2.1 kW for BWR is maintained. The empty fuel rod locations in the lattice are modeled as air. The maximum inner shell temperature (274°F) for the PWR design basis fuel with 2.5 kW heat load (Table 3.4-2) is applied to the boundary of the model.

For each fuel array and fuel rod location configuration, a steady-state thermal analysis is performed using the general purpose ANSYS computer code. The Condition 2 transport case, with the NAC-LWT not located in an ISO container is evaluated. As shown in Table 3.4-10, this

results in higher maximum temperatures for the fuel cladding than transport Condition 1 where the cask is assumed to be inside of the ISO container. Transport Conditions 1 and 2 are described in Section 3.4.1.3.

3.4.1.11 High Burnup PWR and BWR Fuel Rods in a Rod Holder with Damaged Fuel Rods

The NAC-LWT may transport up to 25 PWR or BWR high burnup fuel rods in a rod holder, with up to 14 of the fuel rods classified as damaged. The maximum decay heat for these configurations is 2.3 kW for PWR and 2.1 kW for BWR. The finite element model for the evaluation of the 25 intact fuel rods in a rod holder is described in Section 3.4.1.7. This section provides the thermal evaluation for the configuration containing damaged fuel rods. The analysis conservatively assumes 15 damaged fuel rods, with the remainder of the rod holder containing intact fuel. The model used for this analysis is based on the two-dimensional half-symmetry model described in Section 3.4.1.7 (Condition 2 configuration), as shown in Figure 3.4-12. Modifications were made to the fuel regions to simulate the damaged fuel rods.

The basket design for the high burnup fuel rod transport can accommodate two configurations: a 4×4 matrix of fuel tubes containing 16 rods and a 5×5 matrix of fuel tubes containing 25 rods. Since the decay heat per rod is considered the same, the maximum heat load occurs with the 5×5 matrix and is the configuration evaluated. Thermal analysis is performed for three cases with different locations of the 15 damaged fuel rods. The fuel rod locations are shown in Figure 3.4-17, which shows the matrix region of the thermal model shown in Figure 3.4-12. The nine locations in the half-symmetry model correspond to 15 actual fuel rod locations. The three cases evaluated are:

Case 1: Damaged fuel rods in locations 4 through 12
Case 2: Damaged fuel rods in locations 7 through 15
Case 3: Damaged fuel rods in locations 1 through 9

The inner surface of the inner shell is the boundary of the model. From Table 3.4-2, the maximum inner shell temperature of 274°F for PWR design basis fuel with 2.5 kW heat load for normal transport conditions is applied to the boundary of the model. The maximum temperature of 274°F results from the condition of solar insolation and convection/radiation to surroundings.

To simulate the damaged fuel rods, a 50% compaction of the fuel material in the fuel tubes is considered. It is assumed that the interior region of the fuel rod tube consists of 50% fuel debris and 50% gas. One half of the heat generation rate for the intact fuel rod is conservatively applied to the entire interior region of the fuel rod tube. Since the volume of the interior of the fuel rod

tube is four times that of the volume of an intact fuel rod, the applied heat load for the damaged fuel is two times that of the heat load for an intact fuel rod. In addition, the heat generation rate is multiplied by a peaking factor of 1.22. The material properties in the entire interior of the fuel rod tubes for the damaged fuel are conservatively considered to be the thermal properties of the fuel (rather than 50% fuel and 50% gas), since this results in higher temperatures in the fuel rod tube walls and the surrounding components.

3.4.1.12 Thermal Evaluation for TPBARs

Heat transfer analysis of the NAC-LWT containing TPBARs is performed using a two-dimensional planar finite element analysis and the general purpose ANSYS computer code. The NAC-LWT is transported in an ISO container with solar insolance on the surface of the ISO container during normal conditions of transport. The gas inside the ISO container is air. The cavity of the NAC-LWT is backfilled with helium as required by operational procedures.

There are two TPBAR content conditions requested for certification: the first is for the transport of up to 300 production TPBARs (of which two can be prefailed) in an open consolidation canister; the second is for the transport of up to 55 segmented TPBARs in a welded closed waste container. The 55 segmented TPBARs and debris resulting from PIE are limited to a total heat load of 127 W, based on a minimum of 90 days of cooling (2.31 watts/rod). Therefore, the loaded TPBAR consolidation canister with 300 rods is considered the bounding content condition for this thermal evaluation with each TPBAR limited to a heat load of 2.31 W, which corresponds to a 90-day cooling period (see Appendix 1-C of Chapter 1). This limits the maximum heat load of the NAC-LWT with TPBAR contents to 0.693 kW. The 0.693 kW total heat load is enveloped by the 1.05 kW total heat load for the NAC-LWT TRIGA fuel contents as described in Section 3.4.1.6. Since the NAC-LWT cask ambient conditions are the same for the TPBAR contents as for the TRIGA fuel contents, the maximum temperature of all cask body components for the TPBAR contents are enveloped by the maximum temperatures for the TRIGA fuel contents. Therefore, the cask inner shell temperature of 222°F (Table 3.4-9) for the TRIGA fuel contents bounds the cask inner shell temperature for the TPBAR contents and is used as the bounding condition for the TPBAR thermal evaluation.

The evaluation of the maximum component temperatures for TPBARs is performed using a finite element model as shown in Figure 3.4-18. This model corresponds to the aluminum basket, the consolidation canister containing 300 TPBARs, and the helium inside the cask. The loaded TPBAR consolidation canister bounds the maximum decay heat of the TPBAR waste container containing 55 segmented TPBARs and, therefore, the thermal evaluation bounds all TPBAR content conditions.

Any axial conductance of the contents is conservatively neglected in this two dimensional planar model. The ANSYS PLANE55 and MATRIX50 elements are used. Radiation is considered using radiation matrix elements while convection is conservatively ignored in the following regions.

- Between the outer surfaces of TPBARs.
- Between the inner surface of the consolidation canister and the adjacent TPBARs.
- Between the outer surface of the consolidation canister and the inner surface of the basket.
- Between the outer surface of the basket and the inner surface of the cask inner shell.

A constant temperature of 222°F (Table 3.4-9, Condition 1) was applied to the outer surface of the model, which corresponds to the inner surface of the cask inner shell. During transport, the NAC-LWT is in a horizontal position in which the TPBAR contents are in contact with the inner surface of the basket, while the basket plates are in contact with the inner shell of the cask.

The heat generated by the 300 TPBARs is applied via a heat generation rate to the stainless steel cladding of the TPBARs. A peaking factor of 1.15 is used in the heat generation rate calculation based on a heat load of 2.31 W for each TPBAR.

The thermal analysis demonstrates that the temperature of the TPBARs is maintained within a conservative limit of 300°F for normal conditions of transport. At 300°F, the aluminum retains its capability as a mechanical component.

Maximum component temperatures for the NAC-LWT containing TPBAR contents are summarized in Table 3.4-16. Maximum cask component temperatures for normal conditions are conservatively obtained from the analysis results corresponding to the TRIGA fuel contents, as shown in Table 3.4-9 (Condition 1).

3.4.1.13 PULSTAR Fuel Elements in 28 MTR Basket

Three loading patterns for PULSTAR fuel elements are postulated for the 28 MTR basket configuration.

- Intact fuel assemblies will be directly loaded into 28 MTR basket;
- Intact fuel elements (rods) will be loaded in the fuel rod insert or the PULSTAR cans;
- Damaged fuel elements (rods) or debris will be loaded in the PULSTAR cans.

The heat load in each basket cell is limited to 30 watts. This corresponds to a maximum heat load of 210 watts for each of the four basket modules. The cask cavity is back-filled with helium.

The thermal analysis for the PULSTAR fuel contents in the 28 MTR basket is bounded by the thermal analysis for the TRIGA fuel cluster rods as presented in Section 3.4.1.6. The MTR basket (Section 3.4.1.3) has the same cross-sectional dimensions and basket material as the basket for TRIGA fuel cluster rods. The maximum modular heat load for TRIGA fuel cluster rods is identical to the maximum modular heat load of the PULSTAR fuel contents (210 watts). The bounding condition for the thermal evaluation for the TRIGA fuel cluster rods is "Condition 2" as described in Section 3.4.1.6.2. In the two-dimensional planar model for the TRIGA fuel cluster, the cask cavity is modeled as air. The model conservatively includes an air gap between the fuel cladding and the aluminum tube and between fuel tube assembly and the inner surface of the basket cell, as shown in Figure 3.4-8 and Figure 3.4-9. This is conservative since there is contact between these components, which provides a significant heat transfer path from the fuel to the basket. Note that the aluminum tubes have an insignificant effect on heat transfer, since the air gap controls the heat conduction in the in-plane direction and the model is a two-dimensional planar model, which neglects any heat transfer in axial direction. Since the PULSTAR fuel rod insert is identical to the TRIGA rod insert, the thermal analysis results for TRIGA fuel cluster rods, Condition 2, as presented in Table 3.4-9, are used as the temperature results for the PULSTAR fuel. These temperatures are summarized in Table 3.4-17 for the PULSTAR fuel. The cask body component maximum temperatures with the NAC-LWT configured for the PULSTAR fuel conservatively use the temperatures from Condition 1 and Condition 2 in Table 3.4-17. The maximum temperatures for the cask body and basket are 222°F and 278°F, respectively, which are significantly below the allowable for stainless steel. For the configuration with intact rods or failed rods loaded in a PULSTAR can, the maximum fuel cladding temperature from Table 3.4-17 is conservatively used as the maximum temperature of the fuel can. The maximum fuel cladding temperature is 295°F, which is significantly below the allowable temperature limit of 1,058°F during transport.

3.4.1.14 Thermal Evaluation for ANSTO Fuel

Two types of ANSTO fuel may be loaded in the ANSTO basket in the NAC-LWT cask:

- MOATA plate fuel elements
- Mark III spiral fuel elements

The ANSTO basket consists of six modules with seven fuel tubes in each module. Each fuel tube may be loaded with a MOATA plate bundle or a Mark III spiral fuel assembly. The maximum heat load for a MOATA plate bundle is 0.4 watt (3 watts per assembly is conservatively considered in the thermal evaluation in this section). The maximum heat load is

18 watts per assembly for the Mark III spiral fuel. The corresponding maximum heat load per cask is 0.126 kW for the MOATA plate bundles and 0.756 kW for the Mark III spiral fuel.

The NAC-LWT is supported in an ISO container with solar insolance applied on the surface of the ISO container. The gas inside the ISO container is air. The cavity of the NAC-LWT is actually backfilled with helium as required by operational procedures.

The thermal evaluation for the MOATA plate fuel elements and Mark III spiral fuel is performed using finite element analysis with the ANSYS program. The finite element models for the MOATA plate bundles and Mark III spiral fuel are shown in Figure 3.4-19 and Figure 3.4-20, respectively. Each model corresponds to a quarter-symmetry cross-section of the fuel, the basket and the helium inside the cask cavity. The models are constructed using ANSYS PLANE55 two-dimensional planar elements. The maximum cask inner shell temperature of 222°F for the LWT cask loaded with the TRIGA fuel cluster rods (see Table 3.4-9) is conservatively used as the boundary condition for both models. The heat load used in the evaluation of the TRIGA fuel cluster rods is 1.05 kW per cask (see Section 3.4.1.6), which is significantly higher than the heat load for the MOATA fuel and Mark III spiral fuel. The MOATA plate fuel elements are explicitly modeled with aluminum cladding on both sides of the fuel meat. A volumetric heat generation rate corresponding to 3 watts per assembly is applied to the elements for fuel meat for the MOATA plate fuel.

The MARK III spiral fuel assemblies are modeled as straight plates with effective orthotropic properties. The longitudinal (radial) properties are decreased to reflect the reduction of the length (from the actual curved plates to the straight plates in the model). The material properties for the fuel meat are conservatively used in the transverse (circumferential) direction of the fuel elements in the model (conductivity of the aluminum clad is higher than that for the fuel meat). A volumetric heat generation rate corresponding to 18 watts per assembly is applied to the fuel elements for the Mark III spiral fuel.

The thermal conductivities of the fuel matrix for MTR fuel from Section 3.4.1.3 are used as the conductivities for the fuel meat for the MOATA plate and MARK III spiral fuel elements in the thermal models. These thermal conductivities are conservative since the fuel meat for the MOATA plate fuel and Mark III spiral fuel is composed of uranium and aluminum alloy, which are significantly more conductive than the fuel matrix material for the MTR fuel. Radiation between the basket tube and the cask inner shell is conservatively not considered in the models. For the MOATA fuel, radiation is only considered between fuel plates. For the Mark III spiral fuel, radiation is modeled across the helium gap between the fuel outer tube and the basket tube.

Steady-state thermal analysis is performed to demonstrate that the temperature of the MOATA plate fuel and Mark III spiral fuel is maintained within acceptable limits. A conservative temperature of 400°F is established as the maximum allowable temperature for these aluminum-clad fuel elements, as discussed in Section 3.4.1.3.3 for the MTR fuel.

3.4.2 Maximum Temperatures

Using the models described, temperatures for the cask body and fuel rod cladding are determined for maximum normal operation conditions (2.5 kW decay heat load, 130°F ambient temperature, still air, full insolation). The maximum cask component and fuel rod cladding temperatures for PWR fuel (2.5 kW) are listed in Table 3.4-2. Not all of the cask components are explicitly modeled; their temperatures are obtained by evaluating the analytical model at the component location. Maximum normal operating temperatures for the 1.26 kW MTR fuel and the 1.05 kW TRIGA fuel configurations are shown in Table 3.4-6 and Table 3.4-8, respectively. Maximum normal operating temperatures for high burnup PWR and BWR fuel rods in a rod holder are shown in Table 3.4-10. The maximum component temperatures for DIDO fuel and General Atomics IFM for normal conditions of transport are shown in Table 3.4-12 and Table 3.4-13, respectively. The maximum component temperatures for 25 high burnup PWR and BWR fuel rods in a fuel assembly lattice are shown in Table 3.4-14. The maximum component temperatures for high burnup PWR or BWR fuel with up to 14 damaged fuel rods in a rod holder are shown in Table 3.4-15. Maximum operating component temperatures for the NAC-LWT containing TPBARs are shown in Table 3.4-16. The maximum operating temperatures for the PULSTAR fuel contents in the MTR basket are shown in Table 3.4-17. The maximum component temperatures for the NAC-LWT containing MOATA plate fuel and Mark III spiral fuel are presented in Table 3.4-22.

3.4.3 Minimum Temperatures

As stated in Section 3.4.1, the minimum temperatures in the cask occur with a 0.0 kW decay heat load and the minimum ambient conditions. Under these conditions, a uniform temperature of -40°F will exist in the cask. The maximum thermal stresses in the cask, during normal operations conditions, occur when the design basis decay heat load of 2.5 kW exists in the cask along with the minimum ambient conditions (-40°F ambient temperature and no insolance). The cask component and fuel rod clad temperatures for the 2.5 kW decay heat load with minimum ambient conditions are listed in Table 3.4-3.

3.4.4 Maximum Internal Pressures

3.4.4.1 Maximum Internal Pressure for Design Basis Fuel in Normal Conditions

The NAC-LWT cask is filled to one atmosphere (14.7 psia) upon loading. It is necessary to evaluate the internal pressure of the cask after thermal equilibrium has been attained. Assuming a maximum normal fuel cladding temperature of 472°F (932°R) from Table 3.4-2, 3 percent fuel rods rupture, and 30 percent of the fission gas and 100 percent of the rod backfill gas escape from the ruptured fuel rods, the cask internal pressure is calculated. Table 3.4-4 reports the fission gas inventories for the design basis PWR fuel assembly. Table 5.1-2 reports the design parameters of the design basis PWR fuel. Using information from Table 5.1-2, the void volume of a single fuel rod is calculated as 2.43 in^3 (39.82 cm^3) by subtracting the volume of the fuel pellets from the volume of an empty fuel rod (the plenum spring volume is disregarded). The total fuel assembly void volume is calculated as 495.16 in^3 (8,123.28 cm^3) by multiplying the single fuel rod volume by 204, the number of fuel rods in the fuel assembly. The total fuel assembly void volume, the fission gas inventory information in Table 3.4-4, and the maximum normal transport temperature (472°F) are applied to the ideal gas law (PV = nRT) to obtain the pressure in the unruptured fuel rods due to the fission gases. This fission gas pressure, 1,771.5 psia, is also reported in Table 3.4-4, based on 100% availability of fission gases, later adjusted to 30%. The releasable fission gas pressure and rod backfill pressure (assumed 565 psia) are summed to obtain the total fuel rod pressure.

The cask pressure is obtained using Dalton's Law of Partial Pressures:

$$P = P_A + P_B$$

where:

P = total pressure

P_A = partial pressure of gas A (cask cavity helium gas backfill)

P_B = partial pressure of gas B (fuel rod backfill and fission gas)

The reported cask and fuel rod backfill pressures are at standard temperature (72°F) and must be corrected to the normal transport temperature. Given that the internal volumes of the NAC-LWT Cask and the fuel rods remain constant, the resultant pressure is proportional to the temperature change according to the ideal gas law:

$$P_2 = P_1\left(\frac{T_2}{T_1}\right)$$

where:

P_1 = 14.7 psia (cask backfill pressure)

T_1 = 72°F (532°R) (cask backfill temperature)

T_2 = 472°F (932°R) (maximum normal operating condition cavity gas temperature)

Thus, the cask backfill pressure at normal operating temperature equals:

$$P_2 = 14.7\ \text{psia}\left(\frac{932°R}{532°R}\right)$$

$$P_2 = 25.8\ \text{psia}$$

For the fuel rod backfill pressure at normal operating temperature:

P_1 = 565 psia (fuel rod backfill pressure)

T_1 = 72°F (532°R) (fuel rod backfill temperature)

T_2 = 472°F (932°R) (maximum normal operating condition cavity gas temperature)

and:

$$P_2 = 565\ \text{psia}\left(\frac{932°R}{532°R}\right)$$

$$P_2 = 989.8\ \text{psia}$$

The partial pressure of the cask backfill distributed over the cask free volume (including 3% failed rods) is calculated by:

$$P_{\text{cask backfill}} = P_{\text{initial}}\left(\frac{V_{\text{cask}}}{V_{\text{total}}}\right)$$

where:

$P_{initial}$ = 25.8 psia (temperature adjusted cask backfill pressure)

V_{cask} = 5.196 ft^3 (147,134 cm^3)

$V_{rod\ void}$ = 244 cm^3 (volume of 3% failed fuel rods)

V_{total} = V_{cask} + $V_{rod\ void}$

V_{total} = 147,378 cm^3

Thus, the cask backfill partial pressure at normal operating temperature, including the volume of failed fuel rods equals:

$$P_{cask\ backfill} = 25.8\ psia\left(\frac{147{,}134 cm^3}{147{,}378 cm^3}\right)$$

$$P_{cask\ backfill} = 25.8\ psia$$

The partial pressure of the failed fuel rod gases in the cask cavity is calculated by:

$$P_{fuelrods} = P_{initial}\left(\frac{V_{rodvoid}}{V_{total}}\right)$$

where:

$P_{initial}$ = 1,521.3 psia (fission gas pressure (0.30 x 1,771.5 psia) plus rod backfill pressure (989.8 psia))

$V_{rod\ void}$ = 244 cm^3

V_{total} = 147,378 cm^3

Thus, the failed fuel rod partial pressure at normal operating temperature, including fission gases and the volume of cask cavity void equals:

$$P_{fuelrods} = 1{,}521.3\ psia\left(\frac{243.7 cm^3}{147{,}378 cm^3}\right)$$

$$P_{fuelrods} = 2.5\ psia$$

Summing the two partial pressures yields the total cask pressure.

$$P_{Total} = P_{cask\ backfill} + P_{fuelrods}$$

$$P_{Total} = 25.8\ psia + 2.5\ psia$$

$$P_{Total} = 28.3\ psia$$

3.4.4.2 High Burnup Fuel Rod Canister Maximum Normal Conditions Internal Pressure

The high burnup fuel sealed canister is filled to one atmosphere (14.7 psia) upon loading. The canister internal pressure is calculated assuming that the average helium backfill gas temperature is 600°F (1060 R) and that 3 percent of the fuel rods fail in normal conditions of transport. The temperature of the canister gas is selected to conservatively bound the temperatures given in Table 3.4-10, Table 3.4-14 and Table 3.4-15. On failure, the fuel rods are assumed to release 30% of the fission gas and 100% of the rod backfill gas. To bound both the PWR and BWR analysis, the fuel type with the highest fission source, on a per rod basis, and smallest free gas volume inside the sealed canister is selected. This fuel type is the Exxon 7 × 7 BWR fuel. The fission gas inventory for this fuel is shown in Table 3.4-11, which reports the fission gas inventory for the assembly, and on a per rod basis. The design parameters for the Exxon 7 × 7 fuel rod are:

Parameter	Value
Number of Rods	49
Rod Diameter (in)	0.570
Clad Thickness (in)	0.036
Pellet Diameter (in)	0.4900
Active Fuel Length (in)	150
Rod Length (in)	170

From the values shown, the void volume of a single fuel rod is calculated as 4.82 in^3 (78.99 cm^3) by subtracting the volume of the fuel pellets from the volume of an empty fuel rod (the plenum spring volume is disregarded). For the analysis, 3% of 25 rods is taken to fail, which is 0.75 rods. Conservatively, the number of failed rods is defined as one, which is equal to a 4% fuel rod failure. The equivalent void volume is then equal to one rod, or 4.82 in^3. The fission gas inventory, provided in Table 3.4-11, and the maximum normal transport temperature (600°F) are applied to the ideal gas law (PV = nRT) to obtain the pressure in the unruptured fuel rods due to the fission gases. This fission gas pressure, 4,251 psia (Table 3.4-11), is based on 100% availability of fission gases, which is adjusted to account for the 30 percent release of the fission gas. The releasable fission gas and rod backfill pressures are summed to obtain the total fuel rod pressure.

The ideal gas law is used to analyze the effects of pressure, temperature, volume, and gas inside the cask the ideal gas law states:

$$pV = nRT$$

where:

p = pressure (atm)
V = volume (liters)
n = gram-moles of material
R = gas constant (0.0831 atm-liters/K g-mole)
T = temperature (K)

After the rods rupture, the resultant internal cask pressure is impacted by three sources: the 1-atm inert gas backfill of the canister, the fission product gas escaping from the fuel rods, and the fuel rod inert gas backfill escaping from the ruptured fuel rods. To calculate the resultant internal cask pressure after the fuel rods rupture, partial pressures are calculated using Dalton's law:

$$P = P_a + P_b$$

where:

P = total pressure

P_a = partial pressure of gas A

P_b = partial pressure of gas B

The void volume of the fuel rod is simply the volume contained within the cladding less the fuel volume. The rod is modeled as a cylinder with a 0.570-in outside diameter, a 0.036-in. wall thickness, and a 150-in. active fuel length. The volume of the plenum spring is disregarded. The void volume, which includes the plenum volume, is 4.82 in^3 per rod.

The partial pressure of the canister is calculated by:

$$P_{canister} = P_{initial}\left(\frac{V_{canister}}{V_{total}}\right)$$

where:

$$P_{initial} = P_{atm} * \frac{T_{norm}}{T_{stand}} = 14.7 \text{ psia} * \frac{588.7 \text{ K}}{295.35 \text{ K}} = 29.3 \text{ psia}$$

$P_{initial}$ = 29.3 psia

The minimum free gas volume is calculated as:

$$V_{canister} = 2{,}800\,in^3 - \pi * r_{OD}^2 * L_{rod} * 25\ rods = 2{,}800\,in^3 - \pi * \left(\frac{0.57\,in}{2}\right)^2 * 170\,in. * 25\ rods$$

$$= 2{,}800\,in^3 - 1085\,in^3 = 1715\,in^3$$

$$V_{canister} = 28.1\ liters$$

$$V_{void} = 4.82\,in^3 * (2.54\,cm/in)^3 * 0.001\,liters/cc = 0.079\ liters$$

$$V_{total} = V_{canister} + 25 * 0.04 * V_{void} = 28.1\ liters + 0.04 * 25 * 0.079 = \sim 28.2\ liters$$

$$V_{total} = \sim 28.2\ liters$$

This results in a $P_{canister}$ of 29.3 psia.

Fission product gas inventories were obtained from Table 3.4-11. Using the ideal gas law, the initial pressure of each fission product gas is calculated based upon these inventories, the normal condition temperature (600°F), and the calculated void volume of the fuel (25 rods). The partial pressure of the fuel rod volume is calculated by:

$$P_{fuel\ rods} = P_{initial}\left(\frac{V_{fuel\ rods}}{V_{total}}\right)$$

where:

$$P_{initial} = 0.3 * P_{fission} + P_{backfill}$$

$$P_{fission} = 4251\ psia$$

$$P_{backfill} = P_{initial}^{backfill} * \frac{T_{norm}}{T_{stand}} = 75\ psia * \frac{588.7\,K}{295.35\,K} = 150\ psia$$

$$P_{initial} = \sim 1{,}425\ psia$$

$V_{fuel\ rods}$ = ~0.079 liter (at 4% of the total fuel rod volume)

V_{total} = 28.2 liters = $V_{canister} + 25*0.04(V_{void})$

$$P_{fuel\ rods} = 1425\ psia\left(\frac{0.079\ liter}{28.2\ liters}\right) = \sim 4.00\ psia$$

then:

$$P_{total} = P_{canister} + P_{fuel\ rods} = 29.3\ psia + \sim 4.00\ psia = \sim 33.3\ psia\ (2.3\ atm)$$

An additional analysis was performed for BWR high burnup rods (>45 GWd/MTU) with a 56% failure fraction to envelope damaged fuel rod shipments. This evaluation is conservative since damaged rods are likely to have released their gas inventory prior to shipment.

Following the methodology used for calculating the pressure given above and the calculated canister free gas volume of 29.2 liters, the resulting internal canister pressure from a 56% failed fuel fraction is 82.3 psia (~ 5.6 atm). The calculation follows.

$P_{canister} = P_{initial} * V_{canister} / V_{total}$

$P_{initial} = 29.3$ psia

$V_{canister} = 28.1$ liters

$V_{total} = V_{canister} + 14 * V_{void} = (28.1 \text{ liters}) + 14 * (0.079 \text{ liter}) = 29.2$ liters

$P_{canister} = (29.3 \text{ psia}) * (28.1 \text{ liters}) / (29.2 \text{ liters}) = 28.2$ psia

$P_{fuel\ rods} = P_{initial} * V_{fuel\ rods} / V_{total}$

$P_{initial} = 1{,}425$ psia

$V_{fuel\ rods} = 14 * V_{void} = 1.108$ liters

$P_{fuel\ rods} = (1{,}425 \text{ psia}) * (1.108 \text{ liters}) / (29.2 \text{ liters}) = 54.1$ psia

$P_{total} = P_{canister} + P_{fuel\ rods} = 28.2 \text{ psia} + 54.1 \text{ psia} = 82.3 \text{ psia} = 5.6$ atm

3.4.4.3 25-Rod Maximum Cask Cavity Internal Pressure-Normal Conditions

Following the methodology used for calculating pressure in Section 3.4.4.2, the cask free gas volume is calculated as:

$$V_{cask} = 6{,}534 \text{ in}^3 - \pi * r_{OD}^2 * L_{rod} * 25 \text{ rods} = 6{,}534 \text{ in}^3 - \pi * \left(\frac{0.57 \text{ in}}{2}\right)^2 * 170 \text{ in.} * 25 \text{ rods}$$

$$= 6{,}534 \text{ in}^3 - 1{,}085 \text{ in}^3$$

$$= 5{,}449 \text{ in}^3$$

$V_{cask} = 89.32$ liters

Using this free gas volume in place of $V_{canister}$ and the temperatures in Section 3.4.4.2, the cask cavity pressure resulting from a 3% fuel rod failure is 31 psia (~2.1 atm). This pressure is based on the assumption that the gases in the canister are released to the cask cavity. There are no design basis events that could result in the release of the gas in the canister to the cask cavity.

An additional analysis was performed for a bounding 25 BWR high burnup rod configuration (>45 GWd/MTU) containing up to 14 damaged rods. The damaged fuel rods are conservatively assumed to release the rod gas inventory during transport.

Following the methodology used for calculating the pressures given above and the cask free gas volume of 90.4 liters, the resulting internal cask pressure from a 56% failed fuel fraction is 46.4 psia (~ 3.2 atm). The calculation is outlined below.

$P_{cask} = P_{initial}*V_{cask}/V_{total}$

$P_{initial} = 29.3$ psia

$V_{cask} = 89.3$ liters

$V_{total} = V_{cask} + 14*V_{void} = (89.3 \text{ liters}) + 14*(0.079 \text{ liter}) = 90.4$ liters

$P_{cask} = (29.3 \text{ psia})*(89.3 \text{ liters})/(90.4 \text{ liters}) = 28.9$ psia

$P_{fuel\ rods} = P_{initial}*V_{fuel\ rods}/V_{total}$

$P_{initial} = 1{,}425$ psia

$V_{fuel\ rods} = 14*V_{void} = 1.108$ liters

$P_{fuel\ rods} = (1{,}425 \text{ psia})*(1.108 \text{ liters})/(90.4 \text{ liters}) = 17.5$ psia

$P_{total} = P_{cask} + P_{fuel\ rods} = 28.9 \text{ psia} + 17.5 \text{ psia} = 46.4 \text{ psia} = 3.2$ atm

3.4.4.4 Maximum Cask Cavity Internal Pressure for the General Atomics IFM

The combined heat load of the two GA IFM FHUs is 13 watts. This heat load is distributed between two separate canisters, which have a length of approximately 40 inches. As a result, the heat generation, which would result in a temperature differential between the cavity and ambient, is insignificant.

The internal pressure in the LWT cask cavity is due to the fission gas release from the TRIGA fuel or HTGR fuel pellets in conjunction with the cavity being heated by solar insolance. No credit is taken for the pressure retention capability of the FHUs. The internal pressure that may result from the 20 TRIGA fuel rods in the GA IFM is significantly enveloped by that of the 120 TRIGA fuel rods, which are authorized for transport in the NAC-LWT cask. Likewise, the fission gas release by the HTGR elements is considered to be bounded by the current design basis PWR fuel. Since the free volume for the GA IFM shipment is significantly larger than for the design basis PWR fuel assembly with the PWR basket, the pressure increase in the cavity gas due to the GA IFM shipment is considered to be significantly bounded by the design basis condition in the current NAC-LWT cask. Therefore, the current design pressure of 50 psig for the cask cavity envelopes the cask cavity pressure for the GA IFM contents.

3.4.4.5 TPBAR Shipment Cask Cavity Internal Pressure-Normal Conditions

The method employed in the TPBAR (Tritium Producing Burnable Absorber Rod) shipment evaluation is similar to that employed in the fuel rod evaluations where the cask cavity free volume and molar gas quantities are combined with the ideal gas law (PV=nRT) to determine system pressure. The bounding TPBAR content condition consists of up to 300 production TPBARs (of which two can be prefailed) placed in a consolidation canister and loaded into a NAC-LWT with a TPBAR basket installed in the cavity.

A typical TPBAR is composed of a steel clad rod 0.381 inch in diameter, with a maximum length of 154.15 inches, and a minimum internal free volume of 5.727 inch^3. The TPBARs are located in a consolidation canister composed of three primary pieces: canister body, top insert, and bail. A spacer, attached to the NAC-LWT cask lid, assures that rods remain within the canister envelope and provides support to both the basket and canister under end-drop conditions. The TPBAR basket is a modified NAC-LWT PWR basket that increases the cavity free volume from that provided by a standard PWR basket design.

For conservatism in determining the cask internal pressure, the 298 TPBARs that are not prefailed at loading are assumed to undergo cladding failure during normal transport conditions. Prefailed rods have cladding damage that allows reactor coolant or spent fuel pool water to enter the rod cavity. Cladding failure during transport results in the release of the rod helium backfill gas, helium gas generated during the tritium production, and a portion of the tritium gas produced. For rods not prefailed, the majority of the tritium is locked in the TPBAR structure and is not released during normal or accident conditions of cask transport. Tritium release from intact or in-cask prefailed rods is limited to 55 Ci/rod (0.0019 mole – See Chapter 1, Appendix 1-B) versus a helium release of 0.42 mole per rod after the 90-day cool-down period. A conservative tritium release of 100 Ci per rod is applied in this calculation. After the 90-day cool-down period, the helium release increases according to the decay of tritium.

$$^3\mathrm{He}[\mathrm{moles}](t) = 0.398 \times \left(1 - \exp\left(\frac{-\ln(2)t}{12.33}\right)\right)$$

The remaining two rods in the 300 TPBAR shipment are assumed to be prefailed and waterlogged. These rods contain a maximum of 7.5 moles of H_2O and 0.199 moles of T_2O (1.2 grams H_2), 2% of which dissociate into their constituent gases due to elevated temperatures in the cask cavity (see Chapter 1 appendices). The NAC-LWT is vacuum dried prior to transport, removing water from the cask cavity. This process is expected to remove water from the prefailed rod. The water content is conservatively assumed to remain in the rods for the pressure

calculated. After dissociation, the total gaseous inventory in each prefailed TPBAR is 7.78 moles.

Cask cavity gases after rod failure are therefore comprised of the cask helium backfill (one atmosphere at loading); the combined helium rod backfill, helium generated during the tritium production, helium production from tritium decay, and the tritium release itself (298 rods); and the molar inventory of the two prefailed, waterlogged rods. The total free volume available for the gas is the cask cavity volume plus the internal free volume of the failed rods, minus the canister, spacer, basket, and rod volumes.

Description (Based on 300 Rods Failing)	Volume [cm³]
Cavity (Empty)	4.10E+05
TPBAR Rod (Based on Exterior Rod Dimension)	-8.64E+04
TPBAR Minimum Free Interior	2.82E+04
TPBAR Consolidation Canister	-1.40E+04
TPBAR Basket	-8.49E+04
Cask Cavity Spacer	-5.55E+03
Cask Free volume (300 Rods Failed)	2.47E+05

The free volume in the canister cavity for intact rods is 2.19×10^5 cm^3. Applying a conservative volume 2.4×10^5 cm^3 to calculate the cask backfill molar quantity yields 9.98 moles of helium. The backfill conditions at sealing used in the calculation are one atmosphere pressure and a temperature of 68°F. The backfill pressure is specified in the operating procedure, while 68°F is conservative for the cask with a heat-generating payload.

Again employing the ideal gas law with a total 152 moles of gas (298 rods releasing 0.42 moles of helium and 0.003 mole of tritium, two waterlogged rods releasing 7.78 moles each, plus the 10.27 moles cask backfill), a conservative free volume of 2.47×10^5 cm^3, and the normal condition average gas temperature of 246°F, yields an operating pressure of 276 psig at the end of a 90-day cooldown. For a period of one year following the 90-day cooldown and considering a fixed gas temperature of 246°F, the pressure increases to 289 psig (MNOP). System pressure at cool times greater than 90 days will be lower due to the decreased heat loads associated with the radioactive decay of the payload.

The TPBAR content condition of 55 segmented TPBARs contained in a sealed waste container is bounded by the pressure analyses performed for the fully loaded TPBAR consolidation canister. The contents include segments, debris and vented shrouds, all placed in a vented inner storage container within the welded waste container. Due to the condition of the TPBAR segments and

the cooling period since irradiation, the heat load of the waste container is 0.127 kW, significantly less than the 0.693 kW analyzed for the production TPBAR content condition of 300 TPBARs in an open consolidation canister.

Each of the 55 TPBARs is assumed to contain a maximum of 1.2 grams of tritium at the time of sealing the waste container, and all backfill gases have been vented. For the purpose of the maximum pressure analysis, all of the contained tritium is assumed to decay to He^3, resulting in a total of 66 grams of He^3. Note that the confinement boundary of the welded waste container is assumed to fail during normal transport conditions. Due to the state of the TPBAR segments and the loading of the materials in dry loading conditions, no water will be present in the waste container. Conservatively assuming that the cask free volume and gas temperature for the transport of the waste container is the same as that for the production TPBAR contents listed previously (2.47×10^5 cm^3), the calculated maximum normal operating pressure (MNOP) for the 55 segmented TPBARS in the waste container is less than 65 psia. Therefore, the MNOP for the 55 segmented TPBAR content condition is conservatively bounded by the MNOP of the 300 production TPBARs in the consolidation canister of 289 psig.

Combustible Hazard Assessment

Hydrogen may be released by prefailed, waterlogged TPBARs (TPBARs damaged during in-core use or in-pool storage) primarily in the form of water, tritiated water, and potentially some tritiated methane. Each prefailed TPBAR has the potential to release the tritium assumed to dissociate from tritiated water (0.004 moles) as well as up to 0.15 moles hydrogen gas dissociated from 7.5 moles of H_2O. Both the hydrogen and the tritium gas, as well as the water and tritiated water, will be removed from the cask during vacuum drying prior to helium backfill.

The flammability/ignitability characteristics of tritium (T_2) in the presence of oxygen are substantially the same as for hydrogen (H_2). Hydrogen in air reaches a lower flammability limit at 4% volume.

Tritium escapes intact TPBARs in the form of molecular tritium gas at a rate of less than 0.12 mCi/hr/TPBAR. For a one-year transport period and a 300 TPBAR payload this rate results in a release of less than 0.01 moles of T_2 gas. Given a helium gas back-fill of approximately 10 moles helium (1 atmosphere) no flammability hazard exists for intact TPBARs.

Tritium may be released by event-failed (in-cask failed) TPBARs in the form of tritiated methane (CH_4) or tritiated water. Event-failed TPBARs may release up to 55 Ci of tritium. This translates to approximately 0.002 mole of tritium that may be released from a TPBAR in conjunction with 0.42 mole of helium.

The 55 equivalent TPBARs, in segments and debris, may release up to 100% of the tritium contained in the pellets during transport. The pellets contain approximately 40% of the tritium quantity in the TPBAR. At NAC-LWT normal and accident conditions temperatures, the TPBAR components release tritium primarily as tritiated water with only a small fraction (maximum 2%) as gaseous tritium (see Appendix 1-B of Chapter 1). During a one-year transport, an additional maximum 1% of the tritiated water may undergo radiolysis and dissociate. Conservatively applying a maximum 3% release rate to the 55 equivalent TPBAR total inventory of 66 grams (1.2 grams per rod) yields an inventory of 0.33 moles T_2. Based on an inert gas cask backfill in excess of 10.3 moles, a bounding estimated maximum hydrogen (T_2) volume fraction of 3.1% is calculated. Therefore, no flammability hazard will exist for the 55 segmented TPBAR content condition.

3.4.4.6 Maximum Internal Pressure for PULSTAR Fuel Element Payload

Based on the allowable loading configurations for PULSTAR fuel elements, cask internal pressures are calculated for a payload of 28 intact assemblies and a mixed payload of 14 intact assemblies and the equivalent of 14 canned assemblies. A payload of 28 4×4 intact rod inserts is bounded by either of these evaluated payloads.

The ideal gas law and Dalton's law of partial pressures are used to calculate internal pressures. Cask, can, and element backfill initial conditions are taken as a pressure of 1 atm and a temperature of 68°F.

PULSTAR fuel element and fuel assembly dimensions are summarized in Table 3.4-18. Elements are UO_2 pellets clad with zirconium alloy. A PULSTAR fuel assembly is a 5×5 rectangular array of elements with aluminum upper and lower fittings.

Based on the PULSTAR fuel element, PULSTAR failed fuel can, MTR basket stack, and NAC-LWT cavity dimensions, volumes are calculated and summarized in Table 3.4-19.

The remaining two inputs to the pressure calculation are the temperature and fission gas inventory. For conservatism, the average gas temperature applied is the maximum TRIGA fuel clad temperature of 295°F. The TRIGA temperatures are applicable to the PULSTAR fuel element evaluation as discussed in Section 3.4.1.13. The fission gas inventory is taken from the SAS2H results discussed in Chapter 5 and is shown in Table 3.4-20.

For a payload of 28 intact PULSTAR fuel assemblies, the partial pressures of the cask, element (rod) backfill, and fission gases are summed. The cask free volume is 217 liters and is calculated by subtracting the basket stack volume and the assembly envelope volume (multiplied by 28)

from the cavity volume. The partial pressure of the cask, P_{Cask}, is simply the initial backfill pressure multiplied by the temperature ratio:

$$P_{Cask} = 1\,atm \frac{419.26\,K}{293.15\,K} = 1.430\,atm$$

The cask partial pressure due to a 100% release of element backfill, $P_{RodBackfill}$, is the initial backfill pressure multiplied by the temperature ratio and the backfill-to-cask volume ratio:

$$P_{RodBackfill} = 1\,atm \frac{419.26\,K}{293.15\,K} \frac{2.7\,liters}{217.0\,liters} = 0.018\,atm$$

Only 3% of this pressure contributes to the total pressure under normal conditions.

The cask partial pressure due to a 100% release of the element fission gases, $P_{FissionGas}$, is calculated using the Ideal Gas Law:

$$P_{FissionGas} = \frac{28 \cdot 0.448 \cdot 0.08205 \cdot 419.26}{217} = 1.989\,atm$$

Only 30% of the fission gases are released, and only 3% of the resultant pressure contributes to the total pressure under normal conditions.

The total cask pressure is the sum of the partial pressures, adjusted by the relevant release fractions:

$$P_{Total} = P_{Cask} + 0.03 \cdot P_{RodBackfill} + 0.03 \cdot 0.30 \cdot P_{FissionGas}$$

$$P_{Total} = 1.430 + 0.03 \cdot 0.018 + 0.03 \cdot 0.30 \cdot 1.989 = 1.449\,atm$$

Cask internal pressure for a mixed payload is calculated in a similar fashion, with a smaller cask free volume due to the difference in can and assembly envelope volume, and an assumed 100% failure rate of PULSTAR elements in either the screened or sealed can. The calculated maximum cavity pressure is 1.8 atm. Pressure in the sealed can is based on a 100% failure rate, the can cavity volume, and a payload equivalent in volume to 25 intact PULSTAR fuel elements. Normal condition pressure in the sealed can is 4.4 atm.

A summary of the pressure calculations is given in Table 3.4-21.

3.4.5 Maximum Thermal Stresses

The conditions within the range of normal transport conditions and fabrication that result in the limiting combination of thermal gradient and isothermal stresses have been evaluated. The

analyses are performed in Sections 2.5 through 2.7. The resulting isothermal temperature plots are presented in Section 2.10.3.

3.4.6 Evaluation of Package Performance for Normal Conditions of Transport

Section 3.4 provides analyses of the NAC-LWT cask thermal performance for normal transport conditions. The analyses demonstrate that the NAC-LWT cask thermal performance meets the criteria of 10 CFR 71 for normal transport conditions.

The maximum fuel rod cladding temperature under normal transport conditions is 472°F. This is well below the temperatures that can cause fuel rod cladding deterioration. Components important to safety remain within their safe operating ranges (Section 3.3) during normal transport conditions. Thermally induced stresses (in combination with pressure and mechanical load stresses) are less than allowable stresses as shown in Section 2.6. Thus, the analyses of Section 3.4 demonstrate that the NAC-LWT cask fulfills the heat rejection criteria established in Section 3.1 for normal transport conditions.

Figure 3.4-1 HEATING5 Normal Transport Conditions Thermal Model

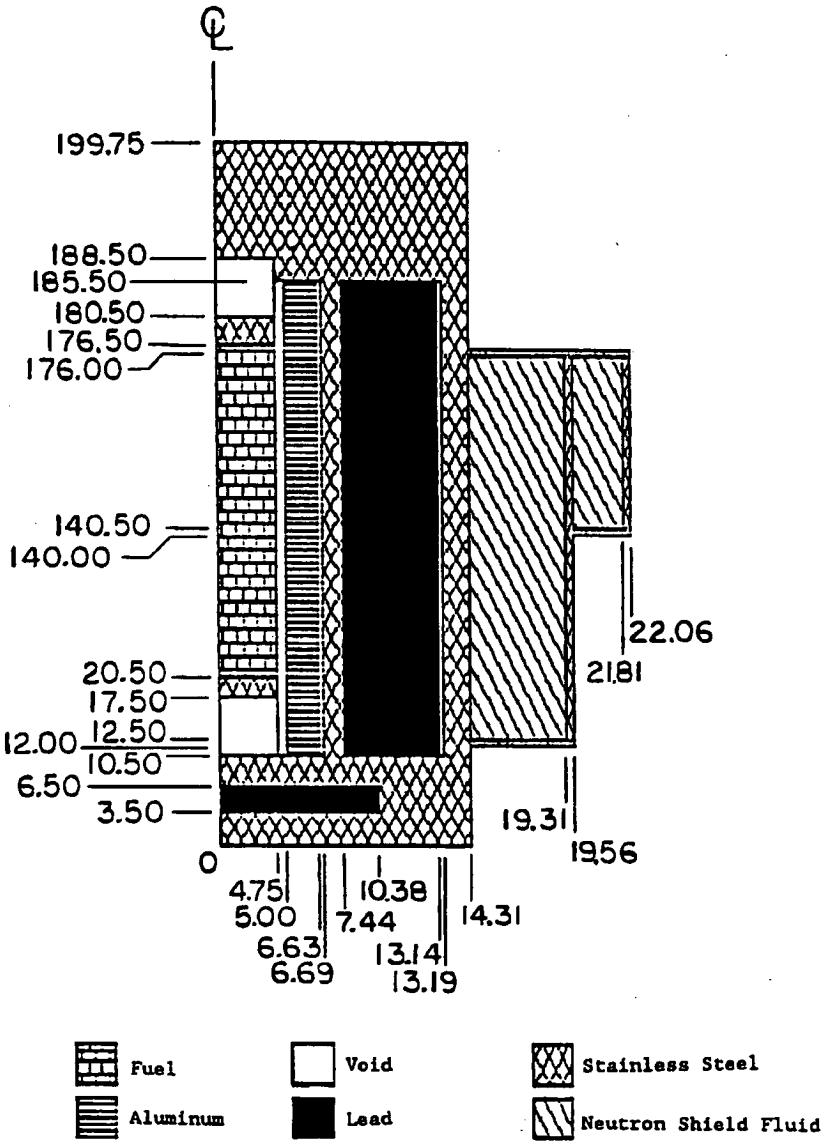

Figure 3.4-2 Design Basis PWR Fuel Assembly Axial Flux Distribution

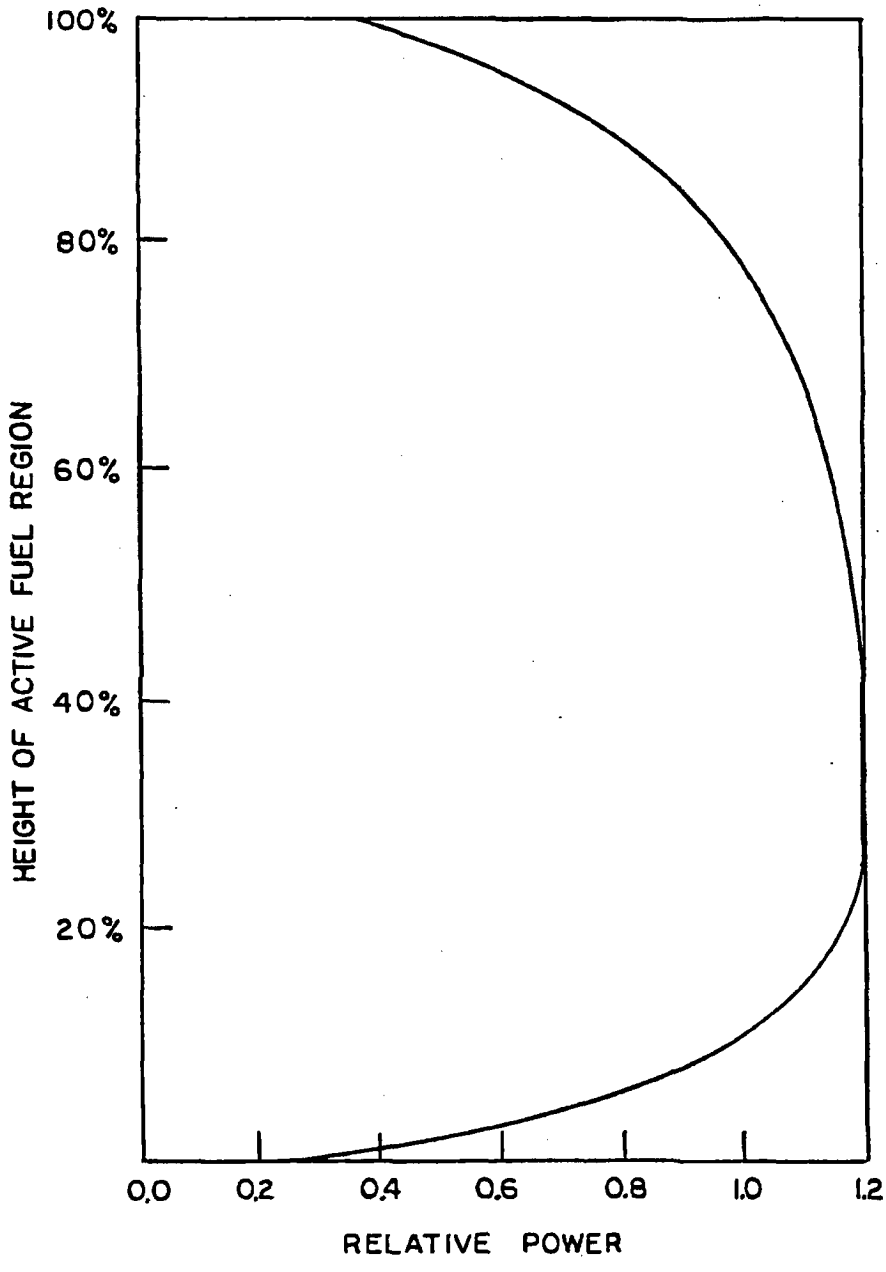

Figure 3.4-3 ANSYS MTR Fuel Design Basis Heat Load Thermal Model (Uniform 30-Watt/Element Configuration Heat Load)

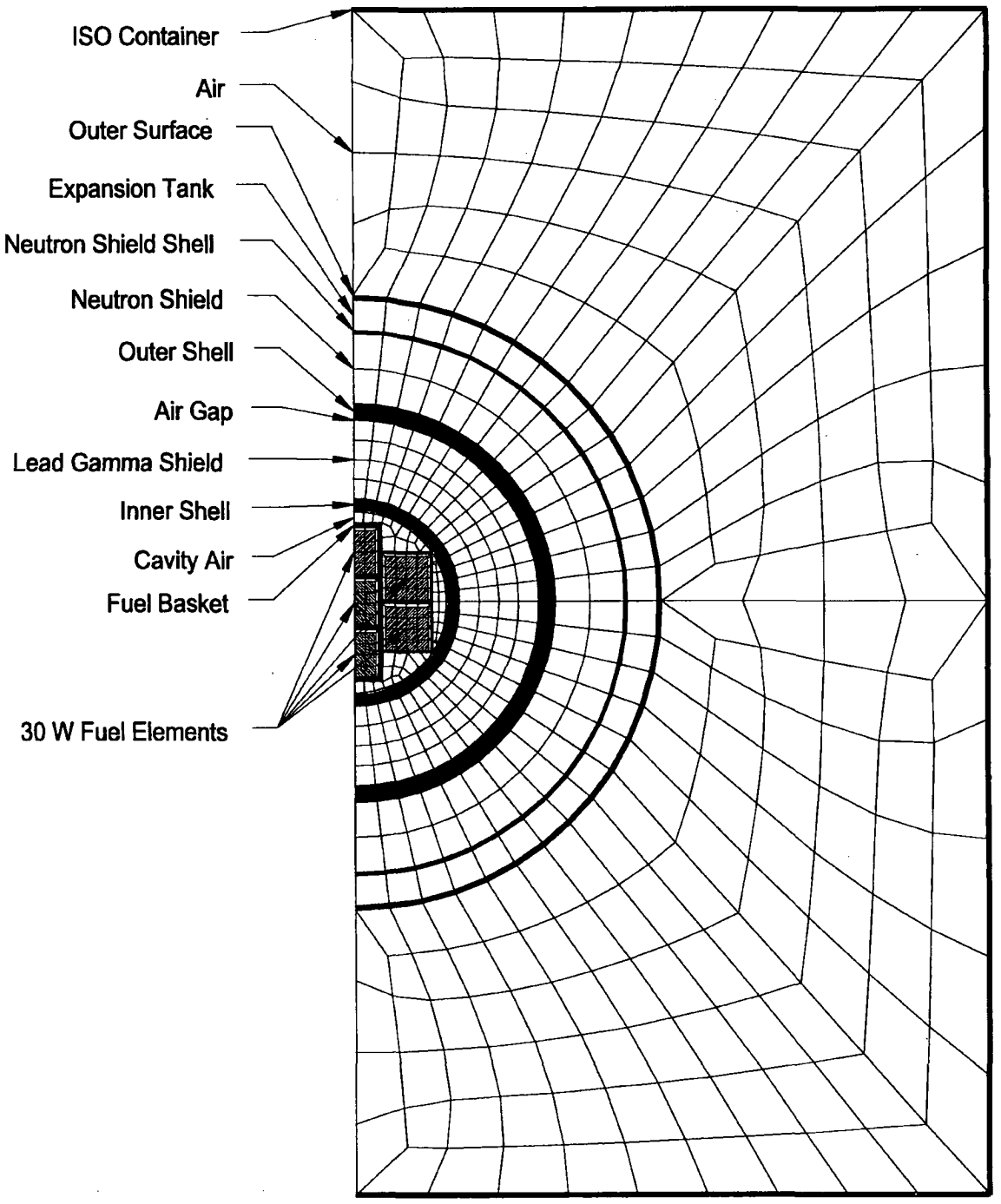

Figure 3.4-4 MTR Fuel Variable Decay Heat ANSYS Thermal Model

(120-Watt / 70-Watt / 20-Watt Configuration Heat Load)

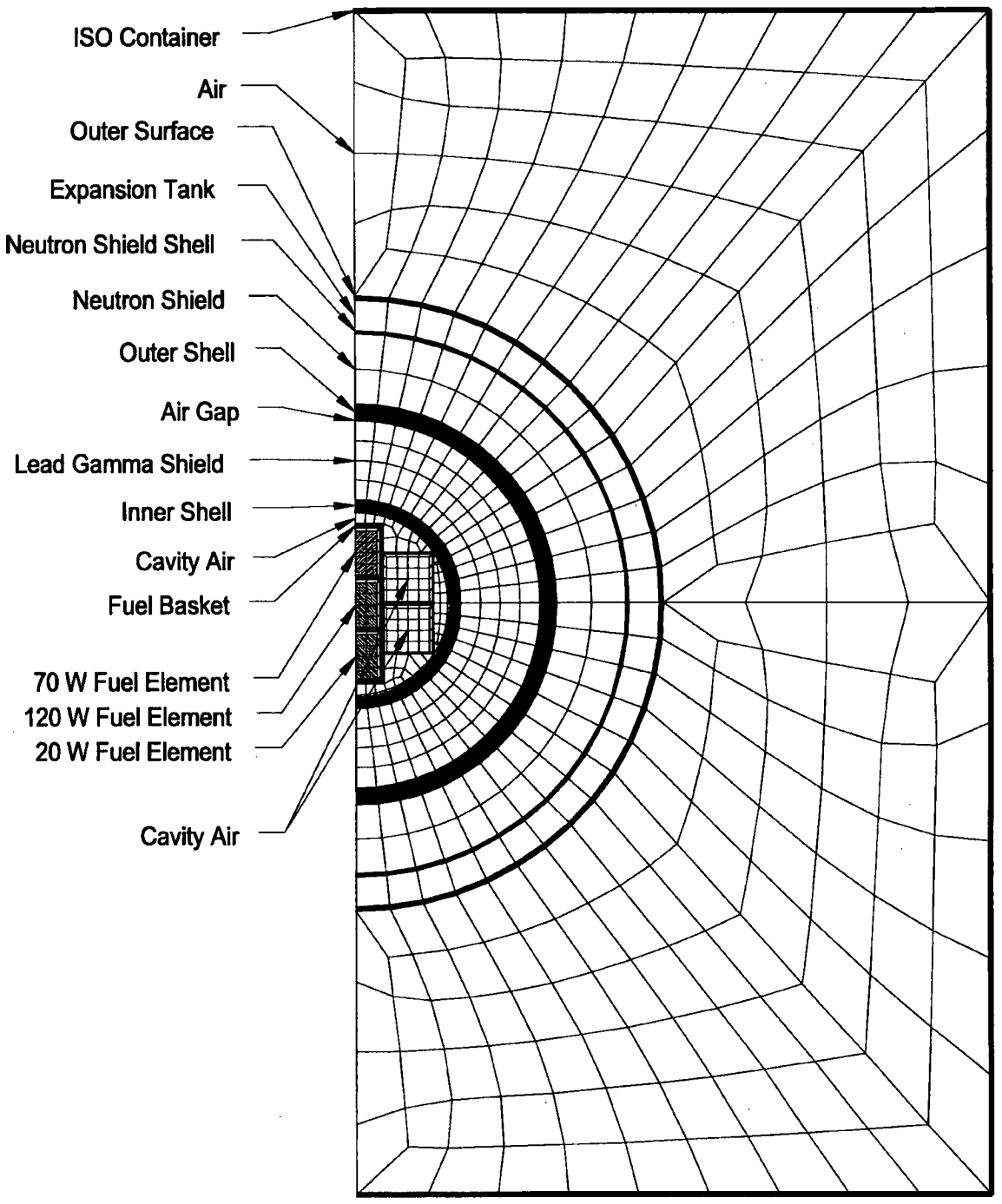

Figure 3.4-5 Thermal Resistance Model for TRIGA Fuel Elements

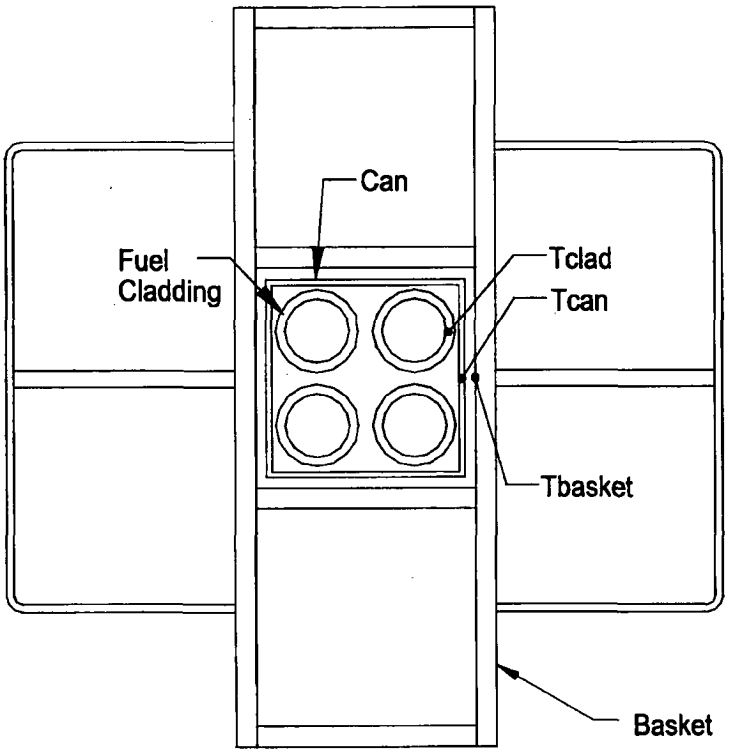

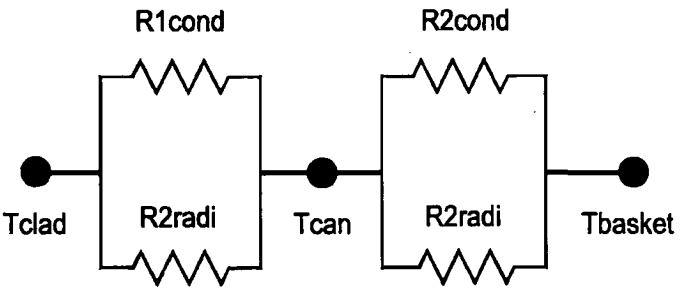

Where:

Rcond = Thermal resistance for conduction

Rradi = Thermal resistance for radiation

Tbasket = Maximum basket temperature

Tcan = Maximum can temperature

Tclad = Maximum fuel cladding temperature

Figure 3.4-6 Modeling Details for the MTR Fuel Assembly Resting on the Surface of the NAC-LWT MTR Basket

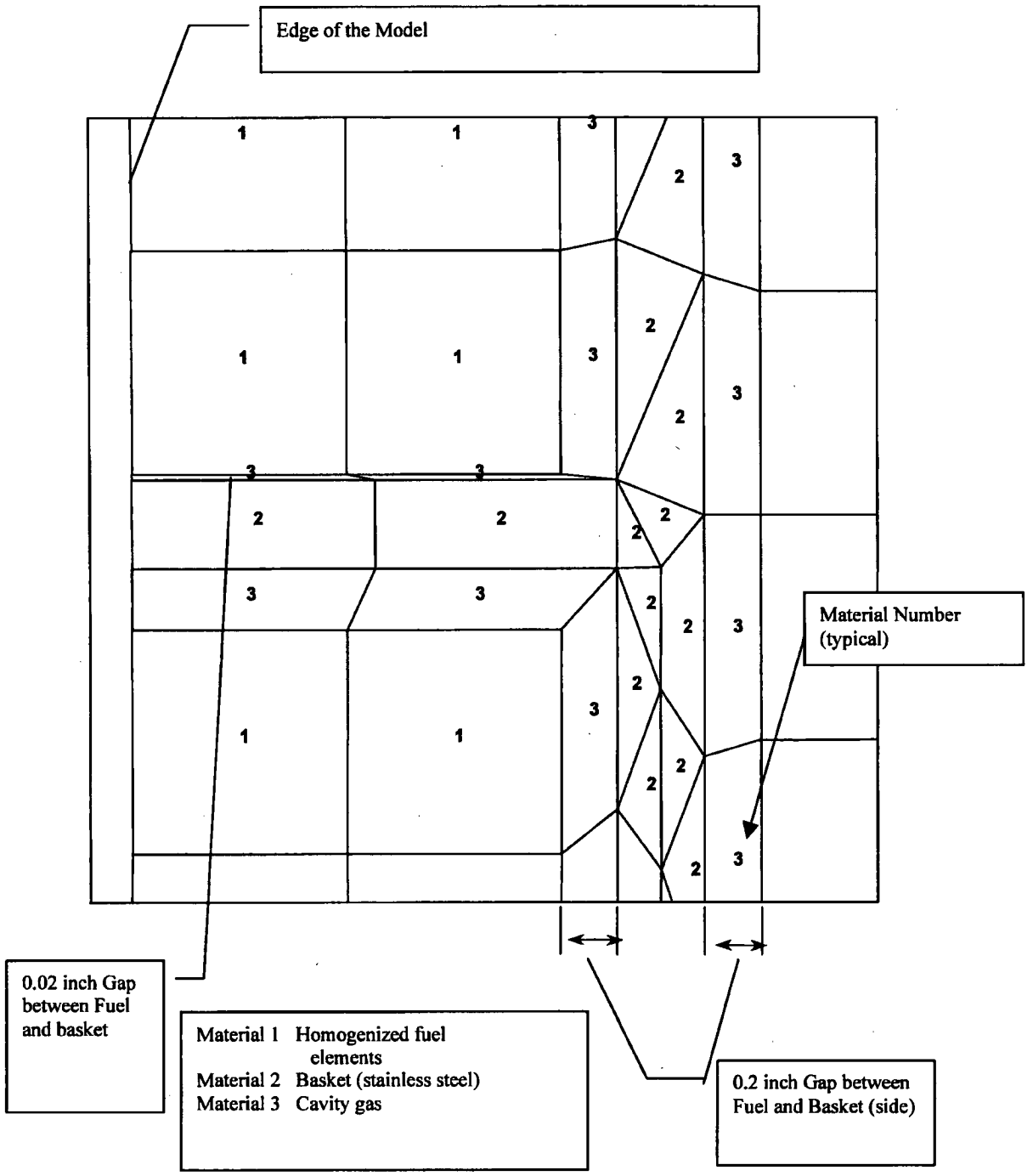

Figure 3.4-7 Finite Element Thermal Model for TRIGA Fuel Cluster Rods

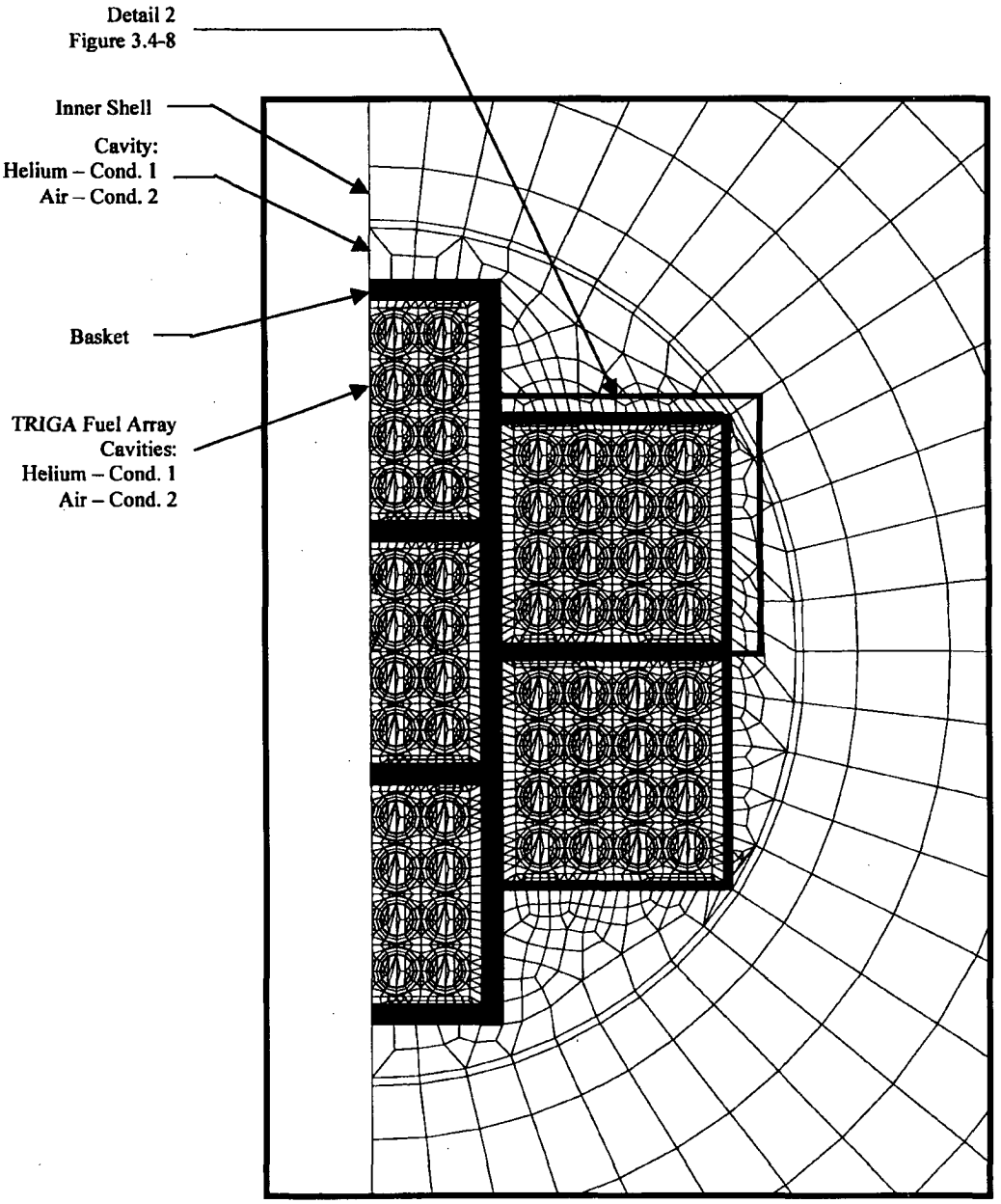

Figure 3.4-8 Details of the TRIGA Fuel Cluster Rods in the Finite Element Model

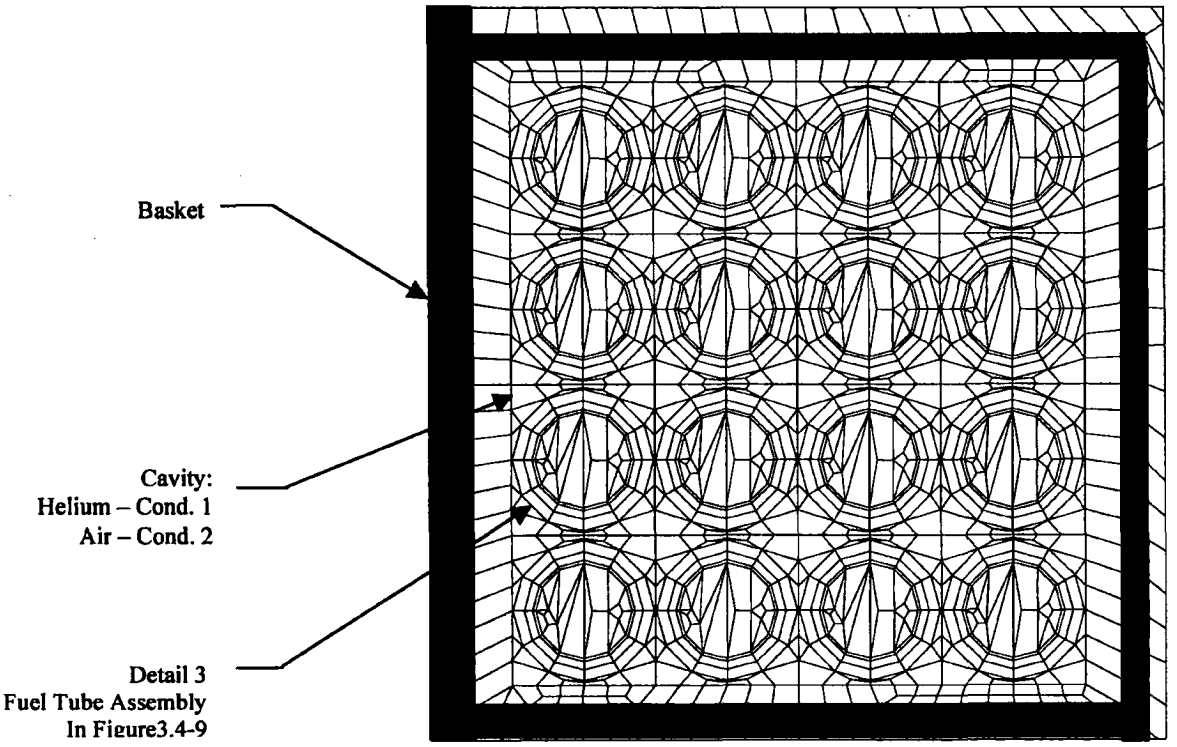

Figure 3.4-9 Individual TRIGA Fuel Cluster Rod Finite Element Model Details

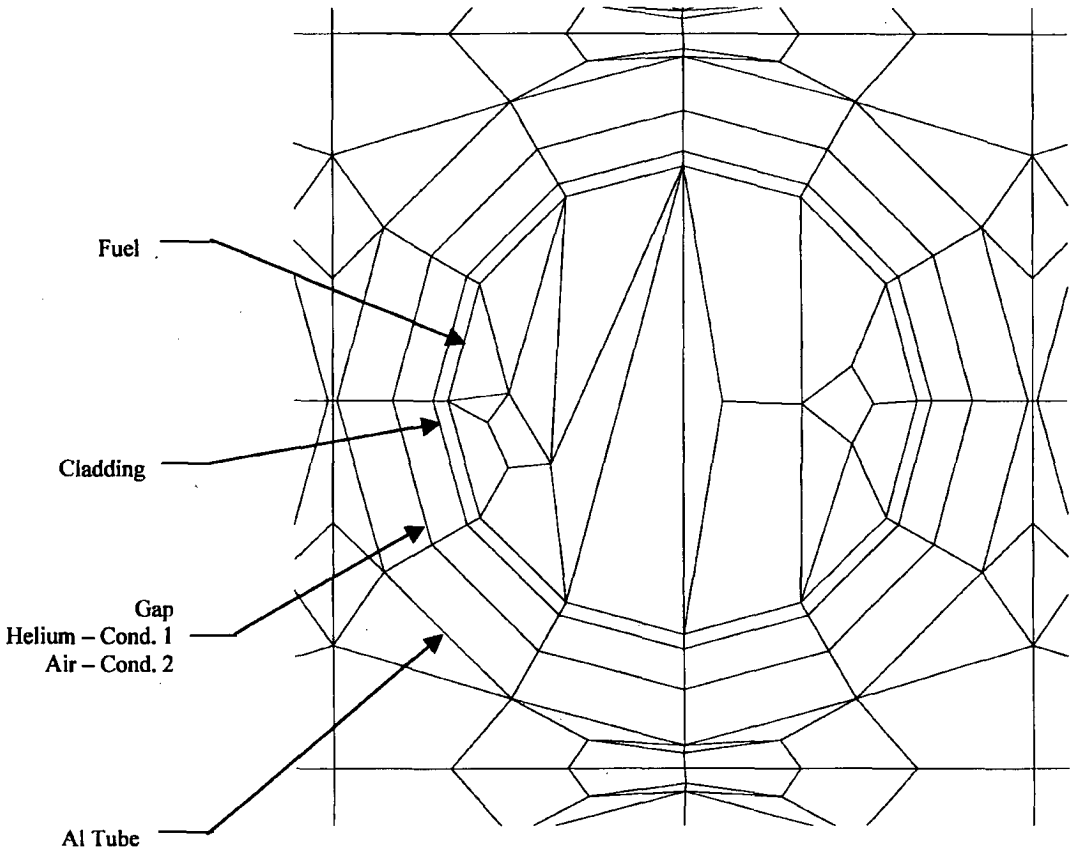

Figure 3.4-10 PWR and BWR High Burnup Fuel Rods Normal Condition ANSYS Thermal Model (Condition 1)

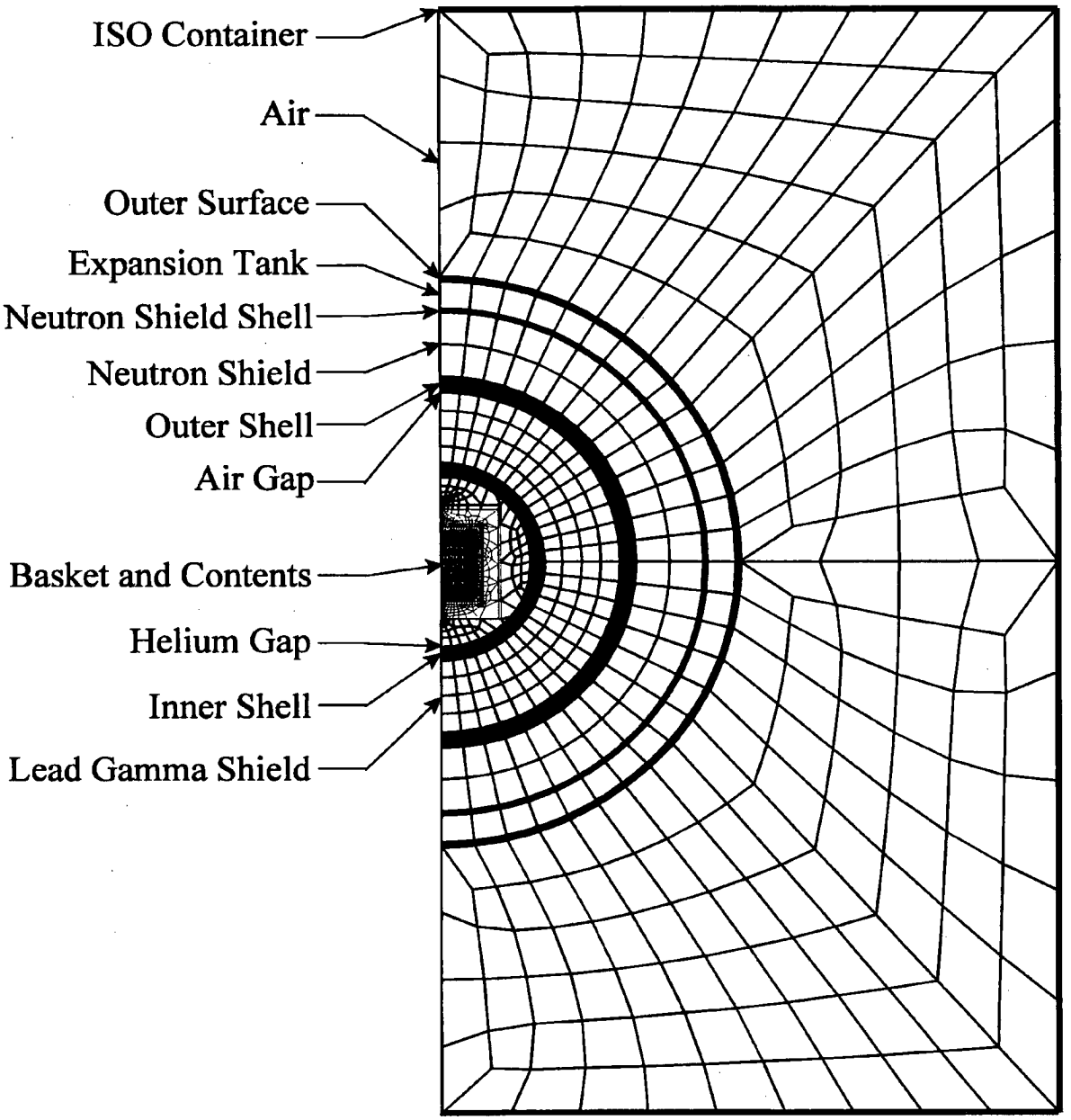

Figure 3.4-11 Close-up of PWR and BWR High Burnup Fuel Rods Normal Condition ANSYS Thermal Model

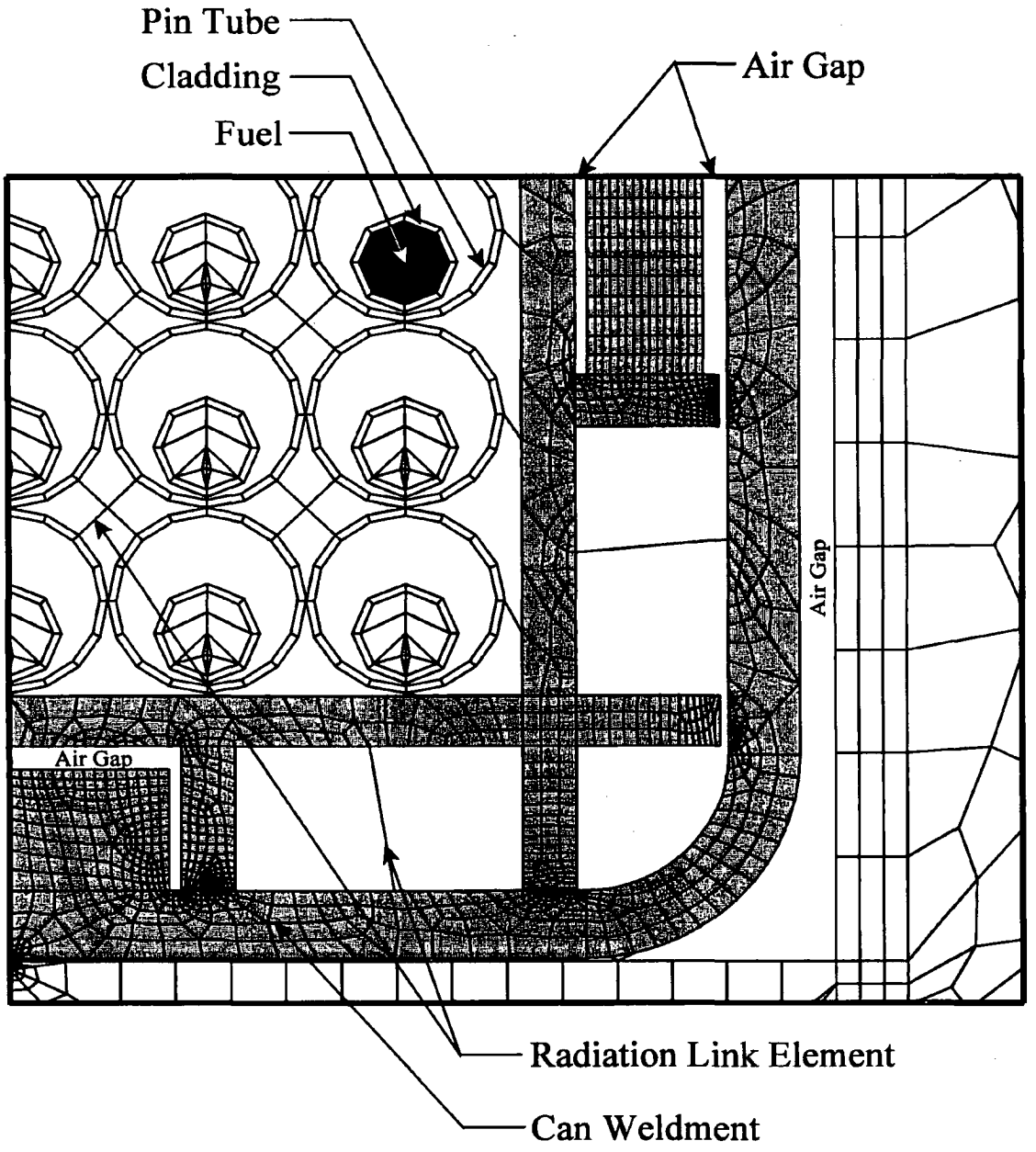

Note: air elements are not shown for clarity.

Figure 3.4-12 PWR and BWR High Burnup Fuel Rods Normal Condition ANSYS Thermal Model (Condition 2)

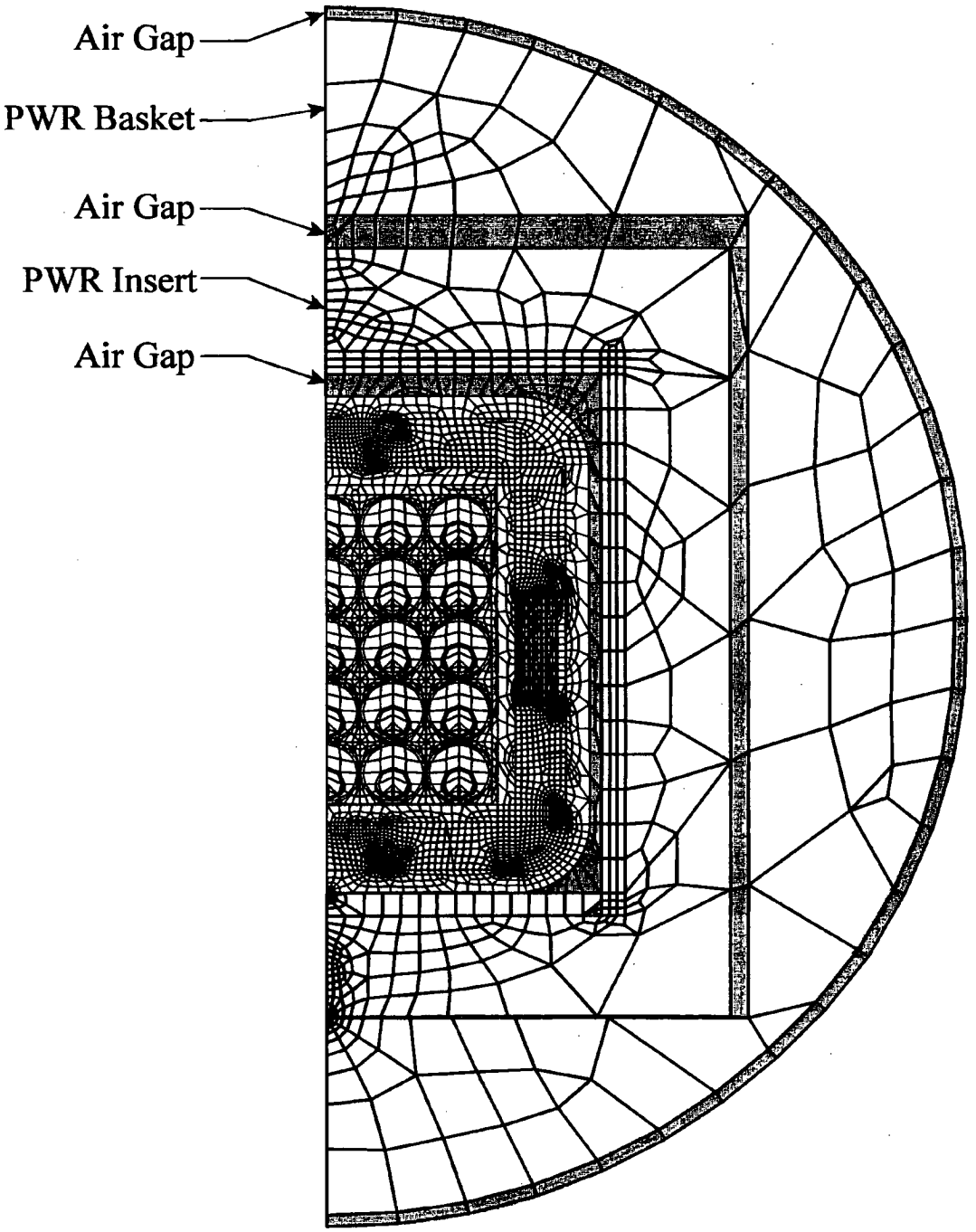

Figure 3.4-13 Finite Element Thermal Model for MTR Fuel Element

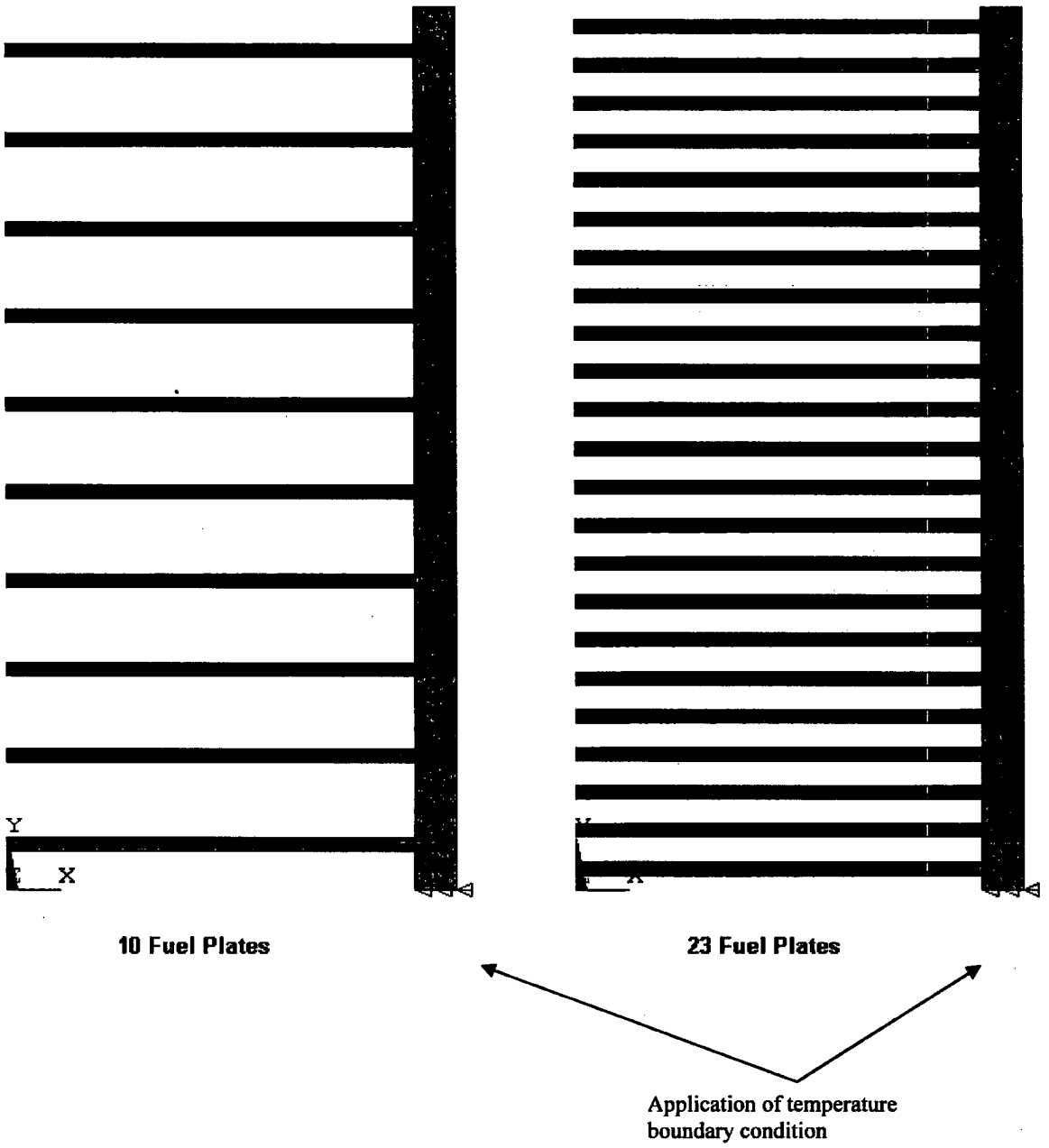

(Air elements omitted for clarity)

Figure 3.4-14 Detailed DIDO Basket Module Finite Element Model

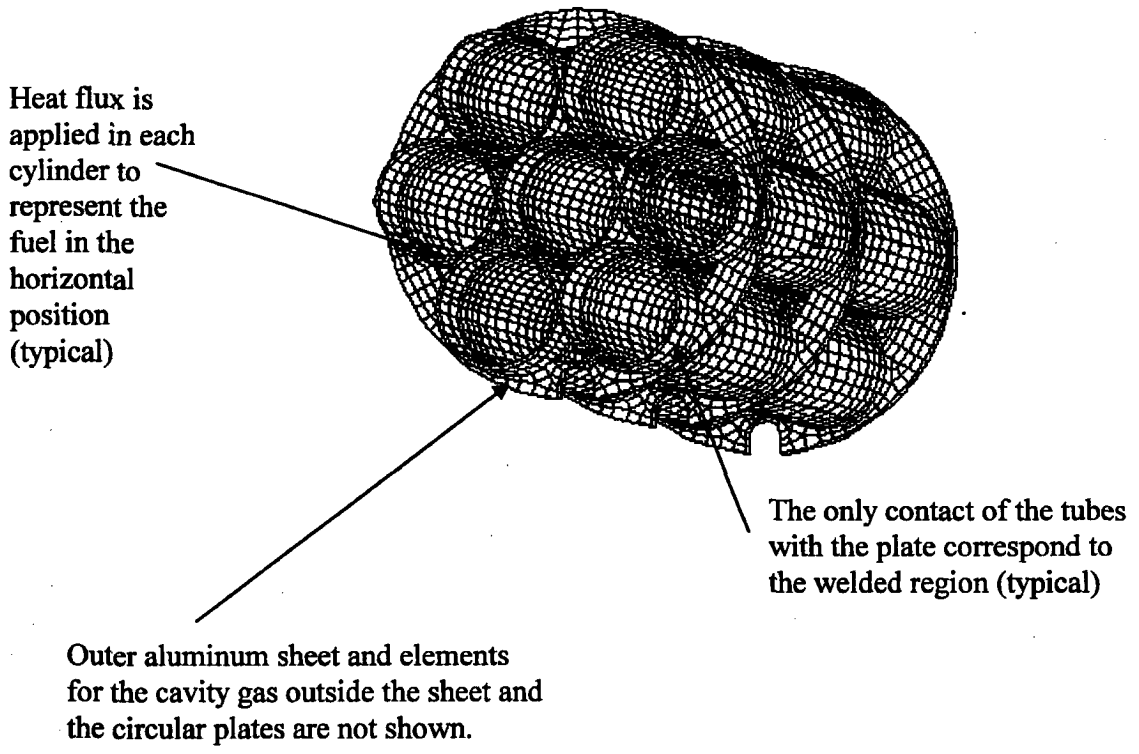

Figure 3.4-15 Detailed DIDO Fuel Assembly Model

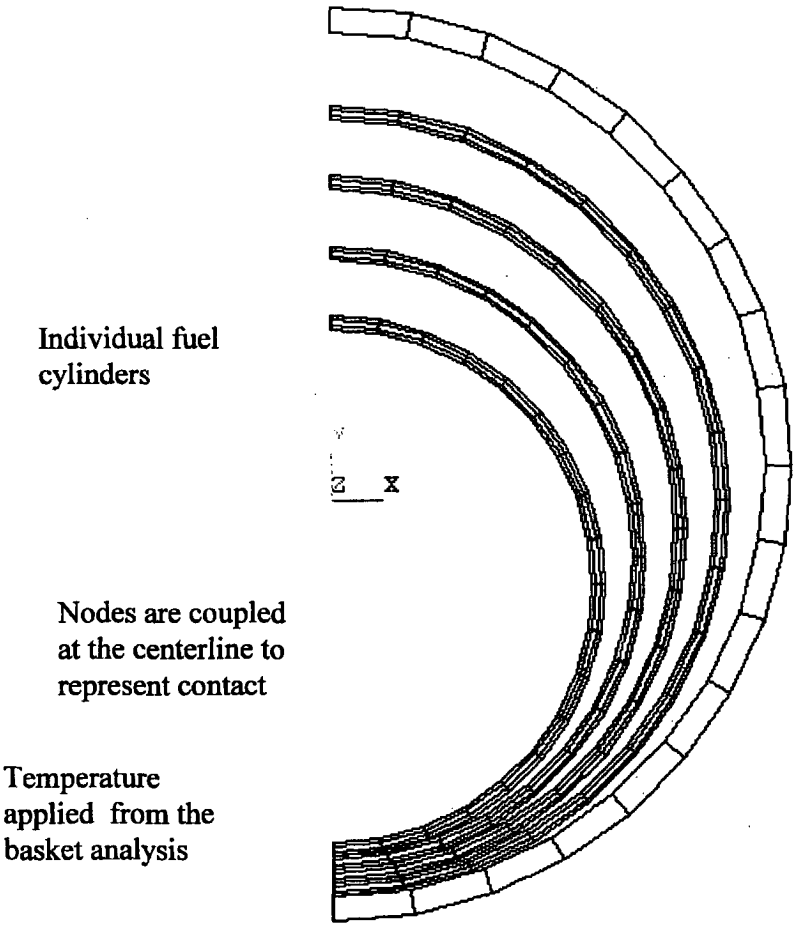

Figure 3.4-16 ANSYS Model for BWR 7 × 7 Fuel Lattice with 25 High Burnup Fuel Rods

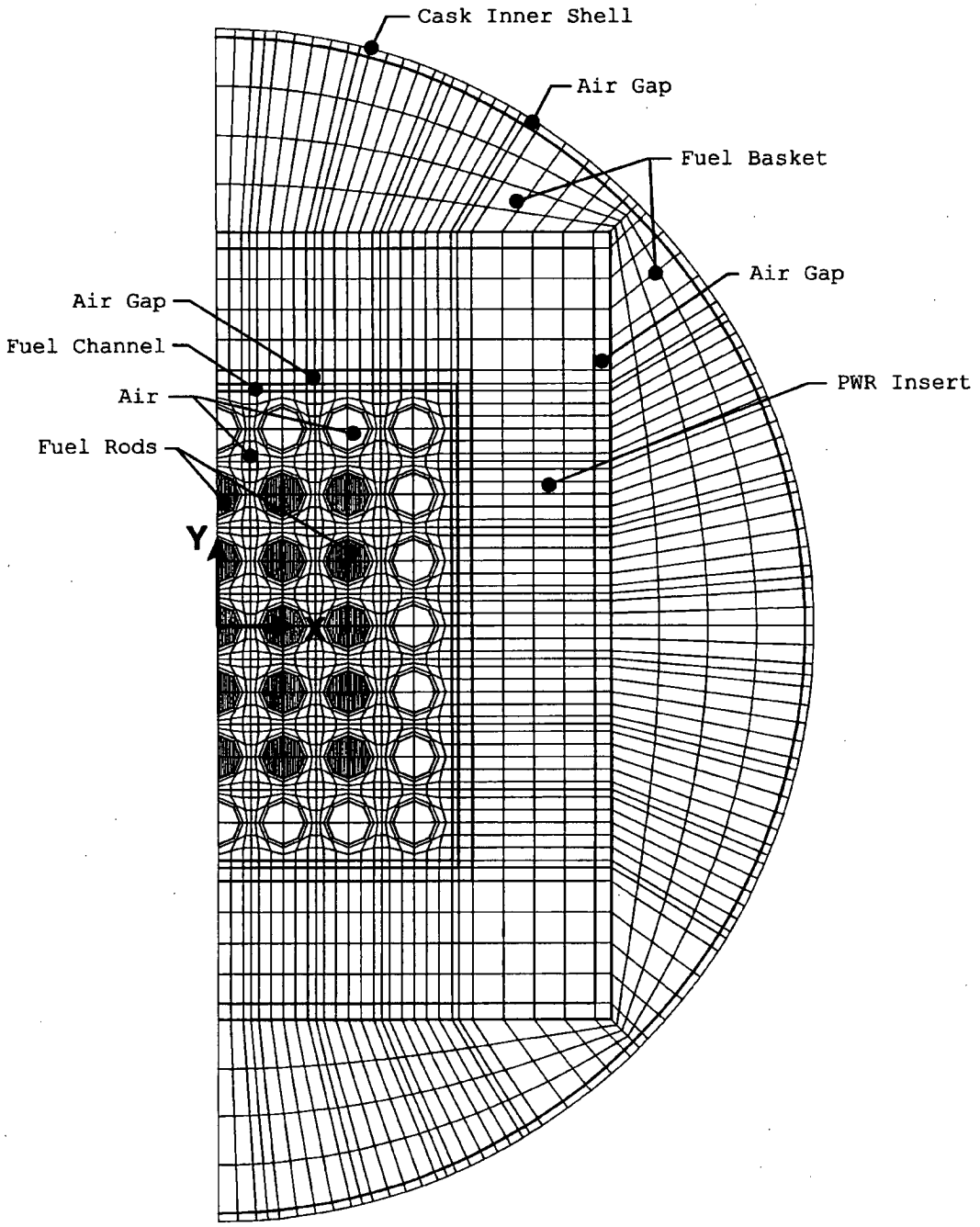

Figure 3.4-17 Fuel Rod Locations in the Thermal Model for Damaged Fuel

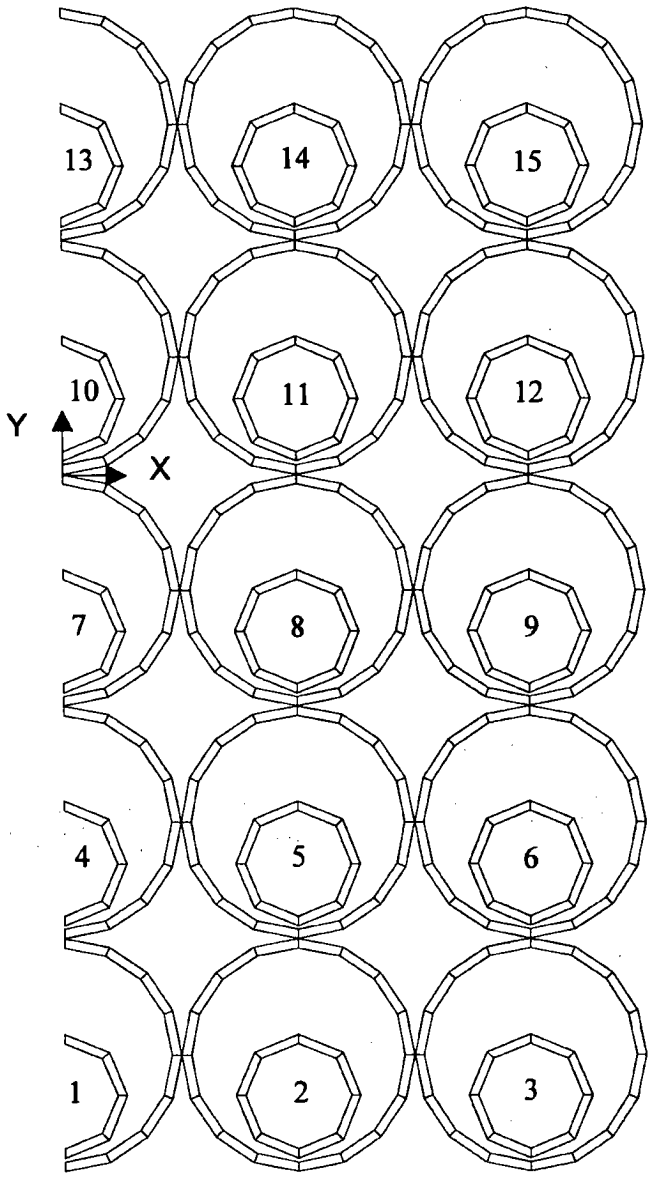

Figure 3.4-18 Finite Element Model for TPBARs

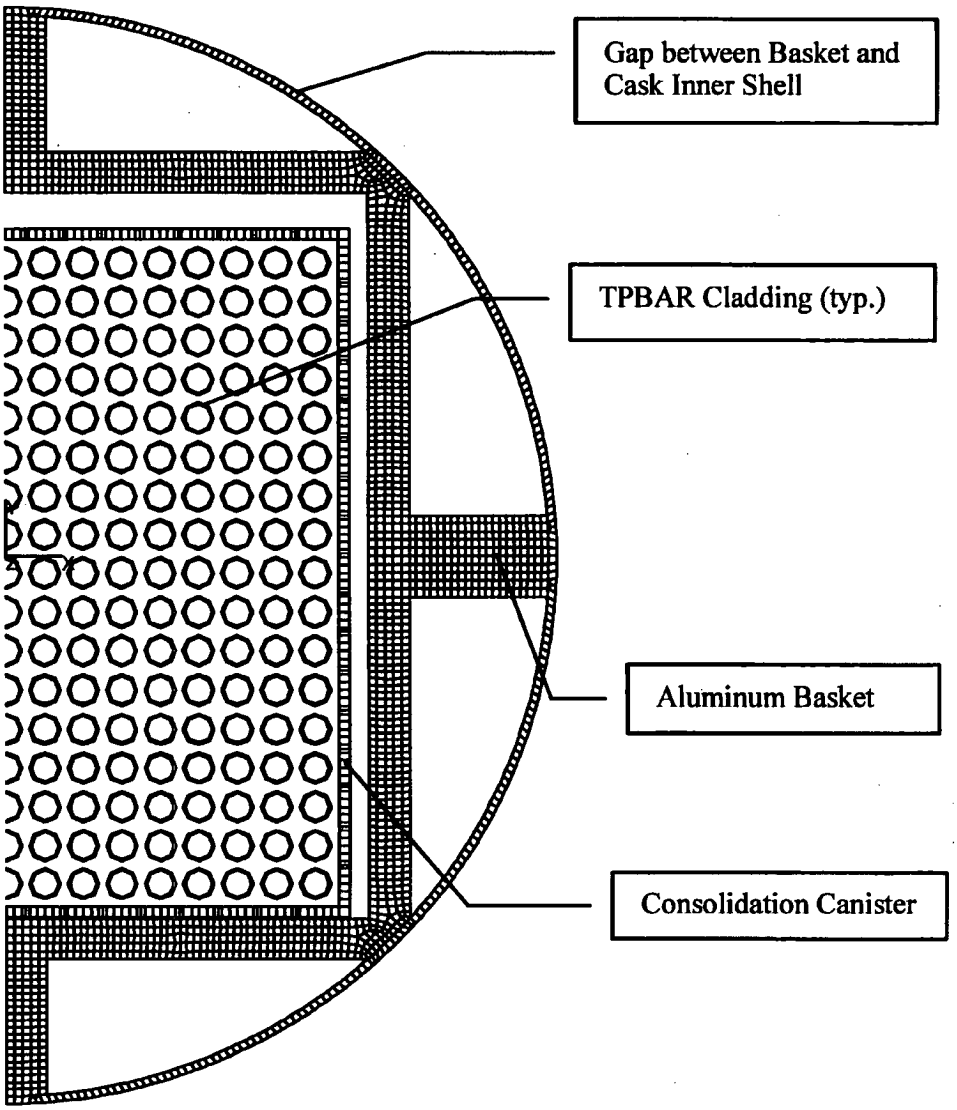

Note: Helium elements, except the gap between the basket and cask inner shell, are not shown for clarity.

Figure 3.4-19 Finite Element Model for MOATA Plate Fuel – ANSTO

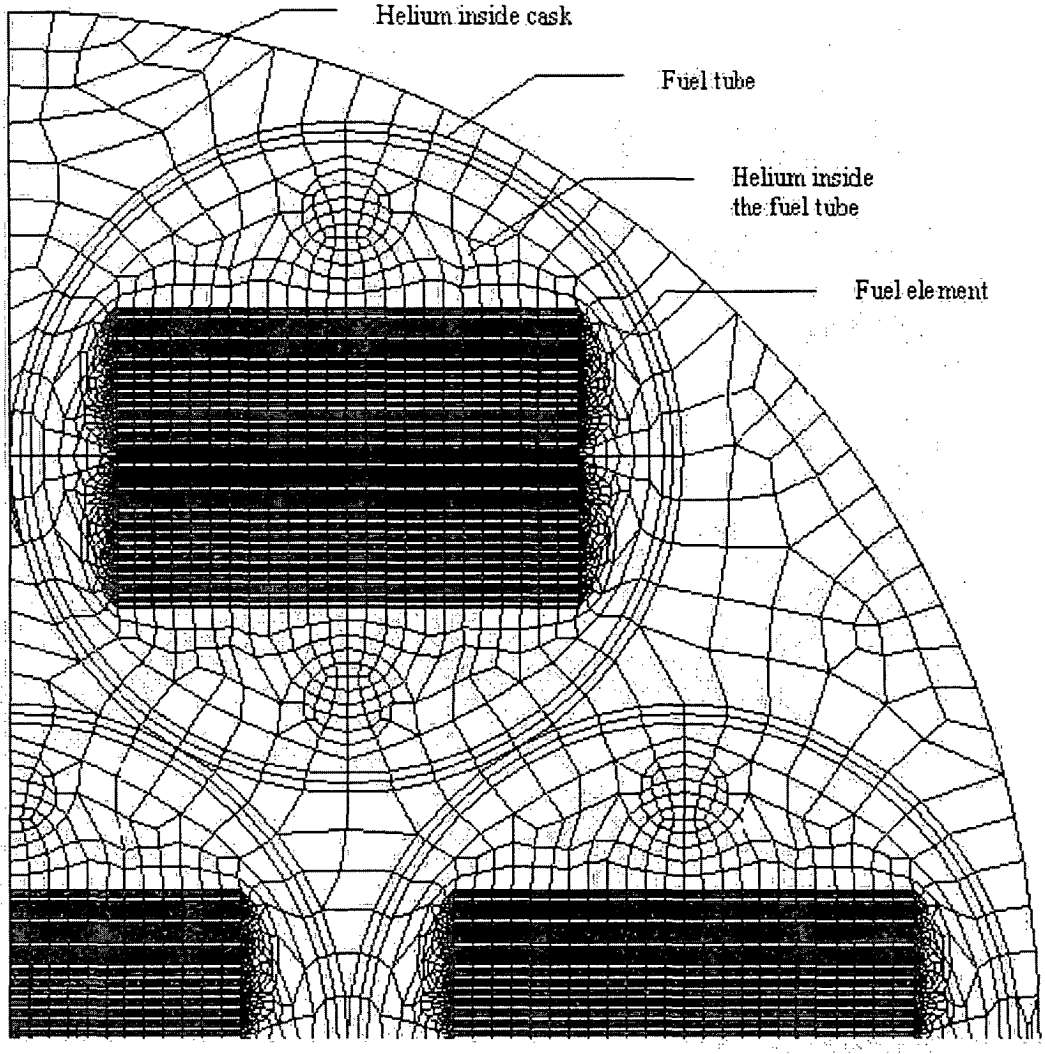

Figure 3.4-20 Finite Element Model for Mark III Spiral Fuel - ANSTO

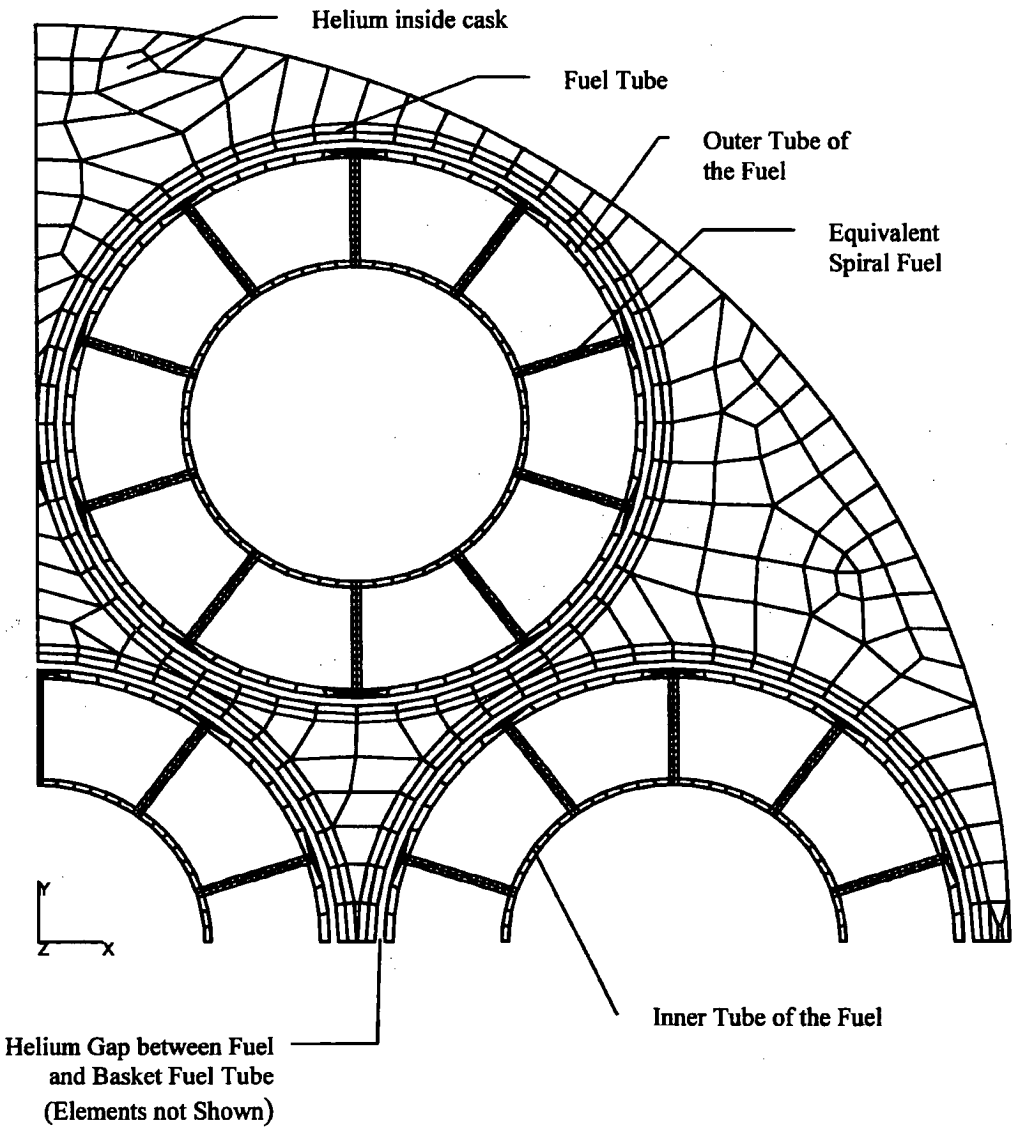

Table 3.4-1 Temperatures for Metallic Fuel Transport

Normal Transport Conditions

Component	Temperature (°F)
O-rings	200
Valves	201
Cask Radial Outer Surface	173
Neutron Shield	252
Radial Lead Gamma Shield	254
Bottom Lead Gamma Shield	210
Inner Stainless Steel Shell	255
Fuel Basket Outer Wall	255
Maximum Fuel Rod Cladding	270

Table 3.4-2 Maximum Component Temperatures – Design Basis PWR Fuel

Normal Transport Conditions

Component	Temperature (°F)
O-rings	227
Valves	231
Cask Radial Outer Surface	229
Neutron Shield	238
Radial Lead Gamma Shield	273
Bottom Lead Gamma Shield	239
Inner Stainless Steel Shell	274
Fuel Basket Outer Wall	276
Maximum Fuel Rod Cladding	472

Table 3.4-3 Limiting Cold Case Component Temperatures – Design Basis PWR Fuel

Normal Transport Conditions

Maximum Decay Heat Load, Minimum Ambient

Component	Temperature (°F)
O-rings	124
Valves	129
Cask Radial Outer Surface	128
Neutron Shield	110
Radial Lead Gamma Shield	167
Bottom Lead Gamma Shield	150
Inner Stainless Steel Shell	167
Fuel Basket Outer Wall	170
Maximum Fuel Rod Cladding	336

Table 3.4-4 Fission Product Gas Inventories and Pressures for Design Basis PWR Fuel Assembly

Fission Product	Inventory per Fuel Assembly (moles)	Initial Pressure (psia)
H-3	0.008	0.615
Kr-80	0.000	0.000
Kr-81	0.000	0.000
Kr-82	0.004	0.308
Kr-83	0.234	17.989
Kr-84	0.687	52.814
Kr-85	0.129	9.917
Kr-86	1.060	81.489
I-127	0.167	12.838
Xe-128	0.010	0.769
I-129	0.704	54.121
Xe-129	0.000	0.000
Xe-130	0.032	2.460
Xe-131	1.641	126.154
Xe-132	4.159	319.728
Xe-134	5.679	436.580
Xe-136	8.529	655.678
Total	**23.044**	**1,771.5**

Table 3.4-5 NAC-LWT Cask Thermal Performance Summary

Normal Transport Conditions

Component	Minimum Temperature °F	Maximum Temperature °F	Safe Operating Range °F
TFE O-rings	-40	227	-40 to +735[1]
Metallic O-rings	-40	227	-40 to +800
Viton® O-rings	-40	227[2]	-40 to +550[3]
Lead gamma shield	-40	273	-40 to +600
Liquid neutron shield	-40	238	-40 to +350

[1] Verified through testing (Certified Test Report D9-3362-1, Applied Technical Services, Inc., Marietta, GA, February 8, 1989)

[2] Normal Transport Condition maximum O-ring temperatures were not calculated. The Viton® O-rings are located in close proximity to the TFE O-rings and there is substantial thermal margin, a new O-ring temperature is not calculated

[3] Verified through testing (Certified Test Report 43939-01, Wyle Laboratories, Inc., Huntsville, AL, February 21, 2000).

Table 3.4-6 MTR Fuel Maximum Component Temperatures – Normal Transport Condition

Conditions: 100°F Ambient Temperature
Solar Insolation
1.26 Kilowatts Decay Heat Load

Condition 1: NAC-LWT (Transported in an ISO Container)
Cavity gas: Helium

Component	Temperature (°F)	
	Design Basis Decay Heat Load [1]	Variable Decay Heat Load [2]
Liquid Neutron Shield	198	198
Outer Shell	199	199
Lead Gamma Shield	212	214
Inner Shell	214	215
Basket (maximum)	256	292
Fuel (maximum)	< 363 [3]	< 363 [3]

Condition 2: NAC-LWT (Transported via Truck Trailer)
Cavity gas: Air

Component	Temperature (°F)	
	Design Basis Decay Heat Load [1]	Variable Decay Heat Load [2]
Liquid Neutron Shield	160	160
Outer Shell	161	160
Lead Gamma Shield	180	180
Inner Shell	181	180
Basket (maximum)	267	312
Fuel (maximum)	< 363 [3]	363

[1] Uniform 30-Watt/Element Configuration Heat Load.
[2] 120-Watt / 70-Watt / 20-Watt Configuration Heat Load.
[3] Fuel not modeled for this condition. Fuel temperature is bounded by the variable decay heat load in air case.

Table 3.4-7 PWR Rods (25 Total) Maximum Component Temperatures – Normal Transport Condition

Conditions: 100°F Ambient Temperature
Cask Inside ISO Container
Solar Insolation
1.41 Kilowatts Decay Heat Load

Component	Temperature (°F)
O-rings	< 249
Valves	< 249
Cask Radial Outer Surface	185
Lead Gamma Shield	248
Inner Shell	249
Outer Shell	235
Basket	252
Liquid Neutron Shield	235
Maximum Cladding Temperature	358

Table 3.4-8 TRIGA Fuel Element Maximum Component Temperatures - Normal Conditions of Transport

Conditions: 100°F Ambient Temperature
Solar Insolation
1.05 Kilowatts Decay Heat Load

Condition 2: NAC-LWT (Transported via Truck Trailer)
Cavity Gas: Air

Component	Temperature (°F)
Liquid Neutron Shield	< 160
Outer Shell	< 161
Lead Gamma Shield	< 180
Inner Shell	< 181
Basket (maximum)	267[1]
Cladding (maximum)	326[1]

[1] As shown in Table 3.4-6, the Condition 2 analysis produces higher basket temperatures than Condition 1. Therefore, the Condition 2 analysis for TRIGA fuel bounds transport of the cask in an ISO container.

Table 3.4-9 TRIGA Fuel Cluster Rod Temperatures – Normal Conditions of Transport

Conditions: 100°F Ambient Temperature
Solar Insolation
1.05 Kilowatts Decay Heat Load

Condition 1: NAC-LWT (Transported in an ISO Container)
Cavity gas: Helium

Component	Temperature (°F)
Liquid Neutron Shield	207
Outer shell	207
Lead Gamma shield	221
Inner shell	222
Basket (maximum)	263
Aluminum insert tube	265
Cladding (maximum)	266

Condition 2: NAC-LWT (Transported via Truck Trailer)
Cavity gas: Air

Component	Temperature (°F)
Liquid Neutron Shield	159
Outer shell	160
Lead Gamma shield	177
Inner shell	178
Basket (maximum)	278
Aluminum insert tube	292
Cladding (maximum)	295

Table 3.4-10 PWR and BWR High Burnup Fuel Rods Maximum Component Temperatures – Normal Transport Condition

Conditions: 100°F Ambient Temperature Solar Insolation
2.1 Kilowatts Decay Heat Load

Condition 1: NAC-LWT (Transported in an ISO Container)
Cavity gas: Helium

Component	Temperature (°F)
Liquid Neutron Shield	306
Outer Shell	308
Lead Gamma Shield	375
Inner Shell	385
Basket (maximum)	387
Cladding (maximum)	671
Aluminum PWR Insert	394
Stainless Steel Can Weldment	500
Average Cavity Gas	506

Condition 2: NAC-LWT (Transported via Truck Trailer)
Cavity gas: Air

Component	Temperature (°F)
Inner Shell	274
Basket (maximum)	280
Aluminum PWR Insert	286
Stainless Steel Can Weldment	538
Cladding (maximum)	896
Average Cavity Gas	541

Table 3.4-11 Fission Product Gas Inventories and Pressures for the Exxon 7 × 7 BWR Fuel Assembly

Fission Product	Inventory per Fuel Assembly (moles)	Initial Partial Pressure per Rod (psia)
H-3	7.670E-03	1.408E+00
Kr-80	0.000E+00	0.000E+00
Kr-81	0.000E+00	0.000E+00
Kr-82	8.110E-03	1.489E+00
Kr-83	1.270E-01	2.331E+01
Kr-84	7.060E-01	1.296E+02
Kr-85	9.590E-02	1.760E+01
Kr-86	9.330E-01	1.713E+02
I-127	1.770E-01	3.249E+01
Xe-128	3.000E-02	5.507E+00
I-129	7.030E-01	1.290E+02
Xe-129	4.260E-04	7.819E-02
Xe-130	9.040E-02	1.659E+01
Xe-131	9.710E-01	1.782E+02
Xe-132	5.030E+00	9.233E+02
Xe-134	5.690E+00	1.044E+03
Xe-136	8.590E+00	1.577E+03
Total	2.32E+01	4.251E+03

Table 3.4-12 DIDO Fuel Maximum Component Temperatures – Normal Transport Condition

Conditions: 100°F Ambient Temperature
Solar Insolation
1.05 Kilowatts Decay Heat Load

Condition 1: NAC-LWT (Transported in an ISO Container)
Cavity gas: Helium

Component	Temperature (°F)
	Design Basis Decay Heat Load
Liquid Neutron Shield	198[1,2]
Outer Shell	199[1,2]
Lead Gamma Shield	212[1,2]
Inner Shell	214[1,2]
Basket (maximum)	299[3]
Fuel (maximum)	306[3]

1 Uniform 30-Watt/Assembly Configuration Heat Load for MTR fuel.
2 Bounding values obtained from Table 3.4-6 for MTR fuel.
3 Uniform 25-Watt/Assembly Configuration Heat Load for DIDO fuel.

Condition 2: NAC-LWT (Transported via Truck Trailer)
Cavity gas: Air

Component	Temperature (°F)
	Design Basis Decay Heat Load
Liquid Neutron Shield	160[1,2]
Outer Shell	161[1,2]
Lead Gamma Shield	180[1,2]
Inner Shell	181[1,2]
Basket (maximum)	327[3]
Fuel (maximum)	338[3]

1 Uniform 30-Watt/Assembly Configuration Heat Load for MTR fuel.
2 Bounding values obtained from Table 3.4-6 for MTR fuel.
3 Uniform 25-Watt/Assembly Configuration Heat Load for DIDO fuel.

Table 3.4-13 General Atomics IFM Maximum Component Temperatures – Normal Transport Condition

Conditions: 100°F Ambient Temperature
Solar Insolation
13 W Decay Heat Load

NAC-LWT (Transported in an ISO Container)

Component	Temperature (°F)
	Design Basis Decay Heat Load
Liquid Neutron Shield	198[1]
Outer Shell	199[1]
Lead Gamma Shield	212[1]
Inner Shell	214[1]
Basket (maximum)	250[2]
FHU contents (maximum)	326[3]

[1] Bounding values obtained from Table 3.4-6 for MTR fuel.
[2] 13-Watt Configuration Heat Load for General Atomics fuel.
[3] Bounding value obtained from Table 3.4-8 for the 1.05 kW TRIGA fuel.

Table 3.4-14 PWR and BWR High Burnup Fuel Rods in a Fuel Assembly Lattice Maximum Component Temperatures—Normal Transport Condition

Conditions: 100°F Ambient Temperature
Solar Insolation
2.1 Kilowatts Decay Heat Load (BWR)
2.3 Kilowatts Decay Heat Load (PWR)
Transport Condition 2 (no ISO container) with air in the cavity

Component	Temperature (°F)
Inner Shell	274
Basket (maximum)	276
Aluminum PWR Insert	336
Cladding (maximum)	664
Average Cavity Gas	430

Table 3.4-15 Maximum Component Temperatures for High Burnup Fuel Rods with Damaged Fuel Rods in a Rod Holder

	Maximum Temperatures (°F)					
Case[1]	Basket	Aluminum Insert	Rod Holder Weldment	Fuel Rod Tube[2]	Fuel Cladding[3]	Cavity Gas Average
Damaged Rods at Locations #4, 5, 6, 7, 8, 9, 10, 11, 12	280	285	523	835	809	479
Damaged Rods at Locations #7, 8, 9, 10, 11, 12, 13, 14, 15	280	286	567	866	653	482
Damaged Rods at Locations #1, 2, 3, 4, 5, 6, 7, 8, 9	280	284	474	743	749	465

[1] See Figure 3.4-17 for fuel rod locations. The nine locations in the half-symmetry model correspond to fifteen actual fuel rod locations.
[2] The structural analysis of the fuel tubes in Section 2.6.7.10.2 uses a maximum temperature of 925°F.
[3] Maximum temperatures are reported for intact fuel rods only.

Table 3.4-16 Maximum Component Temperatures for TPBAR Shipment – Normal Conditions of Transport

Component	Temperature (°F)
Liquid Neutron Shield	207[1]
Outer Shell	207[1]
Lead Gamma Shield	221[1]
Inner Shell	222[1]
TPBARs	290
Aluminum Basket	228
Consolidation Canister	245
Gas (average)	246

[1] Cask component temperature conservatively obtained from Table 3.4-9, Condition 1 for TRIGA Fuel Cluster Rod.

Table 3.4-17 Maximum Component Temperatures - PULSTAR Fuel in MTR Basket

Conditions: 100°F Ambient Temperature
Solar Insolation
840 watts Decay Heat Load
(30 watts in Each Basket Cell)

Condition 1: NAC-LWT (Transported in an ISO Container)
Cavity gas: Helium

Component	Temperature (°F)
Liquid Neutron Shield	207
Outer shell	207
Lead Gamma shield	221
Inner shell	222
Basket (maximum)	263
Aluminum insert tube	265
Cladding (maximum)	266

Condition 2: NAC-LWT (Transported via Truck Trailer)
Cavity gas: Air

Component	Temperature (°F)
Liquid Neutron Shield	159
Outer shell	160
Lead Gamma shield	177
Inner shell	178
Basket (maximum)	278
Aluminum insert tube	292
Cladding (maximum)	295

Notes:
1. The temperatures in this table correspond to the temperatures in Table 3.4-9.
2. PULSTAR fuel can (if used) = 295°F (assume same as fuel cladding temperature).

Table 3.4-18 PULSTAR Fuel Dimensions

Description	Value
Fuel Assembly Height (inch)	38
Fuel Assembly Width (inch)	3.15 × 2.74
Active Fuel Region Height (inch)	24.1
Fuel Rod Diameter (inch)	0.47
Fuel Clad Thickness (inch)	0.0185
Fuel Pellet Diameter (inch)	0.423
Rod Length (inch)	26.2
Plenum Length (inch)	0.5
Number of Fuel Rods	25

Table 3.4-19 PULSTAR Payload Volume Summary

Description	Dimension[cm^3]
Fuel Volume (25 Elements)	1,860
Pellet to Clad Volume (25 Elements)	97
PULSTAR Can Free Volume	1,440
PULSTAR Can Total Volume	4,230
Assembly Envelope Volume	5,370
LWT Cavity Volume	409,300
MTR Basket Stack Volume	41,900

Table 3.4-20 PULSTAR Fuel Assembly Fission Product Gas Inventory

Isotope	Moles
^{4}He	2.28E-03
^{3}H	1.30E-04
^{82}Kr	6.32E-05
^{83}Kr	7.03E-03
^{84}Kr	1.66E-02
^{85}Kr	2.41E-03
^{86}Kr	2.81E-02
^{127}I	2.87E-03
^{128}Xe	1.27E-04
^{129}I	1.42E-02
^{130}Xe	3.11E-04
^{131}Xe	3.91E-02
^{132}Xe	8.49E-02
^{134}Xe	1.27E-01
^{136}Xe	1.23E-01
Total	4.48E-01

Table 3.4-21 PULSTAR Fuel Element Normal Condition Internal Pressure Summary

Description	Free Volume (liters)	Pressure (atm)	Pressure (psia)	Pressure (psig)
Cask Pressure -28 Intact Assemblies	217.0	1.4	21.3	6.6
Cask Pressure -14 Intact Assemblies and 14 Cans	233.0	1.8	27.2	12.5
Can Pressure - PULSTAR Failed Fuel Can	1.53	4.4	65.4	50.7

Table 3.4-22 Maximum Component Temperatures – MOATA Plate Fuel and Mark III Spiral Fuel in ANSTO Basket

Conditions: 100°F Ambient Temperature
Solar Insolation
Heat Load: 126 Watts – MOATA Plate Fuel; 756 Watts – Mark III Spiral Fuel

Component	Temperature (°F)
Liquid Neutron Shield[1]	207
Outer Shell[1]	207
Lead Gamma Shield[1]	221
Inner Shell[1]	222
Basket - MOATA Plate Fuel	230
Fuel Cladding – MOATA Plate Fuel	233
Basket – Mark III Spiral Fuel	248
Fuel Cladding – Mark III Spiral Fuel	250

[1] The cask component temperatures are conservatively obtain from Table 3.4-9 for the TRIGA Fuel Cluster Rod.

3.5 Hypothetical Accident Thermal Evaluation

The hypothetical accident scenario is a series of accidents that occur in a specified order as described in 10 CFR 71.73. The only thermal consequence as a result of the drop and puncture portions of the hypothetical accident is the assumption that the neutron shield is lost prior to the start of the fire. The remainder of the thermal analysis in this section consists of an evaluation of the thermal consequences of the fire portion of the hypothetical accident.

3.5.1 Finite Element Models

There are two finite element models used to evaluate the hypothetical fire accident condition. The axisymmetric thermal model, as described in Section 3.5.1.1, is used to evaluate all configurations except for the PWR and BWR high burnup fuel rod configuration. For the PWR and BWR high burnup fuel rod configuration, a two-dimensional planar finite element model is used. The planar model is described in Section 3.5.1.2.

3.5.1.1 Axisymmetric Thermal Model

The finite element code ANSYS (Revision 5.5) is used to generate a two-dimensional (2-D) axisymmetric finite element model and to perform thermal analyses for the pre-fire, fire and post-fire (cool down) conditions. The ANSYS finite element model is shown in Figure 3.5-1. Figure 3.5-2 and Figure 3.5-3 show the detail of the model at the locations where the thermal insulator is installed in the top and bottom regions. The ANSYS model uses thermal conductivity values for the thermal insulators that are conservative in that they are higher than the values shown in Table 3.2-6 and Table 3.2-8. The thermal insulator protects the lead gamma shield against localized melting during the fire event. As shown, the main components in the radial direction consist of the inner shell, the radial lead, the outer shell, the neutron shield tank and the expansion tank.

The model is constructed using the ANSYS thermal PLANE55 element. Thermal radiation and convection heat transfer at the cask surface is modeled using the PLANE55 and SURF19 elements. Radiation heat transfer across the neutron shield tank and neutron shield expansion tank is modeled using the ANSYS radiation LINK31 element.

The pre-fire condition is defined as the normal transport condition, and a steady-state analysis is performed to determine the temperature field of the cask body. This temperature field is used as the initial condition for the 30 minute fire transient analysis (fire condition), which is followed by a 50-hour cool down period (post-fire condition). Analysis of the 50-hour cool down period ensures that the maximum component temperatures are determined.

The pre-fire analysis considers the convection heat transfer of the liquid neutron shielding inside the shell, but convection heat transfer of the air inside the expansion tank is conservatively neglected. During the fire and post-fire conditions, the liquid neutron shielding is considered to be lost, due to either the pin puncture accident or the failure of the relief valve in the neutron shield tank resulting from high pressure steam produced by the fire. The convection heat transfer of the air in the tank is negligible compared to the radiation heat transfer. The radiation heat transfer across the air-filled tank, and expansion tank, is explicitly modeled using the ANSYS radiation LINK31 element. An emissivity of 0.36 is used for all inner surfaces of the stainless steel neutron shield tank and the expansion tank.

The impact limiters are not discretely modeled, but are represented as thermal boundary conditions. Before the fire accident, adiabatic thermal boundary conditions are conservatively applied to the interface regions between the cask and the impact limiters so that no heat is transferred out of the cask through the impact limiters. During the fire and post-fire periods, the impact limiters are assumed to be removed. In this time period, heat transfer by convection and radiation are modeled in the regions previously covered by the impact limiters. Solar insolation is considered in the model during the pre-fire and post-fire conditions, but neglected during the fire.

The heat input from the fire considers thermal radiation and convection heat transfer. A convection heat transfer coefficient of 0.02446 Btu/hr-in2-°F is applied to account for heat transfer to the cask surface. This value is twice the theoretical value (Wix) to account for uncertainties in the fire accident condition and the data from which the recommended value is derived. These assumptions lead to maximizing the material temperatures and are conservative.

The cask contents (basket and fuel) are not directly modeled. The decay heat generated from the fuel region inside the cask is simulated using an equivalent non-uniform heat flux applied to the inner surface of the cask cavity inner shell, corresponding to the height of the active fuel region. The analysis considers the bounding fuel heat load, 2.5 kW for PWR fuel, and applies the power distribution curve shown in Figure 3.4-2 with a peaking factor of 1.2.

ANSYS 5.5 was used to calculate the maximum post-fire accident temperatures at four new locations for the alternate port cover design. Temperatures calculated for comparable locations on the port cover body vary from those temperatures presented in Table 3.5-1. Changes in the ANSYS 5.5 version and computational solvers account for the differences in calculated results. The transient temperature analysis results are presented in Figure 3.5-12 and Figure 3.5-13.

Exactly the same model described above was rerun using ANSYS 5.5 for the alternate port cover to determine the bolt head and thread temperatures and the temperatures at both O-ring locations. The output is post-processed to determine the maximum average temperatures at specific locations of interest. The temperatures calculated are presented in Table 3.5-1.

3.5.1.2 Two-Dimensional Planar Thermal Model

Thermal analysis of the NAC-LWT cask loaded with PWR and BWR high burnup fuel rods is performed using a two-dimensional planar thermal model. The thermal model is identical to the model utilized to perform the steady state analysis (condition 2, Section 3.4.1.7) for the NAC-LWT cask loaded with PWR and BWR high burnup fuel rods. The detailed model description is contained in Section 3.4.1.7.2.

The Condition 2 model was selected since it initiates the thermal transient with clad temperatures 225°F higher (from Table 3.4-10, 896°F-671°F) than the Condition 1 model steady-state condition. This increase in the initial condition temperature for the cask cavity air-filled condition overcompensates for the higher conductivity of helium as the cavity gas. The effect of the higher helium conductivity heat input during the period of fire exposure is significantly less due to the influence of the parallel heat transfer paths by conduction through the metal contents and by radiation across the gas-filled space. This influence is seen in the transient maximum temperature difference from the higher steady-state temperature of 896°F to the maximum transient temperature of 1,014°F (a change of 118°F), which is significantly bounded by the steady-state temperature condition difference of 225°F, as stated previously. In addition to the conservative modeling introduced by the initial steady-state temperature, during the cooldown portion of the transient, the use of air thermal conductivity in the cavity retards the heat removal from the fuel (as compared to helium conductivity). This also results in a maximum transient temperature higher than when modeling helium as the cavity gas.

A thermal transient analysis for the design basis fuel is performed using the two-dimensional planar thermal model (see Figure 3.4-12). To impose the fire accident condition on this model, a temperature time history was applied to the outer surface of the model, which corresponds to the inner surface of the inner shell. This temperature time history at the inner shell inner surface near the axial midplane is obtained from the fire accident analysis (heat load of 2.5 kW and a peaking factor of 1.2, as described in Section 3.5.2) using the axisymmetric two-dimensional model described in Section 3.5.1.1.

Using a two-dimensional planar model of the cross-section, a 50.5-hour transient analysis is performed with a heat load of 2.1 kW with a peaking factor of 1.22. This represents the bounding heat load for the high burnup PWR and BWR fuel rods.

3.5.2 Package Conditions and Environment

The fire accident is preceded by the cask drop and cask puncture portions of the hypothetical accident. The only damage that occurs as a result of the drop and puncture accident events that are of importance to the cask thermal performance is the damage to the NAC-LWT cask neutron shield. As a result of these events, it is assumed that the integrity of the neutron shield has been damaged to such an extent that the entire contents of the neutron shield are no longer present.

The fuel heat load of 2.5 kW is applied using a nonuniform heat flux with a peaking factor of 1.2. Solar insolation is applied to the outer surfaces of the cask, including the area covered by the impact limiters, during the post-fire conditions, and neglected during the fire condition. The value of solar insolation, based on a 24-hour average to curved surfaces, is:

$$Q_{sun}=1,475/(24\times144) = 0.4268 \text{ BTU/hr-in}^2$$

Convection and radiation heat transfer at the outer surfaces of the cask were considered in the analysis. During the pre-fire (normal) and post-fire periods, the ambient temperature assumed is 100°F, and the cask outer surface emissivity is 0.36. During the fire, the ambient temperature is 1,475°F, and the cask surface emissivity is 0.9. The convection coefficient applied is 0.02446 Btu/hr-in^2-°F.

Using a decay heat of 2.5 kW, the conditions for the hypothetical fire accident are:

Analysis Condition	Loads and Boundary Conditions
Initial steady-state (pre-fire)	• Solar Insolation • Combined convection (using the film coefficient for the cask surface, $0.00125\Delta T^{0.33}$ Btu/hr-in^2-°F) and radiation heat transfer (as defined in Section 3.2.3) between the cask exterior (ε=0.36) and the ambient (100°F) • The surface of the cask in contact with the impact limiter is adiabatic
Fire transient (during fire)	• Ambient temperature 1,475°F with no solar insolation • Combined convective (additional coefficient of 0.02446 Btu/hr-in^2-°F) and radiative heat transfer using a film coefficient (as defined in Section 3.2.3) between the cask exterior (ε=0.9), including the area normally covered by impact limiters, and the fire • Neutron shield fluid lost
Cool down (post-fire)	• Ambient temperature 100°F with solar insolation • Combined convection (using the film coefficient for the cask surface, $0.00125\Delta T^{0.33}$ Btu/hr-in^2-°F) and radiation heat transfer (as defined in Section 3.2.3) between the cask exterior (ε=0.36), including the area covered by the impact limiters, and ambient • Neutron shield fluid lost

3.5.3 Package Temperatures

The temperatures of the cask body resulting from the fire are determined using ANSYS. The heat load used in the transient thermal analysis corresponds to the PWR fuel, since its heat load envelopes all other fuel types that can be transported in the NAC-LWT cask.

The maximum temperatures of the basket and fuel for the different fuel types are determined using the results of the fire transient analysis of the cask body and the maximum temperature differences between the basket and fuel and the inner shell of the cask body as computed in the steady state thermal evaluations.

3.5.3.1 Evaluation for PWR Fuel Contents

The maximum temperatures of the cask body and principal components are evaluated using the ANSYS model described in Section 3.5.1.1. A radial temperature profile is obtained during the postulated 30-minute fire and for a cooldown period of 50 hours. The maximum cask component temperatures for the hypothetical accident are presented in Table 3.5-1.

Maximum time dependent temperatures of different cask components, before, during and after the fire, are shown in Figure 3.5-4 and Figure 3.5-5. The temperatures of the components show a sharp increase during the fire and a sharp decrease that begins right after the fire. After the 50 hour cooling period, the temperatures of the components do not return to the normal conditions of transport values. This is attributed to the loss of the liquid neutron shield during the accident, which results in the loss of the (liquid) convection heat transfer across the tank.

As noted above, the fuel and the fuel basket were not directly modeled in the ANSYS analysis. To determine the maximum temperature of the components inside the basket, the following method is applied:

$$T_{max} = Tis_{max} + \Delta T_{comp}$$

where:

Tis_{max} is the maximum temperature of the inner shell, obtained in the ANSYS transient thermal analysis.

ΔT_{comp} is the difference in maximum temperatures from Table 3.4-2 between the inner shell and the fuel basket outer wall or the fuel rod cladding during normal transport.

The maximum temperatures of fuel cladding and basket wall are:

Component	ΔT_{comp} (°F) [1]	Tis_{max} (°F) [2]	T_{max} (°F)
Fuel basket outer wall	2 (276-274)	505	507
Fuel cladding	198 (472-274)	505	703

[1] Temperatures from Table 3.4-2.

[2] Temperatures obtained in the ANSYS evaluation.

As a result, the maximum average cavity gas temperature can be taken as the average of the maximum basket wall and maximum fuel cladding temperatures. This produces an average cavity gas temperature of 605°F.

As shown in Table 3.5-1, all of the cask component temperatures are within the allowable temperature limit during the fire accident event.

3.5.3.2 Evaluation of MTR Fuel Contents

The temperatures in the MTR fuel basket and MTR fuel plates produced during the fire accident were determined using the two ANSYS finite element models of the NAC-LWT cask for MTR fuel element discussed in Section 3.4.1.3.2. The gas in the NAC-LWT cask cavity is considered to be air. Other conditions applied to the model are the same as those described in Sections 3.5.1 and 3.5.2 for the axisymmetric fire transient model with respect to the liquid neutron shield and outer surface boundary conditions. The accident thermal models for MTR fuel are shown in Figure 3.5-6 and Figure 3.5-7, for the design basis decay heat loading and the variable decay heat loading, respectively. The type, form, design or enrichment of the MTR fuel assemblies has no effect as long as the decay heat load and other fuel characteristics are in compliance with the requirements of Table 1.2-4. The presence and/or use of axial fuel spacers and spacer plates to position the fuel assemblies for ease of handling have no effect on the thermal analyses of the MTR basket assembly.

The transient calculation is performed to determine the maximum temperatures in the MTR fuel elements only for the variable decay heat loading because this is the worst-case condition. The cask model is used to determine the temperature history of the cask components, including the basket. The fuel element model is used to determine the temperature rise between the basket and the hottest point in the fuel element. The capacitance of the fuel element is negligible compared to the very large capacitance of the cask assembly. Therefore, a constant ΔT between basket and fuel is used. The temperature history for the MTR fuel variable heat load fire accident analysis is

shown Figure 3.5-8. The temperature profile within the cask model at the time of the maximum fuel temperature is shown in Figure 3.5-9. The bounding case is an element with 10 fuel plates, a decay heat of 120W and with worst-case dimensions. The maximum temperatures of the components are presented in Table 3.5-2. These results demonstrate that the maximum MTR fuel plate temperature for the variable decay heat loading is 473°F. The MIL-HDBK-5F Specification for 6061-T6 aluminum alloy indicates that the material retains more than 35% of its room temperature yield and ultimate strengths during transient exposure to temperatures as high as 500°F. Therefore, the reduction in strength for the fuel cladding as a result of the fire transient is minor when compared to the values presented in Section 3.4.1.3.3 for aluminum at 400°F. Since the fuel cladding temperatures are maintained significantly below 500°F, it is concluded that the structural integrity of the fuel cladding is maintained. Furthermore, the aluminum cladding of the MTR fuel elements is heated to a temperature of approximately 900°F during the fabrication process and it is clear that the cladding integrity is maintained during that process.

3.5.3.3 Evaluation of TRIGA Fuel Contents

The accident condition temperatures are obtained by applying the temperature differential calculated for the MTR fuel configuration to the TRIGA fuel configuration. To determine the TRIGA accident condition maximum cladding temperature, the temperature difference between the maximum basket temperatures for the normal and accident component temperatures calculated for MTR fuel in Section 3.5.3.2, is added to the maximum cladding temperature calculated for TRIGA fuel in Section 3.4.1.5.

The maximum basket temperature for the MTR fuel design basis heat load fire accident analysis is 374°F, as reported in Table 3.5-2. This temperature is 107°F higher than the normal condition maximum temperature (267°F) reported in Table 3.4-6. The corresponding maximum TRIGA fuel cladding temperature for the fire accident condition is reported in Table 3.5-3 to be 433°F. The MIL-HDBK-5F Specification for 6061-T6 aluminum alloy indicates that the material retains more than 35% of its room temperature yield and ultimate strengths during transient exposure to temperatures as high as 500°F. Therefore, the reduction in strength for the aluminum-clad TRIGA fuel cladding as a result of the fire transient is minor when compared to the values presented in Section 3.4.1.3.3 for aluminum at 400°F. Since the fuel cladding temperatures are maintained significantly below 500°F, it is concluded that the structural integrity of the aluminum-clad TRIGA fuel is maintained. The allowable temperature for stainless steel-clad TRIGA fuel is significantly higher.

The TRIGA fuel generates small amounts of fission gases during reactor operations, but it contains no initial charge of helium gas. Consequently, the internal pressure developed in the accident condition is less for TRIGA fuel than for the design basis PWR fuel.

3.5.3.4 Evaluation of TRIGA Fuel Cluster Rod Contents

The temperatures in the TRIGA fuel cluster rod basket and cladding produced during the fire accident were determined using the ANSYS finite element model of the NAC-LWT for the TRIGA fuel discussed in Section 3.4.1.6 for Condition 2 (air in the cavity and without the ISO container). The gas in the NAC-LWT cask cavity is considered to be air. Other conditions applied to the model are the same as those described in Sections 3.5.1 and 3.5.2 for the axisymmetric fire transient model with respect to the liquid neutron shield and outer boundary conditions.

The temperatures in the basket are bounded by the maximum temperatures of the fuel region. The temperature time history for the fuel region is shown in Figure 3.5-10. The maximum temperature of the clad was determined to be 394°F. This value is below the 800°F limit for the clad or the 400°F limit for the aluminum specified in Section 3.4.1.6. Therefore, the components are determined to be acceptable for the fire accident condition.

3.5.3.5 Evaluation for PWR and BWR High Burnup Fuel Rod Contents in a Rod Holder

The maximum temperatures of the principal components are evaluated using the ANSYS model described in Section 3.5.1.2. The maximum cask component temperatures for the hypothetical accident are identical to those presented in Table 3.5-1 since the bounding temperature history from the analysis of NAC-LWT PWR contents is used as a boundary condition for the analysis for PWR and BWR high burnup fuel rod contents.

Maximum time dependent temperatures of different components, before, during and after the fire, are shown in Figure 3.5-11. For the maximum time dependent temperatures of cask components see Figure 3.5-4 and Figure 3.5-5.

As a result, the maximum average cavity gas temperature for fire accident is calculated as the average of the air contained inside the basket. This produces an average cavity gas temperature of 695°F.

Table 3.5-4 shows the can weldment and fuel rod cladding temperatures during the fire accident event.

3.5.3.6 Evaluation of DIDO Fuel Contents

The DIDO fuel maximum heat load is bounded by the maximum heat load of the MTR fuel. Therefore, in the accident condition, the maximum temperatures of the cask components for the MTR contents will bound the maximum temperatures for the cask components for the DIDO

contents. It is conservative to use the results of the fire transient evaluated in Section 3.5.3.2 for the cask inner shell temperature. The maximum basket and fuel temperatures (T_{max}) for the DIDO fuel for the accident conditions are determined by adding the increase in steady state temperature from the cask inner shell to the maximum temperature of the component ($\Delta T_{component}$) to the maximum cask inner shell temperature ($T_{inner\ shell}$) obtained from the MTR evaluation. The maximum temperatures of the fuel cladding and basket wall are:

Component	$\Delta T_{component}$ (°F)	$T_{inner\ shell}$[1] (°F)	T_{max} (°F)
Fuel basket	146 = 327[2]-181	334	480
Fuel cladding	157 = 338[2]-181	334	491

[1] Obtained from Table 3.5-2 for the uniform heat distribution.
[2] Obtained from Table 3.4-12, Condition 2.

The fuel cladding temperature previously listed is bounded by those determined for the MTR contents. It is concluded that the structural integrity of the fuel cladding is maintained for the fire accident condition.

3.5.3.7 Evaluation for General Atomics Fuel Contents

The General Atomics fuel maximum heat load is bounded by the maximum heat load of the DIDO and MTR fuels. Therefore, in the accident condition, the maximum temperatures of the cask components for the MTR contents will bound the maximum temperatures for the cask components with General Atomics fuel. It is conservative to use the results of the fire transient calculation evaluated in Section 3.5.3.2 for the cask inner shell temperature. The maximum basket temperature (T_{max}) for the General Atomics fuel for accident conditions is determined by adding the increase in steady-state temperature from the cask inner shell to the maximum temperature of the component ($\Delta T_{component}$) to the maximum cask inner shell temperature ($T_{inner\ shell}$) obtained from the MTR evaluation. The maximum temperature of the basket is:

$$T_{max} = (250 - 214) + 334 = 370^{\circ}F$$

where:

334°F is the maximum temperature of the LWT inner shell during a fire accident

This temperature is bounded by those determined for the MTR contents. It is concluded that the structural integrity of the General Atomics basket and contents is maintained for the fire accident condition.

3.5.3.8 Evaluation of PWR and BWR High Burnup Fuel Rods in Fuel Assembly Lattice

The total heat load of the PWR and BWR high burnup fuel rods (up to 25 rods) in a fuel assembly lattice is bounded by that for the PWR and BWR high burnup fuel in a rod holder as evaluated in Section 3.5.3.5. Therefore, in the accident condition, the maximum temperatures of the cask components for the design basis PWR configuration bound the maximum temperatures for the PWR or BWR high burnup fuel rods in the fuel assembly lattice. The fuel cladding is expected to have the same difference in temperature between normal conditions and the accident fire conditions as determined in Section 3.5.3.5. The temperature difference for the fuel cladding between normal and accident conditions for the high burnup fuel in a rod holder is 118°F (1,014°F – 896°F). The maximum fuel cladding temperature is 664°F for high burnup fuel rods in a fuel assembly lattice for normal conditions of transport as evaluated in Section 3.4.1.10 (Table 3.4-14). Therefore, the maximum temperature of the fuel cladding for the 25 fuel rods in the fuel assembly lattice for accident conditions is 782°F (664°F + 118°F).

3.5.3.9 Evaluation of PWR and BWR High Burnup Fuel in a Rod Holder with Damaged Rods

The damaged fuel maximum heat load is equal to the maximum heat load of the PWR and BWR high burnup fuel rods. To determine maximum temperatures of the fuel configuration with damaged fuel rods in the fire accident condition, temperatures from the normal and accident conditions for the PWR and BWR high burnup intact fuel rods (Table 3.4-10 and Table 3.5-4) are used to determine the temperature differentials that are caused by the fire accident. The increase in temperatures is added to the maximum normal conditions temperature for the fuel rods in a rod holder with damaged rods (Table 3.4-15) to compute the maximum fire temperatures. The maximum temperatures of the fuel cladding and stainless steel rod holder are shown in Table 3.5-5. The maximum temperatures for the cask components are bounded by those for the design basis PWR fuel assembly configuration.

3.5.3.10 Evaluation of TPBAR Contents

The maximum heat load of TPBARs is bounded by the maximum heat load of the MTR fuel. Therefore, in the accident condition, the maximum temperatures of the cask components for the MTR contents will bound the maximum temperatures for the cask components for the TPBAR contents. It is conservative to use the results of the fire transient evaluated in Section 3.5.3.2 for the cask inner shell temperature. The maximum component temperatures (T_{max}) for the TPBARs for the accident conditions are determined by adding the temperature difference ($\Delta T_{component}$)

between the cask inner shell and the maximum component temperature for normal conditions to the maximum accident cask inner shell temperature ($T_{inner\ shell}$) obtained from the MTR evaluation. The maximum component temperatures are computed as follows.

Component	$\Delta T_{component}$ (°F)	$T_{inner\ shell}$[2] (°F)	T_{max} (°F)
TPBAR	68 (290[1]-222[1])	334	402
Aluminum Basket	6 (228[1]-222[1])	334	340
Consolidation Canister	23 (245[1]-222[1])	334	357
Gas (average)	24 (246[1]-222[1])	334	358

[1] See Table 3.4-16
[2] See Table 3.5-2

The maximum temperatures of the components are presented in Table 3.5-6.

3.5.3.11 Evaluation of PULSTAR Fuel Elements in 28 MTR Basket

As described in Section 3.4.1.13, the thermal performance of the configuration of PULSTAR fuel elements in the 28 MTR basket is bounded by the thermal performance of the TRIGA fuel cluster rods, condition 2. The temperatures in the TRIGA fuel cluster rod basket and cladding produced during the fire accident were determined and described in Section 3.5.3.4. The temperatures in the basket are bounded by the maximum temperatures of the fuel region. The temperature time history for the fuel region is shown in Figure 3.5-11. The maximum temperature of the cladding was determined to be 394°F. This value is below the 1,058°F limit for the fuel cladding. Therefore, the components for PULSTAR fuel elements in the 28 MTR baskets are determined to be acceptable for the fire accident condition.

3.5.3.12 Evaluation of ANSTO Fuels

The maximum heat load of the spiral fuel assemblies (0.756 kW per cask) is bounded by the maximum heat load of the MTR fuel (1.05 kW per cask). Therefore, in the accident condition, the maximum temperatures of the cask components for the MTR contents will bound the maximum temperatures for the cask components for the ANSTO basket contents. It is conservative to use the results of the fire transient evaluated in Section 3.5.3.2 for the cask inner shell temperature. The maximum basket and fuel temperatures (T_{max}) for the ANSTO fuel contents for the accident condition are determined by adding the temperature difference ($\Delta T_{component}$) between the maximum temperature of the cask inner shell and the component (basket or fuel) for the normal condition to the maximum cask inner shell temperature ($T_{innershell}$)

for the accident condition obtained from the MTR evaluation. The maximum temperatures of the fuel cladding and basket are computed as follows.

Component	$\Delta T_{component}$ (°F)	$T_{innershell}$[1] (°F)	T_{max} (°F)
Fuel basket – MOATA Plate Fuel	8 = 230[2]-222[2]	334	342
Fuel cladding – MOATA Plate Fuel	11 = 233[2]-222[2]	334	345
Fuel basket – Mark III Spiral Fuel	26 = 248[2]-222[2]	334	360
Fuel cladding – Mark III Spiral Fuel	28 = 250[2]-222[2]	334	362

[1] Obtained from Table 3.5-2 for the uniform heat distribution
[2] Obtained from Table 3.4-22

3.5.4 Maximum Internal Pressure

3.5.4.1 Maximum Internal Pressure for Design Basis Fuel in Accident Conditions

The accident internal pressure is calculated assuming an accident with 100 percent fuel rod failure combined with the design basis fire described in 10 CFR 71. The fuel rod failure assumes 30 percent of the fission gas and 100 percent of the backfill gas escapes the ruptured fuel rods.

The internal pressure due to the 100 percent fuel rod rupture is calculated using the method described in Section 3.4.4. The total cask pressure of the cask backfill and failed fuel rods is calculated by a two step procedure. First, the pressures documented under normal conditions in Section 3.4.4 are adjusted to include the increased total free volume associated with 100% fuel rod failure. Then, the revised cask pressure at normal operating temperature is adjusted to accident condition temperatures.

Adjusting the partial pressure of the cask backfill:

$$P_{cask} = P_{initial}\left(\frac{V_{cask}}{V_{total}}\right)$$

where:

$P_{initial}$ = 25.8 psia (normal condition temperature adjusted cask backfill pressure)

V_{cask} = 5.196 ft^3 (147,134 cm^3) [Section 3.4.4]

$V_{rod\ void}$ = 8,123 cm^3 [Section 3.4.4]

V_{total} = 155,257 cm^3 (V_{cask} + $V_{rod\ void}$)

$$P_{cask} = 25.8 \text{ psia} \left(\frac{147{,}134 \text{cm}^3}{155{,}257 \text{cm}^3} \right)$$

$$P_{cask} = 24.4 \text{ psia}$$

Adjusting the partial pressure of the fuel rod backfill and fission gases:

$$P_{fuel\ rods} = P_{initial} \left(\frac{V_{rod\,void}}{V_{total}} \right)$$

where:

$P_{initial}$ = 1,521.3 psia (fuel rod backfill pressure of 989.8 psia plus fission gas pressure of 0.30 x 1771.5 psia)

$V_{rod\ void}$ = 8,123 cm^3

V_{total} = 155,257 cm^3

$$P_{fuel\ rods} = 1{,}521.3 \text{ psia} \left(\frac{8{,}123.28 \text{cm}^3}{155{,}257 \text{cm}^3} \right)$$

$$P_{fuel\ rods} = 79.6 \text{ psia}$$

Summing the two partial pressures yields the total cask pressure at normal operating condition temperature:

$$P_{Total} = P_{cask} + P_{fuel\ rods}$$

$$P_{Total} = 24.4 \text{ psia} + 79.6 \text{ psia}$$

$$P_{Total} = 104.0 \text{ psia}$$

The fuel cladding has the highest temperature of any barrier with which the gas comes in contact during a design basis fire. As shown in Section 3.5.3.1, the maximum average cavity gas temperature is 605°F during the fire accident condition. For conservatism, a temperature of 667°F is used in the calculation of the maximum accident condition internal pressure. Given that the internal volume of the NAC-LWT Cask remains constant during the fire, the resultant pressure is proportional to the temperature change according to the ideal gas law:

$$P_2 = P_1 \left(\frac{T_2}{T_1} \right)$$

Thus, for the design basis fire:

$$P_{fire} = 104.0 \text{ psia} \left(\frac{1127^\circ R}{932^\circ R} \right)$$

$$P_{fire} = 125.8 \text{ psia}$$

3.5.4.2 High Burnup Fuel Rod Canister Maximum Internal Pressure

The high burnup fuel rod canister maximum internal pressure in the accident conditions is calculated assuming 100 percent fuel rod failure combined with the design basis fire maximum temperature. The fuel rod failure assumes release of 30 percent of the fission gas and 100 percent of the backfill gas.

The canister internal pressure is calculated using the method described in Section 3.4.4.2, with the BWR used as the bounding fuel type for the analysis. The total canister pressure is calculated in two steps. First, the pressures documented under normal conditions in Section 3.4.4.2 are adjusted to include the increased total free volume associated with 100 percent fuel rod failure. Then, the canister pressure is adjusted to account for the accident condition temperature.

The partial pressure of the canister volume is calculated by:

$$P_{canister} = P_{initial} \left(\frac{V_{canister}}{V_{total}} \right)$$

where:

$P_{initial}$ = 29.3 psia (from earlier)

$V_{canister}$ = 28.2 liters (from earlier)

V_{void} = 0.079 liter (from earlier)

V_{void} = $25*V_{void} + V_{canister}$ = 30.2 liters

V_{total} = 30.2 liters

Therefore, $P_{canister}$ is equal to 27.4 psia. The partial pressure of the fuel rods is calculated by:

$$P_{fuel\ rods} = P_{initial} \left(\frac{V_{fuel\ rods}}{V_{total}} \right)$$

where:

$P_{initial}$ = 1,425 psia (earlier from Section 3.4.4.2)

$V_{fuel\ rods}$ = $25*V_{void}$

$V_{fuel\ rods}$ = ~1.97 liters (at 100% of the total fuel rod volume)

V_{total} = 30.2 liters ($V_{canister}$ + (25*V_{void}))

then:

$$P_{fuel\ rods} = 1{,}425\ \text{psia}\left(\frac{1.97\ \text{liters}}{30.2\ \text{liters}}\right) = \sim 94\ \text{psia}$$

and

$$P_{total} = P_{canister} + P_{fuel\ rods} = 27.4\ \text{psia} + \sim 94\ \text{psia} = \sim 121\ \text{psia}\ (\sim 8.2\ \text{atm})$$

For the 100% fuel rod failure and the design basis fire accident temperature of 725°F, the pressure is calculated by multiplying the 100% rod failure pressure by the inverse ratio of the normal condition temperature (588.7 K) to the accident temperature (658.15 K). The pressure thus calculated is 135 psia (~9.2 atm)

3.5.4.3 25-Rod Maximum Internal Pressure-Cask Cavity

Using the same methodology used to calculate the cavity pressure in Section 3.5.4.2, the pressure from the 100% fuel rod failure and the design basis fire accident temperature of 725°F is calculated using the cask cavity free gas volume (89.32 liters from earlier). The resulting pressure in the cask cavity, assuming that the gases within the canister are released to the cask cavity, is 67 psia (~4.5 atm).

3.5.4.4 TPBAR Shipment Cask Cavity Internal Pressure-Accident Conditions

Employing the normal condition TPBAR result in Section 3.4.4.5 of 276 psig for the 300 production TPBAR content condition and adjusting system pressure to the average accident gas temperature of 358°F yields a maximum accident condition pressure of 322 psig. For a period of one year following the 90-day cooldown, the pressure for this content condition increases to 337 psig.

Utilizing the same assumptions as presented in Section 3.4.4.5 and the post-accident thermal conditions discussed above, the pressure for the 55 segmented TPBARs in the waste container will be less than 75 psia and, therefore, bounded by the 300 TPBAR content condition.

3.5.4.5 Maximum Internal Pressure for PULSTAR Fuel Payload

Maximum internal pressures under accident conditions are calculated using the same methodology as that employed in Section 3.4.4.6. The accident condition temperature is set to

394°F, and 100 percent of the fuel rods are assumed to fail. The resulting calculated pressures are summarized as follows.

Description	Free Volume (liters)	Pressure (atm)	Pressure (psia)	Pressure (psig)
Cask Pressure -28 Intact Assemblies	217.0	2.3	34.0	19.3
Cask Pressure -14 Intact Assemblies and 14 Cans	233.0	2.4	35.4	20.7
Can Pressure - PULSTAR Failed Fuel Can	1.53	5.0	73.9	59.2

3.5.5 Maximum Thermal Stresses

The most severe thermal stress conditions that occur during the fire test and subsequent cooldown have been evaluated. For conservatism, an internal pressure of 168 psig is used, in the analysis that is performed in Section 2.7.3. The temperatures corresponding to the maximum thermal stresses are reported in Table 3.5-1.

3.5.6 Evaluation of Package Performance for Hypothetical Accident Thermal Conditions

The NAC-LWT cask thermal performance has been assessed for the hypothetical accident, as specified in 10 CFR 71. The O-rings and the lead gamma shields remain within their safe operating ranges. The cask does not suffer any adverse structural consequences as a result of the thermal considerations of the hypothetical accident. The NAC-LWT cask maintains containment and does not exceed the dose rate limits of 49 CFR 173 as a result of the hypothetical accident.

3.5.7 Assessment of the Effects of the Fission Gas Release in the Fire Accident Condition

During the fire, the release of the fission gas is expected to reduce the effective thermal conductivity of the gas in the cavity or inside the sealed canisters. To assess the reduction of the thermal conductivity, the helium conductivity is factored by the ratio of the conservative initial fill pressure of 565 psia (Section 3.4.4) for the PWR fuel assemblies and the end of life pressure (which contains the fill gas plus the fission gas release) of 1,521 psia (Section 3.5.4). This ratio is computed to be 0.37. A conservative ratio of 0.24 is applied to the conductivity of helium, assuming that all fission product gases have a conductivity of zero.

For the temperatures shown, which envelope the maximum temperatures of the cavity gas in the accident condition, the reduced helium properties are larger than the thermal conductivity of air. This is bounding because, as shown in Table 4.2-2, the volume of fission product gas produced by the design basis PWR assembly is higher than that for any other fuel loading.

The data below (Krieth) reflects the comparison of the air conductivity and the factored helium conductivity.

Temperature (°F)	Air Conductivity (K_{air}) (Btu/hr-in-F)	Helium Conductivity (Btu/hr-in-F)	Factored Helium Conductivity (K_{He}) (Btu/hr-in-F)	Ratio K_{He}/K_{air}
300	0.00161	0.00883	0.00212	1.32
400	0.00177	0.00958	0.00230	1.30
500	0.00193	0.01017	0.00244	1.26
600	0.00208	0.01075	0.00258	1.24
700	0.00223	0.01113	0.00267	1.20
800	0.00238	0.01150	0.00276	1.16

The analyses performed for the contents employed air as the gas in the cavity and containers for the accident condition. This demonstrates that the evaluation of the accident condition using air bounds the "reduced helium properties" case.

Figure 3.5-1 Transient Thermal Analysis Finite Element Model of the NAC-LWT

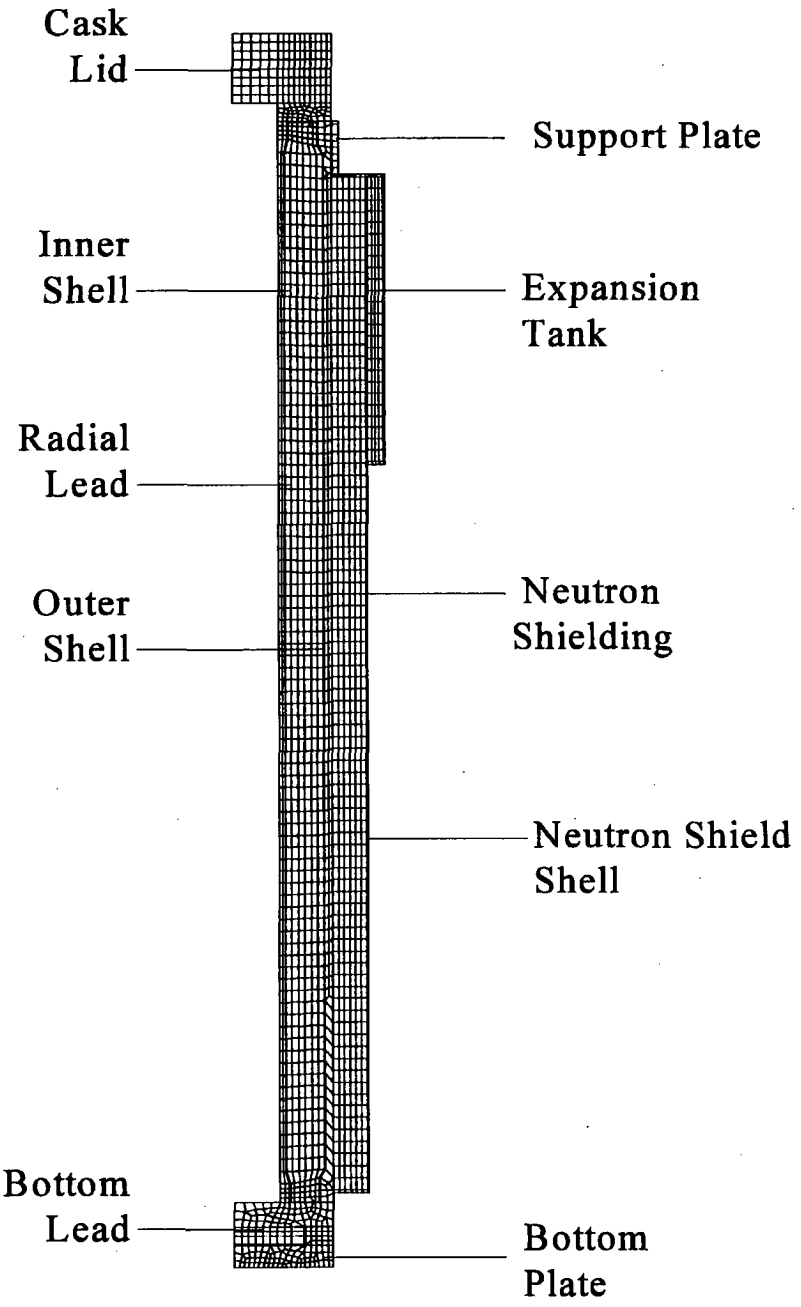

Figure 3.5-2 Top Region of the ANSYS Model

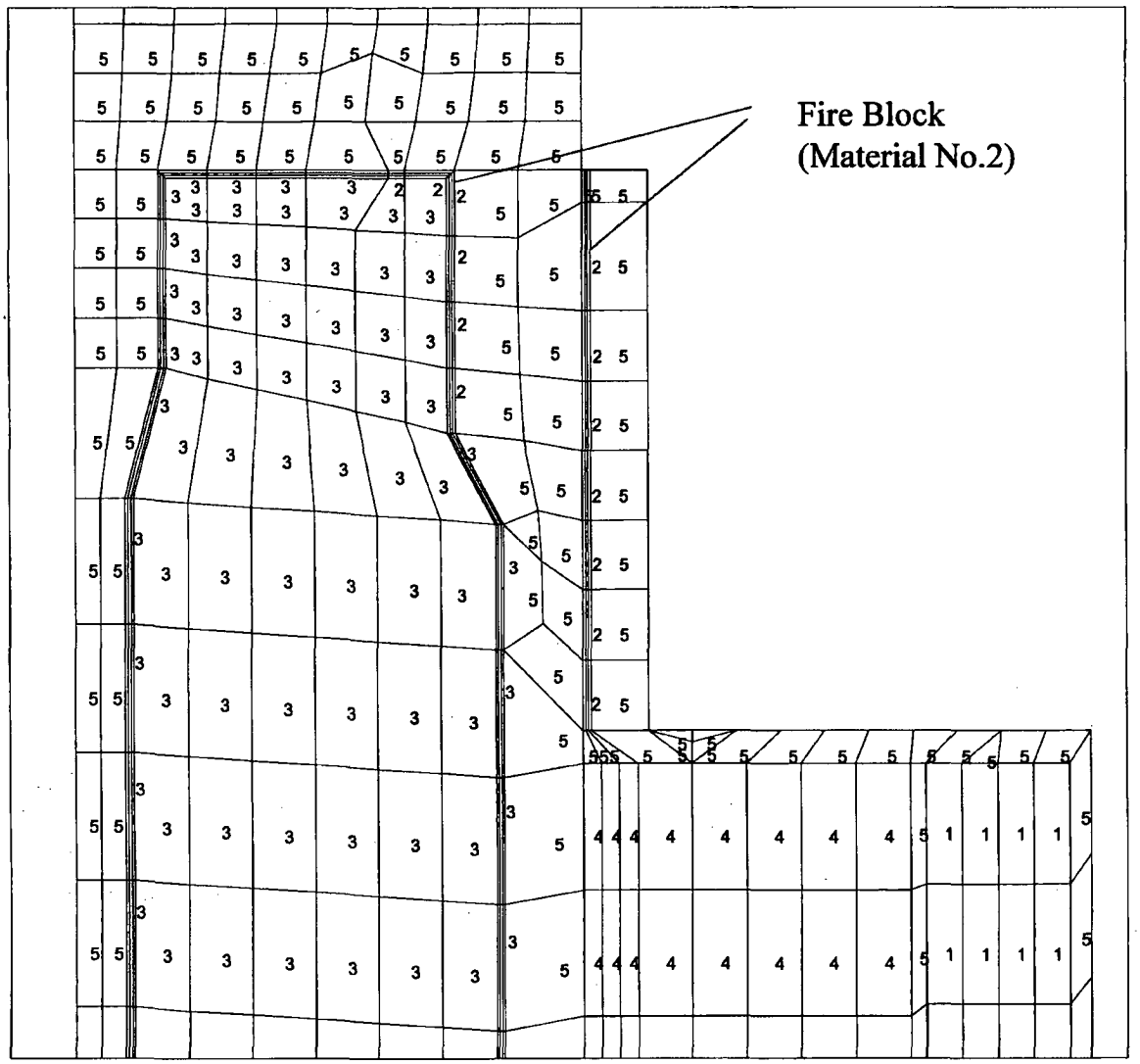

Note: Fire Block is either BISCO FPC or UNIFRAX Fiberfrax Ceramic Fiber Paper

Figure 3.5-3 Bottom Region of the ANSYS Model

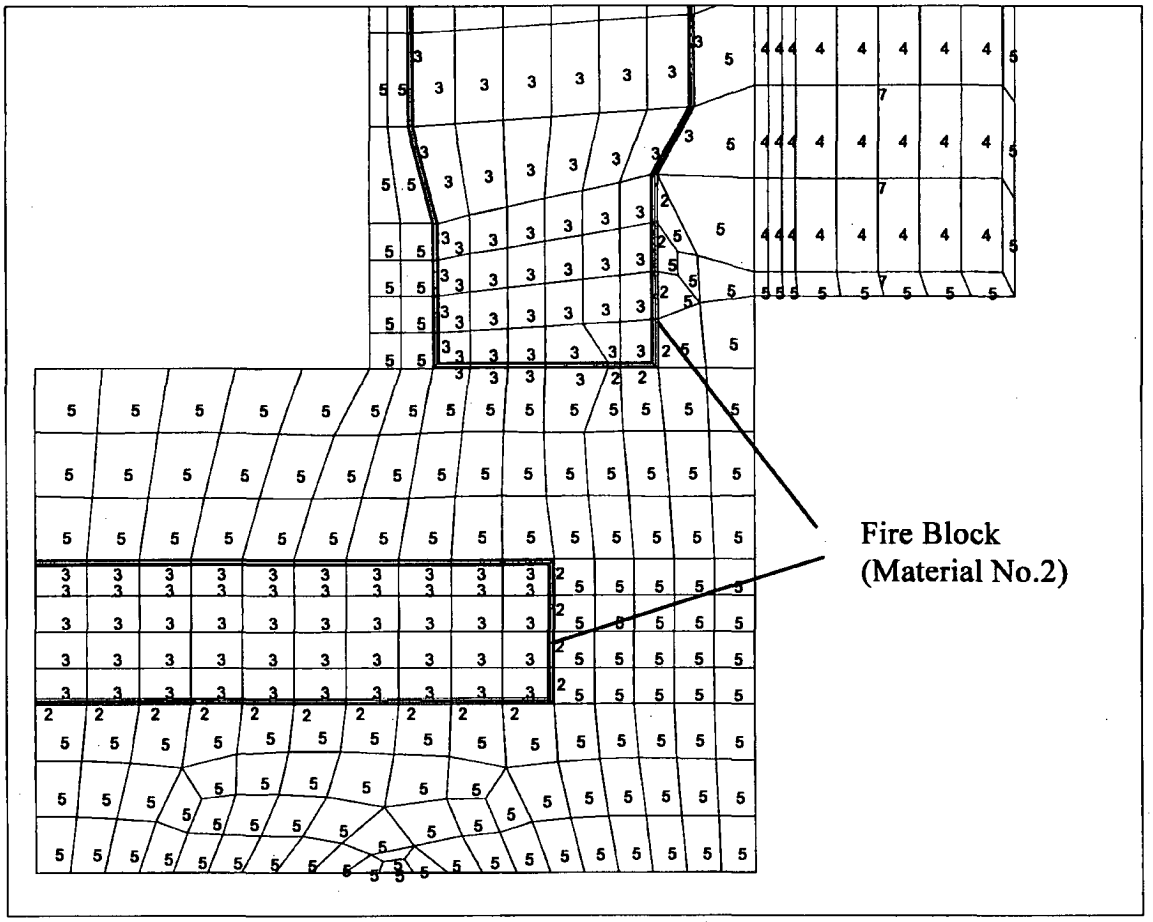

Note: Fire Block is either BISCO FPC or UNIFRAX Fiberfrax Ceramic Fiber Paper

Figure 3.5-4 Temperature History of NAC-LWT O-Rings and Valves in the Hypothetical Fire Event

1. Temperature of the Valves
2. Temperature of the O-Rings

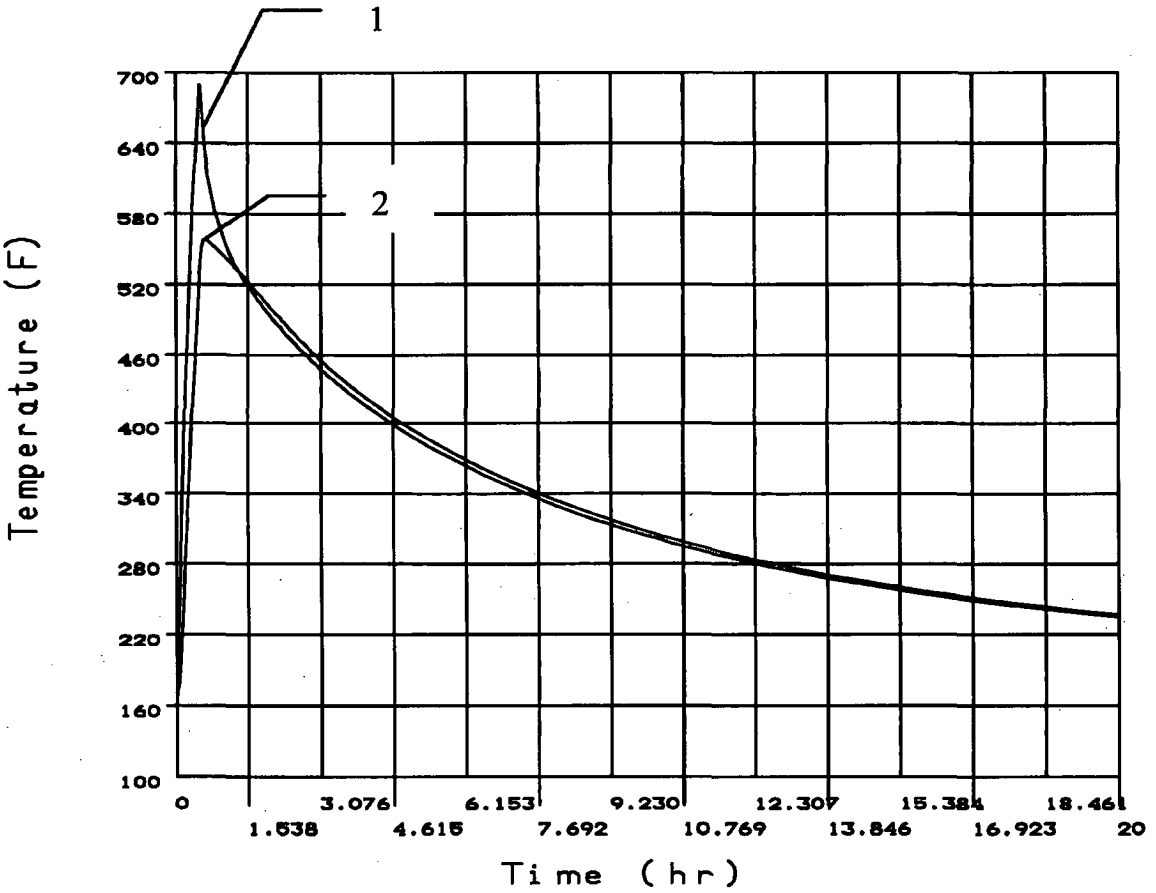

Figure 3.5-5 Temperature History of NAC-LWT Components in the Hypothetical Fire Event

1. Temperature of the Cask Outer Surface
2. Temperature of the Neutron Shield
3. Temperature of the Radial Lead Gamma Shield
4. Temperature of the Bottom Lead Gamma Shield
5. Temperature of the Inner Stainless Steel Shell

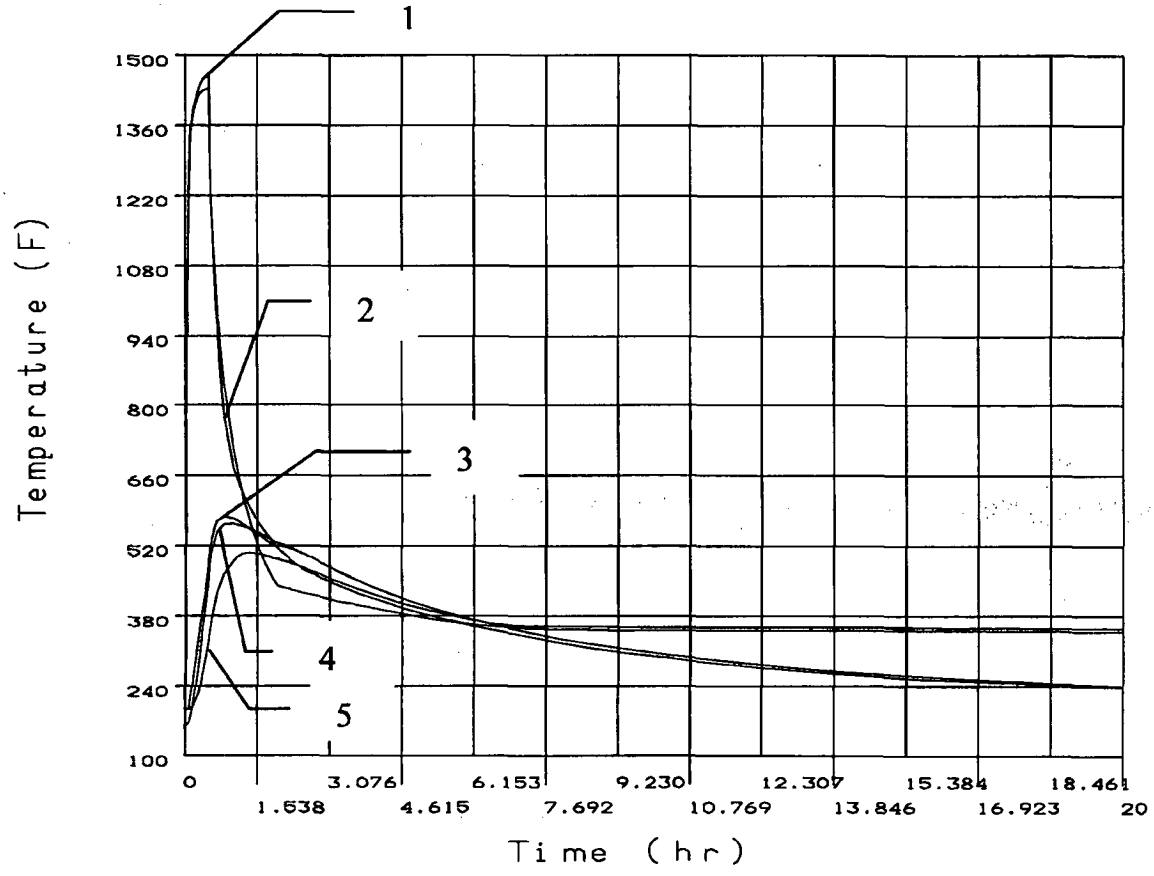

Figure 3.5-6 MTR Fuel Design Basis Heat Load Fire Accident ANSYS Thermal Model (Uniform 30-Watt/Element Configuration Heat Load)

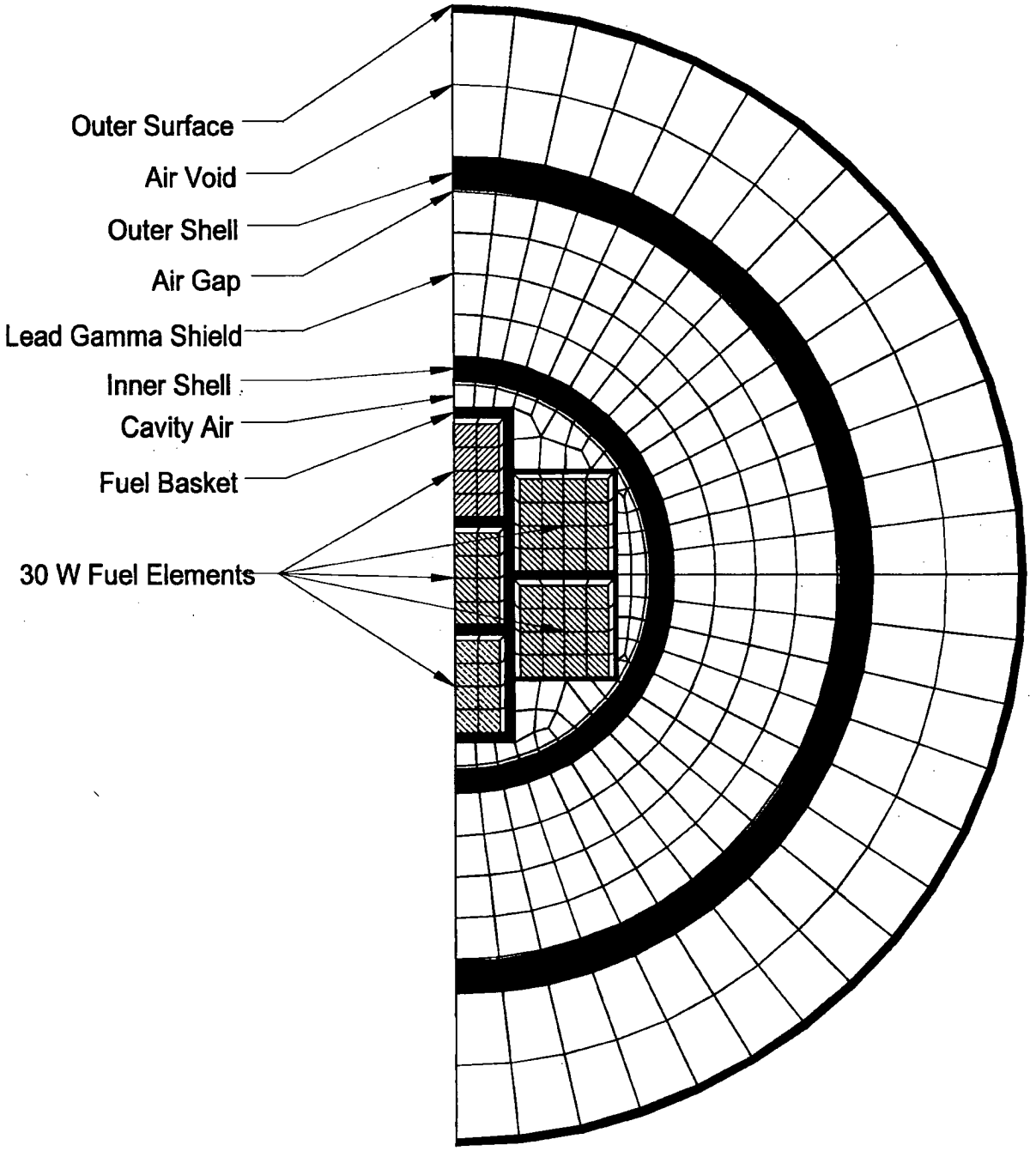

Figure 3.5-7 MTR Fuel Variable Heat Load Fire Accident ANSYS Thermal Model (120-Watt/70-Watt/20-Watt Configuration Heat Load)

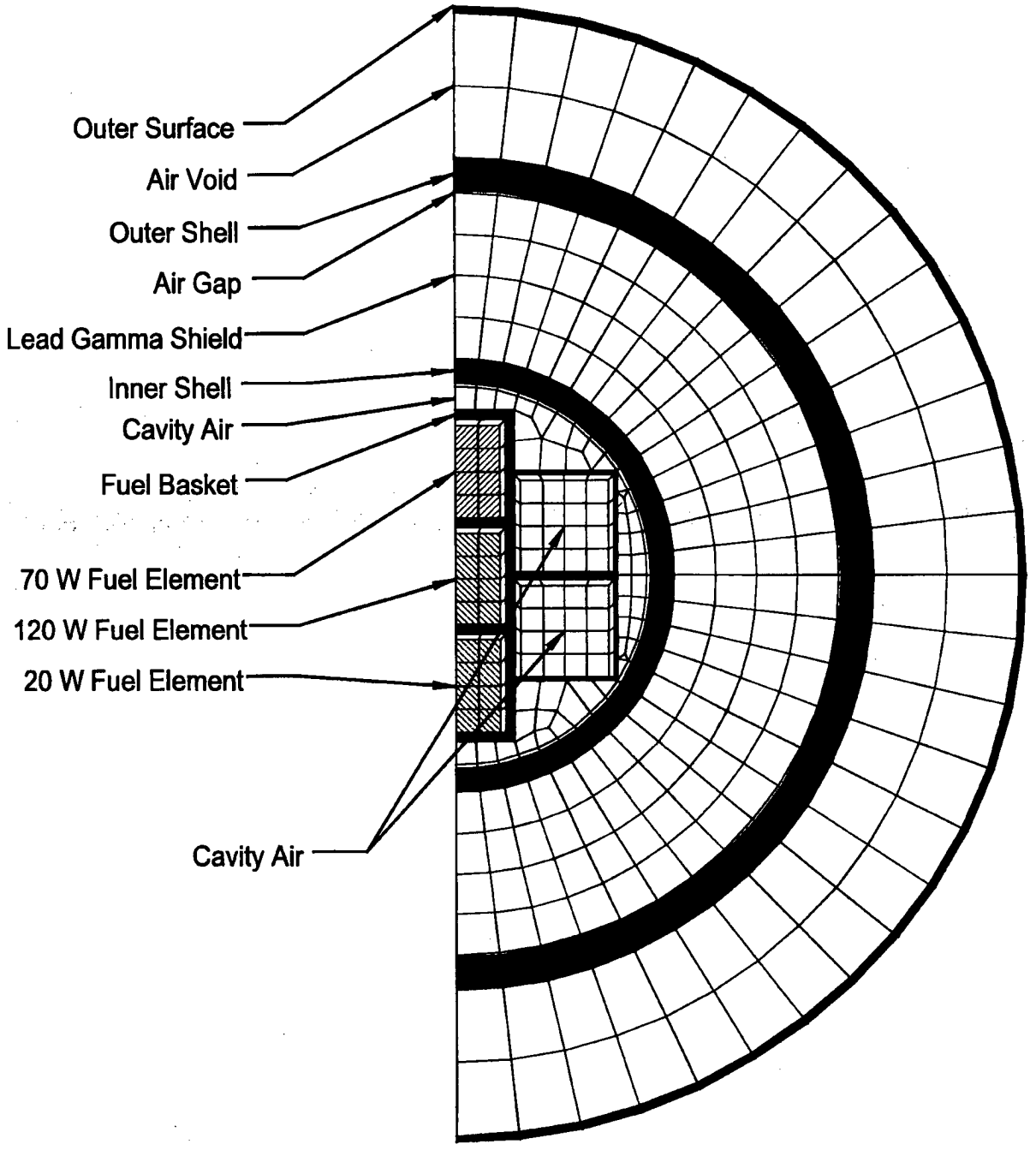

Figure 3.5-8 Temperature History in the MTR Fuel Variable Heat Load Fire Accident Analysis

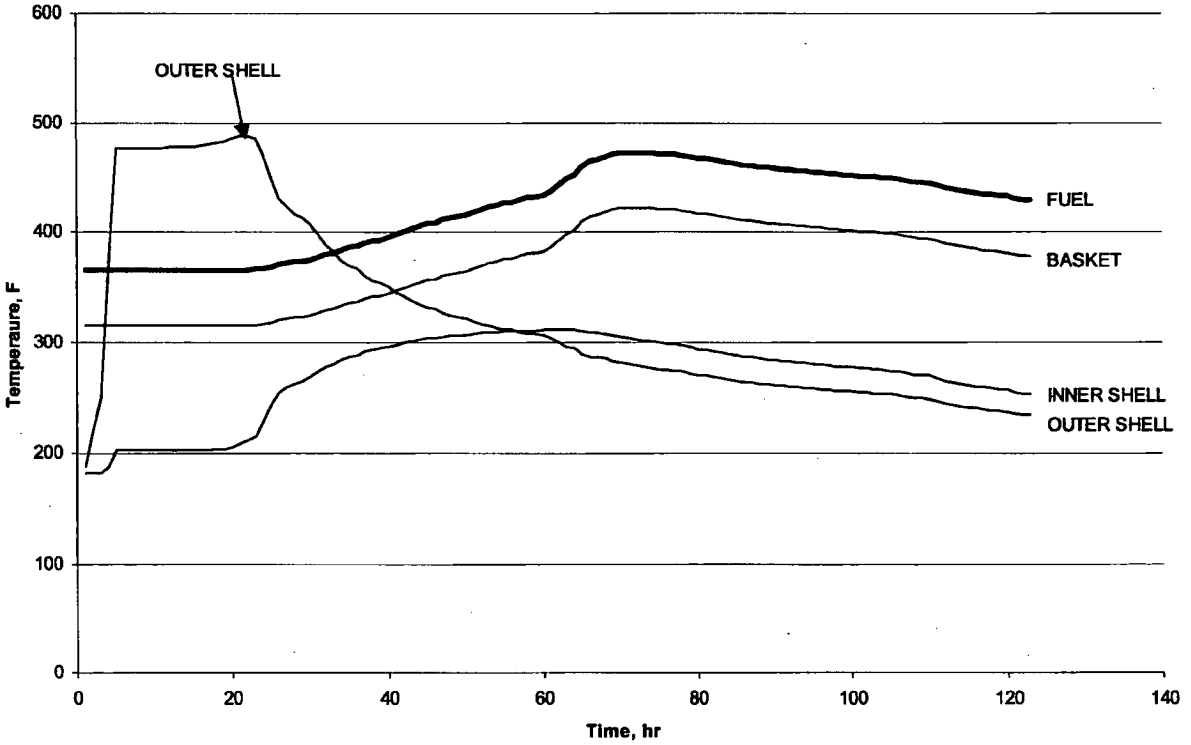

Note: 120-Watt / 70-Watt / 20-Watt Configuration Heat Load. Cavity gas is air with fire applied to cask surface.

Figure 3.5-9 Location of the Maximum Temperature in the MTR Fuel Variable Heat Load

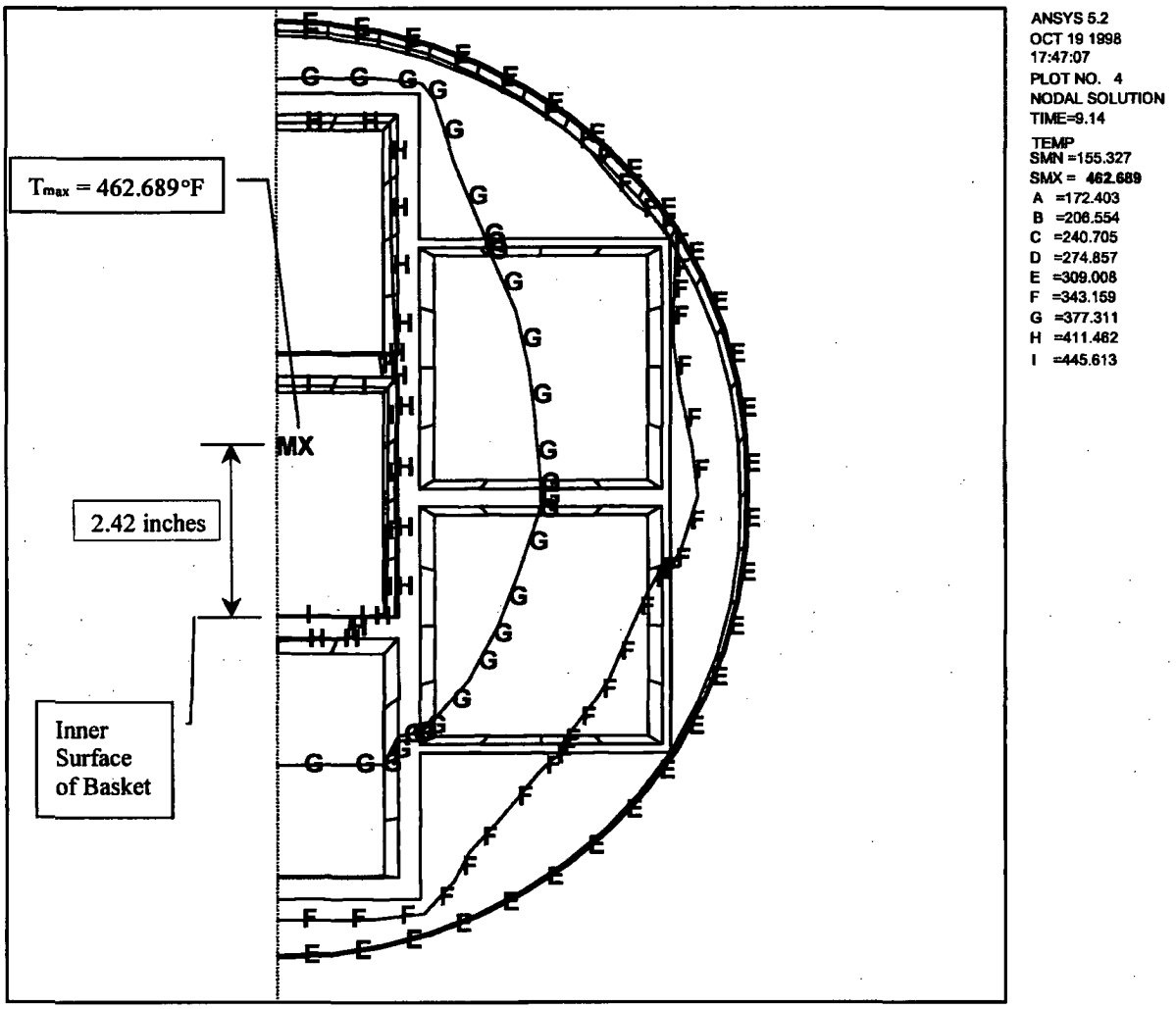

Figure 3.5-10 Temperature History for the TRIGA Fuel Cluster Rods Design Basis Heat Load Fire Accident Analysis

(Uniform 30 watt/basket cell or 210 watt/basket section or 1.05 kW total heat load)
(Cavity gas: Air, Fire is Applied to the Cask Surface)

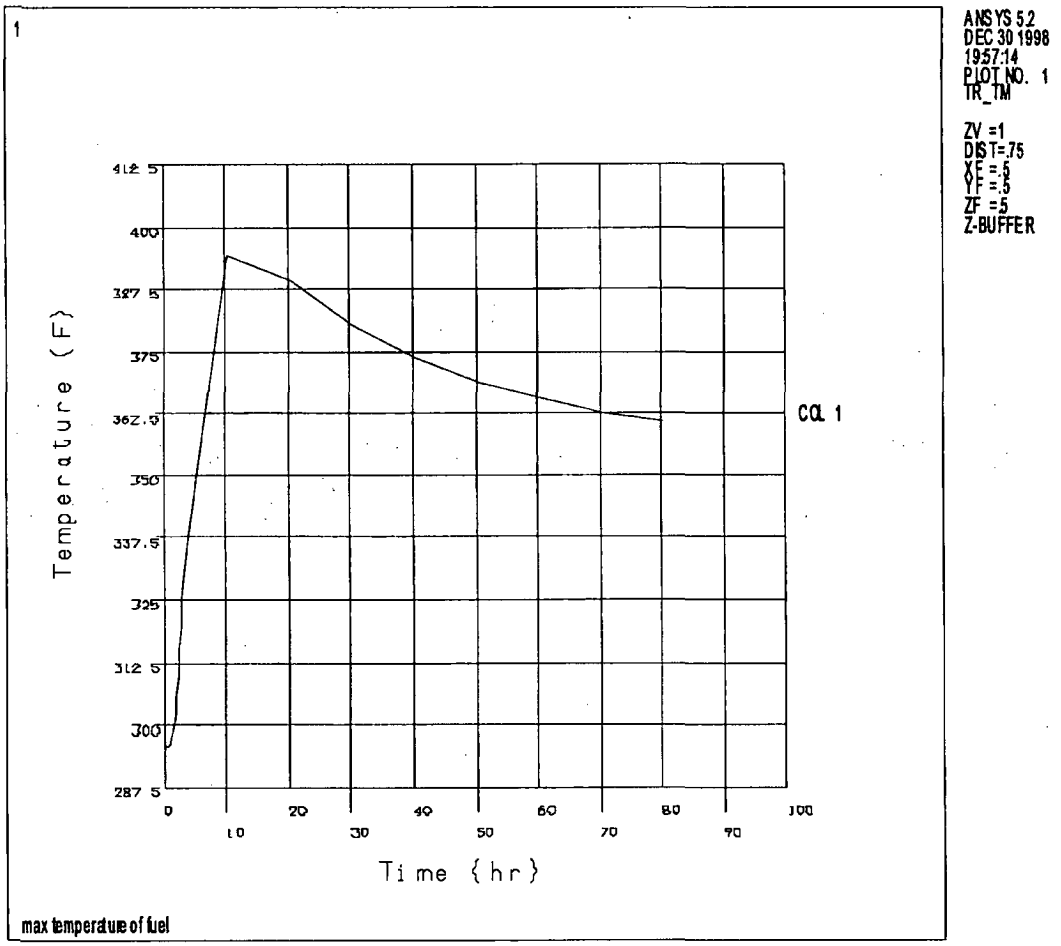

Figure 3.5-11 Temperature History of NAC-LWT Cask Components with PWR and BWR High Burnup Fuel Rods in the Hypothetical Fire Event

1. Average Temperature of Cask Cavity Gas
2. Temperature of the Fuel Cladding
3. Temperature of the Can Weldment
4. Temperature of the Aluminum Structural Component
5. Temperature of the Pin Tube

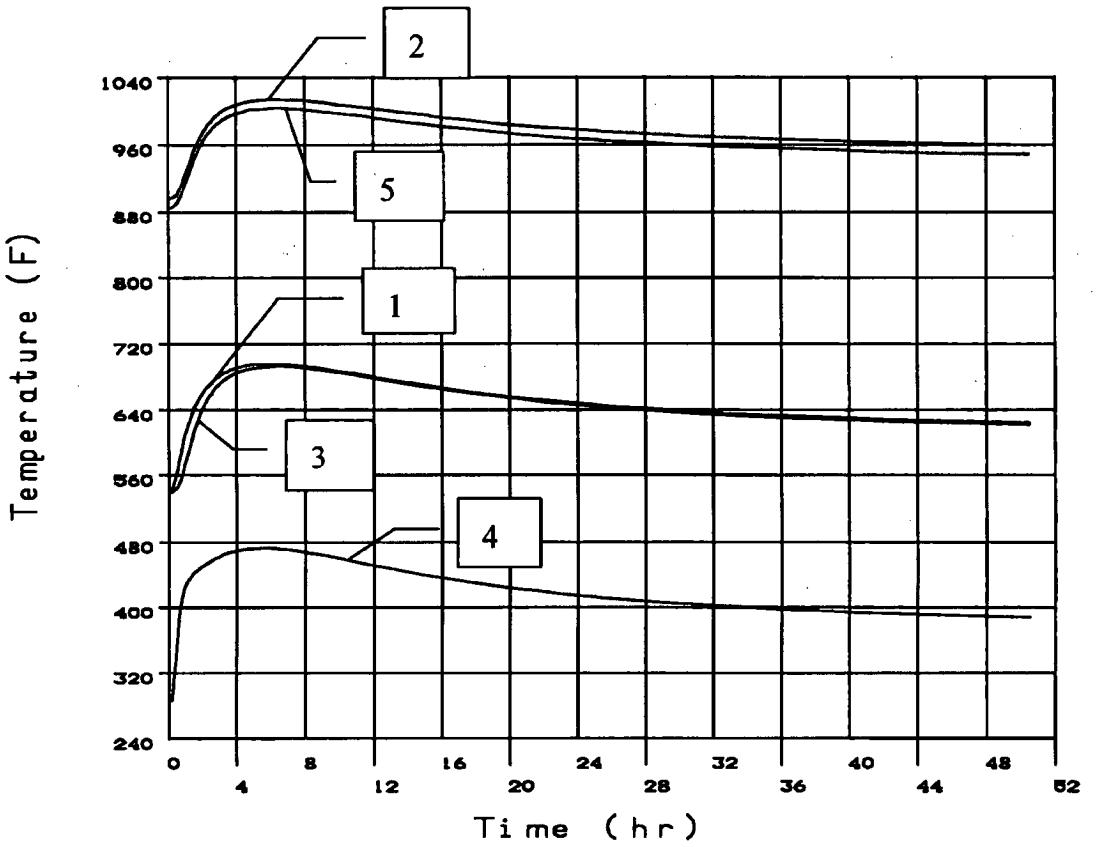

Figure 3.5-12 End of Fire Temperatures of the Alternate Port Cover Components

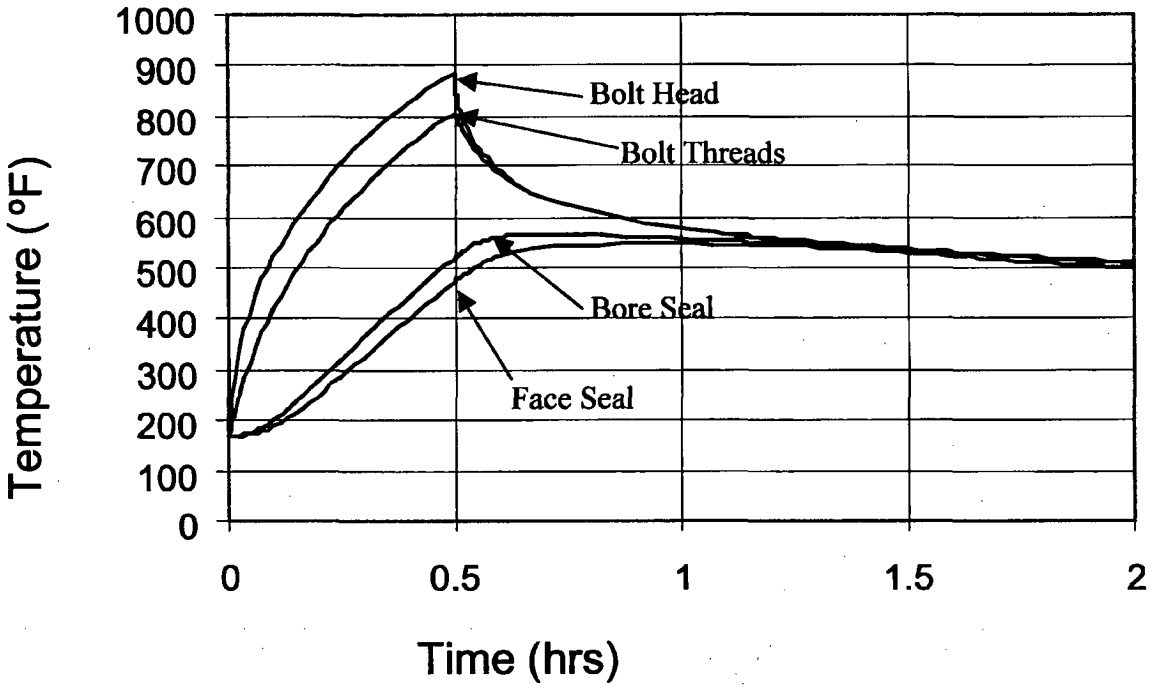

Figure 3.5-13 Transient Temperatures of the Alternate Port Cover Components

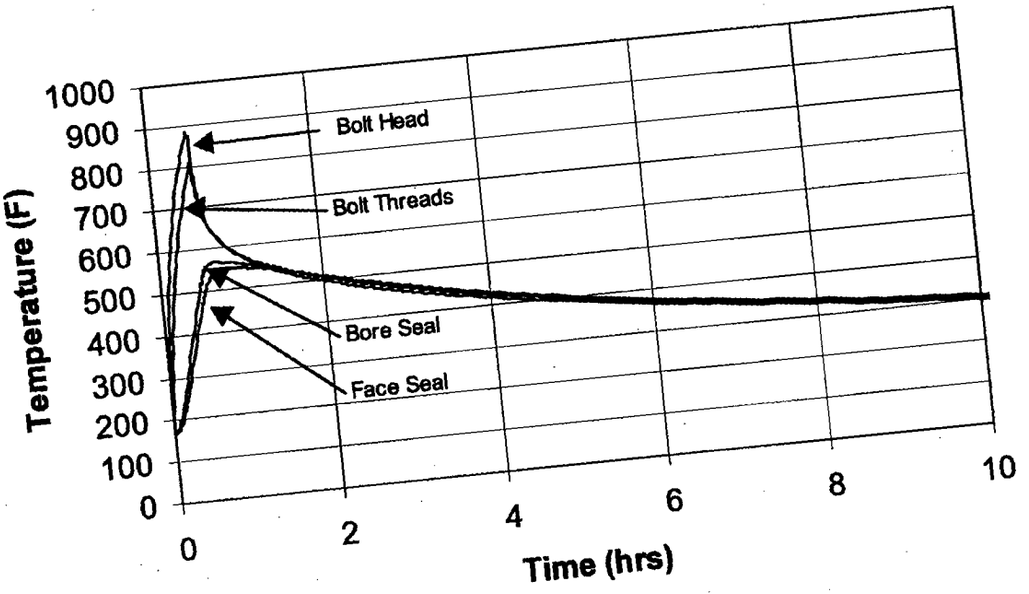

Table 3.5-1 Maximum Component Temperatures (°F) During the Fire Accident (Design Basis PWR Fuel, 2.5 kW Heat Load)

Component	Calculated Temperature	Temperature Limit
O-rings: TFE	558	735
Metallic	571[3]	800
Cask radial outer surface	1460	—[1]
Neutron shield region	1435	—[1]
Radial lead gamma shield	578	600
Bottom lead gamma shield	564	600
Inner stainless steel shell	505	800
Fuel basket outer wall	507	700[2]
Fuel rod cladding	703	1058
Alternate Port Cover	–	–
Bolt head	886	900
Bolt threads	807	900
Port cover O-ring – bore	565[4]	550
Port cover O-ring – face	547	550

Notes:

1. No upper limit established.
2. The primary consideration in establishing the safe operating range of the aluminum is maintaining the integrity of the aluminum. According to MIL-HDBK-5F, it can be shown that aluminum at 700°F retains component performance.
3. The maximum port cover seal temperature is conservatively used to bound the maximum temperature of the metallic seal.
4. Should the bore seal fail post-fire accident, containment would not be breached.

Table 3.5-2 MTR Fuel Fire Accident Maximum Temperatures (°F), 10 Fuel Plate/120W Element Case (Bounding Configuration)

Condition 2: NAC-LWT (Transported via Truck Trailer)
Cavity Gas: Air

Component	Design Basis Heat Loading*	Variable Decay Heat Loading**
Cask Radial Outer Surface	***	***
Lead Shield	***	***
Inner Shell	334	337
Fuel Basket	374	420
Fuel Cladding	385	473

* Uniform 30-Watt/Element Configuration Heat Load.

** 120-Watt/70-Watt/20-Watt Configuration Heat Load.

*** The maximum temperatures for these components are bounded by the design basis reported.

Table 3.5-3 TRIGA Fuel Fire Accident Maximum Temperatures (°F)

Component	Temperature
Fuel Basket	374
Fuel Cladding	433

Table 3.5-4 PWR and BWR High Burnup Fuel Rods Fire Accident Maximum Temperatures (°F)

NAC-LWT (Transported via Truck Trailer)
Cavity Gas: Air

Component	Temperature
Stainless steel Can Weldment	692
Fuel rod cladding	1,014

Table 3.5-5 Maximum Component Temperatures for High Burnup Fuel Rods in a Rod Holder with Damaged Fuel Rods for the Fire Accident

Component	Normal Conditions Temperature[1] (T_{norm})(°F)	Temperature Difference (ΔT) (°F)	Accident Temperature $T_{acc} = T_{norm} + \Delta T$(°F)
Rod Holder Weldment	567	692[2] – 538[3] = 154	721
Fuel Cladding	809	1014[2] – 896[3] = 118	927

[1] Table 3.4-14.
[2] Table 3.5-4.
[3] Table 3.4-10, Condition 2.

Table 3.5-6 TPBAR Fire Accident Maximum Temperatures

Component	Temperature (°F)
TPBARs	402
Aluminum Basket	340
Consolidation Canister	357

3.6 Failed Metallic Fuel Basket – SCOPE Evaluations

The SCOPE thermal analysis computer program is used to evaluate the NAC-LWT cask containing the 2.75-inch inner diameter (I.D.) failed fuel can liner and six 2.75-inch I.D. failed fuel cans loaded with one metallic fuel rod each for a total heat load of 30 watts.

Figure 3.6-1 and Figure 3.6-2 present the input data and the resulting calculated temperatures from the SCOPE analysis. The calculated temperature for the failed fuel can and the liner (basket) is 214°F.

A SCOPE analysis has also been performed for the 4.0-inch I.D. failed fuel can liner (3-hole basket) and three 4.0-inch I.D. failed fuel cans loaded with three metallic fuel rods each, for a total heat load of 45 watts.

Figure 3.6-3 and Figure 3.6-4 present the input data and the results form the SCOPE analysis for transport of nine failed fuel rods. The maximum calculated temperature for the failed fuel can in the nine failed fuel rod configuration is 229°F.

Figure 3.6-1 Failed Fuel Basket SCOPE Input

```
S C O P E  INPUT (IN CARD-IMAGE FORMAT) FOLLOWS:

Evaluation of NAC LWT Containing 6 Failed Fuel Rods (30 WATTS TOTAL HEAT LOAD)
' ==========================================================================
' NELEM   BURNUP    TIME    WHEAT    DHEAT    SRCN    SRCG     ITYPE   NPINS
   21     1600       2       0.0      5.0    6.31+4  1.12+14    1       1
'
' NCAN    ODCAN    TKCAN    HTCAN    HTVOID    HTFUEL
   5       3.0     0.125    12.00      0        12.00
'
' NINSRT    EMINSRT    TKINSRT    TPOISN      TKCGAP    TKIGAP    WTHICK
   5        0.22         0.01       0.0        -0.01      3.75      0.0
'
' NELEM    CASKID
   6        13.375
'
' NISHL  NOSHL  NOLIN  NPIN       TKISHL  TKOSHL  TKOLIN       NGSHLD
   6      6      6     6           0.75     1.2    0.236          1
'
' SPPIN    EMISF    EMISC    TPWMAX    WGHTMX
   1       0.587     0.50      750       200
'
' KTRANS    RHONS    TCNS1    TCNS2    CPNS2
   6        0.071    0.0154   0.0154    0.24
'
' GENERAL FORMAT FOR SHIELDING DATA:
' LTYPE, NUMPTS, (NASSYS(I,LTYPE),TKG(I,LTYPE),TKN(I,LTYPE), I=1,NUMPTS)
' ---------------------------------------------------------------------
'
' SHIELDING DATA FOR 5.75-INCH PB-METAL CASKS
' (ASSUMES A 5-INCH NEUTRON SHIELD)
1 1  6 5.75  5.0
' ---------------------------------------------------------------------
' TERMINATION FLAG (FOR THIS PARTICULAR CASE):
0
```

Figure 3.6-2 Failed Fuel Basket SCOPE Output

```
TITLE:  Evaluation of NAC LWT Containing 6 Failed Fuel Rods (30 WATTS TOTAL HEAT LOAD)


DESCRIPTION OF WASTE MATERIAL

   MELEM       21 (PWR )     MELEM---TYPE OF WASTE MATERIAL (SHOWN IN BRACKETS)
   BU        1600. MWD/MT    BU------AVERAGE BURNUP  (EDIT FOR BOOKEEPING PURPOSES ONLY;  NO LONGER USED)
   TIME       2.00 YEARS     TIME----COOLING TIME  (AGE OF FUEL SINCE DISCHARGE)
   WHEAT  0.0E+00 WATTS/CUFT WHEAT---DECAY HEAT GIVEN OFF BY THE WASTE MATERIAL; NOT USED IF ZERO
   DHEAT  5.0E+00 WATTS/ASSY DHEAT---DECAY HEAT GIVEN OFF BY EACH ASSEMBLY (OR CANISTER); NOT USED IF ZERO
   SRCN   6.3E+04 N/SEC/ASSY SRCN----NEUTRON SOURCE  (EDIT FOR BOOKEEPING PURPOSES ONLY;  NO LONGER USED)
   SRCG   1.1E+14 P/SEC/ASSY SRCG----PHOTON  SOURCE  (EDIT FOR BOOKEEPING PURPOSES ONLY;  NO LONGER USED)

DESCRIPTION OF WASTE CONTAINER

   ITYPE       1             ITYPE---1=CIRC CANISTERS, 2=SQUARE ASSYS (NO CANS), 3=SQR ASSYS WITH SQR CANS
   NPINS       1             NPINS---NUMBER OF FUEL PINS PER ASSEMBLY (IF MELEM DENOTES PWR OR BWR FUEL)
   MCAN        5 ( AL )      MCAN----TYPE OF MATERIAL USED FOR CANISTERS (NO CAN USED IF MCAN=0)
   ODCAN    3.00 INCHES      ODCAN---OUTSIDE DIAM OR WIDTH OF CAN (MCAN.GT.0), OR WIDTH OF ASSEMBLY (MCAN=0)
   TKCAN    .125 INCHES      TKCAN---WALL THICKNESS OF CANISTER (IF MCAN.GT.0)
   HTCAN   12.00 FEET        HTCAN---LENGTH OF CANISTER (ITYPE=1 OR 3), OR LENGTH OF FUEL ASSEMBLY (ITYPE=2)
   HTSABS    .00 FEET        HTSABS--LENGTH OF INTERNAL SHOCK ABSORBERS HOLDING ASSYS OR CANISTERS IN CASK
   HTFUEL  12.00 FEET        HTFUEL--ACTIVE LENGTH OF UO2 FUEL, OR HT OF SOLID WASTE MATL IN CAN (FULL IF 0)

DESCRIPTION OF INSERT

   MINSRT      5 ( AL )      MINSRT--TYPE OF MATERIAL USED FOR INSERT (SHOWN IN BRACKETS)
   EMINST   .220             EMINST--SURFACE EMISSIVITY OF THE INSERT MATERIAL (DIMENSIONLESS)
   TKINST   .010 INCHES      TKINST--THICKNESS OF INSERT BETWEEN ASSEMBLIES (INCLUDES TPOISN)
   TPOISN   .000 INCHES      TPOISN--THICKNESS OF NEUTRON POISON IMBEDDED IN INSERT MATL BETWEEN ASSEMBLIES
   TKCGAP  -.010 INCHES      TKCGAP--THICKNESS OF GAP BETWEEN CANISTER AND INSERT (HE-FILLED IF < 0)
   TKIGAP 3.750 INCHES       TKIGAP--THICKNESS OF GAP BETWEEN INSERT AND THE INNER SHELL (AIR-FILLED IF > 0)
   WTHICK   .000 INCHES      WTHICK--THICKNESS OF THE INSERT BETWEEN CANISTER AND INNER SHELL
   NELEM       6             NELEM---NUMBER OF ASSEMBLIES (OR CANISTERS) PER CASK;  IF ZERO, PERFORM SEARCH
   CASKID  13.38 INCHES      CASKID--INSIDE DIAMETER OF THE CASK (CALCULATED BY CODE IF USER ENTERS 0.0)

DESCRIPTION OF INNER & OUTER SHELL AND THE OUTSIDE LINER

   MISHL       6 ( SS )      MISHL---TYPE OF MATERIAL USED FOR THE INNER SHELL (SHOWN IN BRACKETS)
   MOSHL       6 ( SS )      MOSHL---TYPE OF MATERIAL USED FOR THE OUTER SHELL (SHOWN IN BRACKETS)
   MOLIN       6 ( SS )      MOLIN---TYPE OF MATERIAL USED FOR OUTSIDE LINER AND FINS (IF REQUIRED)
   TKISHL   .750 INCHES      TKISHL--THICKNESS OF INNER SHELL
   TKOSHL  1.200 INCHES      TKOSHL--THICKNESS OF OUTER SHELL
   TKOLIN   .236 INCHES      TKOLIN--THICKNESS OF OUTSIDE LINER

DESCRIPTION OF NEUTRON AND GAMMA SHIELDS

   MNSHLD      0 (SOLID  )   MNSHLD--TYPE OF MATERIAL USED FOR NEUTRON SHIELD (DESCRIBED BELOW IF SOLID)
   MGSHLD      1 ( PB    )   MGSHLD--TYPE OF MATERIAL USED FOR GAMMA SHIELD (SHOWN IN BRACKETS)

DESCRIPTION OF HEAT TRANSFER PARAMETERS FOR FINS (& CASK)

   MFIN        6 ( SS )      MFIN----TYPE OF MATERIAL USED FOR FINS (IF REQUIRED)
   SPFIN   1.000 INCHES      SPFIN---SPACING BETWEEN FINS
   EMISF    .587             EMISF---SURFACE EMISSIVITY OF THE FINS (DIMENSIONLESS)
   EMISC    .500             EMISC---SURFACE EMISSIVITY OF THE CASK (DIMENSIONLESS)
```

Figure 3.6-2 Failed Fuel Basket SCOPE Output (Continued)

```
CASK DESIGN PARAMETERS

   TFMMAX   750.0 DEG.F      TFMMAX--MAXIMUM ALLOWABLE SURFACE TEMPERATURE
   WGHTMX   200.0 KILO.LBS   WGHTMX--MAXIMUM ALLOWABLE WEIGHT OF LOADED CASK
   TAMB     100.0 DEG.F      TAMB----OUTSIDE AMBIENT TEMPERATURE
   NSOLAR       1 INCLUDE    NSOLAR--SOLAR HEATING IN NORMAL STEADY-STATE CALCULATION (INCLUDE/IGNORE=1/0)

KIND OF TRANSIENT THERMAL ANALYSIS TO BE PERFORMED

   KTRANS =     6 OPTION SELECTED BY USER;  OTHER POSSIBLE OPTIONS INCLUDE:

   KTRANS=4 ... ASSUME LIQUID WATER NEUTRON SHIELD IS LOST MANY HOURS BEFORE START OF FIRE (ORIGINAL SCOPE DEFAULT)
   KTRANS=5 ... ASSUME LIQUID NEUTRON SHIELD IS LOST INSTANTLY AT THE START OF THE FIRE (STANDARD NRC SCENARIO)
   KTRANS=6 ... ASSUME A SOLID NEUTRON SHIELD, USE DATA BELOW, AND SWITCH TO NEW THERMAL CONDUCTIVITY DURING FIRE

THERMAL CHARACTERISTICS OF SOLID NEUTRON SHIELD (THE FOLLOWING DATA IS NOT USED UNLESS KTRANS=6)

   RHONS      .07 LBM/CUFT     RHONS--NOMINAL DENSITY OF THE SOLID NEUTRON SHIELD
   TCNS1    .0154 BTU/HR/FT/F  TCNS1--NOMINAL THERMAL CONDUCTIVITY OF THE SOLID NEUTRON SHIELD
   TCNS2    .0154 BTU/HR/FT/F  TCNS2--THERMAL CONDUCTIVITY OF THE SOLID NEUTRON SHIELD DURING AND AFTER THE FIRE
   CPNS2    .2400 BTU/LB/DG.F  CPNS2--HEAT CAPACITY OF THE SOLID NEUTRON SHIELD DURING AND AFTER THE FIRE
```

Figure 3.6-2 Failed Fuel Basket SCOPE Output (Continued)

```
S C O P E -- THE SHIPPING CASK OPTIMIZATION AND PARAMETRIC EVALUATION CODE, VERSION 1.2  (BY J. A. BUCHOLZ, ORNL)

TITLE:  Evaluation of NAC LWT Containing 6 Failed Fuel Rods (30 WATTS TOTAL HEAT LOAD)

COMPONENT DIMENSIONS (INCHES):

  O-LINER =    .236
  N-SHIELD =  5.000
  O-SHELL =   1.200
  G-SHIELD =  5.750
  I-SHELL =    .750
  I-CASK =   16.580
  I-GAP =     3.750
  W-POISN =    .000
  W-INSRT =    .010
  C/P-GAP =    .010
  O-CANSTR =  3.000
  I-CANSTR =  2.750
  Q-LENGTH = 143.750

THERMAL PARAMETERS:

  SOLAR INSOLANCE  =  1 (INCLUDED)
  AMBIENT TEMP     =  100.000 (DEG.F)
  TOTAL DECAY HEAT =    .030 (KW)

                                NOMINAL STEADY STATE TEMPERATURES (DEGREES-F)

SURFACE      O-LINER          N-SHIELD         O-SHELL          PB-SHIELD        I-SHELL
  T        DT   T(MAX)      DT   T(MAX)      DT   T(MAX)      DT   T(MAX)      DT   T(MAX)
-------  ---------------  ---------------  ---------------  ---------------  ---------------
181.16     .00  181.16     24.03  205.19     .01  205.20     .03  205.24     .01  205.25

  GAP   INSERT      INSERT          GAP   CAN       CANISTER          FUEL PIN
  DT    T(MIN)     DT   T(MAX)     DT    T(MIN)     DT   T(MAX)     DT   T(MAX)    DEG.C
-------------  ---------------  ---------------  ---------------  ---------------------
 8.44  213.69     .02  213.71      .09  213.79      .00  213.79     2.13  215.92   102.18

(*) OUTSIDE DIAMETER OF THE CASK BODY =  42.45 INCHES;  NO EXTERNAL COOLING FINS WERE REQUIRED.
    TOTAL WGHT OF CASK LOADED WITH  6 FUEL ASSEMBLIES OR CANISTERS IS APPROXIMATELY  39249 LBS.
```

Figure 3.6-2 Failed Fuel Basket SCOPE Output (Continued)

```
                                PREFIRE TEMPERATURES (DEGREES-F)

TIME...(H.M.S)   *-------INSERT----*--GAP--*----I.SHELL----*---G.SHIELD----*----O.SHELL----*----M.SHIELD----*----O.LINER------*

RADIUS (FT)==>    .3082  .3451  .3783  .6908  .7228  .7533 1.0214 1.2325 1.2835 1.3325 1.5549 1.7492 1.7590 1.7688

                REFERENCE STEADY-STATE TEMPERATURES USED IN CALCULATING TEMP RISE (ASSUMES M-SHLD PRESENT & NO SOLAR HEATING):
  .00  0. 0. 0  136.65 136.64 136.64 124.97 124.96 124.96 124.93 124.92 124.92 124.91 111.35 100.98 100.97 100.97

                INITIAL STEADY-STATE TEMPERATURES AT START OF 30-MINUTE FIRE (SEE ASSUMPTIONS FOR KTRANS=6):
  .00  0. 0. 0  136.65 136.64 136.64 124.97 124.96 124.96 124.93 124.92 124.92 124.91 111.35 100.98 100.97 100.97

INIT TEMP RISE     .00    .00    .00    .00    .00    .00    .00    .00    .00    .00    .00    .00    .00    .00

                                ULTIMATE POSTFIRE TEMPERATURES (DEGREES-F)

TIME...(H.M.S)   *-------INSERT----*--GAP--*----I.SHELL----*---G.SHIELD----*----O.SHELL----*----M.SHIELD----*----O.LINER------*

                ULTIMATE STEADY-STATE TEMPERATURES, LONG AFTER THE 30-MINUTE FIRE IS OVER:
999.0  999.0.0  136.65 136.64 136.64 124.97 124.96 124.96 124.93 124.92 124.92 124.91 111.35 100.98 100.97 100.97

                                TRANSIENT TEMPERATURES (DEGREES-F)

                 *-------INSERT----*--GAP--*----I.SHELL----*---G.SHIELD----*----O.SHELL----*----M.SHIELD----*----O.LINER------*

MAX TEMP RISE:     2.36   2.36   2.36   2.68   2.68   2.68   2.68   2.68   2.69   2.69 750.52 1322.80 1322.85 1322.89
AT TIME (HRS):    31.33  31.00  31.00   4.42   4.42   4.33   4.25   4.08   4.00   3.92    .50    .50    .50    .50

MAX FIRE TEMP:   139.01 139.01 139.00 127.65 127.64 127.64 127.62 127.61 127.60 127.60 861.87 1423.78 1423.82 1423.86


DURING AND AFTER THE 30-MINUTE FIRE:

      MAX GAMMA SHIELD TEMP..... 126 DEG.F =  53 DEG.C
      MAX BASKET INSERT TEMP..... 139 DEG.F =  59 DEG.C
      MAX FUEL PIN CLAD TEMP..... 142 DEG.F =  61 DEG.C

AS PER 10CFR73, SECT 71.73, THE EFFECTS OF SOLAR HEATING WERE
NEGLECTED PRIOR TO, DURING, AND AFTER THE 30-MINUTE FIRE.
```

Figure 3.6-3 Nine Failed Metallic Fuel Rods SCOPE Input

```
S C O P E   INPUT (IN CARD-IMAGE FORMAT) FOLLOWS:

Evaluation of NAC LWT Containing 9 Failed Fuel Rods (45 WATTS TOTAL HEAT LOAD)
' ================================================================================
' MELEM   BURNUP    TIME    WHEAT    DHEAT    SRCN    SRCG      ITYPE   NPINS
   21     1600       2      0.0      15.0    6.31+4  1.12+14     1       1
'
' MCAN    ODCAN    TKCAN    HTCAN    HTVOID    HTFUEL
   5      4.25     0.125    12.00      0        12.00
'
' MINSRT    EMINSRT     TKINSRT     TPOISN       TKCGAP     TKIGAP     WTHICK
   5         0.22         0.01        0.0          0.69       0.188      0.0
'
' NELEM    CASKID
   3        13.375
'
' MISHL  MOSHL  MOLIN  MFIN       TKISHL  TKOSHL  TKOLIN       MGSHLD
   6      6      6      6          0.75     1.2    0.236          1
'
' SPFIN    EMISF     EMISC     TFNMAX     WGHTMX
   1        0.587     0.50       750        200
'
' KTRANS     RHONS     TCNS1     TCNS2     CPNS2
   6         0.071     0.0154    0.0154    0.24
'
' GENERAL FORMAT FOR SHIELDING DATA:
' LTYPE, NUMPTS, (NASSYS(I,LTYPE),TKG(I,LTYPE),TKN(I,LTYPE), I=1,NUMPTS)
' --------------------------------------------------------------------
'
' SHIELDING DATA FOR 5.75-INCH PB-METAL CASKS
' (ASSUMES A 5-INCH NEUTRON SHIELD)
1 1  6 5.75  5.0
' --------------------------------------------------------------------
' TERMINATION FLAG (FOR THIS PARTICULAR CASE):
```

Figure 3.6-4 Nine Failed Metallic Fuel Rods SCOPE Output

PROPERTIES OF MATERIALS CURRENTLY IN THE SCOPE DATA LIBRARY

MATERIAL		DENSITY (LB/CUFT)	CONDUCTIVITY (BTU/HR/FT/F)	HEAT CAPACITY (BTU/LB/F)	TEMPERATURE LIMIT (DEGREES F)	CAPITAL COST ($/LB)
1	PB	708.56	19.3000	.0320	618	7.500
2	FE	488.26	26.0000	.1200	1950	5.000
3	U	1189.25	15.0000	.0280	1450	22.500
4	CU	559.35	210.0000	.0950	1730	1.400
5	AL	168.49	80.0000	.2280	1050	.700
6	SS	494.43	9.6900	.1200	1800	10.000
7	NA	45.00	38.0000	.3000	1400	.500
8	LI	30.00	20.0000	1.0000	1400	27.500
9	PB-L	146.60	.4400	.1560	1200	4.700
10	CONC	707.60	18.0000	.0320	618	.400
11	ALSI	170.00	80.0000	.2000	1065	.880
12	DOWA	62.00	.0760	.5260	600	2.500
13	HE	.00	.1200	1.2400	1400	.000
14	AIR	.08	.0360	.2600	1400	.000
15	H2O	62.43	.3920	1.0000	250	.000
16	HUL3	81.20	.3000	.0660	1000	.000
17	SHOT	370.00	.3500	.0950	1400	.000
18	HUL1	284.00	1.2000	.0660	1000	.000
19	HLWG	212.00	.7000	.1600	1290	.000
20	HUL2	203.00	.6000	.0660	1000	.000
21	PWR	220.90	1.0000	.1000	1650	.000
22	BWR	199.30	1.0000	.1000	1650	.000
23	HLWC	113.00	.2500	.2200	932	.000

NOTE: THIS EDIT WILL BE PRINTED ONLY ONCE, EVEN THOUGH
THE USER MAY HAVE MULTIPLE SETS OF INPUT DATA.

Figure 3.6-4 Nine Failed Metallic Fuel Rods SCOPE Output (Continued)

```
TITLE:  Evaluation of NAC LWT Containing 9 Failed Fuel Rods (45 WATTS TOTAL HEAT LOAD)


DESCRIPTION OF WASTE MATERIAL

   MELEM       21 (PWR )     MELEM---TYPE OF WASTE MATERIAL (SHOWN IN BRACKETS)
   BU        1600. MWD/MT    BU------AVERAGE BURNUP  (EDIT FOR BOOKEEPING PURPOSES ONLY;  NO LONGER USED)
   TIME       2.00 YEARS     TIME----COOLING TIME  (AGE OF FUEL SINCE DISCHARGE)
   WHEAT  0.0E+00 WATTS/CUFT WHEAT---DECAY HEAT GIVEN OFF BY THE WASTE MATERIAL; NOT USED IF ZERO
   DHEAT  1.5E+01 WATTS/ASSY DHEAT---DECAY HEAT GIVEN OFF BY EACH ASSEMBLY (OR CANISTER); NOT USED IF ZERO
   SRCN   6.3E+04 N/SEC/ASSY SRCN----NEUTRON SOURCE  (EDIT FOR BOOKEEPING PURPOSES ONLY;  NO LONGER USED)
   SRCG   1.1E+14 P/SEC/ASSY SRCG----PHOTON  SOURCE  (EDIT FOR BOOKEEPING PURPOSES ONLY;  NO LONGER USED)

DESCRIPTION OF WASTE CONTAINER

   ITYPE        1            ITYPE---1=CIRC CANISTERS, 2=SQUARE ASSYS (NO CANS), 3=SQR ASSYS WITH SQR CANS
   NPINS        1            NPINS---NUMBER OF FUEL PINS PER ASSEMBLY (IF MELEM DENOTES PWR OR BWR FUEL)
   MCAN         5 ( AL )     MCAN----TYPE OF MATERIAL USED FOR CANISTERS (NO CAN USED IF MCAN=0)
   ODCAN     4.25 INCHES     ODCAN---OUTSIDE DIAM OR WIDTH OF CAN (MCAN.GT.0), OR WIDTH OF ASSEMBLY (MCAN=0)
   TKCAN     .125 INCHES     TKCAN---WALL THICKNESS OF CANISTER (IF MCAN.GT.0)
   HTCAN    12.00 FEET       HTCAN---LENGTH OF CANISTER (ITYPE=1 OR 3), OR LENGTH OF FUEL ASSEMBLY (ITYPE=2)
   HTSABS    .00 FEET        HTSABS--LENGTH OF INTERNAL SHOCK ABSORBERS HOLDING ASSYS OR CANISTERS IN CASK
   HTFUEL   12.00 FEET       HTFUEL--ACTIVE LENGTH OF UO2 FUEL, OR HT OF SOLID WASTE MATL IN CAN (FULL IF 0)

DESCRIPTION OF INSERT

   MINSRT       5 ( AL )     MINSRT--TYPE OF MATERIAL USED FOR INSERT (SHOWN IN BRACKETS)
   EMINST    .220            EMINST--SURFACE EMISSIVITY OF THE INSERT MATERIAL (DIMENSIONLESS)
   TKINST    .010 INCHES     TKINST--THICKNESS OF INSERT BETWEEN ASSEMBLIES (INCLUDES TPOISN)
   TPOISN    .000 INCHES     TPOISN--THICKNESS OF NEUTRON POISON IMBEDDED IN INSERT MATL BETWEEN ASSEMBLIES
   TKCGAP    .690 INCHES     TKCGAP--THICKNESS OF GAP BETWEEN CANISTER AND INSERT (AIR-FILLED IF > 0)
   TKIGAP    .188 INCHES     TKIGAP--THICKNESS OF GAP BETWEEN INSERT AND THE INNER SHELL (AIR-FILLED IF > 0)
   WTHICK    .000 INCHES     WTHICK--THICKNESS OF THE INSERT BETWEEN CANISTER AND INNER SHELL
   NELEM        3            NELEM---NUMBER OF ASSEMBLIES (OR CANISTERS) PER CASK;  IF ZERO, PERFORM SEARCH
   CASKID   13.38 INCHES     CASKID--INSIDE DIAMETER OF THE CASK (CALCULATED BY CODE IF USER ENTERS 0.0)

DESCRIPTION OF INNER & OUTER SHELL AND THE OUTSIDE LINER

   MISHL        6 ( SS )     MISHL---TYPE OF MATERIAL USED FOR THE INNER SHELL (SHOWN IN BRACKETS)
   MOSHL        6 ( SS )     MOSHL---TYPE OF MATERIAL USED FOR THE OUTER SHELL (SHOWN IN BRACKETS)
   MOLIN        6 ( SS )     MOLIN---TYPE OF MATERIAL USED FOR OUTSIDE LINER AND FINS (IF REQUIRED)
   TKISHL    .750 INCHES     TKISHL--THICKNESS OF INNER SHELL
   TKOSHL   1.200 INCHES     TKOSHL--THICKNESS OF OUTER SHELL
   TKOLIN    .236 INCHES     TKOLIN--THICKNESS OF OUTSIDE LINER

DESCRIPTION OF NEUTRON AND GAMMA SHIELDS

   MNSHLD       0 (SOLID  )  MNSHLD--TYPE OF MATERIAL USED FOR NEUTRON SHIELD (DESCRIBED BELOW IF SOLID)
   MGSHLD       1 ( PB    )  MGSHLD--TYPE OF MATERIAL USED FOR GAMMA SHIELD (SHOWN IN BRACKETS)

DESCRIPTION OF HEAT TRANSFER PARAMETERS FOR FINS (& CASK)

   MFIN         6 ( SS )     MFIN----TYPE OF MATERIAL USED FOR FINS (IF REQUIRED)
   SPFIN   1.000 INCHES      SPFIN---SPACING BETWEEN FINS
   EMISF    .587             EMISF---SURFACE EMISSIVITY OF THE FINS (DIMENSIONLESS)
   EMISC    .500             EMISC---SURFACE EMISSIVITY OF THE CASK (DIMENSIONLESS)
```

Figure 3.6-4 Nine Failed Metallic Fuel Rods SCOPE Output (Continued)

```
CASK DESIGN PARAMETERS

   TFNMAX   750.0 DEG.F      TFNMAX--MAXIMUM ALLOWABLE SURFACE TEMPERATURE
   WGHTMX   200.0 KILO.LBS   WGHTMX--MAXIMUM ALLOWABLE WEIGHT OF LOADED CASK
   TAMB     100.0 DEG.F      TAMB----OUTSIDE AMBIENT TEMPERATURE
   NSOLAR       1 INCLUDE    NSOLAR--SOLAR HEATING IN NORMAL STEADY-STATE CALCULATION (INCLUDE/IGNORE=1/0)

KIND OF TRANSIENT THERMAL ANALYSIS TO BE PERFORMED

   KTRANS =     6 OPTION SELECTED BY USER;  OTHER POSSIBLE OPTIONS INCLUDE:

   KTRANS=4 ... ASSUME LIQUID WATER NEUTRON SHIELD IS LOST MANY HOURS BEFORE START OF FIRE (ORIGINAL SCOPE DEFAULT)
   KTRANS=5 ... ASSUME LIQUID NEUTRON SHIELD IS LOST INSTANTLY AT THE START OF THE FIRE (STANDARD NRC SCENARIO)
   KTRANS=6 ... ASSUME A SOLID NEUTRON SHIELD, USE DATA BELOW, AND SWITCH TO NEW THERMAL CONDUCTIVITY DURING FIRE

THERMAL CHARACTERISTICS OF SOLID NEUTRON SHIELD (THE FOLLOWING DATA IS NOT USED UNLESS KTRANS=6)

   RHONS      .07 LBM/CUFT      RHONS--NOMINAL DENSITY OF THE SOLID NEUTRON SHIELD
   TCNS1    .0154 BTU/HR/FT/F   TCNS1--NOMINAL THERMAL CONDUCTIVITY OF THE SOLID NEUTRON SHIELD
   TCNS2    .0154 BTU/HR/FT/F   TCNS2--THERMAL CONDUCTIVITY OF THE SOLID NEUTRON SHIELD DURING AND AFTER THE FIRE
   CPNS2    .2400 BTU/LB/DG.F   CPNS2--HEAT CAPACITY OF THE SOLID NEUTRON SHIELD DURING AND AFTER THE FIRE
```